

Infrared Solar Spectroscopic Measurements of Free Tropospheric CO, C<sub>2</sub>H<sub>6</sub>, and HCN  
above Mauna Loa, Hawaii: Seasonal Variations and Evidence for Enhanced Emissions  
from the Southeast Asian Tropical Fires of 1997-1998

C. P. Rinsland,<sup>1</sup> A. Goldman,<sup>2</sup> F. J. Murcray,<sup>2</sup> T. M. Stephen,<sup>2</sup> N. S. Pougatchev,<sup>3</sup> J.  
Fishman,<sup>1</sup> S. J. David,<sup>2</sup> R. D. Blatherwick,<sup>2</sup> P. C. Novelli,<sup>4</sup> N. B. Jones,<sup>5</sup> and B. J.  
Connor<sup>5</sup>

<sup>1</sup>NASA Langley Research Center, Hampton, VA

<sup>2</sup>Department of Physics, University of Denver, Denver, CO

<sup>3</sup>Department of Physics, Christopher Newport University, Newport News, VA

<sup>4</sup>Climate Monitoring and Diagnostics Laboratory, National Oceanic and Atmospheric  
Administration Boulder, CO

<sup>5</sup>National Institute of Water and Atmospheric Research, Lauder, New Zealand



UNIVERSITY of DENVER

Department of Physics

Phone (303) 871-3486 FAX (303) 778-0406

email: kamurcra@du.edu

July 13, 1999

NASA Center for AeroSpace Information  
Parkway Center  
7121 Standard Drive  
Hanover, MD 21076-1320

To Whom It May Concern,

Enclosed please one micro-reproducible copy of our research on NASA grant NSG 1432.

If you need further information please feel free to contact me at the number(s) listed above.

Sincerely Yours,

A handwritten signature in cursive script that reads "Kathy".

Kathleen J. Murcra  
Research Office Manager

Enc.

**Abstract.** High spectral resolution ( $0.003\text{ cm}^{-1}$ ) infrared solar absorption measurements of CO, C<sub>2</sub>H<sub>6</sub>, and HCN have been recorded at the Network for the Detection of Stratospheric Change station on Mauna Loa, Hawaii, (19.5°N, 155.6°W, altitude 3.4 km). The observations were obtained on over 250 days between August 1995 and February 1998. Column measurements are reported for the 3.4-16 km altitude region, which corresponds approximately to the free troposphere above the station. Average CO mixing ratios computed for this layer have been compared with flask sampling CO measurements obtained *in situ* at the station during the same time period. Both show asymmetrical seasonal cycles superimposed on significant variability. The first two years of observations exhibit a broad January-April maximum and a sharper CO minimum during late summer. The C<sub>2</sub>H<sub>6</sub> and CO 3.4-16 km columns were highly correlated throughout the observing period with the C<sub>2</sub>H<sub>6</sub>/CO slope intermediate between higher and lower values derived from similar infrared spectroscopic measurements at 32°N and 45°S latitude, respectively. Variable enhancements in CO, C<sub>2</sub>H<sub>6</sub>, and particularly HCN were observed beginning in about September 1997. The maximum HCN free tropospheric monthly mean column observed in November 1997 corresponds to an average 3.4-16 km mixing ratio of 0.7 ppbv (1 ppbv= $10^{-9}$  per unit volume), more than a factor of 3 above the background level. The HCN enhancements continued through the end of the observational series. Back-trajectory calculations suggest that the emissions originated at low northern latitudes in southeast Asia. Surface CO mixing ratios and the C<sub>2</sub>H<sub>6</sub> tropospheric columns measured during the same time also showed anomalous autumn 1997 maxima. The intense and widespread tropical wild fires that burned during

the strong El Niño warm phase of 1997-1998 are the likely source of the elevated emission products.



## 1. Introduction

The purpose of this paper is to report and interpret a time series of measurements derived from high resolution ( $0.003\text{ cm}^{-1}$ ) infrared solar absorption spectra. The observations were recorded between August 1995 and February 1998 with a Fourier transform spectrometer operated at the Network for the Detection of Stratospheric Change (NDSC) [*Kurylo*, 1991; URL: <http://climon.wwb.noaa.gov>] station on Mauna Loa, Hawaii (latitude  $19.5^{\circ}\text{N}$ ,  $155.6^{\circ}\text{W}$ , altitude 3.4 km). The 3 molecules analyzed are CO,  $\text{C}_2\text{H}_6$ , and HCN. The infrared spectroscopic observations sample a broad altitude region with maximum sensitivity in the upper troposphere. We report partial column for the 3.4-16 km altitude region. This region corresponds approximately to the free troposphere above the station. The seasonal variations of the partial columns are reported and compared with each other, previous measurements, and model calculations.

The molecules included in this investigation are important indicators of tropospheric pollution and transport. They are released at the surface and have mean tropospheric photochemical lifetimes of about a month for both CO and  $\text{C}_2\text{H}_6$  [*McKeen et al.*, 1996, table 1] and about 2.5 years for HCN [*Cicerone and Zellner*, 1983]. Table 1 lists the most important sources for each molecule. As highlighted by this table, biomass burning is an important source for all 3 gases. The lifetimes of CO,  $\text{C}_2\text{H}_6$ , and HCN are relatively short so that they undergo significant seasonal variations that contain important information on the regional distributions of sources and sinks and their variations with time. Carbon monoxide and nonmethane hydrocarbons such as  $\text{C}_2\text{H}_6$  are also important  $\text{O}_3$  precursors. All 3 molecules have strong infrared spectral features that are readily

measured by solar absorption spectroscopy [e.g., *Rinsland et al.*, 1982, 1998a; *Mahieu et al.*, 1995, 1997; *Notholt et al.*, 1999].

The Mauna Loa facility is a well-instrumented, high-altitude station for monitoring of atmospheric constituents, aerosols, meteorological parameters, UV radiation, and solar radiation [*Climate Monitoring and Diagnostics Laboratory (CMDL)*, 1998]. Due to its high elevation, Mauna Loa is located primarily in the free troposphere [*Mendonca*, 1969]. With the exception of the observations from Mauna Loa, the mid-Pacific region is data sparse with few previous measurements of constituents in the free troposphere or time series of observations. Trajectories arriving at MLO within 10 days originate mostly from Asia during winter and spring with the station mostly isolated from Asian influence during summer when some trajectories originate from over Central America within 10 days [*CMDL*, 1998; *Kuniyuki et al.*, 1998]. Fall is a season of transition between easterly trades and westerly flow [*CMDL*, 1998]. Transport of trace gases to the Mauna Loa observatory have been discussed in several recent studies [e.g., *Jaffe et al.*, 1997; *Harris et al.*, 1992, 1998]. Three important aircraft field campaigns have been conducted by NASA's Global Tropospheric Experiment (GTE) to study tropospheric chemistry and transport over the Pacific basin [*Hoell et al.*, 1996, 1997, 1999]. Tropospheric remote sensing measurements have also been obtained in this region during several shuttle flights [*Reichle et al.*, 1986, 1990, 1999; *Connors et al.*, 1999; *Rinsland et al.*, 1998a].

## **2. Infrared Spectroscopic Observations**

The infrared solar absorption measurements at the Mauna Loa observatory (MLO) were recorded with a modified Bruker model 120-HR Fourier transform spectrometer

(FTS) operated at an unapodized spectral resolution of  $0.0035 \text{ cm}^{-1}$  (defined as 0.9 divided by the maximum optical path difference). The instrument, installed in August 1995, is equipped with a computer-controlled solar tracker with a hatched weather-tight enclosure. The system only requires an operator to fill the detector dewars with liquid nitrogen once a day. The system monitors the weather conditions and records solar spectra when conditions are favorable. Observations are scheduled at sunrise and sunset beginning on Monday afternoon through Saturday morning. Under favorable conditions, the morning observations commence at  $85^\circ$  solar zenith angle with a total of 10 measurements recorded in 6 spectral bandpasses. Each observation is obtained from 2 complete interferograms recorded over a 4-minute time period. An additional 4 minutes is required for computer evaluation and processing time of the observation. The database analyzed here covers the August 1995 to February 1998, excluding time periods lost due to instrumental problems. Most measurements were obtained in the morning because of more frequent cloudiness in the afternoon.

Observations from the same site were also obtained between May 1991 and November 1995 with a Bomem model DA3.002 FTS operated typically at  $0.005 \text{ cm}^{-1}$  resolution [e.g., *Goldman et al.*, 1992; *David et al.*, 1994; *Rinsland et al.*, 1994]. Additionally, infrared spectra were recorded at  $0.02 \text{ cm}^{-1}$  resolution on 4 days in February 1987 [*Rinsland et al.*, 1988]. Both sets of earlier measurements were obtained less frequently, and they are generally of lower quality relative to the more recent measurements. Hence, only the measurements recorded with the Bruker interferometer are included in the present investigation.

### 3. Analysis Method and Assumptions

#### a.) Retrieval Algorithm

The infrared solar spectra were analyzed with the SFIT2 algorithm, which has been developed for the retrieval of molecular vertical profiles from ground-based infrared solar absorption spectra. The profiles of one or two molecules are retrieved by simultaneously fitting one or more narrow spectral intervals (microwindows) in one or more solar spectra. The forward and inverse models in SFIT2 have been described previously [Pougatchev *et al.*, 1995; Rinsland *et al.* 1998b]. The algorithm includes a crude model for simulating and fitting the absorption by solar CO lines [Rinsland *et al.*, 1998b, section 3.2.2]. The modeling of instrument performance-related parameters includes a parameter to retrieve the wavelength shift between the measured and calculated spectra and a parameter to fit for the slope of the background in each microwindow. The latter parameter was required primarily because of uncertainties in modeling the absorption by lines outside the fitted regions, particularly those of H<sub>2</sub>O and its continuum.

#### b.) *A priori* Profiles and Covariance Matrix Parameters

Below 12 km, *a priori* profiles for CO and C<sub>2</sub>H<sub>6</sub> were derived by averaging aircraft *in situ* profile measurements obtained near Mauna Loa during 3 GTE missions. The measurements were obtained during the Pacific Exploratory Mission (PEM)-West, phase A, conducted September-October 1991 [Hoell *et al.*, 1996], PEM-West, phase B, conducted during February-March 1994 [Hoell *et al.*, 1997], and PEM-Tropics A conducted between August-October 1996 [Hoell *et al.*, 1999]. Prior CO *in situ* measurements from Mauna Loa show considerable variability throughout the year. A

factor of two seasonal variation at the surface is indicated from time series of CMDL observations [Novelli *et al.*, 1992; 1998]. Similarly, a factor of two seasonal change was indicated from C<sub>2</sub>H<sub>6</sub> infrared total column measurements [Rinsland *et al.*, 1994]. The late winter GTE observations were obtained near maxima in both the CO and C<sub>2</sub>H<sub>6</sub> seasonal cycles. We assumed the mean of the late winter and autumn profiles for both molecules. Above 12 km, the profiles were connected to averages of version 2 profiles measured by the Atmospheric Trace MOlecule Spectroscopy (ATMOS) experiment during the Atmospheric Laboratory for Applications and Science (ATLAS)-3 mission of November 1994 [Gunson *et al.*, 1996]. ATMOS measurements between latitudes of 15°N and 25°N were averaged to derive the *a priori* profiles for CO and C<sub>2</sub>H<sub>6</sub>.

For HCN, a constant mixing ratio of 190 pptv ( $10^{-12}$  per unit volume) was assumed below 16 km. At higher altitudes a vertical distribution scaled to connect smoothly to the reference profile given in Table III of Mahieu *et al.* [1995]. This profile is based on retrievals from ground-based infrared solar spectra recorded at the U.S. National Solar Observatory facility on Kitt Peak, Arizona (31.9°N latitude, 111.6°W longitude, altitude 2.09 km) and the International Scientific Station of the Jungfrauoch (ISSJ) in the Swiss Alps (46.6°N latitude, 8.0°E longitude, altitude 3.58 km) [Mahieu *et al.*, 1995].

Vertical temperature profiles assumed in the analysis were taken from daily mean National Centers for Environmental Prediction (NCEP) measurements. They were smoothly connected to the 1976 U.S. Standard Atmosphere above 65 km. *A priori* volume mixing ratio profiles for interfering species were taken from reference compilations (e.g., Smith [1982]).

### c.) Spectroscopic Parameters and Microwindow Selections

Spectroscopic parameters adopted in the present study were taken from the 1996 HITRAN compilation [Rothman *et al.*, 1998], except for the  $C_2H_6$  parameters which were replaced by improved values [Rinsland *et al.*, 1998b, section 4.1] based on updates to the work of Pine and Stone [1996]. A line of HDO was added at  $4274.81\text{ cm}^{-1}$  to account for an unassigned absorption feature [Rinsland *et al.*, 1998b, section 4.2]. Absorption by this transition is very weak because of the low  $H_2O$  column abundance above the high-altitude Mauna Loa station.

Table 2 lists the microwindows selected for the analysis of each molecule along with a list of the interfering molecules that were fitted. The CO and  $C_2H_6$  windows are identical to those used in a previous investigation [Rinsland *et al.*, 1998b]; simulations of the atmospheric absorption by the individual molecules were displayed in Figs. 5 and 7 of that paper. One of the two windows selected for retrieving profiles of CO contains the strong  $CH_4$  line at  $4285.1553\text{ cm}^{-1}$  [Rinsland *et al.*, 1998b, Fig. 7]. As in the previous study, the profile of  $CH_4$  was also retrieved, though the results for this molecule are not reported here.

The interval for retrieving HCN contains the  $\nu_3$  band P(8) line at  $3287.2483\text{ cm}^{-1}$ . This transition is located in the far wings of the strong  $H_2O$  lines at  $3286.1689$  and  $3288.4829\text{ cm}^{-1}$  with weak transitions of  $CO_2$  and several less significant absorbers nearby [Rinsland *et al.*, 1982]. Fits to the HCN  $\nu_3$  band P(4) line at  $3299.5273\text{ cm}^{-1}$  simultaneously with the P(8) line showed minor inconsistencies. This problem was noted previously by Mahieu *et al.* [1995]. Therefore, we decided not to include the P(4) line in the analysis.

#### d.) Retrieval Characterization

Averaging kernels provide a direct assessment of the theoretical altitude sensitivity of the observations in the absence of errors in the measurements and model parameters [Rodgers, 1990, section 4]. They are a function of the retrieval intervals selected, the spectral resolution of the observations, the assumed signal-to-noise of the measurements, and the selections of the retrieval parameters, such as the *a priori* profile and its covariance matrix. In this work, we assumed the covariance matrix is diagonal and adopted a relative uncertainty equal to 0.5 times the *a priori* mixing ratio in each of the 29 layers in the atmospheric model extending from the surface (3.4 km) to 100 km. Figure 1 shows the averaging kernels for CO, C<sub>2</sub>H<sub>6</sub>, and HCN. The kernels were calculated for the spectral resolution of the measurements and the typical signal-to-noise ratio of 200. Kernels are shown for 3.4-16.0 km and the total column. The boundary at 16 km corresponds to the approximate altitude of the annual mean tropopause above Mauna Loa. As can be seen from this figure, the kernels for the 3.4-16.0 km layer are broad for all 3 molecules with sensitivities that peak in the upper troposphere. The altitudes of the peaks of the 3.4-16.0 km kernels are 11 km for CO, 11 km for C<sub>2</sub>H<sub>6</sub>, and 13 km for HCN, respectively.

#### e.) Error Analysis

In Table 3, we report estimates of the uncertainties in the 3.4-16.0 km columns due to both random and systematic sources of error. The approach used to estimate the uncertainties is the same as adopted previously [Rinsland *et al.*, 1998b].

The sources of random error considered are the temperature uncertainty, uncertainty in the solar zenith angle, the effect of random instrumental noise, and errors in calculating

the absorption by interfering lines. We estimated the uncertainty due to errors in the temperature profile by performed retrievals with 2 K added to the NCEP temperature at each altitude. Changes in the 3.4-16 km columns are shown in the table; the values reported for temperature are the mean offset obtained from retrievals performed with 3 randomly selected spectra on different days. The maximum error due to temperature profile uncertainty was the value of 1.7% obtained for  $C_2H_6$ .

As already mentioned, each spectrum is generated from two coadded scans. The airmass corresponding to the time of each zero path difference crossing is calculated and the values averaged. Errors are introduced by the approximations used to estimate the airmass of each spectrum and also by uncertainties in the time stamping of the individual spectral files (up to 30 sec). Calculations performed for a solar zenith angle of  $75^\circ$  indicate both effects combine to introduce an uncertainty in the calculated air mass of about 1%.

The contribution of instrumental noise was evaluated by generating random numbers with zero mean, a normal distribution, and a root-mean-square deviation equal to 0.005 times the maximum transmission in the spectral interval. The selected noise level is typical of the Mauna Loa observations. Noise generated with 10 different seeds was added to synthetic spectra calculated for a solar astronomical zenith angle of  $60^\circ$ , and the retrievals were repeated for each case. The mean difference between the 3.4-16 km columns retrieved from the noisy spectra and the values obtained without noise is given in the table. As we report only daily average partial columns, the error due to random noise will be generally less than the value in table 3.



Estimates for the random errors due to interfering atmospheric lines reflect the high altitude of Mauna Loa station. Previously, we estimated uncertainties of 7 and 2 % in the tropospheric columns of  $C_2H_6$  above Lauder, New Zealand (45.0°S latitude, 169.7°E longitude, 0.37 km altitude) and Kitt Peak, respectively [Rinsland *et al.*, 1998b, table 1]. The relatively high estimated uncertainties reflected the potential for error in the calculation of the  $H_2O$  absorption line overlapping the target  $C_2H_6$  spectral feature at  $2976.8\text{ cm}^{-1}$  [Rinsland *et al.*, 1998b, Fig. 5]. Hence, our calculated uncertainty due to potential errors in calculating the overlapping interference by  $H_2O$  absorption line is significantly reduced.

Four sources of systematic error were considered: (1) errors in the assumed spectroscopic line parameters, (2) uncertainties in the forward model, (3) errors in the *a priori* profiles, and (4) errors in the instrument line shape function. The improvements in the  $C_2H_6$  spectroscopic parameters reduced the uncertainty in those retrievals from 10% [Rinsland *et al.*, 1994] to 5% [Rinsland *et al.*, 1998b]. The forward model is also the same as adopted previously, and hence the estimated systematic error due to its limitations and approximations is unchanged [Rinsland *et al.*, 1998b]. We estimated the effect of uncertainty in knowledge of the instrument line shape function by generating a synthetic spectrum for each molecule based on the instrument line shape function assumed in the retrievals. We then performed a retrieval from the synthetic spectrum with the coefficient of the “straight line” effective apodization coefficient [Park, 1983] offset from the nominal value of 0.0 to -0.2. This calculation simulates an error in the apodizing function with the error increasing from zero at the zero path difference to 20% at the maximum path difference. Changes in the 0.4-16 km columns were at less than

0.4% for all 3 molecules. Hence, errors in modeling the instrument line shape function introduce only a small error in the calculated 0.4-16 km columns. Narrow lines in the solar spectra showed no evidence for phase errors.

## 4. Results

### a.) Carbon Monoxide (CO)

Figure 2 presents typical spectral fits to the Mauna Loa solar absorption spectra in the two windows used to measure atmospheric CO. The high quality of the Mauna Loa measurements and the success in modeling the atmospheric and solar features can be noted from the low residuals, which are displayed above the measured and best-fit calculated spectra.

Figure 3 displays the time series of Mauna Loa CO measurements. The solid circles show monthly mean mixing ratios (ppbv,  $10^{-9}$  per unit volume) calculated by dividing the 3.4-16 km CO column by the total air column in the same layer. Daily averages were used in these calculations. Low signal-to-noise ratio observations and poor fits to the spectral data have been excluded [Rinsland *et al.*, 1998b, section 5.0]. The open circles show monthly averages of preliminary CO mixing ratios from the CMDL cooperative flask sampling network. The measurements were collected weekly from Mauna Loa and are referenced to the CO CMDL scale [Novelli *et al.*, 1991]. To avoid sampling boundary layer air, the measurements are obtained in the morning before upslope flow begins. Details of the sampling procedures and analytic methods can be found in Novelli *et al.* [1992, 1998]. The flask measurements have been filtered to remove observations subject to sampling errors, analytical problems, and non-background level measurements.

The vertical lines show standard deviations of the measurements. Absence of a vertical marker denotes months when FTS measurements were recorded on a single day. Only the CMDL observations obtained during the time period of the FTS measurements are presented.

The 2.6 years of CO surface and FTS measurements presented in Fig. 3 show significant short-term variations superimposed on a seasonal change of about a factor of two. The August 1995-August 1997 measurements show very similar seasonal cycles with a broad maximum in CO mixing ratio at the surface between January to April. The seasonal variations at the surface are similar those reported for 1990-1995 by *Novelli et al.* [1998, Fig. 4]. Near the peak of the cycle, the surface mixing ratio averaged 10-20% higher than the mean value calculated from the integrated 3.4-16 km spectroscopic columns. This difference implies that the free tropospheric CO mixing ratio profile generally decreased with altitude, consistent with GTE PEM-West B mission CO measurements obtained on February 7 and 8, 1994, near Hawaii [*Hoell et al.*, 1997, table 1]. These measurements are available from the GTE data archive at NASA's Langley Research Center (URL: <http://www-gte.larc.nasa.gov>). The CMDL surface and 3.4-16 km FTS column measurements both show a sharp minimum during late summer. While many factors influence the seasonal variation of tropospheric CO, consistent with previous studies [e.g., *Novelli et al.*, 1998], we note that the seasonal CO maxima and minima occur several months later the corresponding variations expected for OH from seasonal changes in solar insolation. The late summer agreement between the FTS and CMDL mixing ratios implies that the CO mixing ratio profile was on average nearly constant with altitude in the free troposphere. This conclusion is also consistent with the

aircraft profiles measured in October 1991 close to Hawaii during the PEM-West A mission [Hoell *et al.*, 1996, table 2]. The September 1997-February 1998 time period was anomalous in that the monthly averages showed maxima in surface CO (during October) and free tropospheric CO (during November). The agreement between the two sets of mixing ratios in late 1997 implies that the CO vertical mixing ratio profile was nearly uniform in the free troposphere during this anomalous time period.

*Pougatchev and Rinsland* [1995] reported measurements of the CO seasonal variation in two layers deduced from infrared solar spectra recorded between 1982 and 1993. The observations were recorded from Kitt Peak located in Arizona, U.S.A., at 32°N latitude, 112°W, 2.09 km altitude. The lower layer extending from the surface to 400 mbar (~7 km altitude) sampled primarily the free troposphere. The upper layer extended from 400 mbar to the top of the atmosphere. The asymmetrical seasonal variations in both layers are qualitatively similar to the variations indicated from the Mauna Loa surface and infrared spectroscopic measurements. An average ratio of  $2.2 \pm 0.1$  was derived from the Kitt Peak measurements by dividing the average mixing ratio in the lower layer by the average mixing ratio in the upper layer. This ratio implies that within the troposphere there is a more rapid decrease with altitude above Kitt Peak than above Mauna Loa, consistent with the continental location of Kitt Peak and its closer location to sources.

Very few measurements of the seasonal variation of CO in the tropical and subtropical upper troposphere have been reported previously. Measurements of CO mixing ratios have been obtained at altitudes of 8.5-13 km during commercial airline flights between Japan and Australia from April 1993 to July 1996 roughly at 140°W longitude [Matsueda *et al.*, 1998a]. They provided unique measurements of CO variations as a function of

latitude and time in the upper troposphere over the western Pacific. The average CO seasonal cycle for this time period in the 15°N-20°N latitude band [Matsueda *et al.*, 1998a, Fig. 7] was derived by fitting the measurement time series with a linear function combined with three harmonics [Matsueda *et al.*, 1998a, Eq. 1]. The best-fit seasonal component shows a minimum in mid-February with the peak amplitude of 10 ppbv and a maximum at the beginning of May with a peak amplitude of 20 ppbv. Little seasonal variation was observed at these heights during other times of the year [Matsueda *et al.*, 1998a, Fig. 7]. Our measurements of the peak-to-peak amplitude of the seasonal cycle are generally consistent with the aircraft observations, though the times of the maxima and minima are different in the two data sets. The CO late summer minimum apparent in the Mauna Loa 3.4-16 km column measurement time series is not obvious in the aircraft flask sampling observations. The differences in locations of the two sets of observations and the limited samplings of both data sets are likely to contribute to these discrepancies.

To date, the only near global observations of tropospheric CO were obtained by a nadir-viewing Measurement of Air Pollution from Satellites (MAPS) instrument that flew onboard the U.S. Space Shuttle [Reichle *et al.*, 1986, 1990, 1999; Connors *et al.*, 1999]. Table 4 presents the monthly mean 3.4-16 km CO columns derived from our FTS measurements and values calculated from the MAPS observations. The measurements are sorted by month. The number of days included in the calculations is listed in the table. Values from the FTS observations are presented separately for the August 1995-August 1997 and the September 1997-February 1998 time periods.

MAPS observations sample CO in the atmosphere [Pougatchev *et al.*, 1998, Fig. 2] with a vertical sensitivity very similar to our FTS solar observations (Fig. 1). Both sets of

observations are sensitive to changes in middle and upper tropospheric CO but have practically no sensitivity to changes in boundary layer CO levels [Pougatchev *et al.*, 1998, Fig. 2]. In contrast, it should be noted that ground-based infrared measurements of CO are usually performed from a strong CO line at 4.7  $\mu\text{m}$ , which samples the atmosphere with a total column averaging kernel peaked at the surface, not in the upper troposphere [Pougatchev *et al.*, 1998, Fig. 2].

The MAPS instrument measured CO near Mauna Loa during shuttle flights in October 1984, April 1994, and October 1994. Average mixing ratios and standard deviations were computed from a  $1^\circ \times 1^\circ$  gridded product (S. R. Nolf, private communication, 1999). Observations between  $17^\circ\text{N}$  and  $21^\circ\text{N}$  latitude and  $150^\circ\text{W}$  and  $160^\circ\text{W}$  longitude were included. Averaging was performed because many of the MAPS grid points do not have observational values due to the presence of clouds in the field of view or gaps in the spatial coverage during the limited time period of the shuttle flights. This region is located almost entirely over ocean.

We next used our Mauna Loa CO *a priori* profile to calculate a multiplicative factor that relates the mean mixing ratio in the 3.4-16 km layer sampled by the FTS to a partial column integrated over the same altitude range. The Mauna Loa CO *a priori* profile used for the FTS retrievals was assumed. The derived conversion factor between mean CO mixing ratio to the CO column in the 3.4-16 km layer is  $1 \text{ ppbv} = 1.196 \times 10^{16} \text{ molecules cm}^{-2}$ . This approach provides a quantitative correction for the reduced CO column sampled by the FTS observations from the high-altitude Mauna Loa station. Because of the close similarity between the FTS and MAPS averaging kernels and *a priori* profiles, the error in our conversion of MAPS mixing ratio to equivalent 3.4-16 km CO column is

estimated as 3%, significantly less than the 10% accuracy of the MAPS CO observations [Reichle *et al.*, 1999]. Our approach for relating ground-based IR columns and MAPS mixing ratios is consistent with the analysis of Pougatchev *et al.* [1998].

As shown in table 4, the FTS monthly average CO 3.4-16 km columns measured after September 1997 are higher than values from the corresponding months of August 1995–August 1997. The ratio of monthly averages from the two time periods peaked at  $1.43 \pm 0.30$ . This value and uncertainty were calculated from monthly averages and standard deviations for November 1997 relative to values for November 1995 and November 1996. Monthly means of January 1998 and February 1998 FTS measurements are only marginally higher than the corresponding values from the 1995-1997 time period.

Tropospheric CO columns calculated from the MAPS measurements at the location of Mauna Loa show significant variations that are both higher and lower than the FTS averages. It is necessary to compare observations for the same months because of the large seasonal variation in CO. Although no FTS measurements were recorded during the month of April, we estimated a value for that month by averaging the FTS monthly means from March and May of 1995-1997. The MAPS measurement from its April 1994 shuttle flight is higher than the calculated FTS mean by a factor of  $1.17 \pm 0.24$ . The MAPS column for October 1994 is also higher than the FTS value from October 1995 and October 1996 by a factor  $1.24 \pm 0.19$ , but it was  $0.98 \pm 0.20$  times the FTS measurements from October 1997. The MAPS column from October 1984 is the lowest value measured during that month. The ratio of the MAPS October 1984 to the mean of the Mauna Loa March and May measurements from 1995-1997 is  $0.65 \pm 0.12$ .

## b.) Ethane ( $C_2H_6$ )

The top panel of figure 4 illustrates a typical Mauna Loa spectrum and fit in the region analyzed to retrieve the  $C_2H_6$  profiles. The time series of 3.4-16 km columns shows a distinct seasonal cycle that is very similar to the one observed for the 3.4-16 km CO columns. This result is consistent with an analysis of Mauna Loa  $C_2H_6$  observations recorded between November 1991 and July 1993 [Rinsland *et al.*, 1994], even though the two sets of observations were recorded with different instruments, analyzed with different sets of spectroscopic parameters, and different spectral fitting programs were adopted. No significant long-term trend in the  $C_2H_6$  column has been found from either dataset.

Table 5 presents monthly averages of the  $C_2H_6$  3.4-16 km columns from the 1995-1998 series of measurements. As was done for CO, we report values separately for the August 1995-August 1997 and the September 1997-February 1998 time periods. The mean columns were systematically higher during October to December 1997 relative to values for the same months in 1995 and 1996. As for CO, the maximum enhancement was observed in November 1997 with an observed ratio of  $1.43 \pm 0.41$  relative to the corresponding observations from 1995 and 1996. The January and February 1998 measurements show no obvious enhancements relative to the 1995-1997 observations from the same months.

Figure 5 presents a plot of the daily average 3.4-16 km  $C_2H_6$  vs. the daily average CO 3.4-16 km columns. Measurements from all seasons are included with the solid line indicating a fit assuming a linear relation between the two sets of columns. Table 6 compares the correlation coefficients and  $C_2H_6/CO$  slope derived from the Mauna Loa



spectroscopic observations with previous tropospheric spectroscopic column measurements. The previous measurements were obtained from Lauder and Kitt Peak [Rinsland *et al.*, 1998b]. The correlations between the integrated CO and C<sub>2</sub>H<sub>6</sub> tropospheric columns are likely to reflect common principal sources for both molecules (see Table 1) and their similar rates of reaction with OH [Rudolph, 1995]. Also, the C<sub>2</sub>H<sub>6</sub>/CO emission factor of 0.0094 derived from biomass fire measurements [Yokelson *et al.*, 1997, Table 3] is very similar to the slope derived from the Lauder infrared observations during the southern hemisphere burning season. The best-fit Mauna Loa C<sub>2</sub>H<sub>6</sub>/CO 3.4-16 km columns ratio of 0.00935 and the correlation coefficient of 0.927 are also similar to values of 0.0073 and 0.92 deduced from C<sub>2</sub>H<sub>6</sub> and CO mixing ratios measured *in situ* in the western Pacific basin between 10°S and 25°N latitude and above 2 km altitude during February and March 1994 [Blake *et al.*, 1997, Fig. 2].

We have also compared the Mauna Loa CO and C<sub>2</sub>H<sub>6</sub> tropospheric columns with monthly values calculated by integrating profiles predicted for the same location with a global 3-D tropospheric model [Wang *et al.*, 1998]. The model tropospheric columns (Y. Wang, private communication, 1999) reproduce the spring maximum and autumn minimum measured for both CO and C<sub>2</sub>H<sub>6</sub> between August 1995 and August 1997. The ratio of the monthly mean tropospheric columns to the corresponding model values has been calculated for this time period. The mean and standard deviation are 1.06 and 0.08 for CO and 1.61 and 0.21 for C<sub>2</sub>H<sub>6</sub>, respectively. Hence, the model values are in very good agreement with the measured CO tropospheric columns, but the model values are systematically low for C<sub>2</sub>H<sub>6</sub>. The discrepancy for C<sub>2</sub>H<sub>6</sub> is likely to reflect an

underestimation of  $C_2H_6$  emissions from southeast Asia (Y. Wang, private communications, 1999).

Both observational and theoretical evidence indicates that the tropospheric mixing ratios of relatively long-lived hydrocarbons are determined by a combination of OH photochemistry and turbulent mixing during transport [e.g., *McKeen et al.*, 1996]. In general, these processes cannot be distinguished. Although the observed ratio of  $C_2H_2/CO$  has proven to be a highly useful indicator of the combined effects of dynamical mixing and photochemistry, the absorption by  $C_2H_2$  lines is weak in the high-altitude, low-latitude Mauna Loa solar spectra. Hence, it did not prove possible to measure  $C_2H_2$  tropospheric columns throughout the year and use the  $C_2H_2$  to CO ratio to classify air masses, as has been done successfully during GTE field missions [e.g., *Smyth et al.*, 1996].

### c.) Hydrogen Cyanide (HCN)

Figure 6 illustrates fits to the Mauna Loa spectra in the HCN window. The two examples were selected to illustrate observations recorded during the month of November at nearly the same solar zenith angle but with HCN 3.4-16 km column abundances that differ by one order of magnitude.

Figure 7 presents the measured time series of HCN 3.4-16 km partial columns derived from the Mauna Loa measurements. Monthly averages and standard deviations are reported in table 7. As for CO and  $C_2H_6$ , results are reported separately for the August 1995-August 1997 and September 1997-February 1998. As summarized in this table, the variations in HCN are substantially larger than those measured for CO and  $C_2H_6$ .

Higher HCN 3.4-16 km columns were measured throughout the October 1997 to February 1998 time period relative to those from corresponding months between August 1995 and August 1997. A maximum ratio of  $3.37 \pm 1.70$  was calculated from the mean and standard deviation of the November 1997 monthly averages and the corresponding values from both November 1995 and November 1996.

Solid curves in Fig. 7 display the seasonal variation and long-term trend deduced from the best-fits to the measurements. The long-term trend fit suggests a factor of two increase in the 3.4-16 km column over the observation period. However, northern-hemisphere ground-based total columns [Mahieu *et al.*, 1995, 1997] and ATMOS lower stratospheric mixing ratios from solar spectra from 1985 and 1994 [Rinsland *et al.*, 1996] show no evidence for a substantial change in HCN amounts at northern mid-latitudes over multi-year time periods. The apparent trend in the HCN 3.4-16 km column above Mauna Loa is due to the sharp increases observed after about September 1997.

There is now both direct and indirect evidence that HCN is less uniformly distributed in the troposphere than indicated by an early assessment [Cicerone and Zellner, 1983]. Ground-based infrared spectroscopic measurements of HCN recorded from the International Scientific Station of the Jungfraujoch (ISSJ) in the Swiss Alps and Kitt Peak showed variable enhancements in the total column of up to factors of two and three during spring, respectively [Mahieu *et al.*, 1995, Figs. 3, 4; 1997]. The measured line shapes indicated that the springtime HCN enhancements occurred near the surface, and they were attributed to increased vegetative activity. Infrared solar occultation spectra recorded by the Atmospheric Trace Molecule Spectroscopy (ATMOS) Fourier transform spectrometer indicated variable enhancements of up to a factor of 5 in the November

1994 tropical and subtropical upper troposphere [*Rinsland et al.*, 1998a, Fig. 2].

Ground-based measurements of HCN derived from IR solar spectra recorded during a ship cruise between 60°N and 50°S on the central Atlantic also showed a pronounced peak in the total column of HCN. The maximum was observed in the southern tropics during October 1996 [*Notholt et al.*, 1999]. The high HCN columns (corresponding to an average tropospheric mixing ratio of >200 pptv) coincided with elevated levels of CO, C<sub>2</sub>H<sub>6</sub>, and C<sub>2</sub>H<sub>2</sub>, which are well-known emission products of biomass fires [*Yokelson et al.*, 1996, 1997].

The HCN enhancements indicated by the ATMOS and cruise tropical observations have been attributed to increased production of HCN in biomass fires [*Rinsland et al.*, 1998a; *Notholt et al.*, 1999]. Evidence for this link originates primarily from emission factors derived from laboratory fire studies [*Lobert et al.*, 1990, 1991; *Hurst et al.*, 1994a,b; *Yokelson et al.*, 1996, 1997]. Although production efficiencies are observed to vary widely depending on the fuel type and burning phase, we note that from some smoldering organic soils, HCN is the dominant detected nitrogen-containing biomass emission relative to CO [*Yokelson et al.*, 1997]. Usually NH<sub>3</sub> is the major nitrogen-containing emission detected from such fires [*Yokelson et al.*, 1997]. Indirect evidence for elevated HCN upper tropospheric levels has been inferred from the large discrepancies between total reactive nitrogen (NO<sub>y</sub>) levels measured during GTE airborne field campaigns and values calculated by summing the mixing ratios of the individual components thought to comprise NO<sub>y</sub> [*Bradshaw et al.*, 1998]. The observed differences are largest in the middle to upper troposphere [*Bradshaw et al.*, 1998].

Figure 8 compares the Mauna Loa CO, C<sub>2</sub>H<sub>6</sub>, and HCN 3.4-16 km partial columns for the last half of 1997. As can be seen from this plot, the measurements of the 3 molecules are highly correlated. The correlation coefficient between HCN and CO for this time period is 0.95. Tropospheric columns of HCN prior to the beginning of October 1997 average  $2 \times 10^{15}$  molecules cm<sup>-2</sup> with mean 3.4-16 km mixing ratios close to the typical background level of 190 pptv in the free troposphere [Mahieu *et al.*, 1995]. However, highly variable levels of all 3 molecules were observed, particularly during October and November 1997. Sharp peaks in HCN were measured on Oct. 18 and Nov. 15 with the mid-November maximum the larger of the two. The relative enhancements of HCN are by far the largest observed for the three molecules with a maximum HCN 3.4-16 km column of  $9.14 \times 10^{15}$  molecules cm<sup>-2</sup> on November 15. This value corresponds to an average free tropospheric HCN mixing ratio of 0.7 ppbv. After subtracting columns of HCN and CO based on the 1995 and 1996 measurements, we calculate that the November 1997 monthly mean corresponded to an excess HCN/CO 3.4-16 km columns ratio of 0.00982, well within the wide range of values measured from laboratory fires (e.g. 0.00049-0.0581) [Lobert *et al.*, 1991, Table 36.4]. The weekly Mauna Loa CMDL surface CO measurements from October-November 1997 show no obvious evidence for the sharp peaks detected in the infrared column measurements.

## 5.) Trajectory Calculations and Discussion

The correlated variations of CO, C<sub>2</sub>H<sub>6</sub>, and HCN and unusual seasonal cycles observed during the second half of 1997 suggest a common emission origin. The averaging kernels and the observed broad widths of the spectral lines imply that the

enhancements were located primarily in the upper troposphere. In an effort to identify the origin of the high concentrations of the trace gases, we performed back-trajectory calculations with the HYSPLIT4 (Hybrid Single Particle Lagrangian Integrated Trajectory) model [Draxler and Hess, 1997]. Calculations were performed for two altitudes above Mauna Loa, 7 and 11 km. The 6-hourly FLN archive data from the NCEP operational model runs were adopted.

Calculations were performed for up to a 10-day period ending at 0 hr on each of 5 days before and 5 days after the HCN 3.4-16 km column maximum on November 15, 1997. Although there appears to be no consensus on the preferred methodology [Draxler, 1996], we performed runs based on the isentropic and the kinematic assumptions, which should be more realistic in the free troposphere than calculations that assume isobaric vertical motion.

Figure 9 displays the kinematic back trajectories ending at the two altitudes above Mauna Loa. The calculations were terminated shortly after land was encountered. Although there were significant variations among the calculated altitudes and to a lesser extent the geographic paths traversed by the back trajectories, essentially all of the calculated trajectories arrived above Hawaii from the west. The plots show that the low northern hemisphere tropical latitudes of Asia are the most likely origin of the enhanced emissions. Intense and widespread forest fires occurred in tropical Asia during 1997 and early 1998 and impacted a large portion of the population in that region [Liew *et al.*, 1998; Phadnis *et al.*, 1998; UNEP, 1999]. Available satellite imagery and visual reports confirm the existence of widespread biomass burning in southeast Asia [Liew *et al.*, 1998]. Most of our calculated trajectories pass north of Indonesia and Malaysia where

the most intense burning occurred. However, the calculated trajectories are subject to errors in the thermodynamic and wind fields [Merrill, 1996]. Also, there is numerical uncertainty due to the use of the gridded data to represent the continuous flow of air [Draxler, 1996]. As demonstrated by previous studies [Merrill, 1996; Draxler, 1996], the errors accumulate with time and can lead to large uncertainties for long-range trajectory calculations, particularly over oceans where there are few soundings. Sample tests performed by rerunning 10-day back trajectories forward in time from their end point at an altitude of 11 km showed typical differences in calculated longitude and latitude of 15° and 2°, respectively.

Support for a connection between our observations of enhancements in tropospheric CO, C<sub>2</sub>H<sub>6</sub>, and HCN columns and the tropical fires of 1997-1998 comes from the measurements of CO observed in the tropical south Pacific during that time. Increased CO levels were measured at the CMDL station on American Samoa (14.2°S, 170.6°E, elevation 77m) and during shipboard transects between 5°S and 25°S latitude [Novelli, 1998]. Relatively large annual mean CO values were also reported for 1997 from shipboard measurements in the low latitudes of the South China Sea. They reflect the very high CO levels observed during August, September, and October 1997 [CMDL, 1999, section 2.4.2 and table 2.9]. A unique seasonal cycle with an extremely enhanced CO maximum throughout the southern hemisphere was also observed at 8-13 km altitude during aircraft flights over the western Pacific in September and November 1997 [Matsueda *et al.*, 1998b].

The observed enhancements and unusual seasonal variations in the free tropospheric columns of CO, C<sub>2</sub>H<sub>6</sub>, and HCN observed above Mauna Loa may be related to the

occurrence of ENSO (El Niño/Southern Oscillation) events. ENSO events influence air temperature and precipitation patterns [Ropelewski and Halpert, 1987; Halpert and Ropelewski, 1992], which in turn effect the distribution, frequency, and intensity of tropical biomass burning emissions. An index of spatially averaged sea surface temperature anomalies calculated by the Japan Meteorological Agency (JMA) (URL: [http://www.coaps.fsu.edu/pub/JMA\\_SST\\_Index/jma.gif](http://www.coaps.fsu.edu/pub/JMA_SST_Index/jma.gif)) and a classification of ENSO periods by the Center for Ocean-Atmospheric Prediction Studies (COAPS). (URL: [http://www.coaps.fsu.edu/~legler/jma\\_index1.shtml](http://www.coaps.fsu.edu/~legler/jma_index1.shtml)) show the two most intense ENSO events since 1970 took place in 1982-83 and 1997-98. Similar to 1997-98, large amounts of burning took place in southeast Asia and New Guinea during drought conditions in 1982-83 [Malingreau *et al.*, 1985] with elevated levels of tropospheric ozone observed in that region [Fishman *et al.*, 1990; Kim and Newchurch, 1998]. We note that high levels of tropospheric O<sub>3</sub> are often accompanied by enhancements in CO and other trace gases [Browell *et al.*, 1996]. However, de-seasonalized weekly surface flask sampling measurements of CO mixing ratios from Cape Kumukhai and Mauna Loa, Hawaii, and Samoa (14.2°S, 170.6°E) show no obvious enhancements during 1982-83 [Khalil and Rasmussen, 1988, Fig. 1]. These early CO flask sampling measurements may be unreliable because of stability problems [Fraser *et al.*, 1988; Mansbridge *et al.*, 1988], or possibly the prevailing winds did not transport the elevated CO emissions to Samoa or Hawaii. Hence, although a good case can be made for elevated emissions and transport of these emissions from southeast Asia to Mauna Loa in 1997-1998, to our knowledge, no conclusive observational evidence exists for a similar connection during the intense El Niño of 1982-1983.



## 6. Summary and Conclusions

We have analyzed a time series of CO, C<sub>2</sub>H<sub>6</sub>, and HCN infrared solar measurements obtained with the high spectral resolution FTS located at the NDSC primary station on Mauna Loa, Hawaii. The measurements were recorded in solar absorption mode on over 250 days between August 1995 and February 1998. The observations sample a broad altitude region with maximum sensitivity in the upper troposphere. Daily average 3.4-16 km columns are reported for all 3 molecules and compared with previous measurements and model calculations. The comparisons include CO columns calculated for the same altitude and geographic region from the MAPS shuttle measurements in April 1994, October 1984, and October 1994, CMDL surface CO flask measurements from Mauna Loa during the FTS observing period, and GTE aircraft measurements obtained near Hawaii during several campaigns.

Both the FTS and CMDL CO data show significant variability superimposed on changes by a factor of two with season. Prior to about September 1997, both sets of observations show a broad maximum between January and April followed by a sharper minimum in late summer. Differences of 10-20% between mean tropospheric mixing ratios calculated from the FTS column data and measured CMDL surface mixing ratios imply that the CO mixing ratio profile generally decreased with altitude in the troposphere during the first third of the year. In contrast, the CO surface and mean tropospheric mixing ratios agreed during late summer implying that on average tropospheric profile of CO was nearly uniform with altitude during that time. Values during other months are intermediate between these two extremes. Daily average partial columns of CO and C<sub>2</sub>H<sub>6</sub> are highly correlated during all seasons. The best-fit Mauna

Loa  $\text{C}_2\text{H}_6/\text{CO}$  slope derived from spectroscopic column measurements and the  $\text{C}_2\text{H}_6\text{-CO}$  correlation coefficient are similar to values derived from GTE measurements over the western Pacific. The slope of  $\text{C}_2\text{H}_6$  vs. CO correlation is intermediate between the lower values derived from the station in Lauder, New Zealand ( $45^\circ\text{S}$ ), and the higher value derived from solar spectra recorded at Kitt Peak in southern Arizona, U.S.A ( $32^\circ\text{N}$ ).

The 3.4-16 km columns of the 3 molecules were enhanced beginning in about September 1997 with the highest levels observed during November 1997. The largest variations relative to background were observed for HCN with values up to a factor of 3 above background. The observations also indicate that HCN remained elevated up to the end of the observation period. Back-trajectory calculations performed for November 1997 show the low northern latitudes of Asia as the most likely source of the emissions, though contributions from other low latitude areas in the northern hemisphere are probable due to the relatively long lifetimes of all 3 molecules. As biomass burning is an important source for all 3 molecules and widespread burning occurred throughout southeast Asia at that time [Liew *et al.*, 1998; UNEP, 1999; Levine, 1999], we attribute the trace gas enhancements to those fires. Support for this hypothesis also comes from the high CO levels and unusual seasonal cycles measured in the tropical south Pacific at the surface [Novelli, 1998; CMDL, 1999, section 2.4.2] and at 8-13 km altitude [Matsueda *et al.*, 1998b] during the same time period. Additionally, our observations provide further evidence for HCN as an important though highly fuel-composition-dependent emission product of biomass burning [Lobert *et al.*, 1990, 1991; Yokelsen *et al.*, 1996, 1997].

**Acknowledgments.** Research at NASA Langley Research Center was funded by NASA's Upper Atmosphere Research Program and the Atmospheric Chemistry Modeling and Analysis Program. Research at Christopher Newport University was funded by grants from NASA. Research at the NIWA was funded by the New Zealand Foundation for Research, Science, and Technology (contract number CO 1221). We also acknowledge the support of research at MLO-NASA Ames Research Center under NAG-351 and help from the staff of the Mauna Loa observatory. We thank Linda Chiou of Science Applications International Corporation for her assistance with the analysis of the measurements and the preparation of the figures. The trajectory calculations were performed with HYSPLIT4 (Hybrid Single Particle Lagrangian Integrated Trajectory) model, 1997. Web address <http://www.arl.noaa.gov/ready/hysplit4.html>, NOAA Air Resources Laboratory, Silver Spring, MD. We thank Henry Fuelberg of the Department of Meteorology, Florida State University, Tallahassee, and Roland Draxler of the NOAA Air Researches Laboratory, Silver Spring, MD, for helpful discussions concerning the interpretation of trajectory calculations. We also thank Scott R. Nolf of Computer Sciences Corporation for providing the files of MAPS observations, and acknowledge Joel S. Levine for discussions concerning the Indonesian wildfires of 1997-1998. We are especially grateful to Yuhang Wang of Georgia Tech for making available C<sub>2</sub>H<sub>6</sub> and CO tropospheric columns calculated with the Harvard 3-D tropospheric model. Suggestions from Jennifer Logan of Harvard University are acknowledged with thanks.

## References

- Blake, N. J., D. R. Blake, T.-Y. Chen, J. E. Collins, Jr., G. W. Sachse, B. E. Anderson, and F. S. Rowland, Distribution and seasonality of selected hydrocarbons and halocarbons over the western Pacific basin during PEM-West A and PEM-West B, *J. Geophys. Res.*, *102*, 28,315-28,331, 1997.
- Bradshaw, J., S. Sandholm, and R. Talbot, An update on reactive odd-nitrogen measurements made during recent NASA global tropospheric experiment programs, *J. Geophys. Res.*, *103*, 19,129-19,148, 1998.
- Browell, E., M. A. Fenn, C. F. Butler, W. B. Grant, M. B. Clayton, J. Fishman, A. S. Bachmeier, B. E. Anderson, G. L. Gregory, H. E. Fuelberg, J. D. Bradshaw, S. T. Sandholm, D. R. Blake, B. G. Heikes, G. W. Sachse, H. B. Singh, and R. W. Talbot, Ozone and aerosol distributions and air mass characteristics over the south Atlantic basin during the burning season, *J. Geophys. Res.*, *101*, 24,043-24,068, 1996.
- Cicerone, R. J., and R. Zellner, The atmospheric chemistry of hydrogen cyanide (HCN), *J. Geophys. Res.*, *88*, 10,689-10,696, 1983.
- Climate Monitoring and Diagnostics Laboratory (CMDL), Summary Report No. 24, 1996-1997, U.S. Department of Commerce, National Oceanic and Atmospheric Administration, Environmental Research Laboratories, Boulder, CO, December 1998.

Connors, V. S., B. B. Gormsen, S. Nolf, and H. G. Reichle, Jr., Spaceborne observations of the global distribution of carbon monoxide in the middle troposphere during April and October 1994, *J. Geophys. Res.*, in press, 1999.

David, S. J., F. J. Murcray, A. Goldman, C. P. Rinsland, and D. G. Murcray, The effect of the Mt. Pinatubo aerosol on the  $\text{HNO}_3$  column over Mauna Loa, Hawaii, *Geophys. Res. Lett.*, *21*, 1003-1006, 1994.

Draxler, R. R., Boundary layer isentropic and kinematic trajectories during the August 1993 north atlantic regional experiment intensive, *J. Geophys. Res.*, *101*, 29,255-29,268, 1996.

Draxler, R. R., and G. D. Hess, Description of the HYSPLIT\_4 modeling system, *NOAA Tech. Memo. ERL ARL-224*, 27 pp., Natl. Tech. Info. Serv., Springfield, Va, 1997.

Fishman, J. , C. E. Watson, J. C. Larson, and J. Logan, Distribution of tropospheric ozone determined from satellite data, *J. Geophys. Res.*, *95*, 3599-3617, 1990.

Fraser, P. J., R. A. Rasmussen, and M. A. K. Khalil, Atmospheric observations of chlorofluorocarbons, nitrous oxide, carbon monoxide, methane, and hydrogen from the Oregon Graduate Center flask sampling program, 1985-1986, in *Baseline Atmospheric Program 1986*, edited by B. W. Forgan and G. O. Ayers, pp. 67-69, Australian Government Department of Science and Technology, Canberra, Australia, 1988.

Goldman, A., F. J. Murcray, C. P. Rinsland, R. D. Blatherwick, S. J. David, F. H.

Murcray, and D. G. Murcray, Mt. Pinatubo SO<sub>2</sub> column measurements from Mauna Loa,

*Geophys. Res. Lett.*, 19, 183-186, 1992.

Gunson, M. R., M. M. Abbas, M. C. Abrams, M. Allen, L. R. Brown, T. L. Brown, A. Y.

Chang, A. Goldman, F. W. Irion, L. L. Lowes, E. Mahieu, G. L. Manney, H. A.

Michelsen, M. J. Newchurch, C. P. Rinsland, R. J. Salawitch, G. P. Stiller, G. C. Toon,

Y. L. Yung, and R. Zander, The Atmospheric Trace Molecule Spectroscopy (ATMOS) experiment: Deployment on the ATLAS space shuttle missions, *Geophys. Res. Lett.*, 23, 2333-2336, 1996.

Halpert, M. S., and C. F. Ropelewski, Surface temperature patterns associated with the southern oscillation, *J. Climate*, 5, 577-593, 1992.

Harris, J. M., P. P. Tans, E. J. Dlugokencky, K. A. Masarie, P. M. Lang, S. Whittlestone, and L. P. Steele, Variations in atmospheric methane at Mauna Loa observatory related to long-range transport, *J. Geophys. Res.*, 97, 6003-6010, 1992.

Harris, J. M., S. J. Oltmans, E. J. Dlugokencky, P. C. Novelli, B. J. Johnson, and T.

Mefford, An investigation into the source of the springtime tropospheric ozone maximum at Mauna Loa observatory, *Geophys. Res. Lett.*, 25, 1895-1898, 1998.

Hoell, J. M., D. D. Davis, S. C. Liu, R. Newell, M. Shipham, H. Akimoto, R. J. McNeal, R. J. Bendura, and J. W. Drewry, Pacific Exploratory Mission-West A (PEM-West A): September-October 1991, *J. Geophys. Res.*, *101*, 1641-1653, 1996.

Hoell, J. M., D. D. Davis, S. C. Liu, R. F. Newell, H. Akimoto, R. J. McNeal, and R. J. Bendura, The Pacific Exploratory Mission-West phase B: February-March 1994, *J. Geophys. Res.*, *102*, 28,223-28,239, 1997.

Hoell, J. M., D. D. Davis, D. J. Jacob, M. O. Rodgers, R. E. Newell, H. E. Fuelberg, R. J. McNeal, J. L. Raper, and R. J. Bendura, The Pacific Exploratory mission in the Tropical Pacific: PEM-Tropics A, August-September 1996, *J. Geophys Res.*, in press, 1999.

Hurst, D. F., D. W. T. Griffith, J. N. Carras, D. J. Williams, and P. J. Fraser, Measurements of trace gases emitted by Australian savanna fires during the 1990 dry season, *J. Atmos. Chem.*, *18*, 33-56, 1994a.

Hurst, D. F., D. W. T. Griffith, and G. D. Cook, Trace gas emissions from biomass burning in tropical Australian savannas, *J. Geophys. Res.*, *99*, 16,441-16,456, 1994b.

Jaffe, D., A. Mahura, J. Kelley, J. Atkins, P. C. Novelli, and J. Merrill, Impact of Asian emissions on the remote north pacific atmosphere: Interpretation of CO data from Shemya, Guam, Midway, and Mauna Loa, *J. Geophys. Res.*, *102*, 28,627-28,635, 1997.

Khalil, M. A. K., and R. A. Rasmussen, Carbon monoxide in the Earth's atmosphere: indications of a global increase, *Nature*, 332, 242-245, 1988.

Kim, J. H., and M. J. Newchurch, Biomass-burning influence on tropospheric ozone over New Guinea and South America, *J. Geophys. Res.*, 103, 1455-1461, 1998.

Kuniyuki, D. T., R. C. Schnell, S. C. Ryan, and J. M. Harris, Transport of biomass burning smoke from central America to Mauna Loa Observatory, Hawaii, July 1998, *EOS*, 79, F101.

Kurylo, M. J., Network for the detection of stratospheric change, *Proc. Soc. Photo. Opt. Instrum. Eng.*, 1491, 169-174, 1991.

Levine, J. S., The 1997 fires in Kalimantan and Sumatra, Indonesia, *Geophys. Res. Lett.*, 26, 815-818, 1999.

Liew, S. C., O. K. Lim, L. K. Kwoh, and H. Lim, A study of the 1997 fires in South East Asia using SPOT quicklook mosaics, paper presented at the 1998 International Geoscience and Remote Sensing Symposium, July 6-10, Seattle, WA, 3 pp., 1998.

Lobert, J. M., D. H. Scharffe, W. M. Hao, and P. J. Crutzen, Importance of biomass burning in the atmospheric budgets of nitrogen-containing gases, *Nature*, 346, 552-554, 1990.



Lobert, J. M., D. H. Scharffe, W.-M. Hao, T. A. Kuhlbusch, R. Seuwen, P. Warneck, and P. J. Crutzen, Experimental evaluation of biomass burning emissions: Nitrogen and carbon containing compounds, in *Global Biomass Burning: Atmospheric, Climatic and Biospheric Implications*, section IV, Biomass burning: Laboratory studies, pp. 289-304, ed. J. S. Levine, MIT Press Cambridge, Mass., 1991.

Mahieu, E., C. P. Rinsland, R. Zander, P. Demoulin, L. Delbouille, and G. Roland, Vertical column abundances of HCN deduced from ground-based infrared solar spectra: Long-term trend and variability, *J. Atmos. Chem.*, 20, 299-310, 1995.

Mahieu, E., R. Zander, L. Delbouille, P. Demoulin, G. Roland, and C. Servais, Observed trends in total vertical column abundances of atmospheric gases from IR solar spectra recorded at the Jungfraujoch, *J. Atmos. Chem.*, 28, 227-243, 1997.

Malingreau, J. P., G. Stevens, and L. Fellows, Remote sensing of forest fires: Kalimantan and north Borneo, *Ambio*, 14, 314-320, 1985.

Mansbridge, J. V., F. J. Robbins, and P. J. Fraser, Variations in measurements of methane, carbon dioxide, and carbon monoxide from Cape Grim flask samples, in *Baseline Atmospheric Program 1986*, edited by B. W. Forgan and G. O. Ayers, pp. 27-35, Australian Government Department of Science and Technology, Canberra, Australia, 1988.

Matsueda, H., H. Y. Inoue, Y. Sawa, Y. Tsutsumi, and M. Ishii, Carbon monoxide in the upper troposphere over the western Pacific between 1993 and 1996, *J. Geophys. Res.*, *103*, 19,093-19,110, 1998a.

Matsueda, H., H. I. Yoshikawa, and M. Ishii, Enhancement of trace gases in the upper troposphere due to biomass burning in 1997 (abstract), Joint International Symposium on Global Atmospheric Chemistry, University of Washington, Seattle, U.S.A., p. 27, 1998b.

McKeen, S. A., S. C. Liu, E.-Y. Hsie, X. Lin, J. D. Bradshaw, S. Smyth, G. L. Gregory, and D. R. Blake, Hydrocarbon ratios during PEM-WEST A: A model perspective, *J. Geophys. Res.*, *101*, 2087-2109, 1996.

Mendonca, B. G., Local wind circulation on the slopes of Mauna Loa, *J. Appl. Meteorol.*, *8*, 533-541, 1969.

Merrill, J. T., Trajectory results and interpretation for PEM-West A, *J. Geophys. Res.*, *101*, 1679-1690, 1996.

Notholt, J., G. Toon, C. P. Rinsland, N. Pougetchev, N. Jones, B. J. Connor, R. Weller, M. Gautrois, and O. Schrems, Latitudinal variations of trace gas concentrations by solar absorption spectroscopy during a ship cruise, 2. troposphere trace gases, *J. Geophys. Res.*, submitted, 1999.

Novelli, P. C., To what extent does biomass burning drive interannual variations in tropospheric carbon monoxide?, Wengen '98 Workshop on Global Change Research, Department of Geography, University of Fribourg, , proceedings of the workshop on Biomass Burning and its Inter-Relationships with the Climate System, Sept. 28-Oct 2, 1998, p.9.

Novelli, P. C., J. W. Elkins, and L. P. Steele, The development and evaluation of a gravimetric reference scale for measurements of atmospheric carbon monoxide, *J. Geophys. Res.*, 96, 13,109-13,121, 1991.

Novelli, P. C., L. P. Steele, and P. P. Tans, Mixing ratios of carbon monoxide in the troposphere, *J. Geophys. Res.*, 97, 20,731-20,750, 1992.

Novelli, P. C., K. A. Masarie, and P. M. Lang, Distributions and recent changes of carbon monoxide in the lower troposphere, *J. Geophys. Res.*, 103, 19,015-19,033, 1998.

Park, J. H., Analysis method for Fourier transform spectroscopy, *Appl. Opt.*, 22, 835-849, 1982.

Phadnis, G. R., P. K. Bhartia, G. R. Carmichael, J. R. Herman, and J. S. Levine, Regional scale atmospheric impacts of the Indonesian fires of 1997, (Abstract) *EOS Trans. AGU*, 79, Fall Meet., F132, 1998.

Pine, A. S., and S. C. Stone, Torsional tunneling and  $A_1$ - $A_2$  splittings and air broadening of the  ${}^1Q_0$  and  ${}^3Q_3$  subbranches of the  $\nu_7$  band of ethane, *J. Mol. Spectrosc.*, **175**, 21-30, 1996.

Pougatchev, N. S., and C. P. Rinsland, Spectroscopic study of the seasonal variation of carbon monoxide vertical distribution above Kitt Peak, *J. Geophys. Res.*, **100**, 1409-1416, 1995.

Pougatchev, N. S., B. J. Connor, and C. P. Rinsland, Infrared measurements of the ozone vertical distribution above Kitt Peak, *J. Geophys. Res.*, **100**, 16,689-16,697, 1995.

Pougatchev, N. S., N. B. Jones, B. J. Connor, C. P. Rinsland, E. Becker, M. T. Coffey, V. S. Connors, P. Demoulin, A. V. Dzhola, H. Fast, E. I. Grechko, J. W. Hannigan, M. Koike, Y. Kondo, E. Mahieu, W. G. Mankin, R. L. Mittermeier, J. Notholt, H. G. Reichle, Jr., B. Sen, L. P. Steele, G. C. Toon, L. N. Yurganov, R. Zander, and Y. Zhao, Ground-based infrared solar spectroscopic measurements of carbon monoxide during 1994 measurement of air pollution from space flights, *J. Geophys. Res.*, **103**, 19,317-19,325, 1998.

Reichle, H.G., Jr., V. S. Connors, J. A. Holland, W. D. Hypes, H. A. Wallio, J. C. Casas, B. B. Gormsen, M. S. Saylor, and W. D. Hesketh, Middle and upper tropospheric carbon

monoxide mixing ratios as measured by a satellite-borne remote sensor during 1981, *J. Geophys. Res.*, *91*, 10,865-10,887, 1986.

Reichle, H. G., Jr., V. S. Connors, J. A. Holland, R. T. Sherrill, H. A. Wallio, J. C. Casas, E. P. Condon, B. B. Gormsen, and W. Seiler, The distribution of middle tropospheric carbon monoxide during early October 1994, *J. Geophys. Res.*, *95*, 9845-9856, 1990.

Reichle, H. G., Jr., B. Anderson, V. Connors, T. Denkins, D. Forbes, B. Gormsen, D. Neil, S. Nolf, P. Novelli, N. Pougatchev, M. Roell, and P. Steele, Space shuttle based global CO measurements during April and October 1994: MAPS instrument, data reduction, and data validation, *J. Geophys. Res.*, in press, 1999.

Rinsland, C. P., A. Goldman, F. J. Murcray, F. H. Murcray, R. D. Blatherwick, and D. G. Murcray, Infrared measurements of atmospheric gases above Mauna Loa, Hawaii, in February 1987, *J. Geophys. Res.*, *93*, 12,607-12,626, 1988.

Rinsland, C. P., A. Goldman, F. J. Murcray, S. J. David, R. D. Blatherwick, and D. G. Murcray, Infrared spectroscopic measurements of the ethane (C<sub>2</sub>H<sub>6</sub>) total column abundance above Mauna Loa, Hawaii – seasonal variations, *J. Quant. Spectrosc. Radiat. Transfer*, *52*, 273-279, 1994.

Rinsland, C. P., M. A. H. Smith, P. L. Rinsland, A. Goldman, J. W. Brault, and G. M. Stokes, Ground-based spectroscopic measurements of atmospheric hydrogen cyanide, *J. Geophys. Res.*, **87**, 11,119-11,125, 1982.

Rinsland, C. P., E. Mahieu, R. Zander, M. R. Gunson, R. J. Salawitch, A. Y. Chang, A. Goldman, M. C. Abrams, M. M. Abbas, M. J. Newchurch, and F. W. Irion, Trends of OCS, HCN, SF<sub>6</sub>, CHClF<sub>2</sub> (HCFC-22) in the lower stratosphere from 1985 and 1994 Atmospheric Trace Molecule Spectroscopy Experiment measurements near 30°N latitude, *Geophys. Res. Lett.*, **23**, 2349-2352, 1996.

Rinsland, C. P., M. R. Gunson, P.-H. Wang, R. F. Arduini, B. A. Baum, P. Minnis, A. Goldman, M. C. Abrams, R. Zander, E. Mahieu, R. J. Salawitch, H. A. Michelsen, F. W. Irion, and M. J. Newchurch, ATMOS/ATLAS 3 infrared profile measurements of trace gases in the November 1994 tropical and subtropical upper troposphere, *J. Quant. Spectrosc. Radiat. Transfer*, **60**, 891-901, 1998a.

Rinsland, C. P., N. B. Jones, B. J. Connor, J. A. Logan, N. S. Pougatchev, A. Goldman, F. J. Murcray, T. M. Stephen, A. S. Pine, R. Zander, E. Mahieu, and P. Demoulin, Northern and southern hemisphere ground-based infrared spectroscopic measurements of tropospheric carbon monoxide and ethane, *J. Geophys. Res.*, **103**, 28,197-28,218, 1998b.

Rodgers, C. D., Characterization and error analysis of profiles retrieved from remote sounding measurements, *J. Geophys. Res.*, **95**, 5587-5595, 1990.

Ropelewski, C. F., and M. S. Halpert, Global and regional scale precipitation patterns associated with the El Niño/Southern Oscillation, *Mon. Wea. Rev.*, *115*, 1606-1626, 1987.

Rothman, L. S., C. P. Rinsland, A. Goldman, S. T. Massie, D. P. Edwards, J.-M. Flaud, A. Perrin, C. Camy-Peyret, V. Dana, J.-Y. Mandin, J. Schroeder, A. McCann, R. R. Gamache, R. B. Wattson, K. Yoshino, K. V. Chance, K. W. Jucks, L. R. Brown, V. Nemtchinov, and P. Varanasi, The HITRAN molecular spectroscopic database and HAWKS (HITRAN atmospheric workstation): 1996 edition, *J. Quant. Spectrosc. Radiat. Transfer*, *60*, 665-710, 1998.

Rudolph, J., The tropospheric distribution and budget of ethane, *J. Geophys. Res.*, *100*, 11,369-11,381, 1995.

Seiler, W., and R. Conrad, Contribution of tropical ecosystems to the global budgets of trace gases, especially CH<sub>4</sub>, H<sub>2</sub>, CO and N<sub>2</sub>O in *The Geophysiology of Amazonia*, edited by R. Dickirson, Chap. 9, pp.133-160, J. Wiley and Sons, New York, 1987.

Smith, M. A. H., Compilation of atmospheric gas concentration profiles from 0 to 50 km, *NASA Tech. Memo.*, TM 83289, 1982.

Smyth, S., J. Bradshaw, S. Sandholm, S. Liu, S. McKeen, G. Gregory, B. Anderson, R. Talbot, D. Blake, S. Rowland, E. Browell, M. Fenn, J. Merrill, S. Bachmeier, G. Sachse,

J. Collins, D. Thornton, D. Davis, and H. Singh, Comparisons of free tropospheric western Pacific air mass classification schemes for the PEM-West A experiment, *J. Geophys. Res.*, *101*, 1743-1762, 1996.

UNEP (United Nations Environment Programme), Levine, J. S., Bobbe, T., Ray, N., Singh, A., and R. G. Witt, Wildland Fires and the Environment: a Global Synthesis, UNEP/DAIAEW/TR.99-1, 1999.

Wang, Y., D. J. Jacob, J. A. Logan, and C. F. Spivakovsky, Global simulation of tropospheric O<sub>3</sub>-NO<sub>x</sub>-hydrocarbon chemistry, 1. Model formulation, *J. Geophys. Res.*, *103*, 10,713-10,726, 1998.

Yokelson, D. W. T. Griffith, and D. E. Ward, Open-path Fourier transform infrared studies of large scale laboratory biomass fires, *J. Geophys. Res.*, *101*, 21,067-21,080, 1996.

Yokelson, R. J., R. Susott, D. E. Ward, J. Reardon, and D. W. T. Griffith, Emissions from smoldering combustion of biomass measured by open-path Fourier transform infrared spectroscopy, *J. Geophys. Res.*, *102*, 18,865-18,877, 1997.



**Table 1. Summary of the most important tropospheric sources of CO, C<sub>2</sub>H<sub>6</sub>, and HCN**

<b>Molecule</b>	<b>Major Sources</b>	<b>Reference</b>
CO	Biomass burning, fossil fuel combustion, oxidation of CH <sub>4</sub> , oxidation of natural nonmethane hydrocarbons	Seiler and Conrad [1987]
C <sub>2</sub> H <sub>6</sub>	Biomass burning, natural gas losses	Rudolph [1995]
HCN	Biomass burning, vegetation	Lobert <i>et al.</i> [1990, 1991]; Cicerone and Zellner [1983]; Mahieu <i>et al.</i> [1995]

**Table 2. Microwindows and Interferences**

Molecule	Microwindows (cm <sup>-1</sup> )	Interfering Molecules
CO	4274.62-4274.82, 4284.75-4285.18	Solar CO, CH <sub>4</sub> , HDO
C <sub>2</sub> H <sub>6</sub>	2976.62-2976.94	H <sub>2</sub> O, CH <sub>4</sub> , O <sub>3</sub>
HCN	3287.15-3287.35	None

Notes: Except for CH<sub>4</sub>, each interfering molecule was fitted by a multiplicative scaling of the *a priori* volume mixing ratio profile by a single value. The profile of CH<sub>4</sub> was retrieved from the fittings of the two CO windows.

**Table 3. CO, C<sub>2</sub>H<sub>6</sub>, and HCN 3.4-16 km Partial Column Measurement Uncertainties**

*Random Error Budget*

Error Source	Relative Error, %		
	CO	C <sub>2</sub> H <sub>6</sub>	HCN
Temperature	1	2	1
Instrument noise	1	4	12
Zenith angle uncertainty	1	1	<1
Interfering lines	<1	<1	<1
RSS total random error	2	5	12

*Systematic Error Budget*

Error Source	Relative Error, %		
	CO	C <sub>2</sub> H <sub>6</sub>	HCN
Spectroscopic Parameters	2	5	2
<i>A priori</i> profile	1	1	1
Forward model approximations¶	4	2	2
Instrument line shape function	<1	<1	<1
RSS total systematic error	5	5	3

¶ Includes the estimated uncertainty in the retrieval due to errors in computing the absorption by overlapping solar CO lines.

**Table 4. CO 3.4-16 km Column Monthly Mean FTS Measurements from Mauna Loa (MLO/FTS) and Values calculated for the same altitude range and geographic region from MAPS measurements in 1984 and 1994 (in  $10^{18}$  molecules  $\text{cm}^{-2}$ )**

Month	Year	Data Source	Mean Column	Standard Deviation	Number of Days
January	1995-1997	MLO/FTS	1.097	0.083	5
January	1998	MLO/FTS	1.136	0.088	18
February	1995-1997	MLO/FTS	1.076	0.097	15
February	1998	MLO/FTS	1.113	0.079	14
March	1995-1997	MLO/FTS	1.088	0.204	13
April	1994	MAPS	1.261	0.147	---
May	1995-1997	MLO/FTS	1.061	0.147	14
June	1995-1997	MLO/FTS	0.924	0.074	13
July	1995-1997	MLO/FTS	0.790	0.101	13
August	1995-1997	MLO/FTS	0.754	0.087	37
September	1995-1996	MLO/FTS	0.789	0.062	22
September	1997	MLO/FTS	0.800	0.092	18
October	1995-1996	MLO/FTS	0.856	0.093	19
October	1997	MLO/FTS	1.088	0.189	15
October	1984	MAPS	0.710	0.036	---
October	1994	MAPS	1.065	0.116	---
November	1995-1996	MLO/FTS	0.919	0.145	8
November	1997	MLO/FTS	1.318	0.177	10
December	1995-1996	MLO/FTS	1.081	0.055	11
December	1997	MLO/FTS	1.273	0.061	10

**Table 5. Mauna Loa Monthly Mean C<sub>2</sub>H<sub>6</sub> 3.4-16 km Columns (in 10<sup>15</sup> molecules cm<sup>-2</sup>)**

Month	Year	Mean Column	Standard Deviation	Number of Days
January	1995-1997	9.101	1.049	9
January	1998	9.278	1.124	21
February	1995-1997	9.343	1.039	21
February	1998	9.287	0.942	18
March	1995-1997	9.458	1.521	12
May	1995-1997	9.550	1.272	16
June	1995-1997	8.194	1.225	15
July	1995-1997	6.698	1.184	15
August	1995-1997	5.916	0.689	44
September	1995-1996	5.730	0.433	21
September	1997	5.983	0.823	19
October	1995-1996	6.595	1.273	21
October	1997	8.590	1.977	17
November	1995-1996	8.064	2.247	7
November	1997	11.110	1.182	10
December	1995-1996	9.281	0.434	14
December	1997	11.452	1.076	12

**Table 6. Correlation coefficients and C<sub>2</sub>H<sub>6</sub>/CO slopes derived from fits to daily mean tropospheric partial column observations**

Station	Location	Months	Correlation Coefficient	C <sub>2</sub> H <sub>6</sub> /CO Slope (10 <sup>-3</sup> )*
Lauder, New Zealand	45°S, 170°E, 0.37 km altitude	February-March-April	0.400	3.38
Lauder, New Zealand	45°S, 170°E, 0.37 km altitude	May-June-July	0.594	5.52
Lauder, New Zealand	45°S, 170°E, 0.37 km altitude	August-September-October	0.827	6.39
Mauna Loa	19.5°N, 155.6°W, 3.40 km altitude	All	0.927	9.35
Kitt Peak, Arizona, U.S.A.	31.9°N, 111.6°W, 2.09 km altitude	All	0.766	14.2

\* Calculated from 0.37-12 km columns from Lauder, 2.09-14 km columns from Kitt Peak, and 3.4-16 km columns from Mauna Loa.

**Table 7. Mauna Loa Monthly Mean HCN 3.4-16 km Columns (in  $10^{15}$  molecules  $\text{cm}^{-2}$ )**

Month	Year	Mean Column	Standard Deviation	Number of Days
January	1995-1997	2.130	0.340	4
January	1998	4.265	0.463	19
February	1995-1997	1.929	0.485	21
February	1998	3.534	0.466	16
March	1995-1997	1.798	0.598	9
May	1995-1997	3.077	0.510	15
June	1995-1997	2.664	0.692	11
July	1995-1997	2.246	0.467	12
August	1995-1997	1.750	0.412	35
September	1995-1996	1.726	0.501	20
September	1997	2.125	0.658	16
October	1995-1996	1.679	0.400	19
October	1997	3.940	1.769	15
November	1995-1996	1.912	0.870	4
November	1997	6.450	1.411	9
December	1995-1996	1.837	0.398	13
December	1997	5.713	1.107	7

### Figure Captions

Figure 1. Averaging kernels calculated for CO, C<sub>2</sub>H<sub>6</sub>, and HCN. Values are shown for merged layers, 3.4-16 km and the total column, 3.4-100 km.

Figure 2. Sample spectrum and fits in the region of the CO (2-0) band R(3) and R(6) lines at 4274.7047 and 4284.8911 cm<sup>-1</sup>. The measured spectrum was recorded on March 13, 1997. The spectrum has been normalized to the highest signal in each interval. The astronomical zenith angle of the observation is indicated. Residuals (measured minus calculated values) are shown on an expanded vertical scale above each spectral plot. The measured 3.4-16 km CO column equals  $9.99 \times 10^{17}$  molecules cm<sup>-2</sup>.

Figure 3. Monthly average CO mixing ratios (ppbv) in the 3.4-16 km layer derived from the infrared FTS measurements (solid circles) and corresponding values calculated from preliminary CO mixing ratios measured at Mauna Loa by the CMDL cooperative flask sampling network (open circles). Dashed and solid straight lines connect adjacent CMDL and FTS monthly averages, respectively. Vertical lines indicate standard deviations.

Figure 4. Example of a spectrum and the corresponding fit in the interval used to retrieve profiles of C<sub>2</sub>H<sub>6</sub>. The results are shown in the same format as Fig. 2. The interval contains the <sup>P</sup>Q<sub>3</sub> Q branch of the C<sub>2</sub>H<sub>6</sub> ν<sub>7</sub> band at 2976.8 cm<sup>-1</sup>. The spectrum was recorded on February 28, 1998. The astronomical zenith angle of the measurement is indicated.



Figure 5. Daily average 3.4-16 km  $C_2H_6$  vs. CO columns. Measurements from all seasons are included. The solid line shows a fit to the observations assuming the two quantities are linearly related with an extrapolation to a  $C_2H_6$  3.4-16 km column of 0.0 shown as a dashed line. The slope, x-intercept, and correlation coefficient are reported.

Figure 6. Examples of spectra and least-squares best-fits in the microwindow used to retrieve profiles of HCN. The two cases are shown in the same format as Fig. 2. They were selected to illustrate similar airmass observations and the wide range in retrieved HCN 3.4-16.0 km column amounts during the November time period. The upper spectrum corresponds to a 3.4-16 km column of  $9.14 \times 10^{15}$  molecules  $cm^{-2}$  from November 15, 1997, while the observation in the lower panel corresponds to a retrieved 3.4-16 km column of  $8.78 \times 10^{14}$  molecules  $cm^{-2}$ . The spectrum was recorded on November 2, 1996.

Figure 7. Measured HCN 3.4-16 km columns versus time. Daily averages are shown with plus symbols. Corresponding approximate mean mixing ratios are shown on the right vertical axis. Solid curves show least-squares best-fits to the daily-mean 3.4-16 km columns with the seasonal variation and long-term trend displayed separately.

Figure 8. Time series of CO,  $C_2H_6$ , and HCN 3.4-16 km columns for the last half of 1997. Daily averages are shown. Approximate corresponding average mixing ratios for the 3.4-16 km altitude region are shown on the right vertical axis.

Figure 9. Kinematic back-trajectories calculated for up to 10 days originating at Mauna Loa between 10 November and 29 November 1997. Calculations are shown for ending altitudes of 11 km (left) and 7 km (right).

Addresses of Authors

R. D. Blatherwick, S. J. David, A. Goldman, F. J. Murcray, T. M. Stephen, Department of Physics, University of Denver, Denver, CO 80208 (email: [blathe@meeker.ucar.edu](mailto:blathe@meeker.ucar.edu); [Shelle@dove.ucar.edu](mailto:Shelle@dove.ucar.edu); [goldman@acd.ucar.edu](mailto:goldman@acd.ucar.edu); [murcray@ram.phys.du.edu](mailto:murcray@ram.phys.du.edu); [tstephen@du.edu](mailto:tstephen@du.edu))

N. B. Jones and B. J. Connor, NIWA Climate, Private Bag 50061, Omakau, Lauder 9182, New Zealand (email: [jones@kea.lauder.cri.nz](mailto:jones@kea.lauder.cri.nz); [connor@kea.lauder.cri.nz](mailto:connor@kea.lauder.cri.nz))

Paul C. Novelli, Climate Monitoring and Diagnostics Laboratory, National Oceanic and Atmospheric Administration, 325 Broadway, Boulder, CO 80303 (email: [paul@hpsrv.cmdl.noaa.gov](mailto:paul@hpsrv.cmdl.noaa.gov))

N. S. Pougatchev, Department of Physics, Christopher Newport University, Newport News, VA (email: [n.s.pougatchev@larc.nasa.gov](mailto:n.s.pougatchev@larc.nasa.gov))

C. P. Rinsland and J. Fishman, NASA Langley Research Center, Mail Stop 401A, Hampton, VA 23681-2199 (email: [c.p.rinsland@larc.nasa.gov](mailto:c.p.rinsland@larc.nasa.gov); [j.fishman@larc.nasa.gov](mailto:j.fishman@larc.nasa.gov))

Figure 1

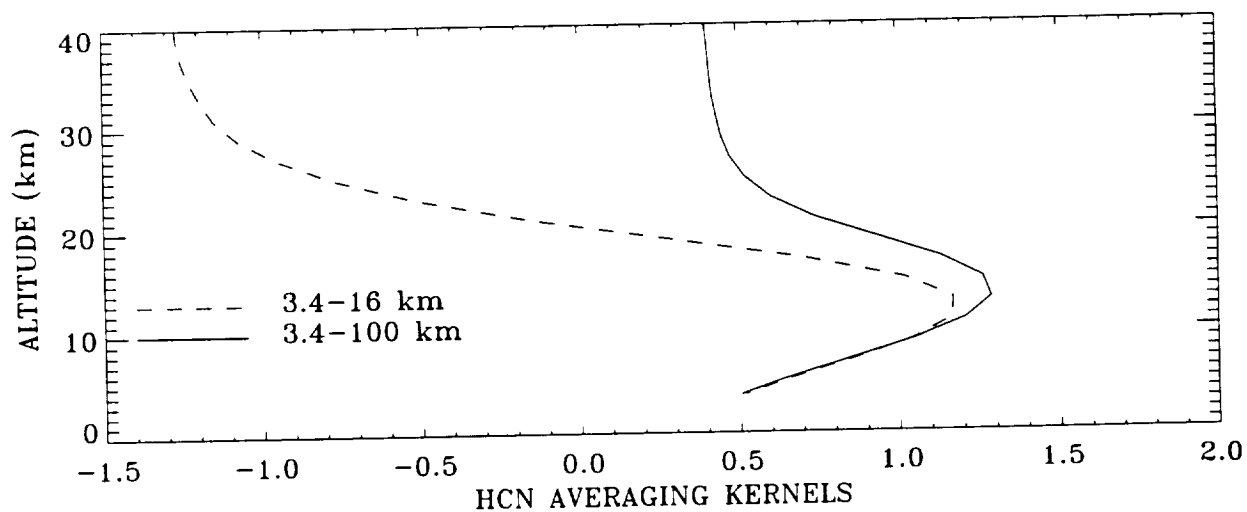
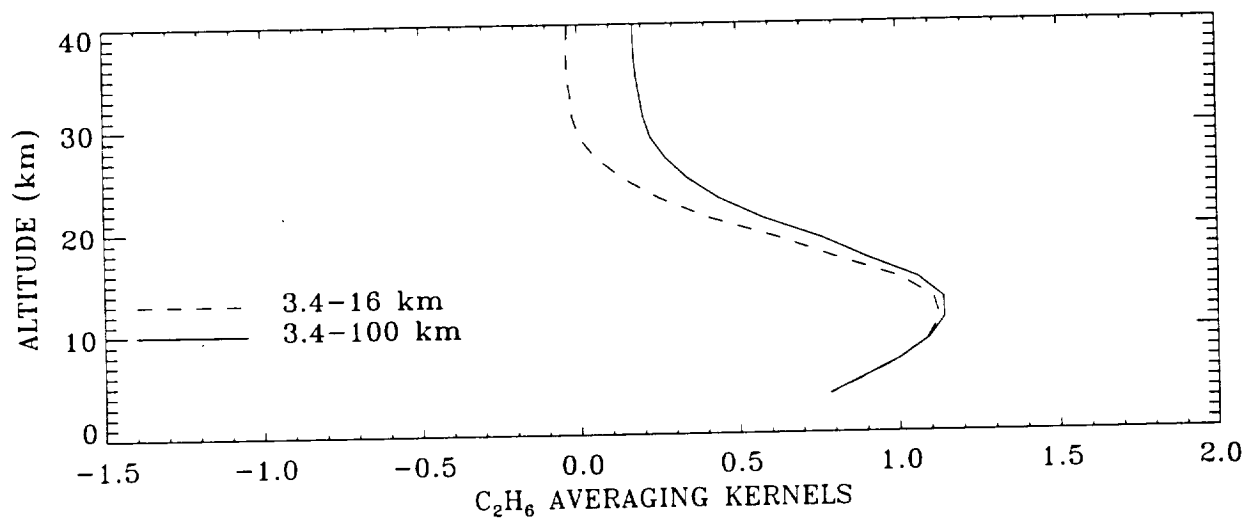
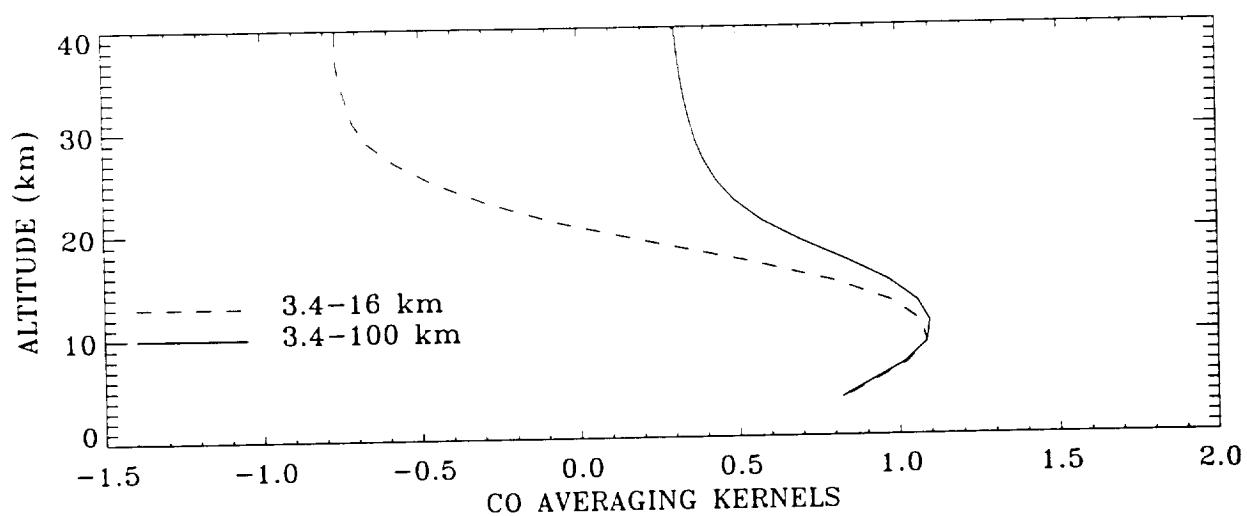


Figure 2

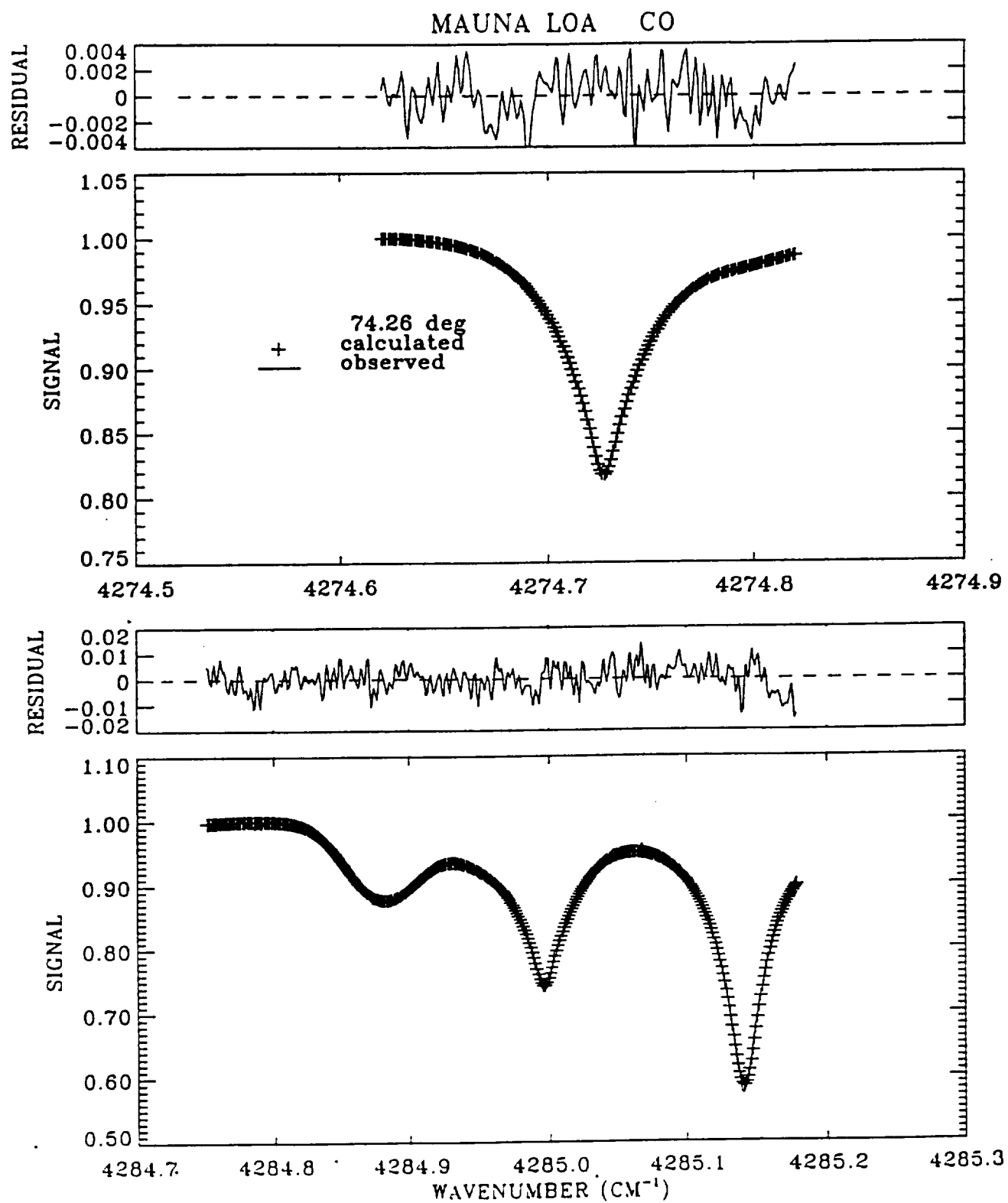


Figure 3

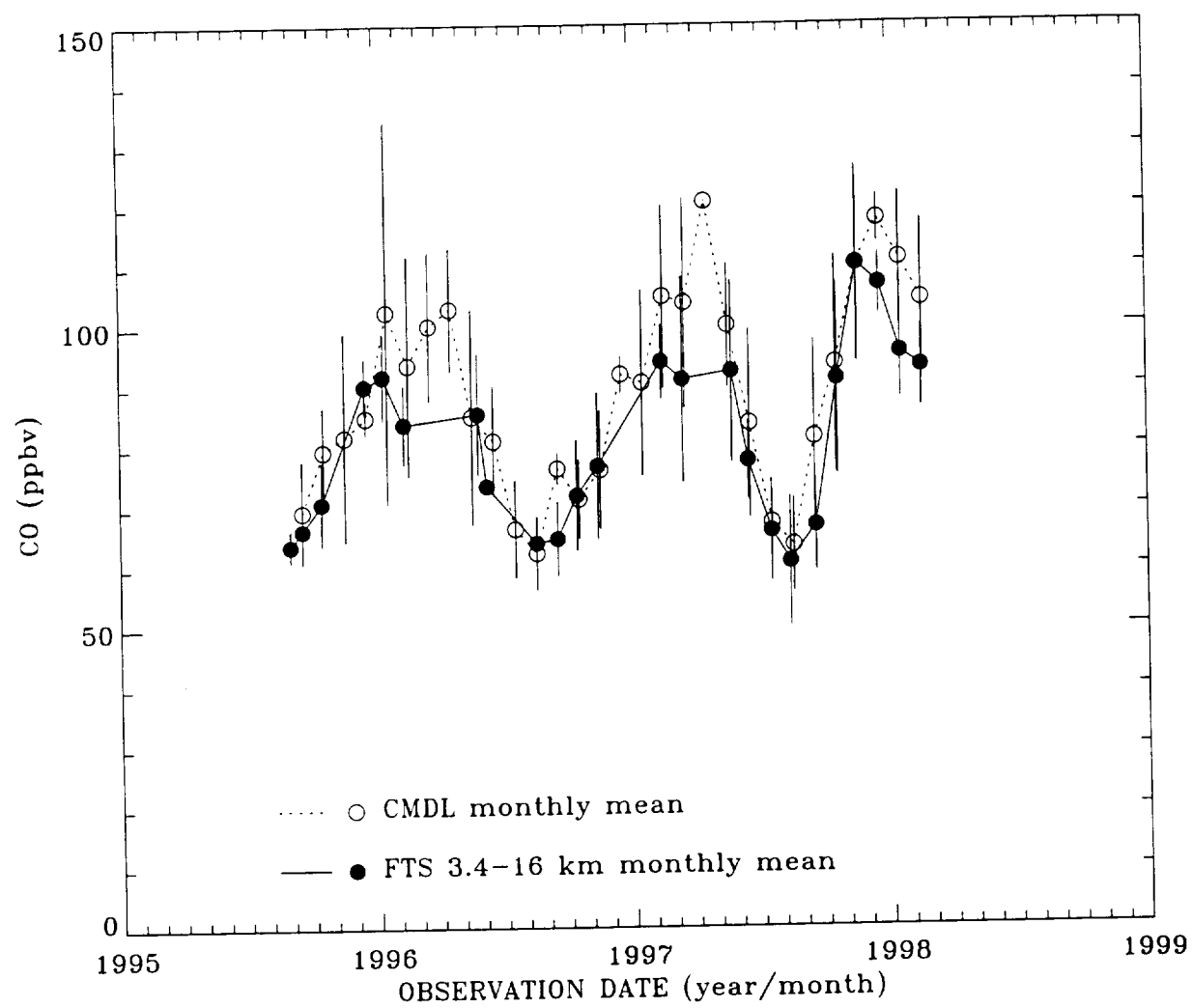


Figure 4

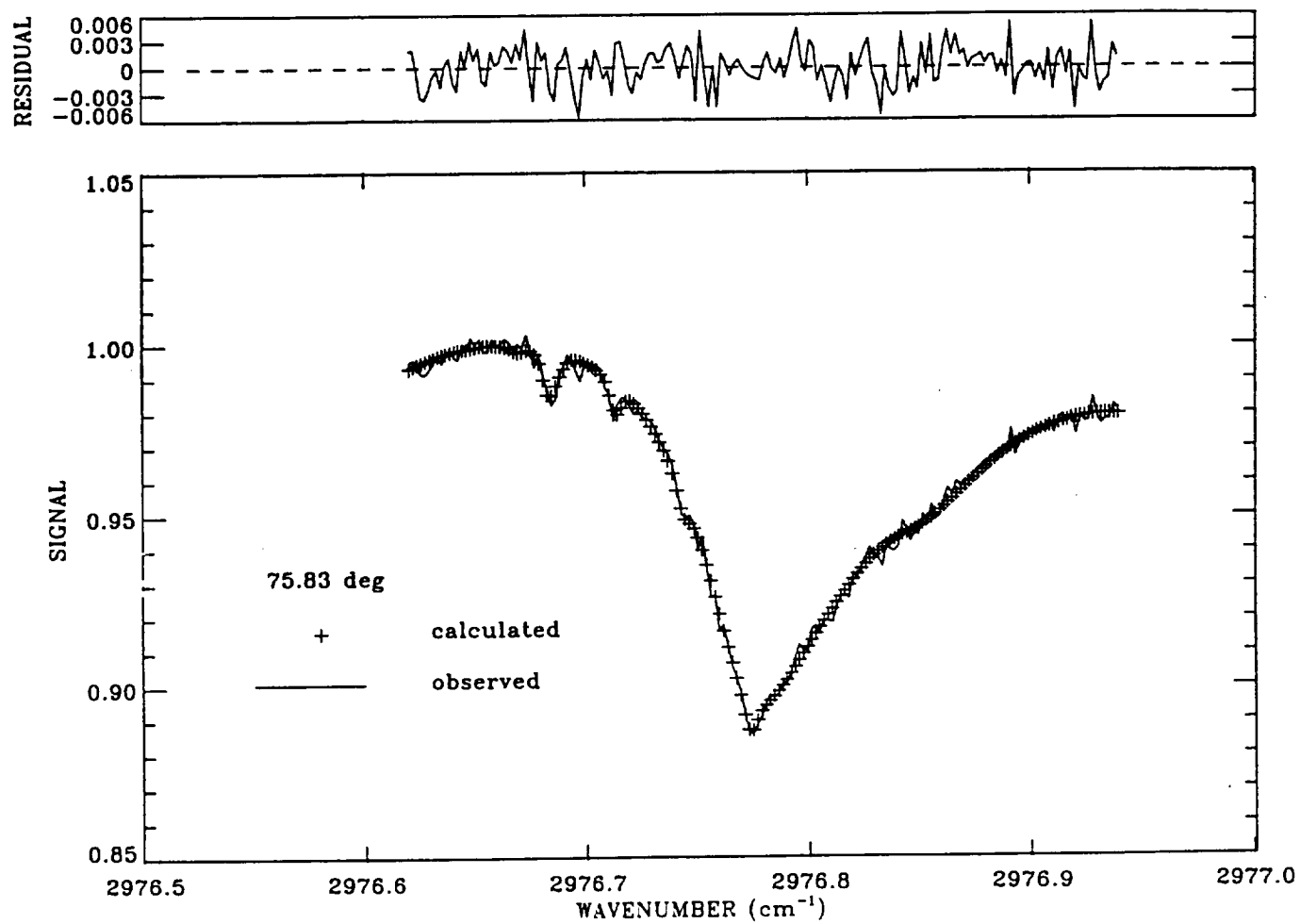


Figure 5

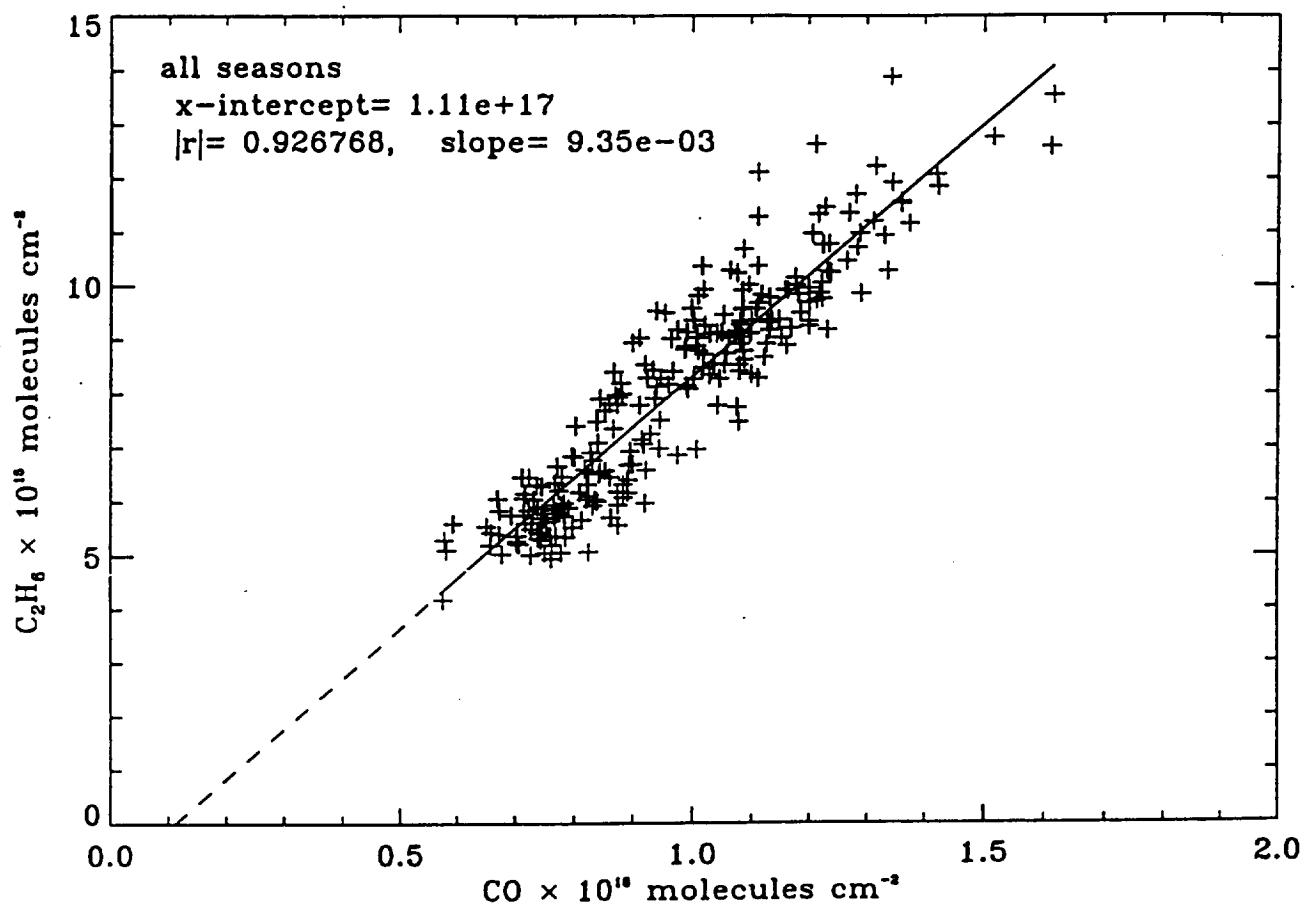




Figure 6

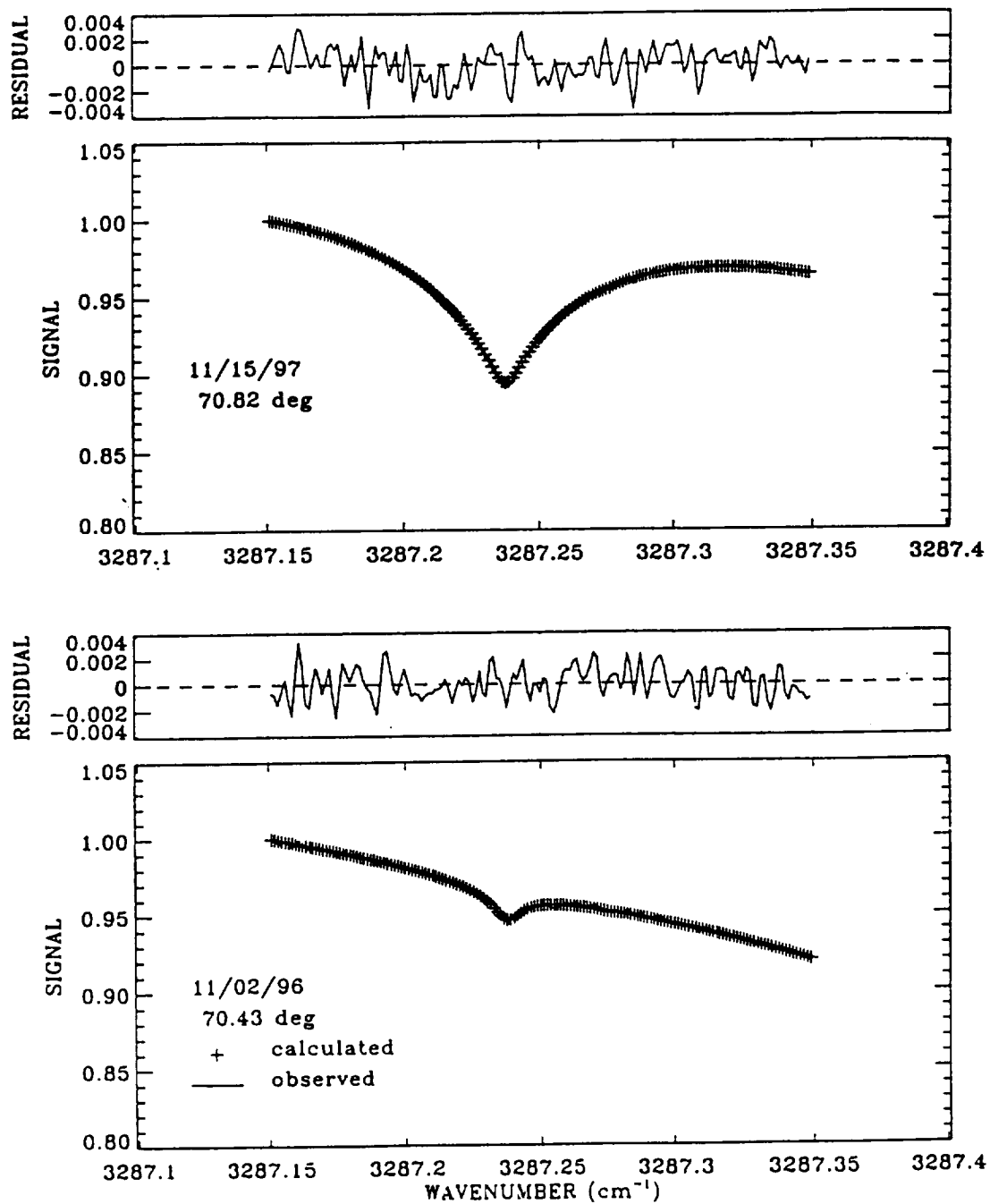


Figure 7

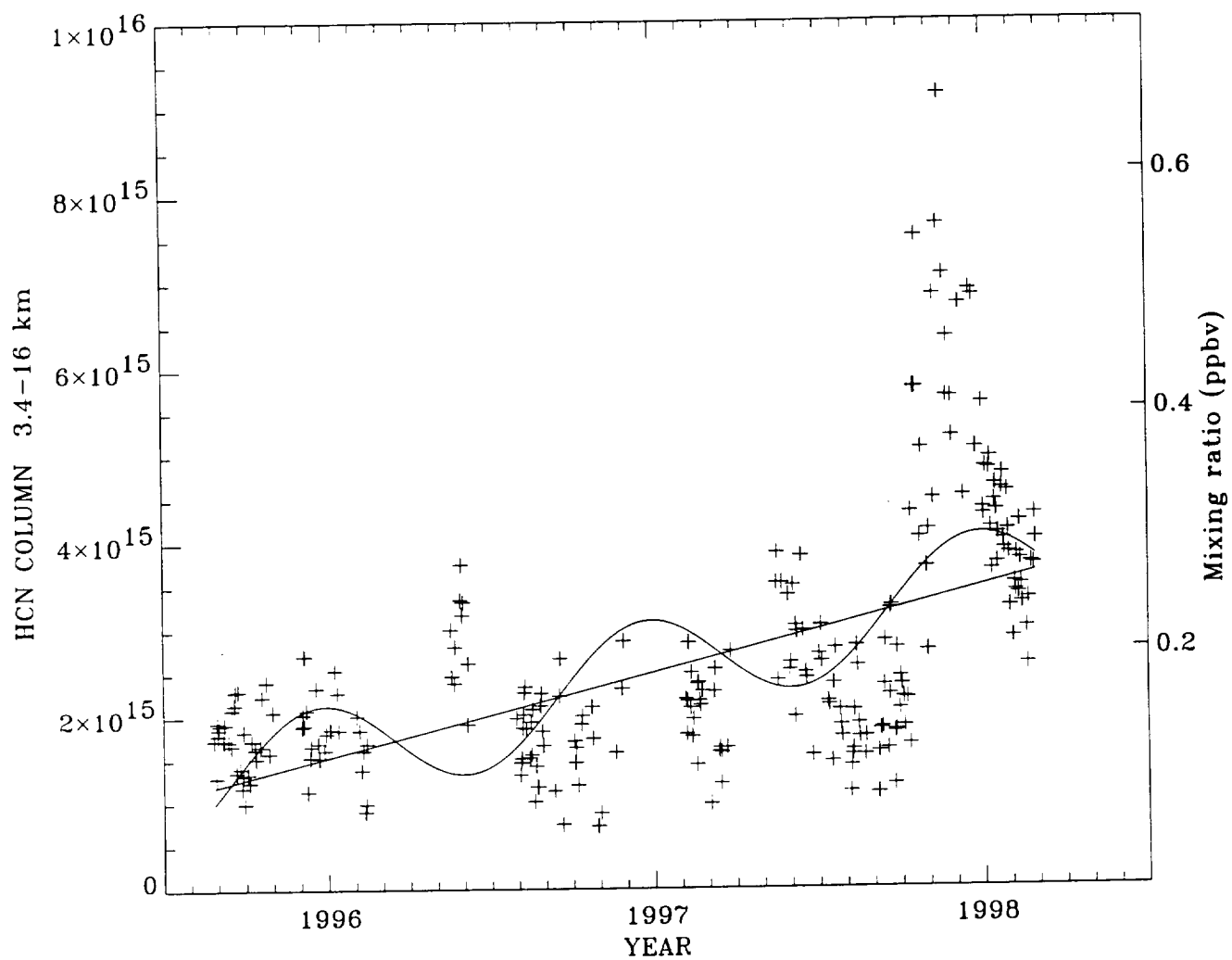


Figure 8

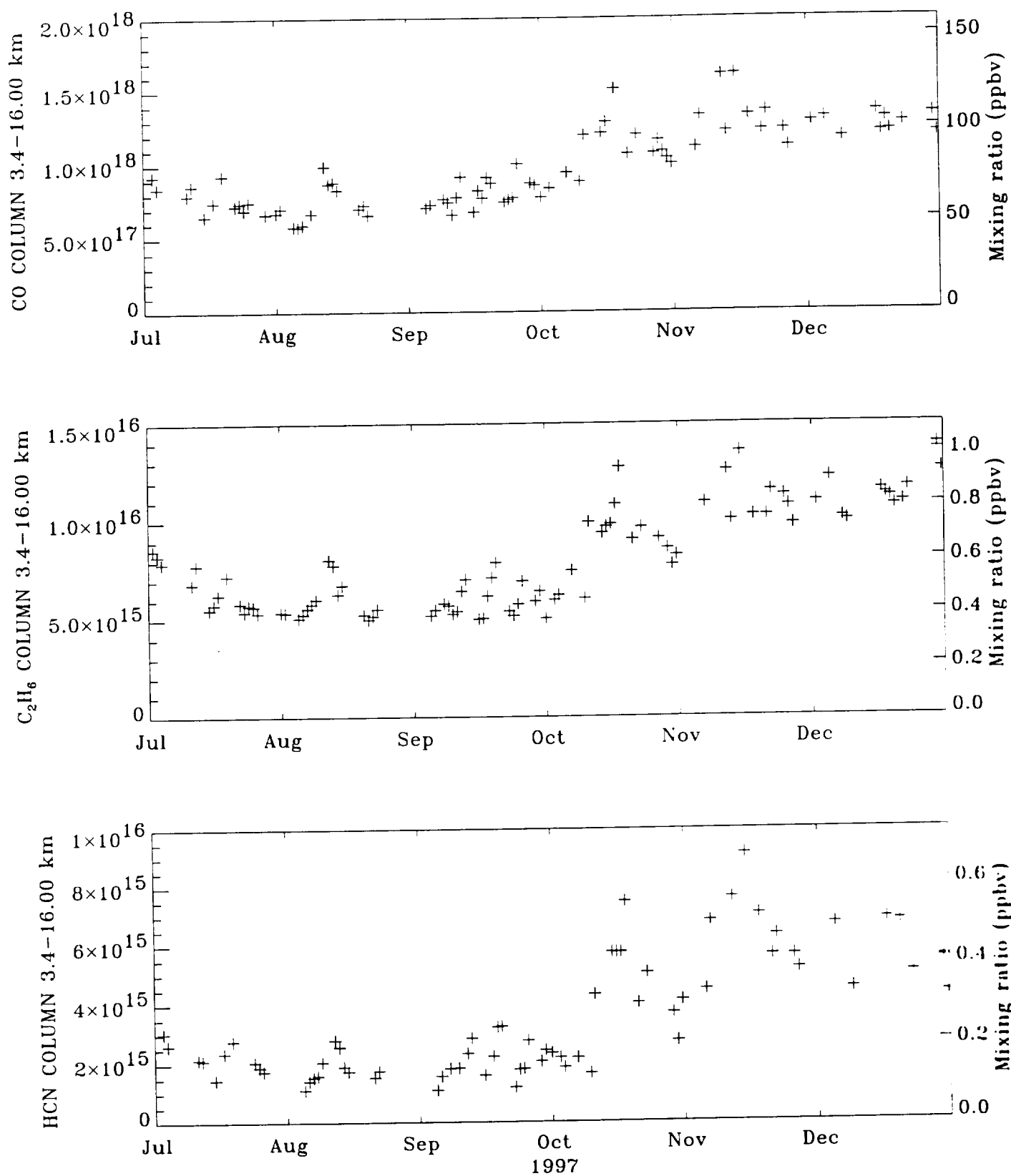
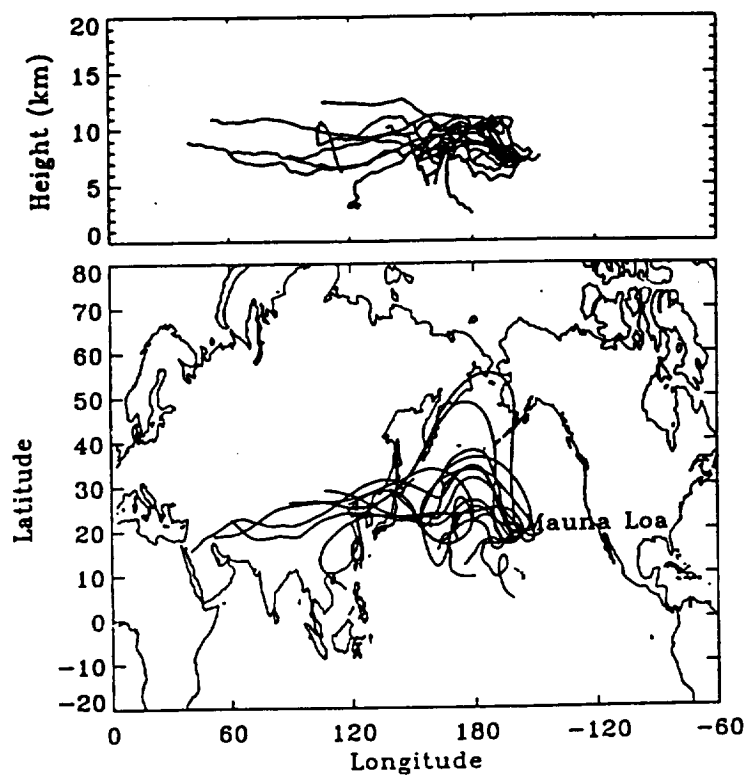
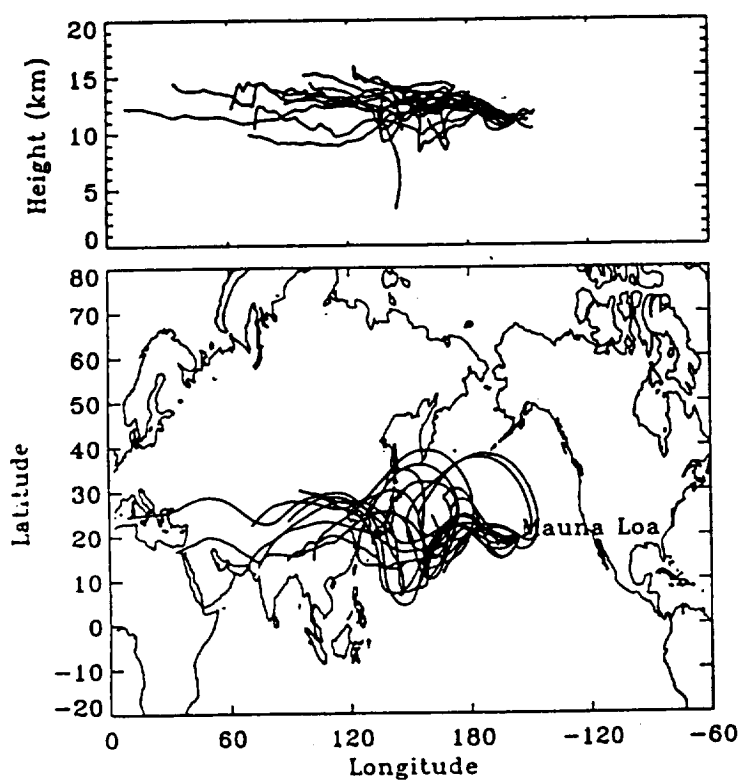


Figure 9







# Northern and Southern Hemisphere Ground-Based Infrared Spectroscopic Measurements of Tropospheric Carbon Monoxide and Ethane

Curtis P. Rinsland,<sup>1</sup> Nicholas B. Jones,<sup>2</sup> Brian J. Connor,<sup>2</sup> Jennifer A. Logan,<sup>3</sup>  
Nikita S. Pougatchev,<sup>4</sup> Aaron Goldman,<sup>5</sup> Frank J. Murcray,<sup>5</sup> Thomas M. Stephen,<sup>5</sup> Alan  
S. Pine,<sup>6</sup> Rodolphe Zander,<sup>7</sup> Emmanuel Mahieu<sup>7</sup>, and Philippe Demoulin<sup>7</sup>

<sup>1</sup>Atmospheric Sciences Division, NASA Langley Research Center, Hampton, Virginia

<sup>2</sup>National Institute of Water and Atmospheric Research, Lauder, New Zealand

<sup>3</sup>Department of Earth and Planetary Sciences and Division of Applied Sciences,  
Harvard University, Cambridge, Massachusetts

<sup>4</sup>Christopher Newport University, Newport News, VA

<sup>5</sup>Department of Physics, University of Denver, Denver, Colorado

<sup>6</sup>Alpine Technologies, Germantown, MD

<sup>7</sup>Institute of Astrophysics and Geophysics, University of Liège, Liège-Cointe,  
Belgium

### Abstract

Time series of CO and C<sub>2</sub>H<sub>6</sub> measurements have been derived from high resolution infrared solar spectra recorded in Lauder, New Zealand (45.0°S, 169.7°E, altitude 0.37 km) and at the U. S. National Solar Observatory (31.9°N, 111.6°W, altitude 2.09 km) on Kitt Peak. Lauder observations were obtained between July 1993 and November 1997 while the Kitt Peak measurements were recorded between May 1977 and December 1997. Both databases were analyzed with spectroscopic parameters that included significant improvements for C<sub>2</sub>H<sub>6</sub> relative to previous studies. Target CO and C<sub>2</sub>H<sub>6</sub> lines were selected to achieve similar vertical samplings based on averaging kernels. These calculations show that partial columns from layers extending from the surface to the mean tropopause and from the mean tropopause to 100 km are nearly independent. Retrievals based on a semiempirical application of the Rodgers optimal estimation technique are reported for the lower layer, which has a broad maximum in sensitivity in the upper troposphere. The Lauder CO and C<sub>2</sub>H<sub>6</sub> partial columns exhibit highly asymmetrical seasonal cycles with minima in austral autumn and sharp peaks in austral spring. The spring maxima are the result of tropical biomass burning emissions followed by deep convective vertical transport to the upper troposphere and long-range horizontal transport. Significant year-to-year variations are observed for both CO and C<sub>2</sub>H<sub>6</sub>, but the measured trends,  $(+0.37 \pm 0.57)\% \text{ yr}^{-1}$  and  $(-0.64 \pm 0.79)\% \text{ yr}^{-1}$ , 1 sigma, respectively, indicate no significant long-term changes. The Kitt Peak data also exhibit CO and C<sub>2</sub>H<sub>6</sub> seasonal variations in the lower layer with trends equal to  $(-0.27 \pm 0.17)\% \text{ yr}^{-1}$  and  $(-1.20 \pm 0.35)\% \text{ yr}^{-1}$ , 1 sigma, respectively. Hence, a decrease in the Kitt Peak tropospheric C<sub>2</sub>H<sub>6</sub> column has been detected, though the CO trend is not significant. Both measurement sets are compared with previous observations, reported trends, and three-dimensional model calculations.



## 1. Introduction

Carbon monoxide (CO) and ethane (C<sub>2</sub>H<sub>6</sub>) are important indicators of tropospheric pollution and transport because they are emitted primarily by anthropogenic sources [Logan et al., 1981; Rudolph, 1995], they have relatively high tropospheric abundances [e.g., Novelli et al., 1992; Blake and Rowland, 1986], and moderately long tropospheric lifetimes. Hough [1991] used a two-dimensional global tropospheric model to estimate mean annual globally averaged tropospheric lifetimes of 52 and 59 days for CO and C<sub>2</sub>H<sub>6</sub>, respectively. These lifetimes are significantly shorter than that of CH<sub>4</sub> (7 years [Hough, 1991]), and hence both gases are less well mixed throughout the troposphere than methane [e.g., Reichle et al., 1986; Singh and Salas, 1982]. However, the lifetimes of CO and C<sub>2</sub>H<sub>6</sub> are long enough for both gases to be possibly influenced by multiple sources, over a large region, potentially with different emission fingerprints [McKeen et al., 1996]. Dilution of emissions with "background" air during transport from distant source regions (especially during vertical mixing) is an important consideration for interpreting measurements at relatively unpolluted locations [Singh and Zimmerman, 1992; McKenna et al., 1995; Smyth et al., 1996]. Both CO and C<sub>2</sub>H<sub>6</sub> share a common initial, principal tropospheric sink, their reaction with OH radicals [Levy, 1971; Crutzen and Gidel, 1983; Ehhalt et al., 1986; Rudolph, 1995] and are convenient chemical species for remote sensing of anthropogenic activity based on strong spectral signatures in the mid-infrared [e.g., Wallace and Livingston, 1990; Zander et al. 1989; Ehhalt et al., 1991]. These absorptions are readily measured in ground-based solar spectra, even at background conditions in the southern hemisphere [e.g., Goldman et al., 1988; Rinsland et al., 1994a; Notholt et al., 1997a].

Nadir-viewing infrared measurements of CO were obtained from the U.S. Space Shuttle in November 1981, October 1984, April 1994, and October 1994 by the Measurement of Air Pollution from Satellite (MAPS) experiment [Reichle et al., 1986; 1990; 1998; Novelli et al., 1998], and a few CO and C<sub>2</sub>H<sub>6</sub> vertical profiles have been derived from Atmospheric Trace Molecule Spectroscopy (ATMOS) Fourier transform spectrometer (FTS) infrared solar occultation observations in May 1985 [Rinsland et al., 1987] and November 1994 [Rinsland et al., 1998], also from the U.S. shuttle. Because of the short duration of U.S. shuttle flights, these observations provide "snapshots" of the CO and C<sub>2</sub>H<sub>6</sub> atmospheric distributions with only indirect information about transport, dilution, and the spatial and temporal variations of CO and C<sub>2</sub>H<sub>6</sub> sources and sinks.

Seasonal variations of CO columns [e.g., Dianov-Klokov and Yurganov, 1989; Zander et al., 1989; Wallace and Livingston, 1990; Pougatchev and Rinsland, 1995a; Yurganov et al., 1997; Notholt et al., 1997b] and C<sub>2</sub>H<sub>6</sub> columns [e.g., Ehhalt et al., 1991; Rinsland et al., 1994a,b; Notholt et al., 1997b] have been derived from ground-based infrared solar absorption spectra. These measurements complement the spaceborne observations (cited above), airborne spectroscopic column measurements [Coffey et al., 1985; Toon et al., 1992], and *in situ* aircraft measurements of CO and C<sub>2</sub>H<sub>6</sub> [e.g. Blake et al., 1997; Talbot et al., 1996; Matsueda et al., 1998] by providing databases covering longer time periods, potentially with information on long-term trends free of drifts in calibration standards [e.g., Mahieu et al., 1997]. Ground-based solar measurements sample a broad altitude range. Hence, they measure plumes of pollution, uplifted by deep convection from the surface to the upper troposphere and transported long distances from sources by the prevailing winds [Dickerson et al., 1987; Heintzenberg and Bigg, 1990; Chatfield et al., 1996; Pickering et al., 1996;

Fuelberg et al., 1998; Matsueda et al., 1998]. Such plumes of pollution, located aloft, are not measured by surface level *in situ* sampling.

Most of the surface emissions of CO and C<sub>2</sub>H<sub>6</sub> originate at northern mid to high latitudes [Logan et al., 1981; Khalil and Rasmussen, 1990; Kanakidou et al., 1991; Rudolph, 1995; Manning et al., 1997]. Surface sources of CO in this latitude range are mainly related to combustion, e.g. automobile exhaust emissions, coal and oil burning, and natural gas losses. Ethane surface emissions in these latitudes are primarily due to natural gas losses (see Rudolph [1995] and the references cited therein).

Tropospheric measurements in the extratropical southern hemisphere (ETSH, defined as 30°S-90°S by Manning et al. [1997] and 35°S-90°S by Rudolph [1995]) show large seasonal variations in both CO [Steele et al., 1996; Novelli et al., 1998; Manning et al., 1997] and C<sub>2</sub>H<sub>6</sub> [Rudolph et al., 1989; Rudolph, 1995; Clarkson et al., 1997]. The dominant cause of these variations is the long range transport of tropical biomass burning surface emissions [e.g., Watson et al., 1990; Heinzenberg and Bigg, 1990; Fishman et al., 1991]. Peak tropical biomass burning north of 5°N usually occurs from March to June and south of the equator between September and December [Hao and Liu, 1994]. *In situ* production of CO from the oxidation of atmospheric CH<sub>4</sub> during transport is also an important source of CO in the ETSH [Manning et al., 1997], but the calculated yield is quite uncertain [Manning et al., 1997; Conny and Currie, 1996]. Although the tropospheric mixing ratios of CO and C<sub>2</sub>H<sub>6</sub> are much higher in the northern hemisphere than in the southern hemisphere [e.g., Logan et al., 1981, Fig. 9; Rudolph, 1995, Fig. 4], the exchange between the hemispheres is limited by the short lifetimes of CO and C<sub>2</sub>H<sub>6</sub> in the tropics (about 1 month) relative to the interhemispheric exchange time (1 to 2 years) [Maiss et al., 1996; Geller et al.,

1997; Manning et al., 1997]. Biogenic emissions of  $C_2H_6$  may be important on a relative basis in remote regions [Hough, 1991; Zimmerman et al., 1978; Singh and Zimmerman, 1992; Rudolph, 1995].

The purpose of this paper is to report multiyear time series of CO and  $C_2H_6$  measurements derived from high resolution infrared solar absorption spectra recorded at two remote stations, both located at midlatitudes, one in the northern hemisphere and the other in the southern hemisphere. A common set of spectroscopic line parameters and analysis procedures were used so that the results from the two sites are consistent. Significant improvements in the  $C_2H_6$  spectroscopic parameters relative to those assumed in previous studies have been incorporated. The observations have been analyzed and characterized with a line-by-line, multilayer algorithm based on the semiempirical version of the optimal estimation technique. The northern and southern hemisphere CO and  $C_2H_6$  columns were derived for two nearly independent layers, the lower extending from the surface to the altitude of the mean tropopause (12 km for Lauder, 14 km for Kitt Peak) and the upper layer extending from the altitude of the mean tropopause to 100 km. Here we report and contrast the northern and southern hemisphere results for the lower layer. The southern hemisphere measurements were obtained with sufficient frequency over a 4.5-year period (1993-1997) to quantify the interannual variability of both gases and comment on the suggestion that tropical biomass burning may be either increasing [Watson et al., 1990; Houghton, 1991; Hao and Liu, 1994; Kim and Newchurch, 1996, 1998] or decreasing [Khalil and Rasmussen, 1994]. Rudolph [1995] highlighted  $C_2H_6$  as a potentially useful gas for that purpose. Owing to their similar lifetimes, the near simultaneous observations of CO and  $C_2H_6$  provide a measure of seasonal changes in the relative importance of surface emissions and *in situ* photochemical CO production from  $CH_4$

oxidation in the tropospheric column. This consideration is particularly important for interpreting measurements from the southern hemisphere, where the seasonal cycles of  $C_2H_6$  and CO destruction by OH are in phase with the seasonal dependence of biomass burning [Rudolph et al., 1989].

We start with a discussion of the observational database (section 2) and the spectral analysis method (section 3). Section 4 describes the spectral regions and line parameters adopted in the analysis. As reported in section 5, after the initial retrievals were run, an objective procedure was used to remove poor quality measurements from the database. Section 6 discusses the error analysis and sensitivity studies. The time series of measurements from both sites are reported and compared with previous observations and model calculations in section 7. Finally, a brief summary of the results is given in section 8.

## 2. Observations

Infrared observations were recorded at the two sites with different instrumentation. Regular infrared observations from Lauder, New Zealand, were obtained as part of a program dedicated to the Network for the Detection of Stratospheric Change (NDSC) [Kurylo, 1991]. Lauder is a designated primary NDSC station. Observations from Kitt Peak are recorded with a facility instrument, which is used for laboratory, atmospheric, and astronomical observations in the visible and infrared. Kitt Peak has been designated as a complementary NDSC station.

## 2.1 Lauder database

The Lauder station (altitude 0.37 km, latitude 45.0°S, longitude 169.7°E) is located in a small town (population ~50) in the middle of the south island of New Zealand in a region of minimal industrial activity. Local burnoffs occur occasionally between about April and September with the majority in August-October. Spectra recorded on days of particularly intense local burnoffs were examined for the presence of spectral features characteristic of short-lived gases emitted by biomass fires (for example, the enhanced IR features studied in the fire spectra of Worden et al. [1997]). None were detected. Infrared spectral features of  $\text{NH}_3$  have been observed in the Lauder solar spectra with a strong, positive correlation between the emissions and the local surface temperature; the most likely source for these emissions is the release of animal excretion at local farms during warm, dry surface conditions [Murcray et al., 1989]. Hence, except for occasional local farming-related emissions, the Lauder site is believed to be representative of background conditions at midlatitudes of the southern hemisphere.

Broadband IR solar absorption spectra were first recorded from Lauder during campaigns in 1985, 1986, and 1987 at a resolution of  $0.02 \text{ cm}^{-1}$  [Murcray et al., 1989]. These observations covered the 3-5  $\mu\text{m}$  and 8-12  $\mu\text{m}$  regions only, and hence included measurements of  $\text{C}_2\text{H}_6$ , but not CO. These relatively low resolution measurements are not included in the present study. Regular high resolution IR solar observations did not begin until September 1990. Initially, these measurements were obtained with a Bruker model 120-HR FTS, which was replaced in September 1992 with a Bruker model 120-M FTS. Observations covering both the CO and  $\text{C}_2\text{H}_6$  regions began with the new instrument in July 1993. The 120-M

spectra are of significantly higher quality than the earlier data, and hence, only the 120-M measurements recorded through November 1997 are reported here.

The Lauder 120-M solar observations were recorded at unapodized resolutions of 0.0035 or 0.007  $\text{cm}^{-1}$  (defined as 0.9 divided by the maximum optical path difference) with a liquid-nitrogen-cooled InSb detector and a KCl beamsplitter. Optical filters were used to limit the spectral bandpasses to 1850-2100  $\text{cm}^{-1}$  (CO fundamental band), 2400 to 3100  $\text{cm}^{-1}$  ( $\text{C}_2\text{H}_6$   $\nu_7$  band), or 4000 to 4300  $\text{cm}^{-1}$  (CO overtone band). The time required to record a single full resolution spectrum was 104 s. The typical signal-to-noise ratio for full resolution Bruker 120-M spectra was about 200:1 near 2000, 2900, and 4200  $\text{cm}^{-1}$ . Most of the spectra were recorded between solar astronomical zenith angles of 45 and 85°. Boxcar apodization was applied.

A major gap in the Lauder measurements occurred between September 1995 and January 1996 when the 120-M instrument was returned to the manufacturer for upgrades and maintenance. Several observational gaps of 2 to 3 months also resulted from failures of the HeNe laser, which measures the optical path difference.

Instrumental performance varied at Lauder with minor phase errors observable in most spectra. Comparisons of ozone lines in the spectra with simulations based on correlative ozonesonde profiles [Rinsland et al., 1996] also indicate that the instrument line shape function is broader at higher wavenumbers than predicted from knowledge of the measurement parameters (maximum optical path difference, applied apodization function, and internal field of view). Modeling of both of these effects has been incorporated in the spectral analysis as described in section 3.

## 2.2 Kitt Peak database

The McMath-Pierce 1-m maximum optical path difference Fourier transform spectrometer [Brault, 1978], on Kitt Peak in southeastern Arizona, U.S.A. (altitude 2.09 km, 31.9°N, 111.6°W), is located on a mountaintop in the Sonora desert, a semiarid region with sparse population. The FTS is a modified Michelson interferometer capable of observations in the 550-45000  $\text{cm}^{-1}$  range using a selection of different beamsplitters, detectors, and optical bandpass filters.

The measurements included in the analysis were recorded with maximum optical path differences greater than 20 cm and solar astronomical zenith angles less than 85°. Liquid nitrogen cooled InSb detectors at the two output ports of the FTS were used. Typical signal-to-noise ratios of full resolution spectra are about 200:1, and 150:1 near 2900 and 4200  $\text{cm}^{-1}$ , respectively. The Kitt Peak infrared atmospheric observations are recorded relatively infrequently, typically 4 runs per year totaling a dozen days, but the database spans 1977 to 1997 with excellent uniformity in observational quality. Except for known problems, which affect relatively few observations (all of which were eliminated from this study), the measured instrument line shape function agrees with the function predicted by theoretical calculations based on the instrumental settings.

## 3. Analysis Method

The Lauder and Kitt Peak spectra were analyzed with the SFIT2 algorithm, which has been codeveloped at NASA Langley and NIWA Lauder for the retrieval of vertical profiles of atmospheric gases from ground-based solar absorption spectra. The profiles of one or more trace gases as well as the column



abundances of interfering species are retrieved by simultaneously fitting one or more microwindows in one or more solar spectra.

Analyses of IR solar spectra with SFIT2 have been reported by Pougatchev et al. [1995b, 1996] and Connor et al. [1996]. The studies of Pougatchev et al. [1995b, 1996] included comparisons of the SFIT2 ozone profile retrievals with correlative ozonesonde measurements. Also, total columns of several gases retrieved with SFIT [Rinsland et al., 1982a, 1984], which has the same forward model as SFIT2, have been compared with retrievals from the same spectra obtained with independently developed NDSC algorithms [Zander et al., 1993].

SFIT2 contains all the components required for retrieval of vertical volume mixing ratio profiles from atmospheric datasets recorded with a ground-based FTS in solar absorption mode (refractive atmospheric ray tracing, forward line-by-line radiative transfer model, FTS instrument model, solar CO absorption model, and the inverse model). Modeling of instrumental performance includes parameters to simulate symmetric and asymmetric distortions of the instrumental line shape function.

### 3.1 Forward Model

Monochromatic transmittances are calculated at a uniform grid spacing of  $<0.0005 \text{ cm}^{-1}$  with a line-by-line model that assumes a Voigt shape [Drayson, 1976] for lines in all atmospheric levels. Refractive ray tracing [Gallery et al., 1983] is used to generate density weighted effective temperatures and pressures for each of 29 layers with upper and lower model boundaries at the surface and 100 km. Vertical layer thicknesses are set to 2 km up to an altitude of 50 km. Higher altitude layer boundaries are at 60, 70, 80, and 100 km.

The FTS instrument response function is modeled by transforming the calculated monochromatic transmittance spectrum to the Fourier domain with a fast Fourier transform. The model interferogram is then multiplied by the applied apodization function and a function to simulate the decrease in fringe visibility with optical path difference due to the finite solid angle of the instrument internal field of view [e.g., Bell, 1972]. In the absence of instrumental distortions, the synthetic spectrum is obtained from the inverse Fourier transform of the model interferogram.

SFIT2 incorporates modeling of the combined effects of symmetric and asymmetric distortions of the line shape function [Guelachvili, 1981]. Several different functional forms have been implemented. Two parameters were introduced to model the Lauder data. One parameter is used to model the symmetric line shape distortions with the straight-line approximation of the effective apodization function [Park, 1983, Eq. 24]. A second parameter is used to model the asymmetric line shape distortions assuming a constant phase error [Park, 1983, section 2B; Guelachvili, 1981, pp. 22]. The Lauder spectra were simulated by Fourier transforming the model interferogram (including the simulated distortion effects) back to the spectral domain.

Atmospheric spectroscopic parameters defined in the format of the HITRAN database [Rothman et al., 1998, Table 3] are read by SFIT2. All are used including the air pressure-shift coefficient and the coefficient of the temperature dependence of the air-broadening coefficient. The isotope code number is read to derive the isotopic mass needed to calculate the Doppler width in each layer. Because of large fractionation effects in the atmosphere, HDO is treated as a separate molecular species. The line intensity in each layer is computed from the variations of the rotational and vibrational partition

functions of the molecule with temperature relative to the reference values at 296 K [Norton and Rinsland [1991, Eqs. 1-3]. An updated set of molecular parameters based on Norton and Rinsland [1991, Table II] is assumed.

All telluric CO lines are overlapped by absorption from solar CO lines. Additional solar CO lines are observable in the solar spectrum because of the high solar temperature and the high dissociation energy of CO. A single layer at 4500 K is assumed to compute the solar CO lines with the Minnaert empirical formula [Kilston, 1975; Rinsland et al., 1982b], given by

$$1/R_\nu = 1/R_c + 1/(K_\nu U) \quad (1)$$

where  $R_\nu$  is the residual intensity (absorbed fraction of solar continuum radiation),  $R_c$  is the limiting residual intensity,  $K_\nu$  is the monochromatic absorption coefficient at wavenumber  $\nu$ , and  $U$  is the solar CO column abundance. Line parameters from HITRAN 1996 [Rothman et al., 1998] were assumed to calculate the solar CO line list at 4500 K.

We further assume that all solar CO lines have a Voigt line shape with the Doppler line width at 4500 K scaled by a multiplicative factor to account for microturbulence in the solar atmosphere. The Lorentz width and the microturbulence scale factor are taken to be the same for all solar CO lines. A wavenumber shift parameter is included to account for the differential Doppler shift of the solar lines with respect to the telluric lines. In summary, five parameters are used in SFIT2 to model the absorption by solar CO lines. The parameters are  $R_c$ ,  $U$ , the Doppler width multiplicative scale factor, the Lorentz width, and the differential wavenumber shift. This model yields calculated solar CO lines with absorbances that match the observed values to  $\pm 5\%$  or better.

### 3.2 Inverse model

The inverse method used in SFIT2 assumes the optimal estimation formalism of Rodgers [1976] modified on the basis of its semiempirical implementation for NDSC microwave profiling of stratospheric  $O_3$  [Parrish et al., 1992; Connor et al., 1995]. Following the nomenclature in these papers, an observing system may be defined conceptually by

$$y = F(x, b) + \epsilon_y \quad (2)$$

where  $y$  is the vector of measurements,  $F$  is the forward model that characterises the measurements in terms of  $x$ , the state vector of parameters to be retrieved,  $b$  is the vector of model parameters which are assumed (not retrieved), and  $\epsilon_y$  is the vector of measurement errors, which are assumed to be normally distributed with zero mean.

The optimal estimation method requires specification of the following 3 inputs for  $x$ : (1)  $x_a$ , the *a priori* state vector; (2)  $S_a$ , the covariance of  $x_a$ ; and (3)  $S_\epsilon$ , the covariance of the measurement errors,  $\epsilon_y$ . The parameters to be retrieved simulate the target atmospheric absorptions, the interfering atmospheric absorptions, and the solar CO absorptions. Parameters are also included to model the instrumental performance.

In practice, the true *a priori* profile and its covariance are not known. In the semiempirical approach to optimal estimation [Parrish et al., 1992; Connor et al., 1995], the selection of the *a priori* mixing ratio profile is based on the best available information. Simulations are then generated and the covariance of the *a priori* state vector is adjusted empirically to yield the desired performance, specifically, spectral fits to the noise level of the measurements with minimal differences between the input vs. retrieved profiles

for the altitude range where the technique has sensitivity and avoidance of nonphysical oscillations in the retrievals. The simulated data are usually based on atmospheric observations, but ideally infinite resolution profiles with the true mean profile and covariances are used.

An additional empirical modification to the method has been applied to set the values for the measurement covariance matrix  $S_e$ . As already noted, formally the measurement errors are assumed to have a normal distribution. We further assume that  $S_e$  is diagonal; i.e. the measurement errors at each wavelength are independent with the variance set for each spectral region on the basis of the measurement signal-to-noise ratio.

**3.2.1. Atmospheric state parameters.** Modeling of the atmospheric state requires specification of the target gas *a priori* mixing ratios in each of the 29 layers in the atmospheric model. Furthermore, all of the selected spectral windows contain significant absorptions by interfering molecules, which were individually modeled by either retrieving their vertical profile or by multiplicatively scaling the *a priori* volume mixing ratio profile by a single factor. Selections of intervals for the  $C_2H_6$  and CO retrievals are discussed in sections 4.1 and 4.2, respectively.

The *a priori* atmospheric volume mixing ratio profiles for CO and  $C_2H_6$  were obtained from several sources. For CO above Lauder, the vertical profile is based on the average of aircraft flask air sample measurements obtained during the months of April and October over Bass Strait and Cape Grim, Tasmania, and analyzed by gas chromatography (L. P. Steele and R. L. Langenfelds, private communication, 1997). These observations have been described by Langenfelds et al. [1996] and Pak et al. [1996] and are reported in the NOAA/CMDL gravimetrically derived CO scale [Novelli et al., 1991, 1998]. The two aircraft

profiles were extended above the highest measurement altitude of 8 km on the basis of the April-May 1985 ATMOS measurements at 48°S [Gunson et al., 1990]. The two profiles are plotted in the paper by Pougatchev et al. [1998, Fig. 3]. The *a priori* profile for  $C_2H_6$  above Lauder was taken as that described by Rinsland et al. [1994a]. This profile below 14 km is based on a seasonal average of the global two-dimensional model profiles calculated for the latitude of Lauder [Kanakidou et al., 1991, Figure 7]. An exponential decline with a 3 km scale height is assumed at higher altitudes based on stratospheric measurements (e.g., Rinsland et al. [1987]).

The CO *a priori* profile for the Kitt Peak analysis is based on an average of tropospheric aircraft samplings at Carr, Colorado (40.9°N, 104.8W) obtained between November 1992 and December 1996 [Tans et al., 1996] and an average of 3 ATMOS/ATLAS 3 profiles measured at 32°N±1° latitude in November 1994 [Gunson et al., 1996]. The Carr measurements, also on the NOAA/CMDL gravimetrically derived CO scale [Novelli et al., 1991, 1998], were used to define the CO *a priori* profile from the surface to 10 km. Observations marked as having analysis or sample problems were excluded. The mean ATMOS measurement defines the *a priori* profile between 16 to 100 km. A spline fit was used to smoothly connect the two profiles in the intermediate altitude regime. The  $C_2H_6$  *a priori* profile above Kitt Peak was adopted from the reference listing of midlatitude northern hemisphere profiles compiled by Smith [1982].

The mixing ratio of CO in the lower stratosphere is fairly constant because of its production from the oxidation of  $CH_4$  is balanced by OH reaction losses. In contrast, there is a steep decline in the  $C_2H_6$  volume mixing ratio above the tropopause because of reactions with both OH radicals and Cl atoms [e.g., Goldman et al., 1984; Rinsland et al., 1987].

Covariances for the CO and C<sub>2</sub>H<sub>6</sub> mixing ratio vectors were taken to be diagonal. Additionally, we expressed the uncertainties relative to the *a priori* mixing ratio in the layer. For CO, the diagonal elements in the S<sub>a</sub> matrix were calculated from  $s_{ii} = (k_i q_{ai})^2$  where  $q_{ai}$  is the corresponding element of the CO *a priori* profile and  $k_i$  equals 0.2 for all layers. This value was tested by generating synthetic spectra for a realistic set of atmospheric profiles and performing retrievals on the synthetic observations. Figure 1 illustrates a comparison for Kitt Peak of 2.09-14 km retrieved columns with the "true" columns. The results are based on individual CO profiles from 82 aircraft flights from Carr, Colorado during all 4 seasons. Each aircraft profile was extrapolated above the flight altitude, as already described. The rms difference between the "true" and retrieved CO 0.37-14 km columns is  $2.735 \times 10^{16}$  molecules cm<sup>-2</sup>, 2% of the 0.37-14 km *a priori* column. As shown in the figure, there is no systematic bias between the "true" and retrieved columns over the full factor of two range in the measurements.

Unfortunately, there are no comparable sets of C<sub>2</sub>H<sub>6</sub> tropospheric profile measurements appropriate for the Kitt Peak or Lauder analysis. We selected  $k_i = 1.0$  for all layers. This weak constraint yields a small relative contribution of the *a priori* profile to the retrieval.

An *a priori* value of 1.0 and a variance of 0.3 were assumed for the factor to multiplicatively scale the *a priori* mixing ratios to retrieve the total column of each molecule with significant interfering absorption. As expected, tests show that the *a priori* variance is a weak constraint (i.e., the relative contribution of the *a priori* to the retrieval is small) provided that the interfering molecule absorbs significantly in the measured spectrum.

3.2.2. Solar CO parameters. As described in section 3.1, 5 parameters are required to model the absorption by solar CO lines with the *a priori* values set on the basis of window-by-window fits to ATMOS exoatmospheric solar spectra, except for the solar-atmospheric differential wavenumber shift, which was set to zero. The parameter values were assumed uncorrelated (off-diagonal elements equal to zero). Very small variances were assumed for  $R_c$  and  $U$ , so that the *a priori* values were adopted in the retrievals. The variances of the other parameters were set large enough to make the retrieved values practically independent of the *a priori* settings; hence, the information used in the retrieval came almost entirely from the measured spectrum.

3.2.3. Instrument performance-related parameters. Model parameters retrieved in the analysis are the wavelength scale calibration factor, the slope of the background (100% transmission line) in each window, and the phase error (Lauder data only). *A priori* values were set to realistic estimates (e.g., zero for the background slope). The individual parameters were assumed to be independent (coefficients of off-diagonal elements set to zero). Variances for the individual parameters were set to large values to avoid underfitting the measured spectrum. The phase error was assumed to be independent of wavenumber in the analysis of the Lauder spectra.

As already mentioned, the Lauder spectra also show an instrument function that is broader than the theoretical one with the discrepancy increasing at higher wavenumbers. The coefficient of the straight line effective apodization parameter used to model the symmetric broadening was assumed, not retrieved. The value for the  $C_2H_6$  region was derived from spectral fits to strong, isolated  $O_3$  lines near the same wavelength with the vertical  $O_3$  profile distribution constrained to agree with same day ozonesonde measurements [Rinsland et al.,



1996]. Based on the measured dependence of the effective apodization coefficient with wavenumber (determined in the same way from  $O_3$  spectral fittings), an extrapolated value was derived for the analysis of the CO (2-0) band lines. The coefficient  $c_0$  [Park, 1983, Eq. 24] was set to -0.35 at  $2976\text{ cm}^{-1}$  ( $C_2H_6$  region) and -1.0 at  $4200\text{ cm}^{-1}$  (CO region).

The Kitt Peak instrumental function is close to the theoretical function calculated from the instrumental settings at the time of measurement. Hence, the theoretical instrument function was assumed ( $c_0=0.0$ ).

#### 3.2.4 Additional assumed parameters

The vertical temperature profiles for Lauder were specified on the basis of daily mean National Centers for Environmental Prediction (NCEP) measurements from 0 to 55 km and smoothly connected to agree with the 1976 U.S. Standard Atmosphere above 65 km. The assumed temperature profiles for Kitt Peak are based on a similar procedure.

The vertical volume mixing ratio profiles for the interfering molecules were assumed from previous observations near the same locations or compilations of reference profiles (e.g., Smith [1982]).

#### 4.0. Spectral Windows and Line Parameters

Selections of the spectral intervals for analysis were based on 4 considerations: (1) the availability of target gas spectral features with minimal interferences from other atmospheric and solar lines, (2) the quality of the available spectroscopic line parameters, (3) a minimal sensitivity of the target spectral features to errors in the vertical temperature profile, and (4) a similar vertical sampling of the atmosphere. The last criterion was dictated by the goal of comparing same day CO and  $C_2H_6$  tropospheric measurements to take

advantage of their very similar tropospheric lifetimes with common principal destruction via reactions with OH radicals [e.g., Kanakidou et al., 1991, Fig. 4; Law and Pyle, 1993, Fig. 1].

The selection of the spectral intervals was also constrained by the existence of only relatively weak absorption features of  $C_2H_6$  in ground-based infrared solar absorption spectra. The most favorable ones for remote sensing are the sharp  $PQ_3$  and  $^1Q_0$  subbranches of the  $\nu_7$  perpendicular band at  $3\ \mu m$  [e.g., Ehhalt et al., 1991; Rinsland et al., 1994a,b]. Lines of CO with a wide range of absorption depths are present in ground-based solar spectra.

Averaging kernels provide a direct assessment of the theoretical altitude sensitivity for an observing system in the absence of errors in the measurements and the model parameters [Rodgers, 1990, section 4]. They show explicitly how the true profile is smoothed in producing the retrieved profile. A perfect measurement system would sample the intended altitude region uniformly with no smoothing; put another way, the averaging kernel for each altitude would be a  $\delta$ -function.

Figure 2 presents partial column averaging kernels for Lauder profile retrievals of  $C_2H_6$  (top) and CO (bottom) obtained with the selected parameters. The assumed *a priori* volume mixing ratio profiles,  $S_a$  covariance matrices, spectral intervals, and spectroscopic parameters are described in sections 4.1 and 4.2. The calculated kernels also depend on the signal-to-noise ratio and the spectral resolution of the measurements [Connor et al., 1996]. Typical Lauder observation values of 200 and  $0.0035\ cm^{-1}$  were assumed, respectively. The kernels for partial columns were first generated for the 29 layer atmospheric model, then combined to derive the curves for 0.37-12, 12-100, and the total column, 0.37-100 km. The boundary at 12 km was selected to correspond with the

average altitude of the tropopause above Lauder. The Lauder tropopause height varies between about and 17 km (G. Bodeker, NIWA Lauder, private communication, 1997). Similarly, the Kitt Peak observations were analyzed in two layers, 2.09-14 km and 14-100 km, with the boundary selected to correspond the approximate average altitude of the tropopause above Kitt Peak.

The Lauder partial column averaging kernels for the two layers (long and short dashed curves in Fig. 2) show little overlap with well separated peaks for the lower and upper layers with maxima at altitudes of 10.9 and 32.7 km for  $C_2H_6$  and 8.0 and 34.2 km for CO, respectively. Hence, the atmosphere is being sampled for  $C_2H_6$  and CO with similar vertical sensitivities, and the measurements of the two regions are nearly independent of each other. The CO calculations in Fig. 2 are based on profile retrievals from two weak lines, the R(3) and R(6) transitions of the (2-0) band.

Figure 3 shows the vertical sampling achieved for CO above Lauder with alternate spectral selections for CO and a different retrieval method. The upper panel shows CO partial column averaging kernels calculated for profile retrievals from the CO R(3) (1-0) line at  $2157.2997\text{ cm}^{-1}$ . This line is two orders of magnitude stronger than the two CO lines used for the Fig. 2 CO calculations. The partial column averaging kernel for the 0.37-12 km layer peaks at 5.5 km. The reduced sensitivity to profile changes in the 12.0-100 km layer results from absorption saturation near line center. The lower panel of Fig. 3 presents CO partial column averaging kernels obtained from the two weak CO lines used in Fig. 2, but the retrievals were performed by multiplicatively scaling the *a priori* mixing ratio in all 29 model layers by a single factor. The 0.37-12 km and 12.0-100 km kernels both peak at 32.6 km with poor sensitivity to CO molecules in the

troposphere. Although not shown, results for  $C_2H_6$  and the multiplicative scaling method are similar (the  $C_2H_6$  absorption is weak).

Results for the Kitt Peak partial and total columns are similar to those presented in Figs. 2 and 3. The spectral windows, molecular and solar interferences, assumed spectroscopy, and the SFIT2 parameter settings are discussed for each molecule in the following 2 subsections.

#### 4.1 Ethane

The retrieval  $C_2H_6$  layer column abundances from the Lauder and Kitt Peak spectra is based on the analysis of the  $PQ_3$  subbranch of the  $\nu_7$  band at  $2976.8\text{ cm}^{-1}$ . This feature is prominent in high resolution infrared solar spectra and has been used frequently for quantification of  $C_2H_6$  atmospheric amounts. In the present work, we report significant updates to the spectroscopy in the  $2976.8\text{--}2977.8\text{ cm}^{-1}$  region.

Pine and Stone [1996] reported the analyses of the  $PQ_3$  and  $^rQ_0$   $C_2H_6$  subbranches from Doppler-limited and air-broadened laboratory spectra recorded at  $161\pm5$  and  $296\pm1$  K and sub-Doppler resolution molecular beam  $C_2H_6$  spectra recorded at an effective temperature of 50 K. The results of their  $PQ_3$  analysis yielded measured positions for individual transitions up to  $J=16$  in the A torsional state and  $J=13$  in the E torsional state.  $A_1$ - $A_2$ -type doublet splittings were measured for  $J\geq8$  and modeled with a power-series expansion in  $J(J+1)$ . Also, air broadening coefficients and pressure shift coefficients in air were measured at 161 and 296 K [Pine and Stone, 1996, Table 1]. A single Lorentz air broadening coefficient and a single air-broadened, pressure-induced shift coefficient were found to fit the absorption by all lines at 161 and 296 K. The measured Lorentz coefficient of  $0.6708\pm0.0043\text{ cm}^{-1}\text{ atm}^{-1}$  at 296 K and a

temperature dependence coefficient  $n$  of  $1.01 \pm 0.03$ , with  $n$  equal to  $\ln(\gamma(T)/\gamma(T_0))/\ln(T_0/T)$  for  $T_0$  equal to 296 K, were derived from the air-broadening data at the two temperatures. These values are significantly lower and higher, respectively, than values of  $0.09$  or  $0.10 \text{ cm}^{-1} \text{ atm}^{-1}$  at 296 K and  $0.75$  assumed previously in our ground-based spectroscopic studies of  $\text{C}_2\text{H}_6$  from Mauna Loa and Lauder [Rinsland et al., 1994a,b]. A value of zero for the pressure shift coefficient of all  $\text{C}_2\text{H}_6$  lines has been assumed in previous analyses of atmospheric solar spectra.

In the present work, we assumed  $\text{C}_2\text{H}_6$   $PQ_3$  subbranch line parameters from the work of Pine and Stone [1996] with extensions to include most of the additional lines in the region (see Pine and Stone [1996], Fig. 9 for a 296 K measurement-calculation comparison without the additional lines). Also, absolute intensities have been derived from the average of two sets of laboratory measurements. We summarize the results here.

The prominent but previously unidentified feature in the Doppler-limited lab data [Pine and Stone, 1996] near  $2976.855 \text{ cm}^{-1}$  has been assigned to the  $\nu_4 + \nu_7 - \nu_4$   $PQ_3$  subbranch. Positions were calculated from Eq. 1 of Pine and Stone [1996] assuming manually adjusted values of  $\nu_0$  for the A and E torsional states and a single value for  $\Delta B$  ( $\Delta D$ ,  $\Delta H$ , and  $\Delta J$  were set to zero). Relative intensities were calculated from the equations and parameters of Dang-Nhu et al. [1984] with  $289 \text{ cm}^{-1}$  added for the vibrational energy of the  $\nu_4$  torsional state [Duncan et al., 1983; Moazzen-Ahmadi et al., 1988, 1992]. The calculated intensity of the hot band  $PQ_3$  subbranch with respect to the intensity of the  $\nu_7$   $PQ_3$  subbranch was scaled by 0.8 to match the observed absorptions at 161 and 296 K. The relative intensities and shapes of both features are well reproduced at the two temperatures with these parameters. Lines of  $\nu_5$  and  $\nu_8 + \nu_{11}$  were added

to the linelist based on the positions and assignments of Pine and Lafferty [1982, Table 2] and the intensity expressions and parameters of Dang-Nhu et al. [1984]. The new linelist accounts for most of the absorptions observed in the  $PQ_3$  region at 161 and 296 K. Furthermore, it is apparent from plots of the measured versus calculated spectra that resonance mixing perturbs the positions and intensities of several assigned lines in the interval. Figure 4 presents comparisons of the measured and calculated Doppler-limited  $C_2H_6$  laboratory spectra at temperatures of 161 and 296 K.

Absolute intensities were derived from an unweighted average of values calculated from the intensity expressions and parameters of Dang-Nhu et al. [1984] and a set of intensities inferred from the laboratory measurements of Pine and Stone [1994]. The results from the more recent measurements are 0.955 times the earlier ones. The discrepancy of the two intensity values primarily reflects the uncertainties in the pressure measurements, at low temperatures in the older study and at low pressure in the newer. The measurements of Rinsland et al. [1986] were not considered because of their low spectral resolution ( $0.06\text{ cm}^{-1}$ ).

The new  $C_2H_6$  spectroscopic parameters adopted here are a significant improvement relative to those assumed in our previous atmospheric studies [Rinsland et al., 1987; Rinsland et al., 1994a,b]. The previous model neglected torsional tunneling and  $A_1$ - $A_2$  splittings. Also, we previously assumed a 296 K Lorentz broadening coefficient  $\approx 30\%$  larger than the value measured for  $PQ_3$  by Pine and Stone [1996]. Further work to estimate the lower state energies of unassigned lines in the vicinity of the  $PQ_3$  subbranch, obtain an improved description of the intensity perturbations in the region, and calculate the

temperature dependent  $C_2H_6$  partition function with improved accuracy is in progress.

Except for  $C_2H_6$ , the spectroscopic parameters were taken from the 1996 HITRAN compilation [Rothman et al., 1998]. The weak temperature-sensitive absorption by the  $H_2^{18}O$  line at  $2976.7839\text{ cm}^{-1}$  (lower state energy of  $1574.679\text{ cm}^{-1}$ ) directly overlaps the  $PQ_3$   $C_2H_6$  subbranch. Parameters for this  $H_2^{18}O$  line were added in HITRAN 1996 [Rothman et al., 1998]. Hence, no update was necessary.

Figure 5 presents molecule-by-molecule simulations and a typical Lauder spectrum in the region of the unresolved  $PQ_3$  subbranch. The  $C_2H_6$  retrievals reported in this paper are based on the fits to the  $2976.62\text{--}2976.94\text{ cm}^{-1}$  interval shown in the figure. The importance of accurate modeling of the interferences, particularly  $H_2O$ , at the low altitude of the Lauder station is evident, as was noted previously [Rinsland et al., 1994a]. Four molecules were fitted in this window:  $C_2H_6$ ,  $H_2O$ ,  $CH_4$ , and  $O_3$ . Only the profile of  $C_2H_6$  was retrieved; a multiplicative *a priori* volume mixing ratio profile scaling factor was retrieved for each of the other 3 gases. The phase error and zero absorption level were also fitted in the Lauder spectra. A sample Lauder fit is presented in Figure 6.

The  $PQ_3$   $C_2H_6$  region of the Kitt Peak spectra is similar to the sample Lauder observations shown in Figs. 5 and 6. However, the interference by  $H_2O$  is significantly weaker because of the higher altitude of Kitt Peak. Columns of  $C_2H_6$  obtained with the new line parameters are 13% less than values obtained with the parameters assumed previously [Rinsland et al., 1994a,b].

## 4.2 Carbon Monoxide

The retrievals are based on spectral fittings of 2 intervals containing the  $^{12}\text{CO}$  R(3) and R(6) (2-0) band lines at 4274.7047 and 4284.8911  $\text{cm}^{-1}$ , respectively. Figure 7 illustrates the intervals for a sample Lauder spectrum along with simulations for  $\text{H}_2\text{O}$ ,  $\text{HDO}$ ,  $\text{CO}$ ,  $\text{CH}_4$ , and solar  $\text{CO}$ . The selected intervals avoid  $\text{CH}_4$  octad lines not included in HITRAN 1996 [Rothman et al., 1998] and yield compatible simultaneous spectral fittings. An unpublished line list shows the importance of the  $\text{CH}_4$  lines missing from HITRAN 1996 [Rothman et al., 1998] in other portions of the 4200-4300- $\text{cm}^{-1}$  region (J.-C. Hilico, private communication, 1997).

The HITRAN 1996 parameters [Rothman et al., 1998] adopted for the  $\text{CO}$  analysis include  $\text{CH}_4$  positions and intensities from Brown and Rothman [1982] with accuracies for single, unblended lines of  $\pm 0.0005 \text{ cm}^{-1}$  and  $\pm 2\%$ , respectively. Air-broadening coefficients and pressure-shift coefficients at 296 K based on the work of Malathy Devi et al. [1993] were assumed for  $\text{CH}_4$  as given on HITRAN 1996 [Rothman et al., 1998]. A weak, unassigned absorption appears at 4274.81  $\text{cm}^{-1}$  in the Lauder and Kitt Peak spectra. A line of  $\text{HDO}$  was added at this position. The retrievals satisfactorily reproduce this weak feature for the range of observational conditions.

The R(3) (2-0) band terrestrial line in the 4274.62-4274.82- $\text{cm}^{-1}$  spectral interval is overlapped by absorption from the corresponding solar  $\text{CO}$  transition with only minor interferences from other gases in the interval. The 4284.75-4285.18  $\text{cm}^{-1}$  spectral interval contains the R(6) terrestrial  $\text{CO}$  line, several solar  $\text{CO}$  lines, and the strong  $\text{CH}_4$  line at 4285.1553  $\text{cm}^{-1}$ . The retrievals were performed by fitting for the vertical profiles of both  $\text{CO}$  and  $\text{CH}_4$ . A multiplicative a priori  $\text{HDO}$  volume mixing ratio profile scaling factor was also



retrieved to account for variations in the absorption by the  $4274.81\text{-cm}^{-1}$  line. An example of a simultaneous fit to the two CO windows in a typical Kitt Peak spectrum is presented in Fig. 8.

### 5.0 Measurement selection criteria

The quality control of retrieved profiles was based on a combination of criteria that measure the goodness of fit and the relative strength of the target absorption feature. The first criterion is the familiar root-mean-square error (rms) between the measured and fitted spectra in the selected intervals. The latter, called the signal strength ratio (ssr), is the observed depth of the target absorption feature relative to the noise measured in a nearby window region. It serves the purpose of identifying spectra in which the target feature is too weak to be measured accurately. As illustrated in Fig. 9, a plot of rms versus ssr produces a scatter plot with points that define an elbow-shaped curve. Values for the maximum rms and minimum ssr are selected near the "elbow" of this curve to weed out unreliable retrievals. As a final step, all profiles that pass the rms/ssr criteria are displayed on a single plot, and any further profiles that are clearly unacceptable (large negative mixing ratio excursions, for example), are removed. This second step generally deletes only about 5% of the remaining measurements, which for a variety of reasons, including poorly modelled interferences, channel spectra, and unwanted instrumental artifacts, produce instabilities in the retrieval process.

### 6.0 Error Analysis

In Table 1, we report our estimates of the effects of both random and systematic errors on the retrieved lower layer CO and  $\text{C}_2\text{H}_6$  partial columns. A single value is given for the two stations where appropriate. We next describe

the procedures and assumptions used in generating the uncertainty estimates.

**6.1. Temperature profile.** As already noted, the analysis regions were selected to contain target lines with intensities insensitive to temperature, and all retrievals were performed assuming NCEP temperature profiles calculated for the date and location of the observations. We generated synthetic spectra for 3 randomly selected days assuming the nominal temperature profile. Retrievals were then performed by adding 2 K to the temperature at each altitude. The magnitude of the mean difference between the true and retrieved partial column is shown in the table; the errors are 1% or less for  $C_2H_6$  and CO.

**6.2. Noise.** Random numbers with zero mean, a normal distribution, and a root-mean-square deviation equal to 0.5% of the maximum transmission were added to synthetic spectra generated for the  $C_2H_6$  and CO analysis regions. The simulated noise is typical of the individual Lauder and Kitt Peak spectra. Ten different seeds were chosen. The retrieved partial columns show no bias with respect to the true partial columns. As shown in the table, the average difference between the noisy and true partial columns range from 2 to 7%. Note that daily averaging further reduces errors due to random instrument noise for both Lauder and Kitt Peak.

**6.3. Interfering atmospheric lines.** As mentioned in section 4.1 and illustrated in Fig. 5,  $H_2O$  is an important interfering molecule with absorption overlapping the target  $C_2H_6$   $P_{Q_3} \nu_7$  band subbranch. The two windows selected for CO contain only minor absorptions by atmospheric molecules.

**6.4. Spectroscopic parameters.** We estimated a 2% uncertainty in the retrievals due to spectroscopic parameters errors in the two microwindows analyzed for CO. This small error estimate is based on the high quality of the CO parameters in the HITRAN 1996 compilation [Rothman et al., 1998] and our

avoidance of intervals containing poorly-modeled, interfering  $\text{CH}_4$  lines. The spectroscopic updates incorporated for  $\text{C}_2\text{H}_6$  in the present analysis are estimated to reduce the errors in the  $\text{C}_2\text{H}_6$  retrievals from 10% [Rinsland et al., 1994a] to 5% with the main source of error the uncertainty in the laboratory pressure measurements.

**6.5. State vector of unknowns.** The retrieval is a linear combination of the true and *a priori* profiles with structures finer than the measurement vertical resolution poorly determined [Connor et al., 1995]. Although we do not know the true  $\text{C}_2\text{H}_6$  and CO atmospheric profiles on the dates of observation, simulations based on correlative observations can be used to show the dependence of the retrieval on the *a priori* profile and the assumed  $S_a$  and  $S_e$  covariances. As illustrated in Fig. 1, retrievals from synthetic spectra generated from a set of correlative vertical profiles and the adopted settings yield partial columns that track the values adopted in the simulations with no deviations from linearity over the factor of two range in the CO 2.09-14 km *a priori* partial columns. Based on these results, we estimate 1% as the error in the lower layer partial column retrieval due the influence of the *a priori* profile and the other state vector parameters.

**6.6. Instrument line shape function.** A synthetic spectrum was calculated for the most common spectral resolution of the Lauder observations. The theoretical instrument line shape function was assumed. A retrieval was performed from this spectrum with the coefficient of the "straight line" effective apodization coefficient [Park, 1983] decreased from the nominal value of 0.0 to -0.1. This case simulates apodization function error that increases linearly from zero at zero path difference to 10% at the maximum optical path difference. Changes of 0.1% in the tropospheric layer partial columns of CO and

$C_2H_6$  were obtained. The Kitt Peak instrument function is well determined so that instrument function errors are negligible for both molecules. The Lauder CO and  $C_2H_6$  0.37-12 km partial columns are much less sensitive to errors in the instrument function than those derived for the Lauder  $O_3$  0.37-12 km column [Pougatchev et al., 1996, Table 1].

**6.7. Forward model.** The forward model in SFIT2 is essentially the same as in SFIT and the algorithms developed at NASA Langley for the analysis of infrared laboratory [Benner et al., 1995] and infrared solar spectra recorded with Fourier transform spectrometers [Norton and Rinsland, 1991]. Based on retrieval comparison exercises that have been performed for atmospheric and laboratory studies [e.g. Zander et al., 1993], we estimate that errors in simulated solar spectra generated with the SFIT2 forward model are unlikely to introduce  $C_2H_6$  and CO lower layer partial column retrieval errors greater than 4% for CO and 2% for  $C_2H_6$ . The larger value was assumed for CO because of the additional uncertainty caused by errors in simulating the absorption by solar CO lines in the windows.

## 7. Results and Discussion

For Lauder, 0.37-12 km partial vertical columns were calculated by integrating the retrieved profiles. For Kitt Peak, the 2.09-14 km partial columns were computed. Daily averages were generated assuming equal weights for all observations; the number of observations per day ranged from 1 to 23 for Lauder  $C_2H_6$ , and the number of observations per day ranged from 1 to 25 for Lauder CO. For Kitt Peak, the corresponding ranges of daily observations were 1 to 13 and 1 to 14.

The daily average partial columns  $C_t$  were fitted with the expression

$$C_t = a_0 + a_1 (t - t_0) + a_2 \cos 2\pi [(t - t_0) - t_1] \quad (3)$$

where  $a_0$  is the mean value,  $t$  is the time of the observation in calendar years,  $t_0$  is the time of the first observation in calendar years,  $a_1$  is the long-term trend,  $a_2$  is the amplitude of the seasonal cycle (assumed to be sinusoidal), and  $t_1$  is the fraction of the calendar year corresponding to the time of the seasonal maximum.

### 7.1 Lauder $C_2H_6$ and CO 0.37-12 km Time Series

The top and middle panels of Fig. 10 present the measured Lauder daily average 0.37-12 km  $C_2H_6$  and CO partial columns between July 1993 to November 1997. The total number of measurement days are 407 for  $C_2H_6$  and 390 for CO. The solid curves show the best-fits to the observations based on Eq. 3. This simple model does a poor job in reproducing the observed highly asymmetrical  $C_2H_6$  and CO seasonal cycles, which show sharp peaks during austral spring and deep minima in austral autumn. Corresponding, peak column-average 0.37-12 km mixing ratios (shown on the right vertical axis) exceeded 0.6 ppbv for  $C_2H_6$  and 100 ppbv for CO. The maximum mixing ratios are as high as measurements in upper tropospheric continental outflow regions between Brazil and Africa during September-October 1992 [Talbot et al, 1996, Tables 2 and 3]. Year-to-year differences are apparent in the Lauder time series with particularly high 0.37-12 km partial CO and  $C_2H_6$  columns observed during October 1994, August 1995, and September-October 1997.

We attribute the sharp peaks to tropical biomass burning emissions lofted to the upper troposphere by deep convection. In the upper troposphere, where the present measurements have their highest sensitivity (Fig. 2), maximum wind

speeds exceeded  $40 \text{ m s}^{-1}$  in the southern subtropical jet stream ( $\sim 30^\circ\text{S}$  latitude) during the September-October 1996 Pacific Exploratory Mission-Tropics (PEM-T) experiment [Fuelberg et al., 1998]. Although typical PEM-T upper tropospheric wind speeds were lower, calculations indicate that the strong, westerly upper tropospheric winds were sufficient to transport southern hemisphere air parcels thousands of km on a time scale of about a week during the mission [Fuelberg et al., 1998]. Once lofted to the upper troposphere, only relatively minor oxidative losses of CO and  $\text{C}_2\text{H}_6$  occur due to the rapid horizontal transport of the emitted plumes.

No statistically significant long-term trend were detected from the Lauder  $\text{C}_2\text{H}_6$  or CO measurement databases. The best-fit trends ( $a_1/a_0$  of Eq. 3) for  $\text{C}_2\text{H}_6$  and CO from daily means between July 1993 and November 1997 are  $(-0.64 \pm 0.79)\%$   $\text{yr}^{-1}$  and  $(0.37 \pm 0.57)\%$   $\text{yr}^{-1}$ , 1 sigma, respectively. Recently, Matsueda et al. [1998] reported a series of upper tropospheric CO mixing ratios measured in situ during commercial aircraft flights at longitudes of  $140^\circ\text{E}$  to  $152^\circ\text{E}$  and latitudes  $30^\circ\text{N}$  to  $30^\circ\text{S}$  (Japan-Australia). A rate of CO decrease of about  $5 \text{ ppbv yr}^{-1}$  was derived from a fit to the  $5^\circ\text{S}$  to  $30^\circ\text{S}$  latitude observations during the 58 sampling flights between July 1994 and June 1996.

Ratios of the  $\text{C}_2\text{H}_6/\text{CO}$  0.37-12 km daily averages are presented in the bottom panel of Figure 10 for the 332 Lauder observation days in common. This plot illustrates that larger relative seasonal changes are observed for  $\text{C}_2\text{H}_6$  than for CO with the seasonal variation of the  $\text{C}_2\text{H}_6/\text{CO}$  0.37-12 km partial columns ratios roughly in phase with the seasonal variations of both gases. The Lauder peak  $\text{C}_2\text{H}_6/\text{CO}$  columns ratio is close to the value of  $6.0 \times 10^{-3}$  measured directly over ( $\leq 1 \text{ km}$ ) active savanna fires in Brazil and Zambia during the same season (September-October 1992 observations), but our peak value is significantly lower

than the enhanced, upper tropospheric ratio of  $12.1 \times 10^{-3}$  determined in the upper troposphere over the south Atlantic basin during the same time period [Talbot et al., 1996].

Time series of  $C_2H_6$  and CO surface measurements of clean marine air at Baring Head, New Zealand ( $41.2^\circ S$ ,  $174.5^\circ E$ ) have been reported recently [Clarkson et al., 1997; Manning et al., 1997]. The Baring Head facility is a remote station located on the edge of an 80-m cliff overlooking Cook Strait at the southern tip of the North Island [Brenninkmeijer, 1993; Clarkson et al., 1997]. We next compare these *in situ* measurements with mean 0.37-12 km mixing ratios derived from our spectroscopic time series.

A sine curve fit to Baring Head  $C_2H_6$  monthly mean measurements collected during southerly winds (to avoid local land sources of pollution) and from measurements at Scott Base, Antarctica ( $77.5^\circ S$ ,  $166.4^\circ E$ ) between 1991 and 1996 yields a peak  $C_2H_6$  mixing ratio of about 0.4 ppbv in September and a minimum of about 0.15 ppbv in March [Clarkson et al., 1997, Fig. 3a], though this curve does not capture the relatively high measurements (0.4-0.6 ppbv) common in the Baring Head data between January and May. The January-May peaks are not seen in the Lauder spectroscopic data. The Baring Head surface  $C_2H_6$  measurements are generally lower than the Lauder 0.37-12 km column average mixing ratios, and the Baring Head measurements do not show the sharp peaks present in the September-October Lauder spectroscopic observations.

The June 1989 to June 1995 monthly average CO mixing ratios at Baring Head show median values ranging from 42 ppbv in March to 65 ppbv in October [Manning et al., 1997, Fig. 1]. The authors comment that while interannual variability was observed, no statistically significant CO trend was detected. As for  $C_2H_6$ , the Lauder CO 0.37-12 km column-averaged mixing ratio show a seasonal cycle with

maxima and minima at times close to those inferred from the Baring Head *in situ* data, but again, our spectroscopic 0.37-12 km daily mean CO mixing ratios show sharp September-October peaks not present in the monthly-averaged surface measurements from Baring Head.

Insight into differences between the Lauder and Baring Head measurements can be obtained from a climatology of CO aircraft measurements obtained over southeast Australia [Pak et al., 1996]. Although this location is quite far from New Zealand, there are no major surface sources in either region, and long range transport can be expected to bring gases originating at a similar set of distant surface sites to these sites. The aircraft CO measurements show tropospheric mixing ratios that increase with altitude throughout the year with the range of the average seasonal cycles increasing with altitude. Increases in CO occur in July and August prior to the observed mixing ratio peak [Pak et al., 1996]. The range in the average CO seasonal cycle above Cape Grim is observed to increase with altitude. The Lauder data do not show the secondary mixing ratio maximum observed in March and April above Cape Grim in CO, CH<sub>4</sub>, and N<sub>2</sub>O [Pak et al., 1996].

Tables 2 and 3 list the Lauder monthly average 0.37-12 km CO and C<sub>2</sub>H<sub>6</sub> columns calculated by averaging the 1993 to 1997 daily means. The listings give the mean characteristics of the temporal variations over this time period, but they do not capture the sharp peaks during austral spring nor do they show the distinct year-to-year differences in the partial columns.

To our knowledge, the only correlative measurements were obtained by the nadir-viewing MAPS gas correlation radiometer instrument [Reichle et al., 1990]. Measurements of CO obtained by the MAPS sensor in April and October 1994 have been analyzed to derive equivalent CO total columns above sites performing



correlative observations, including the Lauder station [Pougatchev et al., 1998]. The MAPS measurements, which have an estimated accuracy of about  $\pm 10\%$  [Pougatchev et al., 1998], correspond to total CO columns above Lauder in April and October of 1.24 and 1.62 (in  $10^{18}$  molecule  $\text{cm}^{-2}$ ), respectively. The averages of our retrieved daily mean total CO columns from observations during the April and October 1994 MAPS missions equal 0.95 and 1.30 (in  $10^{18}$  molecule  $\text{cm}^{-2}$ ), respectively. Our values average 0.78 times the corresponding MAPS values despite the similarity of our total column averaging kernel (Fig. 2) to the MAPS total column averaging kernel [Pougatchev et al., Fig. 2]. We note that our April and October 1994 total columns are 0.92 and 0.94 times those deduced from analysis of Lauder correlative solar spectral measurements of the  $^{12}\text{CO}$  (1-0) band R(3) line by Pougatchev et al. [1998], respectively. The averaging kernel for spectroscopic measurements from this strong line (based on multiplicative scaling of the CO *a priori* profile) decrease with altitude from a maximum of 1.5 at the surface to 0.8 at 8 km [Pougatchev et al., 1998, Fig. 2]. The offsets between the two independently-derived spectroscopic correlative total columns may reflect inaccuracies in the spectroscopic parameters, errors in modeling the overlapping solar CO lines (particularly for the weak lines analyzed in this study), and/or the differences in the vertical sensitivities of the measurements at the moment of the observations, as demonstrated by their averaging kernels. The cause of the larger differences between the two sets of spectroscopic total columns and the total columns inferred from the correlative MAPS measurements may reflect the strong, irregular spatial and temporal variations of atmospheric CO above Lauder (e.g. Fig. 10), and the differences in the times and locations of these measurement sets.

## 7.2 Kitt Peak C<sub>2</sub>H<sub>6</sub> and CO 2.09-14 km time series

Figure 11 illustrates the time series of Kitt Peak 2.09-14 km C<sub>2</sub>H<sub>6</sub> and CO daily average measurements between May 1977 and December 1997. The total number of valid measurement days were 95 for C<sub>2</sub>H<sub>6</sub> and 150 for CO with the number of measurements per day varying from 1 to 14 for CO and from 1 to 13 for C<sub>2</sub>H<sub>6</sub>. The results, displayed in the same format as Figure 10, show a distinct seasonal cycle for both molecules with spring maxima and autumn minima. Significant deviations from the best-fit curves were observed on several days. The trends ( $a_1/a_0$  of Eq. 3) determined from fitting the C<sub>2</sub>H<sub>6</sub> and CO daily mean 2.09-14 km columns are  $(-1.20 \pm 0.35)$  and  $(-0.27 \pm 0.17) \% \text{ yr}^{-1}$ , 1 sigma, respectively. Mean Kitt Peak 2.09-14 km C<sub>2</sub>H<sub>6</sub> and CO mixing ratios are 1.08 and 103 ppbv, respectively. Corresponding Lauder 0.37-12 km values from the 1993 to 1997 dataset are 0.32 and 57 ppbv. Hence, the mean C<sub>2</sub>H<sub>6</sub> and CO tropospheric mixing ratios are higher in the northern hemisphere dataset relative to the southern hemisphere dataset by factors of 3.4 and 1.8, respectively.

Table 4 and 5 list the monthly mean partial CO and C<sub>2</sub>H<sub>6</sub> columns for the 2.09-14 km layer. Unfortunately, the total number of measurement days is significantly fewer than obtained from Lauder. A plot of the Kitt Peak monthly averages from Table 5 shows the CO seasonal variation is asymmetrical with the amplitude of the spring maximum larger than amplitude of the autumn minimum. This conclusion is consistent with the results of Pougatchev and Rinsland [1995a], who analyzed the Kitt Peak measurements with a different retrieval method. The C<sub>2</sub>H<sub>6</sub> measurements show no clear evidence of an asymmetry in the annual cycle. Note that only a single C<sub>2</sub>H<sub>6</sub> measurement was obtained during August.

A substantial downward trend over this time period is indicated for  $C_2H_6$ , but not for CO. In contrast, Ehhalt et al. [1991] reported  $C_2H_6$  column abundances deduced from the analysis of infrared solar spectra recorded at the the International Scientific Station of the Jungfraujoch (ISSJ, 46.55°N, 7.98°E, 3580 m altitude). An exponential tropospheric  $C_2H_6$  column increase rate of  $(0.85 \pm 0.3)\% \text{ yr}^{-1}$  was deduced by comparing 1984-1988 measurements with low spectral resolution measurements from March and April 1951. More recent (1985 to 1995) measurements of  $C_2H_6$  total columns above the ISSJ indicate a mean exponential trend equal to  $(-3.6 \pm 0.4)\% \text{ yr}^{-1}$ , 1 sigma, which reduces to a trend of  $(-2.7 \pm 0.3)\% \text{ yr}^{-1}$ , 1 sigma, when fitting the observations with a model that includes a sine function to account for the seasonal variations [Mahieu et al., 1997].

Wallace and Livingston [1990] derived CO total columns above Kitt Peak by fitting two lines of the (2-0) band in solar spectra recorded between 1979 and 1985. A seasonal cycle with a spring maximum and autumn minimum was observed with no obvious long-term trend. No long-term CO trend was assumed in the analysis of Kitt Peak CO observations reported by Pougatchev and Rinsland [1995]. Although an average CO total column increase rate of about  $1\% \text{ yr}^{-1}$  has been reported from infrared solar spectroscopic measurements above central Europe from 1950-1951 to 1985-1987 [Zander et al., 1989] and above Zvenigorod, Russia, for 1970-1995 [Yurganov et al., 1997], surface measurements at remote sites in both hemispheres show a shift from an upward CO trend during the 1980s to a downward trend in the 1990s [Khalil and Rasmussen, 1994]. The mean trend deduced from the Kitt Peak 1977-1997 CO measurements is consistent with the northern hemisphere 1987-1992 average linear trend of  $(-1.4 \pm 0.9)\% \text{ yr}^{-1}$  reported from surface *in situ* measurements [Khalil and Rasmussen, 1994, Table 1]. More recent

surface measurements from a global network of surface stations show an average northern hemisphere CO surface trend of about  $-0.5 \text{ ppbv yr}^{-1}$  between 1994 and April 1997 (M. A. K. Khalil, private communication, 1998). Fits derived from April 1993 to March 1996 upper tropospheric CO aircraft measurements obtained between Japan and Australia show a downward trend of about  $2 \text{ ppbv yr}^{-1}$  at northern hemisphere latitudes [Matsuda et al., 1998].

The features observed in the northern hemisphere CO surface and upper tropospheric measurements, in particular the trend reversal since the late 1980s, have been noticed in the CO total columns monitored above the ISSJ between 1984 and 1995, i.e. a mean exponential rate of change of  $(-0.54 \pm 0.25)\% \text{ yr}^{-1}$ , 1 sigma; the negative rate is maintained but reduced to  $(-0.18 \pm 0.16)\% \text{ yr}^{-1}$  when fitting the observations with a function combining a sinusoidal and an exponential component [Mahieu et al., 1997]. It should be noted that the CO column minima, which occur above the ISSJ around mid-September, were record low in 1992 and 1993, i.e., during two years following the Mt. Pinatubo volcanic eruption of June 1991.

### 7.3 Correlations between CO and $\text{C}_2\text{H}_6$

The number of Lauder observations is sufficient to examine the correlation between CO with  $\text{C}_2\text{H}_6$  as a function of season. Table 7 presents correlation coefficients and slopes derived by fitting the Lauder 1993-1997 CO and  $\text{C}_2\text{H}_6$  daily mean 0.37-12 km partial column observations to the expression

$$[\text{C}_2\text{H}_6] = a + b [\text{CO}] \quad (4)$$

where  $[]$  denotes the daily-average value.

As expected from the bottom panel of Fig. 10, the minimum value of  $b$  is measured early in the calendar year. This time period shows the lowest correlation between the partial columns of the two species. Table 7 also reports corresponding values derived by fitting all the Kitt Peak 2.09-14 km measurements with Eq. 4. The correlation coefficient of 0.77 is only slightly less than the peak seasonal value derived for Lauder while  $b$  is several times higher than the corresponding value for Lauder.

Slopes derived from fits to Eq. 3 with model calculated columns computed for the locations of Lauder and Kitt Peak (Y. Wang, private communication, 1998) are also shown. The model slopes are lower than the observed values from both sites. Model  $C_2H_6$ -CO correlation coefficients (not shown) derived from the model columns are  $>0.9$ , significantly higher than indicated by the observations.

#### 7.4 Comparisons of the observations with model calculations

Figure 12 presents comparisons of the Lauder and Kitt Peak monthly mean tropospheric measurements with values calculated with a global 3-D tropospheric model [Wang et al., 1998a]. The standard model calculations, which assumed  $2.5 \text{ Tg C}^{-1} \text{ yr}^{-1} C_2H_6$  emitted by biomass burning, are significantly lower than the monthly average Lauder partial columns observed during all seasons. Also, the September-October peak is broader in the model results than in the observations. These differences are consistent with comparisons of the reported Lauder December 1992-March 1994  $C_2H_6$  columns [Rinsland et al., 1994a] and the model results, as displayed in Fig. 15 of Wang et al. [1998b]. The authors comment that the agreement between the measured and calculated Lauder  $C_2H_6$  seasonal cycle is improved with the biomass burning emission rate increased to  $6 \text{ Tg C}^{-1} \text{ yr}^{-1}$ . However, this emissions rate is also higher than the value of  $2.7 \text{ Tg C}^{-1} \text{ yr}^{-1}$ .

derived for the southern hemisphere by Clarkson et al. [1997], and it is outside their estimated budget uncertainty ( $1.6\text{--}5.2\text{ Tg yr}^{-1}$ ). As pointed out by Wang et al. [1998b], the cause of the  $\text{C}_2\text{H}_6$  model-measurement discrepancy is unclear because the model calculations reproduce observations of the southern hemisphere CO seasonal cycle very well (including the present data) and the  $\text{C}_2\text{H}_6/\text{CO}$  biomass burning emissions ratio is well determined from field emission measurements.

In contrast, calculations with the model of Wang et al. [1998a] are significantly higher than the Kitt Peak CO tropospheric column observations throughout the year, but the model reproduces the  $\text{C}_2\text{H}_6$  measurements and their seasonal variation quite well during all seasons. The cause of the Kitt Peak CO model-measurement discrepancy is also unclear, but it is quite likely that the difference is unrelated to the discrepancy noted for Lauder.

## 8. Summary

In this paper we have reported multi-year time series of high spectral resolution infrared solar absorption CO and  $\text{C}_2\text{H}_6$  measurements from remote sites at midlatitudes of the northern and southern hemispheres. Target lines were selected to achieve similar vertical sensitivities based on averaging kernels. The Lauder 1993-1997 CO and  $\text{C}_2\text{H}_6$  columns below 12 km (with peak sensitivities in the upper troposphere) show highly asymmetrical seasonal cycles with a minimum in about February, a maximum near September-October, and distinct year-to-year differences in the seasonal variation. Sharp peaks are observed in the partial columns of both gases near the seasonal maximum. The seasonal variation is larger for  $\text{C}_2\text{H}_6$  than from CO, which is also produced *in situ* by the oxidation of  $\text{CH}_4$ . The elevated values observed in austral spring likely result from the long range transport of tropical biomass burning emissions, principally from Africa

and South America. Near the seasonal maximum, the peak column-average tropospheric mixing ratios of  $C_2H_6$  and CO above Lauder are similar to upper tropospheric values observed in continental outflow regions between Brazil and Africa during the same season. The peak Lauder partial columns are also similar to the annual mean values observed above Kitt Peak. Although year-to-year differences are apparent, no significant trend was detected for either molecule above Lauder. The Kitt Peak 2.09-14 km partial columns also show distinct seasonal cycles with spring peaks in the mixing ratios of the two gases and larger relative seasonal variations for  $C_2H_6$  than CO. An unexpected result of this study is the observed, statistically significant downward trend in the Kitt Peak  $C_2H_6$  tropospheric column. No significant long-term trend in the tropospheric CO column was detected over the 20 year span of the Kitt Peak spectroscopic observations.

**Acknowledgments.** Special thanks to B. M. McNamara of NIWA, Claude Plymate, Jeremy Wagner, and Michael Dulick of the National Solar Observatory (NSO) for recording the high-resolution infrared solar spectra. The NSO is operated by the Association of Universities for Research in Astronomy, Inc. (AURA) under a cooperative agreement with the National Science Foundation (NSF). The McMath FTS solar observations were partially supported by the U. S. Department of Energy CO<sub>2</sub> program, NASA, the Chemical Manufacturers Association, and NSF. Research at the NIWA has been funded by the New Zealand Foundation for Research, Science, and Technology (Contract number CO 1221). Research at NASA Langley has been funded by NASA's Upper Atmosphere Research Program. Research at Christopher Newport University is funded by a grant from NASA. The carbon monoxide aircraft data obtained by the the CSIRO Division of Atmospheric Research GASLAB (version

1-release date 11 March 1997) were obtained by Paul Steele, Ray Langenfelds, and coworkers of the CSIRO Division of Atmospheric Research, and we gratefully acknowledge their use in this investigation. Research at the University of Denver is supported by NASA and NSF. Research at the University of Liège was partially supported by Belgian funds through the Office of Scientific, Technical, and Cultural Affairs, Brussels. We thank Linda Chiou of Science Applications International Corporation for her help with the analysis of the Kitt Peak solar spectra and the preparation of the figures. We are especially grateful to Yuhang Wang of Georgia Tech for sending the Harvard model calculations. Jack Fishman of NASA Langley also provided helpful comments during the development of this manuscript.



### References

- Bell, R. J., *Introductory Fourier Transform Spectroscopy*, Academic Press, New York, 382 pp., 1972.
- Benner, D. C., C. P. Rinsland, V. Malathy Devi, M. A. H. Smith, and D. Adkins, A multispectrum nonlinear least squares fitting procedure, *J. Quant. Spectrosc. Radiat. Transfer*, **53**, 705-721, 1995.
- Blake, D. R., and F. S. Rowland, Global atmospheric concentrations and source strength of ethane, *Nature*, **321**, 231-233, 1986.
- Blake, N. J., Blake, D. R., J. E. Collins, Jr., G. W. Sachse, B. E. Anderson, J. A. Brass, P. J. Riggan, and F. S. Rowland, Biomass burning emissions of atmospheric methyl halide and hydrocarbon gases in the south atlantic region, in *Biomass Burning and Global Change, Vol. 2, Biomass Burning in South America, Southeast Asia, and Temperate and Boreal Ecosystems, and the Oil Fires of Kuwait*, edited by J. S. Levine, pp. 576-594, MIT Press, Cambridge, 1997.
- Brault, J. W., Solar Fourier transform spectroscopy, in *Proceedings of the JOSO Workshop, Future Solar Optical Observations, Needs and Constraints*, Firenze, Italy, edited by G. Godoli, G. Noci, and A. Righin, pp. 33-52, 1978.
- Brenninkmeijer, C. A. M., Measurement of the abundance of  $^{14}\text{CO}$  in the atmosphere and the  $^{13}\text{C}/^{12}\text{C}$  and  $^{18}\text{O}/^{16}\text{O}$  ratio of atmospheric CO with applications in New Zealand and Antarctica, *J. Geophys. Res.*, **98**, 10,595-10,614, 1993.
- Brown, L. R., and L. S. Rothman, Methane line parameters for the 2.3- $\mu\text{m}$  region, *Appl. Opt.*, **21**, 2425-2427, 1982.

- Chatfield, R. B., J. A. Vastano, H. B. Singh, and G. Sachse, A general model of how fire emissions and chemistry produce african/oceanic plumes ( $O_3$ , CO, PAN, smoke) in TRACE A, *J. Geophys. Res.*, 101, 24,279-24,306, 1996.
- Coffey, M. T., W. G. Mankin, A. Goldman, C. P. Rinsland, G. A. Harvey, V. Malathy Devi, and G. M. Stokes, Infrared measurements of atmospheric ethane ( $C_2H_6$ ) from aircraft and ground-based solar absorption spectra in the  $3000\text{-cm}^{-1}$  region, *Geophys. Res. Lett.*, 12, 199-202, 1985.
- Clarkson, T. S., R. J. Martin, and J. Rudolph, Ethane and propane in the southern marine troposphere, *Atmos. Environ.*, 31, 3763-3771, 1997.
- Connor, B. J., A. Parrish, J.-J. Tsou, and M. P. McCormick, Error analysis for the ground-based microwave ozone measurements during STOIC, *J. Geophys. Res.*, 100, 9283-9291, 1995.
- Connor, B. J., N. B. Jones, S. W. Wood, J. G. Keys, C. P. Rinsland, and F. J. Murcray, Retrieval of HCl and  $HNO_3$  profiles from ground-based FTIR data using SFIT2. *Proc. XVIII Quadrennial  $O_3$  Symposium*, Univ. L'Aquila, Italy, 1996.
- Conny, J. M., and L. A. Currie, The isotopic characterization of methane, non-methane hydrocarbons and formaldehyde in the troposphere, *Atmos. Environ.*, 30, 621-638, 1996.
- Crutzen, P. J., and L. T. Gidel, A two-dimensional photochemical model of the atmosphere, 2, The tropospheric budgets of the anthropogenic chlorocarbons, CO,  $CH_4$ ,  $CH_3Cl$  and the effects of various  $NO_x$  sources on tropospheric ozone, *J. Geophys. Res.*, 88, 6641-6661, 1983.
- Dang-Nhu, M., A. S. Pine, and W. T. Lafferty, Les intensités dans les bandes  $\nu_5$ ,  $\nu_7$  et  $\nu_8 + \nu_{11}$  de l'éthane, *Can. J. Phys.*, 62, 512-519, 1984.

- Dianov-Klokov, V. I., and L. N. Yurganov, Spectroscopic measurements of atmospheric carbon monoxide and methane. 2: Seasonal variations and long-term trends, *J. Atmos. Chem.*, **8**, 153-164, 1989.
- Dickerson, R. R., G. J. Huffman, W. T. Luke, L. J. Nunnermacker, K. E. Pickering, A. C. D. Leslie, C. G. Lindsey, W. G. Slinn, T. J. Kelly, P. H. Daum, A. C. Delany, J. P. Greenberg, P. R. Zimmerman, J. F. Boatman, J. D. Ray, and D. E. Stedman, Thunderstorms: An important mechanism in the transport of air pollutants, *Science*, **235**, 460-465, 1987.
- Drayson, S. R., Rapid computation of the Voigt function, *J. Quant. Spectrosc. Radiat. Transfer*, **16**, 611-614, 1976.
- Duncan, J. L., R. A. Kelly, G. D. Nivellini, and F. Tullini, The empirical general harmonic force field of ethane, *J. Mol. Spectrosc.*, **98**, 87-110, 1983.
- Ehhalt, D. H., J. Rudolph, and U. Schmidt, On the importance of light hydrocarbons in multiphase atmospheric systems, in *Chemistry of Multiphase Atmospheric Systems*, NATO ASI Series G: Ecological Sciences, Vol. 6, edited by W. Jaeschke, pp. 321-350, Springer-Verlag, New York, 1986.
- Ehhalt, D. H., U. Schmidt, R. Zander, P. Demoulin, and C. P. Rinsland, Seasonal cycle and secular trend of the total and tropospheric column abundance of ethane above the Jungfraujoch, *J. Geophys. Res.*, **96**, 4985-4994, 1991.
- Fishman, J., K. Fakhruzzaman, B. Cros, and D. Nganga, Identification of widespread pollution in the southern hemisphere deduced from satellite analyses, *Science*, **252**, 1693-1696, 1991.
- Fuelberg, H. E., R. E. Newell, S. P. Longmore, Y. Zhu, D. J. Westberg, and E. V. Browell, A meteorological overview of the PEM-Tropics period, *J. Geophys. Res.*, in press, 1998.

- Gallery, W. O., F. X. Kneizys, and S. A. Clough, Air mass computer program for atmospheric transmittance/radiance calculation: FSCATM, *Environ. Res. Pap.* 828 (AFGL-TR-83-0065), 145 pp., Air Force Geophysics Lab., Bedford, Mass., 1983.
- Geller, L. S., J. W. Elkins, J. M. Lobert, A. D. Clarke, D. F. Hurst, J. H. Butler, and R. C. Myers, Tropospheric SF<sub>6</sub>: Observed latitudinal distribution and trends derived emissions and interhemispheric exchange time, *Geophys. Res. Lett.*, 24, 675-678, 1997.
- Goldman, A., C. P. Rinsland, F. J. Murcray, D. G. Murcray, M. T. Coffey, and W. G. Mankin, Balloon-borne and aircraft infrared measurements of ethane (C<sub>2</sub>H<sub>6</sub>) in the upper troposphere and lower stratosphere, *J. Atmos. Chem.*, 2, 211-221, 1984.
- Goldman, A., F. J. Murcray, F. H. Murcray, D. G. Murcray, and C. P. Rinsland, Measurements of several atmospheric gases above the south pole in December 1986 from high-resolution 3- to 4- $\mu$ m solar spectra, *J. Geophys. Res.*, 93, 7069-7074, 1988.
- Guelachvili, G., Distortions in Fourier spectra and diagnosis, in *Spectrometric Techniques, Vol. II*, pp. 1-62, Academic, New York, 1981.
- Gunson, M. R., C. B. Farmer, R. H. Norton, R. Zander, C. P. Rinsland, J. H. Shaw, and B.-C. Gao, Measurements of CH<sub>4</sub>, N<sub>2</sub>O, CO, H<sub>2</sub>O and O<sub>3</sub> in the middle atmosphere by the atmospheric trace molecule spectroscopy experiment on spacelab 3, *J. Geophys. Res.*, 95, 13,867-13,882, 1990.
- Gunson, M. R., M. M. Abbas, M. C. Abrams, M. Allen, L. R. Brown, T. L. Brown, A. Y. Chang, A. Goldman, F. W. Irion, L. L. Lowes, E. Mahieu, G. L. Manney, H. A. Michelsen, M. J. Newchurch, C. P. Rinsland, R. J. Salawitch, G. P. Stiller, G. C. Toon, Y. L. Yung, and R. Zander, The Atmospheric Trace

- Molecule Spectroscopy (ATMOS) experiment: Deployment on the ATLAS space shuttle missions, *Geophys. Res. Lett.*, **23**, 2333-2336, 1996.
- Hao, W. M., and M.-H. Liu, Spatial and temporal distribution of tropical biomass burning, *Global Biochem. Cycles*, **8**, 495-503, 1994.
- Heintzenberg, J., and E. K. Bigg, Tropospheric transport of trace substances in the southern hemisphere, *Tellus*, **42B**, 355-363, 1990.
- Hough, A., Development of a two-dimensional global tropospheric model: Model chemistry, *J. Geophys. Res.*, **96**, 7325-7362, 1991.
- Houghton, R. A., Biomass burning from the perspective of the global carbon cycle, in *Global Biomass Burning Atmospheric, Climatic and Biospheric Implications*, edited by J. S. Levine, pp. 321-325, MIT Press, Cambridge, 1991.
- Kanakidou, M., H. B. Singh, K. M. Valentin, and P. J. Crutzen, A two-dimensional study of ethane and propane oxidation in the troposphere, *J. Geophys. Res.* **96**, 15,395-15,413, 1991.
- Khalil, M. A. K., and R. A. Rasmussen, The global cycle of carbon monoxide: Trends and mass balance, *Chemosphere*, **20**, 227-242, 1990.
- Khalil, M. A. K., and R. A. Rasmussen, Global decrease in atmospheric carbon monoxide concentrations, *Nature*, **370**, 639-641, 1994.
- Kilston, S., N-type carbon stars and the 3- $\alpha$  process, *Pub. Astron. Soc. Pacific*, **87**, 189-206, 1975.
- Kim, J. H., and M. J. Newchurch, Climatology and trends of tropospheric ozone over the eastern Pacific ocean, *Geophys. Res. Lett.*, **23**, 3723-3726, 1996.
- Kim, J. H., and M. J. Newchurch, Biomass-burning influence on tropospheric ozone over New Guinea and South America, *J. Geophys. Res.*, **103**, 1455-1461, 1998.

- Kurylo, M. J., Network for the detection of stratospheric change, *Proc. Soc. Photo. Opt. Instrum. Eng.*, 1491, 169-174, 1991.
- Langenfelds, R. L., R. J. Francey, L. P. Steele, P. J. Fraser, S. A. Coram, M. R. Hayes, D. J. Beardsmore, M. P. Lucarelli, and F. R. de Silva, Improved vertical sampling of the trace gas composition of the troposphere above Cape Grim since 1991, in *Baseline Atmospheric Program (Australia) 1993*, edited by R. J. Francey, A. L. Dick, and N. Derek, pp. 45-56, Bureau of Meteorology and CSIRO Division of Atmospheric Research, Melbourne, Australia, 1996.
- Law, K. S., and J. A. Pyle, Modeling trace gas budgets in the troposphere 2. CH<sub>4</sub> and CO, *J. Geophys. Res.*, **98**, 18,401-18,412, 1993.
- Levy, H. II, Normal atmosphere: Large radical and formaldehyde concentrations predicted, *Science*, **173**, 141-143, 1971.
- Logan, J. A., M. J. Prather, S. C. Wofsy, and M. B. McElroy, Tropospheric chemistry: A global perspective, *J. Geophys. Res.*, **86**, 7210-7254, 1981.
- Mahieu, E., R. Zander, L. Delbouille, P. Demoulin, G. Roland and C. Servais, Observed trends in total vertical column abundances of atmospheric gases from IR solar spectra recorded at the Jungfraujoch, *J. Atmos. Chem.*, **28**, 227-243, 1997.
- Maiss, M., L. P. Steele, R. J. Francey, P. J. Fraser, R. L. Langenfelds, N. B. A. Trivett, and I. Levin, Sulfur hexafluoride-A powerful new atmospheric tracer, *Atmos. Environ.*, **30**, 1621-1629, 1996.
- Malathy Devi, V., D. C. Benner, M. A. H. Smith, and C. P. Rinsland, Measurements of air-broadening and pressure-shifting of methane lines in the 2.3- $\mu$ m region, *J. Mol. Spectrosc.*, **157**, 95-111, 1993.

- Manning, M. R., C. A. M. Brenninkmeijer, and W. Allan, Atmospheric carbon monoxide budget in the southern hemisphere: Implications of  $^{13}\text{C}/^{12}\text{C}$  measurements, *J. Geophys. Res.*, **102**, 10,673-10,682, 1997.
- Matsueda, H., H. Y. Inoue, Y. Sawa, Y. Tsutsumi, and M. Ishii, Carbon monoxide in the upper troposphere over the western Pacific between 1993 and 1996, *J. Geophys. Res.*, in press, 1998.
- McKeen, S. A., S. C. Liu, E.-Y. Hsie, X. Lin, J. D. Bradshaw, S. Smyth, G. L. Gregory, and D. R. Blake, Hydrocarbon ratios during PEM-WEST A: A model perspective, *J. Geophys. Res.*, **101**, 2087-2109, 1996.
- McKenna, D. S., C. J. Hord, and J. M. Kent, Hydroxyl radical concentrations and Kuwait oil fire emission rates for March 1991, *J. Geophys. Res.*, **100**, 26,005-26,025, 1995.
- Moazzen-Ahmadi, N., H. P. Gush, M. Halpern, H. Jagannath, A. Leung, and I. Ozier, The torsional spectrum of  $\text{CH}_3\text{CH}_3$ , *J. Chem. Phys.*, **88**, 563-577, 1988.
- Moazzen-Ahmadi, N., A. R. W. McKellar, J. W. C. Johns, and I. Ozier, Intensity analysis of the torsional spectrum of  $\text{CH}_3\text{CH}_3$ , *J. Chem. Phys.*, **97**, 3981-3988 1992.
- Murcray, F. J., A. Matthews, A. Goldman, P. Johnston, and C. P. Rinsland,  $\text{NH}_3$  column abundances over Lauder, New Zealand, *J. Geophys. Res.*, **94**, 2235-2238, 1989.
- Norton, R. H., and C. P. Rinsland, ATMOS data processing and science analysis methods, *Appl. Opt.*, **30**, 389-400, 1991.
- Notholt, J., G. C. Toon, R. Lehmann, B. Sen, and J.-F. Blavier, Comparison of Arctic and Antarctic trace gas column abundances from ground-based FTIR spectrometry, *J. Geophys. Res.*, **102**, 12,863-12,869, 1997a.

- Notholt, J., G. C. Toon, F. Stordal, S. Solberg, N. Schmidbauer, E. Becker, A. Meier, and B. Sen, Seasonal variations of atmospheric trace gases in the high Arctic at 79°N, *J. Geophys. Res.*, **102**, 12,855-12,861, 1997b.
- Novelli, P. C., J. W. Elkins, and L. P. Steele, The development and evaluation of a gravimetric reference scale for measurements of atmospheric carbon monoxide, *J. Geophys. Res.*, **96**, 13,109-13,121, 1991.
- Novelli, P. C., L. P. Steele, and P. P. Tans, Mixing ratios of carbon monoxide in the troposphere, *J. Geophys. Res.*, **97**, 20,731-20,750, 1992.
- Novelli, P. C., V. S. Connors, H. G. Reichle, Jr., B. E. Anderson, C. A. M. Brenninkmeijer, E. G. Brunke, B. G. Doddridge, V. W. J. H. Kirchhoff, K. S. Lam, K. A. Masarie, T. Matsuo, D. D. Parrish, H. E. Scheel, and L. P. Steele, An internally consistent set of globally distributed atmospheric carbon monoxide mixing ratios developed using results from an intercomparison of measurements, *J. Geophys. Res.*, in press, 1998.
- Pak, B. C., R. L. Langenfelds, R. J. Francey, L. P. Steele, and I. Simmonds, A climatology of trace gases from the Cape Grim overflights, 1992-1995, in *Baseline Atmospheric Program (Australia) 1994-5*, edited by R. J. Francey, A. L. Dik, and N. Derek, pp. 41-52, Bureau of Meteorology and CSIRO Division of Atmospheric Research, Melbourne, Australia, 1996.
- Park, J. H., Analysis method for Fourier transform spectroscopy, *Appl. Opt.* **22**, 835-849, 1983.
- Parrish, A., B. J. Connor, J. J. Tsou, I. S. McDermid, and W. P. Chu, Ground-based microwave monitoring of stratospheric ozone, *J. Geophys. Res.*, **97**, 2541-2546, 1992.
- Pickering, K. E., A. M. Thompson, Y. Wang, W.-K. Tao, D. P. McNamara, V. W. H. Kirchhoff, B. G. Heikes, G. W. Sachse, J. D. Bradshaw, G. L. Gregory, and



- D. R. Blake, Convective transport of biomass burning emissions over Brazil during TRACE A, *J. Geophys. Res.*, 101, 23,993-24,012, 1996.
- Pine, A. S., and W. J. Lafferty, Torsional splittings and assignments of the Doppler-limited spectrum of ethane in the C-H stretching region, *J. Res. Nat. Bur. Stand.*, 87, 237-256, 1982.
- Pine, A. S., and S. C. Stone, Torsional tunneling and  $A_1$ - $A_2$  splittings and air broadening of the  $^2Q_0$  and  $^2Q_3$  subbranches of the  $\nu_7$  band of ethane, *J. Mol. Spectrosc.*, 175, 21-30, 1996.
- Pougatchev, N. S., and C. P. Rinsland, Spectroscopic study of the seasonal variation of carbon monoxide distribution above Kitt Peak, *J. Geophys. Res.*, 100, 1409-1416, 1995a.
- Pougatchev, N. S., B. J. Connor, and C. P. Rinsland, Infrared measurements of the ozone vertical distribution above Kitt Peak, *J. Geophys. Res.*, 100, 16,689-16,697, 1995b.
- Pougatchev, N. S., B. J. Connor, N. B. Jones, and C. P. Rinsland, Validation of ozone profile retrievals from infrared ground-based solar spectra, *Geophys. Res. Lett.*, 23, 1637-1640, 1996.
- Pougatchev, N. S., N. B. Jones, B. J. Connor, C. P. Rinsland, E. Becker, M. T. Coffey, V. S. Connors, Ph. Demoulin, A. V. Dzhola, H. Fast, E. I. Grechko, J. W. Hannigan, M. Koike, Y. Kondo, E. Mahieu, W. G. Mankin, R. L. Mittermeier, J. Notholt, H. G. Reichle, Jr., B. Sen, L. P. Steele, G. C. Toon, L. N. Yurganov, R. Zander, and Y. Zhao, Ground-based infrared solar spectroscopic measurements of carbon monoxide during the 1994 MAPS flights, *J. Geophys. Res.*, in press, 1998.
- Reichle, H. G., Jr., V. S. Connors, J. A. Holland, W. D. Hypes, H. A. Wallio, J. C. Casas, B. B. Gormsen, M. S. Saylor, and W. D. Hesketh, Middle and

- upper tropospheric carbon monoxide mixing ratios as measured by a satellite-borne remote sensor during November 1981, *J. Geophys. Res.*, **91**, 10,865-10,887, 1986.
- Reichle, H. G., Jr., V. S. Connors, J. A. Holland, R. T. Sherill, H. A. Wallio, J. C. Casas, E. P. Condon, B. B. Gormsen, and W. Seiler, The distribution of middle tropospheric carbon monoxide during early October 1984, *J. Geophys. Res.*, **95**, 9845-9856, 1990.
- Reichle, H. G., B. Anderson, V. Connors, T. Denkins, D. Forbes, B. Gormsen, D. Neil, S. Nolf, P. Novelli, N. Pougatchev, M. Roell, and P. Steele, Space shuttle based global CO measurements during April and October 1994, MAPS instrument, data reduction, and data validation, *J. Geophys. Res.*, in press, 1998.
- Rinsland, C. P., M. A. H. Smith, P. L. Rinsland, A. Goldman, J. W. Brault, and G. M. Stokes, Ground-based infrared spectroscopic measurements of atmospheric hydrogen cyanide, *J. Geophys. Res.*, **87**, 11,119-11,125, 1982a.
- Rinsland, C. P., A. Goldman, F. J. Murcray, D. G. Murcray, M. A. H. Smith, R. K. Seals, Jr., J. C. Larsen, and P. L. Rinsland, Stratospheric N<sub>2</sub>O mixing ratio profile from high-resolution balloon-borne solar absorption spectra and laboratory spectra near 1880 cm<sup>-1</sup>, *Appl. Opt.*, **21**, 4351-4355, 1982b.
- Rinsland, C. P., R. E. Boughner, J. C. Larsen, G. M. Stokes, and J. W. Brault, Diurnal variations of atmospheric nitric oxide: Ground-based infrared spectroscopic measurements and their interpretation with time-dependent photochemical model calculations, *J. Geophys. Res.*, **89**, 9613-9622, 1984.
- Rinsland, C. P., R. Zander, C. B. Farmer, R. H. Norton, and J. M. Russell III, Concentration of ethane (C<sub>2</sub>H<sub>6</sub>) in the lower stratosphere and upper troposphere and acetylene (C<sub>2</sub>H<sub>2</sub>) in the upper troposphere deduced from

- atmospheric trace molecule spectroscopy/spacelab 3 spectra, *J. Geophys. Res.*, **92**, 11,951-11,964, 1987.
- Rinsland, C. P., G. A. Harvey, V. Malathy Devi, K. B. Thakur, J. S. Levine, and M. A. H. Smith, Q branches of the  $\nu_7$  fundamental of ethane ( $C_2H_6$ ): Integrated intensity measurements for atmospheric measurement applications, *Appl. Opt.*, **25**, 2872-2873, 1986.
- Rinsland, C. P., R. Zander, C. B. Farmer, R. H. Norton, and J. M. Russell III, Concentrations of ethane ( $C_2H_6$ ) in the lower stratosphere and upper troposphere and acetylene ( $C_2H_2$ ) in the upper troposphere deduced from atmospheric trace molecule spectroscopy/spacelab 3 spectra, *J. Geophys. Res.*, **92**, 11,951-11964, 1987.
- Rinsland, C. P., N. B. Jones, and W. A. Matthews, Infrared spectroscopic measurements of the total column abundance of ethane ( $C_2H_6$ ) above Lauder, New Zealand, *J. Geophys. Res.*, **99**, 25,941-24,945, 1994a.
- Rinsland, C. P., A. Goldman, F. J. Murcray, S. David, R. D. Blatherwick, and D. G. Murcray, Infrared spectroscopic measurements of the ethane ( $C_2H_6$ ) total column above Mauna Loa, Hawaii, seasonal variations, *J. Quant. Spectrosc. Radiat. Transfer*, **52**, 273-279, 1994b.
- Rinsland, C. P., B. J. Connor, N. B. Jones, I. Boyd, W. Andrew Matthews, A. Goldman, F. J. Murcray, D. G. Murcray, S. J. David, and N. S. Pougatchev, Comparison of infrared and Dobson total ozone columns measured from Lauder, New Zealand, *Geophys. Res. Lett.*, **23**, 1025-1028, 1996.
- Rinsland, C. P., M. R. Gunson, P. Wang, R. F. Arduini, B. A. Baum, P. Minnis, A. Goldman, M. C. Abrams, R. Zander, E. Mahieu, R. J. Salawitch, H. A. Michelsen, F. W. Irion, and M. J. Newchurch, ATMOS/ATLAS 3 infrared profile

- measurements of trace gases in the tropical and subtropical upper troposphere, *J. Quant. Spectrosc. Radiat. Transfer*, accepted, 1998.
- Rodgers, C. D., Retrieval of atmospheric temperature and composition from remote measurements of thermal radiation, *Rev. Geophys. Space Phys.*, **14**, 609-624, 1976.
- Rodgers, C. D., Characterization and error analysis of profiles retrieved from remote sounding measurements, *J. Geophys. Res.*, **95**, 5587-5595, 1990.
- Rothman, L. S., C. P. Rinsland, A. Goldman, S. T. Massie, D. P. Edwards, J.-M. Flaud, A. Perrin, C. Camy-Peyret, V. Dana, J.-Y. Mandin, J. Schroeder, A. McCann, R. R. Gamache, R. B. Wattson, K. Yoshino, K. V. Chance, K. W. Jucks, L. R. Brown, V. Nemtchinov, and P. Varanasi, The HITRAN molecular spectroscopic database and HAWKS (HITRAN atmospheric workstation): 1996 edition, *J. Quant. Spectrosc. Radiat. Transfer*, submitted, 1998.
- Rudolph, J., A. Khedim, and Wagenbach, D., The seasonal variation of light nonmethane hydrocarbons in the antarctic troposphere, *J. Geophys. Res.*, **94**, 13,039-13,044, 1989.
- Rudolph, J., and D. H. Ehhalt, Measurements of C<sub>2</sub>-C<sub>5</sub> hydrocarbons over the north Atlantic, *J. Geophys. Res.*, **86**, 11,959-11,964, 1981.
- Rudolph, J., The tropospheric budget and distribution of ethane, *J. Geophys. Res.*, **100**, 11,369-11,381, 1995.
- Singh, H. B., and L. J. Salas, Measurements of selected light hydrocarbons over the Pacific Ocean, *Geophys. Res. Lett.* **9**, 842-845, 1982.
- Singh, H. B., and P. B. Zimmerman, Atmospheric distribution and sources of nonmethane hydrocarbons, in *Gaseous Pollutants: Characterization and Cycling*, Edited by Jerome O. Nriagu (J. Wyle and Sons, pp. 177-235), 1992.

- Smith, M. A. H., Compilation of atmospheric gas concentration profiles from 0 to 50 km, NASA Tech. Memo., TM 83289, 1982. (Available as NTIS 82N22822 from the Natl. Tech. Inf. Serv., Springfield, Va.)
- Smyth, S., J. Bradshaw, S. Sandholm, S. Liu, S. McKeen, G. Gregory, B. Anderson, R. Talbot, D. Blake, S. Rowland, E. Browell, M. Fenn, J. Merrill, S. Bachmeier, G. Sachse, J. Collins, D. Thornton, D. Davis, and H. Singh, Comparison of free tropospheric western pacific air mass classification schemes for the PEM-West A experiment, *J. Geophys. Res.*, 101, 1743-1762, 1996.
- Steele, L. P., R. L. Langenfelds, M. P. Lucarelli, P. J. Fraser, L. N. Cooper, D. A. Spencer, S. Chea, and K. Broadhurst, Atmospheric methane, carbon dioxide, carbon monoxide, hydrogen and nitrous oxide from Cape Grim flask air samples analyzed by gas chromatography, *Baseline Atmospheric Program (Australia) 1994-1995*, edited by R. J. Francey, A. L. Dick, and N. Derek, pp. 107-110, Bureau of Meteorology and CSIRO Division of Atmospheric Research, Melbourne, Australia, 1996.
- Talbot, R. W., J. D. Bradshaw, S. T. Sandholm, S. Smyth, D. R. Blake, N. R. Blake, G. W. Sachse, J. E. Collins, B. D. Heikes, B. E. Anderson, G. L. Gregory, H. B. Singh, B. L. Lefer, and A. S. Bachmeier, Chemical characteristics of continental outflow over the tropical south atlantic ocean from Brazil and Africa, *J. Geophys. Res.*, 101, 24,187-24,202, 1996.
- Tans, P. P., P. S. Bakwin, T. J. Conway, R. W. Dissly, E. J. Dlugokencky, L. S. Geller, D. W. Guenther, D. F. Hurst, D. R. Kitzik, P. M. Lang, K. A. Masarie, J. B. Miller, P. C. Novelli, C. Prostko-Bell, M. Ramonet, K. W. Thoning, M. Troler, L. S. Waterman, N. Zhang, and C. Zhao, Carbon cycle, in *Climate Monitoring and Diagnostics Laboratory Summary Report No. 23*,

- 1994-1995, U. S. Department of Commerce, National Oceanic and Atmospheric Administration Environmental Research Laboratories, pp. 45-47, 1996.
- Toon, G. C., C. B. Farmer, P. W. Schaper, L. L. Lowes, and R. H. Norton, Composition measurements of the 1989 Arctic winter stratosphere by airborne infrared solar absorption spectroscopy, *J. Geophys. Res.*, **97**, 7939-7961, 1992.
- Wallace, L., and W. Livingston, Spectroscopic observations of atmospheric trace gases over Kitt Peak 2. Nitrous oxide and carbon monoxide from 1979 to 1985, *J. Geophys. Res.*, **95**, 16,383-16,390, 1990.
- Wang, Y., D. J. Jacob, J. A. Logan, and C. S. Spivakovsky, Global simulation of tropospheric  $O_3$ - $NO_x$ -hydrocarbon chemistry, 1. Model formulation, *J. Geophys. Res.*, accepted, 1998a.
- Wang, Y., J. A. Logan, and D. J. Jacob, Global simulation of tropospheric  $O_3$ - $NO_x$ -hydrocarbon chemistry, 2. Model evaluation and global ozone budget, *J. Geophys. Res.*, accepted, 1998b.
- Watson, C. E., J. Fishman, and H. G. Reichle, Jr., The significance of biomass burning as a source of carbon monoxide and ozone in the southern hemisphere tropics: A satellite analysis, *J. Geophys. Res.*, **95**, 16,443-16,450, 1990.
- Worden, H., R. Beer, and C. P. Rinsland, Airborne infrared spectroscopy of 1994 western wildfires, *J. Geophys. Res.*, **102**, 1287-1299, 1997.
- Yurganov, L. N., E. I. Grechko, and A. V. Dzhola, Variations of carbon monoxide density in the total atmospheric column over Russia between 1970 and 1995: Upward trend and disturbances, attributed to the influence of volcanic aerosols and forest fires, *Geophys. Res. Lett.*, **24**, 1231-1234, 1997.

- Zander, R., Ph. Demoulin, D. H. Ehhalt, U. Schmidt, and C. P. Rinsland, Secular increase of the total vertical column abundance of carbon monoxide above central Europe since 1950, *J. Geophys. Res.*, **94**, 11,021-11,028, 1989.
- Zander, R., Ph. Demoulin, E. Mahieu, G. P. Adrian, C. P. Rinsland, and A. Goldman, A., ESMOS II/NDSC - IR spectral fitting algorithms intercomparison exercise, *Proc. Atmospheric Spectroscopy Applications Workshop*, Reims, France, pp. 7-12, Sept. 8-10, 1993.
- Zimmerman, M. R., R. B. Chatfield, J. Fishman, P. J. Crutzen, and P. L. Hanst, Estimates of the production of CO and H<sub>2</sub> from the oxidation of hydrocarbon emissions from vegetation, *Geophys. Res. Lett.*, **5**, 679-682, 1978.

### Figure Captions

Figure 1. Comparison of "true" and retrieved CO 2.09-14 km column amounts (molecules  $\text{cm}^{-2}$ ). The "true" profiles are based on synthetic spectra generated from 82 profiles created from merged aircraft tropospheric and ATMOS measurements. The retrievals were obtained by fitting the synthetic spectra with the *a priori* profile and retrieval algorithm settings described in the text.

Figure 2. Partial column averaging kernels for vertical profile retrievals of  $\text{C}_2\text{H}_6$  (upper panel) and CO (lower panel) from Lauder observations and the spectral intervals used in the present study. Kernels for merged layers of 0.37-12, 12-100, and 0.37-100 km (total column) are presented.

Figure 3. Examples of Lauder CO partial column averaging kernels for other selections of spectral lines and retrieval methods. Upper panel: Kernels for vertical profile retrievals from the strong CO (1-0) R(3) line at  $2157.2997 \text{ cm}^{-1}$ . Lower panel: Kernels for the same CO lines as in Fig. 2, but assuming multiplicative scaling of the *a priori* mixing ratios by a single factor.

Figure 4. Comparison of measured and calculated Doppler-limited  $\text{C}_2\text{H}_6$  laboratory spectra recorded in the region of the  $\text{PQ}_3$  subbranch of the  $\nu_7$  band with a difference-frequency laser spectrometer. The spectra were recorded at 296 K with an absorption path of 69.7 cm (upper panel) and 161 K with an absorption path of 8 m (lower panel). The measured and calculated absorbances are shown with solid and dashed lines at top in each panel; calculated absorbances obtained for



A series, E series, and other lines, offset vertically for clarity, are shown beneath.

Figure 5. Comparison of a Lauder solar absorption spectrum in the  $\text{C}_2\text{H}_6$  measurement interval and simulations of the principal absorbing molecules. The molecule-by-molecule simulations are offset vertically for clarity. The Lauder solar spectrum (bottom) was recorded at an astronomical zenith angle of  $62.61^\circ$  on October 26, 1994, a spectral resolution of  $0.006\text{ cm}^{-1}$ , and a field of view of  $2.95\text{ mrad}$ . An arrow marks the location of the unresolved  $\text{C}_2\text{H}_6\text{ }^{\text{PQ}}_3$  subbranch at  $2976.8\text{ cm}^{-1}$ . Note the overlapping absorption by a weak  $\text{H}_2\text{O}$  line at  $2976.7810\text{ cm}^{-1}$ .

Figure 6. Sample fit to a Lauder solar spectrum in the  $\text{C}_2\text{H}_6\text{ }^{\text{PQ}}_3$  microwindow. The measured spectrum (lower panel), normalized to the peak amplitude in the interval, was recorded at a resolution of  $0.006\text{ cm}^{-1}$  on June 3, 1997. Residuals (measured minus calculated values) are shown on an expanded vertical scale in the upper panel.

Figure 7. Molecule-by-molecule simulations of the absorptions by  $\text{CO}$ ,  $\text{CH}_4$ ,  $\text{H}_2\text{O}$ ,  $\text{HDO}$ , and solar  $\text{CO}$ , offset vertically for clarity, and a Lauder solar spectrum in the 2 intervals used to analyze  $\text{CO}$ . The Lauder spectrum, normalized to the peak signal in each interval, was recorded at an astronomical zenith angle of  $78.05^\circ$  on October 26, 1994, at a resolution of  $0.006\text{ cm}^{-1}$ . The  $(2-0)$  band  $\text{CO}$  lines are identified beneath the measured spectrum.

Figure 8. Example of spectral fittings for the CO (2-0) band R(3) and R(6) lines in a Kitt Peak solar spectrum. The observation was recorded on April 9, 1997, at a spectral resolution of  $0.01\text{ cm}^{-1}$ . The measurements in each interval are normalized to the peak value in the interval. Measured minus calculated residuals are plotted on an expanded scale.

Figure 9. Plot of Kitt Peak root mean square (rms) residual versus signal strength ratio (ssr) for the  $\text{C}_2\text{H}_6\text{ }^{\text{P}}\text{Q}_3$  subbranch at  $2976.8\text{ cm}^{-1}$ . Observations with ssr less than 10 and an rms residual greater than 1 were excluded from further analysis.

Figure 10. Time series of Lauder 0.37-12 km daily average partial columns ( $\text{molecules cm}^{-2}$ ) between July 1993 and November 1997. Plus symbols show the observations; solid curves represent least-squares best-fits to the observations with Equation 3. The best-fit, long-term trend with the seasonal variation removed ( $a_2=0$  in Eq. 3) is shown with a dashed line. Results for  $\text{C}_2\text{H}_6$  and CO are shown in the top and middle panels, respectively, with the corresponding, approximate 0.37-12 km column average mixing ratios indicated on the right vertical axis. Daily average 0.37-12 km  $\text{C}_2\text{H}_6/\text{CO}$  columns ratios are plotted in the bottom panel.

Figure 11. Time series of Kitt Peak 2.09-14 km daily average partial columns ( $\text{molecules cm}^{-2}$ ) between May 1977 and December 1997 and the daily average 2.09-14 km  $\text{C}_2\text{H}_6/\text{CO}$  columns ratios displayed in the same format as in Fig. 10.

Figure 12. Comparison of monthly average tropospheric partial columns of  $C_2H_6$  and CO above Lauder and Kitt Peak (solid lines with open circles and error bars showing standard deviations) and calculations (dotted lines and open triangles) with the 3-dimensional tropospheric model of Wang et al. [1998a].

Table 1. Estimated CO and C<sub>2</sub>H<sub>6</sub> Partial Column Measurement Uncertainties\*

Error Source	CO Error, %	C <sub>2</sub> H <sub>6</sub> Error, %
<i>Random Errors</i>		
Temperature	1	1
Instrumental noise†		
Lauder	2	3
Kitt Peak	3	7
Interfering atmospheric lines		
Lauder	<1	7
Kitt Peak	<1	2
RSS total random error		
Lauder	4	8
Kitt Peak	3	7
<i>Systematic Errors</i>		
Spectroscopic Parameters	2	5
A priori profile	1	1
Forward model approximations‡	4	2
Instrumental line shape function†	<1	<1
RSS total systematic	5	5

\*0.37-12 km layer for Lauder; 2.09-14 km layer for Kitt Peak.

†Calculated with a maximum optical path difference of 150 cm for Lauder and 49 cm for Kitt Peak.

‡Includes the estimated uncertainty in the retrieval due to error in computing the absorption by overlapping solar CO lines.

Table 2. Mean and Standard Deviation (S.D.) of 1993-1997 CO Columns\*, 0.37-12 km, Measured above the Lauder NDSC Station

Month	Mean	S.D.	Number of Days
January	0.86	0.11	24
February	0.85	0.13	29
March	0.79	0.11	37
April	0.82	0.09	38
May	0.85	0.09	43
June	0.86	0.06	25
July	0.91	0.08	32
August	1.02	0.15	56
September	1.20	0.14	23
October	1.25	0.18	41
November	1.03	0.17	34
December	0.84	0.06	8

\* In  $10^{18}$  molecules  $\text{cm}^{-2}$ .

Table 3. Mean and Standard Deviation (S.D.) of 1993-1997 C<sub>2</sub>H<sub>6</sub> Columns\*, 0.37-12 km, Measured above the Lauder NDSC Station

Month	Mean	S.D.	Number of Days
January	3.78	0.68	19
February	4.12	0.79	21
March	3.70	0.71	33
April	4.12	0.69	36
May	4.51	0.64	43
June	5.05	0.58	37
July	5.59	0.76	41
August	6.30	1.26	63
September	7.64	1.35	30
October	7.49	1.37	45
November	5.56	1.23	29
December	4.19	0.59	13

\* In  $10^{15}$  molecules cm<sup>-2</sup>.

Table 4. Mean and Standard Deviation (S.D.) of 1977-1997 CO Columns\*, 2.09-14 km, Measured above Kitt Peak

Month	Mean	S.D.	Number of Days
January	1.44	0.10	18
February	1.44	0.08	9
March	1.85	0.35	8
April	1.71	0.14	9
May	1.50	0.15	25
June	1.31	0.12	16
July	1.18	0.08	9
August	1.07	0.21	7
September	1.07	0.08	17
October	1.32	0.17	10
November	1.28	0.05	7
December	1.32	0.11	15

\* In  $10^{18}$  molecules  $\text{cm}^{-2}$ .

Table 5. Mean and Standard Deviation (S.D.) of 1977-1997 C<sub>2</sub>H<sub>6</sub> Columns\*, 2.09-14 km, Measured above Kitt Peak

Month	Mean	S.D.	Number of Days
January	14.26	1.51	13
February	16.22	1.71	8
March	14.61	7.19	4
April	15.44	1.28	3
May	14.42	2.52	18
June	10.25	2.10	7
July	9.84	3.63	7
August	6.43	0.00	1
September	7.23	2.49	7
October	9.94	2.19	7
November	13.69	3.44	5
December	13.19	1.45	15

\* In 10<sup>15</sup> molecules cm<sup>-2</sup>.



Table 7. Correlation Coefficients and  $C_2H_6/CO$  Slopes derived from fits to daily average Lauder and Kitt Peak partial column measurements and corresponding values obtained with the Harvard model\*

Station	Months	R	b ( $10^{-3}$ )	
			Measured	Model
Lauder	Feb. -Mar. -Apr.	0.400	3.38	3.18
Lauder	May-Jun. -Jul.	0.594	5.52	3.31
Lauder	Aug. -Sep. -Oct.	0.827	6.39	4.44
Lauder	Nov. -Dec. -Jan.	0.822	6.96	5.04
Kitt Peak	All	0.766	14.2	13.2

\*0.37-12 km column for Lauder, 1993-1997. 2.09-14 km column for Kitt Peak, 1977-1997.

Mailing Addresses

Ph. Demoulin, E. Mahieu, and R. Zander, Institute of Astrophysics and Geophysics,  
University of Liège, 4000 Liège-Cointe, Belgium (email: zander@astro.ulg.ac.be)

A. Goldman, F. J. Murcray, and T. M. Stephen, Department of Physics, University  
of Denver, Denver, CO 80208 (email: goldman@acd.ucar.edu;  
fmucray@acd.ucar.edu; tstephen@du.edu)

Nicholas B. Jones and Brian J. Connor, NIWA Climate, Private Bag 50061, Omakau,  
Lauder 9182, New Zealand (e-mail: jones@kea.lauder.cri.nz;  
connor@kea.lauder.cri.nz)

J. A. Logan, Department of Earth and Planetary Sciences, Harvard University, 29  
Oxford Street, Cambridge, MA 02138 (e-mail: jal@io.harvard.edu)

A. S. Pine, Alpine Technologies, 14401 Poplar Hill Road, Germantown, MD 20874  
(alanpine@erols.com)

N. S. Pougatchev, Christopher Newport University, Newport News, VA 23606 (email:  
nikita@riscbox.larc.nasa.gov)

C. P. Rinsland, Atmospheric Sciences Division, NASA Langley Research Center,  
Mail Stop 401A, Hampton, VA 23681-2199 (e-mail: rinsland@riscbox.larc.nasa.gov)

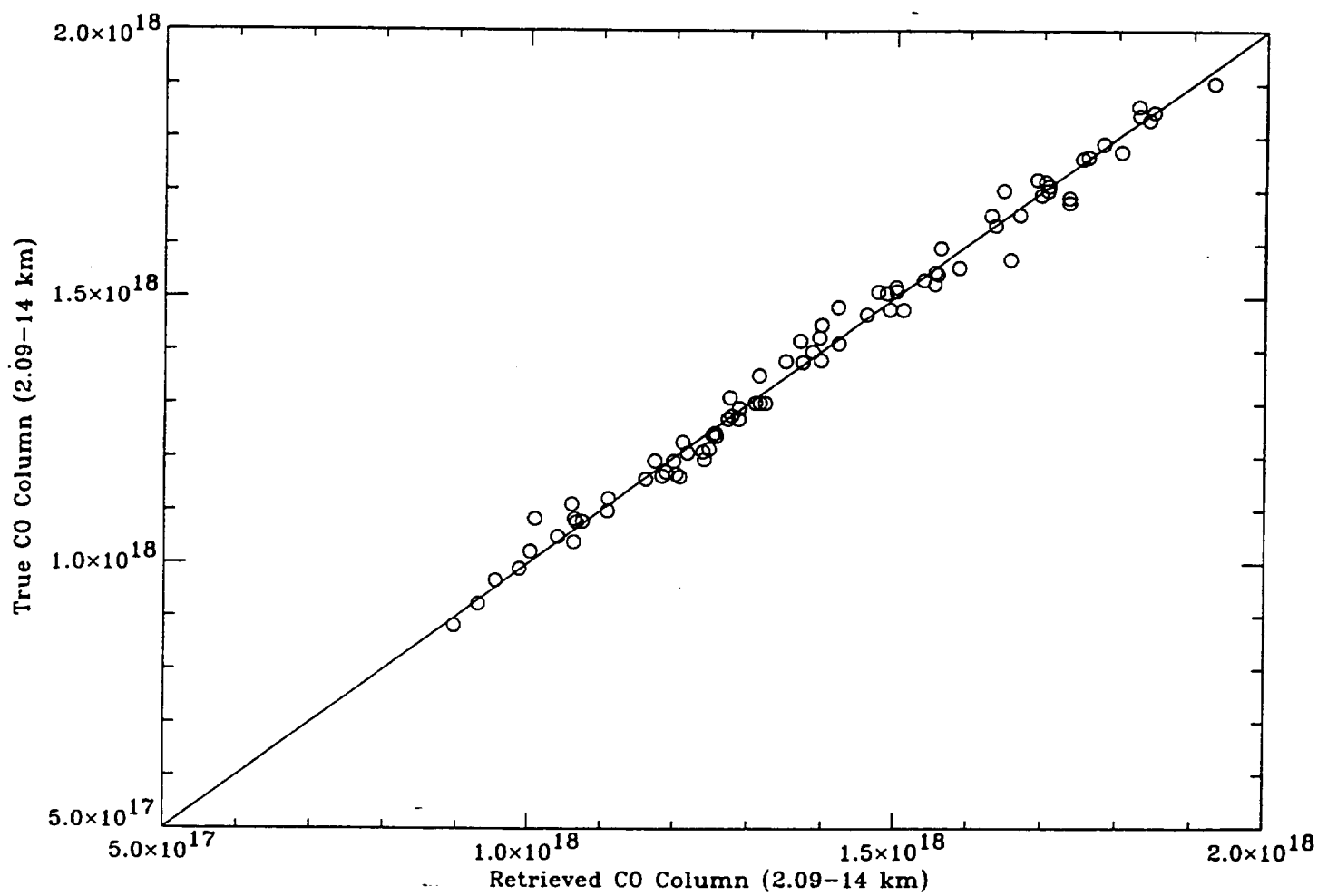
Figure 1

Figure 2

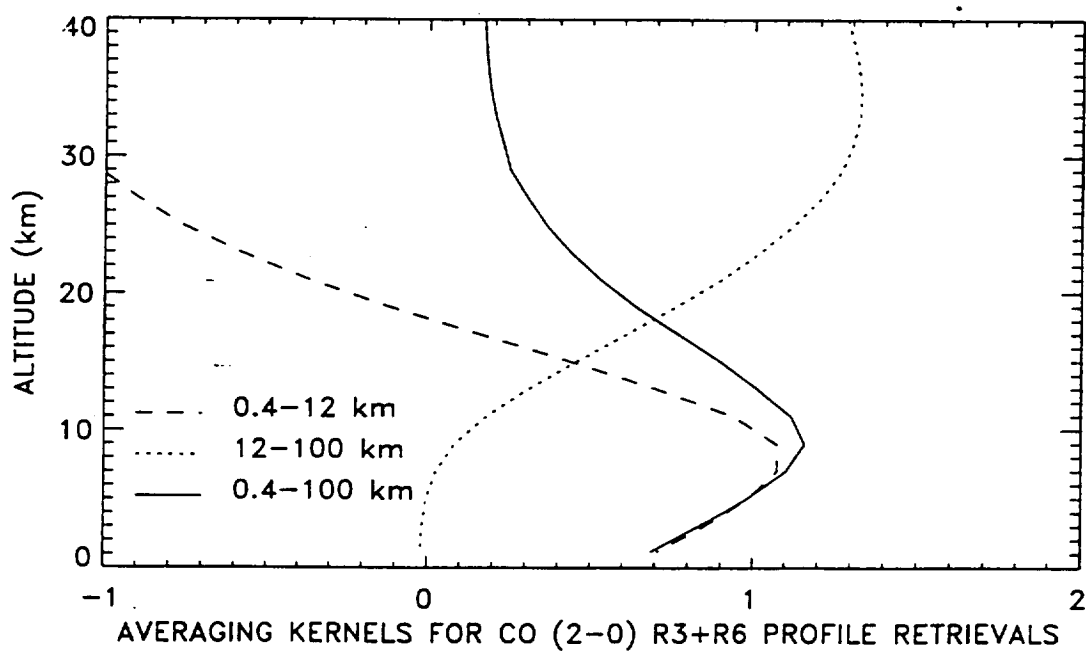
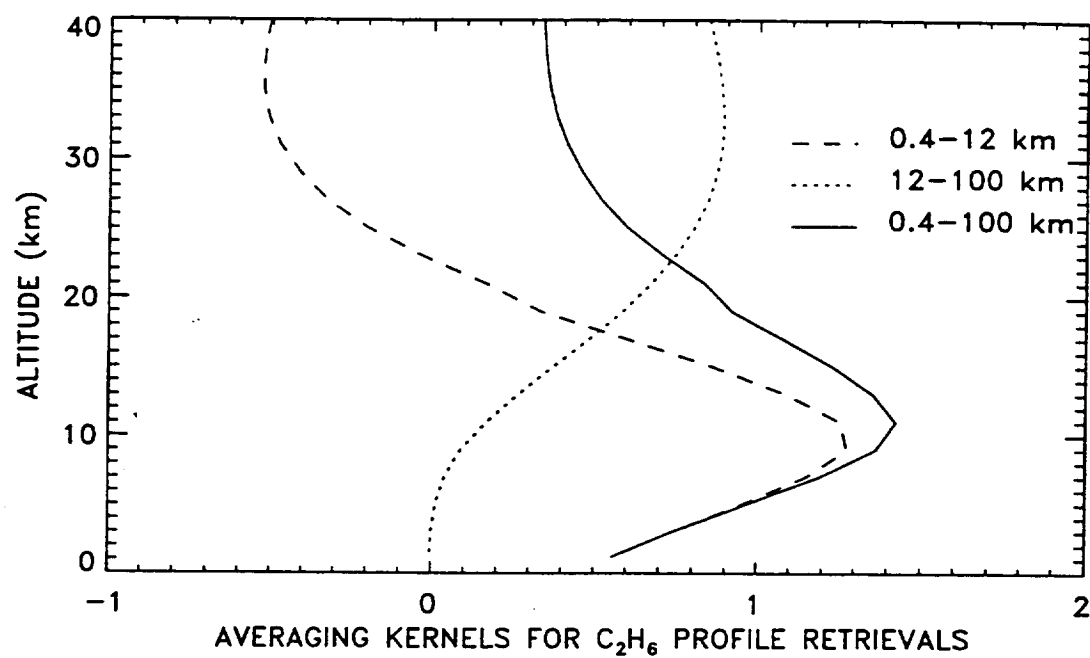
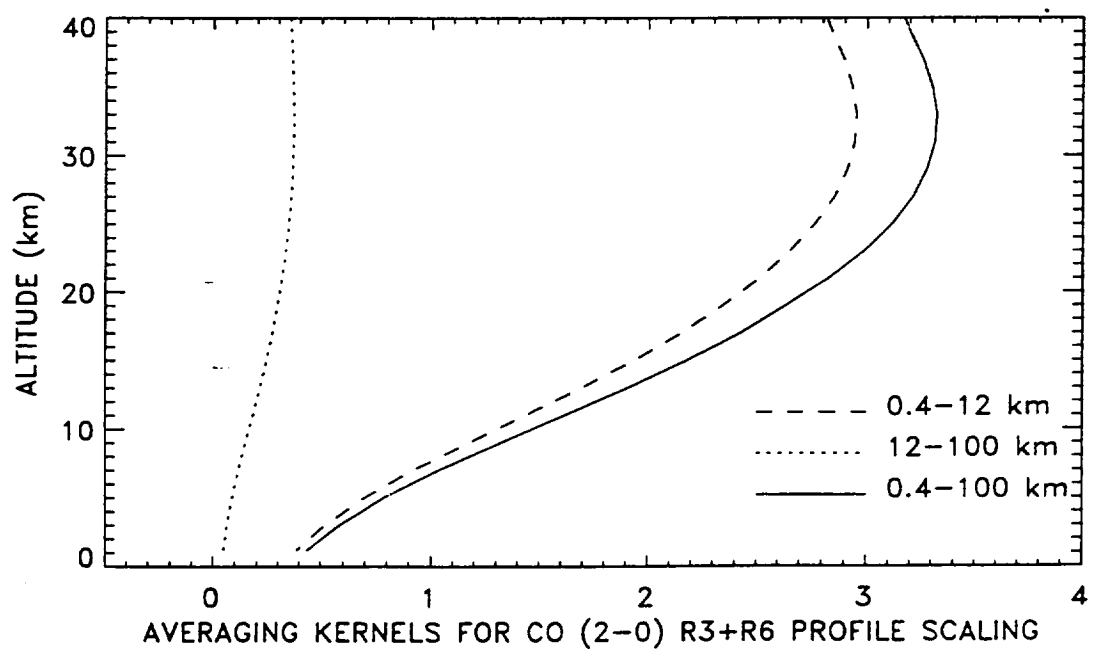
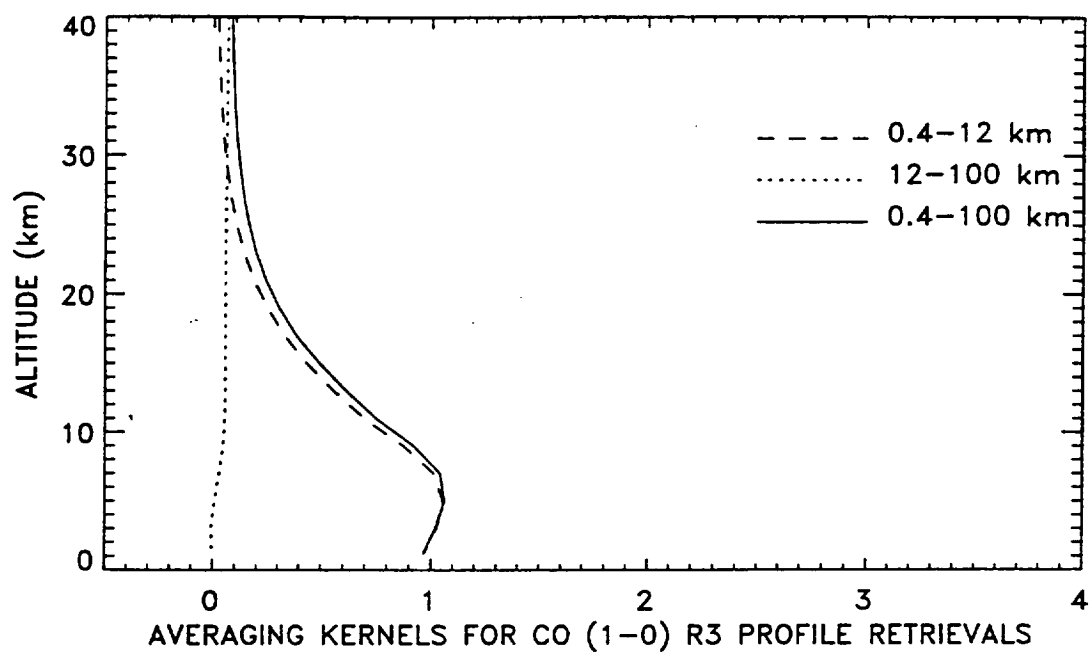
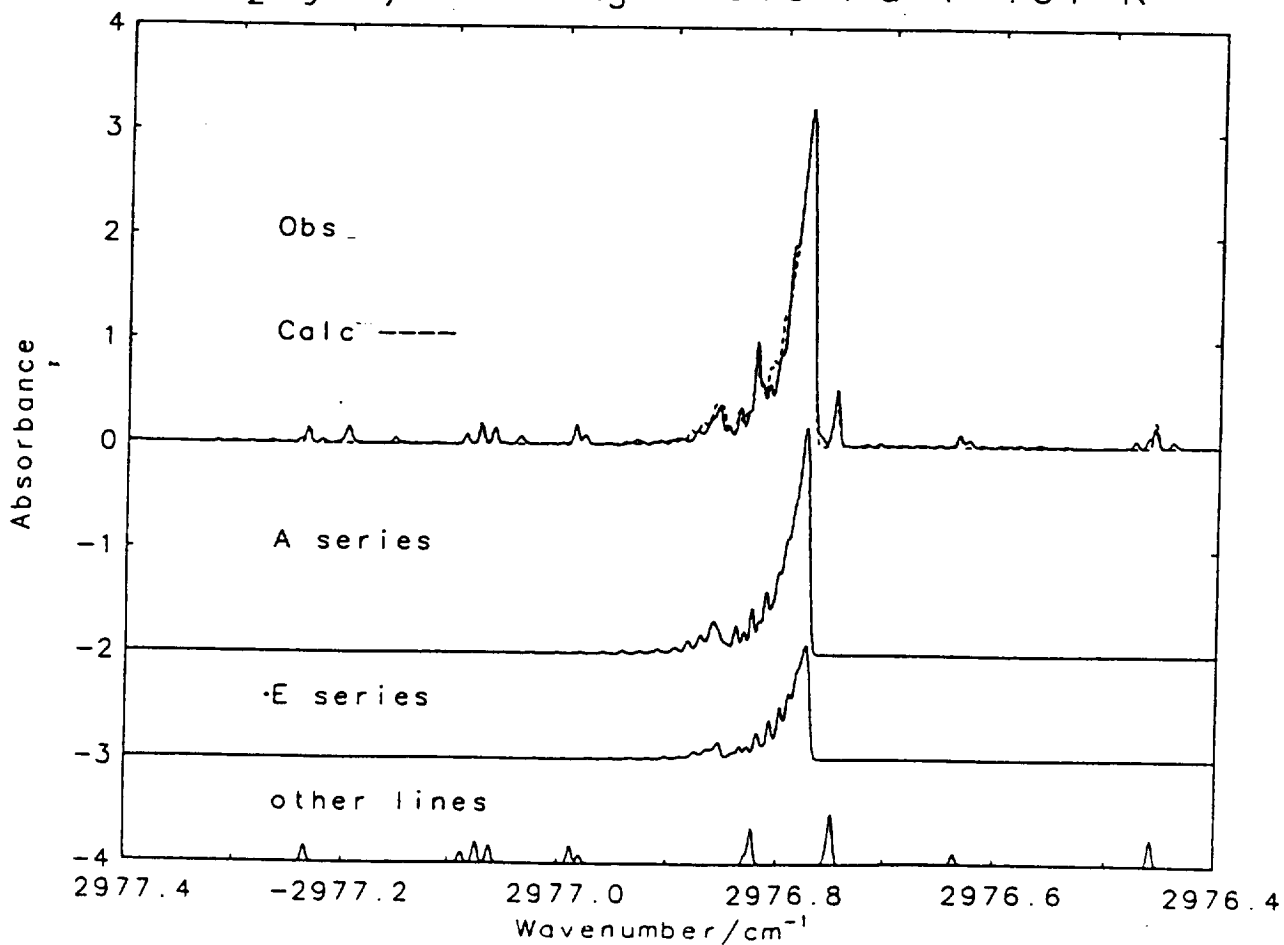
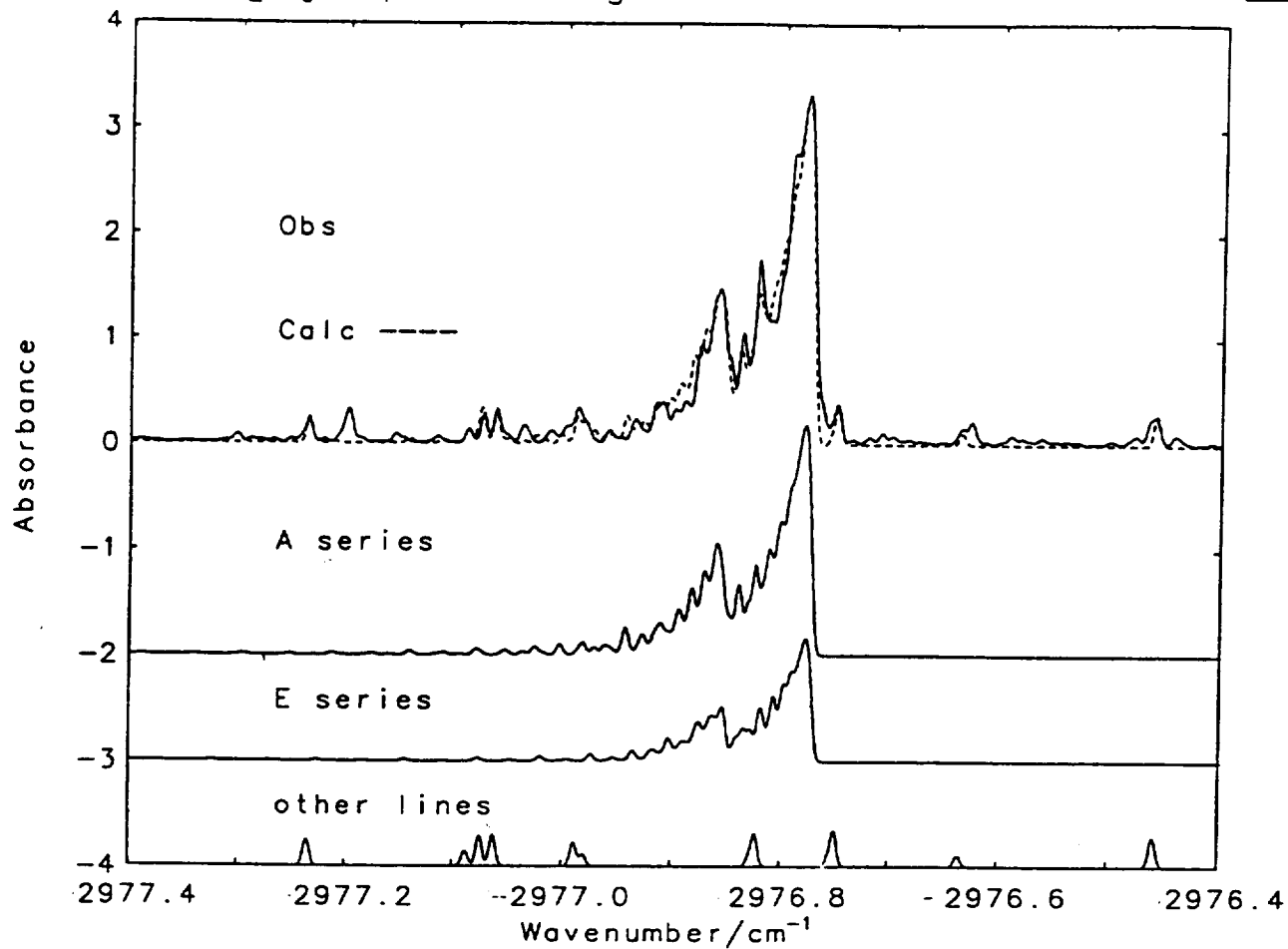


Figure 3





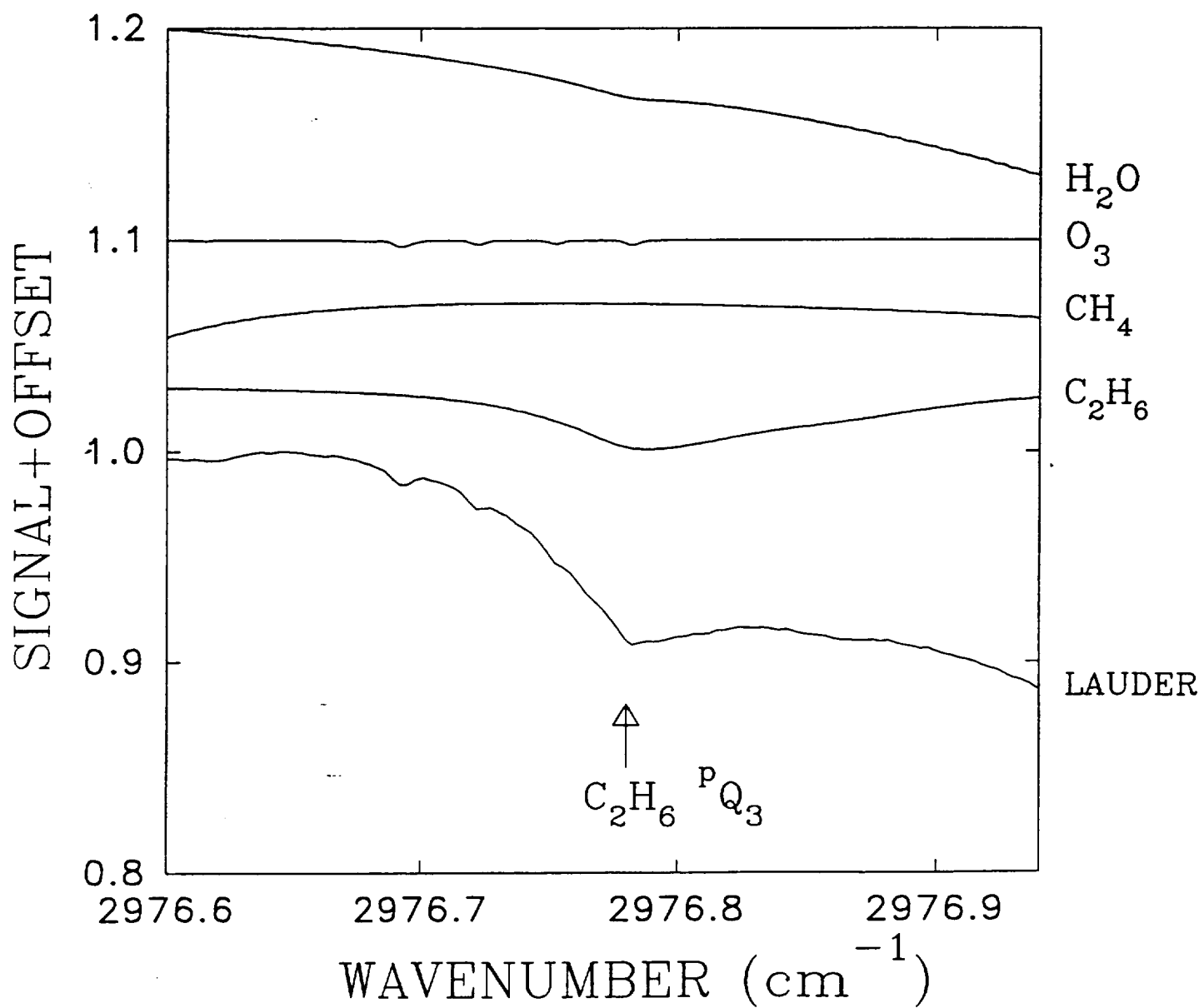


Figure 6

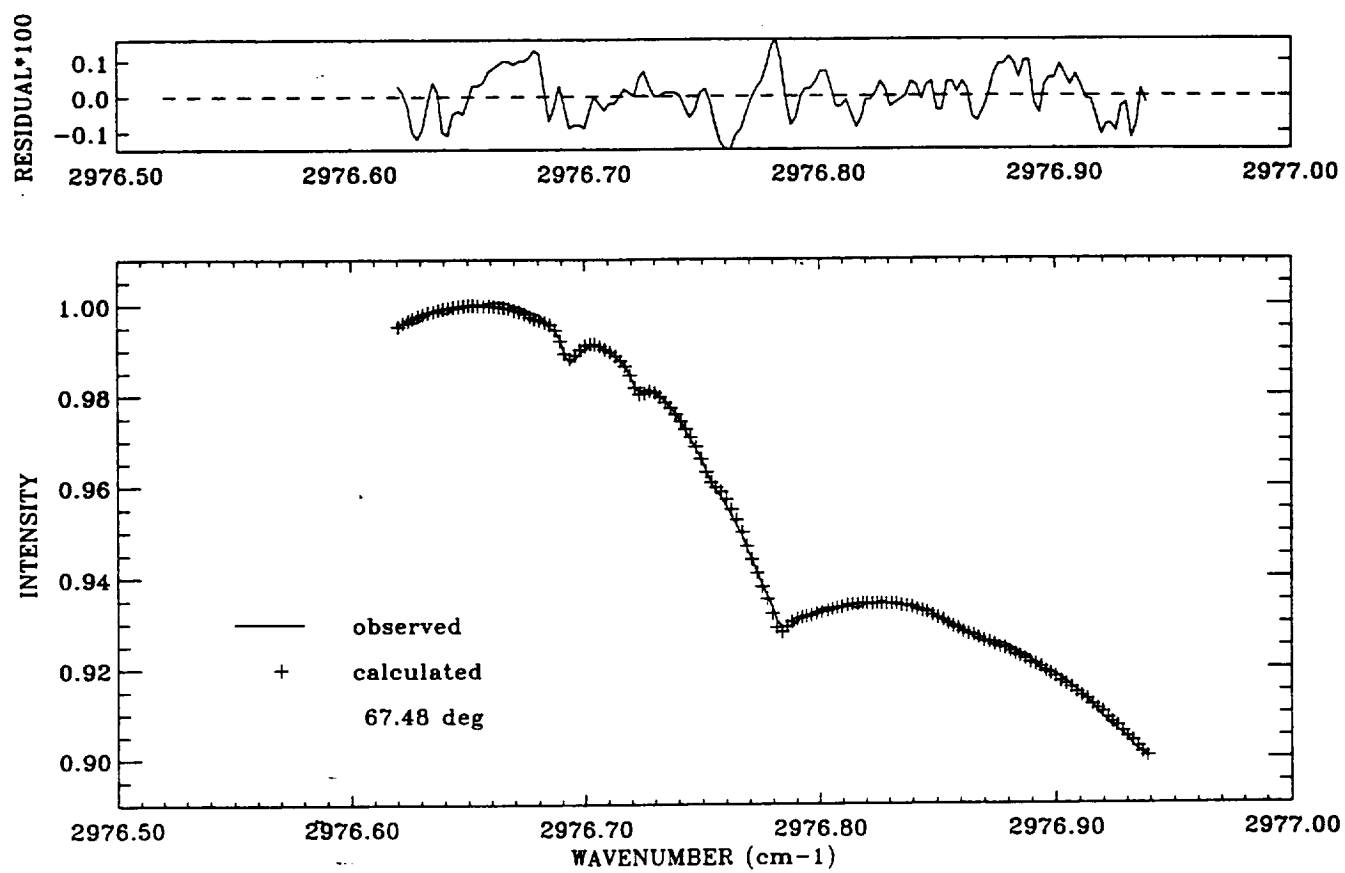




Figure 7

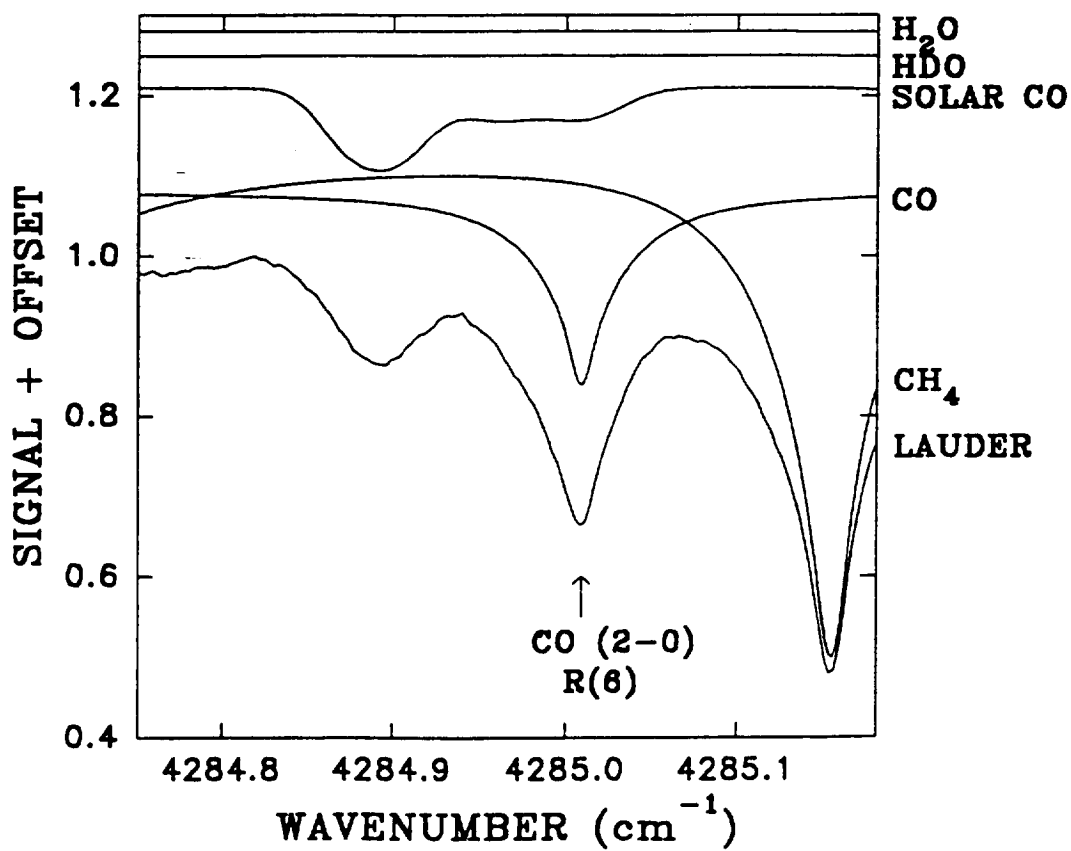
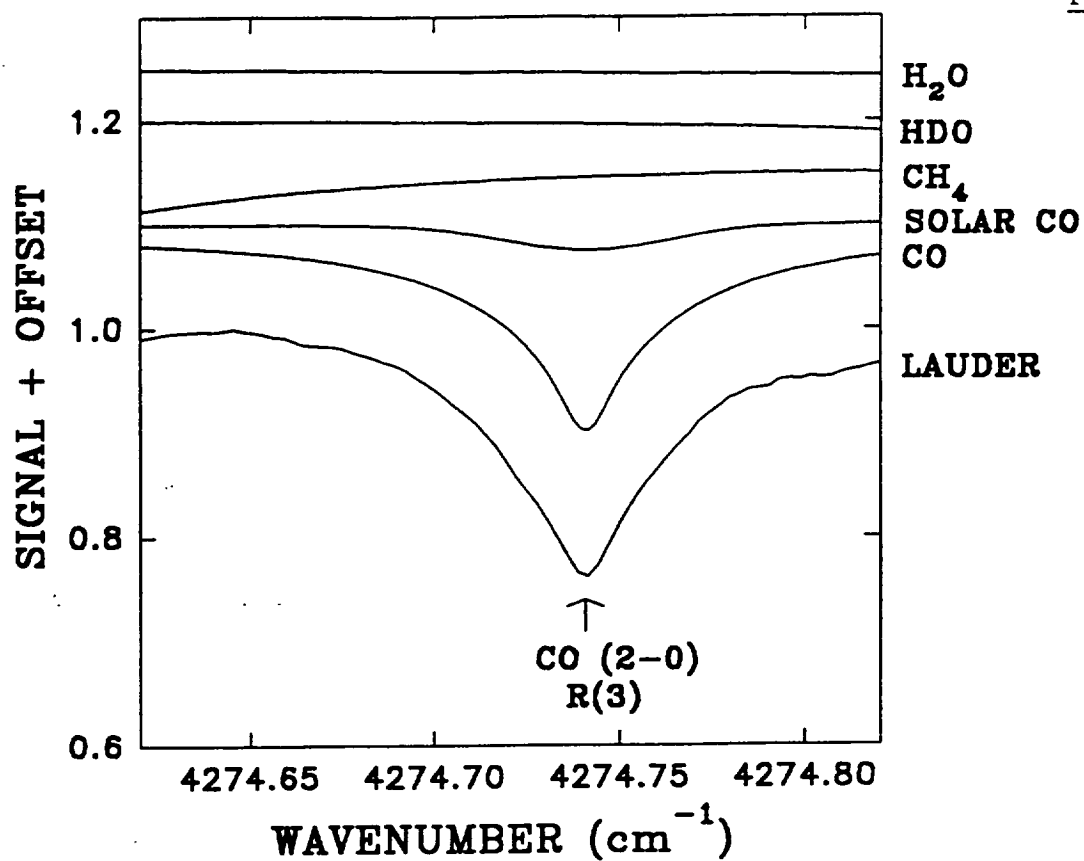


Figure 8

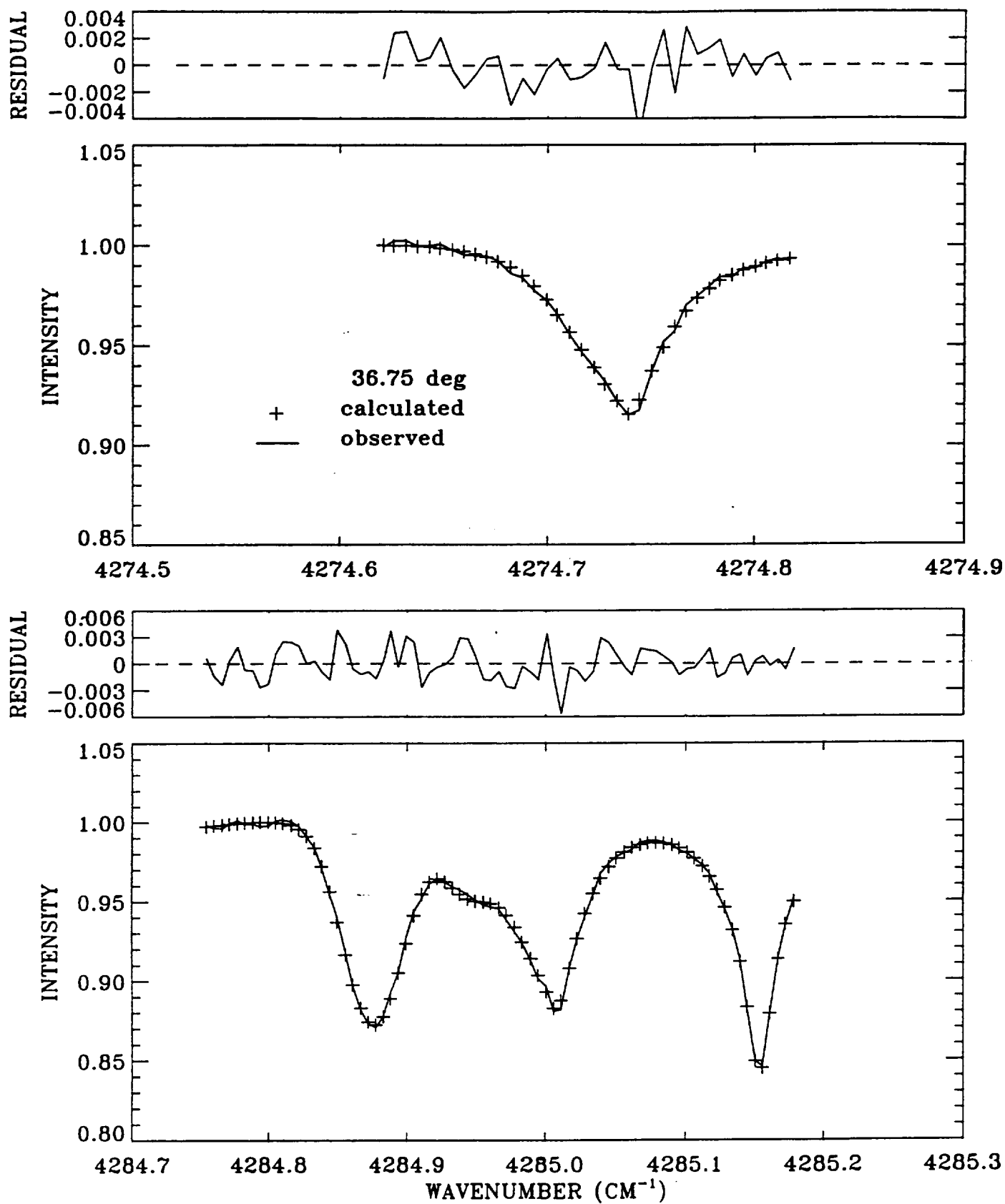


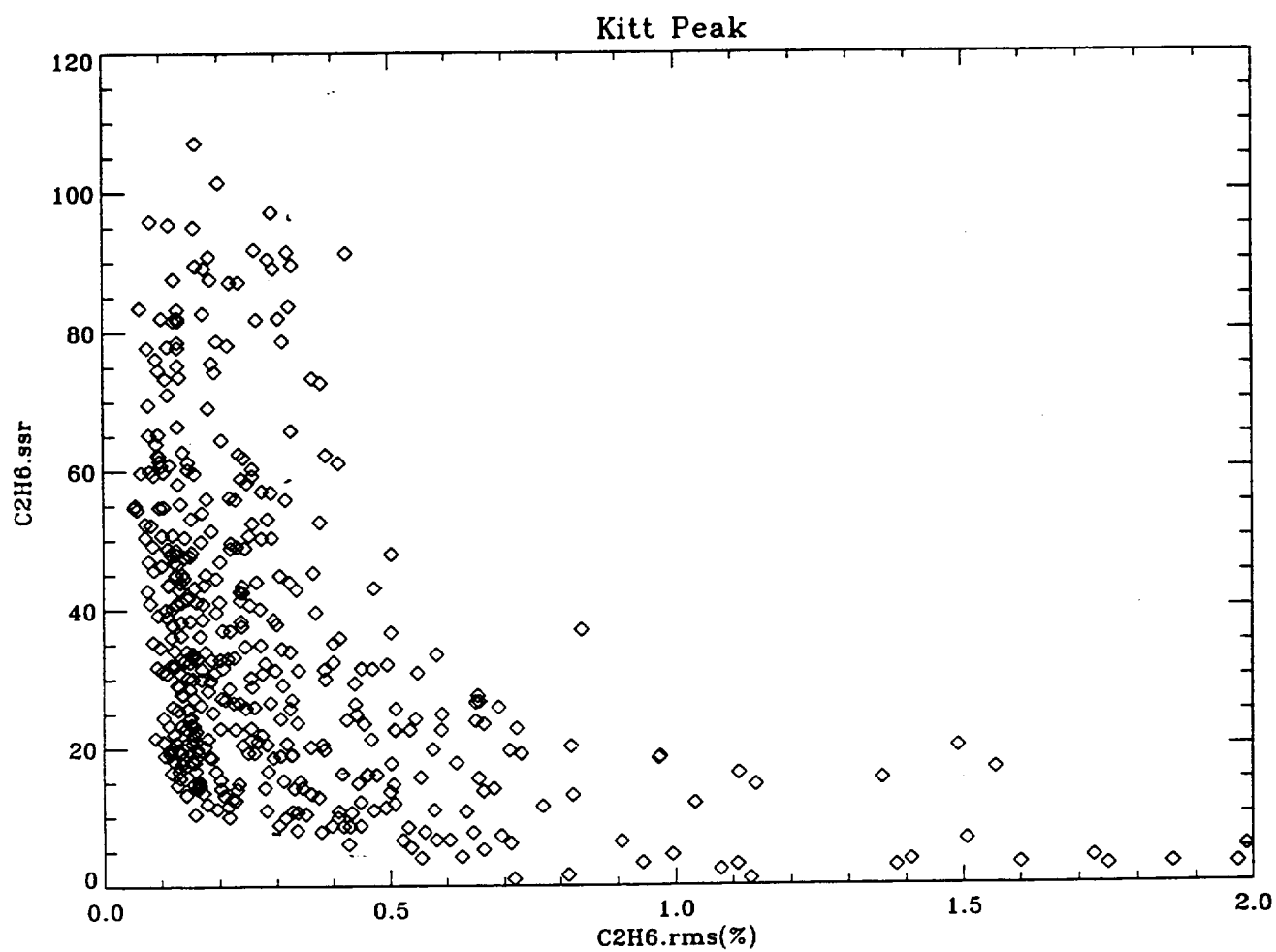
Figure 9

Figure 10

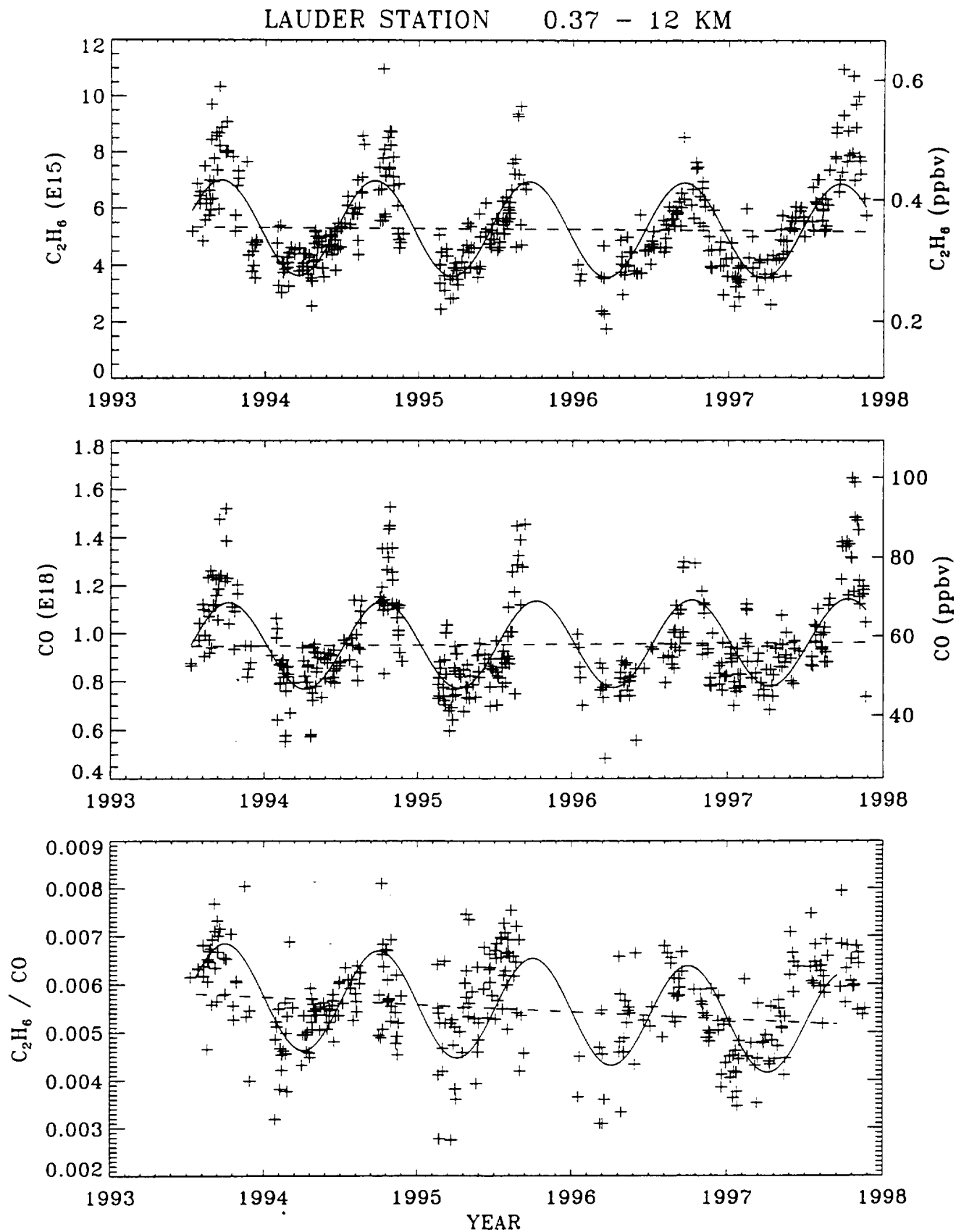


Figure 11

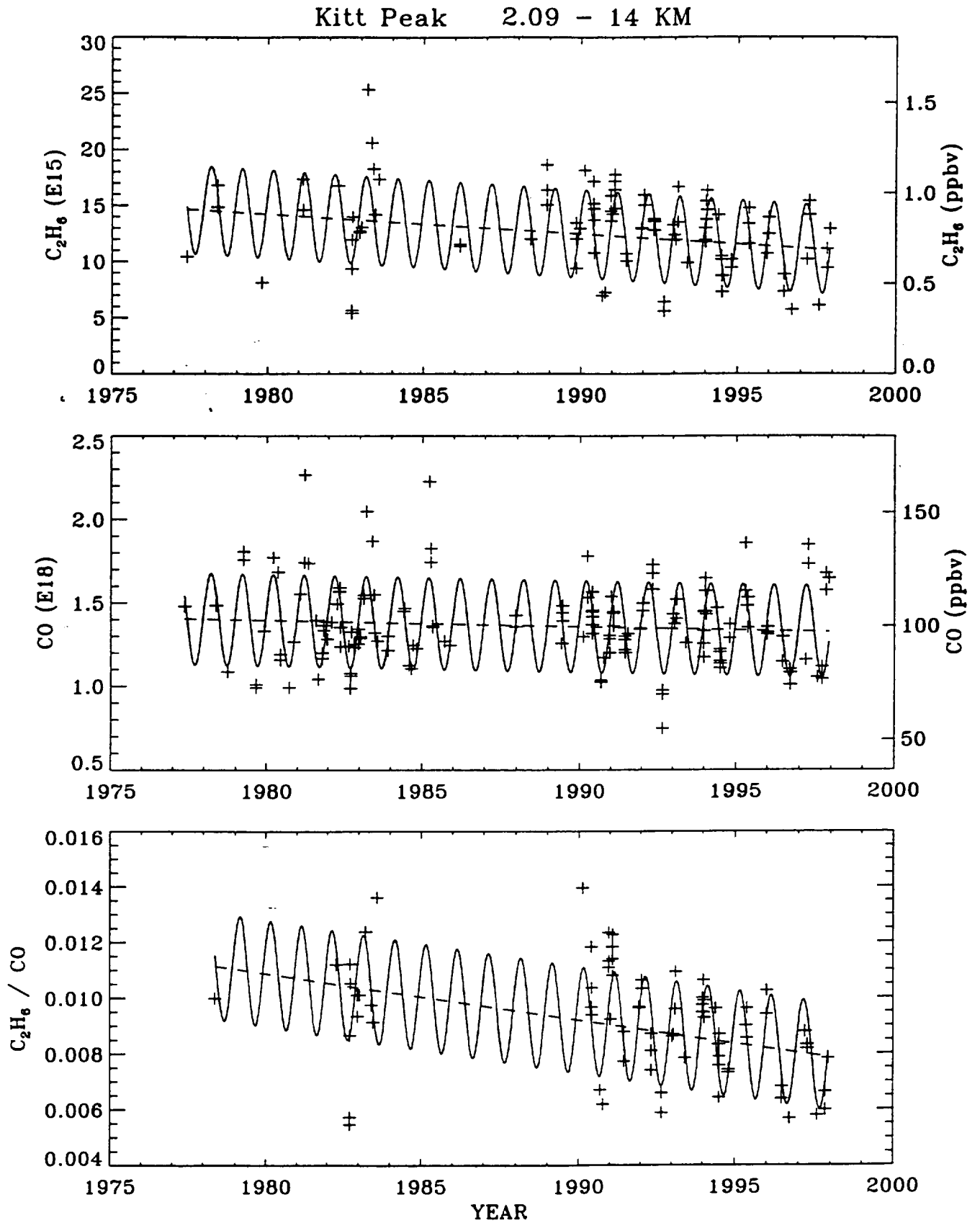
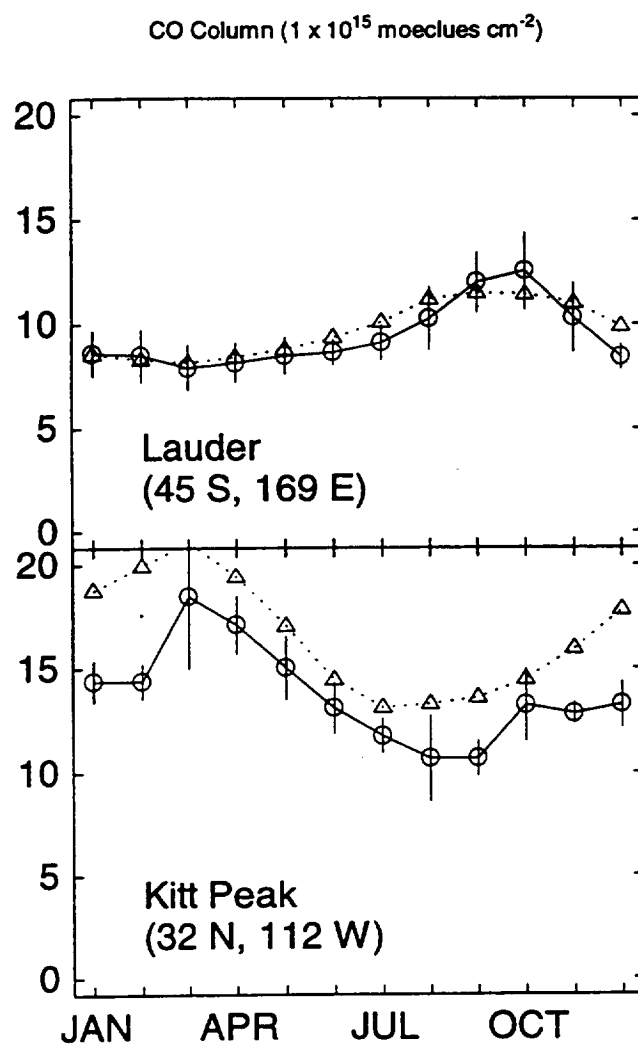
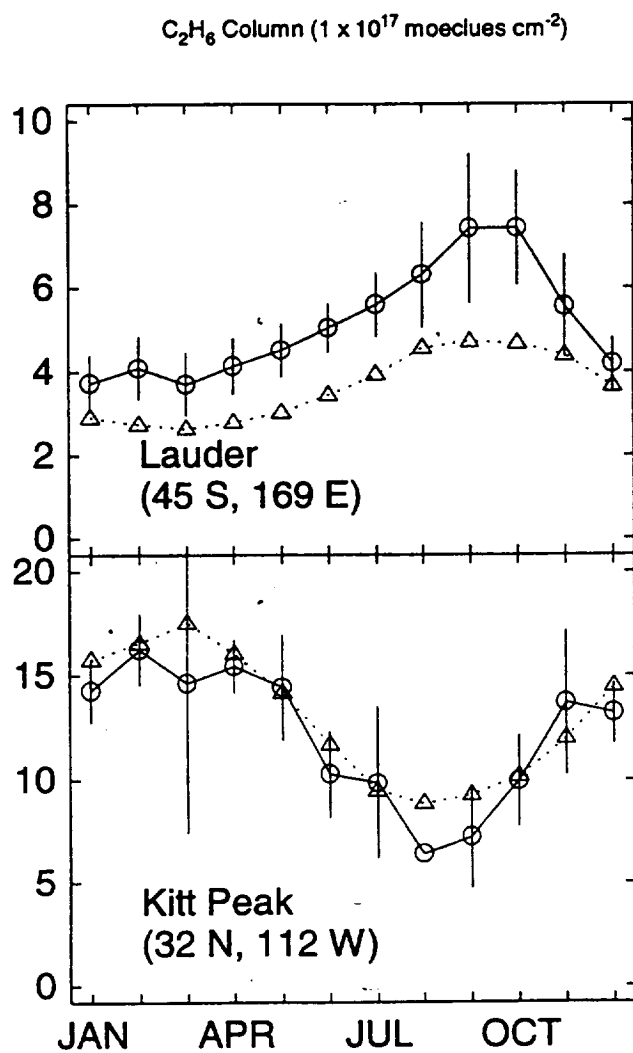


Figure 12









# Measurements of the downward longwave radiation spectrum over the Antarctic Plateau and comparisons with a line-by-line radiative transfer model for clear skies

Von P. Walden

Space Science and Engineering Center, University of Wisconsin, Madison

Stephen G. Warren

Department of Atmospheric Sciences, University of Washington, Seattle

Frank J. Murcray

Department of Physics, University of Denver, Denver, Colorado

**Abstract.** A 1-year field program was conducted at South Pole Station in 1992 to measure the downward infrared radiance spectrum at a resolution of  $1\text{ cm}^{-1}$  over the spectral range 550-1667  $\text{cm}^{-1}$ . The atmosphere over the Antarctic Plateau is the coldest and driest on Earth, where in winter, surface temperatures average about  $-60^\circ\text{C}$ , the total column water vapor is as low as 300  $\mu\text{m}$  of precipitable water, and the clear-sky downward longwave flux is usually less than  $80\text{ W m}^{-2}$ . Three clear-sky test cases are selected, one each for summer, winter, and spring, for which high-quality radiance data are available as well as ancillary data to construct model atmospheres from radiosondes, ozonesondes, and other measurements. The model atmospheres are used in conjunction with the line-by-line radiative transfer model (LBLRTM) to compare model calculations with the spectral radiance measurements. The high-resolution calculations of LBLRTM ( $\approx 0.001\text{ cm}^{-1}$ ) are matched to the lower-resolution measurements ( $1\text{ cm}^{-1}$ ) by adjusting their spectral resolution and by applying a correction for the finite field of view of the interferometer. In summer the uncertainties in temperature and water vapor profiles dominate the radiance error in the LBLRTM calculations. In winter the uncertainty in viewing zenith angle becomes important as well as the choice of atmospheric levels in the strong near-surface temperature inversion. The spectral radiance calculated for each of the three test cases generally agrees with that measured, to within twice the total estimated radiance error, thus validating LBLRTM to this level of accuracy for Antarctic conditions. However, the discrepancy exceeds twice the estimated error in the gaps between spectral lines in the region 1250-1500  $\text{cm}^{-1}$ , where emission is dominated by the foreign-broadened water vapor continuum.

## 1. Introduction

The Antarctic Plateau covers large areas of East Antarctica (above 2000 m) and West Antarctica (above 1500 m). In its longwave radiation budget this region differs from the katabatic wind region [Yamanouchi and Kawaguchi, 1984, 1985] and the maritime Antarctic [Lubin, 1994]. For most of the year a near-surface temperature inversion is present over the plateau, whose strength increases with surface elevation as the atmosphere becomes thinner and less absorptive to infrared radiation. Large radiation losses to space occur throughout most of the year, with frontal activity and the associated cloudiness temporarily reducing the loss at the surface [e.g., Stone *et al.*, 1989; Stone and Kahl, 1991].

Continuous records of meteorological data from the East Antarctic Plateau exist for three stations: 40 years at South Pole ( $90^\circ\text{S}$ ), 40 years at Vostok ( $78^\circ\text{S}$ ,  $107^\circ\text{E}$ ), and 3 years at Plateau ( $79^\circ\text{S}$ ,  $40^\circ\text{E}$ ). Since there is little regional variation in climate

across the plateau, data from one location can represent a large geographical area. Thus, in the absence of data at other locations, atmospheric conditions at South Pole Station may serve to represent the conditions over most of East Antarctica. Recent attempts to model the climate of the Antarctic have met with some success in comparing model output with existing observational data sets [Tzeng *et al.*, 1993, 1994; Genthon, 1994]. For the purpose of this paper the most important characteristic of the atmosphere over the Antarctic interior is that it is the coldest and driest on Earth and thus represents an endpoint of terrestrial climate.

In the 1980s a project on Intercomparison of Radiation Codes used in Climate Models (ICRCCM) was established to compare radiative transfer models, ranging from detailed line-by-line codes to highly parameterized band models [Luther *et al.*, 1988; Ellingson and Fouquart, 1991]. The results of clear-sky calculations for shortwave models were summarized by Fouquart *et al.* [1991] and those for longwave models by Ellingson *et al.* [1991]. The atmospheres used in those comparisons were the five reference atmospheres of the Air Force Geophysics Laboratory (AFGL) [McClatchey *et al.*, 1972] as well as isothermal atmospheres containing only  $\text{CO}_2$  or  $\text{H}_2\text{O}$  as gaseous absorbers. One of the main

Copyright 1998 by the American Geophysical Union.

Paper number 97JD02433.  
0148-0227/98/97JD-02433\$09.00

conclusions of the longwave study was that line-by-line radiative transfer models, although they agree well with each other, do not represent an absolute standard by which to judge less detailed models. Their output must therefore be compared with data from the real atmosphere. Spectral rather than broadband, and radiance rather than flux measurements, would be most useful because the causes of discrepancies between model and observation can be more easily identified if angular and spectral averaging has not been done. Specifically, the study concluded that spectral radiance data of moderate resolution (about  $1\text{ cm}^{-1}$ ) would be particularly valuable for comparison with a variety of radiation codes at various spectral resolutions.

To resolve the differences among the most detailed radiation models, the ICRCCM participants recommended that accurate spectral radiance measurements be made coincidentally with the atmospheric variables necessary to calculate radiance [Ellingson *et al.*, 1991]. Currently, data sets of this type exist for the following locations: (1) Coffeyville, Kansas, where the Spectral Radiance Experiment (SPECTRE) was performed [Ellingson and Wiscombe, 1996], (2) the Southern Great Plains site of the Atmospheric Radiation Measurement (ARM) program [Stokes and Schwartz, 1994; Ellingson *et al.*, 1995], (3) the California coast [Clough *et al.*, 1989a], and (4) the tropical Pacific Ocean [Lubin *et al.*, 1995]. ARM is now establishing a site on the North Slope of Alaska.

The Antarctic Plateau is an ideal location for acquiring spectral radiance data for testing radiative transfer models. Since the atmosphere is so cold and dry ( $\leq 1\text{ mm}$  of precipitable water), the overlap of the emission spectrum of water vapor with that of other gases is greatly reduced. Therefore the spectral signatures of other important infrared emitters, namely,  $\text{CO}_2$ ,  $\text{O}_3$ ,  $\text{CH}_4$ , and  $\text{N}_2\text{O}$ , are quite distinct. In addition, the low atmospheric temperatures provide an extreme test case for testing models. Even in summer the atmosphere is colder and drier than the sub-Arctic winter, the coldest of the five AFGL model atmospheres. The radiation conditions at the surface of the Antarctic Plateau in winter are similar to those at the tropopause at lower latitudes. Routine operations at South Pole Station provide good ancillary data for characterizing the atmosphere throughout the year. The South Pole Weather Office (SPWO) launches radiosondes once or twice per day and makes surface weather observations at least every 6 hours. The Climate Monitoring and Diagnostics Laboratory (CMDL) of the National Oceanic and Atmospheric Administration (NOAA) provides continuous near-surface concentrations of several radiatively active trace gases, as well as ozonesonde profiles once or twice per week.

Many previous Antarctic field programs have reported measurements of broadband radiation fluxes [Hanson, 1960; Hanson and Rubin, 1962; Rusin, 1964; Kopanev, 1967; Kuhn *et al.*, 1977; Yamanouchi *et al.*, 1982; Carroll, 1982; Yamanouchi and Kawaguchi, 1984]. Such broadband measurements, however, are not useful for identifying defects in radiative transfer models. Here our focus is instead on how the radiance varies across the infrared spectrum. In this paper we describe a data set taken at South Pole Station throughout the year of 1992, consisting of spectral infrared radiances together with observations from radiosondes and other instruments to characterize the atmosphere. Particular attention is given to the calibration and uncertainty associated with the radiation measurements. The calibration procedure described here is an improvement over that of Van Allen *et al.* [1996], which used the same instrument at South Pole Station. Their experiment was designed to study stratospheric chemistry,

which did not require the level of accuracy needed here for SPECTRE-type comparisons.

The uncertainties associated with characterizing the atmosphere are also estimated, particularly with regard to temperature and humidity variations in the near-surface layer. Three test cases are constructed, using the highest-quality measurements from the data set, representing the meteorological and infrared radiation conditions in summer, winter, and spring under clear sky. These test cases are used to compare the spectral infrared radiances with calculations of the line-by-line radiative transfer model (LBLRTM) [Clough *et al.*, 1992]. A brief description of LBLRTM is given below as it is applied to this work, including how the model calculations were adjusted for instrumental effects, so that the model results can be compared directly with the observations. The radiance error in the LBLRTM calculations induced by uncertainties in the ancillary data is estimated; the major sources of error are identified for summer and winter conditions. The comparisons for our six test cases (two viewing angles on each of 3 days) are shown, and portions of the spectrum are examined in detail.

## 2. Field Program

Spectral radiance was measured by a Fourier transform interferometer (FTIR), manufactured by Bomem, Inc., and modified at the University of Denver (UD) for outdoor operation at South Pole. It had been successfully operated through a previous winter at South Pole for the purpose of determining concentrations of atmospheric gases important to ozone chemistry [Murcray and Heuberger, 1990, 1991, 1992]. The radiance spectrum was measured at viewing zenith angles of  $45^\circ$  and  $75^\circ$ , and also often at  $60^\circ$ , every 12 hours throughout the year except during blizzard conditions.

The state of the atmosphere is characterized by using various sources of data. Visual sky observations were made by Warren during each FTIR measurement, as well as routinely every 6 hours by the SPWO observers. Vertical profiles of temperature, water vapor, and ozone are constructed by using a combination of radiosonde data from SPWO and CMDL, plus satellite data from the Upper Atmosphere Research Satellite (UARS) [Reber *et al.*, 1993]. Tropospheric concentrations of carbon dioxide, methane, nitrous oxide, and chlorofluorocarbons were obtained from in situ measurements made at the surface by CMDL, and stratospheric concentrations were obtained from UARS.

## 3. Selection of Test Cases

Three days were selected for comparison of spectral radiance measurements to radiative transfer models: January 17, 1992, May 1, 1992, and October 5, 1992. For each day the calibrated radiances at viewing zenith angles of  $45^\circ$  and  $75^\circ$  are determined. The three primary criteria for selection were clear skies with minimal visually observed atmospheric ice crystals, well-calibrated spectral radiance measurements, and time of year. The summer and winter cases were chosen to span the full range of atmospheric conditions over South Pole; the springtime case represents an atmosphere with a depleted ozone profile. Secondary selection criteria include availability of high-quality radiosonde and ozonesonde information and minimal time between the radiosonde launch and the spectral radiance measurements (Table 1). The seasons at South Pole are defined by the annual cycle of surface temperature [Schwerdfeger, 1970; Warren, 1996]: summer

**Table 1.** Characteristics of the Interferometric Measurements and Model Atmospheres for the Three Selected Test Cases

Date	Jan 17, 1992	May 1, 1992	5 Oct 1992
Representative season	summer	winter	spring
Start time of FTIR measurement, UT	2215	2230	1021
Time of radiosonde launch, UT	2214	2131	0941
Total downward longwave flux, $W\ m^{-2}$	121	76	78
Surface air temperature, $^{\circ}C$	-32	-66	-62
Inversion strength, K	5	29	25
Total column water vapor, mm of precipitable water	1.0	0.3	0.3
Carbon dioxide mixing ratio, ppmv	353	353	355
Total column ozone, DU	287	247	147
Methane mixing ratio at the surface, ppbv	1654	1661	1679
Nitrous oxide mixing ratio at the surface, ppbv	308.9	308.6	309.1
CFC-11 mixing ratio at the surface, pptv	265	265	267
CFC-12 mixing ratio at the surface, pptv	491	494	498

DU, Dobson Unit; 1 DU = 0.001 atm cm.

(December-January), autumn (February-March), winter (April-September), and spring (October-November).

On the three days chosen, no visual clouds were observed in any portion of the sky by either the SPWO or Warren. The May 1 case was chosen partly because the amount of clear-sky ice crystal precipitation ("diamond dust") was slight and partly because polar stratospheric clouds (PSCs) normally are not present until later in the winter [Poole and Pitts, 1994]. Polar stratospheric clouds are hard to detect visually from the surface during nighttime, but the assumption that they were absent on May 1 is supported by the lidar data discussed by Cacciani *et al.* [1993].

The primary factor controlling the availability of good sonde data is the type of balloon used. During the winter, plastic balloons were used alternately with standard rubber balloons; plastic balloons typically reach higher altitudes (about 30 km) before bursting but are more expensive. Test cases were chosen for days on which the balloon reached high altitude.

## 4. Spectral Radiance Measurements

### 4.1 Data

A Michelson-type interferometer was used: Bomem model MB-100 with electronics upgraded to an MB-120. Data acquisition from the instrument is controlled by an IBM-PC compatible computer using software developed by Bomem and UD. Modifications made at UD for operation in Antarctica include the following. A mercury-cadmium-telluride (MCT) semiconductor detector, cooled by liquid nitrogen, was installed for high sensitivity at thermal infrared wavelengths. The liquid nitrogen was supplied by a Joule-Thompson expansion cooler using nitrogen gas from high-pressure storage bottles. An external mirror assembly was attached to the interferometer, enabling it to view two external calibration sources and the sky at three zenith angles.

The interferometer is a two-input, two-output instrument. The detector, placed at one of the output ports, records the superposition of infrared radiation from the two input ports, one of which is

an internal reference source; the other is the scene. The output varies as a function of the optical path difference of the scanning mirror; its DC offset is suppressed by the interferometer's electronics by coupling to the variable portion of the signal [Beer, 1992, equation (1.14b)]. The total optical path difference is  $16,384\ (633\ nm) = 1.04\ cm$ ; the wavelength of the interferometer's laser is 633 nm. Typically, the mirror scans about 50 to 100 times successively, with the output from all scans being averaged by a process called co-adding. (This number of co-added scans was necessary to ensure an adequate signal-to-noise ratio for UD's research [Van Allen *et al.*, 1996].) The final co-added record is called an interferogram. The Bomem software apodizes the interferogram using the Hann-window function [Press *et al.*, 1992], and performs a Fourier transform, producing an uncalibrated spectrum for that individual measurement. The spectral resolution of the transformed data is  $1\ cm^{-1}$  (full width at half maximum). The spectral bandwidth of the instrument is limited by the response of the MCT detector and the bandpass of the beamsplitter to the range  $550\text{--}1667\ cm^{-1}$ , or  $6\text{--}18\ \mu m$ . At these limiting wavenumbers the response is about 10% of the peak response at  $900\ cm^{-1}$ .

During a typical spectral radiance measurement the interferometer views four or five different scenes successively. A "measurement sequence" consists of viewing zenith angles of  $45^{\circ}$  and  $75^{\circ}$  (and often  $60^{\circ}$ ), bracketed by views of calibration sources: one at ambient air temperature and another at about 45 K above ambient. A typical measurement sequence takes 20-30 min. The calibration sources are grooved copper plates painted with Aeroglaze Z306, a polyurethane coating. Each source has two thermistors imbedded in the back of the copper disk, sensing its temperature. The cold source has one thermistor at the center of the disk and the other on the periphery. The warm source has a resistive heater attached to the center of its back surface, to elevate its temperature above ambient. One of its thermistors is therefore slightly off center, while the other is on the periphery.

Measurement sequences were performed approximately every 12 hours throughout the year at South Pole and during most routine radiosonde launches made by the SPWO. Measurement

sequences were taken more frequently when the sky was clear, and special observations were made during some ozonesonde and water vapor sonde launches. "Housekeeping" information was recorded routinely during each sequence, consisting primarily of temperature measurements of various parts of the interferometer. These measurements were used to select test cases with good thermal stability, in which the instrument temperature drifted by less than 0.1 K during the measurement sequence [Walden, 1995].

The interferometer was mounted atop the Skylab building at an elevation of approximately 10 m above the upwind snow surface. The instrument was housed in about 10 cm of styrofoam insulation, while the external mirror assembly was exposed to the ambient temperature. Thus the internal temperature of the interferometer varied only slowly as the ambient temperature changed.

## 4.2 Calibration

The method of *Revercomb et al.* [1988] is used to calibrate measurements of the sky. An uncalibrated spectrum,  $C'$ , can be written as a linear function of the measured radiance,  $L$ , as

$$C' = r[L + L^0 e^{i\phi^0}] e^{i\phi}, \quad (1)$$

where  $r$  is the instrument response function of the interferometer,  $L^0$  represents the spectral offset radiance from the instrument itself,  $\phi$  is the phase response of the instrument due to optical and electrical dispersion, and  $\phi^0$  is any anomalous phase incorporated into the offset radiance [Revercomb et al., 1988]. All the variables are functions of frequency. Subscripts  $w$ ,  $c$ , and  $s$  are applied to  $C'$  and  $L$ , referring to warm, cold, and sky (or scene). The uncalibrated spectra for the warm and cold calibration sources,  $C'_w$  and  $C'_c$ , are used to calibrate the measurements of the sky,  $C'_s$ , by taking the real part of the ratio of difference spectra and solving for the scene radiance,  $L_s$ , giving

$$L_s = \gamma[L_w - L_c] + L_c, \quad (2)$$

where

$$\gamma = \text{Re} \left[ \frac{C'_s - C'_c}{C'_w - C'_c} \right]. \quad (3)$$

$L_w$  and  $L_c$  are the radiances emitted and reflected from the calibration sources:

$$L_j = \epsilon_j B(T_j) + (1 - \epsilon_j) B(T_{\text{ambient}}), \quad (4)$$

where  $j$  is either  $w$  or  $c$ .  $B(T)$  represents the Planck radiance at a particular frequency for a given temperature  $T$ ,  $T_j$  is the temperature of the emitting surface of the source,  $\epsilon_j$  is the spectral emissivity of the source, and  $T_{\text{ambient}}$  is the temperature of the ambient outside air.

There are implicit assumptions in equation (1). First, the output from the interferometer's detector is assumed to be linearly related to the input radiance into the interferometer. The possibility of nonlinearities in the detector is not considered in this study, since any resulting bias is probably small compared with the overall radiance uncertainty discussed below.

In addition, the assumption of thermal stability means that the offset radiance  $L^0 e^{i\phi^0}$  is constant within a measurement sequence, so that it can be eliminated by the taking the difference of measurements  $C'$ , which results in the numerator and denominator of equation (3). The maximum acceptable level of thermal drift of the interferometer during measurement sequences to be used for

test cases was chosen such that any radiance errors resulting from thermal drift are negligible compared with those from other error sources. However, a procedure for adjusting measurement sequences with large thermal drift has been developed by Walden [1995].

The radiances from the calibration sources,  $L_w$  and  $L_c$ , must be known accurately, independent of the measurements, for proper calibration of atmospheric radiances. Thus the accuracy of the final calibrated radiances depends on accurate specification of the source temperature and emissivity. The uncertainties in these temperatures and emissivities must also be assessed to estimate the uncertainty in calibrated radiances. The source temperatures and emissivities described below differ from those used by *Van Allen et al.* [1996].

**4.2.1 Temperature of the calibration sources.** The temperature of each calibration source is measured by two thermistors that were calibrated to a temperature reference of the National Institute of Standards and Technology (NIST) by the manufacturer (Yellow Springs Instruments, Inc., Yellow Springs, Ohio). The electronics used to measure the source temperatures were checked by substituting four different high-precision resistors in place of each thermistor. The resistors were chosen to represent a range of temperatures far exceeding the range experienced at South Pole. The voltage recorded by the electronics was converted back to a resistance value, which was then compared with the value of the precision resistors. Analysis of this cross-check procedure indicated that a small additional resistance needed to be added to the inferred resistances to reconcile them with the actual values. In the conversion of resistance to temperature this correction was significant when the resistance being measured was small (less than 1000 ohms). The additional resistance ranged from 9 to 75 ohms and varied from channel to channel within the data acquisition system. Using the thermistor manufacturer's conversion from resistance to temperature, we derived temperature corrections for each thermistor. Figure 1 shows the corrections for the four thermistors on the calibration sources over the range of temperature values experienced by these sources at South Pole in 1992. The corrections are significant at high temperatures, or low thermistor resistance. The corrections are 0.6 K and 1.3 K for the cold source thermistors at their maximum yearly temperature of  $-10^\circ\text{C}$ , and 0.3 K and 1.3 K for the warm source thermistors at  $+35^\circ\text{C}$ .

Figure 2a shows the difference in temperature reported by the two thermistors on the cold calibration source. Since the cold source is at ambient outside temperature, the two thermistors should agree. True temperature differences between the thermistors would be due to random variation of environmental conditions such as wind speed and direction, causing only random scatter in the data. Figure 2a shows instead a consistent pattern of deviation with small scatter; the deviation exceeds the manufacturer's tolerance limit at high temperatures. Figure 2b shows that after correcting for the thermistor electronics bias the cold source temperatures agree well for the entire temperature range throughout the year, thus validating the correction procedure. The true cold source temperature,  $T_c$ , is then estimated by averaging  $T_4'$  and  $T_{10}'$ , where the prime indicates that the correction for the electronics bias has been applied:

$$T_4' = T_4 + \Delta_{c4}, \quad (5)$$

where  $\Delta_{c4}$  is the temperature correction for the thermistor electronics bias of channel 4. A similar expression exists for  $T_{10}'$ .

A similar analysis of the warm source is not possible since temperature gradients do exist within the heated plate, but the success

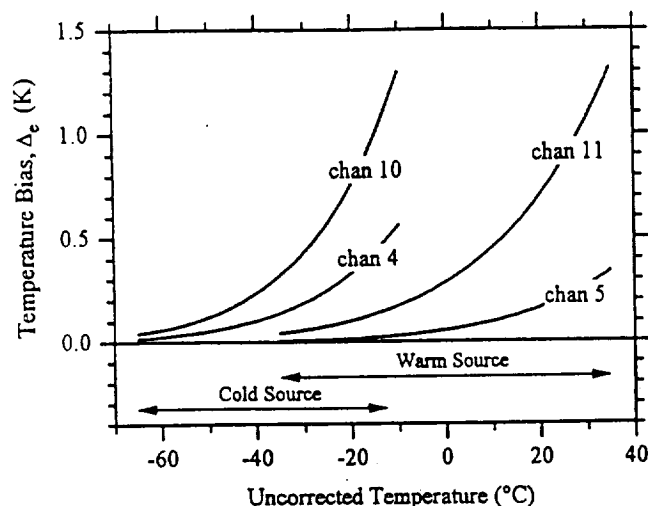


Figure 1. Thermistor electronics temperature bias ( $\Delta_e$ ) for the individual thermistors in the infrared calibration sources. The bias is shown for the range of temperatures experienced at South Pole during 1992. The thermistors are designated by their house-keeping channel number: channels 4 and 10 for the cold source thermistors and channels 5 and 11 for the warm source thermistors. Channels 4, 10, and 11 are 300-ohm thermistors (YSI 44002); channel 5 is a 3000-ohm thermistor (YSI 44005). All thermistors were manufactured by Yellow Springs Instruments, Inc., Yellow Springs, Ohio.

of the electronics bias correction procedure for the cold source argues for its validity in general. We therefore apply the electronics bias correction to the warm source thermistors,  $T_5$  and  $T_{11}$ . However, for the warm source there is an additional correction that must be applied due to thermal gradients within this source. Figure 3a shows that there is a significant temperature difference between the two thermistors on the warm source, which increases as the source temperature (e.g.,  $T_5'$ ) rises above ambient ( $T_c$ ). This behavior is expected because all thermal gradients in the source should be proportional to the difference between its temperature and ambient. Since the two thermistors are at different temperatures, it was necessary to decide which sensor has better accuracy.  $T_5'$  was chosen for two main reasons [Walden, 1995]: it has better sensitivity over most of the range of temperatures experienced during 1992, and the thermistor electronics temperature bias is much smaller for channel 5 than for channel 11 (Figure 1).

In addition to the radial temperature gradient between the thermistors shown in Figure 3a, there is evidence of a temperature difference between  $T_5'$  and the temperature of the emitting surface of the warm source as viewed by the interferometer. Three independent analyses described by Walden [1995, Appendix A] indicate that the portion of the source viewed by the interferometer is actually warmer than  $T_5'$ . This higher temperature is due to the location of the warm source's resistive heater in relation to its thermistors mentioned above, assuming that the interferometer views the center of the copper plate. The results from these analyses are reproduced in Figure 3b. The temperature difference increases as the warm source becomes increasingly warmer than ambient.

A functional form for the thermal gradient temperature bias,  $\Delta_g$ , was determined by performing a linear regression fit to the data shown in Figure 3b. The fit was forced through the origin, since no thermal gradients exist within the calibration source when

it is at ambient temperature. Our final estimate for the temperature of the viewed portion of the warm calibration source,  $T_w$ , is then obtained by applying corrections for both the thermistor electronics ( $\Delta_{e5}$ ) and thermal gradient biases, or

$$T_w \equiv T_5' + \Delta_g = T_5 + \Delta_{e5} + \Delta_g. \quad (6)$$

The larger of these two corrections is  $\Delta_g$ . For the range of warm source temperatures experienced during the year-long field experiment,  $\Delta_g$  was in the range 1–4 K, whereas  $\Delta_{e5}$  was at most 0.3 K.

**4.2.2 Emissivity of the calibration sources.** The spectral emissivity of the UD calibration sources was not directly measured but was inferred from the measured emissivity of a similar source built by Quantic Industries, Inc. (San Carlos, California) while Walden worked there. Both the UD and Quantic sources are grooved copper plates, coated with the same black paint, Aeroglaze Z306. The emissivity of nongrooved plates (constructed independently by Quantic and H. E. Revercomb's group at the University of Wisconsin, but both painted with Aeroglaze) compare well, indicating that perhaps the emissivity in the spectral range 750–1300  $\text{cm}^{-1}$  (the central portion of the interferometer's bandwidth) is not highly sensitive to the paint thickness [Walden, 1995, Appendix A]. The emissivity of the Quantic grooved source in this spectral region was the value used in deriving the thermal gradient bias described above.

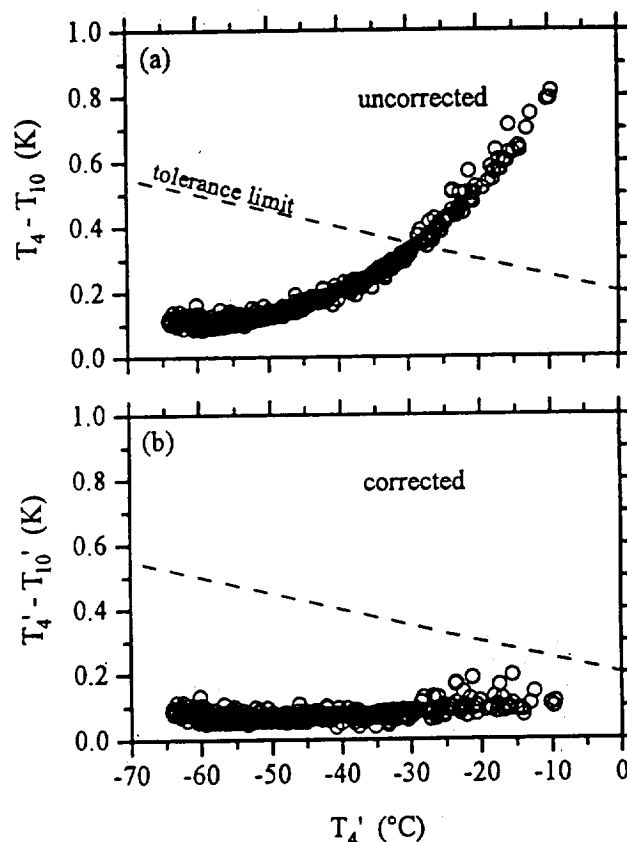


Figure 2. Temperature difference between the cold calibration source thermistors (a) before and (b) after being corrected for the thermistor electronics temperature bias.  $T_4$  and  $T_{10}$  are the uncorrected temperatures from two thermistors recorded in the house-keeping channels 4 and 10.  $T_4'$  and  $T_{10}'$  are the corresponding corrected temperatures. The dashed line is the thermistor manufacturer's interchangeability tolerance, defined as the maximum difference that can occur when two or more thermistors are used to make the same measurement.

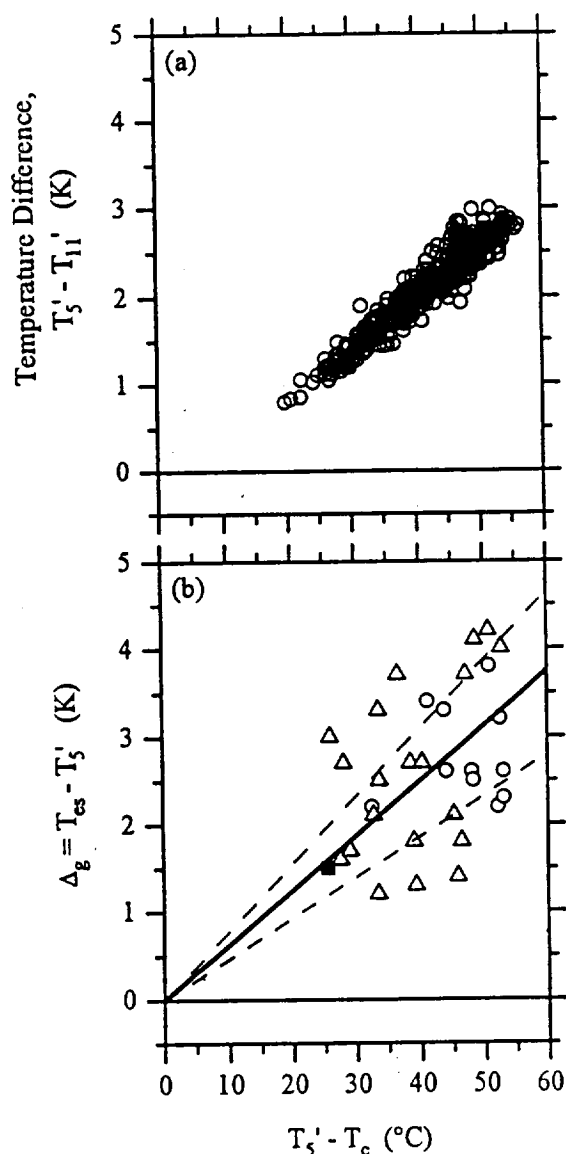


Figure 3. Temperature gradients within the warm calibration source. (a) Temperature difference between the two warm source thermistors plotted against the temperature difference between the warm and cold source temperatures. Since the cold source is at the outside air temperature ( $T_c$ ), the abscissa represents the degree to which the warm source is above ambient.  $T_5'$  and  $T_{11}'$  are the temperatures from housekeeping channels 5 and 11, corrected for the thermistor electronics bias. (b) Thermal gradient temperature bias,  $\Delta_g$ , i.e., the difference in temperature between the emitting surface of the warm source ( $T_{cs}$ ) viewed by the interferometer and  $T_5'$ . The open circles were derived from the supplemental calibrations using a third calibration source, the solid square is from the laboratory test performed by the University of Denver, and the open triangles are from the analysis using the secant method [Walden, 1995]. The solid line is a linear regression fit of the data forced through the origin [ $\Delta_g = 0.062(T_5' - T_c)$ ]. The dashed lines indicate the uncertainty in the best fit slope, which is  $\pm 25\%$ .

At the shortwave and longwave ends of the interferometer's bandwidth ( $550\text{--}750\text{ cm}^{-1}$  and  $1300\text{--}1667\text{ cm}^{-1}$ ) the Quantic source is not a good proxy for the UD sources because the emissivity may be sensitive to the paint thickness; the emissivities of the nongrooved plates in these spectral regions are quite different.

In these spectral regions the emissivity of the UD sources is determined in the following way, using monthly supplemental calibration data taken with a third infrared source, a conical cavity constructed by the University of Wisconsin (hereinafter referred to as the WI source). (The three thermistors used in the WI source had been calibrated to a NIST temperature reference.) The instrument response function given by Revercomb *et al.* [1988] is determined as

$$r = \frac{|C_i' - C_j'|}{L_i - L_j} \quad (7)$$

where  $i$  and  $j$  can represent either the UD sources ( $w$  and  $c$ ) or a series of measurements made with the WI source at different temperatures. Under the assumption that the ambient and instrument temperatures remain constant during the measurement sequence using each experimental setup, equation (4) can be substituted into equation (7) to obtain

$$\beta = r\epsilon = \frac{|C_i' - C_j'|}{B(T_i) - B(T_j)} \quad (8)$$

The quantity  $\beta$  can be determined by using either the two UD sources ( $\beta_{UD}$ ) or the WI source ( $\beta_{WI}$ ). The ratio,  $\beta_{UD}/\beta_{WI}$ , yields the ratio of the spectral emissivities of the sources,  $\epsilon_{UD}/\epsilon_{WI}$ . Here  $\epsilon_{WI}$  is assumed to be 0.9956 independent of wavenumber, as measured at the University of Wisconsin (R. O. Knuteson, personal communication, 1994), and thus  $\epsilon_{UD}$  is determined.

Figure 4 shows the spectral emissivity of the Quantic source and the calibration sources used in this study. The emissivity of the calibration sources is generally between 0.97 and 0.99 but has significant features at  $600$ ,  $1600$ , and  $1650\text{ cm}^{-1}$ . Accounting for these spectral features improves the agreement between the calibrated radiances and radiative transfer calculations described below.

#### 4.3 Calibrated Spectra

Figure 5 shows the calibrated spectra for the six comparison test cases. The contributions of several greenhouse gases are distinctly visible as a result of the small amount of atmospheric water vapor. The  $667\text{ cm}^{-1}$  band of carbon dioxide is bounded by the atmospheric window region at  $800\text{--}1200\text{ cm}^{-1}$  and by the rotational band of water vapor at wavenumbers  $\nu < 600\text{ cm}^{-1}$ . The

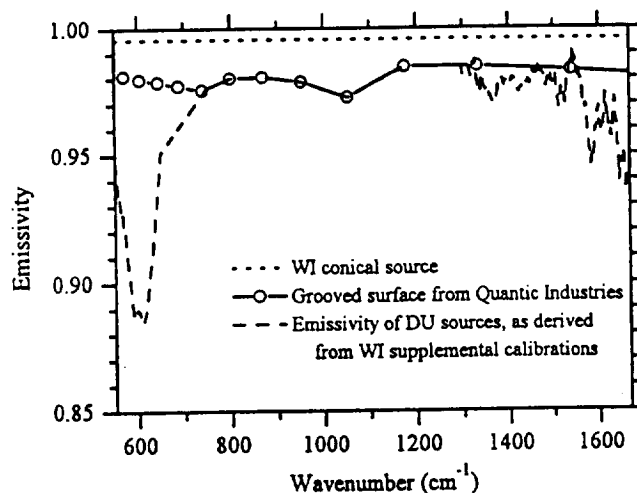


Figure 4. Spectral emissivities of the calibration sources.

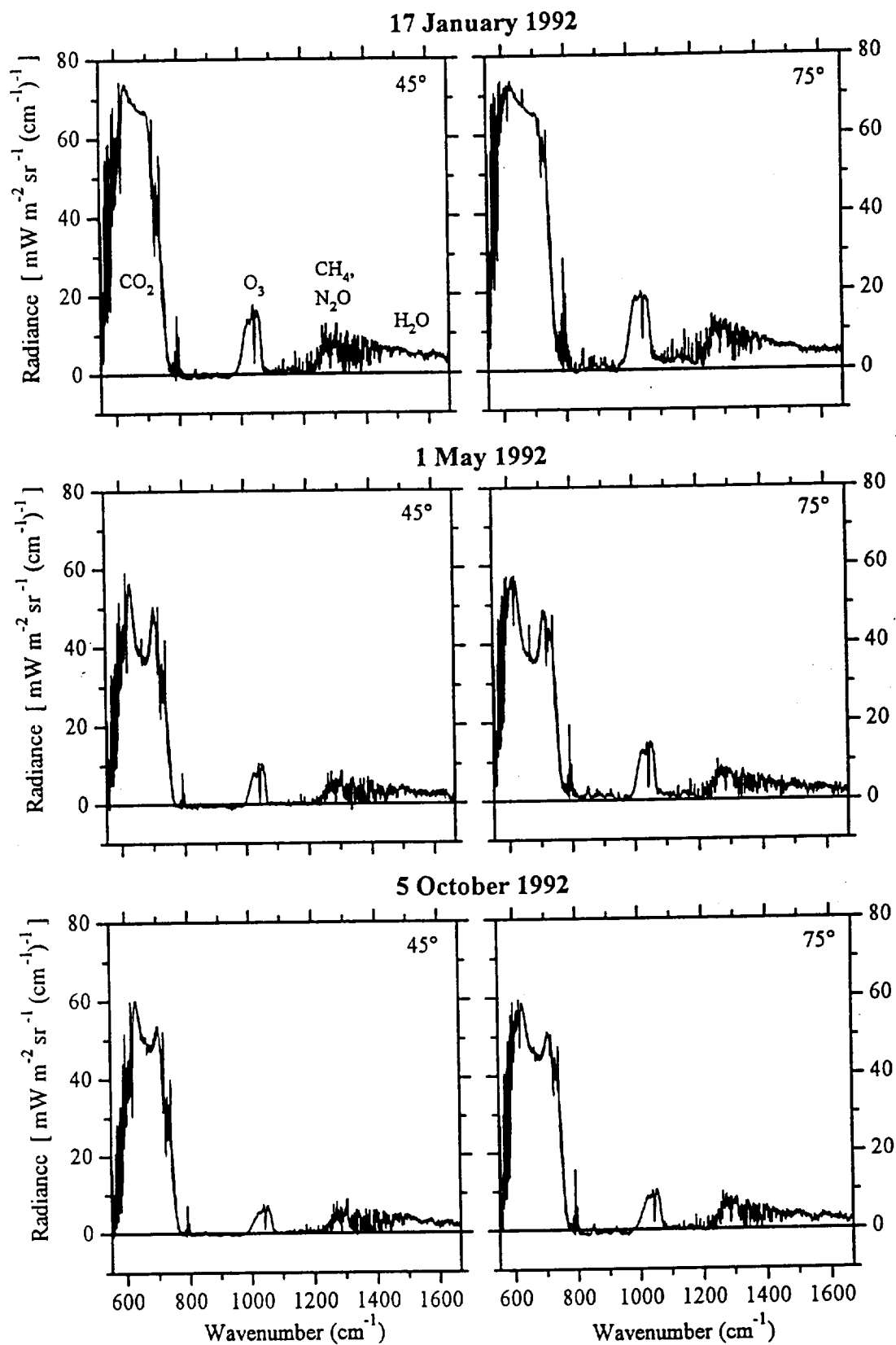


Figure 5. Calibrated radiances for the six test cases. The viewing zenith angles are 45° and 75° for the 3 selected days.

effect of the strong near-surface temperature inversion in winter (May) and spring (October) is most prominent in the center of the carbon dioxide band. Between 800 and 1200  $\text{cm}^{-1}$ , emission from the water vapor continuum is very small. The 1042- $\text{cm}^{-1}$  ozone band stands out in the middle of the window region. Methane and nitrous oxide have emission bands around 1275  $\text{cm}^{-1}$ , and the 1600- $\text{cm}^{-1}$  (6.3  $\mu\text{m}$ ) band of water vapor is visible at  $\nu > 1350 \text{ cm}^{-1}$ .

The total downward infrared fluxes, as measured by a pyrgeometer near the times of the spectral radiance measurements, are given in Table 1.

#### 4.4 Radiance Uncertainties

Variables entering the calibration equations ((2), (3), and (4)) must be assessed for how their uncertainties propagate to uncertainty in the calibrated radiances. The interferometric measurements ( $C_w$ ,  $C_s$ ,  $C_c$ ) are subject to inherent instrument noise associated with the detector and its electronics, which when converted to radiance units is called the noise equivalent spectral radiance (NESR). Radiance errors from the calibration sources ( $L_w$  and  $L_c$ ) are due to uncertainties in the temperatures ( $\sigma_T$ ) and emissivities ( $\sigma_e$ ) of the emitting surfaces. The total estimated radiance error  $\sigma_L$  is given as

$$\sigma_L^2 = \sigma_{LT}^2 + \sigma_{Le}^2 + \text{NESR}^2, \quad (9)$$

where we use  $\sigma_{LT}$  and  $\sigma_{Le}$  for the radiance uncertainties due to temperature and emissivity uncertainties. All the quantities have units of radiance. There is additional error associated with the thermal stability of the interferometer, but on the 3 days used in this study this error is negligible compared with those listed in equation (9).

To determine  $\sigma_{LT}$ , we first estimate the temperature uncertainties in the warm and cold calibration sources,  $\sigma_{Tw}$  and  $\sigma_{Tc}$ . The sky radiance is computed from a calibration using the standard temperatures,  $T_w$  and  $T_c$ , and from another calibration using  $T_w - \sigma_{Tw}$  and  $T_c + \sigma_{Tc}$ . The difference between these two radiances is taken as an estimate of the maximum radiance error due to temperature, since if both  $\sigma_{Tw}$  and  $\sigma_{Tc}$  were added or subtracted from their respective temperatures, the radiance error would be less than that for the case described.

The dominant contributor to  $\sigma_{Tw}$  is the uncertainty in the thermal gradient temperature bias,  $\Delta_g$ , for the warm calibration source. The uncertainty in  $\Delta_g$  is proportional to the uncertainty in the slope shown in Figure 3b and also depends on the temperature difference  $\Delta T$  between the warm and cold sources, i.e., between the warm source and ambient air. The farther the warm source is above ambient, the larger  $\Delta_g$  and its uncertainty;  $\sigma_{Tw}$  increases from 0.4°C at  $\Delta T = 25 \text{ K}$  to 0.8°C at  $\Delta T = 55 \text{ K}$ .

The uncertainty in the cold source temperature,  $\sigma_{Tc}$ , depends on both the uncertainty given by the manufacturer for individual thermistors and the uncertainty in the thermistor electronics bias correction. The manufacturer's uncertainty dominates at low temperatures ( $< -50^\circ\text{C}$ ); the uncertainty ( $1\sigma$ ) for these thermistors (YSI 44002) increases from about 0.1°C at 0°C to 0.2°C at  $-80^\circ\text{C}$ . At high temperatures ( $> -30^\circ\text{C}$ ), the uncertainty in the thermistor electronics bias dominates.

The radiance error due to temperature uncertainties,  $\sigma_{LT}$ , is shown in Figure 6a for the worst (January 17 at  $45^\circ$ ) and best (May 1 at  $75^\circ$ ) error conditions of the six spectra shown in Figure 5. It is largest in the spectral regions where the absolute radiance is small, i.e., where the atmosphere is relatively transparent. This is because errors in the derived sky radiance induced by the errors in the calibration sources are greater when extrapolated to lower

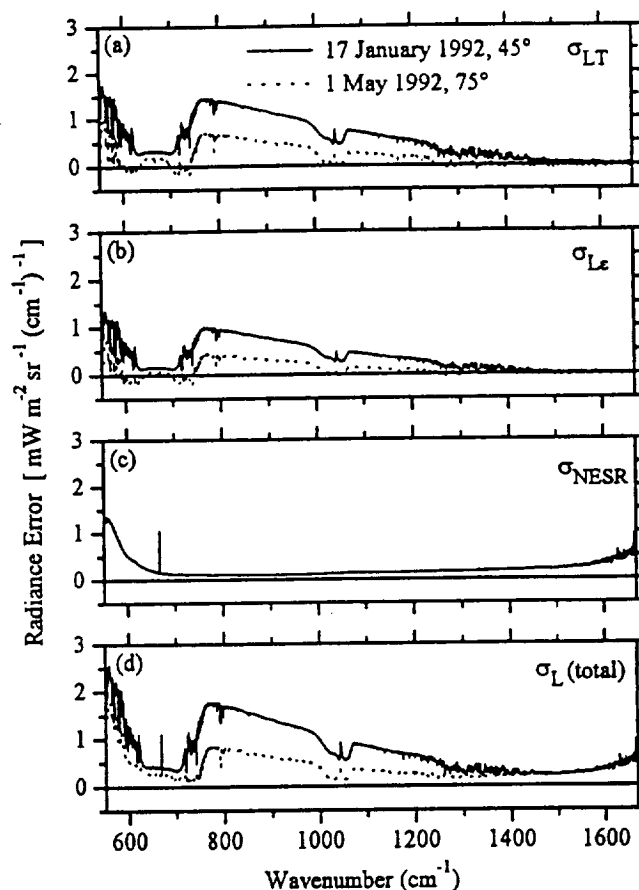


Figure 6. Estimated radiance errors for two of the calibrated spectra shown in Figure 5. The various panels represent contributions to the radiance error listed in equation (9). Here  $\sigma_{NESR}$  is identical for January 17 and May 1.

radiance values. This situation is especially true in summer when the calibration source temperatures are relatively higher than they are in winter when compared with the brightness temperature of the sky.

The radiance error due to the uncertainty in the calibration source emissivities is determined by taking the difference in radiance between a calibration using  $\epsilon$  and a calibration using  $\epsilon + \sigma_e$ . A generous estimate of  $\sigma_e$  is used here;  $\sigma_e = \pm 0.015$ . The corresponding radiance error  $\sigma_{Le}$  is shown in Figure 6b.

The NESR was determined by Walden [1995]; it is significant primarily at the limits of the interferometer's bandwidth (Figure 6c), as a result of the roll-off of the instrument response. The chosen bandwidth of the instrument restricts the NESR to an acceptable level for this study.

The total radiance error (Figure 6d) shows generally the same spectral characteristics as  $\sigma_{LT}$  and  $\sigma_{Le}$ . The radiance error due to temperature uncertainty  $\sigma_{LT}$  constitutes most of the total error, but  $\sigma_{Le}$  provides a sizable contribution. The effect of the NESR becomes significant at the ends of the instrument's bandpass and dominates at high wavenumbers.

#### 5. Specification of Atmospheric Composition and Structure

Model atmospheres are constructed for the times that spectral radiance was measured on January 17, May 1, and October 5. The



trace gases included in our model atmospheres are water vapor, carbon dioxide, ozone, methane, nitrous oxide, oxygen,  $\text{CCl}_3\text{F}$  (CFC-11), and  $\text{CCl}_2\text{F}_2$  (CFC-12). They are included either because they are major infrared emitters in the atmosphere (water vapor, carbon dioxide, ozone, methane, nitrous oxide) or because their concentrations are readily available at South Pole Station (CFC-11, CFC-12). The values are summarized in Table 1 along with other information about the three selected test cases. Detailed information on each model atmospheric profile and their associated uncertainties is given by Walden [1995].

To select times when the sky conditions were most clear, we consult the visual sky observations made by the SPWO and by Warren. Clouds were detected at night when they were illuminated by moonlight or, in the absence of moonlight, by their obscuration of familiar stars. Slight diamond dust was observed by Warren in the interferometer's field of view on May 1 but not on January 17 and October 5. Sunlight was available for the observations on January 1 and October 5. Both the Sun and the moon were below the horizon on May 1.

### 5.1 Temperature

The temperature profiles in the near-surface layer, from the surface (2.8 km above sea level) to 4 km, were obtained from SPWO radiosondes, corrected for thermal lag of the radiosonde's thermistor by the method of Mahesh *et al.* [1997]. The uncertainty in this correction depends upon how rapidly the temperature structure changes with altitude and is therefore greater in winter ( $\pm 0.6^\circ\text{C}$ ) than in summer ( $\pm 0.2^\circ\text{C}$ ). Another concern is the temporal constancy of the temperature within the inversion layer, since the temperatures were not measured coincidentally with the spectral radiances; the times of the FTIR measurement and the radiosonde launch are shown in Table 1. For May 1 the uncertainty is estimated to be  $0.6^\circ\text{C}$ , and  $0.9^\circ\text{C}$  for October 5 [Walden, 1995]. The total uncertainty in the near-surface temperature profile is obtained by combining the two uncertainties discussed above with the inherent temperature uncertainty ( $\pm 0.5^\circ\text{C}$ ) given by the manufacturer of the sonde (Atmospheric Instrumentation Research, Inc., Boulder, Colorado). For the near-surface layer these are  $\pm 0.5^\circ\text{C}$ ,  $\pm 1.0^\circ\text{C}$ , and  $\pm 1.2^\circ\text{C}$  for January 17, May 1, and October 5.

The temperature profiles above 4 km are derived from the SPWO radiosonde data and data from the cryogenic limb array etalon spectrometer (CLAES) and the Halogen Occultation Experiment (HALOE) aboard the UARS [Roche *et al.*, 1993; Russell *et al.*, 1993; Hervig *et al.*, 1995]. The radiosondes for our three case studies reached altitudes of about 30 km. The temperature uncertainty between 4 and 30 km is set to  $\pm 0.5^\circ\text{C}$ , the manufacturer's estimate. Temperatures between 30 km and 60 km were obtained from the UARS data archive at the Distributed Active Archive Center (DAAC) at Goddard Space Flight Center. The time reference data product (3AT) was used. The retrieved temperatures from CLAES have better accuracy ( $1^\circ\text{--}2^\circ\text{C}$ ) than those from HALOE ( $2^\circ\text{--}5^\circ\text{C}$ ) and are therefore used whenever available. Only data with positive quality values are used, meaning that the data are based on actual atmospheric measurements rather than climatology. Even though the UARS instruments view only to a maximum southern latitude of  $80^\circ\text{S}$ , the temperatures from the radiosondes generally agree with those from UARS, where they overlap, to within the estimated uncertainties at the  $2\sigma$  level. This agreement is found as well for water vapor and ozone discussed below.

The temperature profiles for the three model atmospheres are shown in the first two columns of Figure 7; the second column shows the near-surface layer with an expanded vertical scale. The atmosphere is warmest at all altitudes on January 17. By May 1 the stratosphere has cooled as a result of the lack of sunlight. In October the temperatures between 14 and 17 km are below 195 K, cold enough for the formation of type I PSCs. The near-surface temperature structure on January 17 shows a small surface-based inversion, indicating that solar heating of the surface is not providing enough energy to compensate for the loss of longwave radiation. On May 1 with no Sun, and October 5 with low Sun, the surface-based inversion is well developed.

### 5.2 Water Vapor

Water vapor is an extremely important atmospheric constituent, but it is the least well known of the gases measured at South Pole and used in this study. The tethered kite experiments described by Mahesh *et al.* [1997] are used to gain insight into the water vapor content of the near-surface atmosphere. Despite the fact that the carbon hygrometers used for these tests were calibrated only down to  $-40^\circ\text{C}$ , the data suggest that the relative humidity with respect to ice ( $\text{RH}_i$ ) is close to saturation in the near-surface layer. In fact, Schwerdtfeger [1970; 1984] took the frequent occurrence of diamond dust ice crystals as evidence that the lower atmosphere must be at least saturated with respect to ice. On the basis of the tethered hygrometer data we assume that the near-surface inversion layer is saturated with respect to ice, and we bound the atmospheric relative humidity (with respect to ice) in this layer with a range of 90–110%.

Tropospheric humidity was measured by three different instruments: carbon hygrometers used routinely by the SPWO, two frost-point hygrometers launched by NOAA, and capacitive-type Vaisala Humicaps that were packaged with the frost-point hygrometers and ozonesondes. Like the carbon hygrometers the Humicaps are calibrated only down to  $-40^\circ\text{C}$ . The frost-point hygrometers are designed to measure stratospheric humidities and thus are tuned for low absolute humidities (S. J. Oltmans, personal communication, 1993).

On the basis of a small set of intercomparisons between these various instruments it is impossible to draw firm conclusions about the variability of tropospheric humidity. However, the data suggest that the troposphere can be either near saturation or substantially subsaturated in the winter [Walden, 1995]. Because there is no agreement between the SPWO carbon hygrometer and the Vaisala Humicap, some judgment is needed in specification of humidity for the model atmospheres, taking into account the atmospheric processes occurring over the Antarctic Plateau. For all three of our model atmospheres,  $\text{RH}_i$  from 4 to 7 km is assumed to be  $75\% \pm 25\%$ .

The microwave limb sounder (MLS) and HALOE instruments from the UARS are used here to provide water vapor information from about 30 to 60 km, or 100 to 0.1 mbar. Comparisons between MLS data and the two NOAA-CMDL frost-point hygrometers launched from South Pole in 1992 are very good despite the fact that the UARS data are for lower latitudes [Walden, 1995].

Figure 7 (right) shows the humidity profiles for the three model atmospheres. In all cases the troposphere is more humid than the upper atmosphere. The May and October cases have less water vapor in the near-surface layer and the troposphere because of the extreme low temperatures. The total column amount is 1 mm of

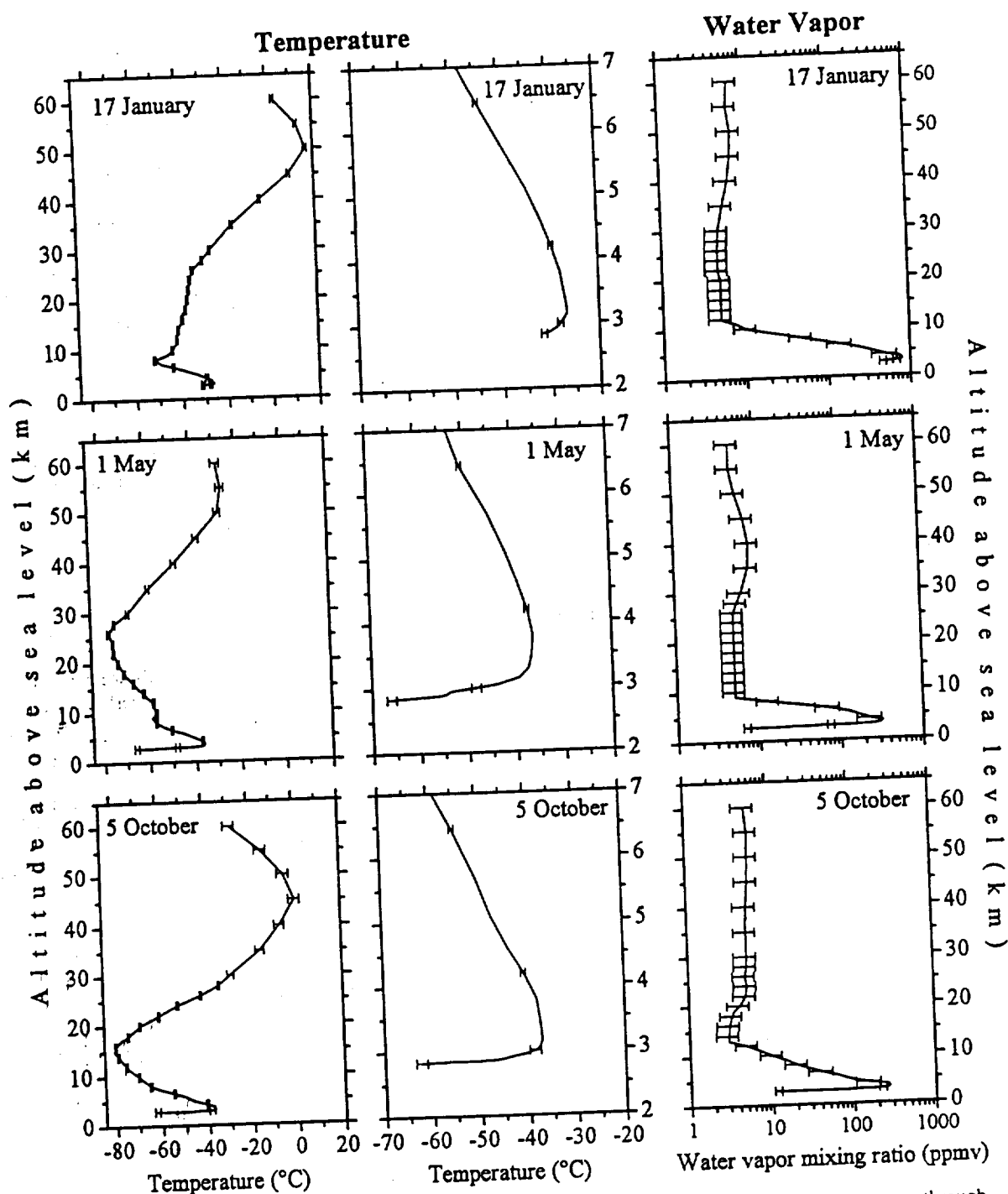


Figure 7. Vertical temperature and humidity profiles for the three model atmospheres: (left) temperature through the entire atmosphere; (middle) temperature in the first 4 km above the surface, and (right) water vapor profiles for the entire atmosphere. Error bars are discussed in the text.

precipitable water on January 17, and 0.3 mm for May 1 and October 5.

### 5.3 Other Gases

Air samples were collected in flasks and analyzed for  $\text{CO}_2$  by NOAA-CMDL [Komhyr et al., 1983, 1985; Thoning et al., 1987]. The values on January 17, May 1, and October 5 were 353.5, 353.5, and 355.0 ppmv, respectively. These mixing ratios are used at all altitudes in the model atmospheres, since  $\text{CO}_2$  is well mixed in the troposphere and stratosphere. As a conservative esti-

mate of the uncertainty we used 2 ppmv, the range of the seasonal cycle.

Ozone profiles were obtained from 68 ozonesondes launched by NOAA-CMDL in 1992, approximately once per week through most of the year but once every 3 days in spring. To specify ozone profiles for the model atmospheres, we interpolate linearly in time between the measured profiles. Since the ozonesondes typically rise only to about 30 km, ozone amounts for 30–60 km are obtained from MLS (205-GHz channel), CLAES (780- $\text{cm}^{-1}$  channel), and HALOE. Overlap of the sonde data with the satellite

data was excellent on January 17 (MLS) and May 1 (CLAES) and good on October 5 (HALOE). For these 3 days, the integrated ozone profiles agree to within 5% with the total ozone reported by CMDL's Dobson spectrophotometer at South Pole and the total ozone mapping spectrometer aboard the Nimbus 7 satellite.

The ozone profiles for the three model atmospheres are shown in Figure 8. On October 5, severe depletion is seen between 12 and 18 km, coincident with the low temperatures in this region. The total column ozone amounts for January 17, May 1, and October 5 are 287, 247, and 147 Dobson units (DU).

Methane mixing ratios at the surface were obtained by analyzing flask samples [Steele *et al.*, 1987; Lang *et al.*, 1990a,b], col-

lected approximately once per week during 1992. Nitrous oxide mixing ratios at the surface were also measured by CMDL (J. Butler, personal communication, 1995). Profiles of tropospheric methane and nitrous oxide were not available, so their mixing ratios from the surface to 10–15 km were set equal to the monthly average surface values. Their seasonal cycles were used to estimate the uncertainty in the mixing ratios in the troposphere, about 30 ppbv for methane and 1 ppbv for nitrous oxide. These uncertainty values were doubled between 10 and 15 km, where it was necessary to match the surface values to UARS data in some cases. Methane above 15 km was obtained from CLAES in January and May and HALOE in October. Concentrations of nitrous

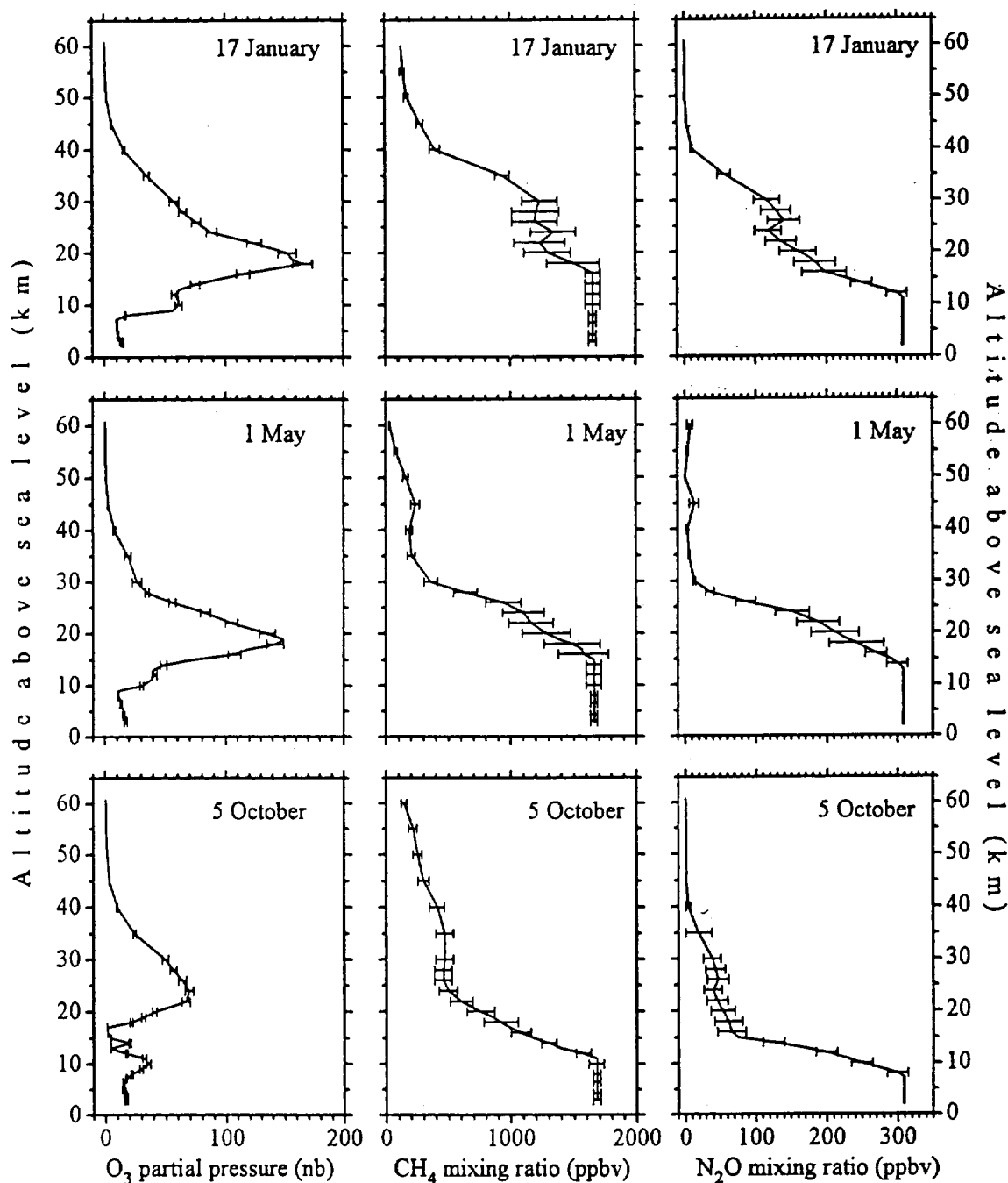


Figure 8. Vertical profiles of ozone, methane, and nitrous oxide for the three model atmospheres. Error bars are discussed in the text.

oxide for the January and May cases came from CLAES. Nitrous oxide data were not available for October 5, so the values above 15 km were set to one third the value of the CLAES data from January 17 in rough agreement with data from Figure 6 of Randall *et al.* [1994]. The estimated relative uncertainty for October 5 is double that of the January case. Figure 8 shows the vertical profiles of methane and nitrous oxide used in the model atmospheres.

The chlorofluorocarbons, CFC-11 and CFC-12, were included in a manner similar to that for  $\text{CH}_4$  and  $\text{N}_2\text{O}$ . Their mixing ratios at the surface were measured by CMDL. The monthly average surface values were used up to about 15 km: about 266 pptv for CFC-11 and 495 pptv for CFC-12. Data from CLAES for January 17 were used above 15 km for all three test cases, since data were not available for May 1 and October 5. Sensitivity studies showed that the downward radiance is insensitive to the uncertainty in the stratospheric concentration but that it is important to specify the observed decrease in concentration above 15 km.

Oxygen was also included to account for its weak emission band from 1390 to 1760  $\text{cm}^{-1}$ . Its mixing ratio was set to 20.95% by volume [Goody and Yung, 1989].

$\text{CCl}_4$  was not included because its contribution to emission at 790  $\text{cm}^{-1}$  appears to be within the estimated radiance uncertainty.  $\text{HNO}_3$  was not included because its tropospheric concentration was not measured at South Pole.

## 6. Radiative Transfer Calculations

### 6.1 Line-By-Line Radiative Transfer Model

This model (LBLRTM) was developed for the ARM program [Clough *et al.*, 1992] and has become a standard in the atmospheric radiation community. It is a vectorized version of FASCOD3 [Clough *et al.*, 1989b] and is used here to calculate radiance in a vertically inhomogeneous, but horizontally homogeneous, atmosphere. Clough *et al.* [1992] described the numerical techniques and approximations used to implement the radiative transfer equation in LBLRTM and also compared its output with another LBL model that was used in the ICRCCM study. LBLRTM has also been compared with accurate spectral radiance measurements taken at midlatitudes [Clough *et al.*, 1989a; 1992]. Example calculations were given by Clough *et al.* [1992] and Clough and Iacono [1995]. Version 3 of LBLRTM, released in April 1996, is employed here in conjunction with the 1992 version of the high-resolution line parameter (HITRAN) database [Rothman *et al.*, 1992].

The input to LBLRTM is provided by the model atmospheres described above. The specified wavenumber range in LBLRTM exceeds the bandwidth of the UD interferometer by at least 25  $\text{cm}^{-1}$ . The zenith angle is set to the value of the angle readout given by UD's interferometer after being adjusted slightly for the measured tilt of the roof upon which the interferometer was mounted. The observation height specified within LBLRTM is 10 m above the surface, because the interferometer occupied a rooftop location 10 m above the surrounding snow surface. The maximum height and vertical resolution of the model atmospheres are specified below. All other values required by LBLRTM are set to the default values; in particular, the line shape calculation uses a Voigt profile that extends to 25  $\text{cm}^{-1}$  from the line centers.

The water vapor continuum is represented by the Clough-Kneizys-Davies (CKD) model, version 2.2. Clough *et al.* [1992] showed the importance of including the self- and foreign-broadening effects of water vapor in a manner consistent with observations. They used the sub-Arctic winter standard atmosphere to

illustrate the particular importance of the foreign continuum for cold atmospheres. The original CKD model [Clough *et al.*, 1989c] has been updated on the basis of comparisons with atmospheric spectral radiance data.

One advantage of using a model for calculating atmospheric radiances is that the full infrared spectrum can be examined, beyond the spectral limits of the measurements. Figure 9 shows radiance calculations for the three model atmospheres at a viewing zenith angle of 45° from 100 to 2000  $\text{cm}^{-1}$  (5 to 100  $\mu\text{m}$ ). In Figure 9a the spectrum is labeled according to contributions from the major radiatively active gases. The radiance is lower in the winter (May 1) and early spring (October 5) than in summer (January 17), because of lower atmospheric temperatures.

The relatively transparent portion of the water vapor rotational band extends from the wing of the carbon dioxide band at 550  $\text{cm}^{-1}$  to around 350  $\text{cm}^{-1}$ . This spectral region is of particular importance to the radiative balance of polar atmospheres. The

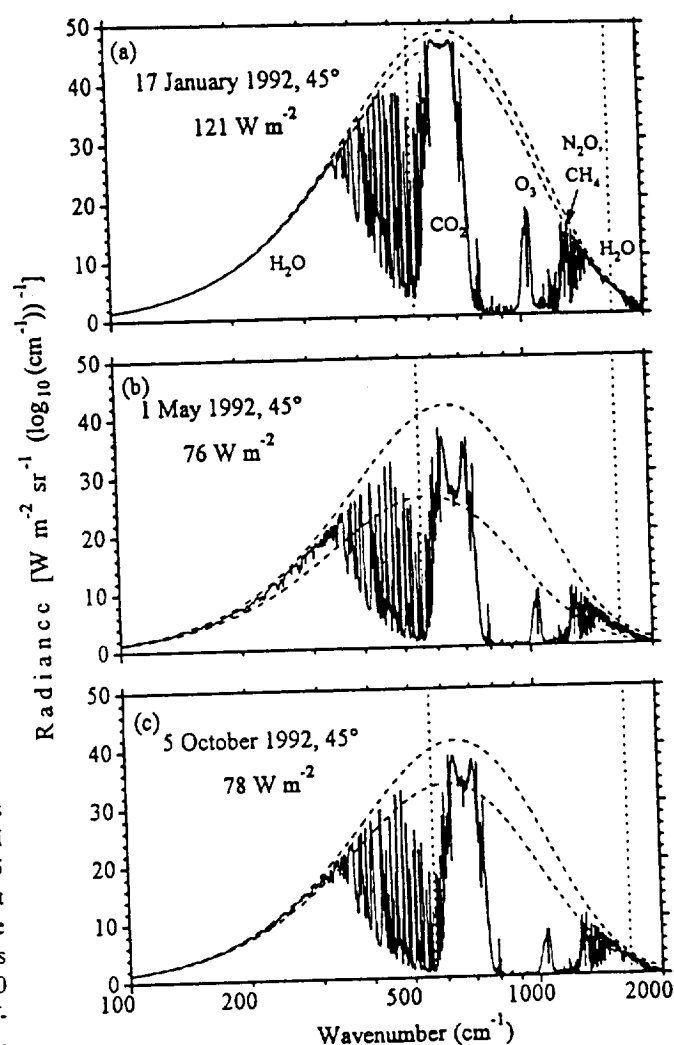


Figure 9. Radiance calculations for the three model atmospheres at a viewing zenith angle of 45° from 100 to 2000  $\text{cm}^{-1}$  (5 to 100  $\mu\text{m}$ ). The vertical dotted lines represent the bandwidth of the measurements obtained by using the UD interferometer. The dashed curves are Planck radiances for the air temperatures at 21 m above the surface (lower curve) and the top of the inversion layer about 1.2 km above the surface (warmer; upper curve). Values are given in the figure for the total downward infrared flux at the surface: they were measured by a pyrgeometer.

emission from the water vapor rotational bands at  $\nu < 350 \text{ cm}^{-1}$  matches a Planck curve well in summer, but not in the winter and spring because of the low water vapor amounts. This fact is somewhat true as well for the vibration-rotation band of water vapor at 1400 to 1600  $\text{cm}^{-1}$ . Even though the atmosphere over the Antarctic Plateau contains at most only 1 mm of precipitable water, and thus emission from the water vapor continuum (between about 600 and 1000  $\text{cm}^{-1}$ ) is small, water vapor is still the primary emitter of thermal radiation to the surface [Walden and Warren, 1994], contributing about two thirds of the total downward flux to the surface. The 667- $\text{cm}^{-1}$  (15- $\mu\text{m}$ ) absorption band of carbon dioxide is important because it is strong and is located near the peak of the Planck function. The near-surface temperature inversion is strongest in May and weakest in January; its effect on the carbon dioxide band is evident. Emission from ozone at 1042  $\text{cm}^{-1}$  is maximum in January; it is lower in May because of low stratospheric temperatures, and even lower in October because of reduced ozone abundance. The emission bands of methane and nitrous oxide around 1100 to 1200  $\text{cm}^{-1}$  are also visible. The  $\text{N}_2\text{O}$  band at 1168  $\text{cm}^{-1}$  contributes in the window region, while emission from both  $\text{CH}_4$  and  $\text{N}_2\text{O}$  overlaps with water vapor between 1200 and 1300  $\text{cm}^{-1}$ .  $\text{CH}_4$  and  $\text{N}_2\text{O}$  are therefore relatively more important in winter, when emission from water vapor is weaker.

The importance of the near-surface air temperature and the various atmospheric window regions is seen by comparing the Planck functions with the spectral radiance. Two Planck functions are plotted: one for the surface air temperature at 2 m and the other for the temperature at the top of the inversion. The peaks of the Planck functions for the January case are centered on the carbon dioxide band, whereas in May and October, when the temperatures are lower, the peaks are on the low-wavenumber side of the band. The carbon dioxide band is relatively more important to the surface energy budget in Antarctica than at other terrestrial locations both for this reason and also because emission from water vapor is small and therefore has little overlap with the  $\text{CO}_2$  band.

The radiance values between the vertical dotted lines in Figure 9 constitute the standard model calculations used throughout this paper because this is the wavenumber region measured by the interferometer. The comparisons discussed below represent the most variable and perhaps most interesting portion of the infrared spectrum, but they do not provide a check on the emission from water vapor at low ( $< 550 \text{ cm}^{-1}$ ) and high ( $> 1667 \text{ cm}^{-1}$ ) wavenumbers.

## 6.2 Matching Calculations to Measurements

To compare spectral radiance observations with the results of a high-spectral-resolution radiative transfer model such as LBLRTM, it is necessary to account for the finite field of view (FOV) of the interferometer and also to match the spectral resolution of the calculations to that of the observations. Steel [1964] and Bell [1972] discuss such corrections in general terms. The discussions by Clough *et al.* [1989a] and Smith *et al.* [1989] apply this theory to comparisons of LBL calculations with interferometric measurements of atmospheric radiance and transmission. In this study, LBLRTM calculations are converted to spectra suitable for comparisons with observed spectral radiances by using the following procedure. LBLRTM calculates a spectrum at its own internal spectral resolution, which is about 0.001  $\text{cm}^{-1}$ . An interferogram is generated from the calculated spectrum, then apodized by using the Hann-window function [Press *et al.*, 1992]. (This apodization function was also applied to the measured interferograms, and for proper comparisons it is necessary to apply the

same apodization function to the calculations.) This interferogram is used to interpolate the spectrum to a wavenumber spacing of 0.01  $\text{cm}^{-1}$ , much finer than the wavenumber grid of the transformed apodized interferogram. This procedure is all done within LBLRTM. The resulting calculated spectrum now matches the spectral resolution of the radiance measurements. A FOV correction [Walden, 1995] is applied by using trapezoidal integration to perform the integral over field of view,

$$L_{\text{LBL}}(\nu') = \int_0^1 \frac{w(\mu)}{\mu} L_a\left(\frac{\nu}{\mu}\right) d\mu \quad (10)$$

where  $L_a$  is the apodized version of the calculated spectrum. The variable of integration,  $\mu$ , is the cosine of the angle  $\theta$  measured from the center of the FOV. The outer limit of the FOV is at  $\theta = \theta_m$ . The weight  $w(\mu)$  is set to the constant value of 1.0 from  $\mu = 0.9996$  ( $\theta_m = 1.5^\circ$ ) to  $\mu = 1$  and set to zero elsewhere. Sensitivity studies show that the calculated spectra described in this study are insensitive to reasonable assumptions about the shape of the FOV and uncertainty in the choice of  $\theta_m$ . Finally, the oversampled, field-of-view-corrected, calculated spectrum is linearly interpolated from its fine wavenumber grid to the coarser grid of the measurements, allowing  $L_{\text{LBL}}$  to be directly compared to  $L_s$  from equation (2).

Before the correction was applied, there were large differences between the observed spectra and the LBLRTM calculations where the spectrum varied rapidly, notably in the wings of the  $\text{CO}_2$  band near 600 and 750  $\text{cm}^{-1}$ . The FOV correction greatly reduced these differences.

The radiances supplied to the ICRCCM project by Walden *et al.* [1997] differ slightly from those reported here in two ways. First, Walden *et al.* [1997] re-calibrated the radiance measurements by adjusting the temperatures of the calibration sources [ $T_w - n \cdot \sigma(T_w)$  and  $T_c + n \cdot \sigma(T_c)$ ], choosing a value of  $n$  as necessary to eliminate most of the negative radiances in the atmospheric window regions:  $n = +1$  for Jan 17 ( $45^\circ$ ), 0 for Jan 17 ( $75^\circ$ ),  $+1$  for May 1 ( $45^\circ$ ), 0 for May 1 ( $75^\circ$ ),  $+1$  for Oct 5 ( $45^\circ$ ),  $+2$  for Oct 5 ( $75^\circ$ ). Second, Walden *et al.* [1997] chose to remove the effect of the FOV from the measurements rather than incorporate it into the calculations. This was done by adjusting the wavenumber scale of the original measurements,  $\nu$ , by  $\nu' = \nu / (\cos \theta_m)$ . This corrects for the wavenumber shift caused by off-axis rays in the interferometer, but does not account for the slight spectral smearing; both effects are described by Bell [1972].

## 7. Uncertainties in the Calculated Radiances

There are many possible sources of error in the LBLRTM calculations. These include uncertainties in the specification of the model atmosphere, the database of absorption line parameters (HITRAN92), the model's numerical techniques, and the treatment of the physics of infrared emission and absorption. Ellingson *et al.* [1991] briefly discussed the three latter sources, finding that LBL models agree well with each other where accurate spectroscopic data are available (e.g., carbon dioxide), indicating that the different numerical techniques used in the various models were all adequate. However, large uncertainties persist where there are deficiencies in the line parameter data, the theory of gaseous absorption, or the specification of the model atmosphere. The purpose of the following error analysis is to place a lower bound on the radiance error in the model calculations by considering only those sources of error induced by uncertainties in the specification of the model atmosphere and in the viewing zenith angle.

### 7.1 Maximum Height of the Model Atmosphere

The error in calculated radiance caused by truncating the model atmosphere is determined by subtracting the radiance for a 60-km atmosphere from those truncated at 30, 40, or 50 km. These radiance differences are negative, since the emission from a truncated atmosphere is less. The radiance errors for a 30-km atmosphere are significant, especially near the  $1042\text{-cm}^{-1}$  ozone band, where they exceed  $-0.8\text{ mW m}^{-2}\text{ sr}^{-1}(\text{cm}^{-1})^{-1}$ . The errors are seen primarily in spectral regions with weak absorption, where emission can come from throughout the atmosphere. The difference in radiance between a 50-km atmosphere and a 60-km atmosphere is very small (less than  $-0.02\text{ mW m}^{-2}\text{ sr}^{-1}(\text{cm}^{-1})^{-1}$ ), so we judge 60 km to be adequate and use this as the maximum height in all further calculations.

### 7.2 Vertical Resolution and Temperature Structure in the Lowest 300 m

Ideally, an altitude grid can be chosen that adequately represents the near-surface temperature inversion over the plateau in winter, when it is steepest. Model atmospheres with extreme inversions and large zenith angles are most sensitive to changes in the vertical resolution, so it is best to use such cases for choosing the vertical resolution. We chose the October 5 atmosphere at a zenith angle of  $75^\circ$ , since its temperature gradient in the lowest 100 m is the steepest of the three model atmospheres. Several different altitude grids between the surface (2.84 km) and 3.15 km are defined: grids with uniform spacings (10, 20, and 30 m) and a variable grid with spacing varying from 5 to 100 m, increasing with altitude. Between 3.15 and 60 km the grid spacing varies from 150 m to 5 km, gradually increasing with altitude, and is held constant in these sensitivity studies. The appropriate vertical resolution is chosen by successively decreasing the uniform altitude spacing in the near-surface layer until the radiance difference between successive runs is smaller than a specified tolerance. This tolerance is chosen as the radiance error induced by uncertainties in the temperature profile, discussed below.

The calculated radiance is sensitive to vertical resolution mainly in spectral regions that are strongly absorbed; i.e., regions in which most of the measured radiance originated in the inversion layer. The 30-m grid causes significant differences, but the 10-m and 20-m grids give almost identical results. Both still show a difference from the variable grid in the  $\text{CO}_2$  band, but this difference is small in comparison with radiance errors caused by the uncertainty in the specification of the temperature profile, discussed next. The calculations shown below use the variable grid.

### 7.3 Radiance Error Due to Uncertainty in Atmospheric Temperature and Composition

With the vertical resolution and the height of the model atmosphere chosen so that they induce little error in the LBLRTM calculations, the radiance error is now determined by performing sensitivity studies by using the model atmosphere data and their uncertainties. Standard spectral radiance calculations are produced using the profile information presented in Figures 7 and 8. Radiance errors are determined by perturbing, one at a time, an individual profile in the model atmosphere by adding its uncertainty. LBLRTM is then run with this perturbed model atmosphere, yielding a radiance spectrum. The radiance errors are found by subtracting the standard radiance case from that obtained with the perturbed atmosphere. The total radiance error is found by taking the square root of the sum of the squares of the radiance differences due to the various profile perturbations.

The results for January 17 at  $45^\circ$  and May 1 at  $75^\circ$ , representing the warmest and coldest atmospheres at South Pole, are shown in Figure 10. These radiance errors represent the range of errors to be expected for clear-sky calculations with LBLRTM for the Antarctic Plateau. Only the four major sources of error are shown in Figure 10; the errors due to uncertainty in concentrations of carbon dioxide, methane, nitrous oxide, CFC-11, and CFC-12 are all negligible in comparison with those shown. The radiance errors for October 5 are similar to those for May 1. The total radiance error in summer is dominated by uncertainties in the temperature and water vapor profiles. In winter the uncertainty in zenith angle (discussed below) is also a major contributor. The total error in calculated radiance for these cases is comparable to the error in measured radiance shown in Figure 6. However, the spectral structure is different. It should be emphasized that the error estimates for the LBLRTM calculations assume the sky is clear. The visual sky observations were initially used to identify clear test cases, but subvisible clouds and aerosols may still have been present in the actual atmosphere. This possibility is examined below.

The uncertainty in zenith angle is due to many sources, some of which are quantified here and some of which are estimated. The angle readout for the interferometer's mirror assembly was accurate to within a few millivolts, or roughly  $0.1^\circ$ . The tilt of the roof during 1992 was estimated as  $0.4^\circ \pm 0.1^\circ$ . Additional sources of uncertainty included the interferometer being mounted in a non-level position and inaccuracy in calibration of the angle readout (which is ideally set to  $0^\circ$  when viewing vertically and  $90^\circ$  when viewing horizontally). One test indicated that the zenith angle was actually  $73.8^\circ$  at the  $75^\circ$  mechanical mirror stop, an offset of  $1.2^\circ$  if it is assumed that the angle readout was set to exactly the  $75^\circ$  voltage during that test (R. Van Allen, personal communication, 1995). When all these sources of uncertainty are taken into account, a generous estimate of the overall zenith angle uncertainty is  $\pm 1.5^\circ$ .

The radiance errors induced by the uncertainty in the zenith angle are most significant in the wintertime. The largest contributions are primarily in regions where gases have intermediate absorption, i.e., the wings of the carbon dioxide band, the weak bands of carbon dioxide ( $975\text{ cm}^{-1}$ ) and nitrous oxide ( $1168\text{ cm}^{-1}$ ), the ozone band, and methane, nitrous oxide, and water between  $1200$  and  $1500\text{ cm}^{-1}$ . Emission from these regions comes from a long path length in the atmosphere and therefore comes on average from a great distance from the observation point. The farther away the emission region, the greater the change in effective emitting temperature due to a given change in zenith angle (if the temperature varies with height). The radiance error is large in the ozone band because most ozone emission comes from the upper troposphere and lower stratosphere. The zenith angle uncertainty induces much less error in summer because of weaker temperature gradients; the error is confined to the wings of the carbon dioxide band.

The uncertainty in the temperature profile produces radiance errors in spectral regions where emission is from altitudes at which the temperature is changing rapidly and where gases are strongly absorbing. Most of the errors in both summer and winter are from emission within the inversion layer (carbon dioxide and water vapor), but there is also a significant contribution in the ozone band.

The radiance errors due to water vapor and ozone are confined to regions in which they emit radiation. The errors are largest where the uncertainty in the individual profile is greatest. Thus, for water vapor, the errors occur in spectral regions where emis-

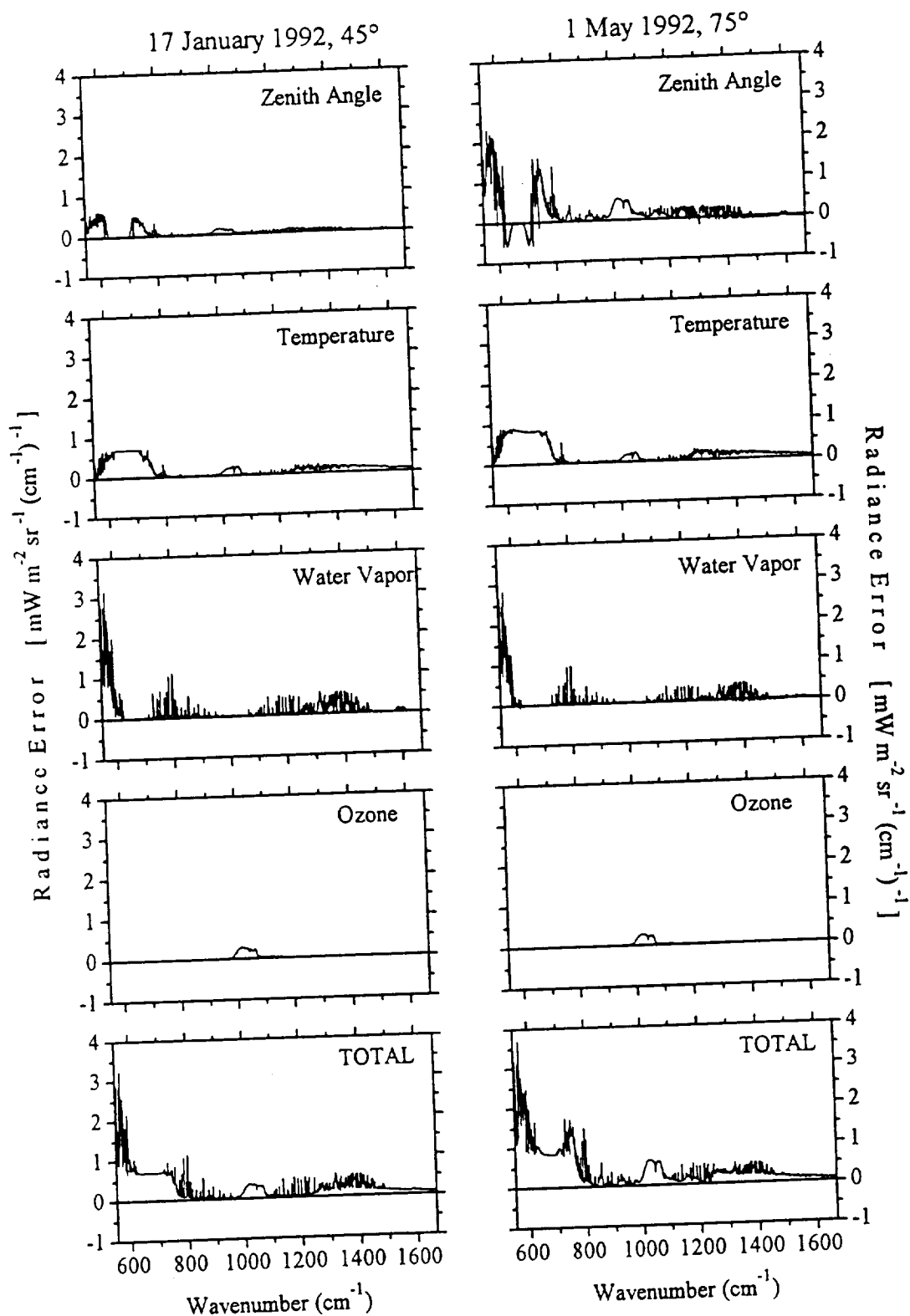


Figure 10. Estimated radiance errors for January 17, 1992, at 45° and May 1, 1992, at 75° based on sensitivity studies using the model atmospheres. The total error is the quadrature sum of the radiance errors induced by the various profile perturbations discussed in the text. The wavenumber range corresponds to the bandwidth of the UD interferometer.

sion is from the free troposphere and stratosphere (above 4 km); i.e., regions of intermediate and weak absorption. LBLRTM is insensitive to changes in water vapor from 625 to 700  $\text{cm}^{-1}$  because of overlap with carbon dioxide. The errors between 550

and 600  $\text{cm}^{-1}$  are large because the Planck function peaks near these wavenumbers and the tropospheric water vapor amounts are quite uncertain. The radiance errors due to uncertainties in ozone concentration are confined to the 1042- $\text{cm}^{-1}$  band.

## 8. Spectral Radiance Comparisons

The measurement and calculation for May 1 at 75° are shown in Figure 11 along with their difference. This case is used for further discussion below, since it is the most extreme model atmosphere in terms of low surface temperature (-66°C), strength of the surface-based temperature inversion (30 K), and low temperatures throughout the atmosphere. Figure 12 shows the radiance differences for all six cases.

The overall agreement between the observations and LBLRTM is good. In absolute radiance, differences are comparable to those reported from SPECTRE [Ellingson and Wiscombe, 1996]. We judge radiance differences to be significant, and requiring explanation, if they exceed twice the estimated combined radiance error from both the measurements and calculations. This situation occurs only in a few spectral regions, discussed below along with a general discussion of the overall comparisons in the following spectral bands: carbon dioxide (550-800  $\text{cm}^{-1}$ ), 11- $\mu\text{m}$  window (800-990  $\text{cm}^{-1}$ ), ozone (990-1070  $\text{cm}^{-1}$ ), 9- $\mu\text{m}$  window (1070-1200  $\text{cm}^{-1}$ ), methane and nitrous oxide (1200-1350  $\text{cm}^{-1}$ ), and water vapor (1350-1500  $\text{cm}^{-1}$  and 1500-1667  $\text{cm}^{-1}$ ). Selected portions of the spectra for May 1 at 75° are plotted in Figure 13 along with the radiance difference and the estimated error in the radiance difference. The error in radiance difference is the square root of the sum of the squares of errors in the measurements and calculations.

### 8.1 Carbon Dioxide

In the carbon dioxide band from 550 to 800  $\text{cm}^{-1}$  (Figures 11 and 12) the agreement is fairly good in all cases. The spurious line at 667  $\text{cm}^{-1}$  often seen in the measurements and in the radiance differences is due to very strong absorption by carbon dioxide where the instrument mostly views its internal temperature. At this frequency the ratio of the difference spectra,  $\gamma$ , is indeterminate; see equations (2) and (3). The spectral structure in the radiance differences between 600 and 725  $\text{cm}^{-1}$ , particularly in May and October when the temperature gradient is large, is probably due to error in specification of the temperature structure and zenith angle. The largest differences in this band are between 550 and 600  $\text{cm}^{-1}$ , shown in Figure 13a. This figure shows that the spectral details in the measurements and calculations agree quite well, giving confidence in the field of view correction and the spectral resolution correction, and indicating that the signal-to-noise ratio is adequate at this end of the interferometer's bandwidth, where the instrument response is dropping rapidly. The large offset between 570 and 600  $\text{cm}^{-1}$  points to a consistent problem in the winter when the calculation is usually larger than the measurement. It is possible that the uncertainty in the calibration source emissivity has been underestimated in this spectral region (see Figure 4). This possibility precludes detection of faults in the radiative transfer model or the spectroscopic data in this spectral region.

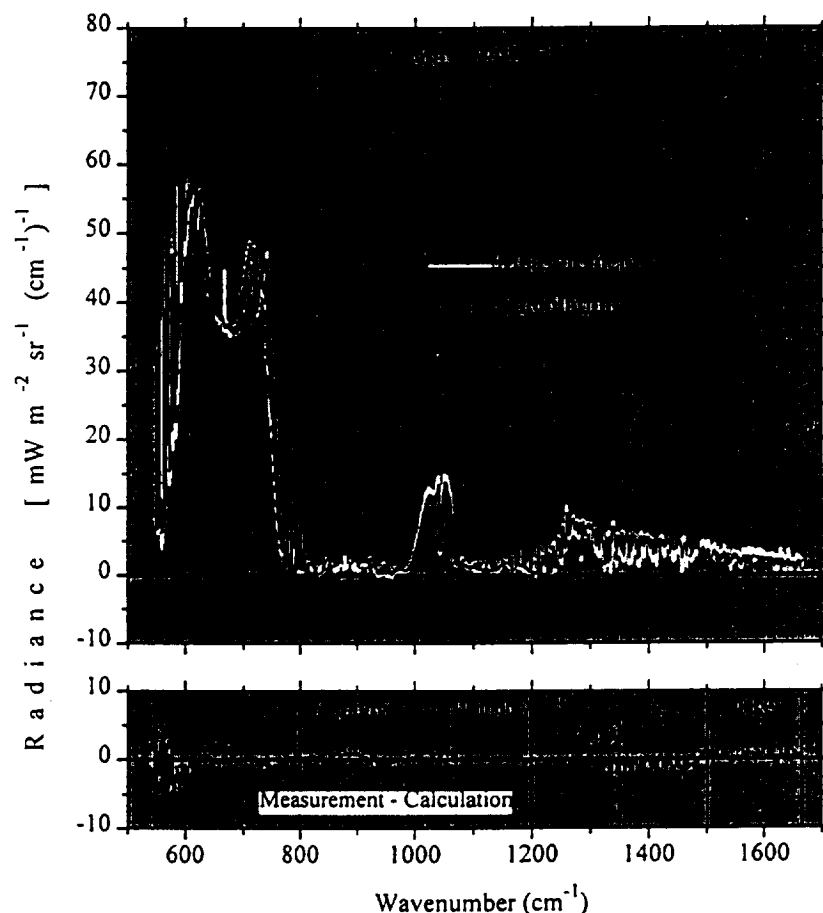


**Figure 11.** Spectral radiance measured by the UD interferometer, compared with LBLRTM calculations for May 1, 1992, at 75°. The lower frame is the radiance difference on the same scale, where the primary infrared emitters in each spectral band are also indicated.



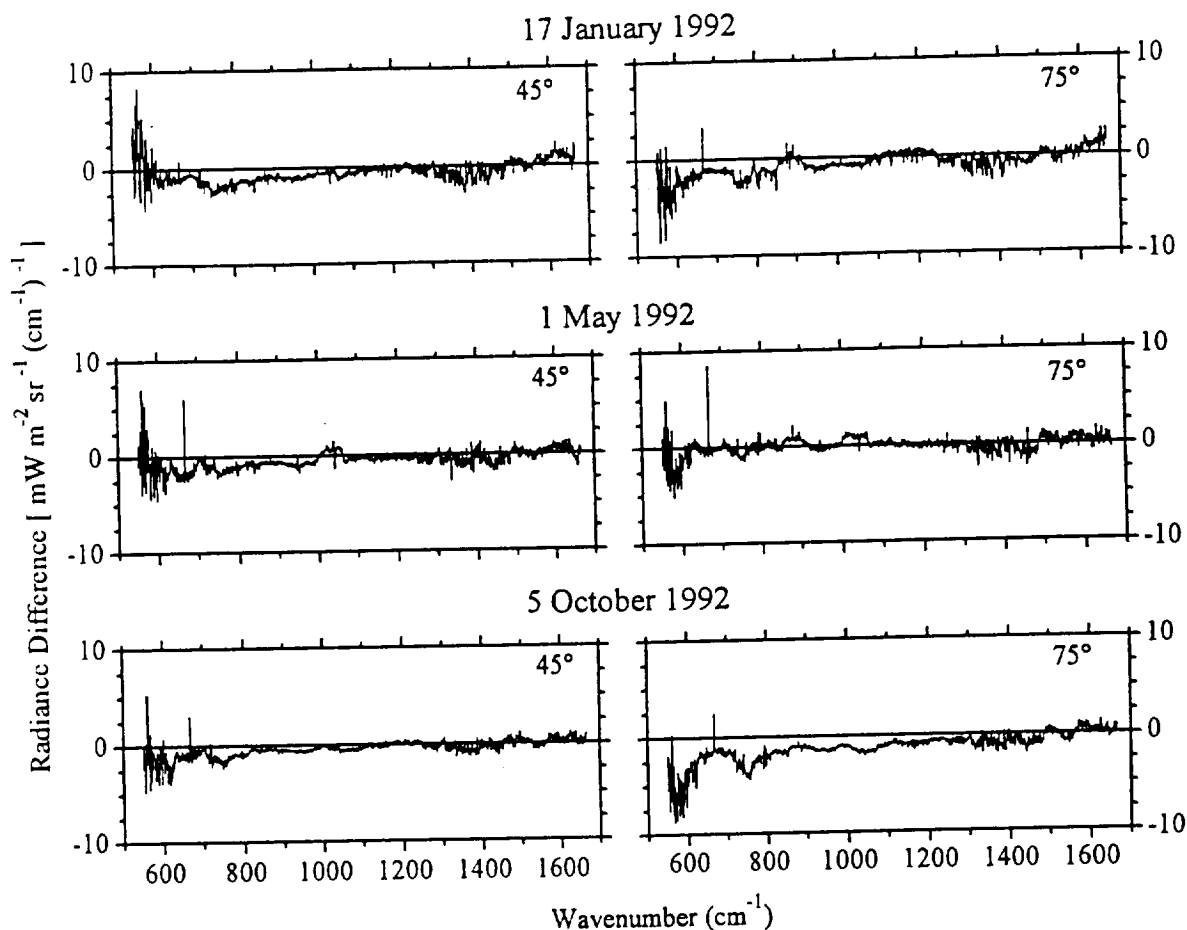


Figure 12. Spectral radiance comparison of LBLRTM calculation with interferometer measurement for the six test cases. The comparisons are shown as radiance differences, measurement minus calculation. The May 1, 1992 case at 75° is the same as the radiance difference shown in Figure 11.

## 8.2 The 11- $\mu$ m Window

The window region is the most transparent portion of the interferometer's bandwidth, and therefore emission from clouds, aerosols, and diamond dust ice crystals are easily detected here. The sky observation for May 1 indicated the presence of diamond dust ice crystals, which is typical for clear skies in winter at South Pole. On October 5, PSCs may have been present over South Pole, since the temperature near 15 km ( $-81^{\circ}\text{C}$ ; Figure 7) was below the threshold (195 K or  $-78^{\circ}\text{C}$ ) at which they are expected to form. Ice crystals and clouds, if present, would cause the measured radiance to exceed the clear-sky calculation, which would give a positive radiance difference (measurement minus calculation). However, the radiance differences plotted in Figures 11 and 12 (and on an expanded scale in Figure 13b) are both positive and negative and not significantly different from zero in this spectral region, suggesting that they are not due to the presence of ice crystals or PSCs. This result is particularly evident in the January and October cases where the calculated radiance exceeds the measured radiance. Since no significant negative radiance differences exist in any of the comparisons, the emission from diamond dust ice crystals and PSCs, if present, is within the estimated error.

In Figure 13b, emissions from CFC-11 and CFC-12 are apparent, as well as water vapor lines. The weak absorption band of carbon dioxide is visible around  $960\text{ cm}^{-1}$ . The radiance difference between 850 and  $900\text{ cm}^{-1}$  is on average larger than other

regions in Figure 13b because nitric acid was not included in the LBLRTM calculation.

## 8.3 Ozone

Ozone emission is seen in Figure 13c. The spectral details correspond well, validating both the HITRAN spectral line parameter data and the FOV and spectral resolution corrections applied to the calculations. The differences seen in Figure 13c are within twice the estimated radiance error. The six comparisons (Figure 12) show no consistent bias in the calculations in relation to the measurements and therefore suggest possible errors in the individual ozone profiles.

## 8.4 The 9- $\mu$ m Window

Ozone and nitrous oxide ( $1168\text{ cm}^{-1}$ ) exhibit weak emission between  $1070$  and  $1200\text{ cm}^{-1}$ , as Figure 13d shows. These Antarctic spectra are ideal for viewing these features, since elsewhere on Earth they are obscured by the water vapor continuum. The radiance differences are generally within the estimated errors.

## 8.5 Methane and Nitrous Oxide

In the portion of the spectrum where nitrous oxide, methane, and water vapor overlap ( $1200$ – $1350\text{ cm}^{-1}$ ) there is good agreement (Figure 13e). The spectral details seen in both the observa-

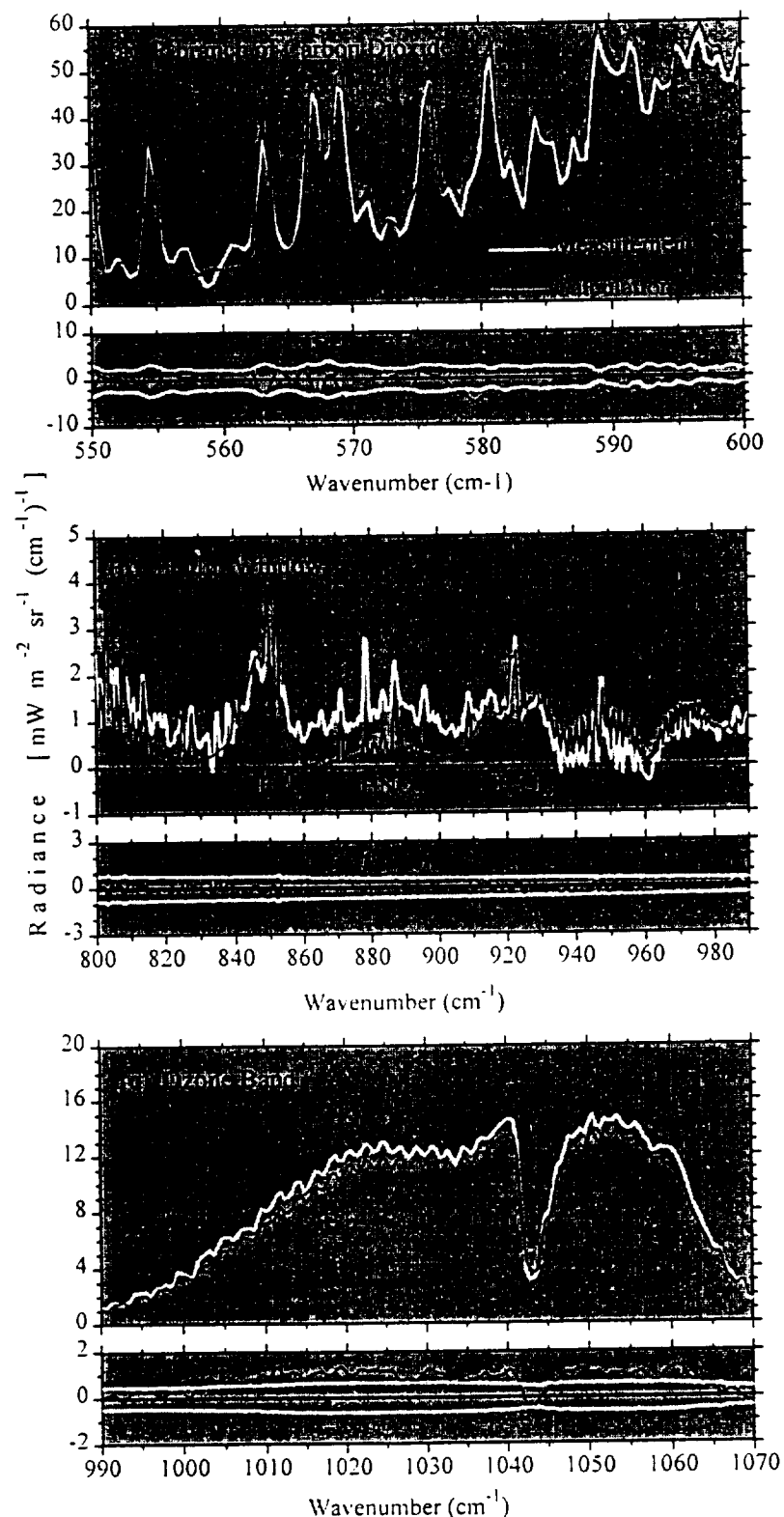


**Figure 13.** Radiance comparisons for May 1, 1992, at 75°. (top) Spectral radiance measured by the DU interferometer plotted with the corresponding LBLRTM calculation; (bottom) Expanded vertical scale of the radiance difference (measurement minus calculation) together with the positive and negative values of the estimated uncertainty in the radiance difference. Each frame displays a different spectral region. Both the horizontal and vertical scales differ from one frame to the next. (a) 550-600  $\text{cm}^{-1}$ . The approximate flux  $F$  in this band is  $4.8 \text{ W m}^{-2}$ , the approximate flux difference (measurement minus calculation)  $\Delta F$  is  $-0.2 \text{ W m}^{-2}$ . (b) 800-990  $\text{cm}^{-1}$ .  $F = 0.5 \text{ W m}^{-2}$ ;  $\Delta F = +0.1 \text{ W m}^{-2}$ . (c) 990-1070  $\text{cm}^{-1}$ .  $F = 2.1 \text{ W m}^{-2}$ ;  $\Delta F = -0.2 \text{ W m}^{-2}$ . (d) 1070-1200  $\text{cm}^{-1}$ .  $F = 0.5 \text{ W m}^{-2}$ ;  $\Delta F = 0.0 \text{ W m}^{-2}$ . (e) 1200-1350  $\text{cm}^{-1}$ .  $F = 2.1 \text{ W m}^{-2}$ ;  $\Delta F = -0.1 \text{ W m}^{-2}$ . (f) 1350-1500  $\text{cm}^{-1}$ .  $F = 2.0 \text{ W m}^{-2}$ ;  $\Delta F = -0.2 \text{ W m}^{-2}$ .

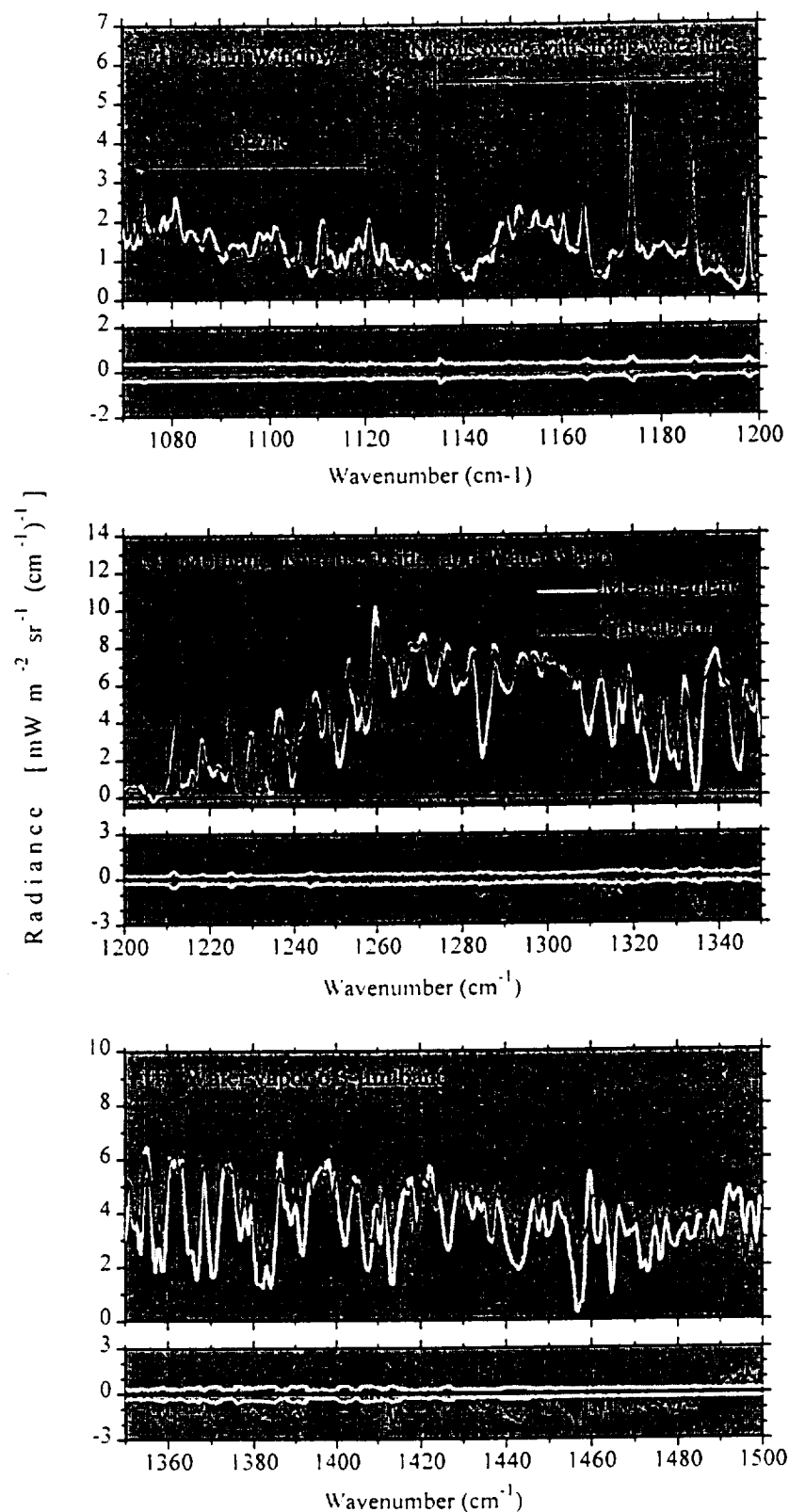


Figure 13. (continued)

tions and BLRTM calculations are similar. The comparisons are quite good between 1200 and 1250 cm<sup>-1</sup>, even at low radiance levels. However, there is a tendency for the calculated radiances to exceed the measurements between spectral lines in the region 1250–1350 cm<sup>-1</sup>.

#### 8.6 Water Vapor

The tendency for calculations to exceed measurements between spectral lines is more pronounced from 1350 to 1500 cm<sup>-1</sup> (Figure 13f), where emission is primarily due to water vapor. In general, the peaks of spectral lines agree well, but there are large offsets

between lines with, in some cases, striking similarities in spectral detail (for instance, around  $1380\text{ cm}^{-1}$ ). Figure 12 shows the calculation generally exceeding the radiance observation (negative radiance differences) from  $1250$  to  $1500\text{ cm}^{-1}$  for all six cases, especially between strong water vapor emission lines. The radiance differences exceed twice the estimated error in all the model atmospheres, regardless of whether the residual calibration bias seen in the measured window radiances is positive or negative.

Sensitivity studies were performed on both the interferometric calibration and the radiative transfer calculations in an attempt to identify the cause of the discrepancies between  $1250$  and  $1500\text{ cm}^{-1}$ . First, the temperature of the warm calibration source was adjusted to achieve better agreement in this spectral region, assuming the LBLRTM calculations were correct. The low values of the measured radiance between spectral lines are more sensitive to the calibration source radiance than are the peaks of the spectral lines. Thus it is possible to fit the measured spectrum to the radiance calculation by changing the warm source temperature. The warm source temperature was chosen as a proxy for changes in the calibration source radiance, since it is typically the largest source of uncertainty in the measured radiances. To minimize the spectrally averaged difference in radiance in this band, the warm source temperature had to be decreased by about  $6\text{ K}$ . This adjustment provided a better match of the low radiances shown in Figure 13f, but it also increased unrealistically the radiance in other parts of the spectrum, particularly the window regions. Furthermore, a decrease in the warm source temperature of this magnitude would imply that the interferometer was viewing a source colder than that reported by the warm source thermistors, contrary to the evidence from three different tests shown in Appendix A of Walden [1995] and summarized in Figure 3b. Therefore miscalibration of the measured radiances cannot explain all of the radiance differences between  $1250$  and  $1500\text{ cm}^{-1}$ .

Second, sensitivity studies with LBLRTM were performed by using different humidity profiles from the surface ( $2.8\text{ km}$ ) to  $7\text{ km}$  above sea level. As discussed above, the uncertainty in the water vapor profiles is large. The calculated spectra are most sensitive to humidity changes below  $7\text{ km}$ , since most of the water vapor is contained in the troposphere. The low radiance values between spectral lines from  $1250$  to  $1500\text{ cm}^{-1}$  are more sensitive to humidity changes than are the peaks of lines, because the peaks are saturated. Therefore the tropospheric humidity can be adjusted to fit the radiance calculation to the measured spectrum. As trial values, the tropospheric relative humidity with respect to ice ( $\text{RH}_i$ ) was set to  $25\%$ ,  $50\%$ ,  $75\%$ , and  $100\%$ . As  $\text{RH}_i$  decreases from  $100\%$  to  $50\%$ , the discrepancies between the calculations and measurements also decrease. However, at  $\text{RH}_i = 25\%$  the peaks of the spectral lines become subsaturated, and the agreement worsens. Therefore good agreement in both the peaks and valleys was impossible, but the best agreement was attained for tropospheric  $\text{RH}_i$  values of  $25\text{--}50\%$ . These low humidity values seem unreasonable, since ice crystal precipitation was observed on every clear day in winter and on most clear days in summer; the presence of precipitation implies saturated conditions somewhere within the lower atmosphere.

Clough *et al.* [1992] and Thériault *et al.* [1994] showed the importance of the foreign-broadened water vapor continuum in this spectral region, particularly in cold atmospheres where the continuum increases the opacity between spectral lines. The oxygen continuum is also important in cold and dry atmospheres from  $1400\text{ cm}^{-1}$  to beyond the high-wavenumber limit of the interferometer [Timofeyev and Tonkov, 1978; Rinsland *et al.*, 1989].

Revercomb *et al.* [1990] and Thériault *et al.* [1994] found that calculations using FASCODE (the predecessor of LBLRTM) and an earlier version of the water vapor continuum model exceeded their measurements, as we also find. Thériault *et al.* [1994] calculated radiance along horizontal paths at temperatures of  $-8^\circ\text{C}$  to  $-4^\circ\text{C}$  and water vapor amounts of  $0.6$  to  $1.2\text{ g cm}^{-2}$ . They suggested that perhaps either the foreign-broadened absorption coefficient has a positive temperature dependence or the temperature dependence of the strengths of nearby water vapor lines is in error. The foreign continuum absorption in the CKD model used here has a slight temperature dependence through density, but the continuum coefficients themselves do not depend on temperature (S. A. Clough, personal communication, 1995).

The final spectral region considered here ( $1500\text{--}1667\text{ cm}^{-1}$ ) shows significant radiance differences (Figures 11 and 12), especially in January. This finding is surprising, since most of this spectral region is strongly absorbed by water vapor and thus should resemble a Planck curve, especially in January when the lowest  $2\text{ km}$  are nearly isothermal. Sensitivity studies show that the choice of emissivity for the calibration sources has little effect on the comparisons. It is possible that the noise equivalent spectral radiance (Figure 6) was underestimated at these wavenumbers. However, since the errors are largest in January and appear to be a bias rather than noise, the radiance differences may be due to slight water vapor variations within the warm and relatively moist instrument during the measurement sequence that are not accounted for in the calibration process. Errors of this type would be most prevalent in spectral regions characterized by strong absorption and emission, e.g., beyond  $1500\text{ cm}^{-1}$ .

## 9. Conclusions

A data set of downward longwave spectral radiance, measured at South Pole Station in 1992, is augmented with ancillary data to describe the atmosphere. An error analysis shows that the primary source of uncertainty in the spectral radiances is the temperature of the warm calibration source; uncertainty in its emissivity also contributes significantly. The overall measurement error is largest in spectral regions that are relatively transparent, particularly the atmospheric window region ( $800\text{--}1250\text{ cm}^{-1}$ ). Three well-calibrated test cases are selected for clear-sky conditions.

The state of the atmosphere at the times of the test cases is constructed from radiosondes, water vapor sondes, and ozonesondes and from surface measurements of carbon dioxide, methane, nitrous oxide, CFC-11, and CFC-12 made at South Pole. Data from the UARS satellite are used to describe the upper atmosphere. Three model atmospheres have been constructed, including estimated uncertainties in all profiles. These data represent the coldest and driest test cases for radiative transfer models for terrestrial conditions.

The line-by-line radiative transfer model LBLRTM was used to calculate spectral radiances, using the ancillary data as input. Before the measurements were compared, the calculations were adjusted for instrumental effects, namely, the spectral resolution of the instrument and its finite field of view. Sources of error in the calculations have been estimated; they are induced by uncertainties in the viewing zenith angle and in the profiles of temperature and the principal radiatively active gases. The major contributors to this error are the uncertainties in the temperature and water vapor profiles. The uncertainty in the viewing zenith angle becomes important in winter, when a steep near-surface temperature inversion persists over the Antarctic Plateau.

The differences in radiance between the measurements and calculations are generally within twice the combined error in the measurements and calculations. However, discrepancies exist at both ends of the interferometer's bandwidth. Another region of discrepancy is between spectral lines from 1250 to 1500  $\text{cm}^{-1}$ , where emission is from the foreign-broadened water vapor continuum. Sensitivity studies show that the discrepancies are probably not solely due to errors in the spectral radiance calibration or to inaccurate specification of the water vapor profiles and therefore suggest errors in either the spectroscopic database or the model of the foreign water vapor continuum, or both. Future field measurements in the polar regions should concentrate on accurately determining temperature and water vapor within the boundary layer. In addition, spectral radiance observations should be extended to wavenumbers as low as 300  $\text{cm}^{-1}$  to fully measure the unsaturated portion of the water vapor rotational band. These suggestions apply in particular to the ARM site on the north slope of Alaska and to the Surface Heat Budget of the Arctic Ocean (SHEBA) experiment [Moritz and Perovich, 1996].

The spectral radiance measurements and their corresponding model atmospheres are available to the modeling community through ICRCCM [Walden et al., 1997].

**Acknowledgments.** We thank Renate Van Allen and John Van Allen of the University of Denver for preparing their interferometer so that it met our needs at South Pole. Kathryn Price helped maintain the interferometer from November 1992 through January 1993. Henry Revercomb provided a reference calibration blackbody, manufactured by his group at the University of Wisconsin. We had many helpful discussions about interferometry with Gary Hansen (University of Hawaii), Robert Knuteson (University of Wisconsin), Jeff Peterson (Carnegie Mellon University), Henry Revercomb, and Renate Van Allen. Kitt Hughes, Bob Koney, B. K. Grant, and Peggy Klinedinst of the South Pole Weather Office provided us with radiosonde data and helped us characterize the response time of the radiosonde's thermistor. We thank Mike O'Neill and John Lowell of NOAA-CMDL for coordinating their launches of water vapor sondes with our interferometer measurements during 1990-1991, and Dale Tysor and David Gaines (also of NOAA-CMDL) for launching ozonesondes and water vapor sondes during 1992. Denise Worthen (University of Washington) measured the tilt of the Skylab roof. We had helpful discussions with R. O. Knuteson regarding field-of-view corrections. S. A. Clough and P. Brown of Atmospheric Environmental Research, Inc., supplied us with the radiative transfer model, LBLRTM, and answered our questions about how to use it with model atmospheres from the Antarctic. S. A. Clough also provided many helpful comments through his review. We acknowledge the Carbon Cycle, Acquisition and Data Management, and Nitrous Oxide and Halocompounds divisions of NOAA-CMDL for providing data. We acknowledge the South Pole Station crews of 1990-1991 and 1991-1992 for their help with our experiments. We thank the Upper Atmosphere Research Satellite (UARS) project (code 916), and the Distributed Active Archive Center (code 902.2) at the Goddard Space Flight Center, Greenbelt, Maryland, for the production and distribution of the UARS data, respectively. Their activities are sponsored by NASA's Mission to Planet Earth Program. This research was supported by NSF grants DPP-88-18570, OPP-91-20380, and OPP-94-21096.

## References

- Beer, R., *Remote Sensing by Fourier Transform Spectroscopy*, John Wiley, New York, 1992.
- Bell, R. J., *Introductory Fourier Transform Spectroscopy* 382 pp., Academic, San Diego, Calif., 1972.
- Cacciani, M., P. di Girolamo, A. di Sarra, G. Fiocco, and D. Fuà, Volcanic aerosol layers observed by lidar at South Pole, September 1991 - June 1992, *Geophys. Res. Lett.*, **20**, 807-810, 1993.
- Carroll, J. J., Long-term means and short-term variability of the surface energy balance components at the South Pole, *J. Geophys. Res.*, **87**, 4277-4286, 1982.
- Clough, S. A., and M. J. Iacono, Calculations of atmospheric fluxes and cooling rates. 2, Application to carbon dioxide, ozone, methane, nitrous oxide, and the halocarbons, *J. Geophys. Res.*, **100**, 16,519-16,535, 1995.
- Clough, S. A., R. D. Worsham, W. L. Smith, H. E. Revercomb, R. O. Knuteson, G. P. Anderson, M. L. Hoke, and F. X. Kneizys, Validation of FASCOD calculations with HIS spectral radiance measurements, in *IRS '88: Current Problems in Atmospheric Radiation* edited by J. Lenoble and J. F. Geleyn, pp. 376-279, A. Deepak, Hampton, Va., 1989a.
- Clough, S. A., F. X. Kneizys, E. P. Shettle, and G. P. Anderson, FASCOD3: Spectral simulation, in *IRS '88: Current Problems in Atmospheric Radiation*, edited by J. Lenoble and J. F. Geleyn, pp. 372-375, A. Deepak, Hampton, Va., 1989b.
- Clough, S. A., F. X. Kneizys, and R. W. Davies, Line shape and the water vapor continuum, *Atmos. Res.*, **23**, 229-241, 1989c.
- Clough, S. A., M. J. Iacono, and J. L. Moncet, Line-by-line calculations of atmospheric fluxes and cooling rates: Application to water vapor, *J. Geophys. Res.*, **97**, 15,761-15,785, 1992.
- Ellingson, R. G., and Y. Fouquart, The intercomparison of radiation codes used in climate models: An overview, *J. Geophys. Res.*, **96**, 8925-8927, 1991.
- Ellingson, R. G., and W. J. Wiscombe, The spectral radiance experiment (SPECTRE): Project description and sample results, *Bull. Am. Meteorol. Soc.*, **77**, 1967-1985, 1996.
- Ellingson, R. G., J. Ellis, and S. Fels, The intercomparison of radiation codes used in climate models: Long wave results, *J. Geophys. Res.*, **96**, 8929-8953, 1991.
- Ellingson, R. G., S. Shen, and J. Warner, Calibration of radiation codes used in climate models: Comparison of clear-sky calculations with observations from the Spectral Radiance Experiment and the Atmospheric Radiation Measurement program, in *Proceedings of the Fourth Atmospheric Radiation Measurement (ARM) Science Team Meeting, 28 February - 3 March 1994, Charleston, South Carolina, DOE CONF-940277*, 47-53, 1995.
- Fouquart, Y., B. Bonnel, and V. Ramaswamy, Intercomparing shortwave radiation codes for climate studies, *J. Geophys. Res.*, **96**, 8955-8968, 1991.
- Genthon, C., Antarctic climate modeling with general circulation models of the atmosphere, *J. Geophys. Res.*, **99**, 12,953-12,961, 1994.
- Goody, R. M., and Y. L. Yung, *Atmospheric Radiation. Theoretical Basis*, 2nd ed., Oxford Univ. Press, New York, 1989.
- Hanson, K. J., Radiation measurement on the Antarctic snowfield: A preliminary report, *J. Geophys. Res.*, **65**, 935-946, 1960.
- Hanson, K. J., and M. J. Rubin, Heat exchange at the snow-air interface at the South Pole, *J. Geophys. Res.*, **67**, 3415-3424, 1962.
- Hervig, M. E., J. M. Russell III, L. L. Gordley, J. Daniels, S. R. Drayson, and J. H. Park, Aerosol effects and corrections in the Halogen Occultation Experiment, *J. Geophys. Res.*, **100**, 1067-79, 1995.
- Komhyr, W. D., L. S. Waterman, and W. R. Taylor, Semiautomatic nondispersive infrared analyzer apparatus for  $\text{CO}_2$  air sample analyses, *J. Geophys. Res.*, **88**, 1315-1322, 1983.
- Komhyr, W. D., R. H. Gammon, T. B. Harris, L. S. Waterman, T. J. Conway, W. R. Taylor, and K. W. Thoning, Global atmospheric  $\text{CO}_2$  distribution and variations from 1968-1982 NOAA/GMCC  $\text{CO}_2$  flask sample data, *J. Geophys. Res.*, **90**, 5567-5596, 1985.
- Kopanev, I. D., The heat balance of the Antarctic continent, in *Polar Meteorology, Tech. Note 87*, pp. 189-195, World Meteorol. Org., Geneva, 1967.
- Kuhn, M., L. S. Kundla, and L. A. Stroschein, The radiation budget at Plateau Station, Antarctica, 1966-1967, in *Meteorological Studies at Plateau Station, Antarct. Res. Ser.*, vol. 25, edited by J. A. Businger, pp. 41-73, AGU, Washington, D.C., 1977.
- Lang, P. M., L. P. Steele, R. C. Martin, and K. A. Masarie, Atmospheric methane data for the period 1983-1985 from the NOAA/GMCC global cooperative flask sampling network, *NOAA Tech. Memo., ERL CMDL-1*, 1990a.
- Lang, P. M., L. P. Steele, and R. C. Martin, Atmospheric methane data for the period 1986-1988 from the NOAA/CMDL global cooperative flask sampling network, *NOAA Tech. Memo., ERL CMDL-2*, 1990b.
- Lubin, D., Infrared properties of the maritime Antarctic atmosphere, *J. Clim.*, **7**, 121-140, 1994.
- Lubin, D., D. Cutchin, W. Conant, H. Grassl, U. Schmid, and W. Biselli, Spectral longwave emission in the tropics: FTIR measurements at the sea surface and comparison with fast radiation codes, *J. Clim.*, **8**, 286-295, 1995.
- Luther, F. M., R. G. Ellingson, Y. Fouquart, S. Fels, N. A. Scott, and W. J. Wiscombe, Intercomparison of Radiation Codes used in Climate Mod-

- els (ICRCCM): Longwave clear-sky results: A workshop summary, *Bull. Am. Meteorol. Soc.*, 69, 40-48, 1988.
- Mahesh, A., V.P. Walden, and S.G. Warren, Radiosonde temperature measurements in strong inversions: Correction for thermal lag based on an experiment at South Pole, *J. Atmos. Oceanic Technol.*, 14, 45-53, 1997.
- McClatchey, R.A., R.W. Fenn, J.E.A. Selby, F.E. Volz, and J.S. Garing, Optical properties of the atmosphere, 3rd ed., *Rep. AFCRL-72-0497*, Air Force Geophys. Lab., Bedford, Mass., 1972.
- Moritz, R.E. and D.K. Perovich (Eds.), *Surface heat budget of the arctic ocean science plan, ARCSS/OAI Rep. Number 5*, 64 pp., Univ. of Washington, Seattle, 1996.
- Murcray, F.J. and R. Heuberger, Infrared atmospheric absorption and emission measurements, *Antarct. J. U.S.*, 25(5), 244-246, 1990.
- Murcray, F.J., and R. Heuberger, Year-round measurement of atmospheric infrared emission at the South Pole, *Antarct. J. U.S.*, 26(5), 278-281, 1991.
- Murcray, F.J. and R. Heuberger, Extended observations of atmospheric infrared absorption and emission, *Antarct. J. U.S.*, 27(5), 278-279, 1992.
- Poole, L.R., and M.C. Pitts, Polar stratospheric cloud climatology based on Stratospheric Aerosol Measurement II observations from 1978 to 1989, *J. Geophys. Res.*, 99, 13,083-13,089, 1994.
- Press, W.H., B.P. Flannery, S.A. Teukolsky, and W.T. Vetterling, *Numerical Recipes: The Art of Scientific Computing*, 2nd ed., Cambridge Univ. Press, New York, 1992.
- Randall, W.J., B.A. Boville, J.C. Gille, P.L. Bailey, S.T. Massie, J.B. Kumer, J.L. Mergenthaler, and A.E. Roche, Simulation of stratospheric N<sub>2</sub>O in the NCAR CCM2: Comparison with CLAES data and global budget analysis, *J. Atmos. Sci.*, 51, 2834-2845, 1994.
- Reber, C.A., C.E. Trevathan, R.J. McNeal, and M.R. Luther, The Upper Atmosphere Research Satellite (UARS) Mission, *J. Geophys. Res.*, 98, 10,643-10,647, 1993.
- Revercomb, H.E., H. Buijs, H.B. Howell, D.D. LaPorte, W.L. Smith, and L.A. Sromovsky, Radiometric calibration of IR Fourier transform spectrometers: Solution to a problem with the high-resolution interferometer sounder, *Appl. Opt.*, 27, 3210-3218, 1988.
- Revercomb, H.E., R.O. Knuteson, W.L. Smith, H.M. Woolf, and H.B. Howell, Spectroscopic inference from HIS measurements of atmospheric thermal emission, in *Optical Remote Sensing of the Atmosphere*, *Tech. Dig. Ser.*, vol. 4, pp. 590-593, Opt. Soc. of Am., Washington, D.C., 1990.
- Rinsland, C.P., R. Zander, J.S. Namkung, C.B. Farmer, and R.H. Norton, Stratospheric infrared continuum absorption observed by the ATMOS instrument, *J. Geophys. Res.*, 94, 16,303-16,322, 1989.
- Roche, A.E., J.B. Kumer, J.L. Mergenthaler, G.A. Ely, W.G. Uplinger, J.F. Potter, T.C. James, and L.W. Stewart, The cryogenic limb array etalon spectrometer (CLAES) on UARS: Experiment description and performance, *J. Geophys. Res.*, 98, 10,763-10,775, 1993.
- Rothman, L.S., et al., The HITRAN molecular database: Editions 1991 and 1992, *J. Quant. Spectrosc. Radiat. Transfer*, 48, 469-507, 1992.
- Rusin, N.P., *Meteorological and Radiational Regime of Antarctica*, translated from Russian by the Israel Program for Scientific Translations, U.S. Dep. of Commerce, Washington, D.C., 1964.
- Russell, J.M., III, L.L. Gordley, J.A. Park, S.R. Drayson, W.D. Hesketh, R.J. Cicerone, A.F. Tuck, J.E. Frederick, J.E. Harries, and P.J. Crutzen, The Halogen Occultation Experiment, *J. Geophys. Res.*, 98, 10,777-10,799, 1993.
- Schwerdtfeger, W., The climate of the Antarctic, in *World Survey of Climatology*, edited by S. Orvig, vol. 14, pp. 253-355, Elsevier Sci., New York, 1970.
- Schwerdtfeger, W., *Weather and Climate of the Antarctic*, Elsevier Sci., New York, 1984.
- Smith, W.L., H.M. Woolf, H.B. Howell, H.-L. Huang, and H.E. Revercomb, The simultaneous retrieval of atmospheric temperature and water vapor profiles: Application to measurements with the high resolution interferometer sounder (HIS), in *RSRM '87: Advances in Remote Sensing Retrieval Methods*, edited by H.E. Fleming and J.S. Theon, pp. 189-202, A. Deepak, Hampton, Va., 1989.
- Steel, W.H., Interferometers without collimation for Fourier spectroscopy, *Appl. Opt.*, 54, 151-156, 1964.
- Steele, L.P., P.J. Fraser, R.A. Rasmussen, M.A.K. Khalil, T.J. Conway, A.J. Crawford, R.H. Gammon, K.A. Masarie, and K.W. Thoning, The global distribution of methane in the troposphere, *J. Atmos. Chem.*, 5, 125-171, 1987.
- Stokes, G.M., and S.E. Schwartz, The Atmospheric Radiation Measurement (ARM) program: Programmatic background and design of the Cloud and Radiation Test Bed, *Bull. Am. Meteorol. Soc.*, 75, 1201-1221, 1994.
- Stone, R.S., and J.D. Kahl, Variations in boundary layer properties associated with clouds and transient weather disturbances at the south pole during winter, *J. Geophys. Res.*, 96, 5137-5144, 1991.
- Stone, R.S., E.G. Dutton, and J.J. DeLuise, Surface radiation and temperature variations associated with cloudiness at the South Pole, *Antarct. J. U.S.*, 24(5), 230-232, 1989.
- Thériault, J.-M., P.L. Roney, D. St-Germain, H.E. Revercomb, R.O. Knuteson, and W.L. Smith, Analysis of the FASCODE model and its H<sub>2</sub>O continuum based on long-path atmospheric transmission measurements in the 4.5-11.5- $\mu$ m region, *Appl. Opt.*, 33, 323-333, 1994.
- Thoning, K.W., P. Tans, T.J. Conway, and L.S. Waterman, NOAA/GMCC calibrations of CO<sub>2</sub>-in-air reference gases: 1979-1985, *NOAA Tech. Memo. ERL ARL-150*, Environ. Res. Lab., Boulder, Colo., 1987.
- Timofeyev, Y.M., and M.V. Tonkov, Effect of the induced oxygen absorption band on the transformation of radiation in the 6  $\mu$ m region in the Earth's atmosphere, *Izv. Acad. Sci. USSR Atmos. Oceanic Phys.*, Engl. Transl., 14, 437-441, 1978.
- Tzeng, R.Y., D.H. Bromwich, and T.R. Parish, Present-day Antarctic climatology of the NCAR Community Climate Model version 1, *J. Clim.*, 6, 205-226, 1993.
- Tzeng, R.Y., D.H. Bromwich, T.R. Parish, and B. Chen, NCAR CCM2 simulation of the modern Antarctic climate, *J. Geophys. Res.*, 99, 23,131-23,148, 1994.
- Van Allen, R., F.J. Murcray, and X. Liu, Mid-infrared measurements of the atmospheric emission over the South Pole using a radiometrically calibrated Fourier transform spectrometer, *Appl. Opt.*, 35, 1523-1530, 1996.
- Walden, V.P., The downward longwave radiation spectrum over the Antarctic Plateau, Ph.D. thesis, Univ. of Washington, Seattle, 1995.
- Walden, V.P., and S.G. Warren, Atmospheric longwave radiation spectrum and near-surface atmospheric temperature profiles at South Pole Station, *Antarct. J. U.S.*, 28(5), 269-271, 1994.
- Walden, V.P., S.G. Warren, F.J. Murcray, and R.G. Ellingson, Infrared radiance spectra for testing radiative transfer models in cold and dry atmospheres: Test cases from the Antarctic Plateau, *Bull. Am. Meteorol. Soc.*, 78, 2246-2247, 1997.
- Warren, S.G., *Antarctica*, in *Encyclopedia of Weather and Climate*, Oxford Univ. Press, New York, 32-39, 1996.
- Yamanouchi, T., and S. Kawaguchi, Longwave radiation balance under a strong surface inversion in the katabatic wind zone, Antarctica, *J. Geophys. Res.*, 89, 11,771-11,778, 1984.
- Yamanouchi, T., and S. Kawaguchi, Effects of drifting snow on surface radiation budget in the katabatic wind zone, Antarctica, *Ann. Glaciol.*, 6, 238-241, 1985.
- Yamanouchi, T., M. Wada, S. Mae, S. Kawaguchi, and K. Kusunoki, The radiation budget at Mizuho Station, Antarctica, 1979, *Ann. Glaciol.*, 3, 327-332, 1982.

F. J. Murcray, Department of Physics, University of Denver, 2112 E. Wesley, Denver, CO 80210 (email: murcray@ram.phys.du.edu)

V. P. Walden, Space Science and Engineering Center, University of Wisconsin-Madison, 1225 W. Dayton Street, Madison, WI 53706 (email: von.walden@ssec.wisc.edu)

S. G. Warren, Department of Atmospheric Sciences, University of Washington, Box 351640, Seattle, WA 98195-1640 (email: sgw@atmos.washington.edu)

(Received October 7, 1996; revised April 23, 1997; accepted August 18, 1997.)



# Retrieval of HCl and HNO<sub>3</sub> Profiles from Ground-based FTIR Data Using SFIT2

Brian J. Connor, Nicholas B. Jones, Stephen W. Wood, J. Gordon Keys

National Institute of Water and Atmospheric Research (NIWA), Lauder, New Zealand

Curtis P. Rinsland

NASA Langley Research Center, Hampton, Virginia, U.S.A.

Frank J. Murcray

Department of Physics, University of Denver, Denver, Colorado, U.S.A.

**Abstract.** A recently developed algorithm, SFIT2, is used to assess profile information available in ground-based FTIR measurements of HCl and HNO<sub>3</sub>, and to analyze spectra recorded at Lauder, New Zealand, and Arrival Heights, Antarctica. It is shown that the altitude range of HCl retrievals may be extended by using multiple spectral lines. A preliminary analysis of a five year record of HNO<sub>3</sub> at Lauder shows that the Pinatubo aerosol caused a large increase of HNO<sub>3</sub> in a layer at about 20-30 km while having little effect at lower altitude.

## 1. Introduction

It has long been understood that ground-based infrared Fourier transform (FTIR) spectra contain information on the altitude profile of the absorbing molecules in the details of the observed lineshape. The current work is part of an ongoing attempt to exploit this information by applying techniques previously used on ground-based microwave emission measurements (e.g. Connor et al., 1995). Results of ozone profile retrievals with SFIT2 have appeared in Pougatchev et al., 1995 and 1996.

SFIT2 is a radiative transfer and profile retrieval algorithm for use with spectra recorded in solar absorption. One or more spectral windows recorded at one or more zenith angles are fit simultaneously. The goodness-of-fit to the measured spectra is controllable, and may vary arbitrarily in different spectral intervals. 1 or 2 trace gas profiles as well as column amounts of interfering species, instrumental background parameters, wavelength calibration factors, and an instrumental lineshape parameter may be retrieved.

## 2. Theoretical results

Ground-based FTIR measurements contain profile information primarily because of the pressure broadening of the spectral lines. This fact limits vertical resolution to about a pressure scale height, and usually limits the altitude range of the retrieved profile to approximately the region where the pressure width is

greater than the Doppler width, or about 25-30 km. Traditionally, ground-based FTIR measurements have been used almost exclusively for determination of the total column amount. This is not as direct a measurement as it might seem, as the integrated absorption cannot be taken directly from the spectrum because only the relative (not absolute) absorption depth is measured. Thus the accuracy of such measurements is limited by the ability to calculate the spectrum with a radiative transfer model which necessarily includes an a priori assumption about the shape of the molecule's height profile. This assumption is often the limiting factor in the accuracy of the resulting column amount. Retrieval of the height profile may be expected to better exploit the information in the spectra, and so improve the accuracy of the column determination.

The theoretical altitude sensitivity of a given measurement may be directly assessed by examination of its averaging kernels (Rodgers, 1990). These are functions which show explicitly how the atmosphere is sampled by the retrieved profile or column. Formally, they are the derivatives of the retrieval with respect to the real profile. A perfect measurement would sample the intended region of the atmosphere uniformly, and not include contributions from outside that region. So for example, the averaging kernel for a perfect column measurement would be equal to 1 at all altitudes, while for a 10-20 km partial column, it would be 1 in that altitude range and 0 elsewhere.

### 2.1 HCl

The HCl averaging kernels are shown in Fig. 1. Kernels for 3 different measurements are shown. The most familiar measurement is the total column determination made by scaling an a priori profile to achieve minimum spectral residuals. The kernel for that measurement is the thick solid line marked by crosses. It shows that the sampling of the atmosphere by the profile scaling technique is highly non-uniform. This provides a good point of reference for the averaging kernels for profile retrieval techniques.

Two sets of averaging kernels for profile retrieval are shown, one for which the analysis uses only the R1 line (2926 cm<sup>-1</sup>; dashed curves) and one using the R1, P5 (2776 cm<sup>-1</sup>), and P7 (2728 cm<sup>-1</sup>) lines simulta-



neously (solid lines). In both cases high signal to noise (500-1000) is assumed. We first describe the R1 only measurement.

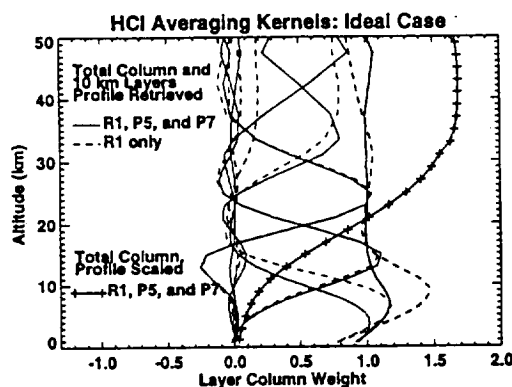


Fig. 1 HCl averaging kernels for high signal-to-noise. Results are shown for a retrieval with 3 spectral lines (R1, P5, and P7) and for the R1 line alone.

Six separate functions (kernels) are plotted, five for partial columns in 10 km thick layers from 0 to 50 km, and one (thick dashes) for the total column. The kernels for the 0-10, 10-20, and 20-30 km partial columns exhibit good sensitivity within their respective ranges and fairly good discrimination outside them. The kernel for 30-40 km, on the other hand, shows an equal response both above and below 40 km, while the 40-50 km kernel shows very poor sensitivity at all altitudes. In short, the R1 line measurement has good sensitivity up to about 30 km. The kernel for the total column is much improved over the profile scaling case, showing that altitudes above about 15 km are well and uniformly sampled. At lower altitudes there is excess sensitivity (molecules will be overcounted) in the upper troposphere.

When the P5 and P7 lines are used along with the R1 the kernels plotted as solid lines result. The tropospheric sensitivity is improved and the upper end of the range is extended to about 40 km. This is an interesting and in part unexpected result. The key fact in interpreting it is that the pressure broadening coefficients of the 3-lines vary over a range of 2.5 times, with the P lines being much narrower than the R1. Therefore they will be more sensitive in the troposphere, since the absorption is less spread out. That the P lines should improve sensitivity in the upper stratosphere is surprising. We believe the explanation is that the differing line widths imply that the lines respond differently to changes in the HCl profile, even at altitudes where the pressure width is less than the Doppler width, so long as the pressure width is still a significant component of the total. By using the three lines simultaneously the algorithm is able to exploit their differing behavior.

In summary, theoretical analysis indicates that high signal-to-noise measurements of HCl should yield good profile information at 10 km resolution up to 30 km if the R1 line is used, and up to 40 km if the P5 and P7 lines are included. Furthermore, use of the profile retrieval algorithm, as opposed to a profile

scaling, greatly improves sampling uniformity in the total column determination, by reducing dependence on the a priori profile shape.

## 2.2 HNO<sub>3</sub>

The left hand panel of Fig. 2 shows the averaging kernels for a high signal-to-noise ratio case, similar to that for HCl in Fig. 1. The spectral interval used is 867-870  $\text{cm}^{-1}$ . It is usually thought that there is little if any profile information in HNO<sub>3</sub> spectra because of the extensive line blending. However, Fig. 2 shows that the 10-20 and 20-30 km regions can be distinguished reasonably well. Further, the total column kernel exhibits more uniform sensitivity for the profile retrieval than for profile scaling, as it did for HCl. However, the partial column averaging kernels are broader and less well defined than for HCl, and the total column kernel shows less sensitivity in the troposphere. So while there is significant profile sensitivity in the HNO<sub>3</sub> spectra, it is less than for the unblended lines of HCl. The profile information which does exist is probably due to the lines being partially resolved and to the use of multiple manifolds.

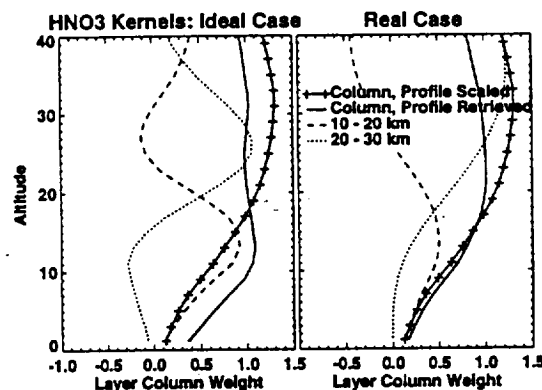


Fig. 2 HNO<sub>3</sub> averaging kernels. The left panel shows results for high signal-to-noise; the right panel for signal-to-noise characteristic of results achieved in practice.

## 2.3 Practical Limitations

Profile retrieval from pressure-broadened line-shapes requires the ability both to make high quality, low noise measurements, and to accurately simulate the observed spectra with a forward model. These are demanding requirements, and unfortunately it has not been possible to achieve in practice the results which might be expected based on the above theoretical analysis. In particular, the information available is limited by our ability to model the measurements and by systematic errors in the measurements themselves. Both effects are manifest by spectral residuals which are non-random, and larger on average than expected from noise. A number of factors are known to contribute here, including the instrument response function, spectroscopic parameters, and forward model approximations. The degradation of the available profile information may be seen in broader and flatter

averaging kernels, implying less discrimination between layers and more influence of the a priori.

For  $\text{HNO}_3$ , as measured at Lauder, the effective signal-to-noise (determined by the magnitude of the spectral residuals) is about 200; the averaging kernels for such measurements are shown on the right-hand panel of Fig. 2. While the comparison to the high signal-to-noise case in the left-hand panel is disappointing, there is still some ability to distinguish the 2 layers, and the total column kernel is still better than that for profile scaling. In the next section we will show results which suggest that useful profile information may be acquired from such measurements in practice as well as in theory.

### 3. Atmospheric Measurements

Despite both theoretical and practical limitations, early results of profile retrievals on atmospheric data are reasonably encouraging. We have made a preliminary analysis of the Lauder  $\text{HNO}_3$  data set, and experimented with a small number of Lauder  $\text{HCl}$  measurements and  $\text{HNO}_3$  measurements from Arrival Heights, Antarctica. It should be noted that this is work-in-progress, and that further developments can be expected.

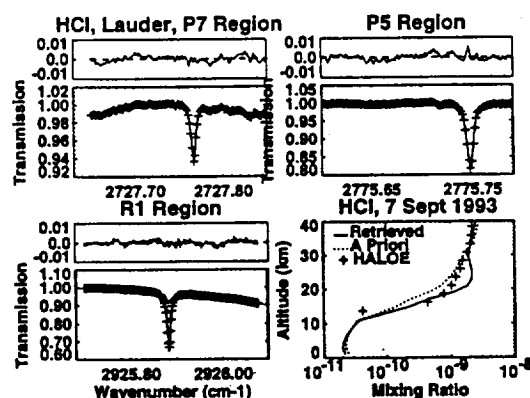


Fig. 3. An  $\text{HCl}$  retrieval from data of 7 September 1993 at Lauder, New Zealand. The 3 spectra shown were fit simultaneously in retrieving the profile shown in the lower right panel.

#### 3.1 $\text{HCl}$

An example of an  $\text{HCl}$  spectrum and profile measured at Lauder is shown in Fig. 3. The spectral data quality is excellent and the calculated spectrum fits the measurement to 1:500 on average. It is interesting to note that all 3 spectral regions are fit reasonably well, although small systematic features do dominate the residuals, the most visible being in the P5 line center. Despite this, while the retrieved profile is generally reasonable, there is a significant discrepancy, up to a factor 1.7, with HALOE  $\text{HCl}$  in the 20-30 km region. The cause of this is still being investigated. A detailed algorithm comparison was recently carried out (A. Goldman, private communication, 1996) which would appear to rule out the algorithm as the principal source of this discrepancy.

Measurements have been made at Lauder (45 S) since 1990 at 0.0035 - 0.007  $\text{cm}^{-1}$  resolution. Fig. 4 shows partial columns in the 10-20 and 20-30 km layers. The data are monthly averages. The solid lines are regression fits to the daily data (not shown) before the Pinatubo eruption and in 1994-95, including annual, semi-annual, and secular terms. Fig 5 shows the ratio of the partial columns. The data show a repeatable annual cycle and a clear response to the Mt. Pinatubo aerosol injection. Further,  $\text{HNO}_3$  behaves differently in the two altitude regions. The annual cycle differs in that the autumnal increase is later in the lower layer. Also, the transient response to the Pinatubo aerosol was much greater in the upper layer.

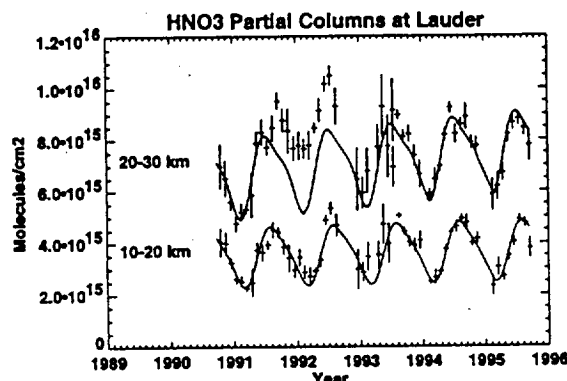


Fig. 4 A time series of  $\text{HNO}_3$  in two layers at Lauder. The data points are monthly means. The solid line is a regression fit to single measurements made before and after the atmosphere was perturbed by the eruption of Mt. Pinatubo.

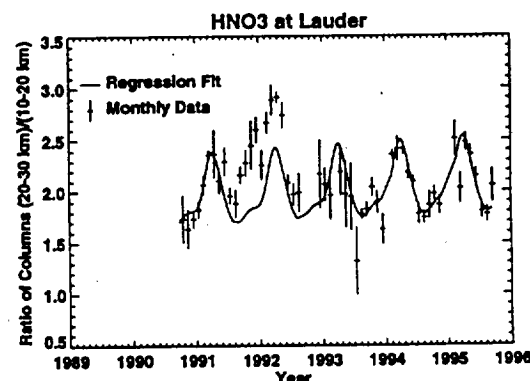


Fig. 5. The ratio of the time series shown in Fig. 4.

$\text{HNO}_3$  measurements are also made routinely at Arrival Heights, Antarctica (78 S). Spectra are recorded at lower resolution ( $0.02 \text{ cm}^{-1}$ ) than at Lauder, and are generally lower quality (Fig. 6). Nevertheless, trials with the 1993 data show a fall to spring change in profile shape roughly consistent with CLAES measurements (Kumer et al., 1996) in 1992, in that the relative decrease in  $\text{HNO}_3$  is greater above 20 km than below.

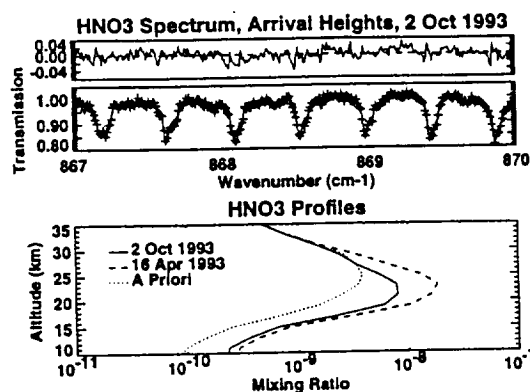


Fig 6. HNO<sub>3</sub> measurements made at Arrival Heights, Antarctica.

#### 4. Conclusions

In summary, a theoretical analysis of the altitude sensitivity of FTIR measurements of HCl and HNO<sub>3</sub> shows that significant profile information exists in both measurements, and that in the case of HCl the range of sensitivity may be extended by use of multiple spectral lines. Experiments with HCl retrievals from Lauder data and HNO<sub>3</sub> retrievals from Arrival Heights have been performed. While the results are generally as expected, there is an apparent anomaly in the HCl profile which is unexplained. Preliminary analysis of a five year time series of HNO<sub>3</sub> data from Lauder shows a behavior in adjacent 10 km layers which is different in the 2 layers, yet repeatable from year to year, and also a response to the Pinatubo aerosol consistent with priori understanding of that event.

**Acknowledgments.** We thank Brian McNamara for recording the spectral data. Funding for this research was provided by the New Zealand Foundation for Science and Technology and by the NASA Upper Atmosphere Research Program.

#### References

- Connor, B.J., A. Parrish, J.J. Tsou, and M.P. McCormick, Error analysis for the ground-based microwave measurements during STOIC, *J. Geophys. Res.*, 100, 9283-9292, 1995.
- Kumer, J.B., et al., Comparison of correlative data with HNO<sub>3</sub> version 7 from the CLAES instrument deployed on the NASA Upper Atmosphere Research Satellite, *J. Geophys. Res.*, 101, 9621-9656, 1996.
- Pougatchev, N.S., B.J. Connor, and C.P. Rinsland, Infrared measurements of the ozone vertical distribution above Kitt Peak, *J. Geophys. Res.*, 100, 16,689-16,698, 1995.
- Pougatchev, N.S., B.J. Connor, N.B. Jones, and C.P. Rinsland, Validation of ozone profile retrievals from ground-based solar spectra, *Geophys. Res. Lett.*, 23, 1637-1640, 1996.
- Rodgers, C.D., Characterization and error analysis of profiles retrieved from remote sounding measurements, *J. Geophys. Res.*, 5587-5595, 1990.
- B.J. Connor, N.B. Jones, S.W. Wood, J.G. Keys, NIWA, Private Bag 50061, Omakau 9182, New Zealand.
- C.P. Rinsland, Mail Stop 401A, NASA Langley Research Center, Hampton, VA 23681, USA
- F.J. Murcray, Department of Physics, University of Denver, Denver, CO 80308, USA

# Retrieval of HCl and HNO<sub>3</sub> Profiles from Ground-based FTIR Data Using SFTT2

Brian J. Connor, Nicholas B. Jones, Stephen W. Wood, J. Gordon Keys

National Institute of Water and Atmospheric Research (NIWA), Lauder, New Zealand

Curtis P. Rinsland

NASA Langley Research Center, Hampton, Virginia, U.S.A.

Frank J. Murcray

Department of Physics, University of Denver, Denver, Colorado, U.S.A.

**Abstract.** A recently developed algorithm, SFTT2, is used to assess profile information available in ground-based FTIR measurements of HCl and HNO<sub>3</sub> and to analyze spectra recorded at Lauder, New Zealand, and Arrival Heights, Antarctica. It is shown that the altitude range of HCl retrievals may be extended by using multiple spectral lines. A preliminary analysis of a five year record of HNO<sub>3</sub> at Lauder shows that the Pinatubo aerosol caused a large increase of HNO<sub>3</sub> in a layer at about 20-30 km while having little effect at lower altitude.

## 1. Introduction

It has long been understood that ground-based infrared Fourier transform (FTIR) spectra contain information on the altitude profile of the absorbing molecules in the details of the observed lineshape. The current work is part of an ongoing attempt to exploit this information by applying techniques previously used on ground-based microwave emission measurements (e.g. Connor et al., 1995). Results of ozone profile retrievals with SFTT2 have appeared in Pougatchev et al., 1995 and 1996.

SFTT2 is a radiative transfer and profile retrieval algorithm for use with spectra recorded in solar absorption. One or more spectral windows recorded at one or more zenith angles are fit simultaneously. The goodness-of-fit to the measured spectra is controllable, and may vary arbitrarily in different spectral intervals. 1 or 2 trace gas profiles as well as column amounts of interfering species, instrumental background parameters, wavelength calibration factors, and an instrumental lineshape parameter may be retrieved.

## 2. Theoretical results

Ground-based FTIR measurements contain profile information primarily because of the pressure broadening of the spectral lines. This fact limits vertical resolution to about a pressure scale height, and usually limits the altitude range of the retrieved profile to approximately the region where the pressure width is

greater than the Doppler width, or about 25-30 km. Traditionally, ground-based FTIR measurements have been used almost exclusively for determination of the total column amount. This is not as direct a measurement as it might seem, as the integrated absorption cannot be taken directly from the spectrum because only the relative (not absolute) absorption depth is measured. Thus the accuracy of such measurements is limited by the ability to calculate the spectrum with a radiative transfer model which necessarily includes an a priori assumption about the shape of the molecule's height profile. This assumption is often the limiting factor in the accuracy of the resulting column amount. Retrieval of the height profile may be expected to better exploit the information in the spectra, and so improve the accuracy of the column determination.

The theoretical altitude sensitivity of a given measurement may be directly assessed by examination of its averaging kernels (Rodgers, 1990). These are functions which show explicitly how the atmosphere is sampled by the retrieved profile or column. Formally, they are the derivatives of the retrieval with respect to the real profile. A perfect measurement would sample the intended region of the atmosphere uniformly, and not include contributions from outside that region. So for example, the averaging kernel for a perfect column measurement would be equal to 1 at all altitudes, while for a 10-20 km partial column, it would be 1 in that altitude range and 0 elsewhere.

### 2.1 HCl

The HCl averaging kernels are shown in Fig. 1. Kernels for 3 different measurements are shown. The most familiar measurement is the total column determination made by scaling an a priori profile to achieve minimum spectral residuals. The kernel for that measurement is the thick solid line marked by crosses. It shows that the sampling of the atmosphere by the profile scaling technique is highly non-uniform. This provides a good point of reference for the averaging kernels for profile retrieval techniques.

Two sets of averaging kernels for profile retrieval are shown, one for which the analysis uses only the R1 line (2926 cm<sup>-1</sup>; dashed curves) and one using the R1, P5 (2776 cm<sup>-1</sup>), and P7 (2728 cm<sup>-1</sup>) lines simulta-

neously (solid lines). In both cases high signal to noise (500-1000) is assumed. We first describe the R1 only measurement.

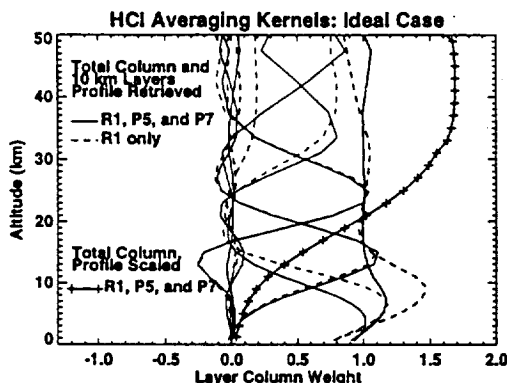


Fig. 1 HCl averaging kernels for high signal-to-noise. Results are shown for a retrieval with 3 spectral lines (R1, P5, and P7) and for the R1 line alone.

Six separate functions (kernels) are plotted, five for partial columns in 10 km thick layers from 0 to 50 km, and one (thick dashes) for the total column. The kernels for the 0-10, 10-20, and 20-30 km partial columns exhibit good sensitivity within their respective ranges and fairly good discrimination outside them. The kernel for 30-40 km, on the other hand, shows an equal response both above and below 40 km, while the 40-50 km kernel shows very poor sensitivity at all altitudes. In short, the R1 line measurement has good sensitivity up to about 30 km. The kernel for the total column is much improved over the profile scaling case, showing that altitudes above about 15 km are well and uniformly sampled. At lower altitudes there is excess sensitivity (molecules will be overcounted) in the upper troposphere.

When the P5 and P7 lines are used along with the R1 the kernels plotted as solid lines result. The tropospheric sensitivity is improved and the upper end of the range is extended to about 40 km. This is an interesting and in part unexpected result. The key fact in interpreting it is that the pressure broadening coefficients of the 3-lines vary over a range of 2.5 times, with the P lines being much narrower than the R1. Therefore they will be more sensitive in the troposphere, since the absorption is less spread out. That the P lines should improve sensitivity in the upper stratosphere is surprising. We believe the explanation is that the differing line widths imply that the lines respond differently to changes in the HCl profile, even at altitudes where the pressure width is less than the Doppler width, so long as the pressure width is still a significant component of the total. By using the three lines simultaneously the algorithm is able to exploit their differing behavior.

In summary, theoretical analysis indicates that high signal-to-noise measurements of HCl should yield good profile information at 10 km resolution up to 30 km if the R1 line is used, and up to 40 km if the P5 and P7 lines are included. Furthermore, use of the profile retrieval algorithm, as opposed to a profile

scaling, greatly improves sampling uniformity in the total column determination, by reducing dependence on the a priori profile shape.

## 2.2 HNO<sub>3</sub>

The left hand panel of Fig. 2 shows the averaging kernels for a high signal-to-noise ratio case, similar to that for HCl in Fig. 1. The spectral interval used is 867-870 cm<sup>-1</sup>. It is usually thought that there is little if any profile information in HNO<sub>3</sub> spectra because of the extensive line blending. However, Fig. 2 shows that the 10-20 and 20-30 km regions can be distinguished reasonably well. Further, the total column kernel exhibits more uniform sensitivity for the profile retrieval than for profile scaling, as it did for HCl. However, the partial column averaging kernels are broader and less well defined than for HCl, and the total column kernel shows less sensitivity in the troposphere. So while there is significant profile sensitivity in the HNO<sub>3</sub> spectra, it is less than for the unblended lines of HCl. The profile information which does exist is probably due to the lines being partially resolved and to the use of multiple manifolds.

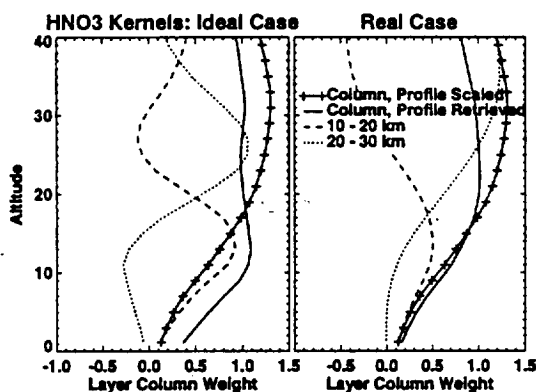


Fig. 2 HNO<sub>3</sub> averaging kernels. The left panel shows results for high signal-to-noise; the right panel for signal-to-noise characteristic of results achieved in practice.

## 2.3 Practical Limitations

Profile retrieval from pressure-broadened line-shapes requires the ability both to make high quality, low noise measurements, and to accurately simulate the observed spectra with a forward model. These are demanding requirements, and unfortunately it has not been possible to achieve in practice the results which might be expected based on the above theoretical analysis. In particular, the information available is limited by our ability to model the measurements and by systematic errors in the measurements themselves. Both effects are manifest by spectral residuals which are non-random, and larger on average than expected from noise. A number of factors are known to contribute here, including the instrument response function, spectroscopic parameters, and forward model approximations. The degradation of the available profile information may be seen in broader and flatter

averaging kernels, implying less discrimination between layers and more influence of the *a priori*.

For HNO<sub>3</sub> as measured at Lauder, the effective signal-to-noise (determined by the magnitude of the spectral residuals) is about 200; the averaging kernels for such measurements are shown on the right-hand panel of Fig. 2. While the comparison to the high signal-to-noise case in the left-hand panel is disappointing, there is still some ability to distinguish the 2 layers, and the total column kernel is still better than that for profile scaling. In the next section we will show results which suggest that useful profile information may be acquired from such measurements in practice as well as in theory.

### 3. Atmospheric Measurements

Despite both theoretical and practical limitations, early results of profile retrievals on atmospheric data are reasonably encouraging. We have made a preliminary analysis of the Lauder HNO<sub>3</sub> data set, and experimented with a small number of Lauder HCl measurements and HNO<sub>3</sub> measurements from Arrival Heights, Antarctica. It should be noted that this is work-in-progress, and that further developments can be expected.

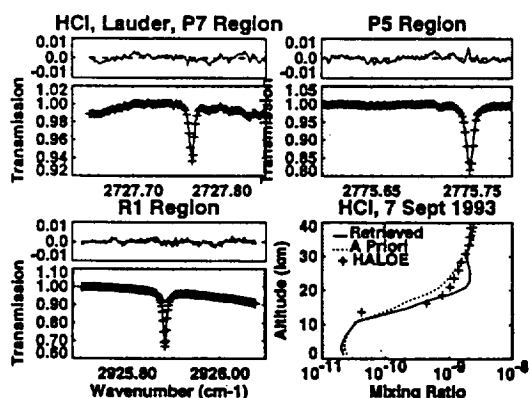


Fig. 3. An HCl retrieval from data of 7 September 1993 at Lauder, New Zealand. The 3 spectra shown were fit simultaneously in retrieving the profile shown in the lower right panel.

#### 3.1 HCl

An example of an HCl spectrum and profile measured at Lauder is shown in Fig. 3. The spectral data quality is excellent and the calculated spectrum fits the measurement to 1:500 on average. It is interesting to note that all 3 spectral regions are fit reasonably well, although small systematic features do dominate the residuals, the most visible being in the P5 line center. Despite this, while the retrieved profile is generally reasonable, there is a significant discrepancy, up to a factor 1.7, with HALOE HCl in the 20-30 km region. The cause of this is still being investigated. A detailed algorithm comparison was recently carried out (A. Goldman, private communication, 1996) which would appear to rule out the algorithm as the principal source of this discrepancy.

#### 3.2 HNO<sub>3</sub>

Measurements have been made at Lauder (45 S) since 1990 at 0.0035 - 0.007 cm<sup>-1</sup> resolution. Fig. 4 shows partial columns in the 10-20 and 20-30 km layers. The data are monthly averages. The solid lines are regression fits to the daily data (not shown) before the Pinatubo eruption and in 1994-95, including annual, semi-annual, and secular terms. Fig 5 shows the ratio of the partial columns. The data show a repeatable annual cycle and a clear response to the Mt. Pinatubo aerosol injection. Further, HNO<sub>3</sub> behaves differently in the two altitude regions. The annual cycle differs in that the autumnal increase is later in the lower layer. Also, the transient response to the Pinatubo aerosol was much greater in the upper layer.

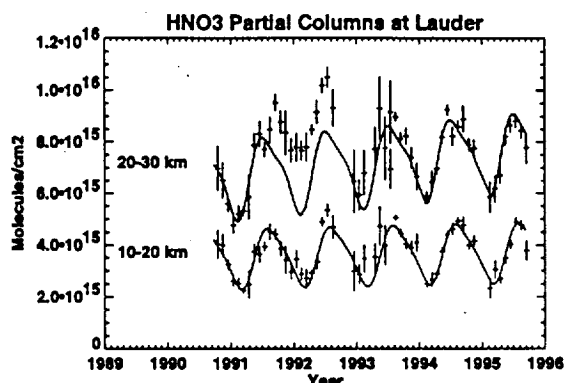


Fig. 4 A time series of HNO<sub>3</sub> in two layers at Lauder. The data points are monthly means. The solid line is a regression fit to single measurements made before and after the atmosphere was perturbed by the eruption of Mt. Pinatubo.

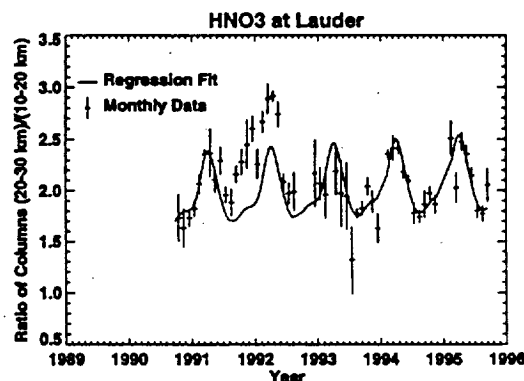


Fig. 5. The ratio of the time series shown in Fig. 4.

HNO<sub>3</sub> measurements are also made routinely at Arrival Heights, Antarctica (78 S). Spectra are recorded at lower resolution (0.02 cm<sup>-1</sup>) than at Lauder, and are generally lower quality (Fig. 6). Nevertheless, trials with the 1993 data show a fall to spring change in profile shape roughly consistent with CLAES measurements (Kumer et al., 1996) in 1992, in that the relative decrease in HNO<sub>3</sub> is greater above 20 km than below.

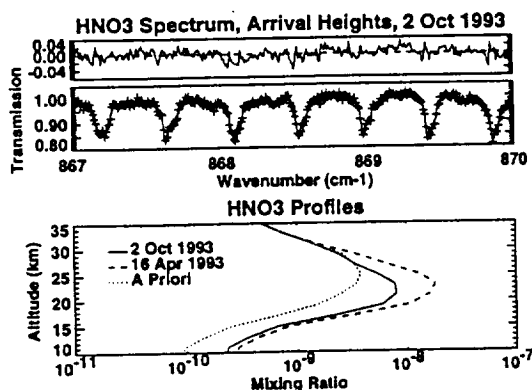


Fig 6. HNO<sub>3</sub> measurements made at Arrival Heights, Antarctica.

#### 4. Conclusions

In summary, a theoretical analysis of the altitude sensitivity of FTIR measurements of HCl and HNO<sub>3</sub> shows that significant profile information exists in both measurements, and that in the case of HCl the range of sensitivity may be extended by use of multiple spectral lines. Experiments with HCl retrievals from Lauder data and HNO<sub>3</sub> retrievals from Arrival Heights have been performed. While the results are generally as expected, there is an apparent anomaly in the HCl profile which is unexplained. Preliminary analysis of a five year time series of HNO<sub>3</sub> data from Lauder shows a behavior in adjacent 10 km layers which is different in the 2 layers, yet repeatable from year to year, and also a response to the Pinatubo aerosol consistent with priori understanding of that event.

**Acknowledgments.** We thank Brian McNamara for recording the spectral data. Funding for this research was provided by the New Zealand Foundation for Science and Technology and by the NASA Upper Atmosphere Research Program.

#### References

- Connor, B.J., A. Parrish, J.J. Tsou, and M.P. McCormick, Error analysis for the ground-based microwave measurements during STOIC, *J. Geophys. Res.*, 100, 9283-9292, 1995.
- Kumer, J.B., et al., Comparison of correlative data with HNO<sub>3</sub> version 7 from the CLAES instrument deployed on the NASA Upper Atmosphere Research Satellite, *J. Geophys. Res.*, 101, 9621-9656, 1996.
- Pougatchev, N.S., B.J. Connor, and C.P. Rinsland, Infrared measurements of the ozone vertical distribution above Kitt Peak, *J. Geophys. Res.*, 100, 16,689-16,698, 1995.
- Pougatchev, N.S., B.J. Connor, N.B. Jones, and C.P. Rinsland, Validation of ozone profile retrievals from ground-based solar spectra, *Geophys. Res. Lett.*, 23, 1637-1640, 1996.
- Rodgers, C.D., Characterization and error analysis of profiles retrieved from remote sounding measurements, *J. Geophys. Res.*, 5587-5595, 1990.
- B.J. Connor, N.B. Jones, S.W. Wood, J.G. Keys, NIWA, Private Bag 50061, Omakau 9182, New Zealand.
- C.P. Rinsland, Mail Stop 401A, NASA Langley Research Center, Hampton, VA 23681, USA
- F.J. Murcray, Department of Physics, University of Denver, Denver, CO 80308, USA







# SPECTROSCOPIC PARAMETERS FOR OZONE AND ITS ISOTOPES: CURRENT STATUS, PROSPECTS FOR IMPROVEMENT, AND THE IDENTIFICATION OF $^{16}\text{O}^{16}\text{O}^{17}\text{O}$ AND $^{16}\text{O}^{17}\text{O}^{16}\text{O}$ LINES IN INFRARED GROUND-BASED AND STRATOSPHERIC SOLAR ABSORPTION SPECTRA

C. P. RINSLAND,<sup>†\*</sup> J.-M. FLAUD,<sup>‡</sup> A. GOLDMAN,<sup>§</sup> A. PERRIN,<sup>‡</sup>  
 C. CAMY-PEYRET,<sup>¶</sup> M. A. H. SMITH,<sup>†</sup> V. MALATHY DEVI,<sup>||</sup> D. C. BENNER,<sup>||</sup>  
 A. BARBE,<sup>\*\*</sup> T. M. STEPHEN<sup>§</sup> and F. J. MURCRAY<sup>§</sup>

<sup>†</sup>NASA Langley Research Center, Mail Stop 401A, Hampton, VA 23681-0001, U.S.A., <sup>‡</sup>Laboratoire de Photophysique Moléculaire, CNRS, Bât. 210, Université Paris-Sud, Campus d'Orsay, 91405 Orsay Cedex, France, <sup>§</sup>Department of Physics, University of Denver, Denver, CO 80208, U.S.A., <sup>¶</sup>Laboratoire de Physique Moléculaire et Applications, CNRS, Boite 76, Université Paris VI, 4 Place Jussieu, 75252 Paris Cedex 05, France, <sup>||</sup>Department of Physics, The College of William and Mary, Williamsburg, VA 23187-8795, U.S.A. and <sup>\*\*</sup>Groupe de Spectrométrie Moléculaire et Atmosphérique, Université de Reims, Equipe Associée au CNRS, UPRESA Q 6089 et ce n'est plus D 1434, UFR Sciences, B. P. 1039, 51687 Reims Cedex 2, France

(Received 5 June 1997)

**Abstract**—We describe the updates to the spectroscopic parameters of ozone and its isotopes in the 1996 HITRAN compilation. Recent published studies not included in HITRAN are also summarized. Finally, we report the identification of infrared lines of the  $\nu_3$  bands of  $^{16}\text{O}^{16}\text{O}^{17}\text{O}$  and  $^{16}\text{O}^{17}\text{O}^{16}\text{O}$  in high-resolution solar spectra recorded by stratospheric balloon-borne and ground-based Fourier transform spectrometers. Published by Elsevier Science Ltd.

## 1. INTRODUCTION

Spectroscopic parameters of ozone are required for virtually all remote-sensing applications involving the chemistry of the troposphere and stratosphere. The vertical distribution of ozone also influence the thermal structure of the atmosphere by absorbing and reemitting radiation in the 8–12  $\mu\text{m}$  window. Hence, the knowledge of the  $\text{O}_3$  vertical distribution is needed for climate research.<sup>1–4</sup> For these reasons, numerous experimental and theoretical investigations have focused on improving our knowledge of infrared, microwave, and electronic ozone spectroscopy.<sup>5,6</sup>

The main purpose of this paper is to document the updates to the ozone spectroscopic parameters in the 1996 HITRAN compilation.<sup>7</sup> A total of 30 bands have been added and nine bands have been modified since the 1992 edition,<sup>8–10</sup> extending the upper wave number limit of the compilation from 3400 to 4100  $\text{cm}^{-1}$ . The updates include lines of the  $^{16}\text{O}^{16}\text{O}^{17}\text{O}$  and  $^{16}\text{O}^{17}\text{O}^{16}\text{O}$  isotopic species which appear in the microwave and infrared sections of the compilation for the first time. However, the new edition does not include the results of many recent studies, and in fact, presently, no parameters are included for the near infrared, visible, and UV spectral regions. Therefore, as a second part of the paper, we provide a brief overview of recent laboratory and modeling work on ozone and its isotopes and highlight areas in need of further investigation. Finally, we present the identification of lines of  $\nu_3$  bands of  $^{16}\text{O}^{16}\text{O}^{17}\text{O}$  and  $^{16}\text{O}^{17}\text{O}^{16}\text{O}$  in high-resolution infrared ground-based and stratospheric solar absorption spectra.

\*To whom all correspondence should be addressed.



# Increase in the vertical column abundance of HCFC-22 (CHClF<sub>2</sub>) above Lauder, New Zealand, between 1985 and 1994

Vanessa J. Sherlock,<sup>1</sup> Nicholas B. Jones,<sup>1</sup> W. Andrew Matthews,<sup>1</sup> Frank J. Murcray,<sup>2</sup> Ronald D. Blatherwick,<sup>2</sup> David G. Murcray,<sup>2</sup> Aaron Goldman,<sup>2</sup> Curtis P. Rinsland,<sup>3</sup> Cirilo Bernardo,<sup>4</sup> and David W. T. Griffith<sup>4</sup>

**Abstract.** Total column abundances of CHClF<sub>2</sub> (HCFC-22) have been retrieved from high-resolution infrared solar absorption spectra recorded at the Network for the Detection of Stratospheric Change (NDSC) station in Lauder, New Zealand (370 m altitude, 45.04°S latitude, 169.68°E longitude). The analysis, based on nonlinear least squares fittings to the unresolved 2ν<sub>6</sub> band Q branch of CH<sup>35</sup>ClF<sub>2</sub> at 829.05 cm<sup>-1</sup>, has been applied to a time series of 670 spectra recorded on 394 days between May 1985 and November 1994. The measurements indicate exponential and linear (referenced to the beginning of 1994) increase rates of (7.5±0.3)% yr<sup>-1</sup> and (5.9±0.2)% yr<sup>-1</sup>, 1σ, corresponding to a doubling of the total column abundance over the 9.5-year measurement period. Of the two models the exponential increase model yields a slightly better fit to the data than the linear model. A HCFC-22 south/north hemispheric ratio of 0.83 ± 0.04, 1σ, is derived by comparing the Lauder column measurements with column measurements from the International Scientific Station of the Jungfraujoch (46.5°N, 8.0°E), after correction for the altitude difference between the two sites. Using a second, independent method in which the N<sub>2</sub>O column serves as a surrogate air mass, we have used the Lauder measurements and similar measurements from Table Mountain (34.4°N) to calculate a south/north ratio of 0.91 ± 0.10.

## Introduction

The role of chlorinated fluorocarbons in the catalytic destruction of stratospheric ozone [Molina and Rowland, 1974; Stolarski and Cicerone, 1974] and greenhouse warming [Ramanathan, 1975] has lead to a series of international agreements [e.g., United Nations Environment Program (UNEP), 1987] limiting their use. Hydrogenated chlorofluorocarbons (HCFCs) are now widely used as replacements in industrial applications. These substitutes are similar to the fully halogenated fluorocarbons in physical and chemical properties, but they have shorter lifetimes due to their reactivity with OH radicals in the troposphere. The reduced radiative forcing and reduced potential for stratospheric ozone destruction [Fisher et al., 1990a, b] have made the HCFCs important replacements until suitable nonchlorinated compounds become available.

The molecule HCFC-22 (CHClF<sub>2</sub>) is widely employed as a substitute for CFC-11 (CCl<sub>3</sub>F) and CFC-12 (CCl<sub>2</sub>F<sub>2</sub>) [Alternative Fluorocarbons Environmental Acceptability Study, (AFEAS), 1995]. Since 1980, atmospheric emissions of HCFC-22 have increased at a rate of about 8.5% yr<sup>-1</sup> [NASA, 1994]. Approximately 3% of the tropospheric anthropogenic organochlorine loading is contained in HCFC-22 [World Meteorological Organization, (WMO) 1991, section 1.11].

Absorption by HCFC-22 was first identified in the infrared by Goldman et al. [1981]. In that work, the narrow, unresolved Q branch of the 2ν<sub>6</sub> band was measured in stratospheric solar occultation spectra recorded with a balloon-borne Fourier transform spectrometer. That investigation was followed by a series of ground-based, balloon-borne, and space-based IR studies (see the summary by Zander et al. [1994]), including recent trend studies based on total columns measured from the International Scientific Station of the Jungfraujoch (ISSJ), Switzerland (altitude 3580 m, 46.5°N latitude, 8.0°E longitude), between June 1986 and November 1992 [Zander et al., 1994], the National Solar Observatory on Kitt Peak (altitude 2090 m, latitude 31.9°N, longitude 111.6°W) near Tucson, Arizona, between December 1980 and April 1992 [Zander et al., 1994], and the Table Mountain Facility (TMF), Wrightwood, California (34.4°N, 117.7°W) [Irion et al., 1994]. In situ measurements have also been used to measure concentrations and the trend of HCFC-22. The most recent set of surface level air-sampling measurements of HCFC-22 were derived from analysis of flasks and archived air samples from sites between 90°S and 82°N latitude [Montzka et al., 1993]. The global trend between 1987 and 1992 was calculated and the southern hemisphere linear trend in 1992 was inferred from the measured interhemispheric difference in HCFC-22 concentration. The interhemispheric HCFC-22 ratio has been estimated recently from simultaneous total column HCFC-22 and N<sub>2</sub>O measurements from IR spectra recorded in California and Antarctica [Irion et al., 1994].

In this paper, we report the analysis of the first extensive time series of HCFC-22 infrared spectroscopic measurements recorded from the southern hemisphere. The observations were obtained from the Network for the Detection of Stratospheric Change (NDSC) station in Lauder, New Zealand (altitude 0.37 km, latitude 45°S, longitude 170°E). The Lauder station is located in a small town (population ~50) in a region of minimal industrial

<sup>1</sup>National Institute of Water and Atmospheric Research, Lauder, New Zealand.

<sup>2</sup>Department of Physics, University of Denver, Denver, Colorado.

<sup>3</sup>NASA Langley Research Center, Hampton, Virginia.

<sup>4</sup>Department of Chemistry, University of Wollongong, Wollongong, New South Wales, Australia.

Copyright 1997 by the American Geophysical Union.

and best fit calculated spectra and presents molecular identifications of the principal absorption features. Residuals (measured minus calculated values) are shown in the top panel on an expanded vertical scale. A total of seven parameters were fitted: a single parameter to scale the initial vertical distribution of each of the four main absorbing molecules (HCFC-22,  $O_3$ ,  $CO_2$ , and  $H_2O$ ), a parameter to retrieve the shift between the wavenumber scales of the measured and the synthetic spectra, and parameters to model the level and slope of the 100% transmission envelope. The residual spectrum shows the adequacy of the present model in reproducing the measured absorption features to the noise level of the data. The 0.5% residuals in the ozone features are attributed to the shortcomings of the monthly mean  $P$ - $T$  profiles and the assumed ozone volume mixing ratio. As for the sensitivity to the assumed  $P$ - $T$  profiles, we estimate that uncertainty in the absorption due to interfering species introduces a random error of 1% in HCFC-22 column retrievals.

A low-frequency channel spectrum has been identified in some of the early spectra. For these cases, additional parameters were included in the analysis to model the relative amplitude, period, and phase of the channel spectrum. The introduction of these additional parameters allowed the channeling to be fitted to the noise level.

Table 1 summarizes the sources of errors and the corresponding uncertainties in the HCFC-22 total columns attributed to the uncertainties in each component. Except for spectra with channeling, the most important sources of random error are the finite signal-to-noise ratio of the data and errors in fitting nearby interfering lines. The uncertainty in the spectroscopic line parameters is the dominant source of systematic error. We have retained the Zander line parameters for comparison purposes, as noted earlier.

## Results

Monthly mean HCFC-22 total vertical column abundances were calculated from the May 1985 to November 1994 measurements, and linear and exponential increases with time

**Table 1.** Error Sources and Uncertainties for a Single Spectrum

	1 $\sigma$ Uncertainty Percent of Total Column	
	HCFC-22 (pre-1990)	HCFC-22 (post-1990)
<b>Random Error Sources</b>		
Temperature-pressure profile	2	1
Finite signal to noise	5	3
Zero transmission offset	2	1
Interfering absorptions	3	2
Error in 100% transmissioin level <sup>†</sup>	3	1
Variability in assumed VMR profile	<2	<2
Root-sum-square total random error	7	4
<b>Systematic Error Sources</b>		
Target molecule line parameters <sup>‡</sup>	7	7
Bias due to assumed VMR profile	2	2
Error in modeling instrument line shape	3	2
Algorithm uncertainty	2	2
Root-sum-square total systematic error	8	8

<sup>†</sup>Uncertainty is 5% for a spectrum with channeling.

<sup>‡</sup>Value for the line parameters uncertainty is from Zander *et al.* [1994].

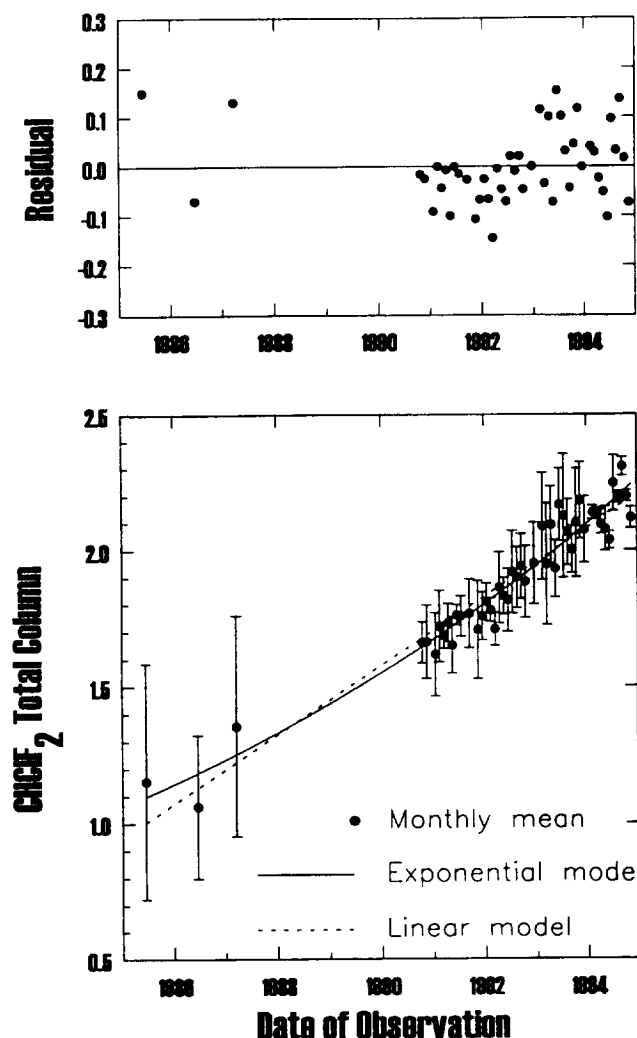


**Figure 2.** Bottom: Monthly mean Lauder HCFC-22 total columns plotted versus time. Error bars show the standard deviations of the measurements. The solid curve and dashed line show best fits to the data assuming exponential and linear increases in the HCFC-22 total column with time, respectively. Top: Total column residuals (measured minus calculated values) plotted versus time on an expanded vertical scale. Residuals obtained assuming an exponential increase with time are shown. The units for the HCFC-22 total columns are  $10^{15}$  molecules  $cm^{-2}$  in both panels.

were fitted to the data. These results are presented in Figure 2 with error bars representing the standard deviations of the monthly means. The number of measurements per month ranged from 6 to 30 for the post-1990 observations with approximately one half of the measurements recorded during 1994. The solid curve in Figure 2 shows the fit to the data derived with the exponential increase model. This curve corresponds to a best fit column increase rate of  $(7.5 \pm 0.3)\% \text{ yr}^{-1}$ ,  $1\sigma$ , and May 1985 and November 1994 total columns (in  $10^{15}$  molecules  $cm^{-2}$ ) of 1.10 and 2.24, respectively. A slightly poorer fit to the measurements is obtained with the linear increase model (dashed line), which returned a best fit column increase rate of  $(5.9 \pm 0.2)\% \text{ yr}^{-1}$ ,  $1\sigma$ , for 1994.0, and May 1985 and November 1994 total columns (in  $10^{15}$  molecules  $cm^{-2}$ ) of 1.02 and 2.18, respectively.

The Lauder monthly average columns show no obvious seasonal cycle, but shorter-term variations are noticeable in the monthly averages from 1993 and 1994. No evidence for a

activity, so that the results should be representative of background conditions. The measurements cover the May 1985 to November 1994 time period and are analyzed here to derive the long-term trend in the HCFC-22 total column. In addition, the south-north hemispheric HCFC-22 ratio is derived from comparisons of the Lauder southern hemisphere HCFC-22 columns with the altitude-corrected columns from two northern hemisphere sites. All columns were derived using the same set of spectroscopic parameters [Zander *et al.*, 1994; Irion *et al.*, 1994]. This paper and the Zander *et al.*, [1994] paper used the same analysis method, Spectrum FIT (SFIT), which is briefly described below in the measurements and data analysis section. The Irion *et al.* [1994] paper used the ATMOS software, described by Norton and Rinsland [1991]. The present results are compared with recently published measurements, trends, and determinations of the interhemispheric HCFC-22 ratio.

### Measurements and Data Analysis

The bulk of the 670 solar spectra analyzed for the HCFC-22 total column was recorded between October 1990 and November 1994 with a Bruker 120 M Fourier transform spectrometer operating at unapodized resolutions of 0.0035 or 0.006  $\text{cm}^{-1}$ , a KCl beam splitter, and a liquid-nitrogen cooled HgCdTe detector. The individual spectra (typical signal-to-noise ratio of 150) cover the 750–950  $\text{cm}^{-1}$  region (October 1990 to March 1993 measurements) or 750–1250  $\text{cm}^{-1}$  (April 1993–November 1994 measurements) and have been used previously to derive total column abundances of  $\text{HNO}_3$  [Jones *et al.*, 1994],  $\text{COF}_2$  [Reisinger *et al.*, 1994], and  $\text{ClONO}_2$  [Reisinger *et al.*, 1995]. These measurements have been supplemented by earlier solar spectra recorded at Lauder during campaigns in May 1985, June 1986, and February 1987 conducted in conjunction with the University of Denver. The campaign measurements cover the 750–1250  $\text{cm}^{-1}$  region and were recorded with a Bomem Fourier transform spectrometer operating at a spectral resolution of 0.02  $\text{cm}^{-1}$  [Murray *et al.*, 1989]. The target HCFC-22 absorption feature in both data sets is the narrow, unresolved  $\text{CH}_3\text{ClF}_2$   $2\nu_6$  band Q branch at 829.05  $\text{cm}^{-1}$ . This feature is relatively weak, and therefore only spectra recorded at astronomical zenith angles above about  $70^\circ$  were analyzed in order to maximize the signal-to-noise ratio in the  $\text{CHClF}_2$  Q branch feature. Only 15 suitable spectra were available from the pre-1990 observations, whereas up to 30 spectra were analyzed from favorable months of 1993 and 1994.

The  $\text{CHClF}_2$  total columns were derived from nonlinear least squares spectral fittings to the 828.7–831.0  $\text{cm}^{-1}$  interval containing the HCFC-22 Q branch and lines of  $\text{H}_2\text{O}$ ,  $\text{CO}_2$ , and  $\text{O}_3$ . The SFIT, PC-based line-by-line retrieval algorithm used in these retrievals [cf. Rinsland *et al.*, 1994] assumes an atmosphere comprised of 29 homogeneous layers with vertical thicknesses of 1 km in the troposphere increasing to 2 km in the stratosphere and 5 to 10 km in the mesosphere. The pressure and temperature, as a function of altitude, are inputs to a ray-tracing program [Gallery *et al.*, 1983] to calculate the total air mass, mass-weighted temperatures, and mass-weighted pressures for each layer along the refracted ray path. For the purposes of this calculation we used monthly mean tropospheric and stratospheric pressure and temperature profiles, as measured by radiosondes launched weekly at the site, in preference to the U.S. Standard Atmosphere pressure-temperature ( $P$ - $T$ ) profiles. Sensitivity studies indicate that the use of monthly mean  $P$ - $T$  profiles introduce a random error of the order of 1% (Table 1) in the retrieved HCFC-22 column.

The volume mixing ratio (VMR) versus altitude distribution assumed for  $\text{CHClF}_2$  is the "reference 1" profile of Zander *et al.* [1994, Table 1]. This profile assumes the mean 1985 ATMOS/Spacelab 3 measurements above 12 km altitude [Zander *et al.*, 1987] and an extension with an almost constant VMR value in the troposphere. The  $\text{CHClF}_2$  total vertical column corresponding to this distribution is  $1.11 \times 10^{15}$  molecules  $\text{cm}^{-2}$ . The vertical profile distributions assumed for other molecules have been taken from reference lists, e.g., Smith [1982]. Spectroscopic line parameters for  $\text{CHClF}_2$  assumed in this work are the same as those described by Zander *et al.* [1994]. Recently, temperature- and pressure-dependent absorption cross sections have been derived for the HCFC-22 829.05- $\text{cm}^{-1}$  Q branch [Varanasi, 1992]. Zander *et al.* [1994] report excellent compatibility between their line parameters and values derived with the high-resolution absorption cross sections of Varanasi [1992]. We have chosen to retain the previous set of spectroscopic parameters in our analysis to maintain consistency with the previously reported IR measurements. The spectroscopic parameters for other gases were taken from a line list essentially the same as the 1992 HITRAN compilation [Rothman *et al.*, 1992].

Figure 1 shows a sample least squares fit derived from a 0.006  $\text{cm}^{-1}$  resolution spectrum. The bottom panel shows the measured

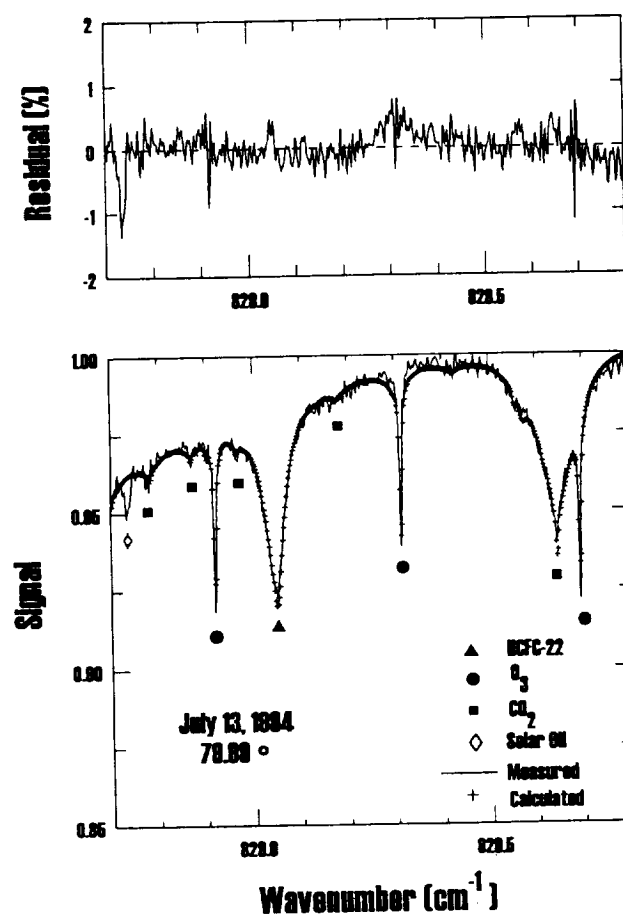


Figure 1. Bottom: Typical post-1990 Lauder solar spectrum in the HCFC-22  $2\nu_6$  band Q-branch region and the corresponding least squares best fit to the data. The measurements were recorded at a resolution of 0.006  $\text{cm}^{-1}$  and an astronomical zenith angle of  $79.99^\circ$  on July 13, 1994. The stronger absorption features are identified beneath the measured spectrum. Top: Differences (measured minus calculated) in percent on an expanded vertical scale.

Table 2. Comparison of Measurements of the Recent HCFC-22 Trend

Location	Method	Time Base	Exponential Trend, % yr <sup>-1</sup>	Linear Trend, % yr <sup>-1</sup>	Reference
Kitt Peak	IR solar	1980-1992	7.00±0.23	6.16±0.20 (1989)	Zander et al. [1994]
Jungfraujoch	IR solar	1986-1992	6.99±0.34	7.45±0.34 (1989)	Zander et al. [1994]
Table Mountain	IR solar	1985-1990	6.7±0.5	5.9±0.8 (1990)	Irion et al. [1994]
Global Mean	In situ	1987-1992	7.3±0.3	5.8±1 (1992)	Montzka et al. [1993]
Lauder	IR solar	1985-1994	7.5±0.3	5.9±0.2 (1994)	this study

seasonal cycle is apparent in the 1985-1988 surface measurements from Cape Grim, Tasmania (41°S) [Montzka et al., 1993, Figure 3], the only previous long-term, southern hemisphere HCFC-22 data set, but published model-calculated total columns for the southern hemisphere predict a ±3% seasonal variation with a peak in August [Irion et al., 1994, Figure 3]. The same model predicts no seasonal variation in the northern hemisphere [Irion et al., 1994, Figure 3], consistent with the analysis by Zander et al. [1994] of their 1986-1992 46.5°N latitude ISSJ total column measurement data set.

In Table 2 the trend in the HCFC-22 total column deduced from the Lauder spectra is compared with recent trend measurements derived from infrared total columns [Zander et al., 1994; Irion et al., 1994] and surface level air-sampling measurements [Montzka et al., 1993]. The agreement between the present results and these previous determinations is excellent.

The HCFC-22 interhemispheric ratio has been derived by two methods. In the first method the infrared total column measurements from Lauder are compared with similar measurements from ISSJ [Zander et al., 1994]. Both studies (and that of Irion et al.) were performed with identical sets of spectroscopic line parameters. The ISSJ observatory is located at 46.5°N, thus we obtain an approximate 45°N-45°S interhemispheric ratio, once altitude differences have been applied. The relative difference in the HCFC-22 column above the two stations was first calculated assuming the same vertical distribution above both sites and a constant volume mixing ratio between 0.37 and 3.58 km, the altitudes of Lauder and ISSJ, respectively. This factor, 1.508, was used to scale the ISSJ total columns derived for mid-year 1991 and 1992 [Zander et al., 1994, Table 3] to correspond to values for the altitude of the Lauder station. The scaled ISSJ columns and the corresponding Lauder measurements are given in Table 3 along with the

computed south/north column ratios. The mean of the two determinations is 0.83. Similarly, Lauder columns were corrected to Jungfraujoch altitudes and interhemispheric ratios recalculated. The ratios agreed to within 2%, providing some confirmation of uniform mixing of HCFC-22 in the lower troposphere, and the long chemical lifetime of HCFC-22 in this region of the atmosphere. Thus given the uncertainty in the determinations of the columns at the two sites and the uncertainty in the assumed vertical profile shapes, this result is estimated to be accurate to better than 5%.

Spectra containing the  $\nu_1+2\nu_2$  band of N<sub>2</sub>O at 2440 cm<sup>-1</sup> have been recorded at Lauder since August 1993, permitting an independent determination of the interhemispheric ratio. Following the development of Irion et al. [1994] in which the N<sub>2</sub>O column serves as a surrogate air mass, we have calculated the HCFC-22/N<sub>2</sub>O column ratio for 56 days in 1994 when spectra in both wavenumber intervals were recorded. To calculate an interhemispheric ratio for HCFC-22, the northern hemisphere HCFC-22/N<sub>2</sub>O ratios derived by Irion et al. were extrapolated to mid 1994, and assuming a negligible latitudinal or interhemispheric gradient in N<sub>2</sub>O [Prinn et al., 1991], this was ratioed with the corresponding ratio from Lauder data. Using this method we have calculated an interhemispheric ratio of 0.91 ± 0.10.

Our values of 0.83 ± 0.04 and 0.91 ± 0.10 may be compared with the south/north hemispheric ratio of 0.88 ± 0.04, 1σ, derived by Irion et al. [1994] from the results of surface-sampling measurements between 82°N and 90°S latitude reported by Montzka et al. [1993], and 0.86 ± 0.08 derived from total column HCFC-22 and N<sub>2</sub>O measurements recorded in California and Antarctica [Irion et al., 1994]. These measurements also show that the largest gradient in the HCFC-22 instantaneous mixing ratio occurs in the tropics and that the midlatitudes data are characteristic of the latitude-weighted interhemispheric difference (S.A. Montzka, personal communication, 1996). Therefore the comparison between the two results is appropriate. All measurements agree within the respective uncertainties.

Table 3. Comparison of Lauder and Scaled ISSJ HCFC-22 Vertical Total Column Measurements (in 10<sup>15</sup> molecules cm<sup>-2</sup>)

Midyear	Lauder Column <sup>†</sup>	ISSJ Column <sup>‡</sup>	Ratio
1991.5	1.74	2.10	0.829
1992.5	1.87	2.23	0.839
1993.5	2.02	--	
1994.5	2.17	--	

<sup>†</sup>Derived from the exponential fit to the measurements.

<sup>‡</sup>A factor of 1.508 has been applied to scale the published ISSJ columns [Zander et al., 1994] to the altitude of the Lauder station.

## Conclusions

In this paper we have reported HCFC-22 total columns derived from the analysis of 670 high-resolution infrared solar absorption spectra recorded on 394 days between May 1985 and November 1994 at the NDSC station in Lauder, New Zealand. The results show a steady, factor of 2.0 increase in the total column over the 9.5-year span of the measurements. The exponential and linear increase rates and 1σ uncertainties of (7.5 ± 0.3)% yr<sup>-1</sup> and (5.9 ± 0.2)% yr<sup>-1</sup> at 1994.0 derived, respectively, from the

measurements are in excellent agreement with previous determinations of the trend through 1992 [Zander et al., 1994; Montzka et al., 1993] and indicate that rapid accumulation of HCFC-22 in the atmosphere continued during 1993 and 1994. Comparisons of total columns measured at the Lauder station with corresponding values measured at ISSJ [Zander et al., 1994] indicate an instantaneous south/north hemispheric ratio of  $0.83 \pm 0.04$ . An independent calculation, based on the ratio of HCFC-22 and  $N_2O$  columns gives an interhemispheric ratio of  $0.91 \pm 0.10$  for HCFC-22. These results are in agreement within the uncertainties with previous determinations based on surface air sampling [Montzka et al., 1993] and infrared total column [Irion et al., 1994] measurements.

**Acknowledgments.** Research at the NIWA is funded by the New Zealand Foundation for Research, Science, and Technology (contract CO 1221). Research at the University of Denver is funded by grants with the National Aeronautics and Space Administration. The authors thank B. M. McNamara for recording the high-resolution infrared solar spectra.

## References

- Alternative Fluorocarbons Environmental Acceptability Study, production, (AFEAS), sales and atmospheric release of fluorocarbons through 1993, Washington, D. C., 1995.
- Fisher, D. A., C. H. Hales, D. L. Filkin, M. K. W. Ko, N. D. Sze, P. S. Connell, D. J. Wuebbles, I. S. A. Isaksen, and F. Stordal, Model calculations of the relative effects of CFCs and replacements on stratospheric ozone, *Nature*, **344**, 508-512, 1990a.
- Fisher, D. A., C. H. Hales, W.-C. Wang, M. K. W. Ko, and N. D. Sze, Model calculations of the relative effects of CFCs and their replacements on global warming, *Nature*, **344**, 513-516, 1990b.
- Gallery, W. O., F. X. Kneizys, and S. A. Clough, *Environ. Res. Pap.* 828 (AFGL-TR-83-0065), 145 pp., Air Force Geophys. Lab., Bedford, Mass., 1983.
- Goldman, A., F. J. Murcray, R. J. Blatherwick, R. D. Bonomo, F. S. Murcray, F. H. Murcray, and D. G. Murcray, Spectroscopic identification of  $CHClF_2$  (F-22) in the lower stratosphere, *Geophys. Res. Lett.*, **8**, 1012-1014, 1981.
- Irion, F. W., M. Brown, G. C. Toon, and M. R. Gunson, Increase in atmospheric  $CHF_2Cl$  (HCFC-22) over southern California from 1985 to 1990, *Geophys. Res. Lett.*, **21**, 1723-1726, 1994.
- Jones, N. B., M. Koike, W. A. Matthews, and B. M. McNamara, Southern hemisphere seasonal cycle in total column nitric acid, *Geophys. Res. Lett.*, **21**, 593-596, 1994.
- Molina, M. J., and F. S. Rowland, Stratospheric sink for chlorofluoromethanes: Chlorine atom-catalysed destruction of ozone, *Nature*, **249**, 810-812, 1974.
- Montzka, S. A., R. C. Myers, J. H. Butler, J. W. Elkins, and S. O. Cummings, Global tropospheric distribution and calibration scale of HCFC-22, *Geophys. Res. Lett.*, **20**, 703-706, 1993.
- Murcray, F. J., W. A. Matthews, A. Goldman, P. V. Johnston, and C. P. Rinsland,  $NH_3$  column abundances over Lauder, New Zealand, *J. Geophys. Res.*, **94**, 2235-2238, 1989.
- National Aeronautics and Space Administration (NASA), Present state of knowledge of the upper atmosphere 1993: An assessment report, *NASA Ref. Publ.* 1337, 1994.
- Norton, R. H., and C. P. Rinsland, ATMOS data processing and science analysis methods, *Appl. Opt.*, **30**, 389-400, 1991.
- Prinn, R., D. Cunnold, R. Rasmussen, P. Simmonds, F. Alyea, A. Crawford, P. Fraser, and R. Rosen, Atmospheric emissions and trends of nitric oxide deduced from ten years of ALE-GAGE data, *J. Geophys. Res.*, **95**, 18369-18385, 1990.
- Ramanathan, V., Greenhouse effect due to chlorofluorocarbons: Climate implications, *Science*, **190**, 50-52, 1975.
- Reisinger, A., N. B. Jones, W. A. Matthews, and C. P. Rinsland, Southern hemisphere ground-based measurements of carbonyl fluoride ( $COF_2$ ) and hydrogen fluoride (HF): Partitioning between fluoride reservoir species, *Geophys. Res. Lett.*, **21**, 797-800, 1994.
- Reisinger, A., N. B. Jones, W. A. Matthews, and C. P. Rinsland, Southern hemisphere midlatitude ground-based measurements of  $ClONO_2$ : Method of analysis, seasonal cycle, and long-term trend, *J. Geophys. Res.*, **100**, 23,183-23,193, 1995.
- Rinsland, C. P., N. B. Jones, and W. A. Matthews, Infrared spectroscopic measurements of the total column abundance of ethane ( $C_2H_6$ ) above Lauder, New Zealand, *J. Geophys. Res.*, **99**, 25,941-25,945, 1994.
- Rothman, L. S., et al., The HITRAN molecular database: Editions of 1991 and 1992, *J. Quant. Spectrosc. Radiat. Transfer*, **48**, 469-507, 1992.
- Smith, M. A. H., Compilation of atmospheric gas concentration profiles from 0 to 50 km, *NASA Tech. Memo.* 83289, NASA Langley Res. Cent., Hampton, 1982.
- Stolarski, R. S., and R. J. Cicerone, Stratospheric chlorine: A possible sink for ozone, *Can. J. Chem.*, **52**, 1610-1615, 1974.
- United Nations Environment Programme (UNEP), Montreal Protocol on Substances that Deplete the Ozone Layer, Final Act, 1987.
- Varanasi, P., Absorption spectra of HCFC-22 around  $829\text{ cm}^{-1}$  at atmospheric conditions, *J. Quant. Spectrosc. Radiat. Transfer*, **47**, 251-255, 1992.
- World Meteorological Organization (WMO), Scientific assessment of ozone depletion: 1991, *WMO Rep. No. 25*, Geneva, 1991.
- Zander, R., C. P. Rinsland, C. B. Farmer, and R. H. Norton, Infrared spectroscopic measurements of halogenated source gases in the stratosphere with the ATMOS instrument, *J. Geophys. Res.*, **92**, 9836-9850, 1987.
- Zander, R., E. Mahieu, P. Demoulin, C. P. Rinsland, D. K. Weisenstein, M. K. W. Ko, N. D. Sze, and M. R. Gunson, Secular evolution of the vertical column abundance of  $CHClF_2$  (HCFC-22) in the earth's atmosphere inferred from ground-based IR solar observations at the Jungfraujoch and at Kitt Peak and comparisons with model calculations, *J. Atmos. Chem.*, **18**, 129-148, 1994.
- R. D. Blatherwick, A. Goldman, D. G. Murcray, and F. J. Murcray, Department of Physics, University of Denver, Denver, CO 80208-0202. (e-mail: blathe@ncar.ucar.edu; goldman@acd.ucar.edu; murcray@ram.phys.du.edu)
- C. Bernardo and D. W. T. Griffith, Department of Chemistry, University of Wollongong, Wollongong, NSW Australia. (e-mail: Dave\_Griffith@uow.edu.au)
- N. B. Jones, W. A. Matthews, and V. J. Sherlock, NIWA Climate, Private Bag 50061, Omakau, Lauder 9182, New Zealand. (e-mail: n.jones@niwa.cri.nz; a.matthews@niwa.cri.nz)
- C. P. Rinsland, NASA Langley Research Center, Mail Stop 401A, Hampton, VA 23681-0001. (e-mail: rinsland@risbox.larc.nasa.gov)

(Received April 14, 1995; revised February 29, 1996; accepted February 29, 1996.)





# University of Denver infrared spectral atlases

A. Goldman, R. D. Blatherwick, F. J. Murcray, and D. G. Murcray

Atmospheric and laboratory atlases of high-resolution infrared absorption spectra have been generated from data obtained with the University of Denver Michelson-type interferometer balloon-borne spectrometer systems. The main objectives of the atlas work have been the identification and the detailed analysis of stratospheric infrared high-resolution spectral features. The stratospheric atlases cover many spectral intervals and provide tables of line positions and species identifications. High Sun spectra are used for identification of solar lines. Latest editions of these atlases include selected sections in the 760–1950- and 800–1700-cm<sup>-1</sup> regions at 0.02- and 0.002-cm<sup>-1</sup> resolutions, respectively. In addition to the stratospheric atlases, ground-based and laboratory spectral atlases have also been produced. The laboratory spectra of many molecules relevant to stratospheric chemistry have been obtained. A number of ongoing spectroscopic studies have been developed on the basis of the atlas work, including studies of solar and atmospheric spectral features. © 1996 Optical Society of America

## 1. Introduction

The spectral atlas project at the University of Denver (DU) has been dedicated to the identification of stratospheric IR spectral features present in high-resolution solar spectra and to the spectroscopic analysis of specific stratospheric molecules such as O<sub>3</sub>, HNO<sub>3</sub>, ClONO<sub>2</sub>, COF<sub>2</sub>, NO<sub>2</sub>, O<sub>2</sub>, C<sub>2</sub>H<sub>6</sub>, and others. The more recent of these studies have been based on balloon-borne solar absorption spectra at 0.002-cm<sup>-1</sup> resolution and corresponding laboratory spectra.

The atlases produced by this work serve as state-of-the-art catalogs of atmospheric absorption features for use by researchers in identifying features in their own data. The line parameters generated from the spectroscopic analysis are essential to the quantification of molecular species from IR spectra. These line parameters have, in most cases, been added to the HITRAN (high-resolution transmission molecular absorption) and other databases used by atmospheric spectroscopists.

Initially, solar spectra for the atlas project were collected from Denver (elevation 1.6 km) and the nearby Mt. Evans (elevation 4.3 km) by the use of a 0.06-cm<sup>-1</sup> resolution (apodized) interferometer system. From these data, the 775–1300- and 1925–

2175-cm<sup>-1</sup> regions of the atlas have been completed and published in two volumes.<sup>1</sup>

A short summary of the atlas work is given in Table 1. In 1978, the atmospheric spectroscopy group at DU started obtaining IR spectra with a 0.02-cm<sup>-1</sup> resolution (apodized) interferometer system. A large number of high-quality spectra have been obtained, including laboratory spectra, ground-based solar spectra, and aircraft-borne and balloon-borne solar spectra. The spectra were obtained in selected intervals in the 550–2300-cm<sup>-1</sup> region. Many of the laboratory spectra at 0.06- and 0.02-cm<sup>-1</sup> resolutions have been published as a CRC handbook.<sup>2</sup>

Numerous excellent 0.02-cm<sup>-1</sup> resolution spectra were also obtained from the South Pole, which is a unique site for IR observations, in December 1978 and December 1980. Thus work was also started on the *Atlas of South Pole IR Solar Spectra*.<sup>3</sup> The first edition of the South Pole Atlas, including the 760–960-cm<sup>-1</sup> region, was published in March 1982. In the next large-format edition the 1220–1340-cm<sup>-1</sup> region was added.<sup>3</sup>

The first large-format edition of the stratospheric atlas, at 0.02-cm<sup>-1</sup> resolution, was published in February 1982.<sup>4</sup> Several updated editions have since been issued, the most recent of which is the September 1987 edition.<sup>4</sup> This atlas now covers the entire spectral region from 760 to 1950 cm<sup>-1</sup>, except for the 960–1060-cm<sup>-1</sup> interval. The total number of spectral features identified as being genuine (telluric or solar) exceeded 14,000. In parallel with the atmospheric spectra work, the laboratory spectra<sup>5</sup>

The authors are with the Department of Physics, University of Denver, Denver, Colorado 80208.

Received 10 July 1995; revised manuscript received 14 November 1995.

0003-6935/96/162821-07\$10.00/0

© 1996 Optical Society of America

Table 1. DU Spectral Atlases

Atlas	Description	Special Spectroscopic Interest
June 1980 Atmospheric	Ground-based, Denver and Mt. Evans 0.06-cm <sup>-1</sup> resolution 0.006-cm <sup>-1</sup> accuracy 775–1300, 1925–2175 cm <sup>-1</sup>	Stratospheric HNO <sub>3</sub> Tropospheric NH <sub>3</sub> Solar emission
December 1983 Atmospheric	South Pole 0.02-cm <sup>-1</sup> resolution 0.002 cm <sup>-1</sup> accuracy 760–960, 1220–1340 cm <sup>-1</sup>	Stratospheric HNO <sub>3</sub> Solar OH Solar emission
September 1987 Atmospheric	Balloon-borne 0.02-cm <sup>-1</sup> resolution 0.002-cm <sup>-1</sup> accuracy 760–1950 cm <sup>-1</sup> except 960–1060	Stratospheric CF <sub>4</sub> , O <sub>2</sub> , HNO <sub>3</sub> , ClONO <sub>2</sub> Solar emission
October 1994 Atmospheric	Balloon-borne 0.002-cm <sup>-1</sup> resolution 0.0002-cm <sup>-1</sup> accuracy 800–810, 934–960, 990–1002, 1220–1230, 1240–1260, 1540–1610, 1680–1690 cm <sup>-1</sup>	Stratospheric COF <sub>2</sub> , O <sub>2</sub> , O <sub>3</sub> + isotopes, HNO <sub>3</sub>
April 1984 Lab	Single cell Low pressure, room temperature 0.02-cm <sup>-1</sup> resolution 0.002-cm <sup>-1</sup> accuracy 760–2000 cm <sup>-1</sup>	Over 30 molecules
1995 Lab	Single cell Low pressure, room temperature 0.002-cm <sup>-1</sup> resolution 0.0002-cm <sup>-1</sup> accuracy 760–3100 cm <sup>-1</sup>	Over 15 molecules

were used not only to support the identification and the quantification of measured atmospheric features but also for molecular spectroscopy analysis. Numerous scientific publications resulting from the atlas work are listed in that report.<sup>4</sup>

In 1986 our atmospheric spectroscopy group at DU began using a new Bomem interferometer system with a total path difference of 250 cm and an unapodized FWHM resolution of 0.002 cm<sup>-1</sup>. The system was modified for balloon-borne measurements of IR solar spectra and has also been used to obtain numerous ground-based solar spectra and laboratory spectra. The 0.002-cm<sup>-1</sup> resolution exceeds both the previous DU and the atmospheric trace molecule spectroscopy (ATMOS) resolutions, and thus the DU balloon-borne spectra obtained since 1986 have revealed many new atmospheric features especially those stratospheric features that are blended at lower resolution and have become an invaluable source for extending the atlases' work and probing the atmospheric trace gases.

Results obtained from the high-resolution atlas studies are presented in the preliminary November 1989 and April 1990 editions of the *Atlas of Very High Resolution Stratospheric IR Absorption Spectra* and the subsequent December 1990, April 1992, April 1993, and October 1994 editions.<sup>6</sup> The spectra are now displayed in frames of 2-cm<sup>-1</sup> intervals, which are needed to show the fine details of the spectra. The tabulated line positions were determined with the same line-marking computer program employed in our previous atlases. For well-

resolved lines, line positions given here have an estimated accuracy of  $\pm 0.0002$  cm<sup>-1</sup> with reference to standard calibration lines of CO<sub>2</sub> and N<sub>2</sub>O.<sup>7,8</sup>

In the April 1993 edition, we added the 1540–1560-cm<sup>-1</sup> region, thus bringing the total number of spectral features identified as being genuine to over 3300. Data for this new addition were recorded during a balloon flight from Palestine, Texas, on 17 June 1991, with the exception of the top displayed scan (high Sun scan), which is from a flight conducted from Ft. Sumner, New Mexico, on 19 April 1989. In the October 1994 edition, we added the 1560–1610-cm<sup>-1</sup> region, thus bringing the total number of spectral features identified as being genuine to over 3500. Numerous publications describing findings from the 0.002-cm<sup>-1</sup> atlas work are listed in the atlas reports.<sup>6</sup>

Since 1990, our atmospheric spectroscopy group at DU has acquired improved Bomem and Bruker 0.002-cm<sup>-1</sup> interferometers. These have been employed for the NASA NDSC (Network for the Detection of Stratospheric Change) and other field measurements programs. Data from these systems have been available for studies that are complementary to the atlas work.

Our ongoing laboratory spectra measurements have produced a large number of 0.002-cm<sup>-1</sup> resolution spectra in selected spectral regions from 750 to 3000 cm<sup>-1</sup>. These include CCl<sub>4</sub>, CCl<sub>2</sub>F<sub>2</sub>, C<sub>2</sub>H<sub>6</sub>, CF<sub>4</sub>, CHCl<sub>3</sub>, CH<sub>2</sub>O, CH<sub>3</sub>Cl, H<sub>2</sub>O<sub>2</sub>, HCOOH, HNO<sub>3</sub>, NO<sub>2</sub>, ClONO<sub>2</sub>, COF<sub>2</sub>, and COCl<sub>2</sub>, which are being prepared for an extended laboratory atlas.<sup>9</sup> These

spectra are used for the identification and the quantification of atmospheric spectral features by either complete spectroscopic quantum-mechanical analysis or semiempirical methods. Several spectral regions, which include previously unidentified features of  $\text{ClONO}_2$ ,  $\text{HNO}_3$ ,  $\text{COF}_2$ , and more, are currently under analysis and will be added to the atlas in the near future.

During the atlas work, a number of atmospheric and solar features were identified, including the first spectral identification of stratospheric  $\text{ClONO}_2$ ,  $\text{CF}_4$ ,  $\text{CHClF}_2$  (F-22),  $\text{C}_2\text{H}_6$ ,  $\text{C}_2\text{H}_2$ ,  $\text{HCOOH}$ , and solar OH. Stratospheric mixing-ratio profiles were retrieved for most of the molecules of atmospheric chemistry interest. Below, however, we present in some detail several of the research topics of current interest that originated on the basis of the atlas work:  $\text{O}_2$  forbidden lines in (0-1)  $X^3\Sigma_g^-$ ,  $\text{HNO}_3$  hot bands, OH pure rotation lines, and solar emission IR lines.

## 2. $\text{O}_2$ Forbidden Lines in (0-1) $X^3\Sigma_g^-$

The first identification and the initial line-parameter calculations of the electric-quadrupole (eq) (0-1) vibration-rotation  $\text{O}_2$  lines in  $X^3\Sigma_g^-$  were made on the basis of a peculiar unidentified triplet near  $1603.8\text{ cm}^{-1}$  in DU balloon-borne  $0.02\text{-cm}^{-1}$  resolution spectra.<sup>10-12</sup> These  $\text{O}_2$  transitions were soon confirmed in laboratory spectra.<sup>13</sup> In an unrelated study, eq lines in the red system  $X^3\Sigma_g^-(0) \rightarrow b^1\Sigma_g^-(0)$  near  $13,200\text{ cm}^{-1}$  were observed in the Kitt Peak solar spectrum.<sup>14</sup> The original  $\text{O}_2$  triplet also appears in the DU  $0.02\text{-cm}^{-1}$  atlas of September 1987.<sup>4</sup> Fig. 1 shows the  $1602\text{--}1604\text{-cm}^{-1}$  frame in the DU  $0.002\text{-cm}^{-1}$  atlas of October 1994.<sup>6</sup>

An intensive search for the (0-1) magnetic-dipole (md) lines resulted in the first positive identification and line-parameter calculations on the basis of both

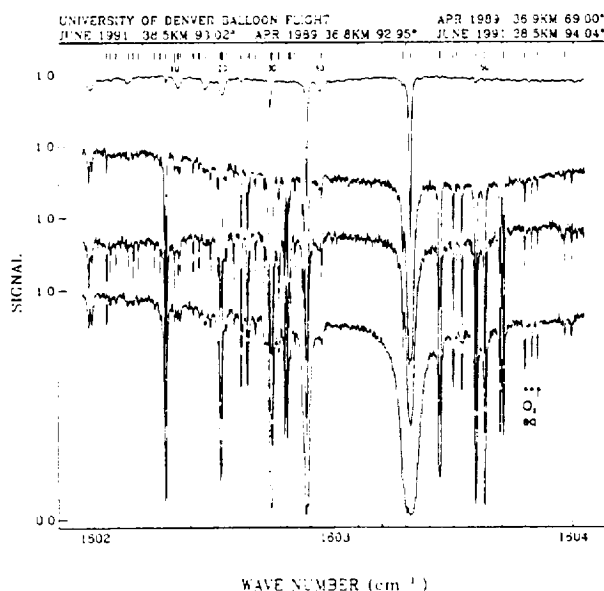


Fig. 1. The  $1602\text{--}1604\text{-cm}^{-1}$  frame of the DU  $0.002\text{-cm}^{-1}$  resolution stratospheric atlas,<sup>6</sup> which shows the  $\text{O}_2$  eq triplet near  $1603.8\text{ cm}^{-1}$ .

ATMOS and DU solar absorption spectra.<sup>15</sup> For both eq and md transitions, the intensity calculations were done<sup>16,17</sup> from Hund's case (b), and a single md moment was used with the energy eigenvectors for the md lines. Subsequent line-intensity calculations of the eq lines in intermediate coupling starting from Hund's case (a) and including vibration-rotation effects on the line intensities showed only minor improvements for a few lines compared with the initial eq intensity calculations in Hund's case (b).<sup>16,17</sup>

Improved energy level constants<sup>18</sup> prompted a new calculation of the line parameters.<sup>19</sup> These results provided improved agreement with DU high-resolution ( $0.002\text{-cm}^{-1}$ ) stratospheric spectra up to all the high  $J$  values observed. However, an ongoing line-intensity problem, which was mostly due to the (0-1) md lines, persisted. The comparisons of synthetic spectra with the observed spectra show excessive calculated intensity in the  $QP$  and  $QR$  lines and missing intensity in the  $QQ$  lines.

The DU  $0.002\text{-cm}^{-1}$  resolution October 1994 atlas<sup>6</sup> shows a number of frames with  $\text{O}_2$  eq and md lines among the other species. The complete identification list is in the Tables volume of the atlas. Figure 2 shows the  $1552\text{--}1553\text{-cm}^{-1}$  section from the atlas, along with a theoretical simulation of the atmospheric components, including the eq and md  $\text{O}_2$  lines. It demonstrates how the  $QR$  and the  $QP$  md lines are overcalculated. Additional quantitative

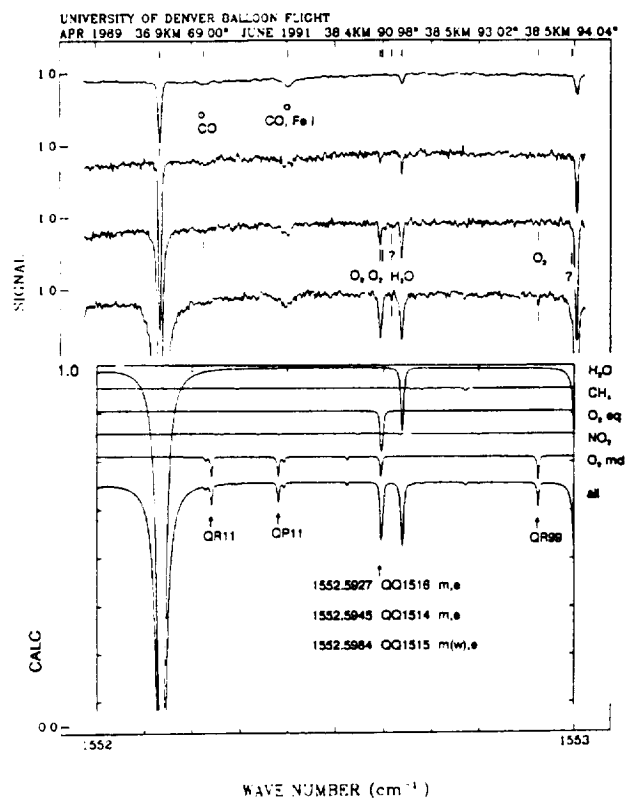


Fig. 2. The  $1552\text{--}1553\text{-cm}^{-1}$  section from the DU  $0.002\text{-cm}^{-1}$  resolution stratospheric atlas<sup>6</sup> and a simulation of absorption by the individual atmospheric molecular species.

spectral fits of the simulations to the observed spectra show how the  $O_2$  md QQ lines are undercalculated.

More recently, intermediate coupling intensity calculations starting from Hund's case (a) were performed for the md lines with both parallel and perpendicular dipole moments.<sup>20,21</sup> These calculations show significant intensity variation as a function of the ratio of the parallel and the perpendicular components and that an optimal ratio of approximately -0.1 improves the agreement with the observed spectra. Figure 3 shows such typical comparisons.

It is also anticipated that the corresponding electric-dipole  $^{16}O^{18}O$  lines will be observable in the atmospheric spectra. Line parameters have been generated on the basis of published  $^{16}O_2$  constants and theoretical isotopic ratios, and a search for these lines is being conducted.

### 3. $HNO_3$ Hot Bands

The stratospheric and laboratory atlases' work has contributed significantly to the study of the  $HNO_3$  bands. The earlier studies are too numerous to be discussed here. Of particular current interest are the recent and the ongoing studies of the hot bands and of the line and band intensities.

In the 25- $\mu m$   $HNO_3$  region dominated by  $\nu_9$ , the HITRAN 1992 compilation provides line parameters only for the  $\nu_9$  band.<sup>22</sup> The  $\nu_9$  line positions are based on the analysis of high-resolution laboratory

spectra,<sup>23</sup> and the total band intensity is derived from previous low-resolution broadband measurements.<sup>24</sup> Recent extensive studies of this region at high resolution led to a revised consistent identification of the hot bands in this region, and line parameters for several of these bands are being generated.<sup>25</sup> New quantitative tunable diode laser measurements of individual intensities of  $\nu_9$  lines and a corresponding total band intensity are in progress.<sup>26</sup>

The new hot-band work in the  $\nu_9$  region also provided interesting new results for the 11- $\mu m$  region dominated by  $\nu_5$  and  $2\nu_9$ . We have been aware, since 1971, of a weak band in the  $HNO_3$  spectra near 830  $cm^{-1}$ . With the recent work, it became possible to assign this absorption to the  $3\nu_9 - \nu_9$  Q-branch and provide quantitative analysis of both laboratory and atmospheric spectra.<sup>27</sup> The high-resolution laboratory spectra of this region clearly show torsional splitting in the  $\nu_3 = 3$  level.

Quantitative analysis of atmospheric spectra of  $HNO_3$  is mostly performed from selected manifolds from the  $\nu_5$ ,  $2\nu_9$  region. The line parameters of these two bands have been improved significantly.<sup>28</sup> They show very good agreement with both laboratory and atmospheric spectra and are included in the HITRAN 1995 compilation. However, the analysis of the hot-band transitions in this region is still incomplete.

HITRAN '92 lists two hot bands<sup>29</sup> at 877 and at 885  $cm^{-1}$ , which are assigned as  $\nu_5 + \nu_9 - \nu_9$  and  $3\nu_9 - \nu_9$ , respectively. The first one is incorrect and has been eliminated from the line data. The second band is clearly seen in our laboratory and stratospheric spectra as a sharp Q-branch centered at 885.425  $cm^{-1}$ . The recent  $\nu_9$  hot-band work allows us to assign it to  $\nu_5 + \nu_9 - \nu_9$  and provides initial line parameters for quantitative simulations. This work is in progress. Individual transitions from the  $\nu_5 - \nu_9 - \nu_9$  are not assigned yet, and additional studies are required. Figures 4 and 5 show recent DU 0.002- $cm^{-1}$  balloon-borne data with the  $\nu_5 + \nu_9 - \nu_9$  analysis. For atmospheric applications, it is fortunate that most of the absorption by this band is concentrated in the narrow Q-branch region, with only weak absorption outside. However, the spectroscopic analysis of the Q-branch is difficult (because of a lack of fine structure) and is still incomplete.

Several recent and ongoing studies have been dedicated to a more accurate and consistent determination of the absolute intensity for the  $HNO_3$  bands in the  $\nu_2$ ,  $\nu_3$ ,  $\nu_4$ , and  $\nu_5$ ,  $2\nu_9$  regions. The work is not complete, and the standing recommendation is to normalize to previous results<sup>30</sup> with the proper hot-band correction.

Further improvements are expected from intensity measurements of individual lines in this region, which is in progress.

### 4. OH Pure Rotation Lines

The first identification of the pure rotation solar OH lines was made from several sets of line quadruplets

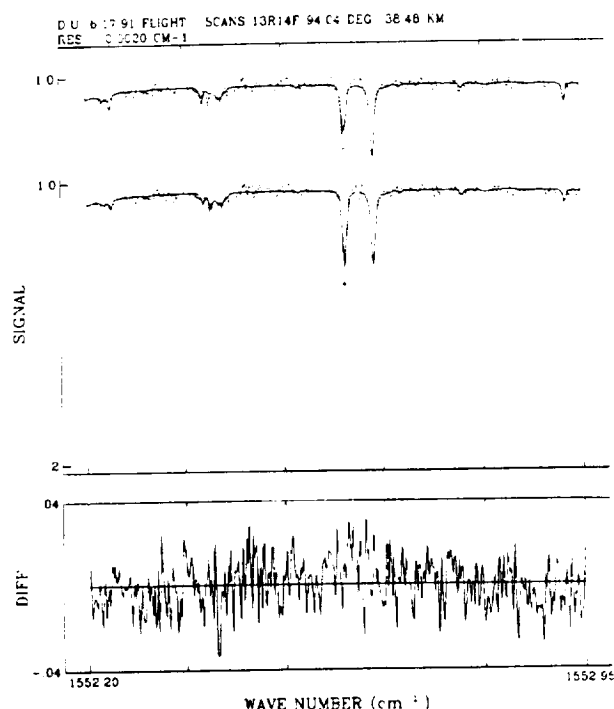


Fig. 3. The 1552.2–1552.95- $cm^{-1}$  section from the 94.04° zenith angle scan from the 6.17.91 DU 0.002- $cm^{-1}$  resolution balloon flight and a simulation of the absorptions by the use of the old and the updated line intensities for  $O_2$  md lines. The difference plot in the lower frame is for the case of the new md lines.

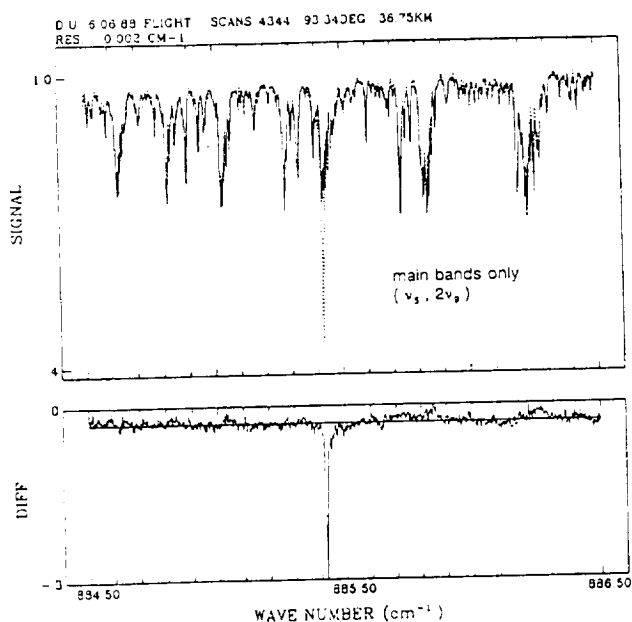


Fig. 4. Spectral least-squares fitting to balloon-borne solar spectra obtained during a DU balloon flight of 6 June 1988, with the recent  $\text{HNO}_3$  line parameters in the  $885\text{-cm}^{-1}$  region. Only the main bands,  $\nu_3$  and  $2\nu_3$ , are included.

in the  $830\text{--}930\text{-cm}^{-1}$  region, which were observed in high Sun solar spectra obtained during the DU March 1981 balloon flight. The lines were assigned as  $X^2\Pi\text{--}0\text{--}0$  and  $(1\text{--}1)$  OH transitions.<sup>31</sup> Subsequently, more  $\Delta v = 0$  lines with  $v = 1, 2$  were identified in the DU March 1981 flight and the DU South Pole atlas.<sup>32</sup> Figure 6 shows the  $920\text{--}930\text{-cm}^{-1}$  interval from the DU September 1987  $0.02\text{-cm}^{-1}$  strato-

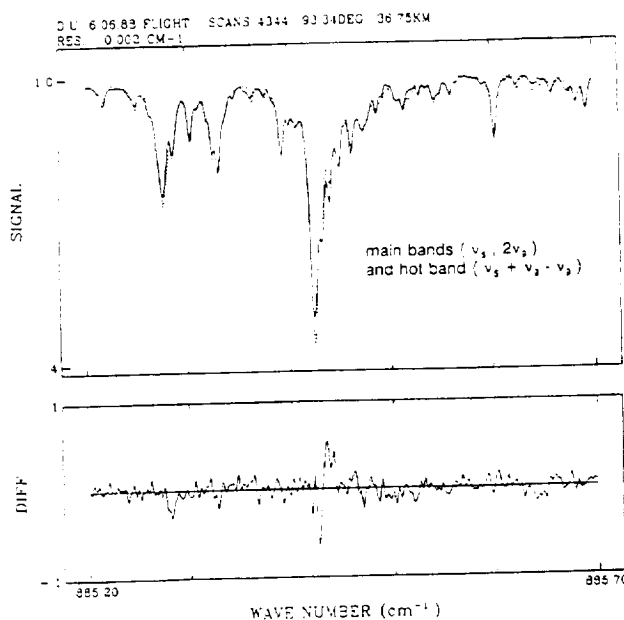


Fig. 5. Spectral least-squares fitting to balloon-borne solar spectra obtained during a DU balloon flight of 6 June 1988, with the recent  $\text{HNO}_3$  line parameters in the  $885\text{-cm}^{-1}$  region. Both the main  $\text{HNO}_3$  bands  $\nu_3$ ,  $2\nu_3$  and the hot band  $\nu_3 + \nu_4 - \nu_5$  preliminary calculation are included.

spheric atlas.<sup>4</sup> The emphasis is on the spectral features of stratospheric species in this region, which are mostly due to  $\text{CF}_2\text{Cl}_2$  (CFC-12) and  $\text{HNO}_3$ . These spectral features are resolved to numerous components at higher resolution, and the detailed identifications are not yet completed for the  $0.002\text{-cm}^{-1}$  resolution stratospheric atlas.

Additional observations and studies of OH and O in the solar photosphere followed, on the basis of the DU spectra<sup>32</sup> and of the Kitt Peak spectra.<sup>33</sup> The latter provided  $\Delta v = 0$  lines up to  $v = 3$ . Further extension of the identification of the solar pure rotation OH lines were accomplished from the ATMOS solar spectra, with lines up to  $v = 4$ .<sup>34</sup>

Line parameters for the pure rotation OH lines were generated since their first identification, with the available state-of-the-art spectroscopic constants and assuming a fixed dipole moment function of  $1.667D$ .<sup>35</sup> Improved absolute intensity by wavefunction calculations and an experimental electric-dipole function<sup>36</sup> led to a recent update of the line intensities,<sup>37</sup> but with the old line-position calculations.<sup>35</sup>

The solar OH pure rotation lines observed in the ATMOS spectra and the recently observed lines in ground-based  $360\text{--}570\text{-cm}^{-1}$  spectra from the Jungfraujoch<sup>38</sup> were combined with other published OH data sets to generate a new set of molecular constants.<sup>39</sup> These latest intensity calculations<sup>37</sup> and molecular constants<sup>39</sup> will next be combined to generate a revised line-parameter set.

It is interesting to note that the pure rotation OH lines were also observed in stellar spectra obtained from Kitt Peak.<sup>40</sup> In the same spectra, the  $12\text{-}\mu\text{m}$  Mg I solar emission lines were also observed (see Section 5 below). More recently, the pure rotation OH lines were observed in the emission spectra of the Earth's nighttime air glow layer at  $\sim 100\text{ km}$ .<sup>41</sup>  $\Delta v = 0$  lines from  $v = 0, 1, 2, 3$  were observed in these spectra and used to derive column densities.<sup>41</sup>

## 5. Solar Emission IR Lines

The  $12\text{-}\mu\text{m}$  solar emission lines were initially observed in DU 1976 ground-based solar spectra at  $811.575$  and  $818.058\text{ cm}^{-1}$  as two suspicious features, which were deleted in the DU June 1980 atlas.<sup>1</sup> This can be seen in the  $800\text{--}825\text{-cm}^{-1}$  frame of the atlas. The features were confirmed by continued investigation of ground-based, aircraft, and balloon-borne spectra obtained with different interferometers and displayed simultaneously.<sup>42</sup> Unknown to the authors, the same features were also observed, but not reported, in the Kitt Peak spectra.

Subsequently these features were identified as high  $l$  Rydberg transitions of Mg I.<sup>43</sup> Additional Mg I and Al I lines were identified,<sup>43</sup> and the emission lines were found to exhibit Zeeman splitting.<sup>43,44</sup> More recently, a number of investigators have worked with both the Kitt Peak and the ATMOS solar spectra on the modeling of line formation in both the quiet Sun and the sunspot penumbra.<sup>45-47</sup> These

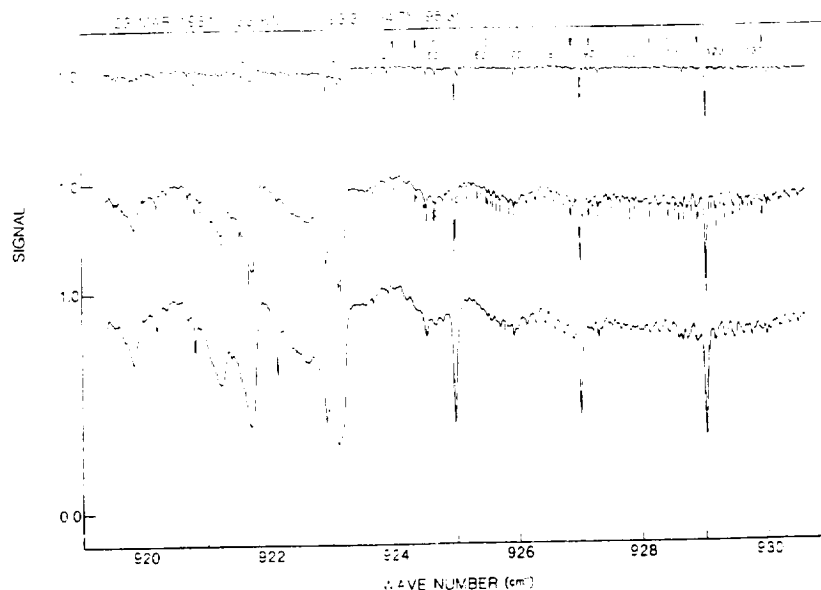


Fig. 6. The 920–930- $\text{cm}^{-1}$  interval from the DU 0.02- $\text{cm}^{-1}$  resolution stratospheric atlas<sup>4</sup> that shows the  $\text{HNO}_3$  and  $\text{CF}_2\text{Cl}_2$  CFC-12 spectral features overlapping the solar pure rotation OH lines. A typical OH quadruplet: lines 37, 40, 51, 55 see atlas<sup>4</sup> tables.

studies provide important results on the solar magnetic fields. As mentioned above, Mg I emission lines were also observed in stellar spectra,<sup>40</sup> albeit as absorption lines.

## 6. Summary

Since 1978, the DU atmospheric spectroscopy group has published several spectral atlases of atmospheric IR spectra obtained from ground-based and balloon-borne platforms as well as from laboratory data.

The spectra in these atlases have provided the first spectroscopic identification and quantification of a number of stratospheric molecular species and have been the basis for the generation of many sets of new spectroscopic line parameters.

The atlas work at DU has been supported by the National Science Foundation, Atmospheric Chemistry Division. Acknowledgment is made to the National Center for Atmospheric Research, which is supported by the National Science Foundation, for computer time used in this research.

## References

1. A. Goldman, R. D. Blatherwick, F. H. Murcray, J. VanAllen, C. M. Bradford, G. R. Cook, and D. G. Murcray, "New atlas of IR solar spectra," *Appl. Opt.* **18**, 604–605 (1979); *New Atlas of IR Solar Spectra*, large-format edition University of Denver, Denver, Col., June 1980.
2. D. G. Murcray and A. Goldman, eds., *Handbook of High Resolution Infrared Laboratory Spectra of Atmospheric Interest* CRC Press, Boca Raton, Fla., 1981.
3. R. D. Blatherwick, F. J. Murcray, F. H. Murcray, A. Goldman, and D. G. Murcray, "Atlas of South Pole IR solar spectra," *Appl. Opt.* **21**, 2658–2659 (1982); *Atlas of South Pole Solar Spectra*, large-format edition University of Denver, Denver, Col., Dec. 1983.
4. A. Goldman, R. D. Blatherwick, F. J. Murcray, J. W. VanAllen, F. H. Murcray, and D. G. Murcray, "Atlas of stratospheric IR absorption spectra," *Appl. Opt.* **21**, 1163–1164 (1982); *Atlas of Stratospheric IR Absorption Spectra*, large-format edition University of Denver, Denver, Col., Feb. 1982; Jan. 1983; Feb. 1985; Nov. 1985; Sept. 1986; Sept. 1987.
5. D. G. Murcray, F. J. Murcray, A. Goldman, F. S. Bonomo, and R. D. Blatherwick, "High resolution IR laboratory spectra," *Appl. Opt.* **23**, 3502 (1984); *High Resolution IR Laboratory Spectra*, large-format edition University of Denver, Denver, Col., April 1984.
6. A. Goldman, R. D. Blatherwick, J. J. Kusters, F. J. Murcray, F. H. Murcray, and D. G. Murcray, *Atlas of Very High Resolution Stratospheric IR Absorption Spectra* Department of Physics, University of Denver, Denver, Col., Dec. 1990; April 1992; April 1993; Oct. 1994, Vol. I, *Line Positions and Identifications*; Vol. II, *The Spectra*.
7. R. A. Toth, "Frequencies of  $\text{N}_2\text{O}$  in the 1100–1440  $\text{cm}^{-1}$  region," *J. Opt. Soc. Am. B* **3**, 1263–1281 (1986).
8. A. G. Maki and J. S. Wells, *Wavenumber Calibration Tables from Heterodyne Frequency Measurements*, NIST Spec. Publ. 821 National Institute of Standards and Technology, U.S. Department of Commerce, Washington, D.C., 1991.
9. D. G. Murcray, F. J. Murcray, A. Goldman, F. S. Bonomo, and R. D. Blatherwick, *Atlas of Very High Resolution Laboratory Spectra* Department of Physics, University of Denver, Denver, Col., 1995.
10. E. Niple, W. G. Mankin, A. Goldman, D. G. Murcray, and F. J. Murcray, "Stratospheric  $\text{NO}_2$  and  $\text{H}_2\text{O}$  mixing ratio profiles from high resolution infrared solar spectra using nonlinear least squares," *Geophys. Res. Lett.* **7**, 489–492 (1980).
11. A. Goldman, J. Reid, and L. S. Rothman, " $\text{O}_2$  and  $\text{N}_2$  lines in the infrared atmospheric absorption spectrum due to the vibration-rotation fundamentals," *Geophys. Res. Lett.* **8**, 77–78 (1981).
12. L. S. Rothman and A. Goldman, "Infrared electric quadrupole transitions of atmospheric oxygen," *Appl. Opt.* **13**, 2182–2184 (1981).
13. J. Reid, R. L. Sinclair, A. M. Robinson, and A. R. W. McKellar, "Observation of electric quadrupole transitions in the fundamental band of  $\text{O}_2$  in the 1600  $\text{cm}^{-1}$  region," *Phys. Rev. A* **24**, 1944–1949 (1981).
14. J. W. Brault, "Detection of electric quadrupole transitions in

- the oxygen A band at 7600Å." *J. Mol. Spectrosc.* **80**, 384–387 (1980).
15. M. Dang-Nhu, R. Zander, A. Goldman, and C. P. Rinsland, "Identification of magnetic dipole transitions of the fundamental band of oxygen," *J. Mol. Spectrosc.* **144**, 366–373 (1990).
16. T. K. Balasubramanian, R. D'Chuna, and K. Narahari Rao, "Line strengths in a  $3\Sigma-3\Sigma$  quadrupole transition with intermediate coupling: application to line intensities in the quadrupole fundamental band of the oxygen molecule," *J. Mol. Spectrosc.* **144**, 374–380 (1990).
17. T. K. Balasubramanian, V. P. Bellary, and R. D'Chuna, "Line strengths for the electric quadrupole fundamental band of the oxygen molecule with rotation-vibration interaction corrections," *J. Mol. Spectrosc.* **153**, 26–31 (1992).
18. G. Rouille, G. Millot, R. Saint-Loup, and H. Berger, "High-resolution stimulated Raman spectroscopy of  $O_2$ ," *J. Mol. Spectrosc.* **154**, 372–382 (1992).
19. C. P. Rinsland, A. Goldman, and J.-M. Flaud, "Infrared spectroscopic parameters of  $COF_2$ ,  $SF_6$ ,  $ClO$ ,  $N_2$  and  $O_2$ ," *J. Quant. Spectrosc. Radiat. Transfer* **48**, 693–699 (1992).
20. T. K. Balasubramanian, V. P. Bellary, and K. Narahari Rao, "Branch intensities in the magnetic dipole rotation-vibration spectrum of the oxygen molecule," *Can. J. Phys.* **72**, 971–978 (1994).
21. A. Goldman, C. P. Rinsland, B. Canova, R. Zander, and M. Dang-Nhu, "Improved spectral parameters for the  $^{16}O_2$  infrared forbidden lines in the  $X^3\Sigma_g^-$  (0–1) band," *J. Quant. Spectrosc. Radiat. Transfer* **54**, 757–765 (1995).
22. A. Goldman and C. P. Rinsland, " $HNO_3$  line parameters: new results and comparisons of simulations with high-resolution laboratory and atmospheric spectra," *J. Quant. Spectrosc. Radiat. Transfer* **48**, 653–666 (1992).
23. A. Goldman, J. B. Burkholder, C. J. Howard, R. Escribano, and A. G. Maki, "Spectroscopic constants for the  $\nu_9$  infrared band of  $HNO_3$ ," *J. Mol. Spectrosc.* **131**, 195–200 (1988).
24. A. Goldman, F. S. Bonomo, W. J. Williams, and D. G. Murcray, "Statistical band model analysis and integrated intensity for the 21.8  $\mu m$  bands of  $HNO_3$  vapor," *J. Opt. Soc. Am.* **65**, 10–12 (1975).
25. A. Perrin, J.-M. Flaud, C. Camy-Peyret, B. P. Winnewisser, A. Goldman, F. J. Murcray, R. D. Blatherwick, F. S. Bonomo, D. G. Murcray, and C. P. Rinsland, "First analysis of the  $3\nu_9-\nu_9$ ,  $3\nu_9-\nu_5$ , and  $3\nu_9-2\nu_9$  bands of  $HNO_3$ : torsional splitting in the  $\nu_9$  vibrational mode," *J. Mol. Spectrosc.* **166**, 224–243 (1994).
26. J. M. Sirota, A. Perrin, M. Weber, D. Steyert, D. Reuter, and J.-M. Flaud, "Absolute line intensities in the  $\nu_9$  region 420 to 460  $cm^{-1}$  of  $HNO_3$  by TDL spectroscopy," presented at the Workshop on Laboratory and Astronomical High Resolution Spectra, Brussels, 29 Aug.–2 Sept. 1994.
27. A. Perrin, J.-M. Flaud, C. Camy-Peyret, A. Goldman, C. P. Rinsland, and M. R. Gunson, "Identification of the  $HNO_3$   $3\nu_9-\nu_9$  band Q branch in stratospheric solar occultation spectra," *J. Quant. Spectrosc. Radiat. Transfer* **52**, 319–322 (1994).
28. A. Goldman, C. P. Rinsland, F. J. Murcray, R. D. Blatherwick, and D. G. Murcray, "High resolution studies of heavy  $NO_y$  molecules in atmospheric spectra," *J. Quant. Spectrosc. Radiat. Transfer* **52**, 367–377 (1994).
29. L. S. Rothman, R. R. Gamache, R. H. Tipping, C. P. Rinsland, M. A. H. Smith, D. C. Benner, V. Malathy Devi, J.-M. Flaud, C. Camy-Peyret, A. Perrin, A. Goldman, S. T. Massie, L. R. Brown, and R. A. Toth, "The HITRAN molecular database: editions of 1991 and 1992," *J. Quant. Spectrosc. Radiat. Transfer* **48**, 469–507 (1992).
30. L. P. Giver, F. P. J. Valero, D. Goorvitch, and F. S. Bonomo, "Nitric-acid band intensities and band model parameters from 610 to 1760  $cm^{-1}$ ," *J. Opt. Soc. Am. B* **1**, 715–722 (1984).
31. A. Goldman, F. J. Murcray, J. R. Gillis, and D. G. Murcray, "Identification of new solar OH lines in the 10–12 micron region," *Astrophys. J.* **248**, L133–L135 (1981).
32. A. Goldman, D. G. Murcray, D. L. Lambert, and J. F. Dominy, "The pure rotation spectrum of the hydroxyl radical and the solar oxygen abundance," *Mon. Not. R. Astron. Soc.* **203**, 767–776 (1983).
33. A. J. Sauval, N. Grevesse, J. W. Brault, G. M. Stokes, and R. Zander, "The pure rotation spectrum of OH and the solar oxygen abundance," *Astrophys. J.* **282**, 330–338 (1984).
34. M. Geller, "A high-resolution atlas of the infrared spectrum of the Sun and the Earth atmosphere from space. Vol. III, *Key to Identification of Solar Features*," NASA Ref. Publ. 1224 (NASA, Washington D.C., 1992).
35. A. Goldman, J. R. Gillis, and J. A. Coxon, "Spectral line parameters for the pure rotation bands of solar OH," *J. Quant. Spectrosc. Radiat. Transfer* **29**, 469–470 (1983).
36. D. D. Nelson, Jr., A. Schiffman, D. J. Nesbitt, J. J. Orlando, and J. B. Burkholder, " $H + O_3$  Fourier-transform infrared emission and laser absorption studies of  $OH(X^2\Pi)$  radical: an experimental dipole moment function and state-to-state Einstein A coefficients," *J. Chem. Phys.* **93**, 7003–7019 (1990).
37. D. Goorvitch, A. Goldman, H. Dothe, R. H. Tipping, and C. Chackerian Jr., "Hydroxyl  $X^2\Pi$  pure rotational transitions," *J. Geophys. Res.* **97**, D18, 20,771–20,786 (1992).
38. C. B. Farmer, L. Delbouille, G. Roland, and C. Servais, "The solar spectrum between 16 and 40 microns," *SJI Tech. Rep. 94-2* San Juan Capistrano Research Institute, San Juan Capistrano, Calif., June 1994.
39. F. Melen, A. J. Sauval, N. Grevesse, C. B. Farmer, L. Delbouille, G. Roland, and C. Servais, "A new analysis of the OH radical spectrum from solar infrared observations," presented at the Workshop on Laboratory and Astronomical High Resolution Spectra, Brussels, 29 Aug.–2 Sept. 1994.
40. D. E. Jennings, D. Deming, G. R. Wiedemann, and J. J. Keady, "Detection of 12-micron Mg I and OH lines in stellar spectra," *Astrophys. J.* **310**, L39–L43 (1986).
41. J. A. Dodd, W. A. M. Blumberg, S. J. Lipson, J. R. Lowell, P. S. Armstrong, D. R. Smith, R. M. Nadile, N. B. Wheeler, and E. R. Huppi, "OH c, N column densities from high-resolution Earthlimb spectra," *Geophys. Res. Lett.* **20**, 305–308 (1993).
42. F. J. Murcray, A. Goldman, F. H. Murcray, C. M. Bradford, D. G. Murcray, M. T. Coffey, and W. G. Mankin, "Observation of new emission lines in the infrared solar spectrum near 12.33, 12.22 and 7.38 microns," *Astrophys. J.* **247**, L97–L99 (1981).
43. E. S. Chang and R. W. Noyes, "Identification of the solar emission lines near 12 microns," *Astrophys. J.* **275**, L11–L13 (1983).
44. J. Brault and R. Noyes, "Solar emission lines near 12 microns," *Astrophys. J.* **269**, L61–L66 (1983).
45. D. Deming, R. J. Boyle, D. E. Jennings, and G. Wiedemann, "Solar magnetic field studies using the 12 micron emission lines. I. Quiet Sun time series and sunspot slices," *Astrophys. J.* **333**, 978–995 (1988).
46. D. Glenar, D. C. Reuter, and D. Deming, "Mg I absorption features in the solar spectrum near 9 and 12 microns," *Astrophys. J.* **335**, L35–L38 (1988).
47. E. S. Chang, E. H. Avrett, P. J. Mauas, R. W. Noyes, and R. Loeser, "Formation of the infrared emission lines of Mg I in the solar atmosphere," *Astrophys. J.* **379**, L79–L82 (1991).





# Comparison of infrared and Dobson total ozone columns measured from Lauder, New Zealand

Curtis P. Rinsland,<sup>1</sup> Brian J. Connor,<sup>2</sup> Nicholas B. Jones,<sup>2</sup> Ian Boyd,<sup>2</sup> W. Andrew Matthews,<sup>2</sup> Aaron Goldman,<sup>3</sup> Frank J. Murcray,<sup>3</sup> David G. Murcray,<sup>3</sup> Shelle J. David,<sup>3</sup> and Nikita S. Pougatchev<sup>4</sup>

**Abstract.** Ozone total columns have been derived from 13 spectral intervals in 5 infrared bands and compared with values deduced from correlative measurements with a Dobson spectrophotometer. The observations were recorded on 10 days in 1994 at the Network for the Detection of Stratospheric Change station in Lauder, New Zealand. The infrared total columns were derived from spectral fittings of unblended, temperature-insensitive ozone lines in high resolution solar absorption spectra. The line parameters on the 1992 HITRAN compilation were assumed with the O<sub>3</sub> and H<sub>2</sub>O relative volume mixing ratio and temperature profiles specified from correlative balloon ozonesonde, microwave O<sub>3</sub>, and radiosonde measurements. The retrieved IR/Dobson total column ratios ranged from 0.96 to 1.02 with the lower wavenumber bands yielding lower ratios. The results do not support the revised O<sub>3</sub> intensity scale currently used to process O<sub>3</sub> infrared measurements from 2 instruments on the Upper Atmosphere Research Satellite.

## Introduction

Accurate measurement of the total vertical column of ozone and its variation with time are crucial experimental problems in environmental science. For several reasons, ground-based infrared solar absorption spectroscopy is an attractive option among the methods in use for measuring O<sub>3</sub>. First, high spectral resolution (<0.005 cm<sup>-1</sup>) is obtainable with modern, commercial Fourier transform spectrometers. Measurements at high resolution make it possible to select unsaturated, temperature-insensitive ozone features with minimal overlap by interfering lines. Suitable transitions are available between 2.3 and 13 μm. Second, extensive laboratory work on ozone in the infrared has been performed during the last several years. These studies have resulted in improved positions, intensities, air-broadening coefficients, and their temperature dependences [Flaud *et al.*, 1992]. Finally, solar absorption spectroscopy avoids the need for radiance calibration since the analysis is performed by fitting the measured spectral features with respect to the local 100% transmittance level. This level is accurately retrieved as part of the spectral fitting procedure. Therefore, biases produced by changes in instrument calibration are avoided.

IR absorption spectroscopy is however affected by uncertainties of several percent in the absolute O<sub>3</sub> line intensities on the

1992 HITRAN compilation [Rothman *et al.*, 1992]. In an attempt to improve the accuracy, Pickett *et al.* [1992] derived absolute intensities for 49 lines in the 9.6 μm ν<sub>3</sub> band based on simultaneous O<sub>3</sub> absorption measurements in the IR and at 253.7 nm, where the absolute cross section is known to 1%. A multiplicative factor of 1.051 for the ν<sub>3</sub> intensities on the 1992 HITRAN compilation [Rothman *et al.*, 1992] was derived, and has been applied in the analysis of the 9.6 μm O<sub>3</sub> measurements recorded by the Halogen Occultation Experiment (HALOE) [Bruhl *et al.*, 1996] and the Improved Stratospheric and Mesospheric Sounder (ISAMS) [Connor *et al.*, 1996] instruments on the Upper Atmosphere Research Satellite (UARS). The 1992 HITRAN parameters are assumed in the analysis for O<sub>3</sub> from the 14 μm UARS CLAES (Cryogenic Limb Etalon Spectrometer) instrument measurements [Bailey *et al.*, 1996].

Additional problems with the infrared approach are the effects of uncertainties in the instrument line shape, the assumed vertical volume mixing ratio distributions of the target and interfering molecules, and the temperature profile [Zander *et al.*, 1994]. The source of line shape problem appears to be optical misalignments in the instrument which cause the actual line shape to differ from the theoretical one calculated on the basis of the internal field of view, the applied apodization function, and the maximum optical path difference. Sensitivity studies have shown that biases of up to several percent in retrieved total columns can result if these effects are not modeled [Zander *et al.*, 1994].

Recently, David *et al.* [1993] compared infrared total columns measured at Mauna Loa, Hawaii, with correlative Dobson spectrophotometer measurements. Based on 2 windows about 0.5 cm<sup>-1</sup> wide centered near 1146 and 1163 cm<sup>-1</sup>, the 1992 HITRAN compilation spectral parameters [Rothman *et al.*, 1992], and an initial O<sub>3</sub> profile based on seasonally averaged measurements, the authors deduced IR total columns on average 1.046 times lower than the Dobson values. Assuming the Pickett *et al.* [1992] scaling of the 1992 HITRAN intensities [Rothman *et al.*, 1992], the average difference increased to 9.9% with the IR columns remaining systematically lower.

The Dobson/IR discrepancy noted above highlights the need for further investigations to ascertain the quality of ozone total columns derived from high resolution IR techniques. We report here comparisons between ozone total columns deduced from 13 spectral intervals covering 5 infrared bands and correlative Dobson total columns. The measurements were recorded on 10 days at the Network for the Detection of Stratospheric Change (NDSC) [Kurylo, 1991] station in Lauder, New Zealand (45.04°S, 169.68°E, 0.37 km a.s.l.). The sample is large enough to determine a statistically meaningful mean IR/Dobson column ratio and root-mean-square deviation of this ratio for each spectral interval. Correlative profile measurements of ozone, temperature, and water vapor have been assumed to minimize errors arising from uncertainties in these parameters.

<sup>1</sup>Atmospheric Sciences Division, NASA Langley Research Center, Hampton, Virginia

<sup>2</sup>NIWA Climate, Lauder, New Zealand

<sup>3</sup>Department of Physics, University of Denver, Denver, Colorado

<sup>4</sup>Christopher Newport University, Newport News, Virginia

Copyright 1996 by the American Geophysical Union.

Paper number 96GL00708

0094-8534/96/96GL-00708\$05.00

## Measurements

The infrared solar spectra were recorded on 10 days between February 14, 1994, and October 21, 1994, with a Bruker 120 M Fourier transform spectrometer operating at unapodized resolutions between 0.0035 and 0.006  $\text{cm}^{-1}$  (defined as 0.9 divided by the maximum optical path difference), a KCl beamsplitter, and a liquid-nitrogen-cooled HgCdTe or InSb detector. The 120 individual spectra were recorded with bandpasses of 750 to 1250  $\text{cm}^{-1}$ , 1880 to 2200  $\text{cm}^{-1}$ , or 2400 to 3200  $\text{cm}^{-1}$ . Between 1 and 10 interferograms were coadded and transformed to derive each spectrum. Measurements between 750 and 1240  $\text{cm}^{-1}$  were recorded with the HgCdTe detector and have a typical signal-to-RMS noise ratio of 200. Spectra in the 1880- to 3200- $\text{cm}^{-1}$  region used the InSb detector, which produced a higher signal-to-RMS noise ratio, typically 700. The measurements included in our analysis were restricted to solar zenith angles less than 80°. A typical measurement was recorded in 5 minutes during which time the airmass changed by 1.5%. Error in the airmass was reduced to less than 1% by calculating an effective solar zenith angle from the average of the angles corresponding to the zero path difference crossing times.

Dobson spectrophotometers [Dobson, 1957] measure total column ozone based on differential solar ultraviolet light absorption in the Huggins band (300–350 nm). Precisions and accuracies of the technique are estimated as 0.3% and 3.0%, respectively [Margitan *et al.*, 1995]. The present results were derived assuming new, standard, effective ozone absorption coefficients [Komhyr *et al.*, 1993] based on laboratory measurements [Bass and Paur, 1985]. The new absorption coefficients yield  $\text{O}_3$  total columns 2.6% lower than values obtained during July 1, 1957, to December 31, 1991, from an earlier set of ozone absorption coefficients (see Komhyr *et al.* [1993] for a discussion).

## Assumptions and Analysis Method

The infrared total columns have been retrieved with the SFIT nonlinear least-squares spectral fitting program developed for analysis of ground-based infrared solar spectra recorded with Fourier transform spectrometers [cf., Rinsland *et al.*, 1984]. The

current version of the program can derive the total columns of up to 5 molecules from a spectral interval by multiplicative scalings of initial volume mixing ratio (VMR) profiles of the target molecules and fittings of instrument performance related parameters. The total column of each molecule is obtained by multiplying the initial vertical column amount by the scale factor. The spectral intervals and the molecules fitted in each are given in Table 1. The intervals contain ozone lines having intensities with minimal sensitivity to temperature errors and minimal blending with telluric and solar features.

The values of 4 instrument-related parameters were obtained from each spectral fit: one parameter accounts for the wavenumber shift between the measured and calculated spectra, two others determine the level and tilt of the 100% transmission curve as a function of wavenumber, and the fourth determines the coefficient of a straight-line effective apodization function [Park, 1983]. The last parameter is important because it allows the calculated instrument function to be adjusted to agree with the shape indicated by the measured spectral lines. Fits yielding effective apodization coefficients significantly different from the nominal value of 1.0 were discarded to eliminate measurements recorded when the instrument was misaligned. We adopted a 29-layer atmospheric model with vertical layer thicknesses of ~1 km in the troposphere, 2 km in the lower and middle stratosphere, and 5 to 10 km in the 35- to 100-km region. Recently, total columns retrieved with SFIT and other independently-developed algorithms have been compared for a prespecified set of spectra and adjustable parameters [Zander *et al.*, 1994].

The initial  $\text{O}_3$  VMR profile is based on same day measurements from Lauder. From the surface to 20 km we assumed the profile measured by an electrochemical concentration cell (ECC) ozonesonde launched between 9 and 10h local time. Between 20 and 24 km, cubic spline interpolation was used to smoothly connect the balloon ozonesonde profile to the profile measured by a microwave radiometer operating at 110.8 GHz. In all cases, the change in  $\text{O}_3$  VMR between 20 and 24 km was reasonably linear, and the error introduced by the interpolation procedure is believed to be <1% in the total column. The microwave measurements were assumed between 24 and 65 km. At higher altitudes, where the microwave instrument lacks

**Table 1.** Spectral Intervals and Comparisons of IR and Dobson Total Columns

Interval ( $\text{cm}^{-1}$ )	Main $\text{O}_3$ Band	Columns Ratio <sup>†</sup>		Interferences
		Mean	St.Dev. <sup>‡</sup>	
764.03–764.43	$\nu_2$	0.962	0.040	---
773.20–773.38	$\nu_2$	0.974	0.042	---
781.08–781.25	$\nu_2$	0.967	0.032	$\text{CO}_2$
1127.60–1129.50	$\nu_1$	0.982	0.032	HDO, $\text{CH}_4$
1146.55–1147.40	$\nu_1$	0.986	0.032	$\text{N}_2\text{O}$ , $\text{H}_2\text{O}$ , HDO
1162.85–1163.50	$\nu_1$	0.983	0.036	$\text{N}_2\text{O}$ , $\text{H}_2\text{O}$ , HDO
1167.50–1167.75	$\nu_1$	0.979	0.035	---
2083.50–2084.72	$\nu_1 + \nu_3$	0.969	0.040	$\text{H}_2\text{O}$ , $\text{CO}_2$
2754.55–2755.45	$\nu_1 + \nu_2 + \nu_3$	0.964	0.031	HDO, $\text{CH}_4$ , solar
2778.90–2779.20	$\nu_1 + \nu_2 + \nu_3$	0.983	0.040	---
2781.60–2781.86	$\nu_1 + \nu_2 + \nu_3$	1.001	0.032	HDO
2792.65–2793.28	$\nu_1 + \nu_2 + \nu_3$	1.018	0.028	$\text{N}_2\text{O}$ , HDO, solar
3040.00–3040.90	$3\nu_3$	1.013	0.027	$\text{H}_2\text{O}$ , $\text{CH}_4$

<sup>†</sup>Ratio of measured IR total column to the Dobson total column measured on the same day.

<sup>‡</sup>Standard Deviation.

sensitivity, cubic spline interpolation was used to smoothly connect the microwave profile to the 1976 U.S. Standard Atmosphere ozone profile [Krueger and Minzner, 1976]. A description of the EEC ozonesonde sensor and estimates of the accuracy and precision of the measurements are given by Komhyr *et al.* [1995] and Barnes *et al.* [1985]. At present, no papers describing the Lauder O<sub>3</sub> microwave measurements have been published. However, this same instrument was used to derive O<sub>3</sub> profiles at Table Mountain, California, during the 1989 Stratospheric Ozone Intercomparison Campaign (STOIC). The precisions, accuracies, and vertical resolutions of the STOIC microwave measurements are 4%, 7%, and 10 km at 55 mbar (~20 km); 5%, 8%, and 10 km at 3 mbar (~40 km); and 6%, 10%, and 17 km at 0.2 mbar (~60 km), respectively [Connor *et al.*, 1995].

The vertical temperature profiles assumed in the IR analysis are also based on a combination of same day measurements and climatology. From the surface to 22 km, we adopted measurements from a meteorological radiosonde flown with the EEC ozonesonde. A spline interpolation procedure was used to smoothly connect this profile with National Meteorological Center temperatures and pressures, which were assumed between 30 and 50 km. Between 50 and 65 km we adopted temperature, density, and pressure profiles from the MAP (Middle Atmosphere Program) Handbook 16 zonal average tabulations [Barnett and Corney, 1985], followed by the 1976 U.S. Standard Atmosphere values from 65 to 100 km. The radiosonde temperatures are estimated to have uncertainties of ~1 K.

The initial H<sub>2</sub>O VMR profile for each day is also a combination of values from the Lauder daily sounding and climatology. The radiosonde measurements were combined with the 1976 U.S. Standard Atmosphere H<sub>2</sub>O profile by assuming the balloon data to an altitude of 20 km, a linear change in the H<sub>2</sub>O VMR between altitudes of 20 and 34 km, and the 1976 U.S. Standard Atmosphere H<sub>2</sub>O profile above 34 km. Initial profiles for the other absorbing molecules are from a variety of sources. Care has been taken to verify the assumed profiles are realistic for the mid-latitude, southern hemisphere location of the Lauder station.

The spectroscopic line parameters used in the analysis were taken from the 1992 HITRAN compilation [Rothman *et al.*, 1992]. The solar features noted in Table 1 were included by adding a line at the appropriate wavenumber and fitting the solar absorption with a one layer model [cf., Rinsland *et al.*, 1984].

## Results and Discussion

Figure 1 shows a sample fit. Absorption by ozone in the region is dominated by the 3 $\nu_3$  band. The maximum discrepancies coincide with the locations of the stronger O<sub>3</sub> lines. Sources of error are inaccuracies in the assumed O<sub>3</sub> line parameters, weak lines missing from the spectroscopic database, and inadequacies in modeling the interfering lines and the instrument line shape. Similar problems occur in other spectral regions.

The mean and standard deviation of ratios calculated by dividing the ozone total columns retrieved from the IR measurements by the same day Dobson values are given for each spectral interval in Table 1. The standard deviations of the ratios are typically 3%, which highlights the consistency between the two datasets despite wide differences in instrumentation and data analysis methods. Although the IR and UV measurements were recorded on the same day, they were in general not coincident in time.

The results in Table 1 indicate IR/Dobson mean column ratios from ~0.96 in the  $\nu_2$  band to ~1.02 in the 3 $\nu_3$  band. At 10  $\mu\text{m}$ ,

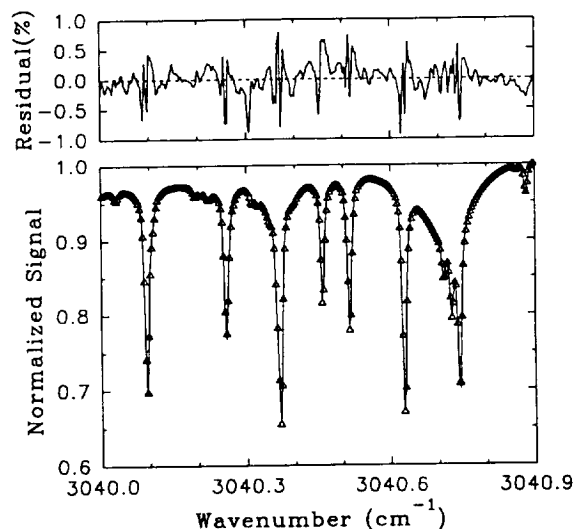


**Figure 1.** Bottom: Measured (solid line) and least-squares, best-fit calculated (open triangles) Lauder solar spectra in the region of the 3 $\nu_3$  band of ozone. The measured spectrum was recorded on April 27, 1994, at an astronomical zenith angle of 62.24°. Top: Measured minus calculated values on an expanded vertical scale. Several CH<sub>4</sub> lines and a H<sub>2</sub>O line at 3040.741 cm<sup>-1</sup> contribute to the measured absorption.

the average of the 4 IR/Dobson ratios is 0.982. Hence, to obtain agreement with the Dobson values, the IR intensities in this region need to be multiplied by 0.982. This factor is higher than the Mauna Loa IR/Dobson ratio of 0.956 deduced by David *et al.* [1993]. However, David *et al.* [1993] note that reprocessing of the Mauna Loa Dobson data with the new, effective O<sub>3</sub> absorption coefficients [Komhyr *et al.*, 1993] would increase the ratio to about 0.98, in excellent agreement with the present results.

The errors that normally arise from uncertainties in the target molecule volume mixing ratio and temperature profiles are negligible in the present work because correlative measurements have been adopted for those quantities. However, 3 other important sources of potential systematic error remain: (1) errors in the spectroscopic parameters, (2) errors in fitting the instrument line shape function, and (3) biases introduced by errors in the retrieval algorithm. Errors in the line intensities are not considered here since the goal is to determine the offset from the IR/Dobson column comparisons. The sensitivity to errors in the air-broadening coefficients and their temperature dependences have been estimated by repeating retrievals with the 1992 HITRAN air-broadening coefficients of ozone [Rothman *et al.*, 1992] multiplied by 1.05. The ozone total columns increased by 0.5%. The uncertainty in the instrument line shape function was estimated by repeating retrievals with the straight-line effective apodization coefficient [Park, 1983] increased or decreased by 0.1 as compared to the retrieved value. Changes in the ozone total columns of -1.5% and +1.5% were obtained, respectively. Total columns retrieved with SFIT agree with values from independently-developed algorithms to about 2% when the same input parameters and fitting options are selected [Zander *et al.*, 1994]. On the basis of these studies, we estimate the uncertainty in the mean IR/Dobson ratios in Table 1 as  $\pm 3\%$ .

The ozone intensity scale on the 1992 HITRAN compilation [Rothman *et al.*, 1992] was transferred from the 10  $\mu\text{m}$  to other IR regions by measuring relative intensities of common lines in overlapping laboratory spectra. The present work suggests that this procedure was successful to within a few percent. Very

precise work will be required to determine if the small, systematic increase in the IR/Dobson column ratio with wavenumber measured in this work results from errors in the  $O_3$  intensities, an artifact in the present analysis, or a combination of both effects.

Recent laboratory measurements are consistent with the present results. Birk *et al.* [1993] compared measured absolute intensities of 26 transitions in the  $O_3$   $v_2$  band with values on the 1992 HITRAN database [Rothman *et al.*, 1992]. The average measured-to-1992 HITRAN ratio was  $0.965 \pm 0.031$ , close to our average ratio of 0.967. Barbe *et al.* [1994] reanalyzed the  $2\nu_1$ ,  $\nu_1 + \nu_3$ , and  $2\nu_3$  bands in the  $1850\text{--}2300\text{-cm}^{-1}$  region based on  $O_3$  amounts calculated from the measured sample pressure and the assumptions that the initial sample contained only  $O_3$  and the only  $O_3$  decay product was  $O_2$ . These new intensities show no significant bias relative to the 1992 HITRAN compilation values [Barbe *et al.*, 1994, Fig. 3]. De Backer and Courtois [1995] used a tunable diode laser spectrometer to measure the intensities of about 40 ozone lines in the  $9.6\text{ }\mu\text{m}$   $\nu_3$  band. They derived an average measured-to-1992 HITRAN ratio of  $0.96 \pm 0.04$  (M. R. De Backer, private communication, 1995). A consistent value for the amount of ozone in the cell was found three ways: (1) UV measurements at  $253.7\text{ nm}$ , (2) measurements of the sample pressure and the assumptions that the initial sample contained only  $O_3$  and the only  $O_3$  decay product was  $O_2$ , and (3) measurement of the  $O_3$  vapor pressure at the temperature of liquid argon, where the  $O_3$  vapor pressure is well known.

## Summary and Conclusions

Average IR-to-Dobson  $O_3$  total column ratios of 0.96 to 1.02 have been derived from 13 intervals in 5 infrared bands and correlative Dobson spectrophotometer measurements. Both sets of measurements, accurate to about  $\pm 3\%$ , were recorded on 10 days in 1994 at the NDSC station in Lauder, New Zealand. Correlative  $O_3$  and  $H_2O$  VMR and temperature profiles were specified in the IR analysis from correlative measurements to minimize systematic errors. The present results do not support the 1.051 multiplicative factor recommended by Pickett *et al.* [1992] for the 1992 HITRAN line intensities in the  $O_3$   $\nu_3$  band [Rothman *et al.*, 1992]. Our results agree with recent laboratory measurements of absolute  $O_3$  intensities and a comparison of Mauna Loa IR total columns with correlative Dobson spectrophotometer measurements [David *et al.*, 1993].

**Acknowledgments.** Research at the NIWA is funded by the New Zealand Foundation for Research, Science, and Technology (Contract number CO 1221). Research at the University of Denver, Christopher Newport University, and NASA Langley Research Center is funded by NASA's Upper Atmosphere Research Program. Special thanks to B. M. McNamara for recording the infrared spectra, T. Beck and D. Keep for obtaining the Dobson measurements, and R. Evans of NOAA's Climate Monitoring and Diagnostic Laboratory for assistance in interpreting the Dobson measurements.

## References

- Bailey, P. L., *et al.*, A comparison of CLAES ozone measurements with correlative measurements, *J. Geophys. Res.*, accepted, 1996.
- Barbe, A., *et al.*, Experimental and theoretical study of the absolute intensities of ozone spectral lines in the range  $1850\text{--}2300\text{ cm}^{-1}$ , *J. Quant. Spectrosc. Radiat. Transfer*, 52, 341–355, 1994.
- Barnes, R. A., A. R. Bandy, and A. L. Torres, Electrochemical concentration cell ozonesonde accuracy and precision, *J. Geophys. Res.*, 90, 7881–7877, 1985.
- Barnett, J., and M. Corney, Middle atmosphere reference model derived from satellite data, *Handb. MAP*, 16, edited by K. Labitzke, J. J. Barnett, and B. Edwards, pp. 47–85, Sci. Comm. for Sol. Terr. Phys. Secr., Univ. of Ill., Urbana, 1985.
- Bass, A. M., and R. J. Paur, The ultraviolet cross-sections of ozone, 1, The measurements, in *Atmospheric Ozone*, edited by C. S. Zerefos and A. Ghazi, pp. 606–610, D. Reidel, Norwell, Mass., 1985.
- Birk, M., *et al.*, Line strengths in the  $\nu_1 - \nu_2$  hot band of ozone, paper K18, Thirteenth Colloquium on High Resolution Spectroscopy, Riccione, Italy, September 1993.
- Bruhl, C., *et al.*, HALOE ozone channel validation, *J. Geophys. Res.*, accepted, 1996.
- Connor, B. J., *et al.*, Error analysis for the ground-based microwave ozone measurements during STOIC, *J. Geophys. Res.*, 100, 9283–9292, 1995.
- Connor, B. J., *et al.*, Ozone in the middle atmosphere as measured by the improved stratospheric and mesospheric sounder, *J. Geophys. Res.*, accepted, 1996.
- David, S. J., *et al.*, Determination of total ozone over Mauna Loa using very high resolution infrared solar spectra, *Geophys. Res. Lett.*, 20, 2055–2058, 1993.
- De Backer, M. R., and D. Courtois, Analysis of some ozone lines in the  $\nu_3$  band with a tunable diode laser spectrometer, paper RA06, 50th International Symposium on Molecular Spectroscopy, Ohio State University, Columbus, OH.
- Dobson, G. M. B., Observer's handbook for the ozone spectrophotometer, *Ann. Int. Geophys. Year*, 5(1), 46–89, 1957.
- Flaud, J.-M., *et al.*, Improved spectroscopic line parameters for the ozone molecule, *J. Quant. Spectrosc. Radiat. Transfer*, 48, 611–615, 1992.
- Komhyr, W. D., C. L. Mateer, and R. D. Hudson, Effective Pass-Pair 1985 ozone absorption coefficients for use with Dobson ozone spectrophotometers, *J. Geophys. Res.*, 98, 20,451–20,465, 1993.
- Komhyr, W. D., *et al.*, Electrochemical concentration cell ozonesonde performance evaluation during STOIC 1989, *J. Geophys. Res.*, 100, 9231–9244, 1995.
- Krueger, A. J., and R. A. Minzner, A mid-latitude ozone model for the 1976 U.S. Standard Atmosphere, *J. Geophys. Res.*, 81, 4477–4481, 1976.
- Kurylo, M. J., Network for the detection of stratospheric change, *Proc. Soc. Photo. Opt. Instrum. Eng.*, 1491, 169–174, 1991.
- Margitan, J. J., *et al.*, Stratospheric ozone intercomparison campaign (STOIC) 1989: Overview, *J. Geophys. Res.*, 100, 9193–9207, 1995.
- Park, J. H., Analysis method for Fourier transform spectroscopy, *Appl. Opt.*, 22, 835–849, 1983.
- Pickett, H. M., D. B. Peterson, and J. S. Margolis, Absolute absorption of ozone in the midinfrared, *J. Geophys. Res.*, 97, 20,787–20,793, 1992.
- Rinsland, C. P., *et al.*, Diurnal variations of atmospheric nitric oxide: Ground-based infrared spectroscopic measurements and their interpretation with time-dependent photochemical model calculations, *J. Geophys. Res.*, 89, 9613–9622, 1984.
- Rothman, L. S., *et al.*, The HITRAN molecular database: Editions of 1991 and 1992, *J. Quant. Spectrosc. Radiat. Transfer*, 48, 469–507, 1992.
- Zander, *et al.*, ESMOS II/NDSC IR spectral fitting algorithms. Intercomparison exercise, Proceedings of the Atmospheric Spectroscopy Applications Workshop, Reims, France, pp. 7–12, 1994.
- C. P. Rinsland, Mail Stop 401A, NASA Langley Research Center, Hampton, VA 23681-0001
- I. Boyd, B. J. Connor, N. B. Jones, and W. Andrew Matthews, NIWA Climate, Private Bag 50061, Omakau, Lauder 9128, New Zealand
- S. J. David, A. Goldman, D. G. Murcray, and F. J. Murcray, Department of Physics, University of Denver, Denver, CO 80308
- N. S. Pougatchev, Christopher Newport University, Newport News, VA 23606-2998

(Received August 17, 1995; revised December 20, 1995; accepted February 15, 1996.)



# Observations of the infrared solar spectrum from space by the ATMOS experiment

M. C. Abrams, A. Goldman, M. R. Gunson, C. P. Rinsland, and R. Zander

The final flight of the Atmospheric Trace Molecule Spectroscopy experiment as part of the Atmospheric Laboratory for Applications and Science (ATLAS-3) Space Shuttle mission in 1994 provided a new opportunity to measure broadband  $625\text{--}4800\text{ cm}^{-1}$ ,  $2.1\text{--}16\text{ }\mu\text{m}$  infrared solar spectra at an unapodized resolution of  $0.01\text{ cm}^{-1}$  from space. The majority of the observations were obtained as exoatmospheric, near Sun center, absorption spectra, which were later ratioed to grazing atmospheric measurements to compute the atmospheric transmission of the Earth's atmosphere and analyzed for vertical profiles of minor and trace gases. Relative to the SPACELAB-3 mission that produced 4800 high Sun spectra (which were averaged into four grand average spectra), the ATLAS-3 mission produced some 40,000 high Sun spectra which have been similarly averaged with an improvement in signal-to-noise ratio of a factor of 3–4 in the spectral region between 1000 and  $4800\text{ cm}^{-1}$ . A brief description of the spectral calibration and spectral quality is given as well as the location of electronic archives of these spectra. © 1996 Optical Society of America

## 1. Introduction

The Atmospheric Trace Molecule Spectroscopy (ATMOS) instrument is a  $0.01\text{-cm}^{-1}$  unapodized resolution Fourier transform spectrometer operating in the infrared for atmospheric observations between  $625$  and  $4800\text{ cm}^{-1}$  ( $2.1\text{--}16\text{ }\mu\text{m}$ ) from the Space Shuttle. Its first flight in 1985 as part of the SPACELAB-3 mission provided a proof of concept for the instrument and measurement technique, with 20 occultations recorded over a 2-day period. The excellent quality of the spectra led to a detailed analysis of the composition of the middle atmosphere, including the profiling of more than 30 gaseous species. The design, performance, and operation of the ATMOS experiment have been documented in the literature.<sup>1–3</sup> In summary, the instrument is a rapid-scanning, double-passed, Michelson

interferometer utilizing cat's eye retroreflectors and a KBr beam splitter to obtain interferograms with a total optical path difference of  $50\text{ cm}$  (nominally 800,000 points, which after transformation produces a spectrum with a dispersion of  $0.007533\text{ cm}^{-1}/\text{pt}$ ).

Although designed in the mid 1970's and delivered in 1982 by Honeywell,<sup>4</sup> the instrument remains state of the art in 1995, and it still exceeds by far the capabilities (in terms of resolution, speed, bandwidth, sampling, and spectral bandpass) of all current implementations of space-based Fourier transform spectrometers. The signal-to-noise ratio of the measurements is maximized through the use of optical bandpass filters, which divide the  $625$  to  $4800\text{-cm}^{-1}$  region into narrower regions that are compatible with the sampling of the laser:  $625\text{--}1500$ ,  $1100\text{--}2000$ ,  $1580\text{--}3400$ ,  $3100\text{--}4800$ , and  $625\text{--}2450\text{ cm}^{-1}$  (the last filter is an addition to the set used in SPACELAB-3). The signal-to-noise ratios of spectra obtained with each of the filters is inversely proportional to frequency, with spectra in the long-wavelength region having a typical signal-to-noise ratio of 300:1, degrading to 50:1 in the  $3100\text{--}4800\text{ cm}^{-1}$  spectral region. The frequency response of the signal-to-noise ratio is largely the consequence of the frequency response of the HgCdTe detector and the modulation efficiency of the interferometer.

The ATMOS instrument obtains a spectrum every  $2.2\text{ s}$  in order to provide adequate vertical resolution

M. C. Abrams is with Science Applications International Corporation-NASA Langley Research Center. C. P. Rinsland is with NASA Langley Research Center, Hampton, Virginia 23681. A. Goldman is with the University of Denver, Denver, Colorado 80208. M. R. Gunson is with the Jet Propulsion Laboratory, California Institute of Technology, Pasadena, California 91109. R. Zander is with the Institute of Astrophysics, University of Liege, Liege, Belgium.

Received 19 October 1995; revised manuscript received 29 January 1996.

0003-6935/96/162747-05\$10.00/0

© 1996 Optical Society of America

during sunrise or sunset observations: pure atmospheric spectra are obtained by ratioing the transmission at a given tangent height against a solar absorption spectrum that averages all spectra observed above a tangent height of 165 km into a single spectrum. Consequently, for each of the solar occultation events, a high signal-to-noise ratio exoatmospheric solar absorption spectrum is obtained. In addition, during each mission, certain observation periods were dedicated to solar-only observations in which 4–40 min of continuous measurements were made by the instrument. Measurements are obtained with a Sun tracker that balances the signals from four quadrants of the solar disk. Hence the observations were nominally obtained at Sun center, with a bore-sighted video camera providing visible wavelength images for confirmation of the position on the solar disk.

The ATMOS Solar Infrared Atlas<sup>5,6</sup> and related studies<sup>7–9</sup> have compiled and analyzed the 1985 observations. Farmer<sup>9</sup> has discussed future plans for solar observations as part of the ATLAS missions, specifically noting the need for improved signal-to-noise ratios possible by increasing the number of observations, and the possibility of investigating the center-to-limb variation in the solar spectrum. The material presented in this paper addresses the first priority, the generation of considerably improved solar spectra. The new spectra illustrate the effectiveness of the dispersion corrections in the formation of accurate observations of the solar spectrum and are compared with spectra from the SPACELAB-3 mission in each of the figures.

## 2. Spectral Calibration

The methodology for correction and transformation of ATMOS spectra has been presented elsewhere.<sup>10–12</sup> During the SPACELAB-3 mission, solar spectra were obtained over a 2-day period during which the Sun-spacecraft velocity remained relatively constant. As a result, the variation in the Sun-spacecraft radial velocity (which produces a Doppler shift) is typically small during individual and between successive observations, and consequently the solar spectra can be averaged together on a point-by-point basis, as has been documented in previous compilations of solar spectra<sup>5</sup> and calibrated line identifications.<sup>6,13</sup> The ATLAS-3 observations were made from a lower altitude orbit (300 km as opposed to 360 km in 1985) and over a 10-day period; consequently, the variation in the Sun-spacecraft velocity was sufficient to prevent point-by-point averaging of high Sun spectra from different observations into grand solar average spectra. Instead, all solar spectra above a tangent height of 165 km were interpolated to a stationary reference frame through the calculation of the Doppler shift, and residual frequency shifts were assessed before averaging.

The canonical dispersion of a Fourier transform spectrometer is  $\Delta\sigma = \sigma_L/2N$ , where  $\sigma_L/2$  is the laser semifrequency and  $N$  is the number of points in the

fast Fourier transform: in the case of the ATMOS interferometer,  $\sigma_L/2 = 7899.0015 \text{ cm}^{-1}$ , yielding a dispersion of  $0.007533 \text{ cm}^{-1} \text{ pt.}$  for a million-point transform. In contrast, to calibrate on-orbit spectra properly for all of the perturbations relative to a laboratory spectrometer, the laser semi-frequency must be corrected for the field of view and the Doppler shift:

$$\sigma_s = \sigma_L w_s [1 + v_s/c] [1 - \Omega^2/4] \quad (1)$$

where  $w_s$  is an empirical stretch factor used for final calibration relative to laboratory standards,  $v_s$  is the spacecraft–Sun velocity,  $c$  is the velocity of light, and  $\Omega$  is the field of view (FOV) of the instrument. The FOV is small compared with the solar disk (approximately 32 mrad as viewed by the instrument; typically the FOV is 0.97 mrad, except for the long-wavelength filter (filter 12, 625–1500  $\text{cm}^{-1}$ , in which a FOV of 2.01 mrad is used to increase the signal-to-noise ratio. These FOV's are smaller than those used during the SPACELAB-3 mission (1.2 and 4 mrad, respectively) and significantly improve the linearity of the measurements. In the presence of residual air within the instrument, the spectral point spacing will be nonuniform and consequently the dispersion will be a function of the frequency

$$\Delta\sigma = \sigma_s \cdot 2Nr_i \quad (2)$$

where  $r_i$  is the refractive index of air obtained with Edlén's formula<sup>14</sup> and depends on the pressure, temperature, and humidity within the instrument (typically this is only relevant during ground calibration and outgassing immediately following launch).

The mean dispersion over a spectral interval between frequencies  $\sigma_1$  and  $\sigma_2$  is

$$\Delta\sigma = (\sigma_2 - \sigma_1) / [\sigma_2 \Delta\sigma_2 - \sigma_1 \Delta\sigma_1] I \quad (3)$$

where  $I$  is the interpolation factor (typically 3 for atmospheric sounding, 1 for solar spectroscopy). The calibration factor,  $w_s$ , allows for the adjustment of the dispersion to match accurately measured line positions, but in practice this complicates the comparison of spectra obtained over the past decade as standards are continually refined. Instead, the SPACELAB-3 correction of 0.999998526 has been assumed for the ATLAS spectra; however, before spectra are averaged, any residual frequency shifts are measured and removed relative to an assumed stationary spectrum to ensure that the line positions and shapes are minimally distorted by the averaging process. Given a correct dispersion, each spectrum is interpolated to a reference frame with a dispersion of  $0.007533067 \text{ cm}^{-1}$  (no interpolation) before averaging.

## 3. Results

Two examples of the ATMOS solar spectra are given, illustrating the similarities and differences between the SPACELAB-3 and ATLAS-3 average solar spec-

tra for (a) molecular transitions and (b) atomic transitions. A notable difference between the 1985 flight and the ATLAS flights was improved purging and reduced outgassing of the instrument, leading to significantly reduced instrumental water vapor lines as illustrated in Fig. 1. The upper panel contains two traces (one scaled by ten in the ordinate to accentuate small features) with four sharp, prominent instrumental lines; in the lower panel, the same lines are greatly reduced in magnitude. The ATLAS-3 spectra are sufficiently free of instrumental lines to permit the averaging of all sunrise and sunset data into a single grand average spectrum. Approximately 10,000 spectra were combined into this average. Figure 1 illustrates several other points: the method of spectral calibration is quite adequate, and although the spectra were accumulated over a 10-day period, it is possible to formulate an average (as indicated above) that does not significantly alter the solar line shapes; in addition, the

lower trace indicates the improvement in signal-to-noise ratio during the ATLAS-3 mission.

In Fig. 1 care has been taken to ensure that the frequency scale, for the SPACELAB-3 spectra, closely matches the calibrations developed by Geller<sup>5,13</sup>; any residual frequency difference between the SPACELAB-3 and ATLAS-3 spectra results from differences in the definitions of the reference frame and should be removable with further calibration. The identification of solar features such as the two strong features in the lower panel as Fe transitions is a continuous process.<sup>13</sup> The improvement in signal-to-noise ratio should permit the identification of new solar features: Fig. 1 illustrates a spectral region containing two weak NH features<sup>15</sup> and instrument lines (marked with the letter I. Figure 1 suggests that many features that are marginally present in the 1985 spectra can be clearly measured and considered for identification. For example, around the NH feature, in addition to the feature

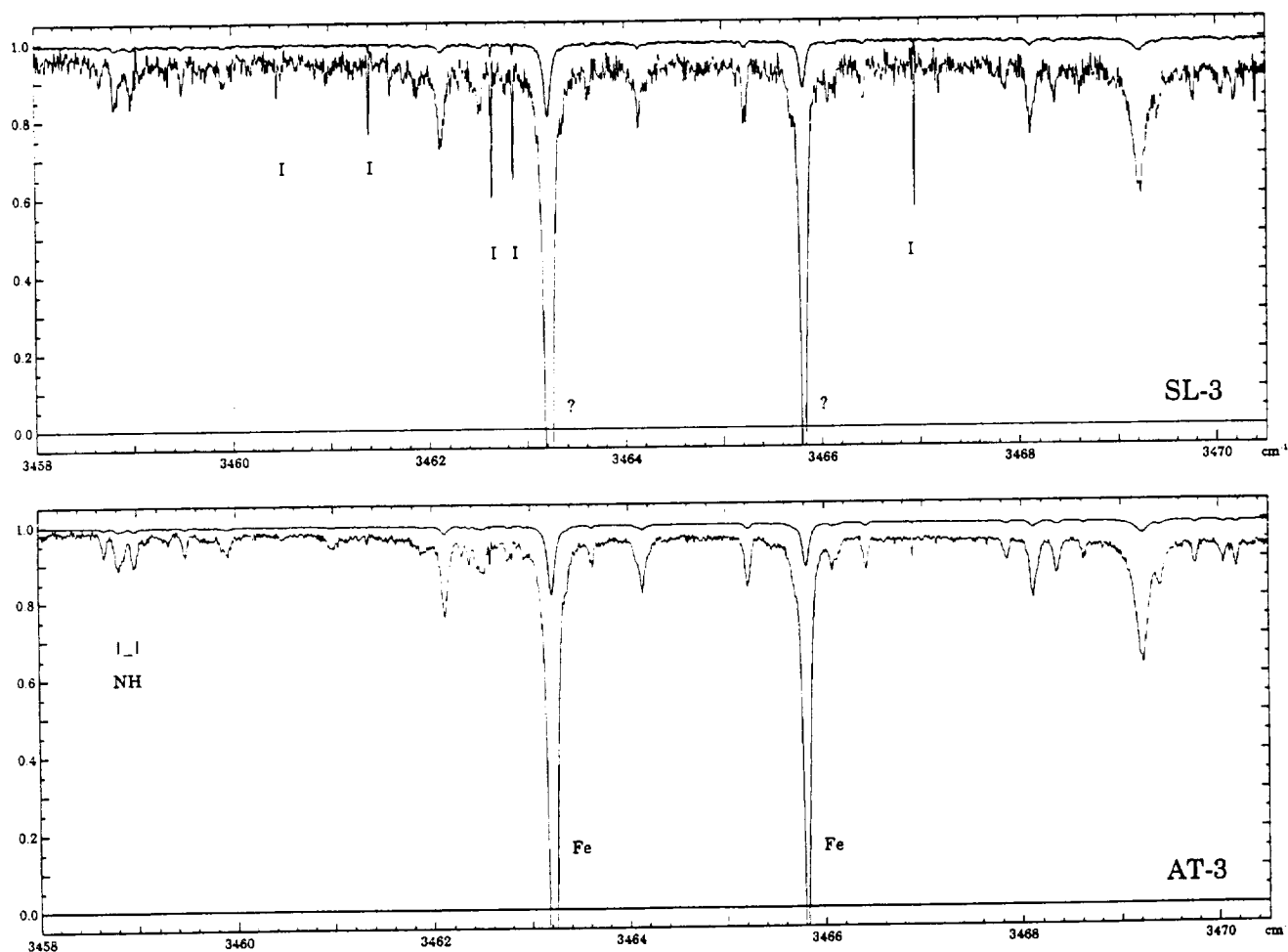


Fig. 1. Portion of the solar spectra observed during SPACELAB-3 upper panel and ATLAS-3 lower panel. The ordinate is normalized intensity and the abscissa is frequency in reciprocal centimeters. In each panel there are two traces, one normalized to unit transmission, the second scaled by a factor of 10 relative to the other curve to accentuate the small-scale structures in the spectra. Three features are significant: the decreased size of the instrumental water vapor lines indicated by the letter I, the decreased noise level and the corresponding increase in the number of identifiable features, and the relative similarity of the line widths and shapes, indicating that the averaging process has not significantly distorted the line shapes. Several marginally resolved 1985 NH features are clearly resolved in the 1994 spectra, as are a number of similar features that are not readily measurable in the 1985 spectra.



identified by Geller at  $3459.92\text{ cm}^{-1}$ , there is a comparable feature at  $3461.0\text{ cm}^{-1}$  in the 1994 spectra that is lost in the noise in the 1985 spectra. Conversely, the 1985 compilation placed a line at  $3461.783\text{ cm}^{-1}$  that is absent from the 1994 spectra, whereas there is a weak feature at  $3461.95\text{ cm}^{-1}$  in the 1994 spectra that is essentially absent from the 1985 spectra although there is a feature that is twice the noise level. The carbon double line identified at  $3469.213$  and  $3469.236\text{ cm}^{-1}$  in the 1985 spectra appears as a single line in the 1994 spectra, and realistically the doublet structure in the 1985 spectra is comparable with the noise in the spectrum.

The improvement in signal-to-noise ratio should allow the identification of weak molecular and atomic features and the determination of more accurate molecular constants. Figure 2 illustrates a spectral region containing four CH spectral features.<sup>16</sup> As in Fig. 1, the recent identification of some unidentified lines (e.g., Fe, in the lower trace of Fig. 2) indicates the evolution of solar spectroscopy, and the lower trace contains a number of features that are statistically significant and warrant investigation (e.g., the weak features between  $3030$  and  $3031.5$

$\text{cm}^{-1}$ ). Positive identification of features as real will require multiple measurements and corroboration from atomic and molecular calculations, especially in cases in which the signal-to-noise ratio is less than 3.

#### 4. Conclusions

Exoatmospheric infrared solar spectra recorded by the ATMOS instrument on board the Space Shuttle are presented and contrasted with earlier measurements made in 1985. The improvement in signal-to-noise ratio mainly resulting from the larger number of spectra is discussed and illustrated, and the method of calibration is presented. Four new spectra, global high Sun averages from the November 1994 ATLAS-3 mission, are available in electronic form and may be obtained from the anonymous File Transfer Protocol sites at Langley Research Center ([arbd4.larc.nasa.gov:pub/atmos](http://arbd4.larc.nasa.gov:pub/atmos)) or the Jet Propulsion Laboratory ([remus.jpl.nasa.gov:pub/incoming\\_solar\\_spectra](http://remus.jpl.nasa.gov:pub/incoming_solar_spectra)). The spectra are stored as ascii files with ancillary information for frequency calibration. Further information about the spectra can be obtained from the lead author

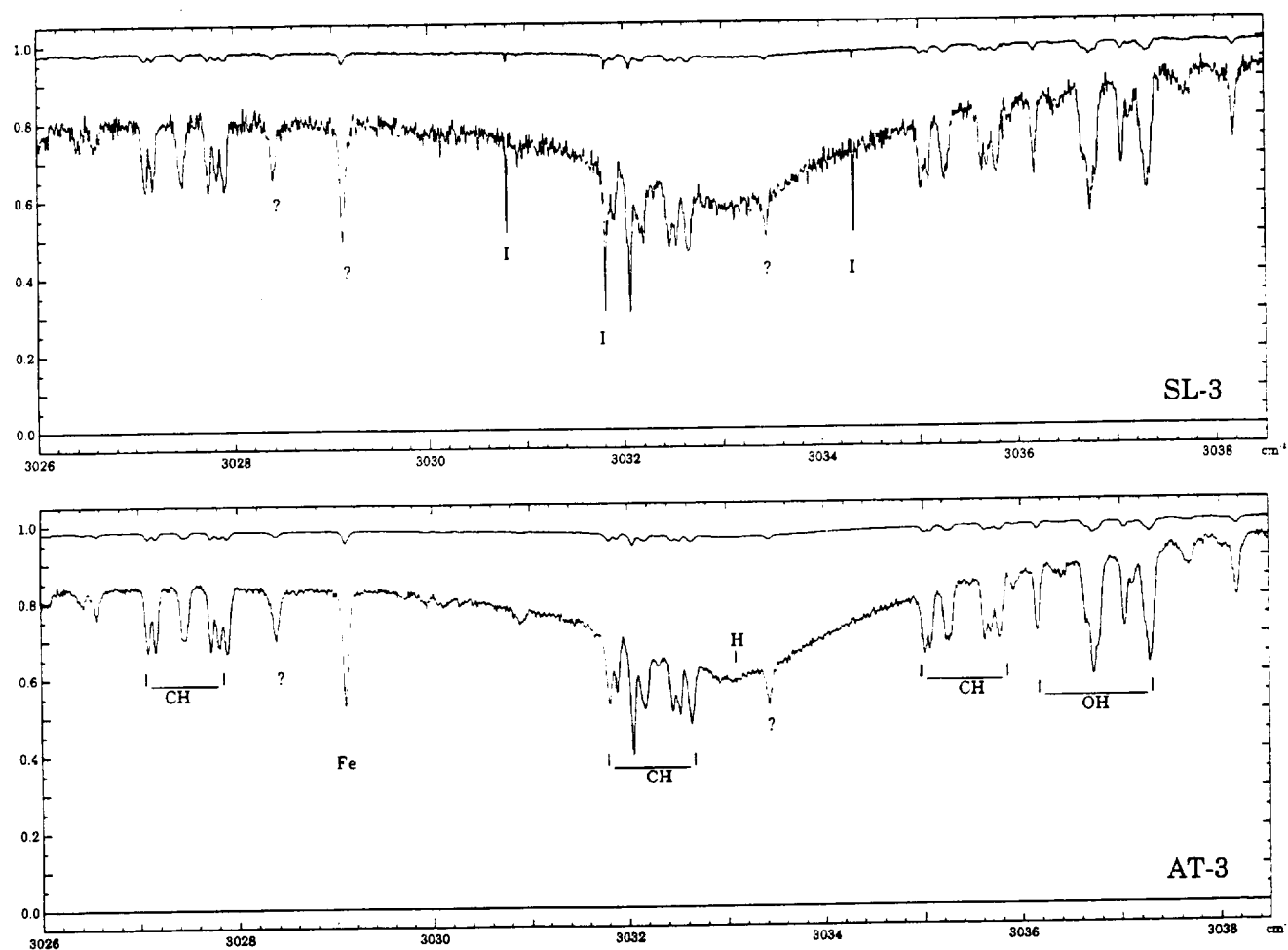


Fig. 2. Spectral region containing several four-component CH features from the (2-1) band, suggesting the increase in rotational coverage to higher  $J$  values possible in the new spectra and hydrogen, iron, and silicon lines. The lines marked with a question mark remain unidentified as of the 1992 compilation. The iron line in the lower panel is a new identification.<sup>13</sup>

m.c.abrams@larc.nasa.gov), and collaborative efforts to measure, calibrate, and catalog these spectra are welcome.

The authors acknowledge contributions from the entire ATMOS data-processing facility and engineering teams. Research at the Jet Propulsion Laboratory, California Institute of Technology, is performed under contract to the National Aeronautics and Space Administration. Contributions by R. Zander were supported by the Belgian Global Change program, which is coordinated by the Services Scientifiques, Techniques et Culturels, Brussels.

## References

1. C. B. Farmer, O. F. Raper, and F. G. O'Callaghan, "Final report on the first flight of the ATMOS instrument during the SPACELAB-3 mission, April 29 Through May 6, 1985," JPL Pub. 87 32 (Jet Propulsion Laboratory, Pasadena, Calif., 1987).
2. M. R. Gunson, R. J. Salawitch, M. C. Abrams, L. R. Brown, T. L. Brown, A. Y. Chang, L. L. Lowes, F. W. Irwin, R. Zandoez, E. Mahieu, C. P. Rinsland, M. J. Newchurch, H. A. Michelsen, A. Goldman, M. M. Abbas, and G. P. Stilles, "The atmospheric trace molecule spectroscopy (ATMOS) experiment deployment on the ATLAS-3 space shuttle mission," to be published in *Geophys. Res. Lett.* (1996).
3. C. B. Farmer, "High resolution infrared spectroscopy of the Sun and the earth's atmosphere from space," *Mikrochim. Acta Wien* **III**, 189-214 (1987).
4. P. G. Morse, "Progress report on the ATMOS sensor: design description and development status," presented at the AIAA Sensor Systems for the 80's Conference, Colorado Springs, Colo., 2-4 December 1980, paper CP807.
5. C. B. Farmer and R. H. Norton, "Atlas of the infrared spectrum of the Sun and the earth atmosphere from space," in *The Sun*, NASA Ref. Pub. 1224 (NASA, Washington, D.C., 1989, Vol. I).
6. M. Geller, "Atlas of the infrared spectrum of the Sun and the earth atmosphere from space," in *Key to Identification of Solar Features*, NASA Ref. Pub. 1224 (NASA, Washington, D.C., 1992), Vol. III.
7. N. Grevesse, A. J. Sauval, C. B. Farmer, and R. H. Norton, "Diatomic molecules in the solar infrared spectrum from ATMOS-SL 3 high resolution observations," presented at the Twenty-Seventh Liege International Astrophysical Colloquium, Liege, Belgium, 23-26 June 1987.
8. N. Grevesse and A. J. Sauval, "The infrared solar spectrum," in *The Infrared Spectral Region of Stars; Proceedings of the Montpellier Colloquium* (Cambridge U. Press, Cambridge, England, 1991), pp. 215-233.
9. C. B. Farmer, "The ATMOS solar atlas," *Infrared Sol. Phys.* **154**, 511-521 (1994).
10. R. H. Norton and C. P. Rinsland, "ATMOS data processing and science analysis methods," *Appl. Opt.* **30**, 389-400 (1991).
11. M. C. Abrams, G. C. Toon, and R. A. Schindler, "A practical example of the correction of Fourier transform spectra for detector nonlinearity," *Appl. Opt.* **33**, 6307-6314 (1994).
12. M. C. Abrams, M. R. Gunson, A. Y. Chang, C. P. Rinsland, and R. Zander, "Remote sensing of the Earth's atmosphere from space with high resolution Fourier transform spectroscopy: development and methodology of data processing for the Atmospheric Trace Molecule Spectroscopy experiment," *Appl. Opt.* **35**, 2774-2786 (1996).
13. M. Geller, "Line identification in ATMOS solar spectra, laboratory and astronomical high resolution spectra," *ASP Conf. Ser.* **81**, 88-95 (1995).
14. N. Edlén, "The dispersion of standard air," *J. Opt. Soc. Am.* **43**, 339-345 (1953).
15. N. Grevesse, D. L. Lambert, A. J. Sauval, E. F. van Dishoeck, C. B. Farmer, and R. H. Norton, "Identification of solar vibration-rotation lines of NH and the solar nitrogen abundance," *Astron. Astrophys.* **232**, 225-230 (1990).
16. F. Melen, N. Grevesse, A. J. Sauval, C. B. Farmer, R. H. Norton, H. Bredohl, and I. Dubois, "A new analysis of the vibration-rotation spectrum of CH from solar spectra," *J. Mol. Spectrosc.* **134**, 305-313 (1989).





## HIGH RESOLUTION STUDIES OF HEAVY NO<sub>x</sub> MOLECULES IN ATMOSPHERIC SPECTRA

A. GOLDMAN,<sup>†</sup> C. P. RINSLAND,<sup>‡</sup> F. J. MURCRAY,<sup>†</sup> R. D. BLATHERWICK,<sup>†</sup> and D. G. MURCRAY<sup>†</sup>

<sup>†</sup>Department of Physics, University of Denver, Denver, CO 80208, and <sup>‡</sup>Atmospheric Sciences Division, NASA Langley Research Center, Hampton, VA 23681-0001, U.S.A.

(Received ?)

**Abstract**—New line parameters for two heavy odd nitrogen molecules HNO<sub>3</sub> in the  $\nu_3/2\nu_2$  region, and ClONO<sub>2</sub> in the  $\nu_4$  region are incorporated in the analysis of high resolution i.r. atmospheric spectra. The line parameters are tested and renormalized vs laboratory spectra, and then applied to retrievals from balloon-borne and ground-based solar absorption spectra.

### INTRODUCTION

High resolution (0.002–0.003 cm<sup>-1</sup>) Michelson type interferometer systems are used at the University of Denver to obtain i.r. solar absorption spectra of the stratosphere during balloon flights, as well as ground-based solar spectra. The stratospheric spectra in the region 700–2200 cm<sup>-1</sup> cover spectral signatures of O<sub>3</sub> (including isotopic species), NO<sub>2</sub>, HNO<sub>3</sub>, O<sub>2</sub>, N<sub>2</sub>, COF<sub>2</sub>, ClONO<sub>2</sub>, SF<sub>6</sub>, and others. For a typical study of new spectral features observable in such spectra see the discussion of the 6 June 1988 flight data by Goldman et al.<sup>1</sup> Ground-based spectra in the 3–12  $\mu$ m region are obtained regularly from Mauna Loa (Hawaii) and Denver (CO), in support of the Network for Detection of Stratospheric Change (NDSC) and the Upper Atmospheric Research satellite (UARS).

In support of the atmospheric observations, numerous laboratory spectra have been obtained with the same interferometer systems. The laboratory spectra cover mostly the region 700–3000 cm<sup>-1</sup> and have also been extended down to 500 or up to 5000 cm<sup>-1</sup>. The molecules covered include CCl<sub>4</sub>, CCl<sub>2</sub>F<sub>2</sub>, CCl<sub>3</sub>F, CF<sub>4</sub>, CHClF<sub>2</sub>, CH<sub>3</sub>Cl, CHCl<sub>3</sub>, CH<sub>2</sub>O, C<sub>2</sub>H<sub>6</sub>, ClONO<sub>2</sub>, COF<sub>2</sub>, COCl<sub>2</sub>, COClF, HCOOH, HNO<sub>4</sub>, H<sub>2</sub>O<sub>2</sub>, NO<sub>2</sub>, HNO<sub>3</sub>, N<sub>2</sub>O<sub>5</sub>, and others. Analysis of stratospheric spectral features, combined with analysis of laboratory molecular absorption spectra, improves the spectral line parameters and leads to more complete line identifications and more accurate retrieval quantification of atmospheric gases.

In the present paper, updates of line parameters and their application to the University of Denver spectra will be presented for the 11  $\mu$ m region of HNO<sub>3</sub> and the 780 cm<sup>-1</sup> region of ClONO<sub>2</sub>.

### RESULTS AND DISCUSSION

Recent updates of line parameters for the HNO<sub>3</sub>  $\nu_3/2\nu_2$  bands, beyond the HITRAN 92 data base,<sup>2</sup> have allowed improved quantitative analysis of atmospheric spectra in the 11  $\mu$ m region. The first update was initiated by A. G. Maki (unpublished) and included Fermi resonance effects on the energy levels but unperturbed intensities. This provided improved modeling of the  $\nu_3$  manifolds in the 860–875 cm<sup>-1</sup> region of the atmospheric spectra, as reported by Goldman et al.<sup>1,2</sup> This set has been used successfully for most retrievals to date from high resolution airborne and ground-based solar spectra. Subsequent update was based on Maki and Wells,<sup>3</sup> who extended the analysis with Fermi resonance, by adding unperturbed intensities to the published energies and line positions. This update covered both bands, with improved agreement in the  $\nu_3$  manifolds and

$Q$ -branch, but the  $2\nu_2$   $Q$ -branch was still poorly modeled. The more recent update, based on the work of Perrin et al.,<sup>4</sup> extended the treatment with both Fermi and Coriolis interactions, including perturbed intensities. With this update the modeling of both the  $\nu_3$  and the  $2\nu_2$   $Q$ -branches is significantly improved, and the  $Q$ -branches are now consistent with most  $P$  and  $R$  manifolds. Line intensity plots for the two latest updates were shown in Fig. 1.

In order to apply these data to atmospheric spectra in a fashion consistent with previous retrievals from these bands and from the other major  $\text{HNO}_3$  bands, the total band intensities were normalized to the measured intensities of Giver et al.,<sup>5</sup> divided by a hot bands factor of 1.30, which amounts to multiplying the Perrin et al. lines<sup>4</sup> (shown in Fig. 1) by 1.43. The hot bands are not analyzed yet, but are not significant in the spectral intervals used for stratospheric retrievals; they are thus not considered in the line list for this study.

Figure 2 shows a typical fitting in the  $\nu_3$  manifolds with the latest lines to data from the University of Denver balloon flight of 6 June 1988. The improvements in the  $Q$ -branches modeling is demonstrated in Fig. 3, also with data from the 6 June 1988 flight. Comparisons with ground-based spectra to be presented elsewhere, also show significant improvements in the spectral fitting. Comparisons with retrievals with the previous two line parameters updates show consistency of better than 4% over the  $860\text{--}870\text{ cm}^{-1}$  manifolds.

The first update of the initial cross-sections for  $\text{ClONO}_2$  (HITRAN 1986) was provided by the work of Ballard et al.,<sup>6</sup> which generated cross-sections in the  $700\text{--}1800\text{ cm}^{-1}$  at  $213\text{--}296\text{ K}$ . These cross-sections were included in the HITRAN 92 data base.<sup>7</sup>

Recent analysis of the  $\nu_4\text{ClONO}_2$  region (the most useful for atmospheric retrievals) by Bell et al.,<sup>8</sup> provided spectroscopic constants for the three main bands in this region,  $\nu_4$   $^{35}\text{ClONO}_2$ ,  $\nu_4$   $^{37}\text{ClONO}_2$ , and  $\nu_4 + \nu_2 - \nu_2$   $^{35}\text{ClONO}_2$ . Based on this analysis, line parameters were generated in the  $\nu_4$  region, with the relative intensities of the three bands normalized to  $0.002\text{ cm}^{-1}$  resolution laboratory spectra taken at the University of Denver, and absolute intensities normalized to the values of Ballard et al.,<sup>6</sup> with the continuum removed (providing consistency of better than 3% with previous retrievals). The new line parameters were then applied to retrievals in the  $780.2\text{ cm}^{-1}$  region from D.U. balloon-borne and ground-based spectra taken at  $0.002\text{--}0.006\text{ cm}^{-1}$  resolution. The new line parameters showed improved agreement with observed data, even though the fine structure is not fully modeled yet. Intensity plots of the normalized line parameters are shown in Fig. 4. Modeling of the  $780.2\text{ cm}^{-1}$  region from University of Denver laboratory data is shown in Fig. 5. Fitting to stratospheric spectra obtained by University of Denver during the 6 June 1988 flight is shown in Fig. 6.

The new line parameters of  $\text{HNO}_3$  and  $\text{ClONO}_2$  were thus applied in retrievals of altitude mixing ratio profiles from sunset spectra obtained during two D.U. balloon flights made on 6 June 1988 (from Palestine, Texas, with float altitude of  $36.7\text{ km}$ ) and 24 July 1992 (Palestine, Texas, float altitude of  $34\text{ km}$ ). Sunset scans were obtained during the 6 June 1988 flight down to  $15.60\text{ km}$  tangent altitude, but only down to  $24.30\text{ km}$  tangent altitude during the 24 July 1992 flight; the Pinatubo aerosol caused loss of the source signal below this altitude. Both flights covered the same spectral interval of  $700\text{--}1350\text{ cm}^{-1}$  with resolution of  $\sim 0.0025\text{ cm}^{-1}$ . The resolution and the signal to noise ratio were slightly better during the 6 June 1988 flight. Spectral fitting results were tested by two non-linear spectral least squares programs, one based on the work of Niple et al.,<sup>9</sup> and one on Rinsland et al.,<sup>10</sup> combined with the onion-peeling method for the mixing ratio profile. The agreement between the two methods is better than 2% in any step of the onion-peeling, assuming the same atmospheric and spectroscopic parameters.

The retrieved mixing ratios are shown in Figs. 7, 8, which also include comparisons with previous results— $\text{HNO}_3$  from D.U.,<sup>11</sup> ATMOS,<sup>12</sup> LIMS,<sup>13</sup> WMO (1986),<sup>14</sup> and BLISS,<sup>15</sup> and  $\text{ClONO}_2$  from ATMOS.<sup>16</sup> The results from the two flights are included in the comparisons of CLAES-UARS retrievals and other correlative measurements and 2-D global model calculations, as reported by Mergenthaler et al.<sup>17</sup> These comparisons show that both  $\text{HNO}_3$  and  $\text{ClONO}_2$  profiles exhibits significant variabilities, not fully modeled yet, even for mid latitudes. In particular, shifts in the altitudes of the peak of the  $\text{ClONO}_2$  profiles such as seen in Fig. 8, also appear in the CLAES results.<sup>17</sup> The improved line parameters will provide a more accurate and consistent quantification of these species from i.r. atmospheric spectra.

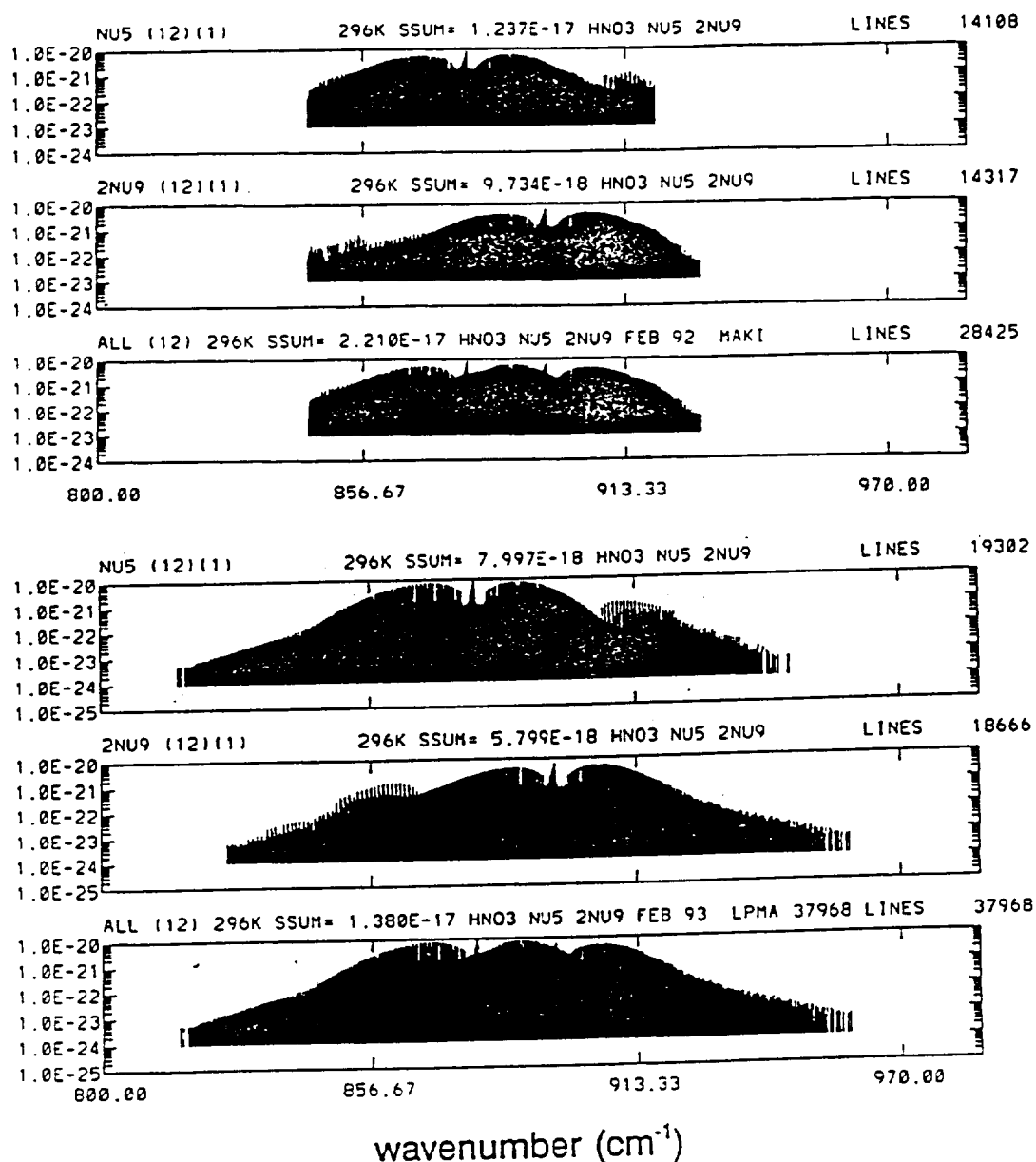


Fig. 1. Line intensity plots for the new sets of HNO<sub>3</sub> line parameters incorporated in the recent analysis of atmospheric spectra for the HNO<sub>3</sub>  $\nu_3/2\nu_3$  bands. The line parameters are based on Maki and Wells<sup>3</sup> and on Perrin et al.<sup>4</sup> The later set is for wider spectral interval and lower intensity cutoff.

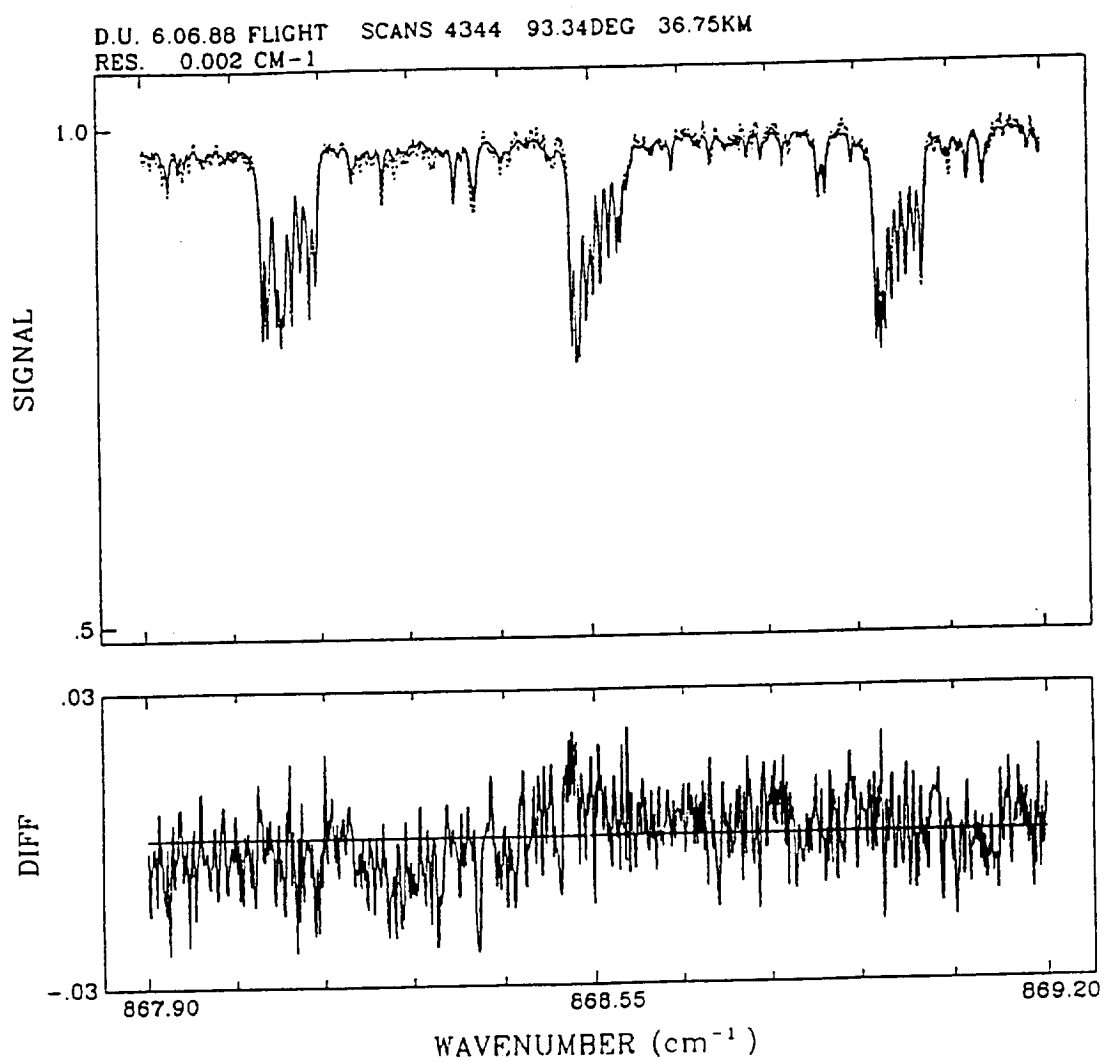


Fig. 2. Sample retrieval of HNO<sub>3</sub> from *P*-branch manifolds in the  $\nu_3$  region by spectral least-squares fitting to balloon-borne solar spectra obtained during D.U. balloon flight of 6 June 1988.

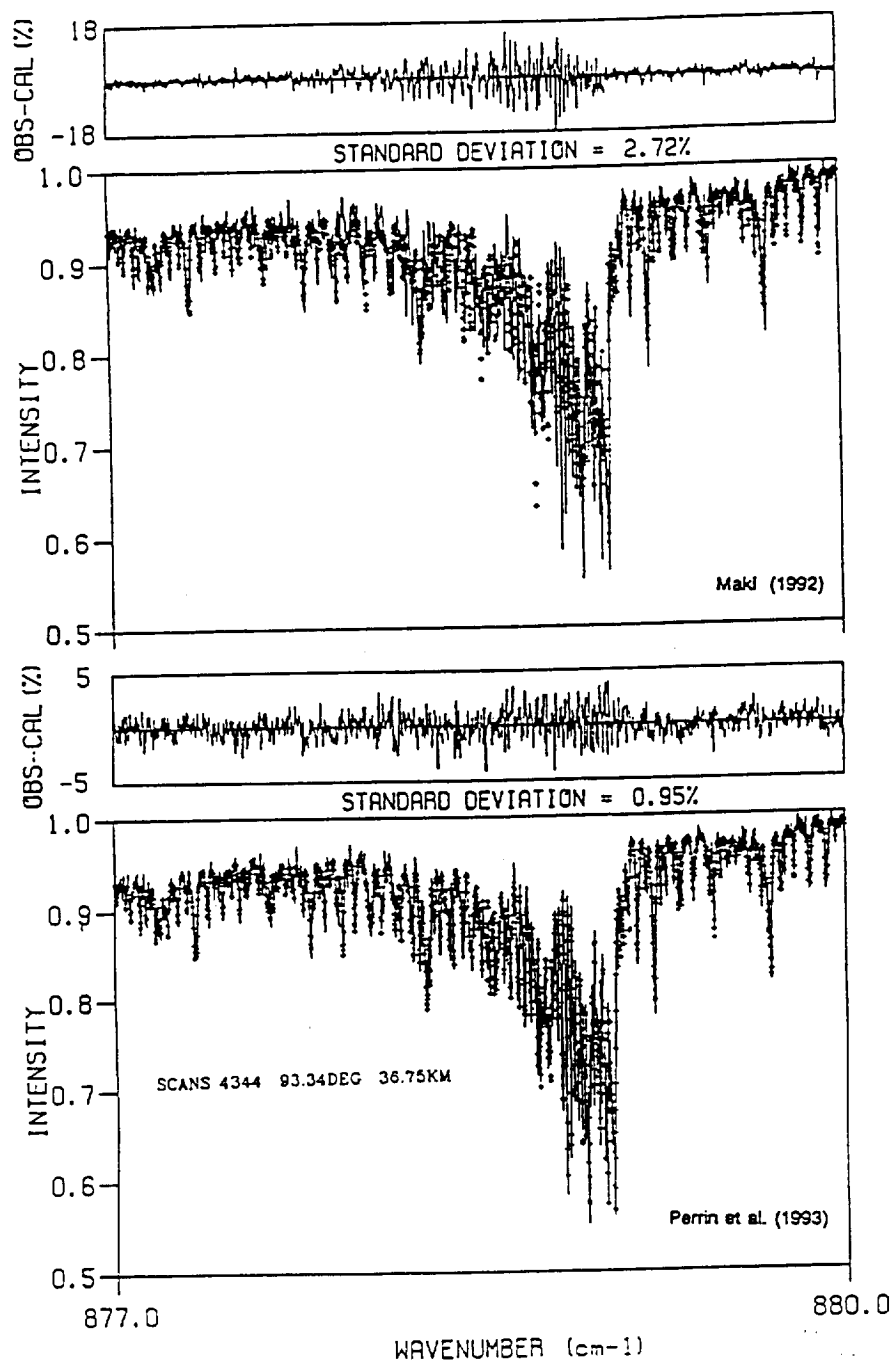


Fig. 3. Comparisons of spectral least-squares fitting to balloon-borne solar spectra obtained during D.U. balloon flight of 6 June 1988, with the recent sets of  $\text{HNO}_3$  line parameters in the  $\nu_3$  Q-branch region.



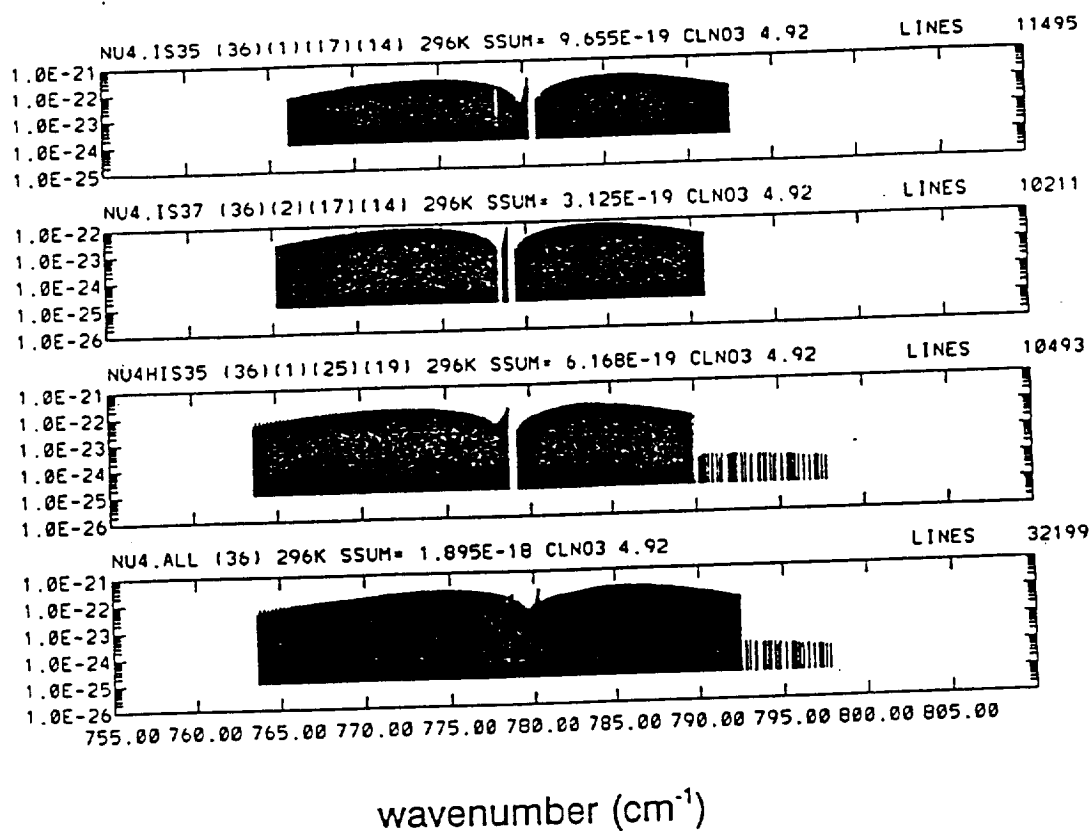


Fig. 4. Line intensity plots of the new  $\text{ClONO}_2$  line parameters incorporated in recent analysis of atmospheric spectra for the  $\nu_4$  bands of  $^{35}\text{ClONO}_2$ ,  $^{37}\text{ClONO}_2$ , and  $\nu_4 + \nu_5 - \nu_9$  of  $^{35}\text{ClONO}_2$ . The line positions are based on the spectroscopic constants of Bell et al<sup>4</sup>, with intensity cutoff for each band of  $5 \times 10^{-3}$  and  $K_{\text{max}} = J_{\text{max}} = 74$ . The relative band intensities are normalized to a University of Denver laboratory spectrum, and absolute intensities normalized to Ballard et al<sup>6</sup> values, with the continuum removed.

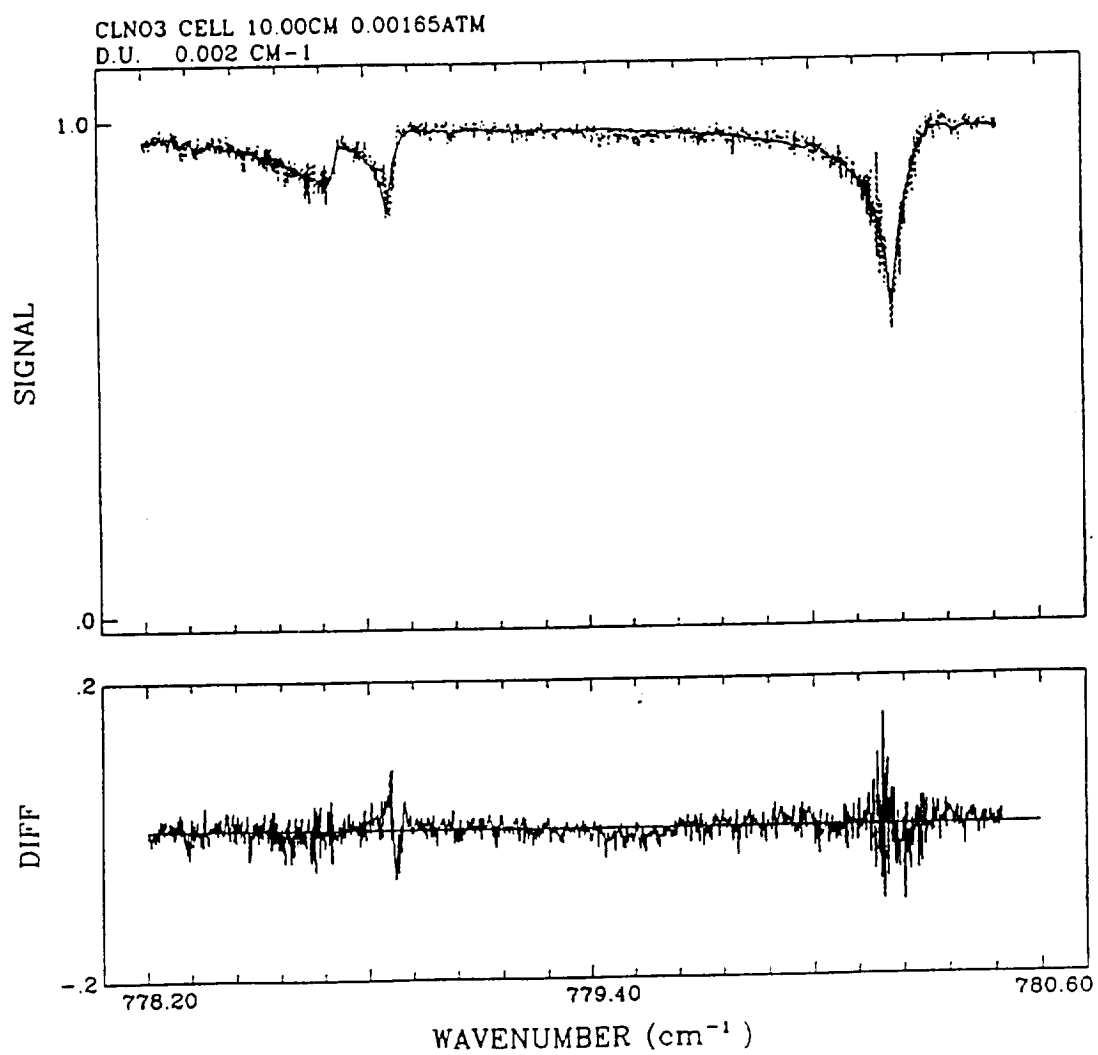


Fig. 5. Spectral least-squares fitting to the ClONO<sub>2</sub> laboratory spectrum with the new line parameters in the  $\nu_4$  <sup>35</sup>ClONO<sub>2</sub> region. Fine structure is not fully accounted for yet.

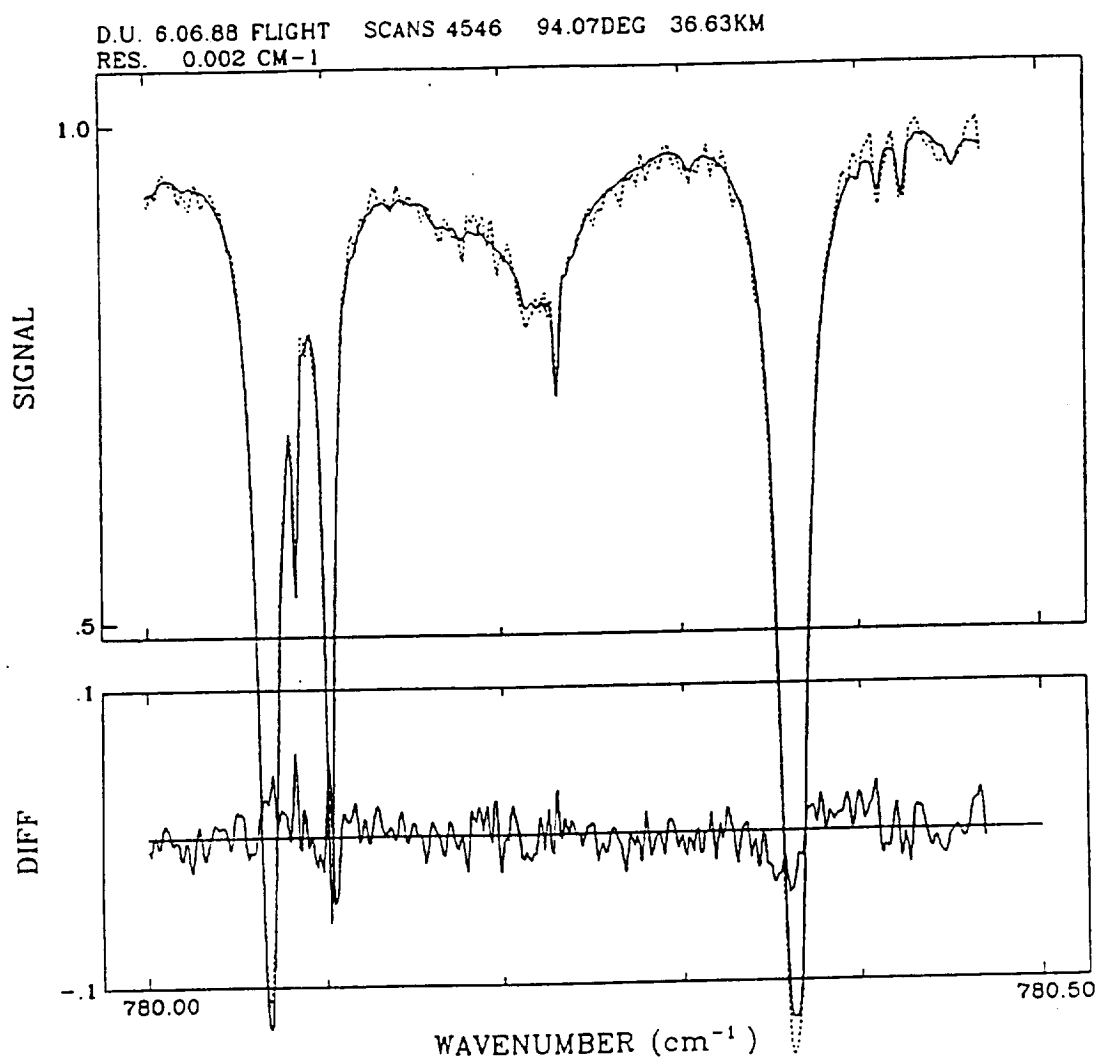


Fig. 6. Sample retrieval of  $\text{ClONO}_2$  by spectral least-squares fitting to balloon-borne solar spectra obtained during University of Denver balloon flight of 6 June 1988.

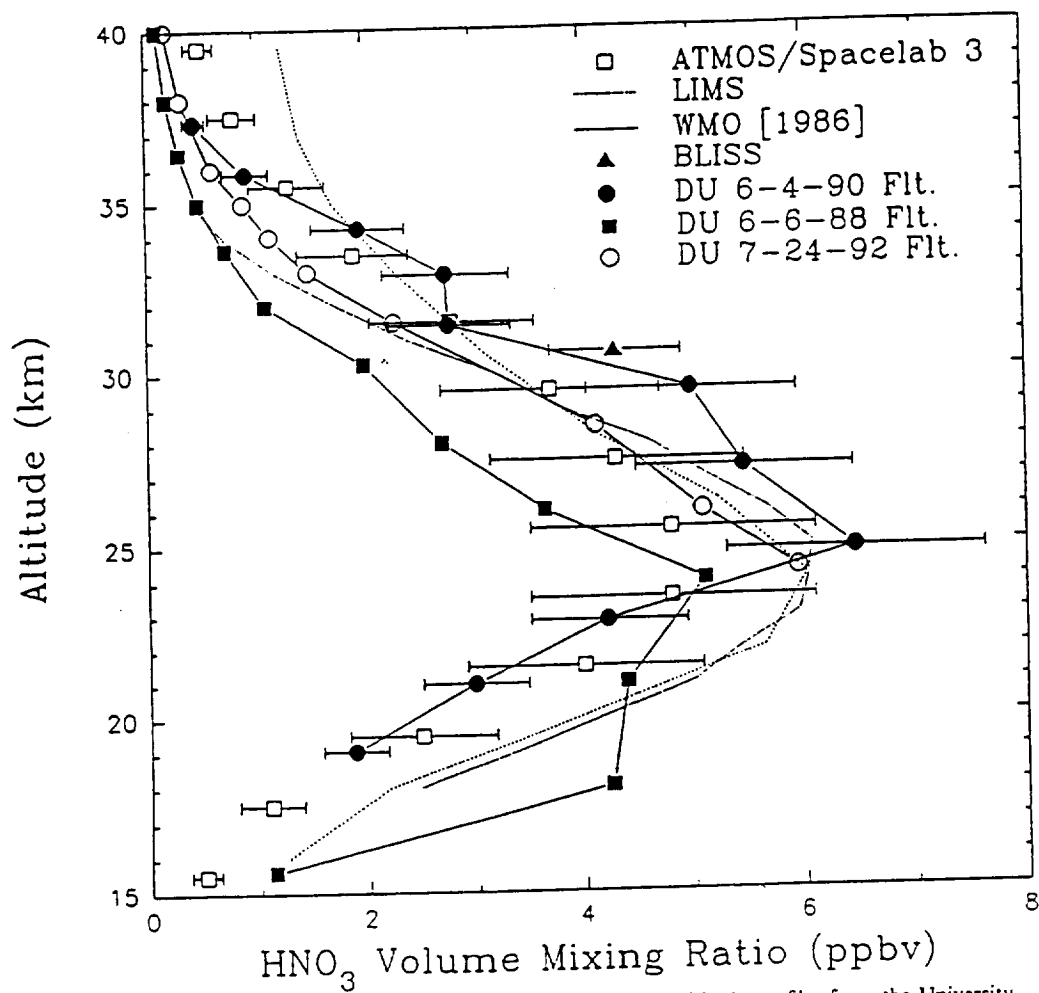


Fig. 7. Comparison of the recent retrievals of  $\text{HNO}_3$  mixing ratio altitude profiles from the University of Denver balloon flights of 6 June 1988 and 24 July 1992. The D.U. 4 June 1990 results were obtained from the  $v_2$  region.<sup>11</sup> The ATMOS, LIMS, WMO (1986) and BLISS results are from Ref. 12-15 respectively.

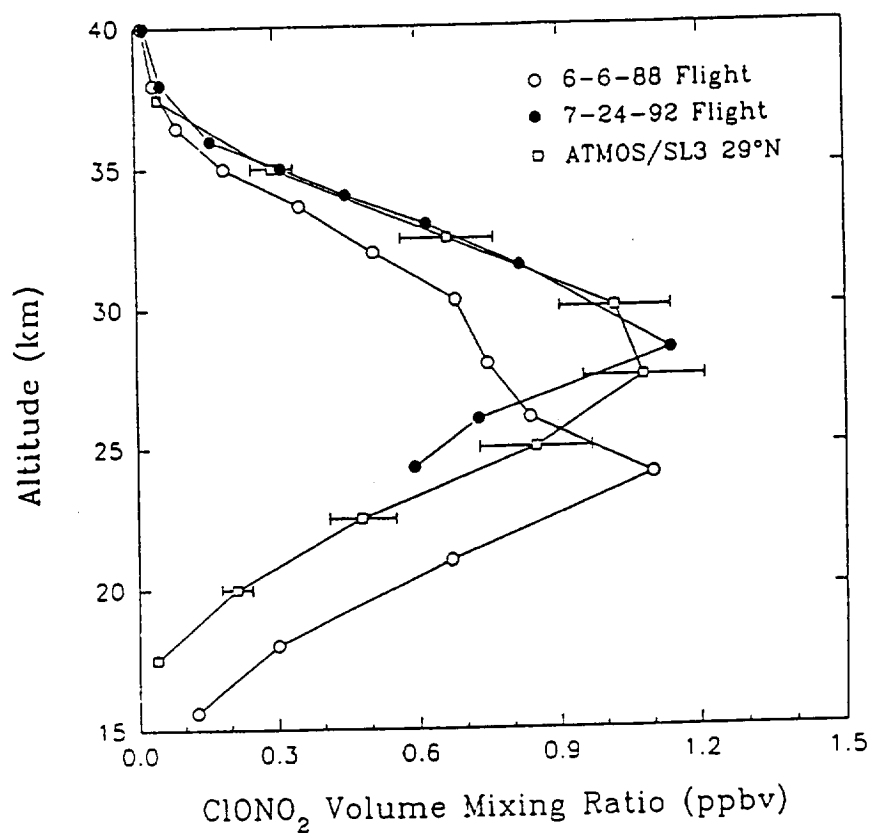


Fig. 8. Comparison of the recent retrievals of  $\text{ClONO}_2$  mixing ratio altitude profiles from the University of Denver balloon flights of 6 June 1988 and 24 July 1992 with previous results of ATMOS.<sup>16</sup>

*Acknowledgements*—This research was supported in part by NSF and in part by NASA. We thank A. G. Maki, J.-M. Flaud, and A. Perrin for providing theoretical results from their HNO<sub>3</sub> studies. Acknowledgement is made to the National Center for Atmospheric Research, which is sponsored by the National Science Foundation, for computer time used in this project.

## REFERENCES

1. A. Goldman, F. J. Murcray, R. D. Blatherwick, J. J. Kusters, F. H. Murcray, D. G. Murcray, and C. P. Rinsland, *J. geophys. Res.* 94, 954 (1989). 14945
2. A. Goldman and C. P. Rinsland, *JQSRT* 48, 653 (1992).
3. A. G. Maki and J. S. Wells, *J. molec. Spectrosc.* 152, 69 (1992).
4. A. Perrin, V. Jaquen, A. Valentin, J.-M. Flaud and C. Camy-Peyret, *J. molec. Spectrosc.* 157, 112 (1993); A. Perrin, J.-M. Flaud, C. Camy-Peyret, V. Jaquen, R. Farrenq, F. Guelachvili, Q. Kou, F. Le Roy, M. Morillon-Chapcy, J. Orphal, M. Badaoui, J.-Y. Mandin, and V. Dana, *J. molec. Spectrosc.* 160, 524 (1993).
5. L. P. Giver, F. P. J. Valero, D. Goorvitch, and F. S. Bonomo, *J. opt. Soc. Am. B.* 1, 715 (1984).
6. J. Ballard, W. B. Johnston, M. R. Gunson, and P. T. Wassel, *J. geophys. Res.* 93, 1659 (1988).
7. S. T. Massie and A. Goldman, *JQSRT* 48, 713 (1992).
8. W. Bell, G. Duxbury, and D. D. Stuart, *J. molec. Spectrosc.* 152, 283 (1992).
9. E. Niple, W. G. Mankin, A. Goldman, D. G. Murcray, and F. J. Murcray, *Geophys. Res. Lett.* 7, 489 (1980).
10. C. P. Rinsland, A. Goldman, F. J. Murcray, D. G. Murcray, M. A. H. Smith, R. K. Seals Jr., J. C. Larsen, and P. L. Rinsland, *Appl. Opt.* 21, 4351 (1982).
11. A. Goldman, F. J. Murcray, R. D. Blatherwick, J. J. Kusters, D. G. Murcray, C. P. Rinsland, J.-M. Flaud, and C. Camy-Peyret, *J. geophys. Res.* 97, 2561 (1992).
12. J. M. Russel III, C. B. Farmer, C. P. Rinsland, R. Zander, L. Froidevaux, G. C. Toon, B. Gao, J. Shaw, and M. Gunson, *J. geophys. Res.* 93, 1718 (1988).
13. J. C. Gille, J. M. Russel III, P. L. Bailey, E. E. Remsberg, L. L. Gordley, W. F. J. Evans, H. Fischer, B. W. Gandrud, A. Girard, J. E. Harries, and S. A. Beck, *J. geophys. Res.* 89, 5179 (1984); J. C. Gille, P. L. Bailey, and C. A. Craig, *Adv. Space Res.* 13, 59 (1993).
14. World Meteorological Organization (WMO), "Atmospheric Ozone 1985—Assessment of our understanding of the processes controlling its present distribution and change," *WMO Rep.* 16, Geneva (1986).
15. R. D. May and C. R. Webster, *J. geophys. Res.* 94, 343 (1989). 16343
16. R. Zander, M. R. Gunson, J. C. Foster, C. P. Rinsland, and J. Namkung, *J. geophys. Res.* 95, 519 (1990). 20519
17. J. L. Mergenthaler, J. B. Kumer, A. E. Roche, R. W. Nightingale, D. G. Murcray, F. J. Murcray, J. W. Williams, and A. Goldman, AGU 1993 fall meeting, San Francisco, Paper A12D-2 (1993).



# INFRARED MEASUREMENTS OF ATMOSPHERIC ETHANE ( $C_2H_6$ ) FROM AIRCRAFT AND GROUND-BASED SOLAR ABSORPTION SPECTRA IN THE $3000\text{ cm}^{-1}$ REGION

M. T. Coffey and W. G. Mankin

National Center for Atmospheric Research, Boulder, Colorado 80307

A. Goldman

University of Denver, Denver, Colorado

C. P. Rinsland and G. A. Harvey

NASA Langley Research Center, Hampton, Virginia

V. Malathy Devi

College of William and Mary, Williamsburg, Virginia

G. M. Stokes

Battelle Observatory, Richland, Washington

**Abstract.** A number of prominent Q-branches of the  $\nu_7$  band of  $C_2H_6$  have been identified near  $3000\text{ cm}^{-1}$  in aircraft and ground-based infrared solar absorption spectra. The aircraft spectra provide the column amount above 12 km at various altitudes. The column amount is strongly correlated with tropopause height and can be described by a constant mixing ratio of 0.46 ppbv in the upper troposphere and a mixing ratio scale height of 3.9 km above the tropopause. The ground-based spectra yield a column of  $9.0 \times 10^{15}$  molecules  $\text{cm}^{-2}$  above 2.1 km; combining these results implies a tropospheric mixing ratio of approximately 0.63 ppbv.

## Introduction

After methane, the most abundant hydrocarbon in the atmosphere is ethane. Its importance for atmospheric chemistry lies principally in its reactions with OH and Cl; it is potentially also a source for atmospheric CO [Chameides and Cicerone, 1978]. In the troposphere, the loss of  $C_2H_6$  is largely by reaction with OH; the lifetime is highly variable, but typical values are approximately 100 days in the lower stratosphere [Rudolph et al., 1981]. In the stratosphere both OH and Cl react with  $C_2H_6$  and the vertical profile of ethane has been used to infer the concentration of chlorine radicals in the lower stratosphere [Rudolph et al., 1981; Aikin et al., 1982; Singh and Salas, 1982]. Measurements of the concentration of ethane near the

tropopause are thus important indicators of radical chemistry.

Recently, infrared measurements of  $C_2H_6$  in the upper troposphere and lower stratosphere were reported based on the analysis of spectra in the  $C_2H_6$   $\nu_9$  band at  $822\text{ cm}^{-1}$  [Goldman et al., 1984]. The same study suggested the identification of the Q-branches of the  $\nu_7$   $C_2H_6$  band near  $3000\text{ cm}^{-1}$ . These absorption features are an order of magnitude stronger than the  $\nu_9$  band Q-branches and thus are important for the remote sensing of  $C_2H_6$  as well as of other trace constituents with spectral features in the same region. In this letter, we present atmospheric spectra with the identification and quantification of the  $C_2H_6$   $\nu_7$  Q-branches. We also present the latitudinal dependence of the  $C_2H_6$  column amount above 12 km as derived from spectra recorded aboard the NCAR Sabreliner aircraft, and a tropospheric amount derived from ground-based spectra recorded at Kitt Peak.

## Analysis

Figure 1 shows atmospheric, calculated, and laboratory spectra in the  $2975\text{--}2990\text{ cm}^{-1}$  region. The aircraft spectrum was recorded in July 1978 at 24 degrees North latitude and an average solar elevation of 2.75 degrees. The three spectra in Figure 1 are all at  $0.06\text{ cm}^{-1}$  resolution. The laboratory spectrum is taken from the laboratory atlas of Murcray and Goldman [1981]. The same atlas also shows a spectrum of the  $\nu_9$  band of  $C_2H_6$  in the  $800\text{ cm}^{-1}$  region recorded under the same conditions, so that the relative intensities of the Q-branches in the two regions are quite apparent. The line-by-line calculation in Figure 1b includes lines of  $CH_4$ ,  $H_2O$ ,  $O_3$ , and  $HCl$  [Rothman et al., 1983a,b], of which  $CH_4$  and  $H_2O$  are the major contributors. The

Copyright 1985 by the American Geophysical Union.

Paper number 5L6437.

0094-8276/85/005L-6437\$03.00



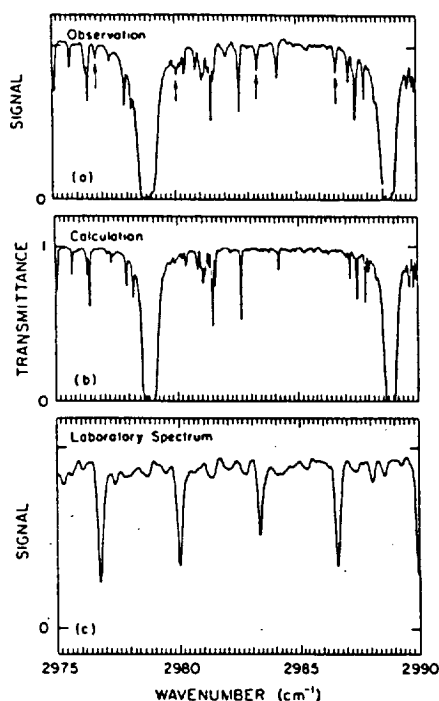


Fig. 1 Spectral region containing the  $R_{Q_0}$  Q-branch of the  $\nu_7$  band of  $C_2H_6$ . Spectrum a is a solar absorption spectrum recorded at  $0.06\text{ cm}^{-1}$  with the NCAR Fourier transform spectrometer from 12 km altitude. The spectrum was recorded in July 1978 at 24 degrees North latitude with an average solar elevation of 2.75 degrees.  $C_2H_6$   $\nu_7$  Q-branches are marked by arrows. Spectrum b is a line-by-line calculation based on line parameters for  $H_2O$ ,  $O_3$ ,  $CH_4$  and  $HCl$  from the 1982 AFGL compilations [Rothman et al., 1983a, b], for conditions corresponding to the observed spectrum in a. Spectrum c is a laboratory spectrum of  $C_2H_6$  also at  $0.06\text{ cm}^{-1}$  resolution [Murray and Goldman, 1981].

features marked by arrows in the aircraft spectrum agree with the  $C_2H_6$  Q-branches in position and relative intensity and are not accounted for in the calculations. The feature at  $2982\text{ cm}^{-1}$  in the observation is due to Si I in the sun's atmosphere. These identifications were further confirmed by comparison of line-by-line simulations with  $0.01\text{ cm}^{-1}$  resolution ground-based spectra obtained at Kitt Peak and additional laboratory spectra. Samples of these spectra are shown in Figure 2 for the interval of  $2976\text{--}2977\text{ cm}^{-1}$ . It should also be noted that our simulations and comparisons with laboratory data showed that several  $CH_4$  line intensities in the  $2990\text{--}3000\text{ cm}^{-1}$  region in the AFGL tape are in large error. These values are being corrected for the next edition.

From studies of spectra such as shown in Figures 1 and 2 we have concluded that several prominent features, as marked with arrows on the figures, are dominated by the  $C_2H_6$  Q-branches. The  $P_{Q_3}$  feature near  $2977\text{ cm}^{-1}$  and the  $R_{Q_0}$  feature near  $2987\text{ cm}^{-1}$  are the most suitable for atmospheric quantification.

Previous search for these features in balloon-borne spectra showed no measurable absorptions [Kendall and Buijs, 1983] for tangent heights down to 19 km. Unlike the  $\nu_9$   $C_2H_6$  Q-branches, line parameters [Rothman et al., 1983b] are not available for the  $\nu_7$  Q-branches, which are not resolved even at very high resolution. Recent studies of laboratory spectra by Pine and Lafferty [1982] and by Dang-Nhu et al. [1984] provide accurate energy levels for the three overlapping vibration-rotation bands in the  $3\text{ }\mu\text{m}$  region ( $\nu_3$ ,  $\nu_7$  and  $\nu_8 + \nu_{11}$  bands) and also approximate intensities for many of the weaker, resolved lines but exclude the Q-branches of atmospheric interest.

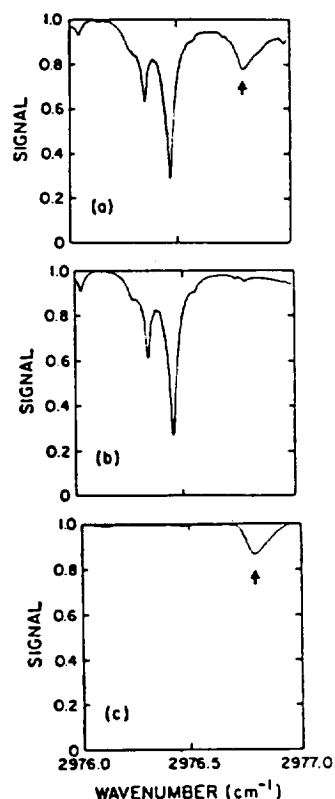


Fig. 2 Spectral region containing the  $P_{Q_3}$  Q-branch of the  $\nu_7$  band of  $C_2H_6$ . Spectrum a is a ground-based solar absorption spectrum recorded at  $0.01\text{ cm}^{-1}$  resolution with the Fourier transform interferometer in the McMath solar telescope complex on Kitt Peak (latitude 31 degrees, 57 minutes North, altitude 2095 m). The spectrum was obtained shortly after sunrise at a mean astronomical zenith angle of 78.72 degrees on February 23, 1981. Spectrum b is a line-by-line simulation calculated with the 1982 AFGL parameters [Rothman et al., 1983a,b] for conditions corresponding to the Kitt Peak atmospheric spectrum a. Spectrum c is a  $0.06\text{ cm}^{-1}$  resolution laboratory spectrum obtained at room temperature with 0.21 Torr of  $C_2H_6$  in a  $5.125\text{ cm}$  absorption path. The  $P_{Q_3}$  Q-branch is marked with an arrow in spectra a and c.

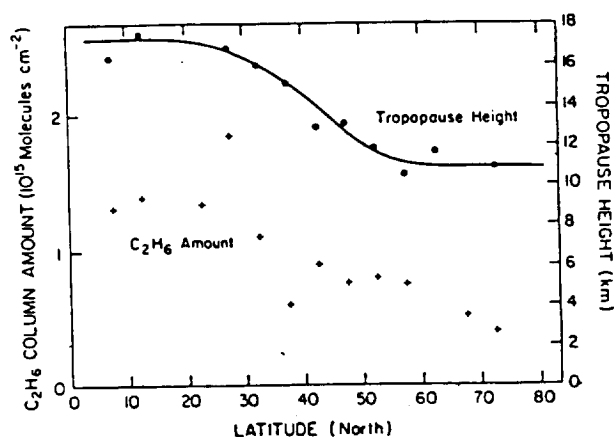


Fig. 3 Latitudinal dependence of the  $C_2H_6$  column amount above 12 km altitude as derived from the aircraft data. Column amounts are averaged from spectra taken over 5 degrees of latitude and represent typically an average of from 8 to 10 individual spectra, some recorded in summer and others in winter. Also shown is the height of the tropopause. The solid circles are the average of winter and summer tropopause heights from the nearest radiosonde observations to the aircraft location.

The  $C_2H_6$  quantification is therefore based on the equivalent width method with the  $PQ_3$  and  $RQ_0$  intensities measured from laboratory spectra. The  $C_2H_6$  Q-branches quantified here are very dense with spectral lines and not broadened significantly by the instrumental spectral resolution. Thus, a small absorption by these Q-branches corresponds to the weak line approximation, where the integrated absorption is proportional to the product of gas amount and the integrated intensity. Assuming linear absorption in the laboratory spectrum of Figure 1 gives an integrated intensity of  $S = 3.23 \pm 0.81 \times 10^{-19} \text{ cm}^{-1}/\text{molecules cm}^{-2}$  (at 296 K) for  $RQ_0$ . Laboratory measurements at NASA Langley, such as in Figure 2c, resulted in an integrated intensity for  $PQ_3$  of  $S = 3.91 \pm 0.64 \times 10^{-19} \text{ cm}^{-1}/\text{molecules cm}^{-2}$  at 296 K. These values have been used in the present analysis.

Aircraft spectra taken over a number of years and a wide range of latitudes show  $C_2H_6$  absorption above the flight level of 12 km. The  $C_2H_6$  column amount is observed to have a maximum at low latitudes and decreases toward the pole. The variation with latitude is strongly correlated with the tropopause altitude as shown in Figure 3.

#### Discussion

The obvious correlation between column amount and tropopause height leads us to attempt to deduce the variation of density of  $C_2H_6$  in the vicinity of the tropopause by fitting the data to the values derived from a simple parametric model profile. We used a model with a constant mixing ratio below the tropopause and an exponential decrease of mixing ratio above the tro-

popause. The two parameters which were fitted are the tropopause mixing ratio and the mixing ratio scale height. The parameters were determined by a least squares fit of the observed columns to the values calculated from the model profile. The resulting best fit was for a mixing ratio at the tropopause of 0.46 ppbv and a scale height of the mixing ratio in the lower stratosphere of 3.9 km. This analysis neglects several important variables, particularly the latitude, but the tropopause height is the most significant variable, and the limited data set does not justify fitting more parameters. The rms difference between the observed and calculated columns is  $0.25 \times 10^{15} \text{ molecules cm}^{-2}$ .

The ground-based measurement in Figure 2 yields a  $C_2H_6$  column of  $9.0 \times 10^{15} \text{ molecules cm}^{-2}$  above the observation altitude of 2.1 km. The aircraft measurement at that latitude indicated  $1.1 \times 10^{15} \text{ molecules cm}^{-2}$  above 12 km. Although the aircraft measurements were made at a different season, if we assume that they are representative of the time of the ground-based observation, the column between 2.1 and 12 km is  $7.9 \times 10^{15} \text{ molecules cm}^{-2}$ , corresponding to a mean mixing ratio of 0.63 ppbv. The ground-based and aircraft results are consistent with previous  $C_2H_6$  sampling measurements [Randolph et al, 1981; Aikin et al., 1982; Singh and Salas, 1982].

**Acknowledgments.** We would like to express our appreciation of the excellent service provided to us by the NCAR Research Aviation Facility.

The National Center for Atmospheric Research is sponsored by the National Science Foundation.

#### References

- Aikin, A. C., J. R. Herman, E. J. Maier, and C. J. McQuillan, Atmospheric chemistry of ethane and ethylene, *J. Geo. phys. Res.*, **87**, 3105-3118, 1982.
- Chameides, W. L., and R. J. Cicerone, Effects of non-methane hydrocarbons in the atmosphere, *J. Geo. phys. Res.*, **83**, 947-952, 1978.
- Dang-Nhu, M., A. S. Pine, and W. J. Lafferty, Les intensités dans les bande  $\nu_5$ ,  $\nu_7$  et  $\nu_8 + \nu_{11}$  de l'éthane  $^{12}C_2H_6$ , *Canad. J. Phys.*, **62**, 512-519, 1984.
- Goldman, A., C. P. Rinsland, F. J. Murcray, D. C. Murcray, M. T. Coffey, and W. G. Mankin, Balloon-borne and aircraft measurements of ethane ( $C_2H_6$ ) in the upper troposphere and lower stratosphere, *J. Atmos. Chem.*, **2**, 211-221, 1984.
- Kendall, D. J. W., and H. L. Buijs, Stratospheric  $NO_2$  and upper limits of  $CH_3Cl$  and  $C_2H_6$  from measurements at  $3.4 \mu m$ , *Nature*, **303**, 221-222, 1983.
- Murcray, D. G., and A. Goldman, Eds., *CRC Handbook of High Resolution Infrared Laboratory Spectra of Atmospheric Interest*, CRC Press, Boca Raton, Florida, 1981.
- Pine, A. S., and W. J. Lafferty, Torsional splittings and assignments of the Doppler-limited spectrum of ethane in the C-H stretching region, *J. Res. N.B.S.*, **87**, 237-256, 1982.

- Rothman, L. S., R. R. Gamache, A. Barbe, A. Goldman, J. R. Gillis, L. R. Brown, R. A. Toth, J.-M. Flaud, and C. Camy-Peyret, AFGL atmospheric absorption line parameters compilation: 1982 edition, Appl. Opt., **22**, 2247-2256, 1983a.
- Rothman, L. S., A. Goldman, J. R. Gillis, R. R. Gamache, H. M. Pickett, R. L. Poynter, N. Husson, and A. Chedin, AFGL trace gas compilation: 1982 version, Appl. Opt., **22**, 1616-1627, 1983b.
- Rudolph, J., D. H. Ehhalt, and A. Tonnissen, Vertical profiles of ethane and propane in the stratosphere, J. Geophys. Res., **86**, 7267-7272, 1981.
- Singh, H. B., and L. J. Salas, Measurement of selected light hydrocarbons over the Pacific Ocean: Latitudinal and seasonal variations, Geophys. Res. Lett., **9**, 842-845, 1982.

(Received January 10, 1985;  
accepted February 7, 1985.)



## Stratospheric $\text{N}_2\text{O}_5$ , $\text{CH}_4$ , and $\text{N}_2\text{O}$ Profiles from IR Solar Occultation Spectra

C. CAMY-PEYRET, J.-M. FLAUD, and A. PERRIN

*Laboratoire de Physique Moléculaire et Applications\*, CNRS Université Pierre and Marie Curie, Paris, France*

C. P. RINSLAND

*Atmospheric Sciences Division, NASA Langley Research Center, Hampton, Virginia, U.S.A.*

A. GOLDMAN and F. J. MURCRAY

*Department of Physics, University of Denver, Denver, Colorado, U.S.A.*

(Received: 23 January 1992; in final form: 3 June 1992)

**Abstract.** Stratospheric volume mixing ratio profiles of  $\text{N}_2\text{O}_5$ ,  $\text{CH}_4$ , and  $\text{N}_2\text{O}$  have been retrieved from a set of  $0.052\text{ cm}^{-1}$  resolution (FWHM) solar occultation spectra recorded at sunrise during a balloon flight from Aire sur l'Adour, France ( $44^\circ\text{ N}$  latitude) on 12 October 1990. The  $\text{N}_2\text{O}_5$  results have been derived from measurements of the integrated absorption by the  $1246\text{ cm}^{-1}$  band. Assuming a total intensity of  $4.32 \times 10^{-17}\text{ cm}^{-1}/\text{molecule cm}^{-2}$  independent of temperature, the retrieved  $\text{N}_2\text{O}_5$  volume mixing ratios in ppbv (parts per billion by volume,  $10^{-9}$ ), interpolated to 2 km height spacings, are  $1.64 \pm 0.49$  at 37.5 km,  $1.92 \pm 0.56$  at 35.5 km,  $2.06 \pm 0.47$  at 33.5 km,  $1.95 \pm 0.42$  at 31.5 km,  $1.60 \pm 0.33$  at 29.5 km,  $1.26 \pm 0.28$  at 27.5 km, and  $0.85 \pm 0.20$  at 25.5 km. Error bars indicate the estimated  $1-\sigma$  uncertainty including the error in the total band intensity ( $\pm 20\%$  has been assumed). The retrieved profiles are compared with previous measurements and photochemical model results.

**Key words.** Atmospheric composition, middle atmosphere, stratosphere, Fourier transform spectroscopy, balloon measurements, nitrogen oxides, methane.

### 1. Introduction

The odd nitrogen family of molecules (primarily  $\text{NO}$ ,  $\text{NO}_2$ ,  $\text{HNO}_3$ ,  $\text{ClONO}_2$ ,  $\text{HO}_2\text{NO}_2$ , and  $\text{N}_2\text{O}_5$ ) is one of three key chemically-coupled families important in the catalytic destruction of ozone in the stratosphere (Crutzen, 1970) (the others are the odd hydrogen and odd chlorine families). Nitrogen pentoxide ( $\text{N}_2\text{O}_5$ ) is a diurnally-varying reservoir of the odd nitrogen family, and the present work reports the accurate measurement of the profile of this molecule at sunrise.

Only a few measurements of  $\text{N}_2\text{O}_5$  have been reported previously. Roscoe (1982) and Evans (1986) reported tentative observations, based on low-resolution sunrise measurements, which were followed by  $0.015\text{ cm}^{-1}$  resolution solar occultation measurements of the  $743$ ,  $1246\text{ cm}^{-1}$ , and  $1720\text{ cm}^{-1}$  bands by the ATMOS Fourier transform spectrometer (FTS) on Spacelab 3 (Toon *et al.*, 1986; Toon,

\* Laboratoire associé aux Universités Pierre et Marie Curie et Paris Sud.

1987; Rinsland *et al.*, 1989), nighttime emission measurements of the  $1246\text{ cm}^{-1}$  band with a balloon-borne FTS (Kunde *et al.*, 1988), and morning emission measurements of the same band with a balloon-borne FTS (Blatherwick *et al.*, 1989).

The present work reports additional measurements of the  $1246\text{ cm}^{-1}$   $\text{N}_2\text{O}_5$  band obtained at sunrise with a high-resolution balloon-borne FTS operating in the solar occultation mode. The  $1246\text{ cm}^{-1}$  band is overlapped by absorption from a number of other atmospheric gases, principally  $\text{CH}_4$  and  $\text{N}_2\text{O}$ , and to a lesser extent molecules such as  $\text{CO}_2$ ,  $\text{H}_2\text{O}$ , and  $\text{COF}_2$ . To obtain accurate corrections for  $\text{CH}_4$  and  $\text{N}_2\text{O}$  interferences, the profiles of both constituents have also been retrieved from the spectra, and those results are also reported.

## 2. Measurements, Data Analysis, and Results

Table I summarizes the most important parameters of the LPMA (Limb Profile Monitor of the Atmosphere) instrument and the balloon flight data of 12 October 1990, which are analyzed here. Instrumental details have been discussed by Camy-Peyret *et al.* (1991); note that a revised set of flight parameters are reported here. Briefly, the LPMA instrument is a rapid-scanning Bomem, Inc. model DA2.01 FTS, which used a HgTdTcd detector and a KCl beamsplitter to cover the  $800$  to  $1400\text{ cm}^{-1}$  region during this balloon flight. The spectral signal-to-rms noise of a single scan exceeded 100 in the region of the  $1246\text{ cm}^{-1}$   $\text{N}_2\text{O}_5$  band. About 40 good spectra were recorded between solar elevation angles of  $-5.42^\circ$  and  $2.47^\circ$  from the float altitude of  $40.1\text{ km}$ . This altitude was derived from measurements by an onboard pressure transducer which were converted to altitude from a correlative pressure-temperature profile (discussed below). The effective instrument resolution was about  $0.052\text{ cm}^{-1}$  FWHM (full width half maximum absorption). The field of view (FOV) of the instrument (see Table I) as determined by an iris of  $0.6\text{ mm}$  at the detector and by the focal length of the output collimator ( $100\text{ mm}$ ) is  $6 \times 10^{-3}\text{ rd}$ , i.e. about  $2/3$  of the angular diameter of the sun. This FOV translates into a vertical span at the limb of about  $2.3\text{ km}$  at a tangent height of  $30\text{ km}$ . The

Table I. Measurement parameters for the 12 October 1990 balloon flight

Parameter	Value
Launch site	Aire sur l'Adour, France ( $43.7^\circ\text{ N}$ , $359.7^\circ\text{ E}$ )
Float altitude	$40.1 \pm 0.2\text{ km}$
Instrument	Bomem DA2.01 Michelson-type interferometer
Spectral coverage	$800\text{--}1400\text{ cm}^{-1}$ ( $7\text{--}12.5\text{ }\mu\text{m}$ )
Spectral resolution	$0.052\text{ cm}^{-1}$ FWHM
Field of view	$6\text{ mrad}$
Aperture	$40\text{ mm}$ diameter (unobscured)
Scan time	$50\text{ s}$
Detector	HgCdTe (cooled to $77\text{ K}$ )
Beam splitter	KCl

vertical resolution is also limited by the time between consecutive zero path difference crossings (in our case  $2 \times 50$ s), which corresponds to a vertical sampling of about 2.5 km at the altitude range of interest.

A pressure-temperature profile calculated by the National Meteorological Center (M. Gelman, private communication, 1991) for the time and location of the balloon flight has been adopted for the analysis. Refracted ray paths for each spectrum were calculated using the FSCATM program (Gallery *et al.*, 1983) and the geometric parameters of the experiment. The time of recording the zero path difference signal was used in computing the solar zenith angles (Park, 1982; Kyle and Blatherwick, 1984).

A nonlinear least-squares spectral fitting procedure (e.g., Rinsland *et al.*, 1982) was used to retrieve the CH<sub>4</sub> and N<sub>2</sub>O profiles. The effective instrument line shape was first determined by least-squares fitting isolated CH<sub>4</sub> lines in a high signal-to-noise spectrum produced by averaging all of the spectra with zenith angles less than 90°. The retrieved instrument function was held fixed during the subsequent retrievals. Independent onion-peeling retrievals were run using each of the spectral intervals listed in Table II. A sample fit is shown in Figure 1. The final profiles have been obtained by averaging the results from the different intervals. Line parameters from the 1991 HITRAN compilation (L. S. Rothman, unpublished results, 1991) were assumed in the analysis.

Figures 2 and 3 show comparisons of the retrieved profiles with in-situ measurements obtained at the same latitude between 1982 and 1985 (Schmidt *et al.*, 1986) and 2-D photochemical model profiles (M. K. W. Ko, private communication, 1991). Error bars represent the total 1- $\sigma$  uncertainty of the present measurements, about 10% for both gases. The error limits were evaluated from sensitivity studies of the effects of uncertainties in each of the assumed parameters. In these studies, retrievals are repeated with each parameter varied by the amount of its estimated uncertainty while all others remain fixed at the assumed values. The total errors are then calculated from the RSS (square root of the sum of the squares) of the indi-

Table II. Spectral intervals used in the CH<sub>4</sub> and N<sub>2</sub>O retrievals

Interval (cm <sup>-1</sup> )	Notes
1242.00–1247.00	CH <sub>4</sub> profile, N <sub>2</sub> O below 30 km <sup>a</sup>
1253.00–1255.30	CH <sub>4</sub> profile, N <sub>2</sub> O below 30 km
1262.63–1262.96	N <sub>2</sub> O above 30 km
1264.62–1264.84	N <sub>2</sub> O above 30 km
1270.01–1270.25	N <sub>2</sub> O above 30 km
1272.73–1273.08	N <sub>2</sub> O above 30 km
1273.60–1273.85	N <sub>2</sub> O above 30 km

<sup>a</sup> Significant interference by H<sub>2</sub>O and CO<sub>2</sub> absorptions. The profiles of both gases were adjusted as part of the fitting procedure.

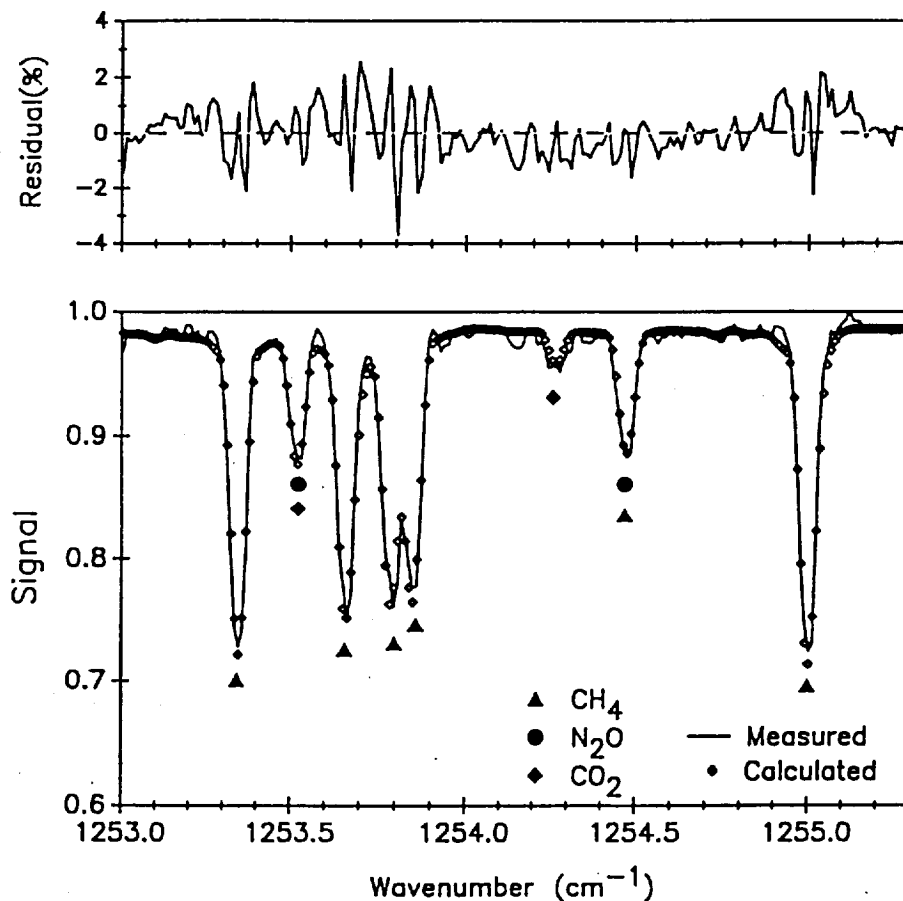


Fig. 1. Sample least-squares fit to a balloon-borne solar spectrum recorded at an astronomical zenith angle of  $92.77^\circ$ , which corresponded to a refracted tangent height of 32.6 km. The bottom panel shows the measured and best-fit calculated spectra while the residuals (measured minus calculated values) are shown on an expanded vertical scale at top. Identifications of the stronger absorption features are given beneath the observed spectrum. No unknown lines appear in this window, and the deviations between measurement and calculation are principally caused by noise and by imperfections in the modeling of the instrument function.

vidual errors. The error sources and the average uncertainty in the retrieved volume mixing ratios resulting from each are (1) uncertainty in the assumed spectroscopic line parameters ( $\pm 4\%$ ), (2) uncertainty in the assumed pressure-temperature profile ( $\pm 2\%$ ), (3) uncertainty in the observational geometry (errors in the pointing angle and balloon float altitude) ( $\pm 5\%$ ), (4) uncertainty due to finite instrument signal-to-noise ( $\pm 5\%$ ), (5) uncertainty in modeling of the instrument line shape function ( $\pm 4\%$ ), and (6) uncertainty due to zero signal level offsets and weak channel spectra ( $\pm 3\%$ ). These last two sources of uncertainty are rather typical of Fourier transform spectra. They are minimal in the present experiment. The



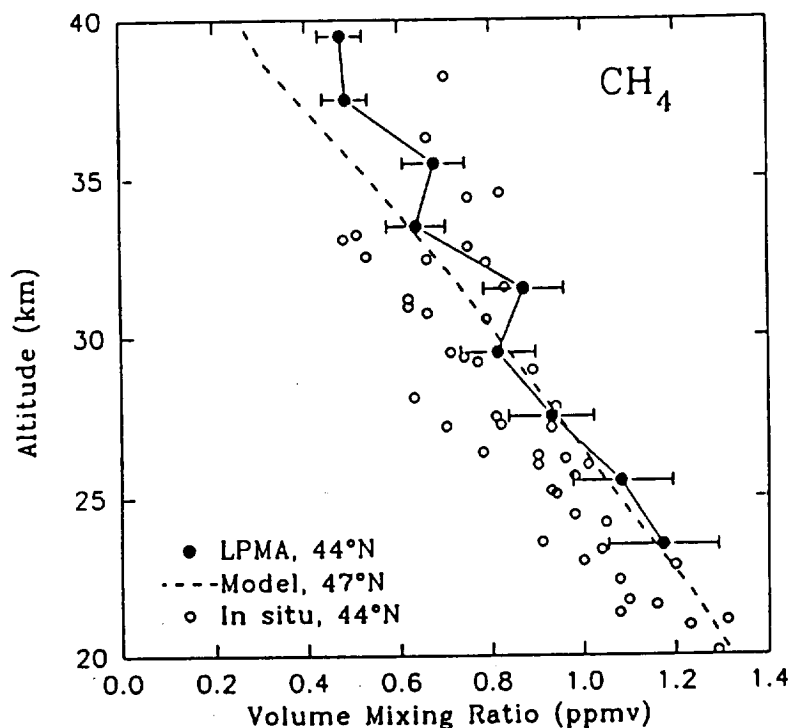


Fig. 2. Comparison of the retrieved LPMA CH<sub>4</sub> profile with in-situ measurements at 44° N obtained between 1982 and 1985 (Schmidt *et al.*, 1986) and a 2-D photochemical model profile computed for 47° N latitude and the date of the LPMA measurements (M. K. W. Ko, private communication, 1991).

zero level can be checked on the edges of the bandpass and at the bottoms of saturated absorption features (H<sub>2</sub>O and O<sub>3</sub> lines). Channel spectra, resulting from the combined effects of using a filter for isolating the spectral region of interest and a germanium window for rejecting the visible-UV part of the solar spectrum, are observable but rather weak. On a relative basis, the agreement between the infrared and in-situ measurements is very good. The mean and the standard deviation of the ratio of the IR volume mixing ratios to the in-situ data are  $1.13 \pm 0.18$  for CH<sub>4</sub> and  $1.34 \pm 0.47$  for N<sub>2</sub>O. The larger standard deviation for N<sub>2</sub>O reflects the larger scatter in the in-situ measurements. About half of the offset between the CH<sub>4</sub> data-sets can be attributed to the long-term increase in CH<sub>4</sub> between the time of the in-situ measurements (1983–1985) and our flight experiment (1990). The rate of CH<sub>4</sub> increase at the surface is about 1% per year (e.g., Khalil and Rasmussen, 1990).

Analysis of the spectra to retrieve the N<sub>2</sub>O<sub>5</sub> profile has followed the procedures described previously (Rinsland *et al.*, 1989). In this method, microwindows spaced about 1 cm<sup>-1</sup> apart between 1210 and 1270 cm<sup>-1</sup>, as given in Table 2 of Rinsland *et al.* (1989), were used to measure the integrated absorption by the N<sub>2</sub>O<sub>5</sub> band. The

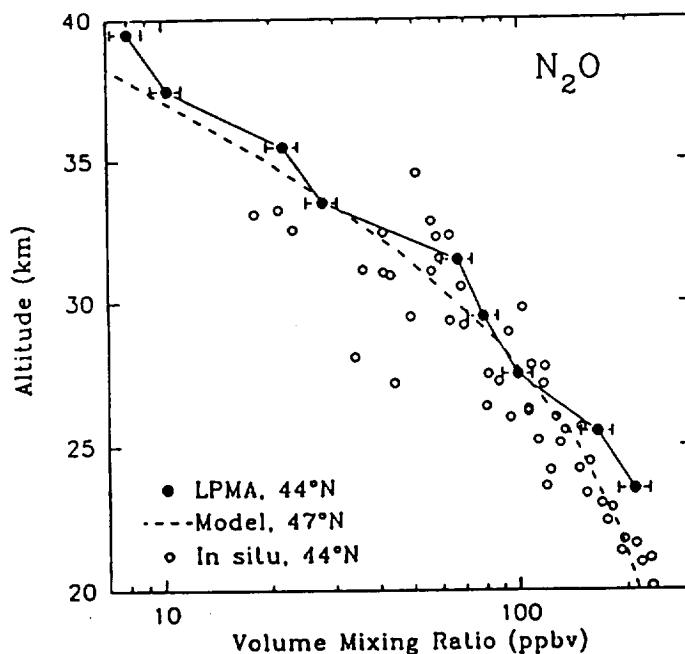


Fig. 3. Comparison of the retrieved LPMA  $\text{N}_2\text{O}$  profile with in-situ measurements at  $44^\circ\text{N}$  obtained between 1982 and 1985 (Schmidt *et al.*, 1986) and a 2-D photochemical model profile computed for  $47^\circ\text{N}$  latitude and the date of the LPMA measurements (M. K. W. Ko, private communication, 1991). Even at the lowest level for which we have retrieved the  $\text{N}_2\text{O}$  mixing ratio, the agreement between our determinations and the in-situ measurements is compatible with the error bars of each technique.

measurements were made on ratio spectra computed by dividing the individual low sun spectra by an average high sun spectrum obtained by coadding all spectra with zenith angles less than  $90^\circ$ . Corrections for residual atmospheric absorption in the microwindows were derived from simulations calculated with the retrieved  $\text{CH}_4$  and  $\text{N}_2\text{O}$  profiles. Reference volume mixing ratio profiles (e.g., the compilation of Smith (1982)) were assumed for calculating the absorption by other gases in this region. All of the species on the 1991 HITRAN compilation (L. S. Rothman, unpublished results, 1991) were included in the calculations.

Figure 4 shows a sequence of microwindow measurements from several of the spectra. The growth of the  $\text{N}_2\text{O}_5$  band absorption with decreasing tangent height is readily apparent. Dashed lines show the fitted 100% transmittance level for two of the spectra. Equivalent widths of the  $\text{N}_2\text{O}_5$  band have been obtained by integrating the absorption between  $1226$  and  $1265\text{ cm}^{-1}$ . The results from spectra with the same zero path difference crossing times agree within the uncertainties and have been averaged. These times correspond to the short period at zero path difference for reverse and forward scans (one sided interferograms) recorded by the present instrument.

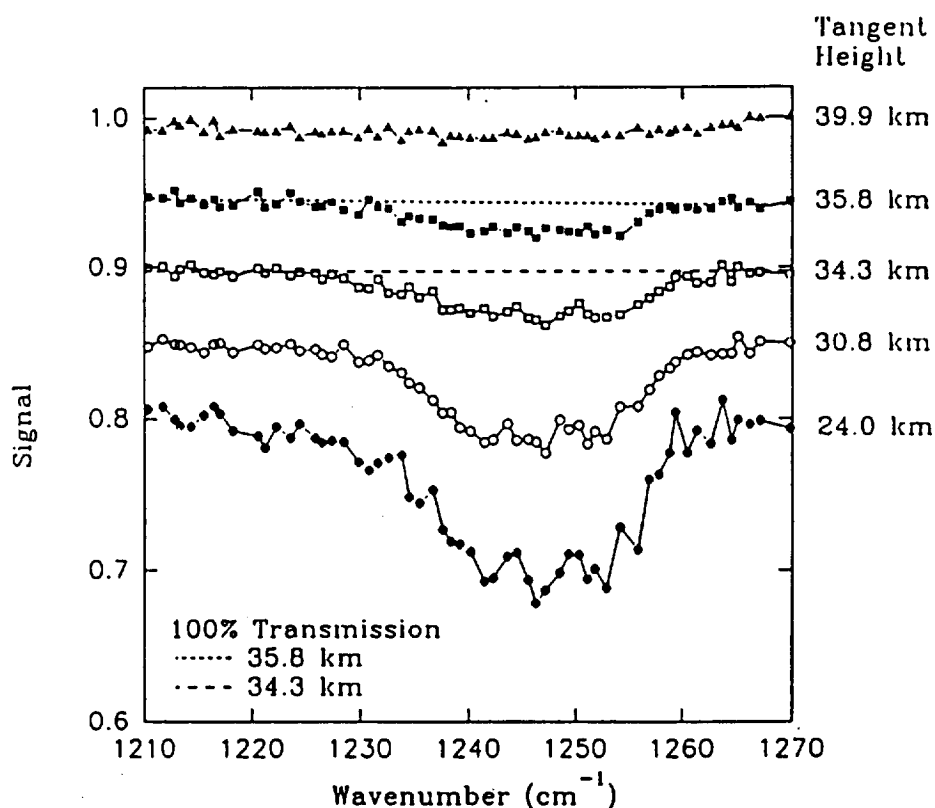


Fig. 4. Examples of microwindow measurements in the region of the  $1246\text{ cm}^{-1}$  band of  $\text{N}_2\text{O}_5$ . The values from each scan, which have been corrected for residual absorption by other gases, are shown on the same scale, but have been offset vertically for clarity. Refracted tangent heights of the spectra are given at right. Dashed lines show 100% transmission levels determined by fitting the microwindow measurements from  $1210$  to  $1226\text{ cm}^{-1}$  and  $1265$  to  $1270\text{ cm}^{-1}$ .

The profile of  $\text{N}_2\text{O}_5$  has been derived from the measured equivalent widths using the onion-peeling retrieval method and an assumed temperature-independent band intensity of  $4.32 \times 10^{-17}\text{ cm}^{-1}/\text{molecule cm}^{-2}$ . This value is the same as adopted previously (Toon *et al.*, 1986; Rinsland *et al.*, 1989). Recently, Roscoe (1991) reviewed the published laboratory and atmospheric measurements of  $\text{N}_2\text{O}_5$  and recommended an integrated  $1246\text{ cm}^{-1}$   $\text{N}_2\text{O}_5$  band intensity of  $4.01 \times 10^{-17}\text{ cm}^{-1}/\text{molecule cm}^{-2}$ . If this lower value is assumed, the published ATMOS measurements and those reported in this study need to be multiplied by a factor of 1.077.

Figure 5 presents a comparison of our retrieved  $\text{N}_2\text{O}_5$  profile with previous published measurements and two photochemical model calculations performed for conditions corresponding to the ATMOS/Spacelab 3 sunrise measurements at  $47^\circ\text{ S}$  on 1 May 1985. Error bars on the LPMA profile increase with altitude, ranging from 22 to 30%. The uncertainty is dominated by the absolute uncertainty of

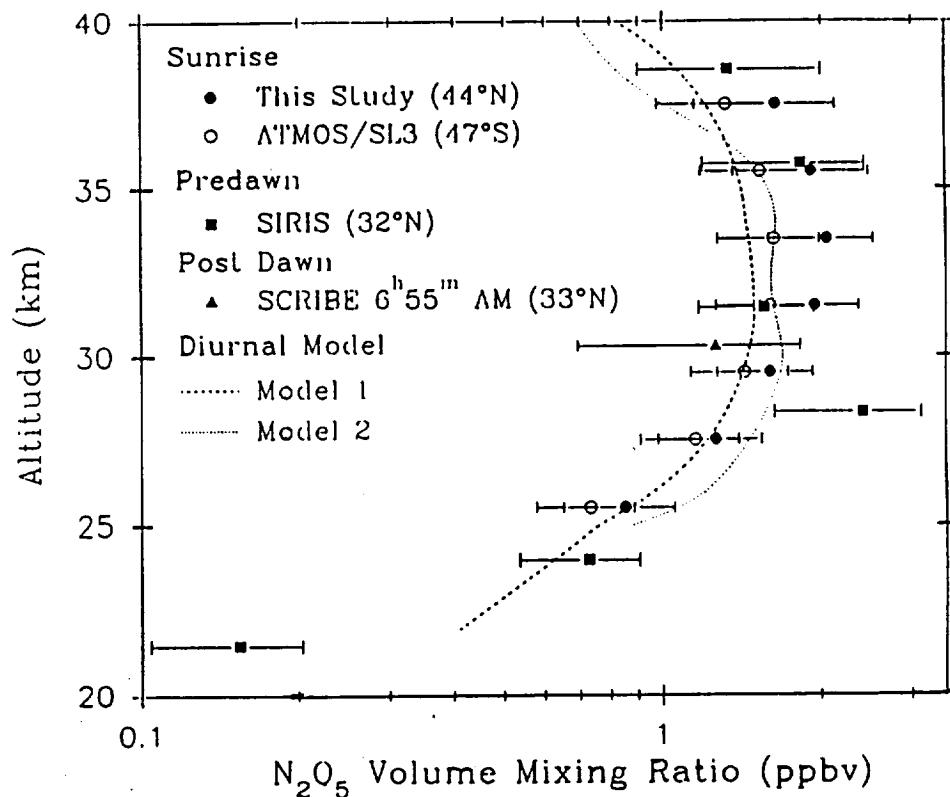


Fig. 5. Comparison of  $\text{N}_2\text{O}_5$  volume mixing ratio profiles measured at sunrise by the LPMA and ATMOS instruments, predawn values retrieved from spectra recorded by the SIRIS instrument (Kunde *et al.*, 1988), a post-sunrise measurement retrieved from a spectrum recorded with the SCRIBE instrument (Blatherwick *et al.*, 1989), and photochemical model calculations generated for the conditions of the ATMOS sunrise measurements (1 May 1985, at 47° S latitude). Error bars indicate the 1-sigma uncertainties of the measurements. Models 1 and 2 denote the model calculations of M. Natarajan (private communication, 1989) and Allen and Delitsky (1990, Fig. 3), respectively. The latter study reported profiles derived with three different values assumed for the  $\text{N}_2\text{O}_5$  absorption cross sections; the curve plotted in this figure (model 2) corresponds to the profile computed with the  $\text{N}_2\text{O}_5$  cross sections recommended by DeMore *et al.* (1987).

20% in the assumed  $\text{N}_2\text{O}_5$  band intensity at stratospheric temperatures. Errors in the equivalent width measurements are also important at the higher tangent altitudes ( $>35$  km), where the  $\text{N}_2\text{O}_5$  absorption is very weak. Below about 31 km, the LPMA profile is in good agreement with the other data. At higher altitudes, the ATMOS volume mixing ratios and photochemical model profiles are lower than the present results, although there is agreement within the measurement errors. A sunrise  $\text{N}_2\text{O}_5$  volume mixing ratio at 30 km has been calculated by Webster *et al.* (1990) from their simultaneous in-situ measurements of NO,  $\text{NO}_2$ ,  $\text{HNO}_3$ ,  $\text{O}_3$ ,  $\text{N}_2\text{O}$ , pressure, and temperature on 13 September 1988, at 32° N latitude. Our measured value of  $1.70 \pm 0.35$  ppbv at the same altitude is significantly lower than

the computed value of  $2.7 \pm 0.4$  ppbv (Webster *et al.*, 1990) (not plotted in the figure). Our measurement results for  $\text{CH}_4$ ,  $\text{N}_2\text{O}$ , and  $\text{N}_2\text{O}_5$  are summarized in Table III. For convenience, the profiles have been interpolated to 2 km altitude spacings. The error limits quoted for all three gases are believed to be conservative.

### 3. Summary and Conclusions

Profiles of  $\text{N}_2\text{O}_5$ ,  $\text{CH}_4$ , and  $\text{N}_2\text{O}$  have been retrieved from  $0.052 \text{ cm}^{-1}$  resolution (FWHM) solar occultation spectra recorded at sunrise near  $44^\circ \text{ N}$  latitude with a balloon-borne Michelson interferometer. The measured profiles have been compared with previous measurements and photochemical model calculations. The agreement is generally good.

The measured spectra contain absorption features of a number of additional stratospheric gases, such as  $\text{HNO}_3$ ,  $^{16}\text{O}_3$ ,  $^{16}\text{O}^{16}\text{O}^{18}\text{O}$ ,  $\text{CCl}_2\text{F}_2$ , and  $\text{CCl}_3\text{F}$ . Work on the analysis of these gases as well as spectra recorded during other balloon flights is in progress.

### Acknowledgements

The authors thank M. K. W. Ko of AER, Inc., Cambridge, Mass., U.S.A., for sending  $\text{CH}_4$  and  $\text{N}_2\text{O}$  photochemical model profiles to compare with the LPMA measurements. Financial support by Programme Atmosphère Moyenne of CNRS together with support from CEC/STEP funding through the SIUBEX project are acknowledged for the balloon flight and instrumentation. Research at the University of Denver is supported by the National Aeronautics and Space Administration.

Table III. Retrieved volume mixing ratio profiles

Altitude (km)	Pressure (mbar)	Temperature (K)	Volume mixing ratio		
			$\text{CH}_4$ (ppmv)	$\text{N}_2\text{O}$ (ppbv)	$\text{N}_2\text{O}_5$ (ppbv)
39.5	3.0	246.2	0.48 (5)	8.0 (7)	—
37.5	4.0	241.7	0.49 (5)	10.3 (10)	1.64 (49)
35.5	5.3	237.0	0.68 (7)	22 (2)	1.92 (56)
33.5	7.1	231.5	0.64 (6)	28 (3)	2.06 (47)
31.5	9.5	226.0	0.87 (9)	66 (6)	1.95 (42)
29.5	12.8	223.0	0.81 (8)	79 (8)	1.60 (33)
27.5	17.5	220.4	0.93 (9)	99 (10)	1.26 (28)
25.5	23.8	217.9	1.08 (11)	165 (17)	0.85 (20)
23.5	32.4	215.6	1.17 (12)	209 (21)	—

ppmv =  $10^{-6}$  per unit volume, ppbv =  $10^{-9}$  per unit volume. Values enclosed in parentheses are 1- $\sigma$  total uncertainties in units of the last quoted digit.

## References

- Allen, M. and Delitsky, M. L., 1990, Stratospheric NO, NO<sub>2</sub>, and N<sub>2</sub>O<sub>5</sub>: A comparison of model results with Spacelab 3 atmospheric trace molecule spectroscopy (ATMOS) measurements, *J. Geophys. Res.* **95**, 14077–14082.
- Blatherwick, R. D., Murcray, D. G., Murcray, F. H., Murcray, F. J., Goldman, A., Vansasse, G. A., Massie, S. T., and Cicerone, R. J., 1989, Infrared emission measurements of morning stratospheric N<sub>2</sub>O<sub>5</sub>, *J. Geophys. Res.* **94**, 18337–18340.
- Camy-Peyret, C., Flaud, J.-M., and Perrin, A., 1991, Balloon-borne solar occultation Fourier transform spectrometry for measurements of stratospheric trace species, *ESA Publ. SP-317*, pp. 179–186.
- Cantrell, C. A., Davidson, J. A., McDaniel, A. H., Shetter, R. E., and Calvert, J. G., 1988, Infrared absorption cross sections for N<sub>2</sub>O<sub>5</sub>, *Chem. Phys. Lett.* **148**, 358–363.
- Crutzen, P. J., 1970, The influence of nitrogen oxides on atmospheric ozone content, *Quart. J. R. Met. Soc.* **96**, 320–325.
- DeMore, W. B., Molina, M. J., Sander, S. P., Golden, D. M., Hampson, R. F., Kurzio, M. J., Howard, C. J., and Ravishankara, A. R., 1987, Chemical kinetics and photochemical data for use in stratospheric modeling, *JPL Publ.* **87-41**.
- Evans, W. F. J., 1986, Observation of the 8- $\mu$ m N<sub>2</sub>O<sub>5</sub> thermal emission feature in the stratosphere, *Appl. Opt.* **25**, 1866–1868.
- Gallery, W. O., Kneizys, F. X., and Clough, S. A., 1981, Air mass computer program for atmospheric transmittance/radiance calculation: FSCATM, AFGL-TR-83-0065, Environmental Research Paper No. 828, Air Force Geophysics Laboratory, Hanscom Air Force Base, Mass.
- Khalil, M. A. K. and Rasmussen, R. A., 1990, Atmospheric methane: Recent global trends, *Environ. Sci. Technol.* **24**, 549–553.
- Kunde, V. G., Brasunas, J. C., Maguire, W. C., Herman, J. R., Massie, S. T., Abbas, M. M., Herath, L. W., and Shaffer, W. A., 1988, Measurement of nighttime stratospheric N<sub>2</sub>O<sub>5</sub> from infrared emission spectra, *Geophys. Res. Lett.* **15**, 1177–1180.
- Kyle, T. G. and Blatherwick, R., 1984, Smearing of interferograms in Fourier transform spectroscopy, *Appl. Opt.* **23**, 261–263.
- Park, J. H., 1982, Effect of interferogram smearing on atmospheric limb sounding by Fourier transform spectroscopy, *Appl. Opt.* **21**, 1356–1366.
- Rinsland, C. P., Goldman, A., Murcray, F. J., Murcray, D. G., Smith, M. A. H., Seals, R. K. Jr., Larsen, J. C., and Rinsland, P. L., 1982, Stratospheric N<sub>2</sub>O mixing ratio profile from high-resolution balloon-borne solar absorption spectra and laboratory spectra near 1880 cm<sup>-1</sup>, *Appl. Opt.* **21**, 4351–4355.
- Rinsland, C. P., Toon, G. C., Farmer, C. B., Norton, R. H., and Namkung, J. S., 1989, Stratospheric N<sub>2</sub>O<sub>5</sub> profiles at sunrise and sunset from further analysis of the ATMOS/Spacelab 3 solar spectra, *J. Geophys. Res.* **94**, 18341–18349.
- Roscoe, H. K., 1982, Tentative observation of stratospheric N<sub>2</sub>O<sub>5</sub>, *Geophys. Res. Lett.* **9**, 901–902.
- Roscoe, H. K., 1991, Review and revision of measurements of stratospheric N<sub>2</sub>O<sub>5</sub>, *J. Geophys. Res.* **96**, 10879–10884.
- Schmidt, U., Jebsen, C., Johnen, F. J., Khedim, A., Klein, E., Knapska, D., Kulassa, G., Rudolph, J., Schumacher, G., and Schunck, E., 1986, Stratospheric observations of long-lived trace gases at midlatitudes 1982–1985 (data report), Kernforschungsanlage Jülich GmbH, Institut für Chemie: Atmosphärische Chemie, Jülich, Germany.
- Smith, M. A. H., 1982, Compilation of atmospheric gas concentration profiles from 0 to 50 km, NASA Tech Memo., TM 83289. (Available as NTIS 82N22822 from the Natl. Tech. Inf. Serv., Springfield, Va.)
- Toon, G., 1987, Reply: Detection of stratospheric nitrogen species, *Nature* **330**, 427.
- Toon, G. C., Farmer, C. B., and Norton, R. H., 1986, Detection of stratospheric N<sub>2</sub>O<sub>5</sub> by infrared remote sounding, *Nature* **319**, 570–571.
- Webster, C. R., May, R. D., Toumi, R., and Pyle, J. A., 1990, Active nitrogen partitioning and the nighttime formation of N<sub>2</sub>O<sub>5</sub> in the stratosphere: Simultaneous in-situ measurements of NO, NO<sub>2</sub>, HNO<sub>3</sub>, O<sub>3</sub>, and N<sub>2</sub>O using the BLISS diode laser spectrometer, *J. Geophys. Res.* **95**, 13851–13866.



## DETERMINATION OF TOTAL OZONE OVER MAUNA LOA USING VERY HIGH RESOLUTION INFRARED SOLAR SPECTRA

Shelle J. David, Sheryl A. Beaton, Mary H. Anderberg and Frank J. Murcray

Department of Physics, University of Denver

**Abstract.** A very high resolution infrared Fourier transform spectrometer has been used to record solar spectra at the Mauna Loa Observatory in Hawaii. Spectra are normally taken one day a week at sunrise. These spectra have been analyzed for ozone and  $\text{N}_2\text{O}$  total columns, and the ozone column compared with the value reported by the Mauna Loa Dobson spectrophotometer. Aside from the FTIR reporting about 5% lower values than the Dobson (which may be due to a systematic difference in the treatment of tropospheric ozone), the FTIR and Dobson agree to within 2.7% (RMS) during this period.

### Introduction

Ozone has long been recognized as one of the most important atmospheric trace gases. Early interest in the compound was due to its role in atmospheric radiation exchange. As a result, measurement of ozone column abundances and profiles were generally supported by various national meteorological offices. Long-term ozone records are somewhat sporadic because of the variation of national funding.

Stratospheric ozone absorbs much of the solar UV-B radiation before it reaches the earth's surface, thus reducing the likelihood of skin cancer in humans. The possibility that changes in ozone could have serious health effects was first raised as a serious issue in conjunction with the environmental effects of the SST (supersonic transport). Since that time, research on the ozone layer has concentrated on determining the extent to which man's activities can result in the depletion of the stratospheric ozone layer.

Ozone also has several strong absorption bands in the middle infrared, some of which occur in regions that would otherwise be nearly transparent ("atmospheric windows"). Thus, in addition to heating the stratosphere by absorbing solar UV, ozone plays a significant role in the atmospheric greenhouse effect.

While the initial measurement of atmospheric ozone by observing the absorption of solar radiation in the ultraviolet was performed by Fabry and Buisson [1913, 1921], the first extensive, systematic measurement program was carried out by Dobson and his collaborators [Dobson, et al. 1926, 1927, 1929, 1930]. Dobson was also responsible for development of instrumentation for the measurement of the total column on a routine basis [Dobson, 1957]. As noted, the importance of ozone in atmospheric processes

was recognized by the meteorological community and instruments of the Dobson design were installed at meteorological observatories around the world. Upgraded versions of these instruments are still in use at many locations. The Dobson instrument and processing algorithm have been the subject of many studies to determine the absolute accuracy of the measured column. With properly maintained and operated instruments, relative accuracy of 1% or better can be achieved [Grass et al., 1992]. The absolute accuracy is more difficult to estimate. The standard coefficients used differ by 3% from more recent values, while other known error sources are about 1% [WMO, 1988].

Ozone has strong absorption around  $9.6\ \mu\text{m}$  due to the  $\nu_1$  and  $\nu_3$  vibration rotation bands. These bands occur in the  $8\text{--}12\ \mu\text{m}$  atmospheric window. The bands are very complex, consisting of thousands of individual absorption lines. As recently as 1986, the molecular parameters required to accurately calculate the ozone absorptions were known to be incorrect. A new analysis of the available experimental data by Flaud et al. [1992] has greatly improved parameters for these bands. Also, instrumentation has been developed within the last decade that can measure isolated single absorption lines and their shapes. For the first time, accurate ozone amounts can be determined from observations of the absorption of solar radiation in the infrared.

The Network for Detection of Stratospheric Change (NDSC) (see Kurylo, 1991) is establishing an observing station at Mauna Loa Observatory (MLO), Hawaii. As part of a preliminary study, we have been recording infrared solar absorption spectra in the  $8\text{--}14\ \mu\text{m}$  region once a week since November, 1991. The instrument being used is a very high resolution Fourier transform interferometer system (FTIR). MLO has an automated Dobson instrument which has been measuring total column ozone amounts for many years. In this study we do a preliminary comparison of the results obtained with the FTIR and the Dobson techniques.

### Instrumentation

The solar spectrometer used in this study is a slightly modified commercial FTIR system built by BOMEM, Inc. of Quebec, Canada. It has a 2.50 m maximum path difference. For most of the data used in this study, spectra were obtained at 5 millikayser resolution (200 m path difference with apodization). The interferometer is controlled by a personal computer and the data is recorded on the hard disk. At the end of a run the data are transferred to digital audio tapes (DAT). One DAT remains at MLO for backup, and a copy is mailed to Denver about once a month.

Copyright 1993 by the American Geophysical Union.

Paper number 93GL02470  
0094-8534/93/93GL-02470\$03.00



The interferometer is housed in a small dome. Solar radiation is directed through the wall into the interferometer entrance by an automatic biaxial solar tracker. Currently, the system must be started by an operator. Since many of the chemical constituents of interest to the NDSC occur in trace amounts, long atmospheric paths are desired. MLO staff record spectra shortly after sunrise once each week, weather permitting. Normally, the observations are made on Wednesday. Occasionally, data are taken more frequently by University of Denver personnel while servicing the instrument or for satellite intercomparisons.

### Analysis

A non-linear least squares spectral fitting algorithm (SFIT) has been adapted for use on IBM compatible personal computers by C. P. Rinsland (NASA Langley, private communication). The program performs a line-by-line layer-by-layer calculation using the HITRAN molecular data base [Rothman, 1992], or other parameters as desired. The program adjusts the amount of ozone by multiplying a starting ozone profile by a scaling factor. When the best fit is achieved, the total amount of ozone (and any other chemical compounds with absorptions in the spectral interval) is calculated. The program also adjusts several instrument parameters including the 100% transmission level and frequency shift. Figure 1 shows an

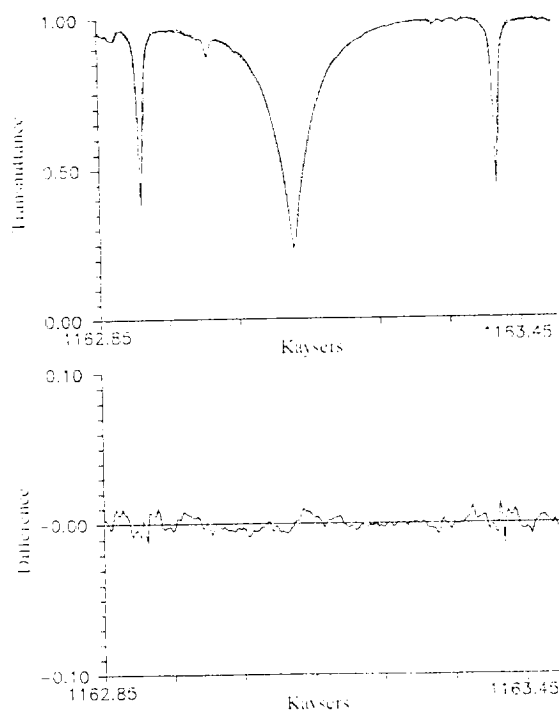


Fig. 1. Top: Example of a solar spectrum (dotted line) used in this analysis, along with the calculated best fit spectrum (solid line). The spectrum was collected at 6:38 local time on May 13, 1992. Solar zenith angle 79.6°. Bottom: Difference between the observed and calculated spectra.

example of a solar spectrum, along with the calculated best fit spectrum. The ozone lines chosen were isolated and only weakly temperature dependent. This region includes two prominent ozone absorptions, several weaker ozone lines, and a strong line due to  $N_2O$ . Input for the calculations includes the atmospheric temperature and water vapor profile from the Hilo, Hawaii radiosonde launch on the morning of the observation, the HITRAN 1992 database, and an initial ozone profile based on a seasonal average of ozone sonde data (S. Oltmans, NOAA CMDL, personal communication, 1992). The  $N_2O$  profile was the ATMOS midlatitude zonal average [Gunson et al. 1990], with a 6 km upward shift to account for the high tropopause over Hawaii. The difference between the observed and calculated spectra is shown below the spectra on an expanded scale. The residuals show a predominantly random noise component except for a few points near the ozone lines with larger excursions. The larger residuals are probably due to the real ozone altitude profile being different than the average profile used by the algorithm, but the total column is insensitive to the shape of the stratospheric part of the profile.

Each day's data consists of 3 spectra covering 800 to 1250 Kaysers, collected at 3 different solar zenith angles. Two small spectral intervals are fitted for each of the spectra. The intervals and lines used are listed in Table 1. These fits result in 6 ozone and  $N_2O$  values, unless some of the spectra are discarded. Spectra are rejected if they appear unusual, or if the residuals are too large. The individual fit values are averaged to determine the ozone and  $N_2O$  columns. Each column amount included here is the average of at least 2 separate fits.

### Results

The Dobson data used here was supplied by the WMO World Ozone Data Center (Toronto, Canada). The mean total ozone column determined by the FTIR is 4.6% lower than the Dobson. After multiplying FTIR results by 1.046, the RMS difference between the FTIR and Dobson is 2.7%. Figure 2 shows the total column ozone measured by the two techniques (after multiplying the FTIR by 1.046) for the period November 1, 1991 through September 6, 1992, when measurements were available on the same day. Measurements were made using both tech-

Table 1. Significant ozone lines used in the calculation. Frequency is in Kaysers (wavenumbers), strengths are in Kaysers/(molecule  $cm^{-2}$ ) at 296K.

Region 1 1145.85-1146.45		Region 2 1162.85-1163.45	
Frequency	Strength	Frequency	Strength
1145.9136	2.10E-22	1162.9140	3.29E-22
1145.9470	2.47E-22	1163.0110	2.52E-23
1146.1352	8.34E-23	1163.4222	2.57E-22
1146.1807	1.26E-22		
1146.2613	4.27E-22		
1146.4715	3.95E-22		

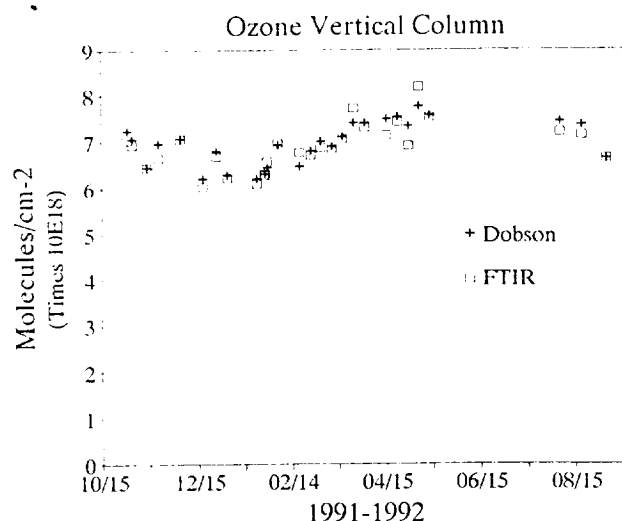


Fig. 2. Total column ozone measured by the FTIR and Dobson techniques, after multiplying the FTIR values by 1.046.

niques on 29 days. Even though the observations were made on the same day, they are not coincident in time, and the natural variability of ozone column is fairly large.

### Discussion

The agreement between the FTIR and Dobson after removing the bias is surprisingly good. We have not yet done a detailed error budget for the retrievals, however, the  $\text{N}_2\text{O}$  columns have an RMS deviation of less than 2.2%. The absolute accuracy of the ozone column retrieved depends upon several factors, including the line parameters and systematic errors in the retrieval. For the comparison done here, the absolute accuracy of the line intensities is of less importance than the accuracy relative to the UV cross-sections used by the Dobson instrument. Since the determination of the infrared intensities is almost always done by measuring the ozone amount using the UV cross-sections, the IR to UV accuracy is quite high. Pickett et al. [1992] claim 1% on the average for this process. However, individual lines, which are used here, may differ by as much as 5%. Our two intervals are self consistent to less than 2%. Pickett et al. also find that the ozone line intensities for this band on the HITRAN database should be multiplied by 1.051. This would further reduce the column reported by the FTIR making it 9.9% lower than the Dobson. On the other hand, we believe that using recent values of absorption for the Dobson data processing would reduce the FTIR and Dobson discrepancy by about 3%.

The techniques respond differently to changes in the vertical distribution of ozone. Surface ozone, monitored at MLO, can change by more than a factor of 2. If this change occurred throughout the troposphere, a significant ( $\approx 10\%$ ) difference in the total column would result. We use a tropospheric ozone profile which increases slightly with altitude up to the tropopause, with a surface value of 45 ppbv. Because of pressure broadening of the ozone

lines at low altitudes, this FTIR retrieval would report almost the same column for larger or smaller tropospheric amounts. The Dobson technique would report a change in the column.

Although we know of no other direct comparisons between infrared and Dobson techniques, UV and FTIR instruments have been compared on aircraft [Margitan et al., 1989], and aircraft borne FTIR systems compared to TOMS [Toon et al., 1992]. Toon et al. noted a 5% bias between infrared and TOMS ozone values outside of the Arctic vortex. They attribute the difference to a discrepancy in infrared and ultraviolet cross sections, however, they notice the opposite bias inside the vortex. The infrared line intensities used may have to be adjusted due to the recent changes. Margitan et al. report a comparison of FTIR and UV measurements from aircraft over Antarctica. They noted very good agreement on one flight, and some separation between two different FTIR instruments on a second flight. However, their ozone line intensities would have to be increased by either 9% (to match the 1992 HITRAN database) or 14% (to agree with Pickett et al.), resulting in too low FTIR reported columns.

### Conclusions

The results of this study are extremely encouraging, even though it is based on a relatively small sample of overlapping measurements. The two techniques differ so widely in instrumentation, analysis, and spectroscopic properties, that the agreement to such high precision reinforces accuracy of both.

We have difficulty accounting for the 10% bias implied by the Pickett et al. values for the line strengths.

The data set is expanding rapidly, and further work is in progress. Comparison between FTIR and Dobson data will be done for other sites, and we are also trying to improve the FTIR retrieval for tropospheric effects.

**Acknowledgments.** The Mauna Loa Observatory is operated by the Climate Monitoring and Diagnostics Laboratory of NOAA, which provided space and manpower for the collection of this data. We are particularly grateful to Bob Uchida for operating the instrument at sunrise every Wednesday. This research was partially supported by NASA. Some of the analysis was funded by the National Institutes for Global Environmental Change of the Department of Energy.

### References

- Dobson, G. M. B. and D. N. Harrison, Measurements of the amount of ozone in the Earth's atmosphere and its relation to other geophysical conditions, *Proc. Roy. Soc. A110*, 660-693, 1926.
- Dobson, G. M. B., D. N. Harrison and J. Lawrence, Measurements of the amount of ozone in the Earth's atmosphere and its relation to other geophysical conditions, part II, *Proc. Roy. Soc. A114*, 521-541, 1927.
- Dobson, G. M. B., D. N. Harrison and J. Lawrence, Measurements of the amount of ozone in the Earth's

- atmosphere and its relation to other geophysical conditions, part III, *Proc. Roy. Soc.*, *A122*, 456-486, 1929.
- Dobson, G. M. B., Observations of the amount of ozone in the Earth's atmosphere and its relation to other geophysical conditions, part IV, *Proc. Roy. Soc.*, *A129*, 411-433, 1930.
- Dobson, G. M. B., Observers handbook for the ozone spectrophotometer, *Ann. Int. Geophys. Year*, *5*, 90 1957.
- Fabry, C. and M. Buisson, L'absorption de l'ultraviolet par l'ozone et al limite du spectre solaire, *J. Phys. Rad.*, *3*, 196-206, 1913.
- Fabry, C. and M. Buisson, Etude de l'extremite ultraviolette du spectre solaire., *J. Phys. Rad.*, *2*, 197-226, 1921.
- Flaud, J.-M., C. Camy-Peyret, A. Perrin and C. P. Rinsland, Improved spectroscopic line parameters for the ozone molecule, *J. Quant. Spectrosc. Radiat. Transfer*, *48*, 611, 1992.
- Grass, R. D., W. D. Komhyr, G. L. Koenig, and R. D. Evans, Results of international Dobson spectrophotometer calibrations at the LKO, Arosa, Switzerland, 1990, *Proc. Quadrennial Ozone Symposium*, in press, 1992.
- Gunson, M. R., C. B. Farmer, R. H. Norton, R. Zander, C. P. Rinsland, J. H. Shaw and B.-C. Gao, Measurements of CH<sub>4</sub>, N<sub>2</sub>O, CO, H<sub>2</sub>O, and O<sub>3</sub> in the middle atmosphere by the atmospheric trace molecule spectroscopy experiment on Spacelab 3, *J. Geophys. Res.*, *95*, 13,867-13,882, 1990.
- Kurylo, M. J., Network for the detection of stratospheric change, *Proc. Soc. Photo. Opt. Instrum. Eng.*, *1491*, 169-174, 1991.
- Margitan, J. J. G. A. Brothers, E. V. Browell, D. Cariolle, M. T. Coffey, J. C. Farman, C. B. Farmer, G. L. Gregory, J. W. Harder, D. J. Hoffman, W. Hypes, S. Ismail, R. O. Jakoubek, W. Komhyr, S. Kooi, A. J. Drueger, J. C. Larsen, W. Mankin, M. P. McCormick, G. H. Mount, M. H. Proffitt, A. R. Ravishankara, A. L. Schmeltekopf, W. L. Starr, G. C. Toon, A. Torres, A. F. Tuck, A. Wahner and I. Watterson, Intercomparison of ozone measurements over Antarctica, *J. Geophys. Res.*, *94*, 16,557-16,569, 1989.
- Pickett, H. M., D. B. Peterson and J. S. Margolis, Absolute absorption of ozone in the midinfrared, *J. Geophys. Res.*, *97*, 20787-20793, 1992.
- Rothman, L. S., R. R. Gamache, R. H. Tipping, C. P. Rinsland, M. A. H. Smith, D. C. Benner, V. M. Devi, J.-M. Flaud, C. Camy-Peyret, A. Perrin, A. Goldman, S. T. Massie, L. R. Brown and R. A. Toth, The HITRAN molecular database: Editions of 1991 and 1992, *J. Quant. Spectrosc. Radiat. Transfer*, *48*, 469-507, 1992.
- Toon, G. C., C. B. Farmer, P. W. Schaper, L. L. Lowes and R. H. Norton, Composition measurements of the 1989 arctic winter stratosphere by airborne infrared solar absorption spectroscopy, *J. Geophys. Res.*, *97*, 7939-7961, 1992.
- WMO, Report of the international ozone trends panel 1988, WMO Global Ozone Research and Monitoring Project, Report no. 18, Volume 1, 439 pp., 1981.
- M. H. Anderberg, S. A. Beaton, S. J. David, F. J. Murcray, Department of Physics, University of Denver, Denver, CO 80208-0202

(Received: July 12, 1993

Accepted: August 9, 1993)



# The $\nu_2$ and $2\nu_2 - \nu_2$ bands of $^{14}\text{N } ^{16}\text{O}_2$ : Electron Spin-Rotation and Hyperfine Contact Resonances in the (010) Vibrational State

A. PERRIN,\* J.-M. FLAUD,\* C. CAMY-PEYRET,\* A. GOLDMAN,† F. J. MURCRAY,†  
R. D. BLATHERWICK,† AND C. P. RINSLAND‡

\*Laboratoire de Physique Moléculaire et Applications,<sup>1</sup> CNRS, Université P. et M. Curie, Bte 76,  
4 Place Jussieu, 75252 Paris Cedex 05, France; †Department of Physics, University of Denver,  
Denver, Colorado 80208; and ‡Atmospheric Sciences Division, NASA Langley Research Center,  
Hampton, Virginia 23681-0001

High-resolution Fourier transform spectra covering the 720–920  $\text{cm}^{-1}$  spectral region have been used to perform a reanalysis of the  $\nu_2$  band ((010)–(000) vibrational transition) together with the first analysis of the  $2\nu_2 - \nu_2$  hot band of nitrogen dioxide ((020)–(010) vibrational transition). The high-quality spectra show that, for numerous  $\nu_2$  lines, the hyperfine structure is easily observable in the case of resonances due to the hyperfine Fermi-type operator. By performing a full treatment of the spin-rotation and of the hyperfine operators, a new line list of the  $\nu_2$  band (positions and intensities) has been generated, and it is in excellent agreement with the experimental spectrum. Also, a thorough analysis of the  $2\nu_2 - \nu_2$  hot band has been performed leading to an extended set of new (020) spin-rotation levels. These levels, together with the {(100), (020), (001)} spin-rotation levels deduced previously from the analysis of the  $\nu_1$ ,  $2\nu_2$ , and  $\nu_3$  cold bands performed in the 6.3- to 7.5- $\mu\text{m}$  spectral range [A. Perrin, J.-M. Flaud, C. Camy-Peyret, A.-M. Vasserot, G. Guelachvili, A. Goldman, F. J. Murcray, and R. D. Blatherwick, *J. Mol. Spectrosc.* **154**, 391–406 (1992)] were least-squares fitted, allowing one to derive a new set of vibrational band centers and rotational, spin-rotation, and interaction constants for the {(100)(020)(001)} interacting states of  $^{14}\text{N } ^{16}\text{O}_2$ . © 1993 Academic Press, Inc.

## 1. INTRODUCTION

The cold  $\nu_2$  band and the  $2\nu_2 - \nu_2$  first hot band of nitrogen dioxide, located at 13  $\mu\text{m}$ , correspond, respectively, to the (010)–(000) and (020)–(010) vibrational transitions of this molecule; consequently, in order to have accurate line positions it is necessary to have precise parameters for both the upper and the lower vibrational states involved in these transitions.

For the (000) and (010) vibrational states, the most recent spectroscopic parameters were obtained from a simultaneous fit of the available microwave or double resonance data (Refs. (1–8) and (9, 10) for the (000) and (010) state, respectively) and of the infrared spin-rotation energy levels obtained from recent analyses of Fourier transform spectra recorded in the far infrared (11) and in the 13.3- $\mu\text{m}$  (12) spectral regions.

In the analysis of the (000)–(000) band, even at the high resolution of the far-infrared experimental spectra, the hyperfine structure is usually *not* detectable, except in cases of *local* resonances due to the Fermi contact hyperfine operator. Accordingly, the line list (11, 13, 14) of the pure rotation region of  $\text{NO}_2$  ( $\sim 0$ –200  $\text{cm}^{-1}$ ) was generated by explicitly taking into account the spin-rotation and hyperfine structures.

On the other hand, this effect could not be observed so accurately in the 13.3- $\mu\text{m}$  experimental spectrum which was used in Ref. (12) for the analysis of the  $\nu_2$  band,

<sup>1</sup> Laboratoire associé aux Universités P. et M. Curie et Paris-Sud.

and consequently the line list (12-14) generated in the 13.3- $\mu\text{m}$  spectral range did *not* include the hyperfine structure.

For the (020) vibrational state, the most recent spectroscopic parameters were obtained from a recent analysis (15) of the  $\nu_1$ ,  $2\nu_2$ , and  $\nu_3$  bands ((100)-(000), (020)-(000), and (001)-(000) vibrational transitions, respectively) using Fourier transform spectra (15, 16) covering the 6.3- $\mu\text{m}$  region. Actually the (001) state is involved in a strong Coriolis interaction with the (020) and (100) states, and the very weak  $2\nu_2$  band borrows its intensity from the strong  $\nu_3$  band. In fact, only the  $K_a = 0-2$  subbands for  $N \leq 46$  (because they appear in a clear window between  $\nu_1$  and  $\nu_3$ ) and the  $K_a = 6$  subband for  $19 \leq N \leq 62$  (because the corresponding (020) levels are strongly resonating with levels of (001) state) could be analyzed at 6.7  $\mu\text{m}$  (15-17). Finally, it must be pointed out that for the energy level calculations of the {(100), (020), (001)} interacting vibrational states, both the spin-rotation and the vibrational Coriolis-type interactions were explicitly taken into account, but that the hyperfine structure was not considered:

(i) For the *A*-type  $\nu_3$  band, which is by far the strongest band at 6.3  $\mu\text{m}$ , the hyperfine resonances affect only some  $\nu_3$  nonresolved doublets, the spin splittings of which vanish in the upper and lower levels of the transition. In this case, the hyperfine structure is blended within the total line width, and the hyperfine components cannot be observed.

(ii) Because of the weakness of the  $\nu_1$  and  $2\nu_2$  bands the hyperfine structures cannot be precisely measured on the spectra and consequently the hyperfine resonances were not considered for these bands.

Using new high-resolution Fourier transform spectra recorded in the 13.3- $\mu\text{m}$  spectral region, we report in this paper a reanalysis of the  $\nu_2$  band (with a full treatment of the hyperfine structure), together with a first analysis of the hot  $2\nu_2 - \nu_2$  band of  $^{14}\text{N}^{16}\text{O}_2$ .

## II. EXPERIMENTAL DETAILS

The spectra were recorded in the 720-960  $\text{cm}^{-1}$  spectral range at 0.002  $\text{cm}^{-1}$  resolution with the BOMEM Fourier transform spectrometer of the University of Denver. The optical path length was 1 m, and two spectra were recorded at  $\text{NO}_2$  pressures of 1 and 2 Torr. The calibration of the spectra was performed by means of  $\text{N}_2\text{O}$  absorption lines (18, 19) in the 1150-1250  $\text{cm}^{-1}$  region, and the accuracy of the positions of unblended lines is estimated to be  $\sim 0.0002 \text{ cm}^{-1}$ .

## III. ANALYSIS AND LINE POSITION CALCULATIONS

### The $\nu_2$ Band

The analysis was started by comparing the experimental line positions to the line list calculated in Ref. (12). Overall, the agreement was excellent except for transitions in which the upper or the lower state are involved in a hyperfine Fermi resonance. Consequently, a new line list was generated for the  $\nu_2$  band, taking into account not only the electron spin-rotation interaction, but also, as described in Ref. (11) for the (000) state, the magnetic hyperfine hamiltonian (i.e., the Fermi contact operator together with the spin-spin dipolar interaction operators) and the nuclear quadrupole interaction. For this calculation we used the vibrational band center, rotational, spin-rotation, and hyperfine constants of Ref. (12) and Ref. (11), respectively, for the upper and lower state of the transition.

The agreement this time proved to be excellent for all the lines. However, we observed a  $-0.0004 \text{ cm}^{-1}$  global shift of the observed line positions relative to the calculated

ones, which is due to a slightly different calibration of the spectra used in the present work (18, 19) compared to that used (20) in 1988. This leads to a different vibrational band center of the  $\nu_2$  band:  $E_{(0)0} = 749.652561 \text{ cm}^{-1}$  (instead of  $749.652961 \text{ cm}^{-1}$  obtained previously in Ref. (12)).

To show the quality of the experimental spectra and of the calculations performed in the present work, we show in Figs. 1 and 2 portions around  $771.8$  and  $758.0 \text{ cm}^{-1}$  of the experimental spectra together with line-by-line calculations performed using either the line list generated in Ref. (12) (no hyperfine structure) or the line list derived here (full treatment of the hyperfine operators). In both regions, the improvement brought by the new calculation is very clear.

In the first spectral region, the complex hyperfine structure appears clearly in the  $N = \text{even } {}^RQ_{K_a=1}$  subband. At  $771.30$  and  $771.64 \text{ cm}^{-1}$  it is due to a strong hyperfine resonance involving the  $(010)[22\ 2\ 20]$  and  $(010)[20\ 2\ 18]$  rotational levels. At  $772 \text{ cm}^{-1}$ , since the resonance is weaker, one observes mainly a broadening of the  $N = 18$  doublet structure. The same hyperfine effect can be clearly observed in Fig. 2 around  $758 \text{ cm}^{-1}$  for lines belonging to the  ${}^RQ_{K_a=0}$  subband. It is worth stressing that in both cases the new calculation, which involves the hyperfine operators, reproduces the experimental spectrum with high accuracy.

### The $2\nu_2 - \nu_2$ Band

Lines from the  $2\nu_2 - \nu_2$  band were already observed in the experimental spectrum (12) which was used in 1988 for the analysis of the  $13.3\text{-}\mu\text{m}$  band of nitrogen dioxide. However, because this hot band is weak and because the  $(020)$  spectroscopic parameters available at that time were not precise enough (only the  $K_a = 0, 1, 2$   $(020)$  series were derived from the analysis of the  $2\nu_2$  band performed at  $6.6 \mu\text{m}$  (17)), only a few lines involving the  $K_a = 0, 1, 2$   $(020)$  rotational series could be analyzed at  $13.3 \mu\text{m}$ .

The  $(020)$  parameters were recently significantly improved from a new analysis of the  $\{\nu_1, 2\nu_2, \nu_3\}$  interacting bands (15). Indeed, more lines involving the  $K_a = 0, 1, 2$  series were assigned; also, lines involving the  $K_a = 6$  rotational series of  $(020)$ , which borrow their intensities from  $\nu_3$  through a Coriolis interaction, were observed (15, 16).

Consequently, from the  $\{(100), (020), (001)\}$  and  $(010)$  parameters obtained in Ref. (15) and Ref. (12) respectively, it has been possible to better predict the  $2\nu_2 - \nu_2$  line positions, as performed in the present analysis.

Because the  $2\nu_2 - \nu_2$  band is rather weak, only transitions of this band involving  $N \leq 30$  rotational quantum number could be identified in the spectrum. For transitions involving the  $K_a = 0-2$  and  $K_a = 6$   $(020)$  energy levels, the agreement between the observed and the predicted line positions was excellent, but this was not completely the case for lines involving the  $K_a = 3-5$   $(020)$  rotational levels since small discrepancies (up to  $0.0030 \text{ cm}^{-1}$ ) were observed. Using these new data, we then determined the vibrational band centers, rotational, spin-rotation, and coupling constants of the  $\{(100), (020), (001)\}$  resonating states. As in Ref. (15) the Hamiltonian matrix explicitly takes into account both the Coriolis and the spin-rotation interactions. For this least-squares fit calculation, the 164  $(020)$  new spin-rotation energy levels obtained in the present work for  $K_a \leq 6$  and  $N \leq 30$  were combined to the 3230  $(100)$   $(001)$  and  $(020)$  energy levels obtained in Ref. (15).

Table I gives the list of vibrational energies and rotational, spin-rotation, and coupling constants deduced from the fit, together with their estimated uncertainty. The

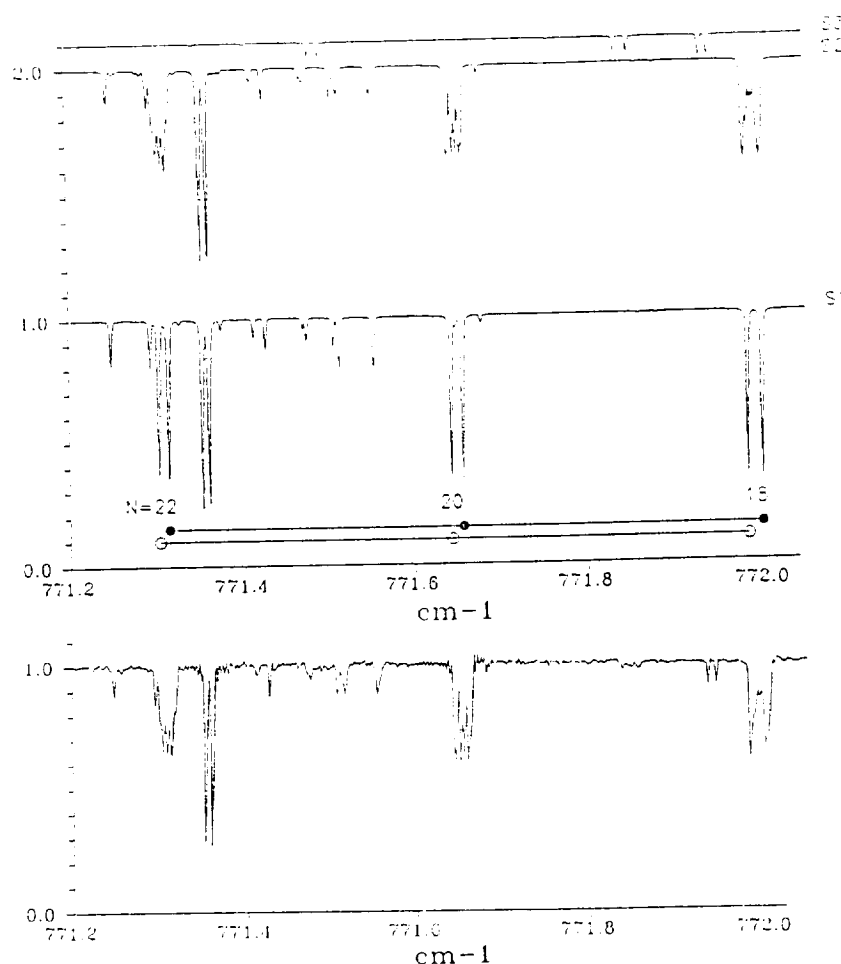


FIG. 1. Experimental spectrum (bottom trace) of nitrogen dioxide around  $771\text{ cm}^{-1}$  and calculated spectra of the absorption due to the  $^{14}\text{N}^{16}\text{O}_2$  isotopic species: trace S1 and S2 are for the  $\nu_2$  band, respectively, without and with taking into account the hyperfine structure; trace S3 is for the  $2\nu_2 - \nu_2$  hot band (no calculation of the hyperfine structure). All spectra have the same vertical scale but are displaced for clarity. On trace S1 we have marked the rotational transitions belonging to the  $^RQ_{K_2-1}$  subband (black dots and open circles correspond to  $J = N + \frac{1}{2}$  and  $J = N - \frac{1}{2}$ , respectively). The agreement between observation and calculation is excellent.

corresponding statistical analysis of the results is given in Table II. It is clear that significant improvements were obtained in the present calculation for the (020) spin-rotation levels and to a lesser extent for the (001) levels compared with the results obtained previously (15): the percentages of experimental energy levels which are reproduced within  $0.001\text{ cm}^{-1}$  are now 84.5 and 79.1% instead of 69.5 and 77% for (020) and (001), respectively.

#### IV. SYNTHETIC SPECTRA

This section presents the calculations<sup>2</sup> which have been performed in order to generate a precise line list of absorption lines of  $^{14}\text{N}^{16}\text{O}_2$  in the  $13.3\text{-}\mu\text{m}$  region.

<sup>2</sup> Both calculations were performed for a reference temperature of 296 K using a  $Z(296\text{ K}) = 13\,617.9$  partition function (this value includes the nitrogen nuclear degeneracy).



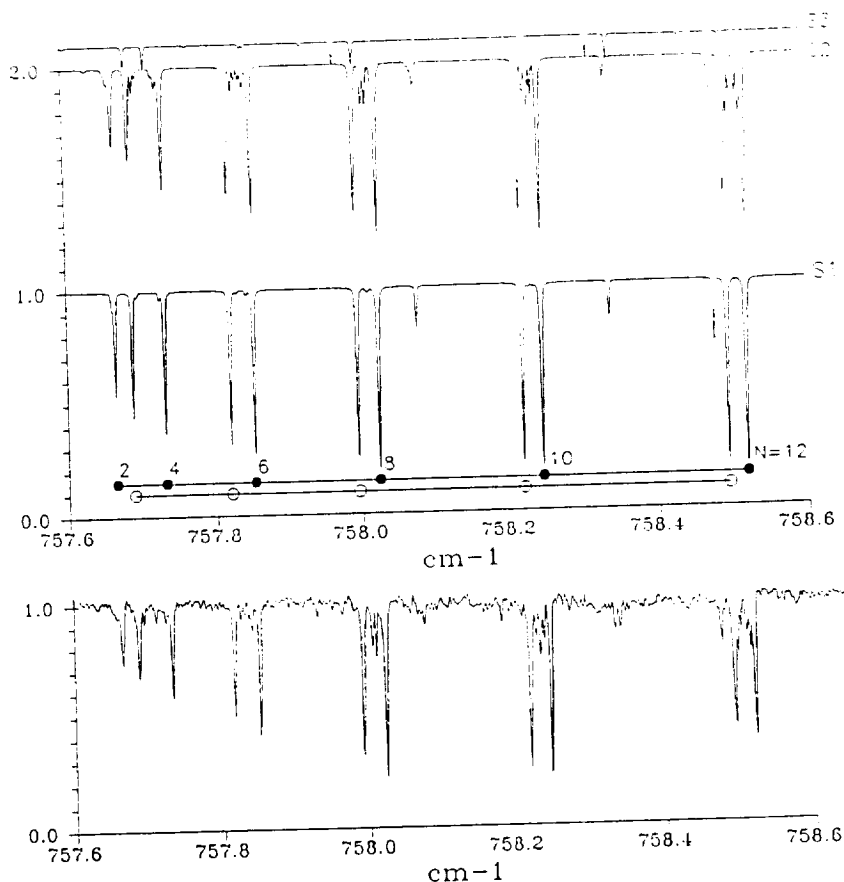


FIG. 2. Experimental spectrum (bottom trace) of nitrogen dioxide around  $758\text{ cm}^{-1}$  and calculated spectra of absorption due to the  $^{14}\text{N } ^{16}\text{O}_2$  isotopic species: trace S1 and S2 are for the  $\nu_2$  band, respectively, *without* and *with* taking into account the hyperfine structure; trace S3 is for the  $2\nu_2 - \nu_2$  hot band (no calculation of the hyperfine structure). All spectra have the same vertical scale but are displaced for clarity. On trace S1, we have marked the rotational transitions belonging to the  $^RQ_{K'_a=0}$  subband, (black dots and open circles are for  $J = N + \frac{1}{2}$  and  $J = N - \frac{1}{2}$ , respectively). The agreement between observation and calculation is excellent.

### $\nu_2$ Band

For the calculation of the  $\nu_2$  band we used the  $\nu_2$  transition moment operator obtained in Ref. (21):

$${}^{(000)(010)}\mu'_z = -0.04272\varphi_x - 0.403 \times 10^{-3} \{i\varphi_y, N_z\} + 0.1083 \times 10^{-3} \{\varphi_z, iN_y\}. \quad (1)$$

Also, for this calculation the effect of the hyperfine structure was *explicitly* taken into account, as described in Ref. (11), through the standard tensorial formalism using a  $\mathbf{F} = \mathbf{J} + \mathbf{I}$  and  $\mathbf{J} = \mathbf{N} + \mathbf{S}$  coupling scheme.

Finally, 30 620 line intensities were calculated with an intensity cutoff of  $0.1 \times 10^{-24}\text{ cm}^{-1}/\text{molecule cm}^{-2}$  and the following ranges of quantum numbers and energies:

$$\begin{aligned} N &\leq 65 & K'_a &\leq 13 \\ E' &\leq 2600\text{ cm}^{-1} & E'' &\leq 2000\text{ cm}^{-1} \end{aligned}$$

TABLE I

Vibrational Energies and Rotational, Spin-Rotation, and Coupling Constants for the  $\{(100), (020), (001)\}$  Interacting Vibrational States of  $^{14}\text{N } ^{16}\text{O}_2$

	1 0 0	0 2 0	0 0 1
$E_v$	1319.76589 $\pm$ 0.00012	1498.34688 $\pm$ 0.00027	1616.84918 $\pm$ 0.00089
$A_v$	8.0932898 $\pm$ 0.0000082	8.778705 $\pm$ 0.000054	7.7742509 $\pm$ 0.000080
$B_v$	0.43133685 $\pm$ 0.0000067	0.4335453 $\pm$ 0.0000015	0.43092954 $\pm$ 0.0000022
$C_v$	0.40928232 $\pm$ 0.0000037	0.4086528 $\pm$ 0.0000017	0.40637082 $\pm$ 0.0000018
$\Delta E_v$	(0.285392 $\pm$ 0.000015) $\times 10^{-2}$	(0.43885 $\pm$ 0.00037) $\times 10^{-2}$	(0.252448 $\pm$ 0.000018) $\times 10^{-2}$
$\Delta E_{v,K}$	(-0.20710 $\pm$ 0.00012) $\times 10^{-4}$	(-0.24104 $\pm$ 0.00011) $\times 10^{-4}$	(-0.18874 $\pm$ 0.00010) $\times 10^{-4}$
$\Delta E_{v,K}^{\prime}$	(0.30118 $\pm$ 0.00071) $\times 10^{-6}$	(0.29919 $\pm$ 0.00043) $\times 10^{-6}$	(0.30278 $\pm$ 0.00074) $\times 10^{-6}$
$\Delta E_{v,K}^{\prime\prime}$	(0.518 $\pm$ 0.012) $\times 10^{-5}$	(0.861 $\pm$ 0.063) $\times 10^{-5}$	(0.4657 $\pm$ 0.0070) $\times 10^{-5}$
$\Delta E_{v,K}^{\prime\prime\prime}$	(0.2987 $\pm$ 0.0040) $\times 10^{-7}$	(0.3111 $\pm$ 0.0024) $\times 10^{-7}$	(0.3417 $\pm$ 0.0037) $\times 10^{-7}$
$H_v^{\prime}$	(0.33722 $\pm$ 0.00011) $\times 10^{-5}$	(0.7503 $\pm$ 0.0067) $\times 10^{-5}$	(0.27939 $\pm$ 0.00013) $\times 10^{-5}$
$H_{v,K}^{\prime}$	(-0.2823 $\pm$ 0.0014) $\times 10^{-7}$	-0.44346 $\times 10^{-7}$	(-0.2596 $\pm$ 0.0013) $\times 10^{-7}$
$H_{v,K}^{\prime\prime}$	(0.220 $\pm$ 0.087) $\times 10^{-10}$	-0.8928 $\times 10^{-10}$	(0.1044 $\pm$ 0.0072) $\times 10^{-9}$
$H_{v,K}^{\prime\prime\prime}$	(0.330 $\pm$ 0.071) $\times 10^{-12}$	0.1777 $\times 10^{-12}$	(0.350 $\pm$ 0.013) $\times 10^{-12}$
$h_v^{\prime}$	(0.378 $\pm$ 0.029) $\times 10^{-7}$		(0.562 $\pm$ 0.028) $\times 10^{-7}$
$h_{v,K}^{\prime}$	-0.2571 $\times 10^{-10}$		(0.21 $\pm$ 0.14) $\times 10^{-10}$
$h_v^{\prime\prime}$	0.10727 $\times 10^{-12}$		(0.127 $\pm$ 0.0067) $\times 10^{-12}$
$L_v^{\prime}$	(-0.55356 $\pm$ 0.00027) $\times 10^{-8}$	-0.13633 $\times 10^{-7}$	(-0.48653 $\pm$ 0.00031) $\times 10^{-8}$
$L_{v,K}^{\prime}$	(0.3250 $\pm$ 0.0041) $\times 10^{-10}$		(0.3482 $\pm$ 0.0064) $\times 10^{-10}$
$L_{v,K}^{\prime\prime}$	(0.325 $\pm$ 0.041) $\times 10^{-12}$		(0.87 $\pm$ 0.27) $\times 10^{-13}$
$P_v^{\prime}$	0.867 $\times 10^{-11}$		0.867 $\times 10^{-11}$
$Q_v^{\prime}$	-0.8439 $\times 10^{-14}$		-0.8439 $\times 10^{-14}$
$e_{v,K}^{\prime}$	0.183418 $\pm$ 0.000052	0.21947 $\pm$ 0.00037	0.172433 $\pm$ 0.000044
$e_{v,K}^{\prime\prime}$	(0.230 $\pm$ 0.013) $\times 10^{-3}$	(0.176 $\pm$ 0.018) $\times 10^{-3}$	(0.2660 $\pm$ 0.0043) $\times 10^{-3}$
$e_{v,K}^{\prime\prime\prime}$	(-0.3327 $\pm$ 0.0013) $\times 10^{-2}$	(-0.334 $\pm$ 0.0015) $\times 10^{-2}$	(-0.31510 $\pm$ 0.00041) $\times 10^{-2}$
$\Delta E_{v,K}^{\prime\prime\prime}$	(-0.18430 $\pm$ 0.00036) $\times 10^{-3}$	(-0.306 $\pm$ 0.012) $\times 10^{-3}$	(-0.16757 $\pm$ 0.00031) $\times 10^{-3}$
$\Delta E_{v,K}^{\prime\prime\prime\prime}$	0.6005 $\times 10^{-6}$		0.6005 $\times 10^{-6}$
$\Delta E_{v,K}^{\prime\prime\prime\prime\prime}$	0.1678 $\times 10^{-5}$		0.1678 $\times 10^{-5}$
$\Delta E_{v,K}^{\prime\prime\prime\prime\prime\prime}$	0.6322 $\times 10^{-9}$		0.6322 $\times 10^{-9}$
$\Delta E_{v,K}^{\prime\prime\prime\prime\prime\prime\prime}$	0.3769 $\times 10^{-6}$		0.3769 $\times 10^{-6}$
$\Delta E_{v,K}^{\prime\prime\prime\prime\prime\prime\prime\prime}$	0.244 $\times 10^{-9}$		0.244 $\times 10^{-9}$
$H_v^{\prime\prime}$	0.29673 $\times 10^{-6}$		0.29673 $\times 10^{-6}$
$L_v^{\prime\prime}$	-0.3568 $\times 10^{-9}$		-0.3568 $\times 10^{-9}$

$$h_{(001)(020)}^{\prime\prime} = (-0.294552 \pm 0.000088) \times 10^{-1}$$

$$h_{(001)(020)}^{\prime\prime\prime} = (0.736_9 \pm 0.031) \times 10^{-7}$$

$$h_{(001)(100)}^{\prime\prime} = -0.656287_3 \pm 0.000064$$

$$h_{(001)(100)}^{\prime\prime\prime} = (-0.9193_6 \pm 0.0096) \times 10^{-4}$$

$$h_{(001)(100)}^{\prime\prime\prime\prime} = (-0.256_6 \pm 0.033) \times 10^{-5}$$

Note. All the results are in  $\text{cm}^{-1}$  and the quoted errors correspond to one standard deviation. The constants with no errors were held fixed during the fit.

The total band intensity was found to be  $S_{(010)-(000)} = 0.542 \times 10^{-18} \text{ cm}^{-1}/\text{molecule cm}^{-2}$  at 296 K.

Because of the rather high proportion of so-called  $\Delta F \neq \Delta J \neq \Delta N$  "forbidden" transitions which were not considered in the 1988 calculation (12), the present calculated lines are more numerous than those in 1988 (30 620 instead of  $8065 \times 3$ , taking into account the  $(2I + 1) = 3$  nitrogen nuclear degeneracy).

### $2\nu_2 - \nu_2$ Band

For the hot  $2\nu_2 - \nu_2$  band, only the spin-rotation fine structure was considered and its vibrational transition moment constant was determined using the following relation, valid up to the second order of approximation:

$${}^{(020)(010)}\mu_z' = \sqrt{2} \times {}^{(010)(000)}\mu_z' \quad (2)$$

The  $2\nu_2 - \nu_2$  line intensities were calculated in the following ranges:

TABLE II  
Statistical Analysis of the Results for the Energy Levels Calculation

	(100)	(020)	(001)
Number of experimental spin-rotation levels	1187	374	1833
$0 \leq \delta E < 1 \times 10^{-3}$	65.8%	84.5%	79.1%
$1 \times 10^{-3} \leq \delta E < 2 \times 10^{-3}$	25.7%	12.8%	15.4%
$2 \times 10^{-3} \leq \delta E < 7.0 \times 10^{-3}$	7.4%	2.7%	5.6%

$\delta E = |E_{\text{calc}} - E_{\text{expt}}|$  in  $\text{cm}^{-1}$

$$N \leq 60 \quad K_a'' \leq 10$$

$$E' \leq 3200 \text{ cm}^{-1} \quad E'' \leq 2600 \text{ cm}^{-1}$$

Also, in order to be consistent with the  $\nu_2$  calculation, the intensity cutoff was chosen to be  $0.3 \times 10^{-24} \text{ cm}^{-1}/\text{molecule cm}^{-2}$  at 296 K, taking into account the  $3I + 1 = 3$  nitrogen nuclear degeneracy.

Finally, 4388 lines were calculated for the  $2\nu_2 - \nu_2$  band and the sum of all the intensities was found to be  $S_{(020)-(010)} = 0.2735 \times 10^{-19} \text{ cm}^{-1}/\text{molecule cm}^{-2}$  at 296 K.

#### V. CONCLUSION

Using high-resolution Fourier transform spectra, a new analysis of the  $\nu_2$  band of  $^{14}\text{N } ^{16}\text{O}_2$  involving the hyperfine structure has been performed for the first time together with the first extensive analysis of the  $2\nu_2 - \nu_2$  band of this molecule, leading to a very accurate representation of the absorption of  $^{14}\text{N } ^{16}\text{O}_2$  in the  $13.3\text{-}\mu\text{m}$  region. It must be mentioned that lines of the  $\nu_2$  band of  $\text{NO}_2$  are visible in the University of Denver balloon flight spectra of June 1988 (22), and knowledge of their parameters (and lines of the hot band) may be important in attempts to detect the weakly absorbing lines of stratospheric ClO in the infrared (23).

RECEIVED: January 27, 1993

#### REFERENCES

1. G. R. BIRD, J. C. BAIRD, A. W. JACHE, J. A. HODGENSON, R. F. CURL, Jr., A. C. KUNKLE, J. W. BRANSFORD, J. RASTRUP-ANDERSON, AND J. ROSENTHAL, *J. Chem. Phys.* **40**, 3378-3390 (1964).
2. R. M. LEE, R. F. CURL, AND J. C. BAKER, *J. Chem. Phys.* **45**, 2037-2040 (1966).
3. P. A. BARON, P. D. GODFREY, AND D. O. HARRIS, *J. Chem. Phys.* **60**, 3723-3724 (1974).
4. W. C. BOWMAN AND F. C. DE LUCIA, *J. Chem. Phys.* **77**, 92-107 (1982).
5. O. I. BASKAKOV, M. V. MOSKIENKO, AND S. F. DYUBKO, *Opt. Spectrosc. (USSR)* **53**, 270-272 (1982).
6. T. TANAKA, A. D. ENGLISH, R. W. FIELDS, D. A. JENNINGS, AND D. O. HARRIS, *J. Chem. Phys.* **59**, 5217-5218 (1973).
7. J. M. BROWN, T. C. STEIMLE, M. E. COLES, AND R. F. CURL, Jr., *J. Chem. Phys.* **74**, 3668-3672 (1981).
8. N. SEMMOUD-MONNANTEUIL, J.-M. COLMONT, A. PERRIN, J.-M. FLAUD, AND C. CAMY-PEYRET, *J. Mol. Spectrosc.* **134**, 176-182 (1989).
9. L. W. HRUBESH AND R. F. CURL, *J. Mol. Spectrosc.* **61**, 144-146 (1976).

10. Y. MORINO, M. TANIMOTO, S. SAITO, E. HIROTA, R. AWATA, AND T. TANAKA, *J. Mol. Spectrosc.* **98**, 331-348 (1983).
11. A. PERRIN, J.-M. FLAUD, C. CAMY-PEYRET, B. CARLI, AND M. CARLOTTI, *Mol. Phys.* **63**, 791-810 (1988).
12. A. PERRIN, C. CAMY-PEYRET, J.-M. FLAUD, AND J. KAUPPINEN, *J. Mol. Spectrosc.* **130**, 168-182 (1988).
13. A. PERRIN, C. CAMY-PEYRET, AND J.-M. FLAUD, *J. Quant. Spectrosc. Radiat. Transfer* **48**, 645-651 (1992).
14. L. S. ROTHMAN, R. R. GAMACHE, R. H. TIPPING, C. P. RINSLAND, M. A. H. SMITH, D. CHRIS BENNER, V. MALATHY-DEVI, J.-M. FLAUD, C. CAMY-PEYRET, A. PERRIN, A. GOLDMAN, S. T. MASSIE, L. R. BROWN, AND R. A. TOTH, *J. Quant. Spectrosc. Radiat. Transfer* **48**, 469-507 (1992).
15. A. PERRIN, J.-M. FLAUD, C. CAMY-PEYRET, A.-M. VASSEROT, G. GUELACHVILI, A. GOLDMAN, F. J. MURCRAY, AND R. D. BLATHERWICK, *J. Mol. Spectrosc.* **154**, 391-406 (1992).
16. R. A. TOTH, *J. Opt. Soc. Amer. B* **9**, 433-461 (1992).
17. A. PERRIN, J.-M. FLAUD, AND C. CAMY-PEYRET, *J. Mol. Spectrosc.* **118**, 174-179 (1986).
18. R. A. TOTH, *J. Opt. Soc. Amer. B* **3**, 1263-1281 (1986).
19. A. G. MAKI AND J. S. WELLS, "Wavenumber Calibration Tables from Heterodyne Frequency Measurements," NIST Special Publication 821, 1992.
20. G. GUELACHVILI AND K. NARAHARI RAO, "Handbook of Infrared Standards," Academic Press, Orlando, 1986.
21. V. MALATHY DEVI, P. P. DAS, A. BANO, K. NARAHARI RAO, J.-M. FLAUD, C. CAMY-PEYRET, AND J.-P. CHEVILLARD, *J. Mol. Spectrosc.* **88**, 251-258 (1981).
22. A. GOLDMAN, F. J. MURCRAY, R. D. BLATHERWICK, J. J. KOSTERS, F. H. MURCRAY, F. G. MURCRAY, AND C. P. RINSLAND, *J. Geophys. Res. D* **94**, 14945-14955 (1989).
23. C. P. RINSLAND AND A. GOLDMAN, *J. Quant. Spectrosc. Radiat. Transfer* **48**, 685-692 (1992).



# The $\nu_2$ and $2\nu_2 - \nu_2$ bands of $^{14}\text{N } ^{16}\text{O}_2$ : Electron Spin-Rotation and Hyperfine Contact Resonances in the (010) Vibrational State

A. PERRIN,\* J.-M. FLAUD,\* C. CAMY-PEYRET,\* A. GOLDMAN,† F. J. MURCRAY,†  
R. D. BLATHERWICK,† AND C. P. RINSLAND‡

\*Laboratoire de Physique Moléculaire et Applications,<sup>1</sup> CNRS, Université P. et M. Curie, Bte 76,  
4 Place Jussieu, 75252 Paris Cedex 05, France; †Department of Physics, University of Denver,  
Denver, Colorado 80208; and ‡Atmospheric Sciences Division, NASA Langley Research Center,  
Hampton, Virginia 23681-0001

High-resolution Fourier transform spectra covering the 720–920  $\text{cm}^{-1}$  spectral region have been used to perform a reanalysis of the  $\nu_2$  band ((010)–(000) vibrational transition) together with the first analysis of the  $2\nu_2 - \nu_2$  hot band of nitrogen dioxide ((020)–(010) vibrational transition). The high-quality spectra show that, for numerous  $\nu_2$  lines, the hyperfine structure is easily observable in the case of resonances due to the hyperfine Fermi-type operator. By performing a full treatment of the spin-rotation and of the hyperfine operators, a new line list of the  $\nu_2$  band (positions and intensities) has been generated, and it is in excellent agreement with the experimental spectrum. Also, a thorough analysis of the  $2\nu_2 - \nu_2$  hot band has been performed leading to an extended set of new (020) spin-rotation levels. These levels, together with the  $\{(100), (020), (001)\}$  spin-rotation levels deduced previously from the analysis of the  $\nu_1$ ,  $2\nu_2$ , and  $\nu_3$  cold bands performed in the 6.3- to 7.5- $\mu\text{m}$  spectral range [A. Perrin, J.-M. Flaud, C. Camy-Peyret, A.-M. Vasserot, G. Guelachvili, A. Goldman, F. J. Murcay, and R. D. Blatherwick, *J. Mol. Spectrosc.* **154**, 391–406 (1992)] were least-squares fitted, allowing one to derive a new set of vibrational band centers and rotational, spin-rotation, and interaction constants for the  $\{(100)(020)(001)\}$  interacting states of  $^{14}\text{N } ^{16}\text{O}_2$ . © 1993 Academic Press, Inc.

## I. INTRODUCTION

The cold  $\nu_2$  band and the  $2\nu_2 - \nu_2$  first hot band of nitrogen dioxide, located at 13  $\mu\text{m}$ , correspond, respectively, to the (010)–(000) and (020)–(010) vibrational transitions of this molecule; consequently, in order to have accurate line positions it is necessary to have precise parameters for both the upper and the lower vibrational states involved in these transitions.

For the (000) and (010) vibrational states, the most recent spectroscopic parameters were obtained from a simultaneous fit of the available microwave or double resonance data (Refs. (1–8) and (9, 10) for the (000) and (010) state, respectively) and of the infrared spin-rotation energy levels obtained from recent analyses of Fourier transform spectra recorded in the far infrared (11) and in the 13.3- $\mu\text{m}$  (12) spectral regions.

In the analysis of the (000)–(000) band, even at the high resolution of the far-infrared experimental spectra, the hyperfine structure is usually *not* detectable, except in cases of *local* resonances due to the Fermi contact hyperfine operator. Accordingly, the line list (11, 13, 14) of the pure rotation region of  $\text{NO}_2$  ( $\sim 0$ –200  $\text{cm}^{-1}$ ) was generated by explicitly taking into account the spin-rotation and hyperfine structures.

On the other hand, this effect could not be observed so accurately in the 13.3- $\mu\text{m}$  experimental spectrum which was used in Ref. (12) for the analysis of the  $\nu_2$  band,

<sup>1</sup> Laboratoire associé aux Universités P. et M. Curie et Paris-Sud.

and consequently the line list (12–14) generated in the 13.3- $\mu\text{m}$  spectral range did not include the hyperfine structure.

For the (020) vibrational state, the most recent spectroscopic parameters were obtained from a recent analysis (15) of the  $\nu_1$ ,  $2\nu_2$ , and  $\nu_3$  bands ((100)–(000), (020)–(000), and (001)–(000) vibrational transitions, respectively) using Fourier transform spectra (15, 16) covering the 6.3- $\mu\text{m}$  region. Actually the (001) state is involved in a strong Coriolis interaction with the (020) and (100) states, and the very weak  $2\nu_2$  band borrows its intensity from the strong  $\nu_3$  band. In fact, only the  $K_a = 0$ –2 subbands for  $N \leq 46$  (because they appear in a clear window between  $\nu_1$  and  $\nu_3$ ) and the  $K_a = 6$  subband for  $19 \leq N \leq 62$  (because the corresponding (020) levels are strongly resonating with levels of (001) state) could be analyzed at 6.7  $\mu\text{m}$  (15–17). Finally, it must be pointed out that for the energy level calculations of the {(100), (020), (001)} interacting vibrational states, both the spin–rotation and the vibrational Coriolis-type interactions were explicitly taken into account, but that the hyperfine structure was not considered:

(i) For the A-type  $\nu_3$  band, which is by far the strongest band at 6.3  $\mu\text{m}$ , the hyperfine resonances affect only some  $\nu_3$  nonresolved doublets, the spin splittings of which vanish in the upper and lower levels of the transition. In this case, the hyperfine structure is blended within the total line width, and the hyperfine components cannot be observed.

(ii) Because of the weakness of the  $\nu_1$  and  $2\nu_2$  bands the hyperfine structures cannot be precisely measured on the spectra and consequently the hyperfine resonances were not considered for these bands.

Using new high-resolution Fourier transform spectra recorded in the 13.3- $\mu\text{m}$  spectral region, we report in this paper a reanalysis of the  $\nu_2$  band (with a full treatment of the hyperfine structure), together with a first analysis of the hot  $2\nu_2 - \nu_2$  band of  $^{14}\text{N}^{16}\text{O}_2$ .

## II. EXPERIMENTAL DETAILS

The spectra were recorded in the 720–960  $\text{cm}^{-1}$  spectral range at 0.002  $\text{cm}^{-1}$  resolution with the BOMEM Fourier transform spectrometer of the University of Denver. The optical path length was 1 m, and two spectra were recorded at  $\text{NO}_2$  pressures of 1 and 2 Torr. The calibration of the spectra was performed by means of  $\text{N}_2\text{O}$  absorption lines (18, 19) in the 1150–1250  $\text{cm}^{-1}$  region, and the accuracy of the positions of unblended lines is estimated to be  $\sim 0.0002 \text{ cm}^{-1}$ .

## III. ANALYSIS AND LINE POSITION CALCULATIONS

### *The $\nu_2$ Band*

The analysis was started by comparing the experimental line positions to the line list calculated in Ref. (12). Overall, the agreement was excellent except for transitions in which the upper or the lower state are involved in a hyperfine Fermi resonance. Consequently, a new line list was generated for the  $\nu_2$  band, taking into account not only the electron spin–rotation interaction, but also, as described in Ref. (11) for the (000) state, the magnetic hyperfine hamiltonian (i.e., the Fermi contact operator together with the spin–spin dipolar interaction operators) and the nuclear quadrupole interaction. For this calculation we used the vibrational band center, rotational, spin–rotation, and hyperfine constants of Ref. (12) and Ref. (11), respectively, for the upper and lower state of the transition.

The agreement this time proved to be excellent for all the lines. However, we observed a  $-0.0004 \text{ cm}^{-1}$  global shift of the observed line positions relative to the calculated

ones, which is due to a slightly different calibration of the spectra used in the present work (18, 19) compared to that used (20) in 1988. This leads to a different vibrational band center of the  $\nu_2$  band:  $E_{(010)} = 749.652561 \text{ cm}^{-1}$  (instead of  $749.652961 \text{ cm}^{-1}$  obtained previously in Ref. (12)).

To show the quality of the experimental spectra and of the calculations performed in the present work, we show in Figs. 1 and 2 portions around  $771.8$  and  $758.0 \text{ cm}^{-1}$  of the experimental spectra together with line-by-line calculations performed using either the line list generated in Ref. (12) (no hyperfine structure) or the line list derived here (full treatment of the hyperfine operators). In both regions, the improvement brought by the new calculation is very clear.

In the first spectral region, the complex hyperfine structure appears clearly in the  $N = \text{even } {}^RQ_{K_a=1}$  subband. At  $771.30$  and  $771.64 \text{ cm}^{-1}$  it is due to a strong hyperfine resonance involving the  $(010)[22\ 2\ 20]$  and  $(010)[20\ 2\ 18]$  rotational levels. At  $772 \text{ cm}^{-1}$ , since the resonance is weaker, one observes mainly a broadening of the  $N = 18$  doublet structure. The same hyperfine effect can be clearly observed in Fig. 2 around  $758 \text{ cm}^{-1}$  for lines belonging to the  ${}^RQ_{K_a=0}$  subband. It is worth stressing that in both cases the new calculation, which involves the hyperfine operators, reproduces the experimental spectrum with high accuracy.

### The $2\nu_2 - \nu_2$ Band

Lines from the  $2\nu_2 - \nu_2$  band were already observed in the experimental spectrum (12) which was used in 1988 for the analysis of the  $13.3\text{-}\mu\text{m}$  band of nitrogen dioxide. However, because this hot band is weak and because the  $(020)$  spectroscopic parameters available at that time were not precise enough (only the  $K_a = 0, 1, 2$   $(020)$  series were derived from the analysis of the  $2\nu_2$  band performed at  $6.6 \mu\text{m}$  (17)), only a few lines involving the  $K_a = 0, 1, 2$   $(020)$  rotational series could be analyzed at  $13.3 \mu\text{m}$ .

The  $(020)$  parameters were recently significantly improved from a new analysis of the  $\{\nu_1, 2\nu_2, \nu_3\}$  interacting bands (15). Indeed, more lines involving the  $K_a = 0, 1, 2$  series were assigned; also, lines involving the  $K_a = 6$  rotational series of  $(020)$ , which borrow their intensities from  $\nu_3$  through a Coriolis interaction, were observed (15, 16).

Consequently, from the  $\{(100), (020), (001)\}$  and  $(010)$  parameters obtained in Ref. (15) and Ref. (12) respectively, it has been possible to better predict the  $2\nu_2 - \nu_2$  line positions, as performed in the present analysis.

Because the  $2\nu_2 - \nu_2$  band is rather weak, only transitions of this band involving  $N \leq 30$  rotational quantum number could be identified in the spectrum. For transitions involving the  $K_a = 0-2$  and  $K_a = 6$   $(020)$  energy levels, the agreement between the observed and the predicted line positions was excellent, but this was not completely the case for lines involving the  $K_a = 3-5$   $(020)$  rotational levels since small discrepancies (up to  $0.0030 \text{ cm}^{-1}$ ) were observed. Using these new data, we then determined the vibrational band centers, rotational, spin-rotation, and coupling constants of the  $\{(100), (020), (001)\}$  resonating states. As in Ref. (15) the Hamiltonian matrix explicitly takes into account both the Coriolis and the spin-rotation interactions. For this least-squares fit calculation, the 164  $(020)$  new spin-rotation energy levels obtained in the present work for  $K_a \leq 6$  and  $N \leq 30$  were combined to the 3230  $(100)$   $(001)$  and  $(020)$  energy levels obtained in Ref. (15).

Table I gives the list of vibrational energies and rotational, spin-rotation, and coupling constants deduced from the fit, together with their estimated uncertainty. The



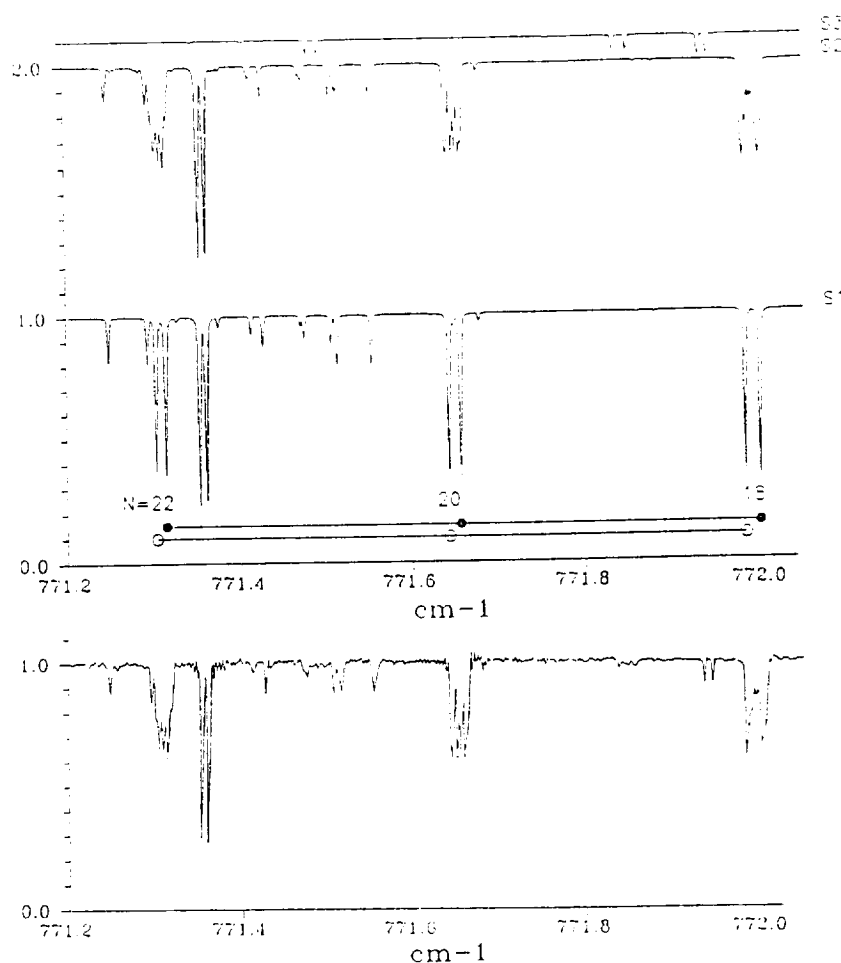


FIG. 1. Experimental spectrum (bottom trace) of nitrogen dioxide around  $771\text{ cm}^{-1}$  and calculated spectra of the absorption due to the  $^{14}\text{N } ^{16}\text{O}_2$  isotopic species: trace S1 and S2 are for the  $\nu_2$  band, respectively, *without* and *with* taking into account the hyperfine structure; trace S3 is for the  $2\nu_2 - \nu_3$  hot band (no calculation of the hyperfine structure). All spectra have the same vertical scale but are displaced for clarity. On trace S1 we have marked the rotational transitions belonging to the  $^RQ_{K_2=1}$  subband (black dots and open circles correspond to  $J = N - \frac{1}{2}$  and  $J = N + \frac{1}{2}$ , respectively). The agreement between observation and calculation is excellent.

corresponding statistical analysis of the results is given in Table II. It is clear that significant improvements were obtained in the present calculation for the (020) spin-rotation levels and to a lesser extent for the (001) levels compared with the results obtained previously (15): the percentages of experimental energy levels which are reproduced within  $0.001\text{ cm}^{-1}$  are now 84.5 and 79.1% instead of 69.5 and 77% for (020) and (001), respectively.

#### IV. SYNTHETIC SPECTRA

This section presents the calculations<sup>2</sup> which have been performed in order to generate a precise line list of absorption lines of  $^{14}\text{N } ^{16}\text{O}_2$  in the  $13.3\text{-}\mu\text{m}$  region.

<sup>2</sup> Both calculations were performed for a reference temperature of 296 K using a  $Z(296\text{ K}) = 13\,617.9$  partition function (this value includes the nitrogen nuclear degeneracy).

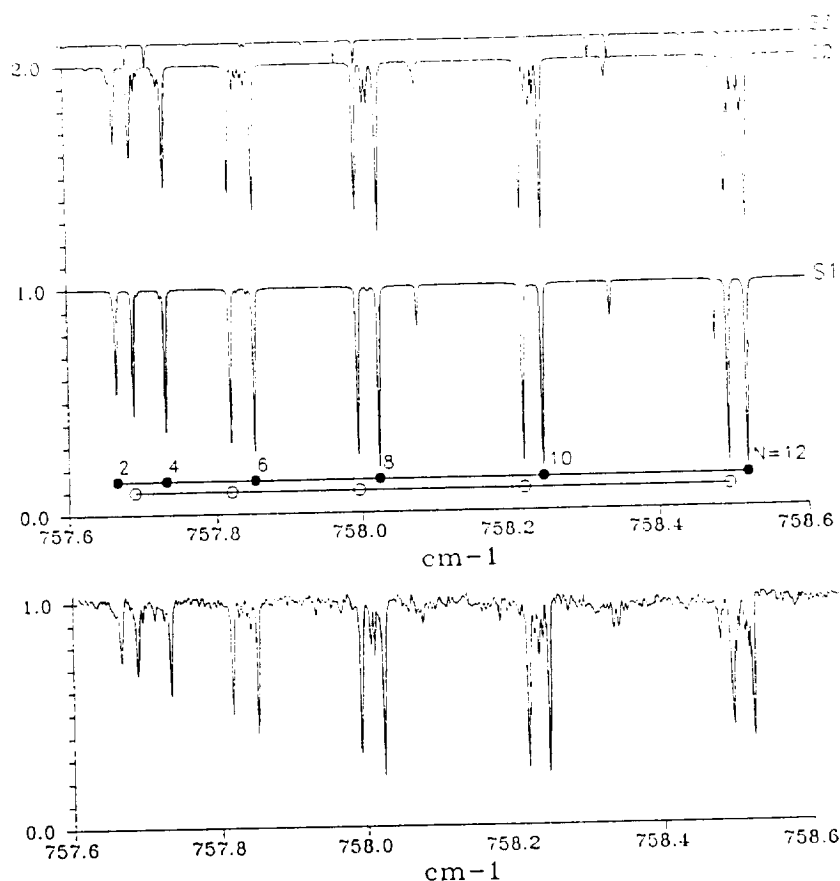


FIG. 2. Experimental spectrum (bottom trace) of nitrogen dioxide around  $758\text{ cm}^{-1}$  and calculated spectra of absorption due to the  $^{14}\text{N } ^{16}\text{O}_2$  isotopic species: trace S1 and S2 are for the  $\nu_2$  band, respectively, *without* and *with* taking into account the hyperfine structure; trace S3 is for the  $2\nu_2 - \nu_2$  hot band (no calculation of the hyperfine structure). All spectra have the same vertical scale but are displaced for clarity. On trace S1, we have marked the rotational transitions belonging to the  $^RQ_{K_a''=0}$  subband, (black dots and open circles are for  $J = N + \frac{1}{2}$  and  $J = N - \frac{1}{2}$ , respectively). The agreement between observation and calculation is excellent.

### $\nu_2$ Band

For the calculation of the  $\nu_2$  band we used the  $\nu_2$  transition moment operator obtained in Ref. (21):

$${}^{(000)(010)}\mu'_z = -0.04272\varphi_N - 0.403 \times 10^{-3} \{i\varphi_N, N_z\} + 0.1083 \times 10^{-3} \{i\varphi_z, N_y\}. \quad (1)$$

Also, for this calculation the effect of the hyperfine structure was *explicitly* taken into account, as described in Ref. (11), through the standard tensorial formalism using a  $\mathbf{F} = \mathbf{J} + \mathbf{I}$  and  $\mathbf{J} = \mathbf{N} + \mathbf{S}$  coupling scheme.

Finally, 30 620 line intensities were calculated with an intensity cutoff of  $0.1 \times 10^{-24}\text{ cm}^{-1}/\text{molecule cm}^{-2}$  and the following ranges of quantum numbers and energies:

$$\begin{aligned} N &\leq 65 & K_a' &\leq 13 \\ E' &\leq 2600\text{ cm}^{-1} & E'' &\leq 2000\text{ cm}^{-1} \end{aligned}$$

TABLE I

Vibrational Energies and Rotational, Spin-Rotation, and Coupling Constants for the  
 $\{(100), (020), (001)\}$  Interacting Vibrational States of  $^{14}\text{N } ^{16}\text{O}_2$

	1 0 0	0 2 0	0 0 1
$E_v$	1319.76589 $\pm$ 0.00012	1498.34688 $\pm$ 0.00027	1616.84918 $\pm$ 0.00089
$A_v$	8.0932898 $\pm$ 0.000082	8.778705 $\pm$ 0.00054	7.7742509 $\pm$ 0.000080
$B_v$	0.43133685 $\pm$ 0.0000067	0.4335453 $\pm$ 0.0000015	0.43092954 $\pm$ 0.0000022
$C_v$	0.40928232 $\pm$ 0.0000037	0.4086528 $\pm$ 0.0000017	0.40637082 $\pm$ 0.0000018
$\Delta_v^s$	(0.285392 $\pm$ 0.000015) $\times 10^{-2}$	(0.43885 $\pm$ 0.00037) $\times 10^{-2}$	(0.252448 $\pm$ 0.00018) $\times 10^{-2}$
$\Delta_{K_a}^s$	(-0.20710 $\pm$ 0.00012) $\times 10^{-4}$	(-0.24104 $\pm$ 0.00011) $\times 10^{-4}$	(-0.18874 $\pm$ 0.00010) $\times 10^{-4}$
$\Delta_{K_c}^s$	(0.30118 $\pm$ 0.00071) $\times 10^{-6}$	(0.29919 $\pm$ 0.00043) $\times 10^{-6}$	(0.30278 $\pm$ 0.00074) $\times 10^{-6}$
$\delta_K^s$	(0.518 $\pm$ 0.012) $\times 10^{-5}$	(0.861 $\pm$ 0.063) $\times 10^{-5}$	(0.4657 $\pm$ 0.0070) $\times 10^{-5}$
$\delta_{K_a}^s$	(0.2987 $\pm$ 0.0040) $\times 10^{-7}$	(0.3111 $\pm$ 0.0024) $\times 10^{-7}$	(0.3417 $\pm$ 0.0037) $\times 10^{-7}$
$H_K^s$	(0.33722 $\pm$ 0.00011) $\times 10^{-5}$	(0.7503 $\pm$ 0.0067) $\times 10^{-5}$	(0.27939 $\pm$ 0.00013) $\times 10^{-5}$
$H_{K_a}^s$	(-0.2823 $\pm$ 0.0014) $\times 10^{-7}$	(-0.44346 $\pm$ 0.007) $\times 10^{-7}$	(-0.2596 $\pm$ 0.0013) $\times 10^{-7}$
$H_{K_c}^s$	(0.220 $\pm$ 0.087) $\times 10^{-10}$	(-0.8928 $\pm$ 0.007) $\times 10^{-10}$	(0.1044 $\pm$ 0.0072) $\times 10^{-9}$
$H_{K_a K_c}^s$	(0.330 $\pm$ 0.071) $\times 10^{-12}$	0.1777 $\times 10^{-12}$	(0.350 $\pm$ 0.013) $\times 10^{-12}$
$h_K^s$	(0.378 $\pm$ 0.029) $\times 10^{-7}$		(0.562 $\pm$ 0.028) $\times 10^{-7}$
$h_{K_a}^s$	-0.2571 $\times 10^{-10}$		(0.21 $\pm$ 0.14) $\times 10^{-10}$
$h_{K_c}^s$	0.10727 $\times 10^{-12}$		(0.1277 $\pm$ 0.0067) $\times 10^{-12}$
$L_K^s$	(-0.55356 $\pm$ 0.00027) $\times 10^{-8}$	-0.13633 $\times 10^{-7}$	(-0.48653 $\pm$ 0.00031) $\times 10^{-8}$
$L_{K_a K_c}^s$	(0.3250 $\pm$ 0.0041) $\times 10^{-10}$		(0.3482 $\pm$ 0.0064) $\times 10^{-10}$
$L_{K_c}^s$	(0.325 $\pm$ 0.041) $\times 10^{-12}$		(0.87 $\pm$ 0.27) $\times 10^{-13}$
$P_K^s$	0.867 $\times 10^{-11}$		0.867 $\times 10^{-11}$
$Q_K^s$	-0.8439 $\times 10^{-14}$		-0.8439 $\times 10^{-14}$
$\epsilon_{K_a}^s$	0.183418 $\pm$ 0.000052	0.21947 $\pm$ 0.00037	0.172433 $\pm$ 0.000044
$\epsilon_{K_b}^s$	(0.230 $\pm$ 0.013) $\times 10^{-1}$	(0.176 $\pm$ 0.018) $\times 10^{-1}$	(0.2660 $\pm$ 0.0043) $\times 10^{-1}$
$\epsilon_{K_c}^s$	(-0.3327 $\pm$ 0.0013) $\times 10^{-2}$	(-0.334 $\pm$ 0.0015) $\times 10^{-2}$	(-0.31510 $\pm$ 0.00041) $\times 10^{-2}$
$\Delta_{K_a}^{s,s}$	(-0.18430 $\pm$ 0.00036) $\times 10^{-3}$	(-0.306 $\pm$ 0.012) $\times 10^{-3}$	(-0.16757 $\pm$ 0.00031) $\times 10^{-3}$
$\Delta_{K_a K_c}^{s,s} + \Delta_{K_c}^{s,s}$	0.6005 $\times 10^{-6}$		0.6005 $\times 10^{-6}$
$\Delta_{K_a K_c}^{s,s}$	0.1678 $\times 10^{-5}$		0.1678 $\times 10^{-5}$
$\Delta_{K_c}^{s,s}$	0.6322 $\times 10^{-9}$		0.6322 $\times 10^{-9}$
$\delta_K^{s,s}$	0.3769 $\times 10^{-6}$		0.3769 $\times 10^{-6}$
$\delta_{K_a}^{s,s}$	0.244 $\times 10^{-9}$		0.244 $\times 10^{-9}$
$H_K^{s,s}$	0.29673 $\times 10^{-6}$		0.29673 $\times 10^{-6}$
$L_K^{s,s}$	-0.3568 $\times 10^{-9}$		-0.3568 $\times 10^{-9}$

$$h_{(001)(020)}^{\nu_2} = (-0.294552 \pm 0.000088) \times 10^{-1}$$

$$h_{(001)(020)}^{\nu_2} = (0.736_9 \pm 0.031) \times 10^{-7}$$

$$h_{(001)(001)}^{\nu_2} = -0.656287_9 \pm 0.000064$$

$$h_{(001)(001)}^{\nu_2} = (-0.9193_6 \pm 0.0096) \times 10^{-4}$$

$$h_{(001)(100)}^{\nu_2} = (0.256_6 \pm 0.033) \times 10^{-5}$$

Note. All the results are in  $\text{cm}^{-1}$  and the quoted errors correspond to one standard deviation. The constants with no errors were held fixed during the fit.

The total band intensity was found to be  $S_{(010)-(000)} = 0.542 \times 10^{-18} \text{ cm}^{-1}/\text{molecule cm}^{-2}$  at 296 K.

Because of the rather high proportion of so-called  $\Delta F \neq \Delta J \neq \Delta N$  "forbidden" transitions which were not considered in the 1988 calculation (12), the present calculated lines are more numerous than those in 1988 (30 620 instead of  $8065 \times 3$ , taking into account the  $(2I + 1) = 3$  nitrogen nuclear degeneracy).

### $2\nu_2 - \nu_2$ Band

For the hot  $2\nu_2 - \nu_2$  band, only the spin-rotation fine structure was considered and its vibrational transition moment constant was determined using the following relation, valid up to the second order of approximation:

$${}^{(020)(010)}\mu_z' = \sqrt{2} \times {}^{(010)(000)}\mu_z' \quad (2)$$

The  $2\nu_2 - \nu_2$  line intensities were calculated in the following ranges:

TABLE II  
Statistical Analysis of the Results for the Energy Levels Calculation

	(100)	(020)	(001)
Number of experimental spin-rotation levels	1187	374	1833
$0 \leq \delta E < 1 \times 10^{-3}$	65.8%	84.5%	79.1%
$1 \times 10^{-3} \leq \delta E < 2 \times 10^{-3}$	26.7%	12.8%	15.4%
$2 \times 10^{-3} \leq \delta E < 7.0 \times 10^{-3}$	7.4%	2.7%	5.6%

$$\delta E = |E_{\text{obs}} - E_{\text{calc}}| \text{ in cm}^{-1}$$

$$N \leq 60 \quad K'_a \leq 10$$

$$E' \leq 3200 \text{ cm}^{-1} \quad E'' \leq 2600 \text{ cm}^{-1}$$

Also, in order to be consistent with the  $\nu_2$  calculation, the intensity cutoff was chosen to be  $0.3 \times 10^{-24} \text{ cm}^{-1}/\text{molecule cm}^{-2}$  at 296 K, taking into account the  $3I + 1 = 3$  nitrogen nuclear degeneracy.

Finally, 4388 lines were calculated for the  $2\nu_2 - \nu_2$  band and the sum of all the intensities was found to be  $S_{(020)-(010)} = 0.2735 \times 10^{-19} \text{ cm}^{-1}/\text{molecule cm}^{-2}$  at 296 K.

#### V. CONCLUSION

Using high-resolution Fourier transform spectra, a new analysis of the  $\nu_2$  band of  $^{14}\text{N } ^{16}\text{O}_2$  involving the hyperfine structure has been performed for the first time together with the first extensive analysis of the  $2\nu_2 - \nu_2$  band of this molecule, leading to a very accurate representation of the absorption of  $^{14}\text{N } ^{16}\text{O}_2$  in the  $13.3\text{-}\mu\text{m}$  region. It must be mentioned that lines of the  $\nu_2$  band of  $\text{NO}_2$  are visible in the University of Denver balloon flight spectra of June 1988 (22), and knowledge of their parameters (and lines of the hot band) may be important in attempts to detect the weakly absorbing lines of stratospheric ClO in the infrared (23).

RECEIVED: January 27, 1993

#### REFERENCES

1. G. R. BIRD, J. C. BAIRD, A. W. JACHE, J. A. HODGENSON, R. F. CURL, Jr., A. C. KUNKLE, J. W. BRANSFORD, J. RASTRUP-ANDERSON, AND J. ROSENTHAL, *J. Chem. Phys.* **40**, 3378-3390 (1964).
2. R. M. LEE, R. F. CURL, AND J. C. BAKER, *J. Chem. Phys.* **45**, 2037-2040 (1966).
3. P. A. BARON, P. D. GODFREY, AND D. O. HARRIS, *J. Chem. Phys.* **60**, 3723-3724 (1974).
4. W. C. BOWMAN AND F. C. DE LUCIA, *J. Chem. Phys.* **77**, 92-107 (1982).
5. O. I. BASKAKOV, M. V. MOSKIENKO, AND S. F. DYUBKO, *Opt. Spectrosc. (USSR)* **53**, 270-272 (1982).
6. T. TANAKA, A. D. ENGLISH, R. W. FIELDS, D. A. JENNINGS, AND D. O. HARRIS, *J. Chem. Phys.* **59**, 5217-5218 (1973).
7. J. M. BROWN, T. C. STEIMLE, M. E. COLES, AND R. F. CURL, Jr., *J. Chem. Phys.* **74**, 3668-3672 (1981).
8. N. SEMMOUD-MONNANTEUIL, J.-M. COLMONT, A. PERRIN, J.-M. FLAUD, AND C. CAMY-PEYRET, *J. Mol. Spectrosc.* **134**, 176-182 (1989).
9. L. W. HRUBESH AND R. F. CURL, *J. Mol. Spectrosc.* **61**, 144-146 (1976).

10. Y. MORINO, M. TANIMOTO, S. SAITO, E. HIROTA, R. AWATA, AND T. TANAKA, *J. Mol. Spectrosc.* **98**, 331-348 (1983).
11. A. PERRIN, J.-M. FLAUD, C. CAMY-PEYRET, B. CARLI, AND M. CARLOTTI, *Mol. Phys.* **63**, 791-810 (1988).
12. A. PERRIN, C. CAMY-PEYRET, J.-M. FLAUD, AND J. KAUPPINEN, *J. Mol. Spectrosc.* **130**, 168-182 (1988).
13. A. PERRIN, C. CAMY-PEYRET, AND J.-M. FLAUD, *J. Quant. Spectrosc. Radiat. Transfer* **48**, 645-651 (1992).
14. L. S. ROTHMAN, R. R. GAMACHE, R. H. TIPPING, C. P. RINSLAND, M. A. H. SMITH, D. CHRIS BENNER, V. MALATHY-DEVI, J.-M. FLAUD, C. CAMY-PEYRET, A. PERRIN, A. GOLDMAN, S. T. MASSIE, L. R. BROWN, AND R. A. TOTH, *J. Quant. Spectrosc. Radiat. Transfer* **48**, 469-507 (1992).
15. A. PERRIN, J.-M. FLAUD, C. CAMY-PEYRET, A.-M. VASSEROT, G. GUELACHVILI, A. GOLDMAN, F. J. MURCRAY, AND R. D. BLATHERWICK, *J. Mol. Spectrosc.* **154**, 391-406 (1992).
16. R. A. TOTH, *J. Opt. Soc. Amer. B* **9**, 433-461 (1992).
17. A. PERRIN, J.-M. FLAUD, AND C. CAMY-PEYRET, *J. Mol. Spectrosc.* **118**, 174-179 (1986).
18. R. A. TOTH, *J. Opt. Soc. Amer. B* **3**, 1263-1281 (1986).
19. A. G. MAKI AND J. S. WELLS, "Wavenumber Calibration Tables from Heterodyne Frequency Measurements," NIST Special Publication 821, 1992.
20. G. GUELACHVILI AND K. NARAHARI RAO, "Handbook of Infrared Standards," Academic Press, Orlando, 1986.
21. V. MALATHY DEVI, P. P. DAS, A. BANO, K. NARAHARI RAO, J.-M. FLAUD, C. CAMY-PEYRET, AND J.-P. CHEVILLARD, *J. Mol. Spectrosc.* **88**, 251-258 (1981).
22. A. GOLDMAN, F. J. MURCRAY, R. D. BLATHERWICK, J. J. KOSTERS, F. H. MURCRAY, F. G. MURCRAY, AND C. P. RINSLAND, *J. Geophys. Res. D* **94**, 14945-14955 (1989).
23. C. P. RINSLAND AND A. GOLDMAN, *J. Quant. Spectrosc. Radiat. Transfer* **48**, 685-692 (1992).



# Atmospheric Sulfur Hexafluoride: Sources, Sinks and Greenhouse Warming

MALCOLM K. W. KO,<sup>1</sup> NIEN DAK SZE,<sup>1</sup> WEI-CHYUNG WANG,<sup>1,2</sup> GEORGE SHIA,<sup>3</sup> AARON GOLDMAN,<sup>4</sup>  
FRANK J. MURCRAY,<sup>4</sup> DAVID G. MURCRAY,<sup>4</sup> AND CURTIS P. RINSLAND<sup>5</sup>

Model calculations using estimated reaction rates of sulfur hexafluoride (SF<sub>6</sub>) with OH and O(<sup>1</sup>D) indicate that the atmospheric lifetime due to these processes may be very long (25,000 years). An upper limit for the UV cross section would suggest a photolysis lifetime much longer than 1000 years. The possibility of other removal mechanisms are discussed. The estimated lifetimes are consistent with other estimated values based on recent laboratory measurements. There appears to be no known natural source of SF<sub>6</sub>. An estimate of the current production rate of SF<sub>6</sub> is about 5 kt/yr. Based on historical emission rates, we calculated a present-day atmospheric concentrations for SF<sub>6</sub> of about 2.5 parts per trillion by volume (pptv) and compared the results with available atmospheric measurements. It is difficult to estimate the atmospheric lifetime of SF<sub>6</sub> based on mass balance of the emission rate and observed abundance. There are large uncertainties concerning what portion of the SF<sub>6</sub> is released to the atmosphere. Even if the emission rate were precisely known, it would be difficult to distinguish among lifetimes longer than 100 years since the current abundance of SF<sub>6</sub> is due to emission in the past three decades. More information on the measured trends over the past decade and observed vertical and latitudinal distributions of SF<sub>6</sub> in the lower stratosphere will help to narrow the uncertainty in the lifetime. Based on laboratory-measured IR absorption cross section for SF<sub>6</sub>, we showed that SF<sub>6</sub> is about 3 times more effective as a greenhouse gas compared to CFC 11 on a per molecule basis. However, its effect on atmospheric warming will be minimal because of its very small concentration. We estimated the future concentration of SF<sub>6</sub> at 2010 to be 8 and 10 pptv based on two projected emission scenarios. The corresponding equilibrium warming of 0.0035°C and 0.0043°C is to be compared with the estimated warming due to CO<sub>2</sub> increase of about 0.8°C in the same period.

## 1. INTRODUCTION

The Earth's atmosphere contains a trace amount (~few parts per trillion) of SF<sub>6</sub>. Earliest measurements [Krey *et al.*, 1977; Singh *et al.*, 1977] indicated concentrations of less than 1 part per trillion by volume (pptv) in the 1970s. Although there is no continuous long-term global monitoring of this gas, intermittent samplings [Singh *et al.*, 1977, 1979; Leifer *et al.*, 1982] and sampling of ocean water [Watson and Liddicoat, 1985] have indicated an increasing trend. Recent papers by Rinsland *et al.* [1990a, b] and Zander *et al.* [1991] provided additional evidence for the increasing trend. The possibility that SF<sub>6</sub> may contribute to the global warming was raised by Ramanathan *et al.* [1985, 1987], but no quantitative assessment was made by the authors.

Assessment of the greenhouse warming impact of the species requires knowledge on its radiative property and information on its lifetime and atmospheric budget so that its future abundance in the atmosphere can be predicted. Our understanding of the life cycle (or budget) of atmospheric SF<sub>6</sub> was hampered, in part, by the lack of global emission data. This paper discusses some of its commercial application and usage and provides an estimate of worldwide production of SF<sub>6</sub>, from which a global emission rate is derived and extrapolated for the next 20 years. The second

objective of the paper is to estimate the atmospheric lifetime of SF<sub>6</sub> using several different approaches: estimates based on a known mechanism (e.g., photolysis and atmospheric oxidation) and/or mass balance method. The third objective is to calculate the radiative forcing of SF<sub>6</sub> based on our recent laboratory infrared absorption cross section and to compute the expected warming over the time period 1950–2010 according to several emission scenarios.

## 2. USES OF SULFUR HEXAFLUORIDE AND SOURCES OF ATMOSPHERIC EMISSIONS

### 2.1. Applications for Sulfur Hexafluoride and Emission Sources

Sulfur hexafluoride has a unique combination of chemical, physical, and electrical properties which make it ideally suited for some very specialized industrial applications. By far, its largest use (approximately 80% of production) is for insulation of electrical equipment. The material's high dielectric strength and unique arc-quenching ability have enabled the development of safe, reliable gas-insulated high-voltage circuit breakers, substations, transformers, and transmission lines. Sulfur hexafluoride provides an effective alternative to insulating oils (which suffer from high maintenance costs, disposal problems, and safety problems due to the flammable oil). SF<sub>6</sub>-insulated equipment also has important advantages over vacuum- or air-insulated equipment which require more space and are not well suited for switching very high voltages.

There are two main sources of emission from SF<sub>6</sub>-insulated electrical equipment. SF<sub>6</sub> can escape from the container through seals and gaskets. Older equipment is prone to leak in this manner as it is typically pressurized to 0.015–0.03 N m<sup>-2</sup> (100–200 psi) with SF<sub>6</sub>. Newer designs for SF<sub>6</sub>-filled switchgear allow operation at near-ambient pressure and have greatly improved seals giving rise to leakage rates of less than 1%/yr. Emissions may occur when SF<sub>6</sub>-

<sup>1</sup>Atmospheric and Environmental Research, Incorporated, Cambridge, Massachusetts.

<sup>2</sup>Now at State University of New York, Albany.

<sup>3</sup>Buffalo Research Laboratory, Allied-Signal Incorporated, Buffalo, New York.

<sup>4</sup>Department of Physics, University of Denver, Denver, Colorado.

<sup>5</sup>Atmospheric Science Center, NASA Langley Research Center, Hampton, Virginia.

TABLE 1. Estimated Production Rate of SF<sub>6</sub>

Year	Kiloton/Year	Year	Kiloton/Year
1953	0.01	1975	1.50
1954	0.03	1976	1.82
1955	0.04	1977	2.14
1956	0.05	1978	2.50
1957	0.05	1979	2.82
1958	0.10	1980	3.14
1959	0.16	1981	3.45
1960	0.16	1982	3.82
1961	0.19	1983	3.82
1962	0.33	1984	4.00
1963	0.44	1985	4.00
1964	0.55	1986	4.50
1965	0.68	1987	4.50
1966	0.68	1988	5.00
1967	0.68	1989	5.00
1968	0.64		
1969	0.73		
1970	0.77		
1971	0.91		
1972	1.09		
1973	1.18		
1974	1.18		

The 62.6 kt SF<sub>6</sub> released to date. Assumes all SF<sub>6</sub> produced are emitted to the atmosphere in the same year.

filled equipment is opened for servicing, which typically occurs after several years of operation. Earlier many utilities simply vented the SF<sub>6</sub> to the atmosphere prior to servicing. The rapid increase in the concentration of atmospheric SF<sub>6</sub> observed during the 1980s may largely be attributable to these sources. However, present standard industry practice minimizes losses as the gas is evacuated from the equipment, purified, and stored until the equipment is ready to be refilled. The recent improvements in equipment and gas recycling will tend to mitigate future increases.

Another use (5–10% of production) is in blanketing or degassing molten reactive metals [MacNeal *et al.*, 1990]. Sulfur hexafluoride can be used to replace CFCs or chlorine in aluminum degassing. Dilute blends (5 vol % or less) of SF<sub>6</sub> and an inert gas (nitrogen or argon) are bubbled through molten aluminum to remove solid impurities and entrapped hydrogen. Almost no sulfur hexafluoride escapes the molten metal as it readily reacts to form aluminum fluoride. Blanketing of magnesium during alloying and casting is another but much smaller application. Unlike aluminum degassing, most of the SF<sub>6</sub> is not consumed during this process.

There are a number of smaller applications for sulfur hexafluoride. One of significance to atmospheric scientists has been its use as a tracer. Because of sulfur hexafluoride's very large electron capture cross section, detection of this gas below the parts per trillion range is possible. It has been used as tracers of pollutants in urban areas [Drivas and Shair, 1974; Vandeborghet *et al.*, 1982] and as a discharge testing agent for halon 1301 fire suppression systems.

## 2.2. Historical Production and Release Data

Yearly production or sale volumes have never been reported; however, a rough estimate puts the 1989 world production rate at about 5 kt/yr. Estimates for the historical release rate are available for the years 1953 to 1974 [see Krey *et al.*, 1976]. The emission estimate shown in Table 1 was assembled by combining the emission estimates by Krey *et*

*al.* [1976] for the period prior to 1974 with a roughly linear interpolation for the years 1974–1989 using the emission rate for 1974 and the estimated production rate for 1989. These estimates are only approximate because the amount of gas that is banked inside electrical equipment is highly uncertain. While this bank has never been thoroughly investigated, it appears that it could contain more than 50% of each year's production, particularly for the past 5 to 10 years. Thus the values given after 1974 should be considered as the upper limits, assuming none of the SF<sub>6</sub> is banked. The emission by 1989 could be as low as 2.5 kt if 50% of the production are indeed banked. The previously mentioned improvements in electrical equipment design (better seals) and gas recycling practices during maintenance combined with the retirement of older (more leak prone) equipment will eventually mean that nearly all the SF<sub>6</sub> that goes into this application will never be released.

## 3. ATMOSPHERIC LIFETIMES AND ABUNDANCE OF SF<sub>6</sub>

Two approaches have been used to estimate the atmospheric lifetime of trace gases. The first one utilizes a numerical model to calculate the lifetime based on our knowledge of specific removal mechanism such as reactions with reactive species (O(<sup>1</sup>D), OH), photolysis, hydrolysis, etc. [cf. Cicerone, 1979]. Alternatively, the lifetime may be derived, without knowing the specific removal mechanism, from the observed trends of the concentrations in the atmosphere together with the knowledge of the historical emission rates [cf. Krey *et al.*, 1977; Prinn *et al.*, 1983; Cunnold *et al.*, 1983]. Other more indirect approaches include consideration of the vertical distribution and/or interhemispheric asymmetries. This information is often helpful in pointing to the existence of other possible sources or sinks in the atmosphere.

### 3.1. Observed Abundance and Lifetime

Measurements of the tropospheric concentrations of SF<sub>6</sub> have been reported by Singh *et al.* [1977, 1979, 1983], Rasmussen *et al.* [1981], Rasmussen and Khalil [1983], and Watson and Liddicoat [1985]. Additional data have been reported using remote sensing techniques from space platform [Rinsland *et al.*, 1990a], balloon platform [Rinsland *et al.*, 1990b], and ground-based stations [Zander *et al.*, 1991]. Stratospheric concentrations from aircraft sampling program Project Airstream have been reported by Krey *et al.* [1977] and Leifer *et al.* [1982]. Additional information on the vertical distribution of SF<sub>6</sub> were reported from the ATMOS data [Rinsland *et al.*, 1990a] and balloon data [Rinsland *et al.*, 1990b]. These results are summarized in Figures 1–3.

Results reported by Singh *et al.* [1977, 1979, 1983] indicate that the average surface concentrations for 1977 and 1981 were 0.31 and 0.9 pptv, respectively, for the northern hemisphere and 0.27 and 0.8 pptv, respectively, for the southern hemisphere. The data reported by Zander *et al.* [1991] show the average tropospheric concentration at 32°N were 1.76 pptv in 1981 and 3.18 pptv in 1990. The results from Rinsland *et al.* [1990a, b] show average concentrations between 12 and 18 km of 1.17 pptv in 1981 and 2.02 pptv in 1988. Each data set, taken by itself, shows an increasing trend in the SF<sub>6</sub> concentration. As summarized by Zander *et al.* [1991], trends in the atmospheric concentration of SF<sub>6</sub> have been reported based on the individual



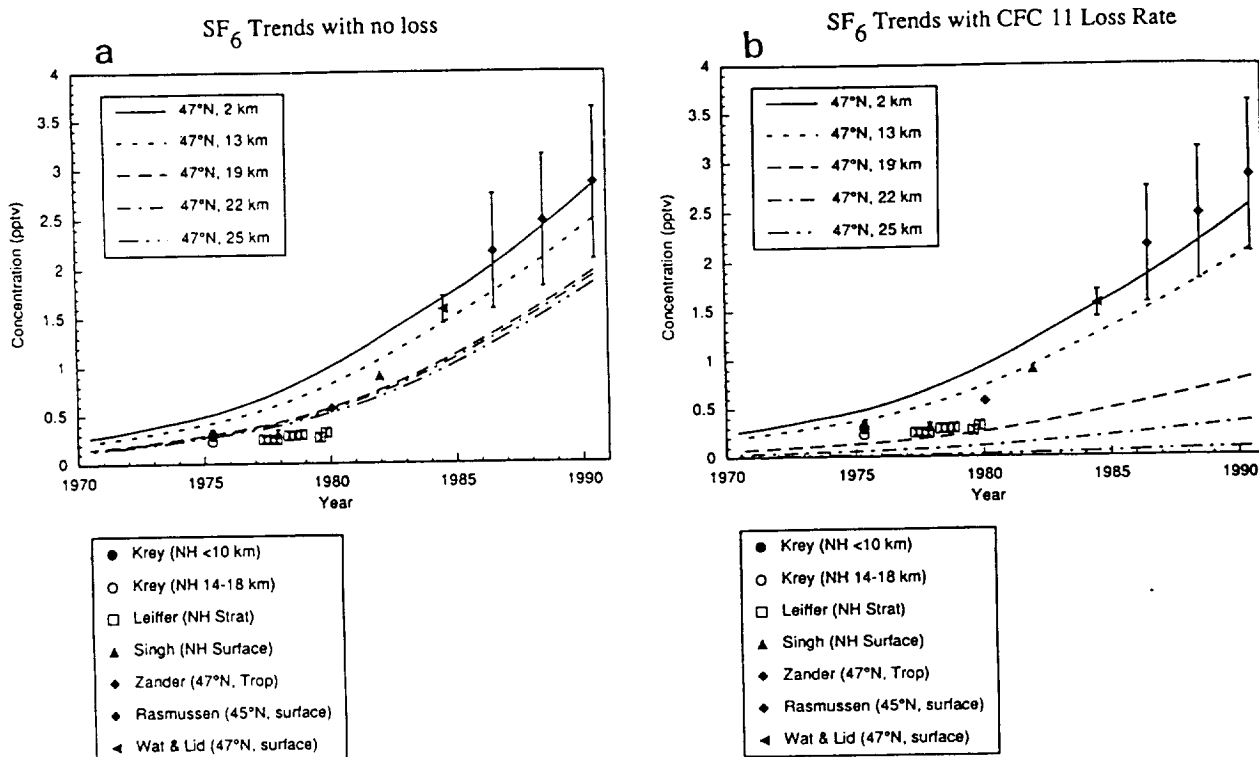


Fig. 1. The calculated mixing ratio of SF<sub>6</sub> at 47°N for selected altitudes. (a) From case 1, calculated assuming no photochemical removal. (b) Calculated assuming that the local photochemical removal rate is the same as that of CFC 11. The observed concentrations are included for comparison. Since we are comparing the results to a zonal mean mode, we decided to show only the average concentration cited by the authors rather than individual data points.

data sets. Because the data were obtained at different geographical locations and because of possible differences in absolute calibration, it is difficult to combine the data sets to form time series for trend analysis. *Watson and Liddicoat* [1985] also reported seawater concentration and derived a trend for the atmospheric concentration based on the concentration profile of SF<sub>6</sub> in the water. However, in the absence of reliable estimates for historical emission rates, it remains difficult to derive a lifetime from the trends.

*Krey et al.* [1977] used the aircraft data between 1974 and 1975 to estimate the tropospheric and stratospheric burdens of SF<sub>6</sub> and CFC 11. A two-box model was used to calculate the burdens for this time period using historical emission rates between 1953 and 1975. Comparison of the observed and calculated burdens led *Krey et al.* [1977] to conclude that SF<sub>6</sub> and CFC 11 have similar stratospheric lifetimes of about 2 years, which translated into an atmospheric lifetime of about 30 years. However, there is considerable uncertainties in both the emission rates and the observed burden derived from the observations.

Indeed, the derived lifetime for CFC 11 appears to be in conflict with recent findings. The analysis of *Cunnold et al.* [1986] used ground-based data of CFC 11 at five monitoring stations over a 5-year period between 1978 and 1983. Regression analysis comparing the observed trends at the five stations with the calculated trends from a nine-box model yielded a lifetime for CFC 11 of 74(+31, -17) years. A lifetime as short as 59(+18, -11) years was obtained using the data from a single station. Recent updated estimates based on 10 years of data are 41 and 47 years depending on analysis method used [*Kaye and Penkett*, 1993].

### 3.2. Kinetic Data and Estimates for Atmospheric Lifetime

*Ravishankara et al.* [1992] reported a measured rate for reaction with O(<sup>1</sup>D) ( $1.8 \times 10^{-14} \text{ cm}^3 \text{ s}^{-1}$ ), estimated upper limit for reaction with OH ( $<5 \times 10^{-19} \text{ cm}^3 \text{ s}^{-1}$ ), and measured photolysis cross section at Ly  $\alpha$  wavelength ( $1.8 \times 10^{-18} \text{ cm}^2$ ). *Ravishankara et al.* [1992] calculated a lifetime due to photolysis of about 13,500 years and a lifetime due to reaction with free electrons in the mesosphere of about 4200 years. Their best estimate for the atmospheric lifetime due to photochemical reactions in the atmosphere is 3200 years.

Using the AER two-dimensional model, which explicitly calculates the OH and O(<sup>1</sup>D) concentrations, we calculated the steady state atmospheric lifetime of SF<sub>6</sub> to be longer than 60,000 years. With the upper limit value for the OH reaction, reactions with OH and O(<sup>1</sup>D) contribute about equal amounts to the removal rate. According to *Hertzberg* [1966], SF<sub>6</sub> absorbs UV radiation only below 110 nm. Measurements made on the UV cross section indicate an upper limit of  $2 \times 10^{-22} \text{ cm}^2$  between 185 and 300 nm (R. Bray, private communication, 1989). If one assumes a UV absorption cross section of  $2 \times 10^{-22} \text{ cm}^2$  for wavelength less than 240 nm and zero for wavelength longer than 240 nm, one obtains a photolysis lifetime of about 1000 years. This estimated lifetime will be much longer as the cutoff shift to wavelengths shortward of 240 nm. Other removal mechanisms include electron capture and ion reactions [see *Fershenfeld*, 1971]. If these reactions are assumed to be effective only in the ionosphere, estimated lifetimes will be of the order of  $10^5$  years.

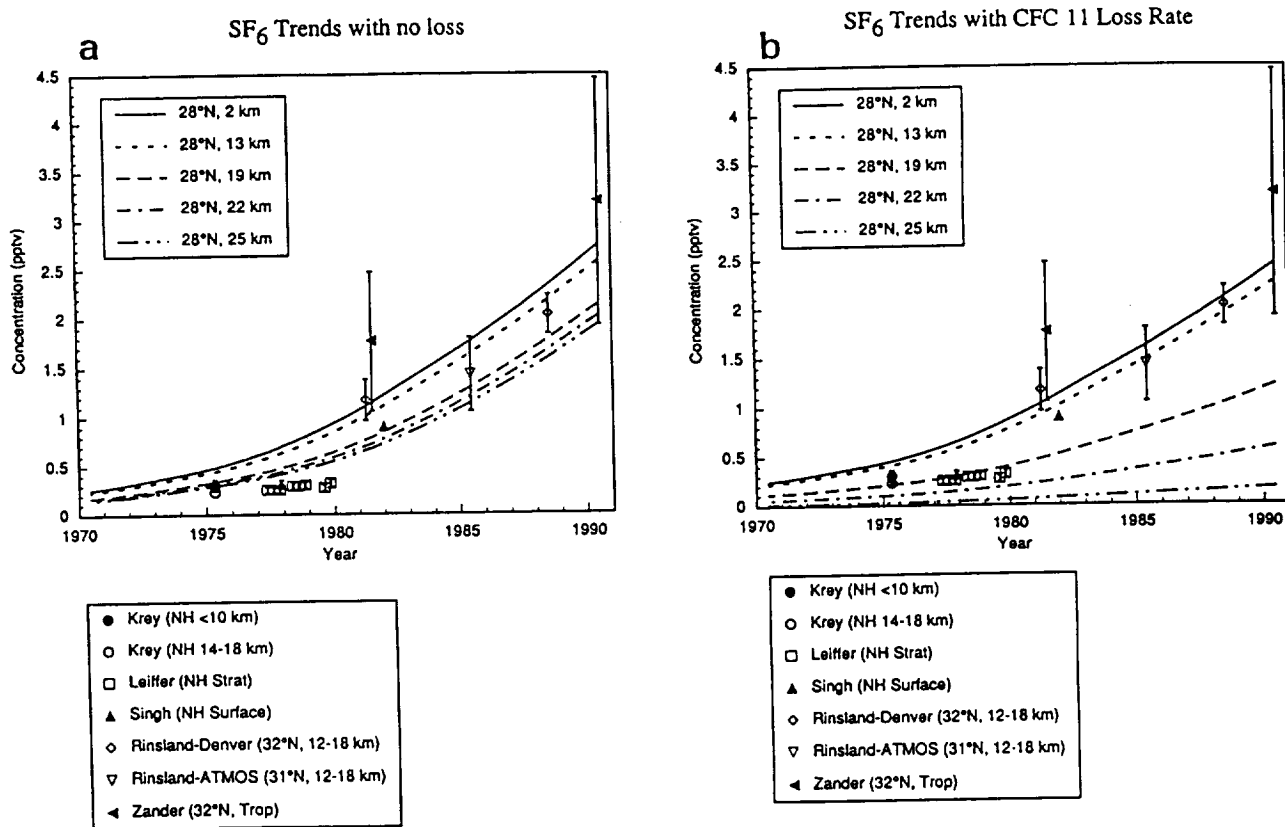


Fig. 2. Same as Figure 1 except the results are for 28°N.

Apart from atmospheric removal processes, surface removal mechanisms should also be considered. *Watson and Liddicoat* [1985] reported a Henry's coefficient in distilled water at 20°C of  $1.7 \times 10^{-4}$  (mol/liter/atmosphere). Their

measured atmospheric concentration and seawater concentration would imply a Henry's coefficient of  $2.0 \times 10^{-4}$  (mol/liter/atmosphere) assuming equilibrium. Unless there is a fast hydrolysis rate ( $k > 10^{-7} \text{ s}^{-1}$ ), lifetime due to ocean

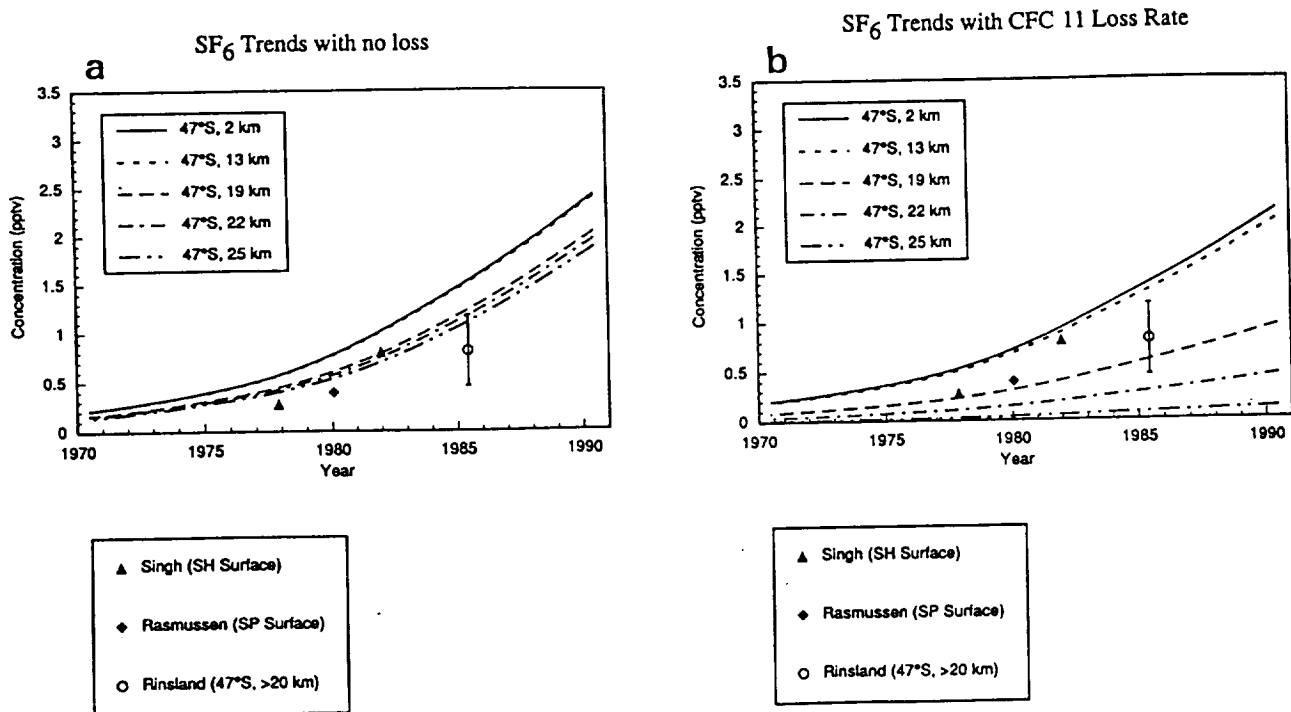


Fig. 3. Same as Figure 1 except the results are for 47°S.

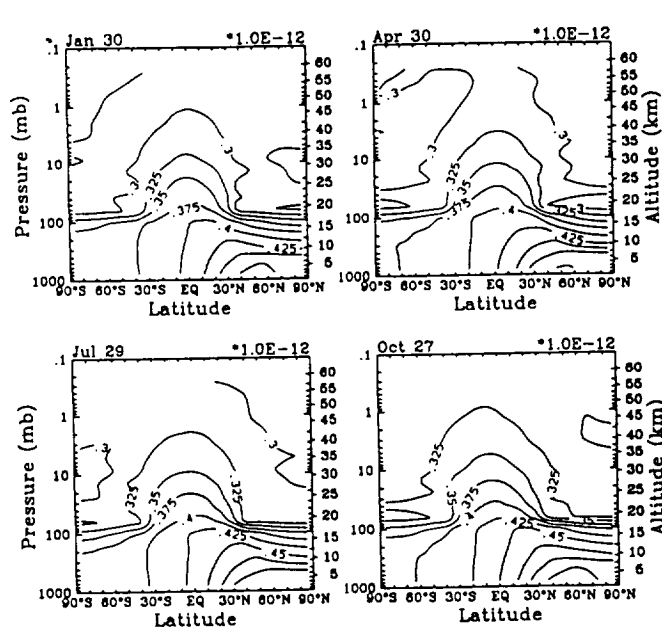


Fig. 4. Calculated mixing ratio for SF<sub>6</sub> for 1975 assuming no photochemical removal mechanism. The emission rates are as given in Table 1.

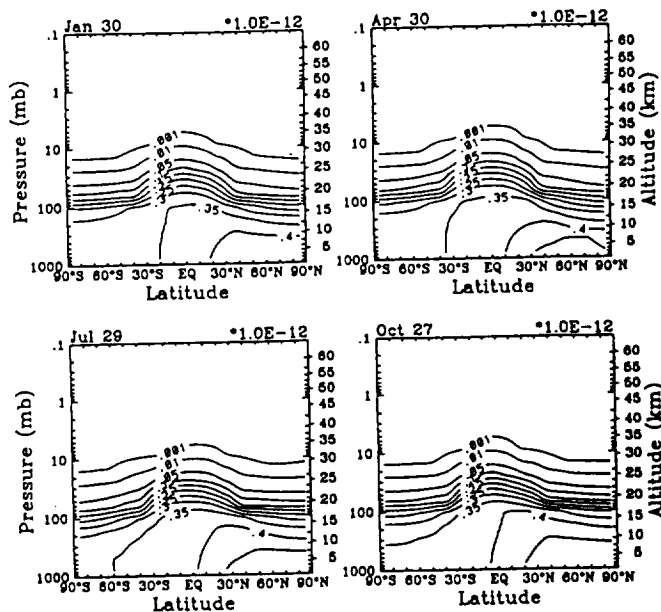


Fig. 5. Calculated mixing ratio for SF<sub>6</sub> for 1975 assuming that the local photochemical removal rate is the same as that of CFC 11. The emission rates are as given in Table 1.

removal is also estimated to be of the order of 10<sup>4</sup> years and longer. (See *Wine and Chameides* [1989] and *Butler et al.* [1991] for a discussion of estimating ocean removal lifetime.) The same argument would indicate that lifetime due to washout is long. We do not have any estimate for lifetime due to dry deposition. The lifetime is likely to be long based on the inert nature of SF<sub>6</sub>.

### 3.3. Model Results

With the emission rates given in Table 1, we used the AER two-dimensional model [Ko et al., 1991; Weisenstein et al., 1992] to calculate the atmospheric concentration of SF<sub>6</sub>. Results from two simulations will be presented. In both cases the emissions are assumed to be restricted to the northern hemisphere between 23° and 62°N. Case 1 corresponds to the calculation assuming no photochemical removal in the atmosphere. In case 2 the photochemical removal rate for SF<sub>6</sub> is assumed to be identical to that of CFC 11, corresponding to a model-calculated steady state atmospheric lifetime of 49 years.

The calculated latitude-height cross sections for the mixing ratio of SF<sub>6</sub> for 1975 are shown in Figures 4 and 5 for cases 1 and case 2, respectively. The calculated tropospheric burden is about 0.4 pptv with variations over latitude and altitude. In both cases the mixing ratio at the southern mid-latitude is typically about 20% smaller than the mixing ratio at northern latitude. The burden in case 2 is 10% smaller than that in case 1. The largest difference between the two cases is seen in the stratosphere with case 2 showing a much sharper vertical gradient reflecting the effect from the imposed stratospheric removal. The calculated concentrations in case 1 show little variation with altitude above 19 km indicating that SF<sub>6</sub> is well mixed in the stratosphere. The altitude profiles for the average mixing ratio in the northern hemisphere are shown in Figure 6 together with the derived average profile for the northern hemisphere reported by *Krey et al.* [1977, Table 2]. Note that even in case 1 the

mixing ratio is not uniform in the troposphere because the species is not in steady state. The vertical profile shows that the concentration at 25 km is typically 70% of the tropospheric concentration in case A. The calculated scale heights in cases 1 and 2 around 20 km are consistent with the 1974–1975 Project Airstream data [Krey et al., 1977] and the mixing ratio profile derived from the ATMOS data [Rinsland et al., 1990a].

The calculated annually averaged concentrations of SF<sub>6</sub> between 1970 and 1990 at selected altitudes for 47°N, 28°N, and 47°S are shown in Figures 1–3, respectively. Included in the figures are the observations discussed in the previous section. Note that since the emission is increasing with time, the stratospheric mixing ratio consistently lags behind the tropospheric mixing ratio by about 4 years for case 1.

In an ideal situation where the emission history and the atmospheric concentration are precisely known, comparison

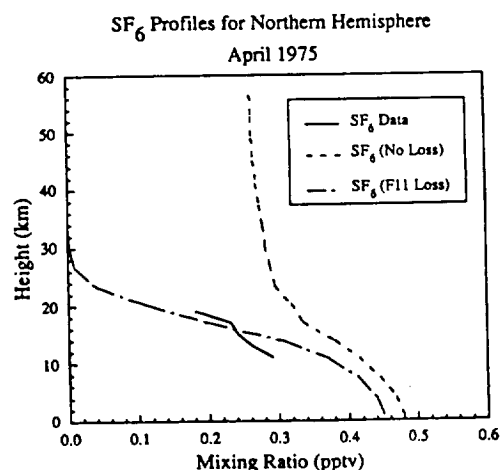


Fig. 6. Calculated vertical profiles of the average mixing ratio of SF<sub>6</sub> for the northern hemisphere. The profiles of *Krey et al.* [1977] are included for comparison.

of the calculated concentration with observation could provide validation of the assumed lifetime. Two features could be used in the comparison. The first is the calculated burden at any point in time. The second is the vertical gradient of the mixing ratio.

Comparison of the measured concentrations indicates that an uncertainty of at least 10% exists in the burden derived from measured concentrations. The emission data in Table 1 indicate that 62.6 kt of SF<sub>6</sub> would have accumulated in the atmosphere if there is no removal. An assumed lifetime of 49 years and 100 years would imply that the burden by 1989 is 15 and 10% smaller, respectively. Given these uncertainties, we estimate that it is difficult to use the observed burdens to distinguish lifetimes longer than 100 years. In addition, the uncertainty in the calculated burden due to uncertainty in the emission rate is of the same order. If we assumed that only a portion of the manufactured SF<sub>6</sub> is released to the atmosphere and that the fraction varies linearly from 1 in 1976 to 0.5 in 1989, the accumulated burden in 1989 (assuming no removal) would be 48.7 kt, or 22% smaller. Given the uncertainty associated with deriving atmospheric burden from sampled data and the uncertainty in the emission rate, the available data base on the observed concentration of SF<sub>6</sub> is of limited utility in distinguishing among lifetimes of 100 years or longer.

The second approach is the analysis of vertical gradient in the stratosphere. The model results showed that the calculated concentration in the lower stratosphere for cases 1 and 2 could differ by a factor of 3 (0.5 pptv versus 1.5 pptv) in the present-day stratosphere. In the past this approach has been faced with the difficulty of determining whether the data collected from limited locations and times represent the climatological mean. Recent works associated with the various aircraft campaigns [Schoeberl *et al.*, 1989; Hartmann *et al.*, 1989; Plumb and Ko, 1992] showed that simultaneously measured values of a dynamical or chemical tracer could be used to help interpret the measured values. Concentrations of N<sub>2</sub>O, a good chemical tracer, is available from the Project Airstream data that cover the time period from 1974 to 1979 [Krey *et al.*, 1977; Leifer *et al.*, 1982]. Work is under progress in collaboration with R. Leifer (Environmental Measurement Laboratory, Department of Energy (DOE)) to reexamine the data. Additional data in the lower stratosphere around the ER 2 altitude will be extremely useful in differentiating the lifetimes.

#### 4. IR ABSORPTION DATA AND GREENHOUSE CALCULATION

##### 4.1. Absorption Band Data

SF<sub>6</sub> has been identified, along with CF<sub>4</sub> and C<sub>2</sub>F<sub>6</sub> as one of many man-made species whose concentration may be increasing and may have a greenhouse effect [e.g., Ramanathan *et al.*, 1985]. Measurement was made in the Allied-Signal Laboratory (R. Bray, private communication, 1989) to obtain the spectral absorption coefficient at 0.125 cm<sup>-1</sup> resolution in the spectral region 640–1225 cm<sup>-1</sup> taken at background N<sub>2</sub> pressure of 0.01, 0.1, and 1.0 atmosphere at room temperature. The major band has band limits 915–960 cm<sup>-1</sup>. The spectra in this region for the 0.01 atmosphere background case is shown in Figure 7. The spectra for the other backgrounds are almost identical. The integrated band strength is given in Table 2, together with

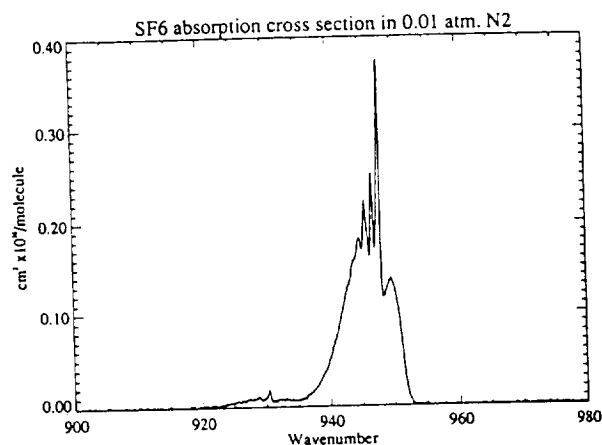


Fig. 7. Absorption cross section of SF<sub>6</sub>.

reported measurements from previous work. The values reported in this work are typically 10 to 20% larger than previous measurements.

##### 4.2. Long-Wave Flux

Because of the small gas concentration in the atmosphere we use the mean absorption coefficient approximation to calculate the radiation flux for the individual absorption bands. In this treatment the layer absorption in the frequency interval  $\Delta n_i$  is approximated by

$$A_i = 1 - \exp(-k_i u)$$

where  $u$  is the gas amount in the layer and  $k_i = S_i/\Delta n_i$  is the mean absorption coefficient over the band with band strength  $S_i$ .

The validity of the mean absorption coefficient approximation can be verified by comparing the results with more detailed calculations employing the high-resolution data. The previous results using molecules with a similar absorption feature suggest that the mean absorption coefficient approximation is a good approximation for concentration up to a few parts per billion by volume (ppbv).

##### 4.3. Greenhouse Effect

The mean absorption coefficients calculated from the spectral data were used in the AER one-dimensional RC model [Wang and Molnar, 1985] to calculate the direct surface warming due to SF<sub>6</sub> with a uniform concentration of 1 ppbv. In the calculation it is assumed that SF<sub>6</sub> does not

TABLE 2. Integrated Band Strength of SF<sub>6</sub>

Reference	Band Strength, cm <sup>-2</sup> atm <sup>-1</sup> at STP
Schatz and Hornig [1953]	4800
Schachtschneider [1960]	4702
Kim <i>et al.</i> [1980]	6072
Brodbeck <i>et al.</i> [1980]	4908
Dunn <i>et al.</i> [1982]	4742
Chapados and Birnbaum [1988]	4845
McDowell <i>et al.</i> [1986]	4729
This study, 0.01 atm N <sub>2</sub> pressure	5898
This study, 0.1 atm N <sub>2</sub> pressure	5456
This study, 1.0 atm N <sub>2</sub> pressure	5425

TABLE 3. Global Warming Potential (GWP) of SF<sub>6</sub> for Various Assumed Lifetimes

Species	Lifetimes, years	GWP		
		20	100	500
CFC 11	55	4500	3400	1400
SF <sub>6</sub>	55	13500	10200	4200
SF <sub>6</sub>	200	15300	17400	14000
SF <sub>6</sub>	2000	16000	21600	33800
SF <sub>6</sub>	5000	16100	21900	37200
SF <sub>6</sub>	∞	16100	22100	38100

affect the concentrations of other greenhouse gases through photochemical interaction. The data with the largest integrated band strength (i.e., data taken at N<sub>2</sub> background of 0.01 atmosphere) was used to calculate the upper limit of the SF<sub>6</sub> greenhouse effect. The results indicate a greenhouse warming of 0.43°C/ppbv, compared to 0.14°C/ppbv for CFC 11 calculated using the same model [Fisher *et al.*, 1990]. The results suggest that on a per parts per billion by volume basis the greenhouse effect is larger than that of CFC 11 by a factor of 3. Note that the calculations do not account for the temperature dependence of absorption data.

Values for the global warming potential (GWP) [see *Intergovernmental Panel on Climate Change* (IPCC), 1990] for different integration time horizons are given in Table 3. Since we are not certain about the lifetime for SF<sub>6</sub>, we have calculated the result for a range of lifetimes. The GWP for CFC 11 is also given in the table for comparison.

#### 5. SCENARIO CALCULATIONS

To assess the potential greenhouse effects from future SF<sub>6</sub> emissions, calculations were made to obtain the equilibrium surface warming for two hypothetical emission scenarios. The emission rates are given in Table 4. In both scenarios 1 and 2 it was assumed that even with growing demand, the atmospheric release rate would stabilize after the year 2000.

TABLE 4. Projected Emission Rate for SF<sub>6</sub> in Kilotons

Year	Scenario 1	Scenario 2
1990	5.5	5.5
1991	5.9	5.9
1992	6.4	6.4
1993	6.4	6.8
1994	6.4	6.8
1995	6.4	6.8
1996	6.4	6.8
1997	6.4	8.2
1998	6.4	9.1
1999	6.4	10
2000	6.8	10
2001	6.8	10
2002	6.8	10
2003	6.8	10
2004	6.8	10
2005	6.8	10
2006	6.8	10
2007	6.8	10
2008	6.8	10
2009	6.8	10
2010*	6.8	10

\*Assume constant after 2010.

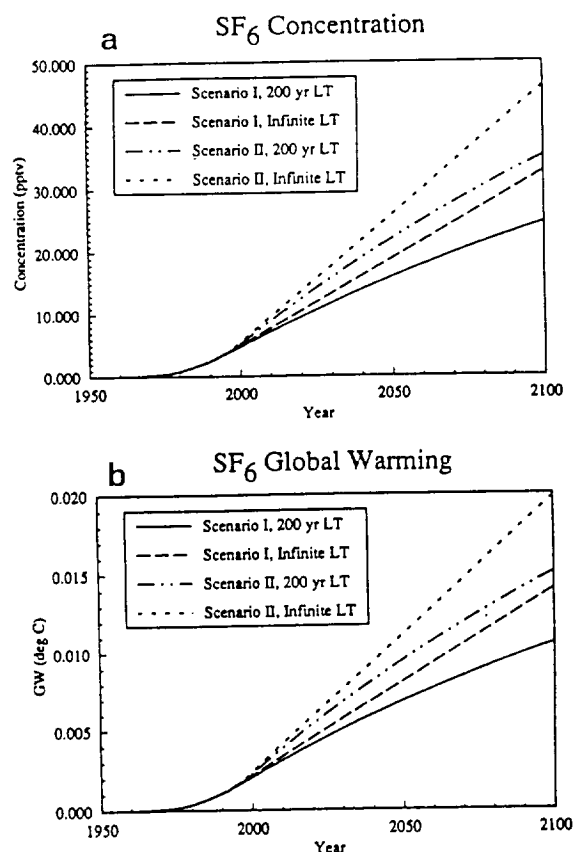


Fig. 8. (a) The calculated surface concentration and (b) equilibrium warming between the years 1950 and 2100 for two emission scenarios as described in Tables 1 and 2. Results are shown for lifetimes of 25,000 years and 200 years.

With improvements in the design of electrical equipment, gas recycling, other conservation measures, and the awareness of potential climate impact, this assumption does not seem unreasonable.

The calculated concentrations between 1950 and 2100 are shown in Figure 8a for two cases corresponding to an effective infinite lifetime (i.e., no removal) and a lifetime of 200 years. The latter case is included for comparison purpose. There is no observational evidence to indicate that the atmospheric lifetime is shorter than 1000 years. The corresponding equilibrium warming given by the product of the concentration and our calculated warming of 0.43°C/ppbv is shown in Figure 8b. The equilibrium warming corresponds to the equilibrium response to the instantaneous forcing due to presence of the greenhouse gas. This is sometimes referred to as the potential realizable warming [see Hansen *et al.*, 1989]. Actual temperature response will be different because of time delay due to the heat capacity of the Earth climate system and the time scale for transport of heat into the deep ocean. The calculated equilibrium warming by 2100 is about .004°C. These values are to be compared with the estimated equilibrium warming for the other trace gases in the same period as summarized in Table 5.

The projected warming due to CO<sub>2</sub> and other trace gases in 2100 is estimated to be between 2°C to 5°C depending on assumed emission [see IPCC, 1990]. The projected SF<sub>6</sub> warming is about 0.02°C.

TABLE 5. Greenhouse Warming Due to Increases in CO<sub>2</sub>, CFC 11, and CFC 12 Between 1950 and 2010

Species	Change in Concentrations	Estimated Warming, °C
CO <sub>2</sub>	300–368 ppmv*	0.82†
CFC 11	0–286 pptv‡	0.04§
CFC 12	0–544 pptv‡	0.11§

\*Based on assumed increase of 0.4%/yr after 1990.

†Based on estimates from Lacis *et al.* (1981).

‡Projected concentrations from the World Meteorological Organization [1990] report based on the assumption that the emissions of CFC 11 and CFC 12 will be reduced to 5% of the current emission rates by the year 2000.

§Based on 0.14°C/ppbv and 0.20°C/ppbv for CFC 11 and CFC 12, respectively.

## 6. CONCLUDING REMARKS

The atmospheric lifetime of SF<sub>6</sub> due to photochemical removal by any known mechanism is estimated to be longer than a thousand years. However, lifetime as short as 200 years cannot be ruled out immediately based on the limited measured tropospheric concentrations and emission rates. Based on stratospheric measurements obtained in the 1970s, a lifetime similar to that of CFC 11 has been suggested [Krey *et al.*, 1977]. This appears to be unlikely based on preliminary analysis of more recent stratospheric data. Refinement of worldwide emission data together with additional measurement of SF<sub>6</sub> in the lower stratosphere and/or long-term monitoring from ground-based stations will be useful in reducing the uncertainty associated with the lifetime and will provide a more accurate determination of the global warming potential. However, based on the experience of the Atmospheric Lifetime Experiment-Global Atmospheric Gases Experiment (ALE-GAGE) program [Cunnold *et al.*, 1983, 1986], this may require monitoring over a time period of the order of half the expected lifetime.

The infrared absorption cross section of SF<sub>6</sub> is reported and found to be in good agreement with previously reported band strengths. Calculations showed that SF<sub>6</sub> is 3 times more effective as a greenhouse gas compared to CFC 11 on a per molecule basis. However, based on projected emission scenarios, the calculated concentration is small. The expected warming from SF<sub>6</sub> through 2010 is small (0.004°C) compared to the warming from CO<sub>2</sub> and other trace gases (0.8°C).

The discussion presented here illustrates a multidiscipline approach in which the laboratory kinetic data, emission information from the manufacturers, and field measurements are interpreted in the context of the present-day atmosphere. This approach could be used to evaluate other greenhouse gases. The utility and limitation of this method will depend on the quality of the data for each individual species.

**Acknowledgments.** We thank Carl Howard for discussion on the estimates for the reactions of OH and O(<sup>1</sup>D) with SF<sub>6</sub>. Work at AER was funded by Allied-Signal Incorporated and NASA NASW-4428.

## REFERENCES

- Brodbeck, C., I. Rossi, H. Strapelias, and J.-P. Bouanich, Infrared spectral absorption intensities in the  $\nu_3$  and  $\nu_4$  regions of SF<sub>6</sub>, *Chem. Phys.*, **54**, 1–7, 1980.
- Butler, J. H., J. W. Elkins, T. M. Thompson, B. D. Hall, T. H. Swanson, and V. Koropalov, Oceanic consumption of CH<sub>3</sub>CCl<sub>3</sub>: Implications for tropospheric OH, *J. Geophys. Res.*, **96**, 22,347–22,355, 1991.
- Chapados, C., and G. Birnbaum, Infrared absorption of SF<sub>6</sub> from 32 to 3000 cm<sup>-1</sup> in the gaseous and liquid states, *J. Mol. Spectrosc.*, **132**, 323–351, 1988.
- Cicerone, R. J., Atmospheric carbon tetrafluoride: A nearly inert gas, *Science*, **206**, 59–61, 1979.
- Cunnold, D. M., R. G. Prinn, R. A. Rasmussen, P. G. Simmonds, F. N. Alyea, A. J. Crawford, P. J. Fraser, and R. D. Rosen, The atmospheric lifetime experiment, 3, Lifetime methodology and application to 3 years of CFCl<sub>3</sub> data, *J. Geophys. Res.*, **88**, 8379–8400, 1983.
- Cunnold, D. M., R. G. Prinn, R. A. Rasmussen, P. G. Simmonds, F. N. Alyea, C. A. Cardelino, A. J. Crawford, P. J. Fraser, and R. D. Rosen, Atmospheric lifetime and annual release estimates for CFCl<sub>3</sub> and CF<sub>2</sub>Cl<sub>2</sub> from 5 years of Atmospheric Lifetime Experiment data, *J. Geophys. Res.*, **91**, 10,797–10,817, 1986.
- Drivas, P. J., and F. H. Shair, A tracer study of pollutant transport and dispersion in the Los Angeles area, *Atmos. Environ.*, **8**, 1155–1163, 1974.
- Dunn, D. S., K. Scanlon, and J. Overend, The absolute intensities of the binary combination bands in the infrared spectrum of sulfur hexafluoride, *Spectrochim. Acta, Part A*, **38**, 841–847, 1982.
- Fershenfeld, F. C., Ion chemistry of SF<sub>6</sub>, *J. Chem. Phys.*, **54**, 438, 1971.
- Fisher, D. A., C. H. Hales, W.-C. Wang, M. K. W. Ko, and N. D. Sze, Model calculations of the relative effects of CFCs and their replacements on global warming, *Nature*, **344**, 513–516, 1990.
- Hansen, J., A. Lacis, and M. Prather, Greenhouse effect of chlorofluorocarbons and other trace gases, *J. Geophys. Res.*, **94**, 16,417–16,421, 1989.
- Hartmann, D. L., K. R. Chan, B. L. Gary, M. R. Schoeberl, P. A. Newman, R. L. Martin, M. Loewenstein, J. R. Podolske, and S. E. Strahan, Potential vorticity and mixing in the south polar vortex during spring, *J. Geophys. Res.*, **94**, 11,625–11,640, 1989.
- Hertzberg, G., *Molecular and Spectra and Molecular Structure, vol. 1, Spectra of Polyatomic Molecules*, 2nd ed., Van Nostrand Reinhold, New York, 1966.
- Intergovernmental Panel on Climate Change, World Meteorological Organization, *Climate Change: The IPCC Scientific Assessment*, edited by J. T. Houghton, G. J. Jenkins, and J. J. Ephraums, pp. iii–364, Cambridge University Press, New York, 1990.
- Kaye, J., and S. Penkett (Eds.), Report on concentrations, lifetimes and trends of CFCs, halons, and related species, *NASA Tech. Rep.*, in press, 1993.
- Kim, K., R. S. McDowell, and W. T. King, Integrated infrared intensities and transition moments in SF<sub>6</sub>, *J. Chem. Phys.*, **73**, 36–41, 1980.
- Ko, M. K. W., N. D. Sze, and D. K. Weisenstein, The use of satellite data to constrain the model-calculated atmospheric lifetime for N<sub>2</sub>O: Implications for other trace gases, *J. Geophys. Res.*, **96**, 7547–7552, 1991.
- Krey, P. W., R. J. Lagomarsino, L. E. Toonkel, and M. Schonberg, Atmospheric residence time of SF<sub>6</sub>, *Rep. HASL-302*, pp. 1–50–1–57, U.S. Energy Res. and Dev. Admin., New York, 1976.
- Krey, P. W., R. J. Lagomarsino, and L. E. Toonkel, Gaseous halogens in the atmosphere in 1975, *J. Geophys. Res.*, **82**, 1753–1766, 1977.
- Lacis, A., J. Hansen, P. Lee, T. Mitchell, and S. Lebedeff, Greenhouse effect of trace gases, *Geophys. Res. Lett.*, **8**, 1035–1038, 1981.
- Leifer, R., R. Larsen, and L. Toonkel, Trends in stratospheric concentrations of trace gases in the northern hemisphere during the years 1974–1979, *Geophys. Res. Lett.*, **9**, 755–758, 1982.
- MacNeal, J. R., T. P. Rack, and R. R. Corns, Process for degassing aluminum melts with sulfur hexafluoride, U.S. Pat. Off. patent no. 4,959,101, Washington, D. C., Sept. 25, 1990.
- McDowell, R. S., B. J. Krohn, H. Flicker, and M. Vasquez, Vibrational levels and anharmonicity in sulfur hexafluoride, I, Vibrational band analysis, *Spectrochim. Acta, Part A*, **42**, 351–369, 1986.
- Plumb, R. A., and M. K. W. Ko, Interrelationships between mixing ratios of long-lived stratospheric constituents, *J. Geophys. Res.*, **97**, 10,145–10,156, 1992.

- Prinn, R. G., P. G. Simmonds, R. A. Rasmussen, R. D. Rosen, F. N. Alyea, C. A. Cardelino, A. J. Crawford, D. M. Cunnold, P. J. Fraser, and J. E. Lovelock, The atmospheric lifetime experiment, I, Introduction, instrumentation, and overview, *J. Geophys. Res.*, **88**, 8353–8367, 1983.
- Ramanathan, V., R. J. Cicerone, H. B. Singh, and J. T. Kiehl, Trace gas trends and their potential role in climate change, *J. Geophys. Res.*, **90**, 5547–5566, 1985.
- Ramanathan, V., et al., Climate-chemical interactions and effects of changing atmospheric trace gases, *Rev. Geophys.*, **25**, 1441–1482, 1987.
- Rasmussen, R. A., and M. A. K. Khalil, Rare trace gases at the South Pole, *Antarct. J. U.S.*, **18**, 250–252, 1983.
- Rasmussen, R. A., M. A. K. Khalil, and R. W. Dalluge, Atmospheric trace gases in Antarctica, *Science*, **211**, 285–287, 1981.
- Ravishankara, A. R., S. Solomon, A. A. Turnipseed, and R. F. Warren, Atmospheric lifetimes of long-lived species, *Science*, **259**, 194–199, 1993.
- Rinsland, C. P., L. R. Brown, and C. B. Farmer, Infrared spectroscopic detection of sulfur hexafluoride (SF<sub>6</sub>) in the lower stratosphere and upper troposphere, *J. Geophys. Res.*, **95**, 5577–5585, 1990a.
- Rinsland, C. P., A. Goldman, F. J. Murcray, R. D. Blatherwick, J. J. Kusters, D. G. Murcray, N. D. Sze, and S. T. Massie, Long-term trends in the concentrations of SF<sub>6</sub>, CHClF<sub>2</sub>, and COF<sub>2</sub> in the lower stratosphere from analysis of high-resolution infrared solar occultation spectra, *J. Geophys. Res.*, **95**, 16,477–16,490, 1990b.
- Schachtschneider, J. H., Simultaneous transitions and intermolecular forces, dissertation, Univ. of Minn. at Minneapolis, St. Paul, 1960.
- Schatz, P. N., and D. F. Hornig, Bond moments and derivatives in CF<sub>4</sub>, SiF<sub>4</sub>, and SF<sub>6</sub> from infrared intensities, *J. Chem. Phys.*, **21**, 1516–1530, 1953.
- Schoeberl, M. R., et al., Reconstruction of the constituent distribution and trends in the Antarctic polar vortex from ER-2 flight observations, *J. Geophys. Res.*, **94**, 16,815–16,845, 1989.
- Singh, H. B., L. J. Salas, and L. A. Cavanagh, Distribution, sources and sinks of atmospheric halogenated compounds, *J. Air Pollut. Control Assoc.*, **27**, 333–336, 1977.
- Singh, H. B., L. J. Salas, H. Shigeishi, and E. Scribner, Atmospheric halocarbons, hydrocarbons, and sulfur hexafluoride: Global distributions, sources, and sinks, *Science*, **203**, 899–903, 1979.
- Singh, H. B., L. J. Salas, and R. E. Stiles, Selected man-made halogenated chemicals in the air and oceanic environment, *J. Geophys. Res.*, **88**, 3675–3683, 1983.
- Vandeborgh, B., J. Kretzschmar, and T. Rymen, On the use of SF<sub>6</sub> tracer releases for the determination of fugitive emissions, in *Proceedings of Second European Symposium on Physico-Chemical Behaviour of Atmospheric Pollutants, Varese, Italy, 29 September–1 October, 1981*, edited by B. Versino and H. Ott, pp. 517–523, D. Reidel, Norwell, Mass., 1982.
- Wang, W.-C., and G. Molnar, A model study of the greenhouse effects due to increasing atmospheric CH<sub>4</sub>, N<sub>2</sub>O, CF<sub>2</sub>Cl<sub>2</sub>, and CFC<sub>13</sub>, *J. Geophys. Res.*, **90**, 12,971–12,980, 1985.
- Watson, A. J., and M. I. Liddicoat, Recent history of atmospheric trace gas concentrations deduced from measurements in the deep sea: Application to sulfur hexafluoride and carbon tetrachloride, *Atmos. Environ.*, **19**, 1477–1484, 1985.
- Weissenstein, D. K., M. K. W. Ko, and N. D. Sze, The chlorine budget of the present-day atmosphere: A modeling study, *J. Geophys. Res.*, **97**, 2547–2559, 1992.
- Wine, P. H., and W. L. Chameides, Possible atmospheric lifetimes and chemical reaction mechanisms for selected HCFCs, HFCs, CH<sub>3</sub>CCl<sub>3</sub>, and their degradation products against dissolution and/or degradation in seawater and cloudwater, Appendix, AFEAS report, in *Scientific Assessment of Stratospheric Ozone*, vol. 2, Rep. 20, pp. 273–295, Global Ozone Res. and Monit. Proj., World Meteorol. Organ., Geneva, 1989.
- World Meteorological Organization (WMO), Scientific assessment of stratospheric ozone: 1989, Rep. 20, Global Ozone Res. and Monit. Project, Geneva, 1990.
- Zander, R., C. P. Rinsland, and P. Demoulin, Infrared spectroscopic measurements of the vertical column abundance of sulfur hexafluoride, SF<sub>6</sub>, from the ground, *J. Geophys. Res.*, **96**, 15,447–15,454, 1991.
- A. Goldman, D. G. Murcray, and F. J. Murcray, Department of Physics, University of Denver, Denver, CO 80208.
- M. K. W. Ko and N. D. Sze, Atmospheric and Environmental Research, Incorporated, 840 Memorial Drive, Cambridge, MA 02139.
- C. P. Rinsland, Atmospheric Science Center, NASA Langley Research Center, Hampton, VA 23681.
- G. Shia, Buffalo Research Laboratory, Allied-Signal Incorporated, Buffalo, NY 14210.
- W.-C. Wang, State University at New York, 100 Fuller Road, Albany, NY 12205.

(Received August 22, 1992;  
revised January 15, 1993;  
accepted January 22, 1993.)





# MT. PINATUBO SO<sub>2</sub> COLUMN MEASUREMENTS FROM MAUNA LOA

A. Goldman,<sup>1</sup> F. J. Murcray,<sup>1</sup> C. P. Rinsland,<sup>2</sup> R. D. Blatherwick,<sup>1</sup>  
S. J. David,<sup>1</sup> F. H. Murcray,<sup>1</sup> and D. G. Murcray<sup>1</sup>

**Abstract.** Absorption features of the  $\nu_1$  band of SO<sub>2</sub> have been identified in high resolution infrared solar absorption spectra recorded from Mauna Loa, Hawaii, on July 9 and 12, 1991, shortly after the arrival of the first eruption plume from the Mt. Pinatubo volcano in the Philippines. A total SO<sub>2</sub> vertical column amount of  $(5.1 \pm 0.5) \times 10^{16}$  molecules cm<sup>-2</sup> on July 9 has been retrieved based on nonlinear least-squares spectral fittings of 9 selected SO<sub>2</sub> absorption features with an updated set of SO<sub>2</sub> spectral parameters. A SO<sub>2</sub> total column upper limit of  $0.9 \times 10^{16}$  molecules cm<sup>-2</sup> deduced from measurements on September 20-24, 1991, is consistent with the dispersion of the SO<sub>2</sub> cloud and the rapid conversion of the SO<sub>2</sub> vapor into volcanic aerosol particles.

## Introduction

Lidar observations at Mauna Loa Observatory (MLO), Hawaii, indicate the initial arrival of the Mount Pinatubo volcanic plume above that station on July 1, 1991, followed by 3 generalized pulses or waves on approximately July 3, July 24, and August 9 [DeFoor et al., 1991]. Fortuitously, we recorded broadband IR solar spectra on July 9-12, 1991, shortly after the arrival of the first pulse. These observations provided a rare opportunity to measure a number of molecular constituents during the early phases of the evolution of massive volcanic plume. The present paper reports quantitative analysis of SO<sub>2</sub> absorption features identified in these spectra. Additional observations from MLO recorded on May 11 and September 20-24, 1991, show no detectable SO<sub>2</sub> features, and are analyzed to obtain SO<sub>2</sub> total column upper limits.

## Observations and Analysis

Table 1 summarizes the observations from MLO (19.53°N, 155.58°W, altitude 3400 m) analyzed in this work. The solar spectra were recorded with a Bomem model DA3.002 Michelson interferometer system capable of operating at resolutions up to 0.002 cm<sup>-1</sup> (full width half maximum instrumental line shape). The observing runs were conducted as part of an effort to obtain a baseline of measurements at MLO for the Network for the Detection of Stratospheric Change (NDSC) [Kurylo, 1991]. Daily NDSC IR solar measurements are anticipated to commence at MLO next year.

<sup>1</sup> Department of Physics, University of Denver

<sup>2</sup> ASD, NASA Langley Research Center

Numerous features of the  $\nu_1$  band of SO<sub>2</sub> (centered at 1157.71 cm<sup>-1</sup>) have been identified between 1150 and 1190 cm<sup>-1</sup> in the July solar spectra. Figure 1 shows several of these features in the 1154- and 1162-cm<sup>-1</sup> regions. The features are marked by symbols beneath a spectrum from July 9 (top scan), but they are absent in the spectra from May 11 (middle scan) and September 22 (bottom scan). Transitions of O<sub>3</sub> and N<sub>2</sub>O are also identified in Figure 1. Note that the SO<sub>2</sub> and O<sub>3</sub> lines are narrow, indicating maximum concentrations in the layers of low pressure broadening (i.e., the upper atmosphere). The  $\nu_1$  band is about one order of magnitude weaker in intensity than the  $\nu_3$  band, which is the strongest SO<sub>2</sub> band in the infrared. Unfortunately, the  $\nu_3$  band (centered at 1362.06 cm<sup>-1</sup>) is strongly masked from the ground because of strong attenuation by water vapor and methane absorption. Features of the SO<sub>2</sub>  $\nu_3$  and  $\nu_1$  bands have been identified in airborne solar absorption spectra of the Mt. Pinatubo plume recorded on July 8-14, 1991, over the Caribbean [Mankin et al., 1991]. Features of the  $\nu_3$  band were used in the retrievals of the aircraft spectra.

Improved spectroscopic parameters for the SO<sub>2</sub>  $\nu_1$  band have been generated for this investigation. The line positions were computed from the work of Guelachvili et al. [1984, 1987]. The new line positions are accurate to 0.0004 cm<sup>-1</sup> and differ by 0.003 cm<sup>-1</sup> from the values on the 1986 HITRAN database [Rothman et al., 1987]. The band intensity of  $3.519 \times 10^{-18}$  cm<sup>-1</sup>/(molecule cm<sup>-2</sup>) at 296 K on the 1986 HITRAN compilation [Rothman et al., 1987] has been retained since no clear revision could be noted based on the published papers (summarized by Smith et al. [1985]). The same positions and band intensity have also been assumed on the 1991 HITRAN compilation (L. S. Rothman, manuscript in preparation, 1991). As a first approximation, we adopted a constant air-broadening coefficient of 0.13 cm<sup>-1</sup> atm<sup>-1</sup> at 296 K based on averages of the measurements of Hinkley et al. [1972] and the theoretical calculations of Tejwani [1972a,b]. The calculations of Tejwani [1972a,b] and recent tunable diode laser measurements [Kuhnemann et al., 1991] indicate that the air-broadening coefficients generally decline with increasing  $J$  quantum number; incorporation of this decrease will be considered in the next line parameters compilation update. Most of the SO<sub>2</sub> line groups used here for the spectral quantification have ground state energies in the range of 20-300 cm<sup>-1</sup>, which correspond to less than 1% intensity change per 1K at stratospheric temperatures. The integrated lines absorption is small and thus insensitive to the halfwidths. The lines of the SO<sub>2</sub>  $\nu_1$  band are located in a region of relatively strong atmospheric absorption by O<sub>3</sub>, H<sub>2</sub>O, N<sub>2</sub>O, HDO, and CH<sub>4</sub> lines. Hence, accurate spectroscopic parameters for these gases were also required in the analysis. We adopted the spectroscopic parameters from the 1991 HITRAN compilation (L. S. Rothman, manuscript in preparation, 1991) for these gases.

Copyright 1992 by the American Geophysical Union.

Paper number 92GL00073  
0094-8534/92/92GL-00073\$03.00

TABLE 1. Summary of Results

Observation Date (of 1991)	Spectral Resolution (cm <sup>-1</sup> )	SO <sub>2</sub> Vertical Column Amount (in 10 <sup>16</sup> molecules cm <sup>-2</sup> )
May 11	0.004	< 0.9
July 9	0.010	(5.1 ± 0.5)
September 20-24	0.004	< 0.9

The improvements in the quality of the O<sub>3</sub> parameters [Flaud et al., 1990a,b] were particularly important for accurate fitting of the spectra. Thus, all the spectral features are well modeled in the simultaneous fitting of SO<sub>2</sub> and the other trace gases.

The SO<sub>2</sub> total columns were retrieved with a nonlinear least-squares spectral fitting algorithm [cf. Rinsland et al., 1991a,b]. The total vertical column amount of a gas is retrieved from a spectrum by scaling an assumed relative

volume mixing ratio (VMR) profile by a single multiplicative factor for all altitudes, which is iteratively adjusted along with the values of a number of instrumental parameters (e.g., a wavenumber shift between the measured and calculated spectra) until the sum of the squares of the residuals (measured minus calculated signals) is minimized. The total column amount is calculated by summing the scaled vertical absorber column amounts in all layers.

The reference volume mixing ratio profiles reported by Smith [1982] were assumed in our analysis. The profile for SO<sub>2</sub> is a background profile corresponding to a SO<sub>2</sub> total column above MLO of  $1.1 \times 10^{15}$  molecules cm<sup>-2</sup>, well below our detection limit (see below). The Mauna Loa lidar measurements of DeFoor et al. [1991] indicate that the Pinatubo aerosols in early July were confined to a narrow altitude band in the lower stratosphere. We assumed that the SO<sub>2</sub> was co-located with the aerosols and approximated the SO<sub>2</sub> plume by a 4-km thick layer centered at 20 km based on the lidar profiles presented in Figure 2 of DeFoor et al. [1991]. The VMR of SO<sub>2</sub> was assumed constant in this layer. Tests indicate that the retrieved total columns are dominated by the stratospheric layer and are insensitive to realistic changes in the assumed altitude and vertical thickness of the Pinatubo SO<sub>2</sub> layer. Since the local 100%

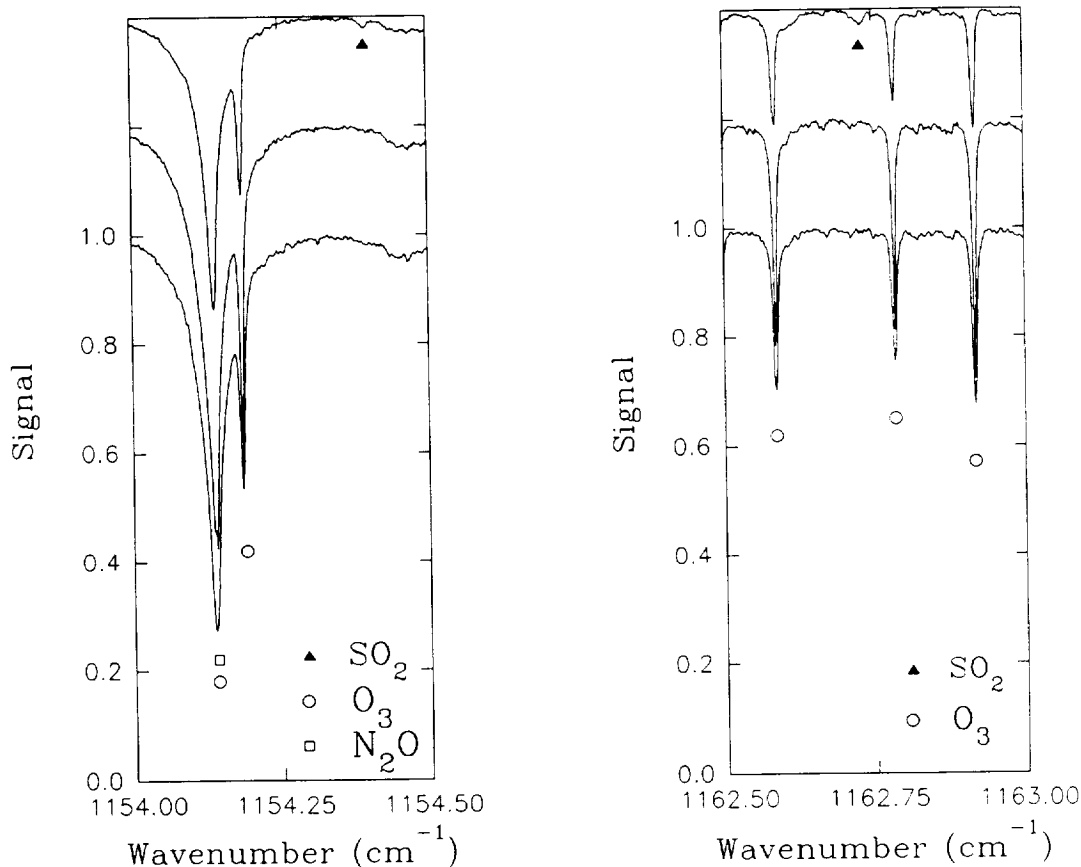


Fig. 1. Comparison of three infrared solar absorption spectra recorded at MLO. The dates (of 1991), solar astronomical zenith angles, and FWHM resolutions of the spectra are July 9, 46.5°, and 0.01 cm<sup>-1</sup> (top); May 11, 68.1°, and 0.004 cm<sup>-1</sup> (middle), and September 22, 66.2°, and 0.004 cm<sup>-1</sup> (bottom). Solid triangles mark indicate SO<sub>2</sub> features in the July 9 spectrum. Features of O<sub>3</sub> and N<sub>2</sub>O are also identified. The scans are offset vertically for clarity.

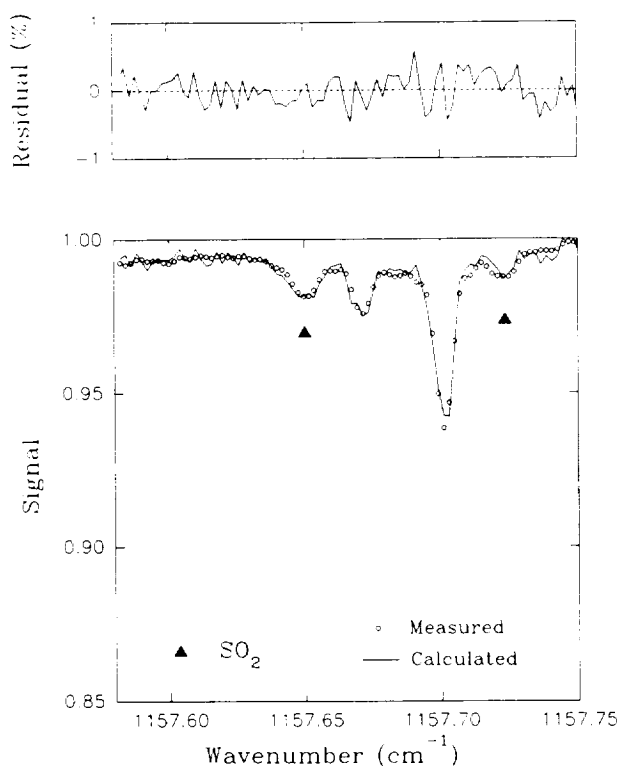


Fig. 2. Sample least-squares fit to the 46.5° solar zenith angle spectrum from July 9, 1991. The signals in the lower panel are normalized to the highest amplitude in the interval. Residuals are measured minus calculated values on an expanded vertical scale. Features of SO<sub>2</sub> are marked; the other absorptions are produced by O<sub>3</sub> lines.

transmission level is retrieved in the fitting procedure, the retrievals are not affected by the broad band attenuation of aerosols from the eruption.

Figure 2 illustrates a typical least-squares fit from a spectrum recorded on July 9 (the best out of the few available scans). The average of the total columns retrieved from nine narrow ( $<0.3 \text{ cm}^{-1}$  wide) intervals between 1154 and 1180  $\text{cm}^{-1}$  was adopted as the final result. An absolute uncertainty (1 sigma) of 10% was computed from the root-sum-square of the following error sources and their magnitudes: (1) SO<sub>2</sub> spectroscopic line parameters uncertainties ( $\pm 5\%$ ), (2) uncertainty in the assumed SO<sub>2</sub> vertical distribution ( $\pm 3\%$ ), (3) temperature profile uncertainties ( $\pm 2\%$ ), (4) interferences from other molecules ( $\pm 3\%$ ), and (5) instrumental effects (zero level offsets, instrument line shape uncertainties, etc.) ( $\pm 7\%$ ). The upper limits for the May and September observations were derived by increasing the SO<sub>2</sub> VMR in the 4-km thick stratospheric layer until features more than 3 times the RMS noise level of the measured spectra were produced in simulations generated for the same conditions.

### Results and Discussion

The retrieved total columns and upper limits are given in Table 1. The July 9 SO<sub>2</sub> vertical total column of  $5.1 \times 10^{16}$

molecules  $\text{cm}^{-2}$  (1.9 Dobson units) corresponds to a mean SO<sub>2</sub> VMR in the assumed 4-km thick stratospheric layer of 66 ppbv (parts per billion by volume). This value provides a clear indication of the high average SO<sub>2</sub> concentrations in the plume above Mauna Loa at the time of our measurements; background SO<sub>2</sub> VMRs measured in the lower stratosphere are  $\sim 100$  times less [Inn et al., 1981]. The SO<sub>2</sub> features were also seen in spectra recorded on July 12, but the reduced signal-to-noise ratio of the available data preclude an accurate measurement of the SO<sub>2</sub> total column. The total column upper limit of  $0.9 \times 10^{16}$  molecules  $\text{cm}^{-2}$  derived from the September 20 to 24 observations is a factor of 6 lower than the July 9 measurement. The absence of observable SO<sub>2</sub> in September is attributed to the rapid dispersion of the gas cloud and the rapid conversion of SO<sub>2</sub> into aerosols. Bluth et al. [1991] used TOMS measurements of SO<sub>2</sub> to estimate that the total amount SO<sub>2</sub> had declined by one third 14 days after the Pinatubo eruption.

The strong inhomogeneities and the rapid temporal changes in the plume indicated by lidar [DeFoor et al., 1991; Winker and Osborne, 1991] and SAGE II measurements [McCormick and Veiga, 1991] obtained during July indicate the difficulties inherent in comparing our SO<sub>2</sub> measurement with those obtained in the Caribbean during the same time period. Nevertheless, our measurement is close to the total columns of  $2.0 \times 10^{16}$  to  $3.7 \times 10^{16}$  molecules  $\text{cm}^{-2}$  obtained using IR solar absorption spectroscopy [Mankin et al., 1991]. The mean SO<sub>2</sub> column of 2.5 Dobson units derived from measurements with a differential, vertically-looking UV correlation spectrometer [Hoff, 1991] is also in good agreement with our result.

A set of simulations were generated to search for absorption features of the H<sub>2</sub>S  $\nu_2$  band in the window region between 1210 and 1250  $\text{cm}^{-1}$ . These calculations were based on the H<sub>2</sub>S line parameters from the 1984 GEISA compilation [Husson et al., 1986]. No H<sub>2</sub>S features were found above the noise level of the spectra, and an upper limit of  $2 \times 10^{17}$  molecules  $\text{cm}^{-2}$  has been estimated from the 46.46° solar zenith angle spectrum recorded on July 9, 1991. The upper limit is very high because the H<sub>2</sub>S  $\nu_2$  band is weak.

The results of this study have shown that high resolution ground-based IR observations can be used to measure SO<sub>2</sub> total columns from large volcanic plumes. While the sensitivity of the technique is not particularly high for SO<sub>2</sub> (only total columns above  $1 \times 10^{16}$  molecules  $\text{cm}^{-2}$  are readily measurable), the regular series of observations planned at the NDSC stations might allow future large events to be monitored. Such measurements, especially if combined by simultaneous lidar observations from the same site, could be valuable for studying the conversion of SO<sub>2</sub> into stratospheric aerosols. The IR observations of SO<sub>2</sub> could also be used to verify the calibration of SO<sub>2</sub> measurements by satellite instruments, such as TOMS.

**Acknowledgments.** Research at the University of Denver was supported by NASA and NSF. Acknowledgment is made to the National Center for Atmospheric Research, which is supported by NSF, for computer time used in this research.

## References

- Bluth, G., S. Doiron, C. Schnetzler, L. Walter, and A. Krueger, Global tracking of the June, 1991 Mount Pinatubo eruption clouds, *Geophys. Res. Lett.*, this issue, 1991.
- DeFoor, T. E., E. Robinson, and S. Ryan, Early lidar observations of the June 1991 Pinatubo eruption plume at Mauna Loa Observatory, Hawaii, *Geophys. Res. Lett.*, this issue, 1991.
- Flaud, J.-M., C. Camy-Peyret, C. P. Rinsland, M. A. H. Smith, and V. Malathy Devi, "Atlas of Ozone Spectral Parameters from Microwave to Medium Infrared," Academic Press, Boston, MA, 1990a.
- Flaud, J.-M., C. Camy-Peyret, C. P. Rinsland, V. Malathy Devi, M. A. H. Smith, and A. Goldman, Improved line parameters for ozone bands in the 10- $\mu$ m region, *Appl. Opt.*, **29**, 3667-3671, 1990b.
- Guelachvili, G., O. N. Ulenikov, and G. A. Ushakova, Analysis of the  $\nu_1$  and  $\nu_3$  absorption bands of  $^{32}\text{S}^{16}\text{O}_2$ , *J. Mol. Spectrosc.*, **108**, 1-5, 1984.
- Guelachvili, G., O. V. Naumenko, and O. N. Ulenikov, Analysis of the SO<sub>2</sub> absorption Fourier spectrum in regions 1055 to 2000 and 2200 to 2550 cm<sup>-1</sup>, *J. Mol. Spectrosc.*, **125**, 128-139, 1987.
- Hinkley, E. D., A. R. Calawa, P. L. Kelley, and S. A. Clough, Tunable-laser spectroscopy of the  $\nu_1$  band of SO<sub>2</sub>, *J. Appl. Phys.*, **43**, 3222-3224, 1972.
- Hoff, R. M., Differential SO<sub>2</sub> column measurements of the Mt. Pinatubo volcanic plume, *Geophys. Res. Lett.*, this issue, 1991.
- Husson, N., A. Chedin, N. A. Scott, D. Bailly, G. Graner, N. Lacome, A. Levy, C. Rossetti, G. Tarrago, C. Camy-Peyret, J. M. Flaud, A. Bauer, J. M. Colmont, N. Monnanteuil, J. C. Hilico, G. Pierre, M. Loete, J. P. Champion, L. S. Rothman, L. R. Brown, G. Orton, P. Varanasi, C. P. Rinsland, M. A. H. Smith and A. Goldman, The GEISA spectroscopic line parameters data bank in 1984, *Ann. Geophys.*, **4**, A, 185-190, 1986.
- Inn, E. C. Y., J. F. Vedder, and D. O. O'Hara, Measurement of stratospheric sulfur constituents, *Geophys. Res. Lett.*, **8**, 5-8, 1981.
- Kurylo, M. J., Network for the detection of stratospheric change, *SPIE*, **1491**, 168-174, 1991.
- Kuhnemann, F., Y. Heiner, B. Sumpf, and Ka. Herrmann, Line broadening in the  $\nu_3$  band of SO<sub>2</sub> studied with diode laser spectroscopy, *J. Mol. Spectrosc.*, in press, 1991.
- Mankin, W. G., M. T. Coffey, and A. Goldman, Airborne observations of SO<sub>2</sub>, HCl, and O<sub>3</sub> in the stratospheric plume of the Pinatubo volcano in July 1991, *Geophys. Res. Lett.*, this issue, 1991.
- McCormick, M. P., and R. E. Veiga, SAGE II measurements of early Pinatubo aerosols, *Geophys. Res. Lett.*, this issue, 1991.
- Rinsland, C. P., R. Zander, and P. Demoulin, Ground-based infrared measurements of HNO<sub>3</sub> total column abundances: Long-term trend and variability, *J. Geophys. Res.*, **96**, 9379-9389, 1991a.
- Rinsland, C. P., J. S. Levine, A. Goldman, N. D. Sze, M. K. W. Ko, and D. W. Johnson, Infrared measurements of HF and HCl total column abundances above Kitt Peak, 1977-1990: Seasonal cycles, long-term increases, and comparisons with model calculations, *J. Geophys. Res.*, **96**, 15,523-15,540, 1991b.
- Rothman, L. S., R. R. Gamache, A. Goldman, L. R. Brown, R. A. Toth, H. M. Pickett, R. L. Poynter, J.-M. Flaud, C. Camy-Peyret, A. Barbe, N. Husson, C. P. Rinsland, and M. A. H. Smith, The HITRAN database: 1986 edition, *Appl. Opt.*, **26**, 4058-4097, 1987.
- Smith, M. A. H., Compilation of atmospheric gas concentration profiles from 0 to 50 km, NASA Tech. Memo., TM 83289, 1982. (Available as NTIS 82N22822 from the Natl. Tech. Inf. Serv., Springfield, Va.)
- Smith, M. A. H., C. P. Rinsland, B. Fridovich, and K. Narahari Rao, Intensities and collision broadening parameters from infrared spectra, Chap. 3 in *Molecular Spectroscopy: Modern Research*, Vol. III, K. Narahari Rao, editor, Academic Press, 1985.
- Tejwani, G. D. T., Computed linewidths of SO<sub>2</sub>, research report no. UTPA-ERAL-02, November 1972, Department of Physics and Astronomy, University of Tennessee, Knoxville, 1972a.
- Tejwani, G. D. T., Calculation of pressure-broadened linewidths of SO<sub>2</sub> and NO<sub>2</sub>, *J. Chem. Phys.*, **57**, 4676-4681, 1972b.
- Winker, D. M., and M. T. Osborn, Airborne lidar observations of the Pinatubo volcanic plume, *Geophys. Res. Lett.*, this issue, 1991.
- A. Goldman, F. J. Murcray, R. D. Blatherwick, S. J. David, F. H. Murcray, and D. G. Murcray, Department of Physics, University of Denver, Denver, CO 80208.
- C. P. Rinsland, Atmospheric Sciences Division, NASA Langley Research Center, Hampton, VA 23665

(Received: October 21, 1991;

Accepted: December 2, 1991)



## The Fundamental Quadrupole Band of $^{14}\text{N}_2$ : Line Positions from High-Resolution Stratospheric Solar Absorption Spectra

The purpose of this note is to report accurate measurements of the positions of *O*- and *S*-branch lines of the (1-0) vibration-rotation quadrupole band of molecular nitrogen ( $^{14}\text{N}_2$ ) and improved Dunham coefficients derived from a simultaneous least-squares analysis of these measurements and selected infrared and far infrared data taken from the literature. The new measurements have been derived from stratospheric solar occultation spectra recorded with Fourier transform spectrometer (FTS) instruments operated at unapodized spectral resolutions of 0.002 and 0.01  $\text{cm}^{-1}$ .

The motivation for the present investigation is the need for improved  $\text{N}_2$  line parameters for use in IR atmospheric remote sensing investigations. The *S* branch of the  $\text{N}_2$  (1-0) quadrupole band is ideal for calibrating the line-of-sight airmasses of atmospheric spectra since the strongest lines are well placed in an atmospheric window, their absorption is relatively insensitive to temperature and is moderately strong (typical line center depths of 10 to 50% in high-resolution ground-based solar spectra and in lower stratospheric solar occultation spectra), and the volume mixing ratio of nitrogen is constant in the atmosphere and well known. However, a recent investigation has shown the need to improve the accuracies of the  $\text{N}_2$  line positions, intensities, air-broadened half-widths, and their temperature dependences to fully exploit this calibration capability (1). The present investigation addresses the problem of improving the accuracy of the  $\text{N}_2$  line positions.

Nitrogen is a homonuclear diatomic molecule, and therefore electric dipole pure rotation and vibration-rotation transitions within the  $^1\Sigma_g^+$  ground electronic state are forbidden. For this reason, the vibrational and rotational constants of the ground electronic state have remained poorly determined with most of the reported values derived from medium-resolution Raman spectra recorded in the far infrared (2-4) and infrared (3-5) regions. Reuter *et al.* (6) used a White cell to achieve an absorption path length of 434 m and a FTS to obtain measurements of line positions in the *O* and *S* branches of the (1-0) vibration-rotation quadrupole band. The positions derived in Ref. (6) were significantly more precise than achieved previously, and the use of standard IR calibration techniques yielded a wavenumber calibration superior to those of the Raman investigations. Measurements with line position accuracies of 0.003 to 0.010  $\text{cm}^{-1}$  were reported from analysis of a spectrum recorded at 0.01- $\text{cm}^{-1}$  resolution. The results were limited in accuracy by the weakness of the  $\text{N}_2$  lines in the measured spectrum (maximum line center absorption of a few tenths of one percent).

The stratospheric measurements reported here were obtained from solar spectra recorded during flights by two different instruments. The first set of data was acquired from orbit on April 30-May 1, 1985, by the atmospheric trace molecule spectroscopy (ATMOS) instrument, a high speed FTS operating at an unapodized spectral resolution of 0.01  $\text{cm}^{-1}$  during its first Shuttle mission onboard Spacelab 3. For an overview of the ATMOS instrument and experiment and the Spacelab 3 results, see the review paper by Farmer (7). ATMOS-related data processing and science analysis methods are described in a paper by Norton and Rinsland (8). The other set of measurements was obtained with a FTS achieving an unapodized resolution of 0.002  $\text{cm}^{-1}$  onboard a balloon platform. The instrument is a modified commercial interferometer operated by the atmospheric spectroscopy group at the University of Denver. Solar observations were recorded both prior to and during sunset from a float altitude of  $36.6 \pm 0.5$  km during a flight from the National Scientific Balloon Facility in Palestine, Texas, on June 4, 1990. A description of the instrumentation and examples of spectra from several balloon flights can be found in the paper by Murcray *et al.* (9).

The positions of unblended  $\text{N}_2$  lines between *S*(4) and *S*(20) (2373 to 2492  $\text{cm}^{-1}$  region) have been measured from ATMOS spectra recorded with a filter covering approximately 1580 to 3400  $\text{cm}^{-1}$ . The continuum signal-to-rms noise in the  $\text{N}_2$  *S*-branch region is  $\sim 100$  in an individual spectrum. The stronger  $\text{N}_2$  *S*-branch lines first appear above the noise level at a tangent altitude of  $\sim 40$  km (10). Because the atmospheric density increases exponentially with decreasing altitude, the nitrogen lines strengthen rapidly

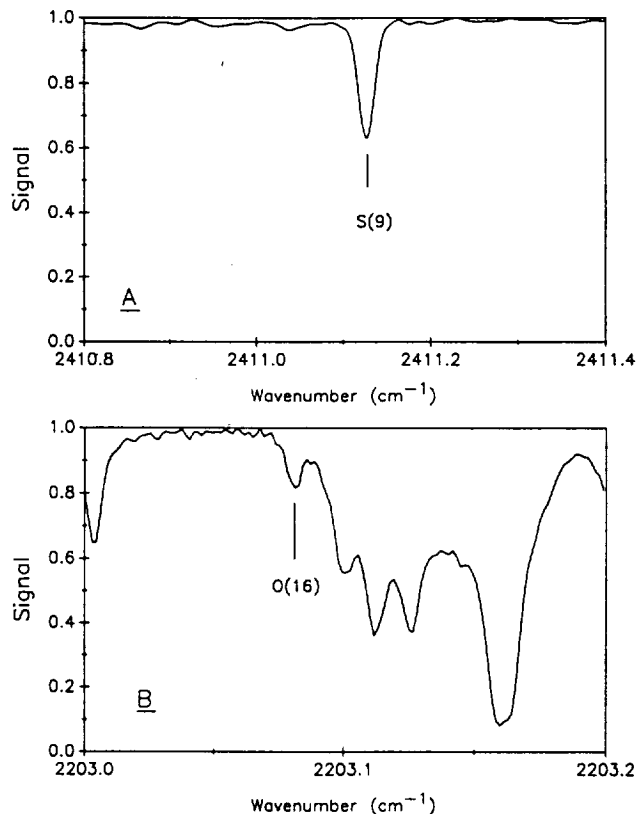


FIG. 1. Examples of  $^{14}\text{N}_2$  (1-0) band quadrupole lines in the ATMOS and University of Denver infrared stratospheric solar occultation spectra. The upper panel (A) shows the region of the S(9) line in a zonal average ATMOS spectrum with tangent altitude of 19.7 km. The slight decrease in signal to lower wavenumbers is caused by continuous absorption produced by the  $\text{N}_2$  pressure-induced (1-0) band and sub-Lorentzian absorption by the overlapping far wings of the intense  $\text{CO}_2$   $\nu_3$  fundamental band (11). The region of the O(16) line is plotted in the lower panel (B). The spectrum was recorded at a tangent altitude of 23.4 km with the University of Denver FTS. The nitrogen lines are identified and marked with vertical ticks in both panels.

with decreasing tangent altitude. The most accurate measurements are obtained from spectra recorded near a tangent altitude of 20 km where the stronger S-branch lines are prominent features in the ATMOS spectra (10).<sup>1</sup> At that altitude, the atmospheric pressure is  $\sim 40$  Torr, so that the effect of pressure-induced line shifts should be small. At lower tangent altitudes, the signal-to-noise ratio is decreased by continuum absorption resulting from the collision-induced fundamental vibration-rotation band of  $\text{N}_2$  and sub-Lorentzian absorption produced by the superposition of the far wings of the intense  $\text{CO}_2$   $\nu_3$  fundamental band (11). Also, the absorption by other telluric gases generally increases with decreasing tangent altitude so that interference effects become more of a limitation. For the present work, to improve the signal-to-noise ratio, we derived the line positions from zonal average ATMOS spectra obtained by coadding nearly equal tangent altitude spectra recorded during four sunset occultations near  $30^\circ\text{N}$  latitude. The line positions were measured with

<sup>1</sup> To receive this NASA publication, write to authors. A few copies have also been kept on deposit in the Editorial Office of the *Journal of Molecular Spectroscopy*.

a second derivative line finder algorithm and calibrated using accurate line positions reported for the  $N_2O$   $\nu_3$  (12) or  $\nu_1 + 2\nu_2$  bands (13). Nitrogen line positions from 1 to 4 ATMOS zonal spectra have been averaged for use in the subsequent analysis; the corresponding uncertainties were estimated on the basis of the standard deviation of the individual measurements and the calculated uncertainty derived from the formula given by Reuter *et al.* (6). A minimum uncertainty limit of  $0.0002 \text{ cm}^{-1}$  was adopted to account for the uncertainty in the absolute wavenumber calibration.

The balloon-borne solar spectra were recorded with a filter covering the  $1580$  to  $2230 \text{ cm}^{-1}$  region and hence provide measurements of only high- $J$   $N_2$  lines in the  $O$  branch. A total of 6  $N_2$  lines between  $O(13)$  and  $O(19)$  were selected for measurement based on comparisons of the solar spectra with synthetic spectrum calculations. All of the measured transitions are calculated to be free of significant blending by other telluric lines. The  $O(20)$   $N_2$  line also appears to be present, but it is at the limit of detection and was not included in the analysis. As the  $N_2$  lines occur near the edge of the band-pass filter, the continuum signal-to-rms noise ratio of a single spectrum decreases from  $\sim 100$  at the  $O(19)$  line to  $\sim 50$  at the  $O(13)$  line. The positions of the  $N_2$  lines were measured from one to three spectra recorded between tangent altitudes of  $28.1$  and  $18.0 \text{ km}$ . Mean values were used in the subsequent analysis. Calibration of the individual solar spectra was achieved by comparing measured positions of strong, isolated lines (e.g.,  $H_2O$  and  $CO_2$  transitions) with values derived from stratospheric spectra recorded with the same instrument during an earlier balloon flight. The calibration of this earlier dataset, which covers  $1400$  to  $1960 \text{ cm}^{-1}$ , is based on  $H_2O$  standard positions (14), scaled by the multiplicative factor recommended by Brown and Toth (15). The frequency scale of the new flight data was also checked using accurate  $NO_2$   $\nu_3$  band line positions (16), as well as direct comparisons of measured  $H_2O$  line center positions with the data of Brown and Toth (15). A second derivative line finder was used here to determine the location of the line centers. Uncertainties were estimated as described earlier. Figure 1 presents examples of the  $N_2$  lines in the ATMOS (A) and University of Denver (B) stratospheric solar spectra.

The line position measurements were analyzed with the Dunham formula for the upper and lower state term values (17)

$$F(v, J) = \sum_{ij} Y_{ij}(v + \frac{1}{2})^i [J(J+1)]^j \quad (1)$$

TABLE I  
Dunham Coefficients<sup>a</sup> for  $^{14}N_2$

Dunham Coefficient	This Study		Ref. 6	Ref. 5
	Case A	Case B		
$Y_{01}$	1.9982673(43)	1.9982369(56)	1.998286(13)	
$Y_{02} \times 10^6$	-5.761(10)	-5.747(14)	-5.763(40)	
$Y_{03} \times 10^{12}$	0.	4.78 <sup>b</sup>	0.	
$Y_{10}$	2329.91170(20)	2329.91156(21)	2329.91239(70)	
$Y_{11} \times 10^2$	-1.73717(9)	-1.73030(19)	-1.73121(67)	1.72978
$Y_{12} \times 10^6$	0.	-1.01(56)	0.	-0.832
$Y_{21} \times 10^5$	0.	-3.28(20) <sup>c</sup>	-3.28(20) <sup>c</sup>	-4.15
Weighted Error	$2.72 \times 10^{-4}$	$2.67 \times 10^{-4}$	$1.99 \times 10^{-3}$	

a) Values in parentheses are standard deviations in units of the last quoted digit of the coefficient.

b) Calculated from case A Dunham coefficients and Eq. 2 of Reuter *et al.* (5); value was held fixed in the analysis.

c) Taken from Lofthus and Krupenie (18); value was held fixed in the analysis.



with the coefficients  $Y_{ij}$  obtained from a weighted linear least-squares fit of the stratospheric measurements and additional data selected from reported laboratory experiments. Each weight was given by  $1/\sigma^2$ , where  $\sigma$  is the estimated uncertainty. The additional data were required because the stratospheric dataset covers only a limited range of transitions in the  $O$  and  $S$  branches. Three additional datasets were included: the ground state Raman measurements of Bendtsen (3), the Raman (1-0) band  $O$ -branch measurements of Bendtsen (3), and the quadrupole  $O$ - and  $S$ -branch (1-0) band measurements of Reuter *et al.* (6). The  $Q$ - and  $S$ -branch (1-0) band Raman measurements of Bendtsen (3) were excluded from the fit because they show a bias of about  $+0.009 \text{ cm}^{-1}$  with respect to our measured line positions and our fitting results; this offset was noted previously by Reuter *et al.* (6). Similarly, the calibrated coherent anti-Stokes Raman (CARS) (1-0) band  $Q$ -branch measurements of Gilson *et al.* (5) were excluded from the fit because of a calibration bias in the data (also about  $+0.009 \text{ cm}^{-1}$ ). No obvious offset was noted between our measurements and the  $O$ -branch (1-0) band positions from Ref. (3) so we retained those data in the analysis.

Table I presents the two sets of Dunham coefficients obtained from the least-squares analysis. Set A was obtained by fitting the coefficients  $Y_{10}$ ,  $Y_{01}$ ,  $Y_{11}$ , and  $Y_{02}$  with all other Dunham coefficients constrained to zero. For set B, the coefficient  $Y_{12}$  was fitted in addition to the same four Dunham coefficients. Also,  $Y_{21}$  was fixed at the value  $-3.28 \times 10^{-5}$ , as determined by Lofthus and Krupenie (18), and  $Y_{03}$  was set to  $4.78 \times 10^{-12}$ , a value estimated from Dunham's theory (17) by substituting the  $Y_{01}$  and  $Y_{11}$  values from set A and the  $Y_{10}$  value of  $2358.5665 \text{ cm}^{-1}$  from Ref. (5) into Eq. (2) of Reuter *et al.* (6). The  $Y_{10}$  value from our analysis was not used in these calculations because only two vibrational states were studied in this work.

TABLE II  
Experimental Line Positions<sup>a</sup> for  $^{14}\text{N}_2$

$v'$	$J'$	$v''$	$J''$	Measured Position	R	U	$v'$	$J'$	$v''$	$J''$	Measured Position	R	U
0	2	0	0	11.9344 <sup>b</sup>	-2.9	10.0	1	9	0	11	2244.8345 <sup>c</sup>	-5.2	3.0
0	3	0	1	19.8941 <sup>b</sup>	-0.9	10.0	1	8	0	10	2253.0967 <sup>c</sup>	-0.1	3.0
0	4	0	2	27.8517 <sup>b</sup>	-0.3	10.0	1	7	0	9	2261.3203 <sup>b</sup>	-1.5	10.0
0	5	0	3	35.8084 <sup>b</sup>	0.4	10.0	1	6	0	8	2269.5146 <sup>c</sup>	0.2	3.0
0	6	0	4	43.7629 <sup>b</sup>	0.0	10.0	1	5	0	7	2277.6737 <sup>b</sup>	-0.6	10.0
0	7	0	5	51.7163 <sup>b</sup>	0.2	10.0	1	4	0	6	2285.8056 <sup>b</sup>	4.3	10.0
0	8	0	6	59.6658 <sup>b</sup>	-1.8	10.0	1	3	0	5	2293.8986 <sup>b</sup>	3.5	10.0
0	9	0	7	67.6162 <sup>b</sup>	-0.9	10.0	1	2	0	4	2301.9561 <sup>b</sup>	0.7	10.0
0	10	0	8	75.5643 <sup>b</sup>	0.1	10.0	1	1	0	3	2309.9851 <sup>b</sup>	3.2	10.0
0	11	0	9	83.5061 <sup>b</sup>	-2.5	10.0	1	0	0	2	2317.9750 <sup>b</sup>	0.7	10.0
0	12	0	10	91.4513 <sup>b</sup>	1.1	10.0	1	6	0	4	2372.9433	-1.6	2.4
0	13	0	11	99.3881 <sup>b</sup>	-0.5	10.0	1	8	0	6	2388.3288	0.2	0.2
0	14	0	12	107.3242 <sup>b</sup>	0.7	10.0	1	9	0	7	2395.9652	-0.2	0.2
0	15	0	13	115.2546 <sup>b</sup>	-0.1	10.0	1	10	0	8	2403.5651	0.0	0.2
0	16	0	14	123.1839 <sup>b</sup>	2.0	10.0	1	11	0	9	2411.1273	-0.0	0.3
0	17	0	15	131.1061 <sup>b</sup>	1.2	10.0	1	12	0	10	2418.6519	-0.1	0.2
0	18	0	16	139.0205 <sup>b</sup>	-2.8	10.0	1	13	0	11	2426.1389	0.2	0.2
0	19	0	17	146.9378 <sup>b</sup>	1.0	10.0	1	14	0	12	2433.5871	-0.1	0.2
0	20	0	18	154.8418 <sup>b</sup>	-3.5	10.0	1	15	0	13	2440.9973	0.0	0.2
1	17	0	19	2177.6601	1.1	1.0	1	16	0	14	2448.3709 <sup>c</sup>	2.4	3.0
1	16	0	18	2186.1621	-1.2	0.8	1	17	0	15	2455.7008	0.1	0.2
1	15	0	17	2194.6277 <sup>b</sup>	-9.9	30.0	1	18	0	16	2462.9934	-0.2	0.3
1	14	0	16	2203.0818	0.1	0.4	1	19	0	17	2470.2474 <sup>c</sup>	0.5	7.0
1	13	0	15	2211.4956	0.2	0.5	1	20	0	18	2477.4619 <sup>c</sup>	1.6	3.0
1	12	0	14	2219.8781	-0.2	0.5	1	21	0	19	2484.6349	1.4	1.9
1	11	0	13	2228.2309	0.7	0.9	1	22	0	20	2491.7658	-0.5	1.3
1	10	0	12	2236.5481 <sup>c</sup>	-2.6	3.0							

a) Measured line positions are in  $\text{cm}^{-1}$ , R is the residual (measured minus calculated) in  $10^{-3} \text{ cm}^{-1}$  obtained with the set B constants given in Table I, and U is the estimated uncertainty in  $10^{-3} \text{ cm}^{-1}$ . Uncertainties for transitions from Refs. (3,6) are taken from Table I of Ref. (6). Uncertainties from the present work have been estimated as described in the text.

b) These measurements are taken from Ref. (3).

c) These measurements are taken from Ref. (6).

and all higher-order pure vibrational Dunham coefficients were constrained to values of zero. This procedure produces a fitted coefficient that is an underestimate of  $Y_{10}$ . In Table I, we also give the weighted fitting error  $(N \sum w_i \delta_i^2 / m \sum w_i)^{1/2}$ , where  $N$  is the number of lines,  $m$  is the number of degrees of freedom, and  $\delta_i$  is the observed minus calculated wavenumber for line  $i$  (6).

Examination of the values in Table I indicates that the uncertainties in the case A coefficients are slightly smaller than those of case B. The case A and case B values are consistent among themselves, but the coefficients from the two solutions are sometimes slightly outside the range of the calculated uncertainties. Table I also lists previously reported values for the Dunham coefficients. The accuracies of  $Y_{01}$ ,  $Y_{02}$ ,  $Y_{10}$ , and  $Y_{11}$  have been improved by about a factor of 3 compared to the results in Ref (6). No error estimates were given for the Dunham coefficients listed in Ref. (5), but the present values are generally consistent with those results. The  $Y_{12}$  coefficient determined in case B has an uncertainty of  $\sim 50\%$ . Within this uncertainty, the measured value of  $-1.01 \times 10^{-8}$  agrees with a value of  $-7.9 \times 10^{-9}$  calculated from Eq. (3) of Reuter *et al.* (6), the case B values of  $Y_{11}$  and  $Y_{01}$ , and the values of  $Y_{10}$  and  $Y_{20}$  reported by Gilson *et al.* (5).

Table II presents the measurement results and the residuals of the case B weighted least-squares best fit to the data. The case A results, which are not reported, are very similar. For most lines, the residual (measured minus calculated) position is less than the estimated uncertainty. The residuals of both the far infrared and infrared data show no obvious trend with  $J$ . Reuter *et al.* (6) noted that the pure rotational lines showed a slight negative bias in the residuals of their fit, but this offset does not appear in the present results nor is it obvious in ground state combination differences computed from the stratospheric infrared line positions.

We examined published  $0.0033\text{-cm}^{-1}$  resolution stratospheric emission spectra for the presence of the ground state  $v = 0-0$  quadrupole lines of  $N_2$ . The  $7\text{--}40\text{ cm}^{-1}$  interval covered in the atlas of Baldecchi *et al.* (19, 20) and the few small higher wavenumber intervals in Refs. (21-23) show only the  $S(1)$  and  $S(4)$  lines at  $19.895$  and  $43.763\text{ cm}^{-1}$  in regions nearly free of interfering telluric features (see Fig. 13 of Ref. (19) and Fig. 2 of Ref. (23)). The absence of any significant features at the predicted positions of these transitions indicates that the  $N_2$  pure rotational quadrupole band is extremely weak.

#### ACKNOWLEDGMENTS

Research at the Jet Propulsion Laboratory (JPL), California Institute of Technology, was performed under contract to the National Aeronautics and Space Administration. Research at the University of Denver was funded by NASA and the National Science Foundation (NSF). The Ministère de l'Éducation Nationale, Belgium, partially supported the investigations at the University of Liège.

#### REFERENCES

1. PH. DEMOULIN, C. B. FARMER, C. P. RINSLAND, AND R. ZANDER, *J. Geophys. Res.*, accepted for publication.
2. R. J. BUTCHER, D. V. WILLETTS, AND W. J. JONES, *Proc. R. Soc. London A* **324**, 231-245 (1971).
3. J. BENDTSEN, *J. Raman Spectrosc.* **2**, 133-145 (1974).
4. B. P. STOICHEFF, *Can. J. Phys.* **32**, 630-634 (1954).
5. T. R. GILSON, I. R. BEATTIE, J. D. BLACK, D. A. GREENHALGH, AND S. N. JENNY, *J. Raman Spectrosc.* **9**, 361-368 (1980).
6. D. REUTER, D. E. JENNINGS, AND J. W. BRAULT, *J. Mol. Spectrosc.* **115**, 294-304 (1986).
7. C. B. FARMER, *Mikrochim. Acta [Wien]* **III**, 189-214 (1987).
8. R. H. NORTON AND C. P. RINSLAND, *Appl. Opt.* **30**, 389-400 (1991).
9. F. J. MURCRAY, J. J. KOSTERS, R. D. BLATHERWICK, J. OLSON, AND D. G. MURCRAY, *Appl. Opt.* **29**, 1520-1525 (1990).
10. C. B. FARMER AND R. H. NORTON, unpublished.
11. C. P. RINSLAND, R. ZANDER, J. S. NAMKUNG, C. B. FARMER, AND R. H. NORTON, *J. Geophys. Res.* **94**, 16,303-16,322 (1989).
12. R. A. TOTH, *J. Opt. Soc. Am. B Opt. Phys.* **4**, 357-374 (1987).
13. R. A. TOTH, unpublished results, 1991.
14. G. GUELACHVILI AND K. NARAHARI RAO, "Handbook of Infrared Standards," Academic Press, Orlando, FL, 1986.

15. L. R. BROWN AND R. A. TOTH, *J. Opt. Soc. Am. B Opt. Phys.* **2**, 842-856 (1985).
16. L. R. ZINK, M. VANEK, AND J. S. WELLS, unpublished.
17. J. L. DUNHAM, *Phys. Rev.* **41**, 721-731 (1932).
18. A. LOFTHUS AND P. H. KRUPENIE, *J. Phys. Chem. Ref. Data* **6**, 113-307 (1977).
19. M. G. BALDECCHI, B. CARLI, F. MENCARAGLIA, A. BONETTI, AND M. CARLOTTI, *J. Geophys. Res.* **89**, 11,689-11,704 (1984).
20. M. G. BALDECCHI, B. CARLI, F. MENCARAGLIA, A. BARBIS, A. BONETTI, AND M. CARLOTTI, *J. Geophys. Res.* **93**, 5303-5318 (1988).
21. B. CARLI, F. MENCARAGLIA, AND A. BONETTI, *Int. J. Infrared Millimeter Waves* **3**, 385-394 (1982).
22. B. CARLI, F. MENCARAGLIA, A. BONETTI, B. M. DINELLI, AND F. FORNI, *Int. J. Infrared Millimeter Waves* **4**, 475-488 (1983).
23. B. CARLI AND J. H. PARK, *J. Geophys. Res.* **93**, 3851-3865 (1988).

C. P. RINSLAND

*NASA Langley Research Center  
Atmospheric Sciences Division  
Mail Stop 401A  
Hampton, Virginia 23665-5225*

R. ZANDER

*Institute of Astrophysics  
University of Liège  
4200 Liège-Ougrée  
Belgium*

*Department of Physics  
University of Denver  
Denver, Colorado*

A. GOLDMAN  
F. J. MURCRAY  
D. G. MURCRAY

M. R. GUNSON  
C. B. FARMER

*Jet Propulsion Laboratory  
California Institute of Technology  
Mail Stop 183-301  
4800 Oak Grove Drive  
Pasadena, California  
Received March 4, 1991*



Analysis of Atmospheric Trace Constituents  
from High Resolution Infrared Balloon-Borne and  
Ground-Based Solar Absorption Spectra

A. Goldman, F.J. Murcray, C.P. Rinsland\*, R.D. Blatherwick,  
F.H. Murcray, and D.G. Murcray

Department of Physics, University of Denver  
Denver CO 80208

\*Atmospheric Sciences Division, NASA Langley Research Center  
Hampton VA 23665

ABSTRACT

Recent results and ongoing studies of high resolution solar absorption spectra will be presented. The analysis of these spectra is aimed at the identification and quantification of trace constituents important in atmospheric chemistry of the stratosphere and upper troposphere.

Analysis of balloon-borne and ground-based spectra obtained at  $0.0025\text{ cm}^{-1}$  covering the  $700\text{--}2200\text{ cm}^{-1}$  interval will be presented. Results from ground-based  $0.02\text{ cm}^{-1}$  solar spectra, from several locations such as Denver, South Pole, M. Loa, and New Zealand will also be shown. The  $0.0025\text{ cm}^{-1}$  spectra show many new spectroscopic features. The analysis of these spectra, along with corresponding laboratory spectra, improves the spectral line parameters, and thus the accuracy of trace constituents quantification. The combination of the recent balloon flights, with earlier flights data since 1978 at  $0.02\text{ cm}^{-1}$  resolution, provides trends analysis of several stratospheric trace species. Results for  $\text{COF}_2$ ,  $\text{F}_2$ ,  $\text{SF}_6$  and other species will be presented. Analysis of several ground-based solar spectra provides trends for  $\text{HCl}$ ,  $\text{HF}$  and other species.

The retrieval methods used for total column density and altitude distribution for both ground-based and balloon-borne spectra will be presented. These are extended for the analysis of the ground-based spectra to be obtained by the high resolution interferometers of the Network for Detection of Stratospheric Change (NDSC). Progress of the University of Denver studies for the NDSC will be presented. This will include intercomparison of solar spectra and trace gases retrievals obtained from simultaneous scans by the high resolution ( $0.0025\text{ cm}^{-1}$ ) interferometers of BRUKER and BOMEM.

1. INTRODUCTION

The technique of infrared solar spectra has been used for many years to obtain information about the column abundance and vertical distribution of atmospheric gases. To maximize retrieval of this information, nonlinear multiparameters spectral least squares fitting methods have been developed, and since 1980 became an important tool in our research.<sup>1-4</sup> Subsequent studies (see below), conducted with higher resolution and signal to noise spectra, allowed to further enhance these analysis methods.

The spectral least square programs can fit simultaneously several spectral regions of several spectral scans, with three kinds of parameters: (i) instrumental parameters, such as resolution and background contours with channel and phase corrections, (ii) atmospheric (or laboratory) parameters such as the temperature and gas amounts in isothermal layers, and (iii) spectral line parameters such as line positions, intensities and half widths. The programs allow the initial parameters to remain fixed or vary within a constrained range of a priori values. The fitted parameters include the scaling of the initial mixing ratio distribution functions which determine the gas amount.

The atmospheric spectroscopy group at the University of Denver has been studying atmospheric infrared absorption with several types of balloon-borne, aircraft and ground-based spectrometers for many years. The instrumentation used in recent experiments includes  $0.002\text{--}0.003\text{ cm}^{-1}$  (unapodized) resolution FTS systems<sup>5</sup> and  $0.0005\text{ cm}^{-1}$  resolution tunable diode LHS system<sup>6</sup> for atmospheric solar absorption spectra. Ground-based measurements have been made from various

locations, e.g. Denver, New Mexico, Hawaii, New Zealand, the South Pole, and McMurdo, during several seasons over the last few years. Balloon flights were made from several locations in the U.S. and Europe. The field measurements are supplemented by extensive laboratory spectra, mostly taken with the field spectrometers. The analysis of these spectra has been very successful in the identification and quantification of atmospheric trace gases, some monitored since 1980, and upgrading the theoretical capabilities of atmospheric spectroscopy. Analysis of the data includes detailed atlases with complete identifications of the individual atmospheric and solar lines, molecular spectroscopic constants and line parameters analysis of selected bands, theoretical line-by-line and cross sections simulations of emission and absorption spectra, and spectral least-squares fitting using the most current atmospheric absorption parameters. These show good agreement with the data in many spectral intervals and also many new spectral features in the stratospheric spectrum. In this paper, samples of our recent  $0.002\text{--}0.003\text{ cm}^{-1}$  data and analysis leading to advances in atmospheric spectroscopy will be discussed. Quantification of several trace gases since 1980 will be summarized from  $0.02\text{ cm}^{-1}$  and  $0.002\text{ cm}^{-1}$  data.

Work in progress with new BRUKER and BOMEM interferometer systems towards the NDSC (Network for Detection of Stratospheric Change) will be presented, including intercomparisons, and further developments in the retrieval methods.

## 2. RESULTS

### 2.1 Balloon-borne spectra

We have studied the new infrared spectroscopic observations of several important stratospheric trace gases obtained with a  $0.002\text{ cm}^{-1}$  resolution interferometer system now covering the  $700\text{--}2200\text{ cm}^{-1}$  region.<sup>7-8</sup> Most stratospheric species are measurable in these spectra. The main molecules studied are  $\text{O}_3$ ,  $\text{HNO}_3$ ,  $\text{ClONO}_2$ ,  $\text{HO}_2\text{NO}_2$ ,  $\text{NO}_2$ ,  $\text{COF}_2$ ,  $\text{SF}_6$  and  $\text{CHClF}_2$ . The stratospheric solar spectra, ground-based solar spectra, and laboratory spectra reveal new details of the absorption by these molecules which are important in determining the photochemistry and the heat balance of the atmosphere. It has been possible to assign numerous previously unidentified features to these gases in the stratospheric spectra and to incorporate several new sets of spectral line parameters and cross sections from their simulation.

Many of these features were not accounted for in the previous line parameters compilations, and will be included in future data bases, HITRAN91 and GEISA91. A number of spectral regions have been atlased in detail.<sup>9</sup> Fig. 1 shows a sample from the atlas. The high resolution  $10\text{ }\mu\text{m}$  spectra have been analyzed with the new ozone line parameters<sup>10</sup> to determine the isotopic ratios of  $^{16}\text{O}^{16}\text{O}^{18}\text{O}$  and  $^{16}\text{O}^{18}\text{O}^{16}\text{O}$  in the stratosphere.

The excellent agreement between the highly precise laboratory and stratospheric spectra provided significant new evidence for absorption by the  $\text{HO}_2\text{NO}_2$   $802.7\text{ cm}^{-1}$  Q branch in the lower stratosphere. The improved resolution of the flights measurements reveals additional details of the interference in the  $\text{ClONO}_2$   $780.2\text{ cm}^{-1}$   $\nu_4$  Q branch region, including the identification of overlapping  $\text{HNO}_3$   $\nu_8$  features. New analysis of the  $\text{COF}_2$   $\nu_6$  band and the  $\nu_4$  band, and recent analysis of the  $\text{HNO}_3$   $\nu_8$  and  $\nu_8 + \nu_9$  bands have been applied to both laboratory and stratospheric spectra. New features of other trace gases (e.g.  $\text{ClONO}_2$ ,  $\text{HNO}_3$  and  $\text{CF}_4$  in the  $1280\text{ cm}^{-1}$  region) have been identified in the stratospheric spectra and are currently under study with new line parameters and cross-sections.

The  $5\text{--}7\text{ }\mu\text{m}$  spectra are also being studied for numerous new  $\text{O}_3$  features. Updated line parameters of  $\text{HNO}_3$   $\nu_2$ ,  $\text{O}_3$   $5\text{ }\mu\text{m}$  bands, and  $\text{H}_2\text{O}$   $\nu_2$  bands are now used for new retrievals of  $\text{HNO}_3$ . The  $\text{NO}_2$  spectral lines in the  $6\text{ }\mu\text{m}$  region show the need for further update. The combination of the high resolution flight data with other solar spectral data allows improvements in the spectral line parameters of the reference gases  $\text{O}_2$  and  $\text{N}_2$ , but further studies are needed.<sup>11-12</sup>

The long time span covered by medium and high resolution infrared atmospheric absorption measurements generated considerable interest in studying trends of atmospheric trace gases. Thus, an analysis of both recent  $0.002\text{ cm}^{-1}$  spectra and previous  $0.02\text{ cm}^{-1}$  spectra provided long term trends for  $\text{SF}_6$ ,  $\text{CHClF}_2$ , and  $\text{COF}_2$  over the last decade. Exponential increase rates of  $(7.4 \pm 1.9)\%$ ,  $(9.4 \pm 1.3)\%$  and  $(10.3 \pm 1.8)\%$  year<sup>-1</sup> were found.<sup>13</sup>

### 2.2 Ground-based spectra

We have performed quantitative analysis of the absorption by a number of minor and trace constituents in  $0.02\text{ cm}^{-1}$

resolution solar absorption spectra geographical locations.<sup>13-20</sup> In addition to various measurements from Denver, these include the total vertical column amounts of H<sub>2</sub>O (and isotopes), CO<sub>2</sub>, O<sub>3</sub>, N<sub>2</sub>O, CH<sub>4</sub>, CHClF<sub>2</sub>, NO, NO<sub>2</sub>, HCl, and HNO<sub>3</sub> from M. Loa, Hawaii, in February 1987; O<sub>3</sub>, N<sub>2</sub>O, HNO<sub>3</sub>, CO<sub>2</sub>, CH<sub>4</sub>, and CF<sub>2</sub>Cl<sub>2</sub> in December 1980 and November-December 1986 from the South Pole; HCl, NO, NO<sub>2</sub>, and C<sub>2</sub>H<sub>6</sub> in December 1986 from the S. Pole, and HCl, HNO<sub>3</sub>, O<sub>3</sub>, ClONO<sub>2</sub> and NO<sub>2</sub> from McMurdo, Antarctica during the spring 1987 ozone hole. In the M. Loa measurements it was found that the average tropospheric concentrations deduced for CO<sub>2</sub>, N<sub>2</sub>O and CH<sub>4</sub> are very consistent with correlative NOAA GMCC surface data.

Of particular interest is the observed increase in the CF<sub>2</sub>Cl<sub>2</sub> column amount above the S. Pole over the 6 year period, corresponding to  $(3.6 \pm 2.1)\%$  year<sup>-1</sup>. The column amount of HNO<sub>3</sub> for both 1980 and 1986 were not significantly different. Other data sets, such as from the National Solar Observatory (NSO) at Kitt Peak were used for monitoring trends of HF and HCl from 0.02-0.005 cm<sup>-1</sup> spectra obtained during the 1977-1990 period. Linear increase rates of  $(10.7 \pm 1.1)\%$  year<sup>-1</sup> and  $(4.9 \pm 0.7)\%$  year<sup>-1</sup> have been obtained for HF and HCl respectively.

We have also been conducting 0.002-0.003 cm<sup>-1</sup> resolution solar absorption ground-based measurements, for periodic observations and monitoring of the atmosphere from Denver. The initial measurements were made with the balloon-borne BOMEM FTS system.<sup>5</sup> Typical results are shown in Figures 2-5. More recently, dedicated BOMEM and BRUKER FTS have been used, one of which will be moved to Mauna Loa as soon as the NDSC station becomes operational. Preliminary results are shown in Figures 6-10.

The analysis of the ground-based spectra shows that the trace gases of interest to the NDSC can be well monitored from selected spectral intervals of multiscans measurements, with temperatures and geometry and instrumental performance monitored from reference gases. It is apparent that no more than scale height vertical resolution can usually be expected for the altitude distribution of the trace gases, and in some cases only the tropospheric and stratospheric components could be separated. The translation of the statistical errors of the spectral least squares fitting to absolute errors estimates from a priori constraints and accuracies requires further studies.

### 3. CONCLUSIONS

High resolution stratospheric spectra show many new spectral features not observed in previous lower resolution spectra. This requires new analysis of laboratory and atmospheric spectra and improved theoretical calculations for many molecular bands of atmospheric interest. Atmospheric spectra remain a powerful source for observing and monitoring our changing atmosphere.

Retrieval methods based on spectral least squares are best suited for spectroscopic quantification, but further development are desired.

### 4. ACKNOWLEDGMENTS

Research was at the University of Denver supported in part by NSF and in part by NASA. Acknowledgement is made to the National Center for Atmospheric Research, which is sponsored by the National Science Foundation, for computer time used in this work. We thank A. Maki, L.R. Brown, J.-M. Flaud, and C. Camy-Peyret, and others for collaboration on new spectral line parameters, and to N.D. Sze, M. Ko, R. Cicerone and others for providing photochemical modeling.

### 5. REFERENCES

1. E. Niple, W.G. Mankin, A. Goldman, D.G. Murcray, and F.J. Murcray, "Stratospheric NO<sub>2</sub> and H<sub>2</sub>O Mixing Ratio Profiles from High Resolution Infrared Solar Spectra Using Nonlinear Least Squares," *Geophys. Res. Lett.*, 7, 489-492, 1980.
2. A. Goldman, D.G. Murcray, F.J. Murcray, and E. Niple, "High Resolution IR Balloon-Borne Solar and Laboratory Spectra in the HNO<sub>3</sub> 1720-cm<sup>-1</sup> Region: An Analysis," *Appl. Opt.*, 19, 3721-3724, 1980.
3. C.P. Rinsland, A. Goldman, F.J. Murcray, D.G. Murcray, M.A. H. Smith, R.K. Scals, Jr., J.C. Larsen, and P.L. Rinsland, "Stratospheric N<sub>2</sub>O Mixing Ratio Profile from High-Resolution Balloon-Borne Solar Absorption Spectra and

Laboratory Spectra Near 1880  $\text{cm}^{-1}$ ," *Appl. Opt.*, 21, 4351-4355, 1982.

4. A. Goldman, F.G. Fernald, F.J. Murcray, F.H. Murcray, and D.G. Murcray, "Spectral Least Squares Quantification of Several Atmospheric Gases from High Resolution Infrared Solar Spectra Obtained at the South Pole," *J. Quant. Spectrosc. Radiat. Transfer*, 29, 189-204, 1983.

5. F.J. Murcray, J.J. Kusters, R.D. Blatherwick, J. Olson, and D.G. Murcray, "High Resolution Solar Spectrometer System for Measuring Atmospheric Constituents," *Appl. Opt.*, 29, 1520-1525, 1990.

6. C.T. McElroy, A. Goldman, P.F. Fogel, and D.G. Murcray, "Heterodyne Spectrophotometry of Ozone in the 9.6- $\mu\text{m}$  Band using a Tunable Diode Laser," *J. Geophys. Res.*, 95, D5, 5567-5575, 1990.

7. A. Goldman, F.J. Murcray, D.G. Murcray, J.J. Kusters, C.P. Rinsland, C. Camy-Peyret, J.-M. Flaud, and A. Barbe, "Isotopic Abundances of Stratospheric Ozone from Balloon-Borne High-Resolution Infrared Solar Spectra," *J. Geophys. Res.*, 94, 8467-8473, 1989.

8. A. Goldman, F.J. Murcray, R.D. Blatherwick, J.J. Kusters, F.H. Murcray, D.G. Murcray, and C.P. Rinsland, "New Spectral Features of Stratospheric Trace Gases Identified from High Resolution Infrared Balloon-Borne and Laboratory Spectra," *J. Geophys. Res.*, 94, 14,945-14,955, 1989.

9. A. Goldman, R.D. Blatherwick, J.J. Kusters, F.J. Murcray, F.H. Murcray, and D.G. Murcray, "Atlas of Very High Resolution Stratospheric IR Absorption Spectra, Volume I, Line Positions and Identifications, Volume II, The Spectra," *Department of Physics, University of Denver*, Dec., 1990.

10. J.-M. Flaud, C. Camy-Peyret, C.P. Rinsland, V. Malathy Devi, M.A.H. Smith, and A. Goldman, "Improved Line Parameters for the Ozone Bands in the 10 $\mu\text{m}$  Spectral Region," *Appl. Opt.*, 29, 3667-3671, 1990.

11. M. Dang-Nhu, R. Zander, A. Goldman, and C.P. Rinsland, "Identification of Magnetic Dipole Infrared Transitions of the Fundamental Band of Oxygen," *J. Molec. Spectrosc.*, 144, 366-373, 1990.

12. C.P. Rinsland, R. Zander, Ph. Demoulin, A. Goldman, M.R. Gunson, and C.B. Farmer, "The Fundamental Quadrupole Band of  $^{14}\text{N}_2$ : Line Positions from High Resolution Solar Absorption Spectra," To be submitted, 1991.

13. C.P. Rinsland, A. Goldman, F.J. Murcray, R.D. Blatherwick, J.J. Kusters, D.G. Murcray, N.D. Sze, and S.T. Massie, "Long-Term Trends in the Concentration of  $\text{SF}_6$ ,  $\text{CHClF}_2$ , and  $\text{COF}_2$  in the Lower Stratosphere from Analysis of High-Resolution Infrared Solar Occultation Spectra," *J. Geophys. Res.*, 95, D10, 16,477-16,490, 1990.

14. F.J. Murcray, F.H. Murcray, A. Goldman, D.G. Murcray, and C.P. Rinsland, "Infrared Measurements of Several Nitrogen Species above the South Pole in December 1980 and November-December 1986," *J. Geophys. Res.*, 92, 13,373-13,376, 1987.

15. A. Goldman, C.P. Rinsland, F.J. Murcray, F.H. Murcray, and D.G. Murcray, "Measurements of Atmospheric Gases above the South Pole in December 1986 from High-Resolution 3 to 4  $\mu\text{m}$  Solar Spectra," *J. Geophys. Res.*, 93, D6, 7069-7074, 1988.

16. C.P. Rinsland, A. Goldman, F.J. Murcray, F.H. Murcray, R.D. Blatherwick, and D.G. Murcray, "Infrared Measurements of Atmospheric Gases Above Mauna Loa, Hawaii, in February 1987," *J. Geophys. Res.*, 93, D10, 12,607-12,626, 1988.

17. C.P. Rinsland, A. Goldman, F.J. Murcray, F.H. Murcray, "Increased  $\text{CF}_2\text{Cl}_2$  (CFC-12) Absorption above the South Pole," *Appl. Opt.*, 27, 627-630, 1988.

18. F.J. Murcray, A. Matthews, A. Goldman, P. Johnston, and C.P. Rinsland, " $\text{NH}_3$  Column Abundances over Lauder, New Zealand," *J. Geophys. Res.*, 94, 2235-2238, 1988.

19. F.J. Murcray, A. Goldman, R.D. Blatherwick, A. Matthews and N. Jones, " $\text{HNO}_3$  and  $\text{HCl}$  Amounts over McMurdo during the Spring of 1987," *J. Geophys. Res.*, 94, D14, 16,615-16,618, 1989.

20. C.P. Rinsland, J.S. Levine, R. Zander, A. Goldman, N.D. Sze, M.K.W. Ko, and D.W. Johnson, "Infrared Measurements of  $\text{HF}$  and  $\text{HCl}$  Total Column Abundance above Kitt Peak, 1977-1990: Seasonal Cycles, Increases in Total Columns Ratio, and Comparisons with Two-Dimensional Model Calculations," submitted to *J. Geophys. Res.*, Nov. 1990.



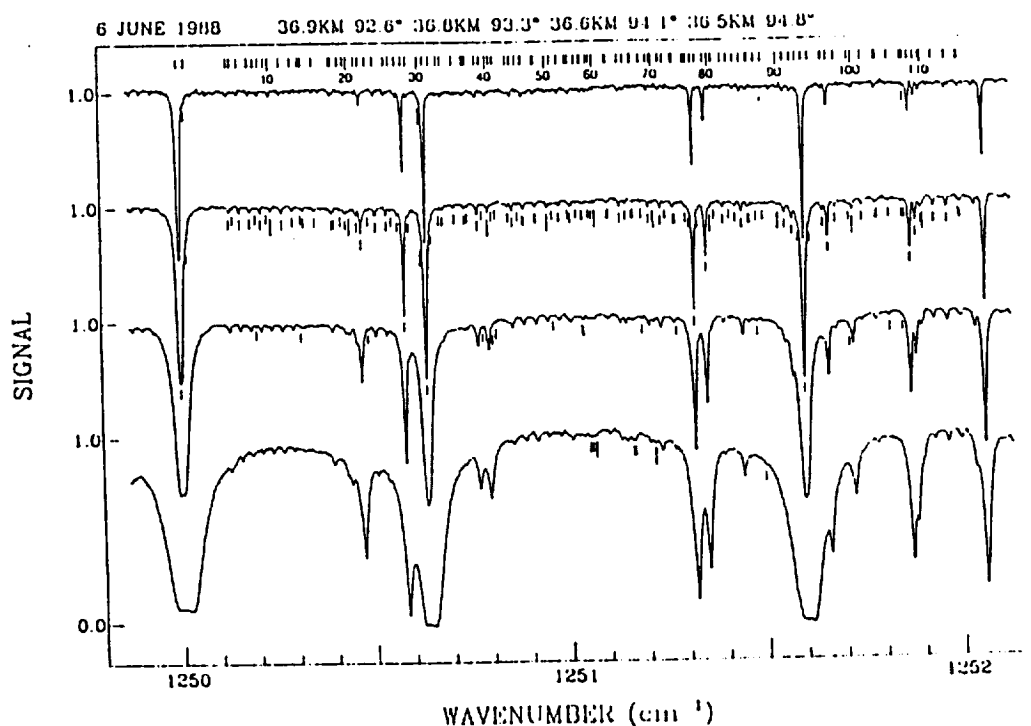


Fig.1. Sample spectra from the new atlas of high resolution ( $0.002 \text{ cm}^{-1}$ ) stratospheric IR absorption spectra in the  $1250\text{--}1252 \text{ cm}^{-1}$ . The spectral region contains several manifolds of the  $\text{COF}_2 \nu_4$  band.

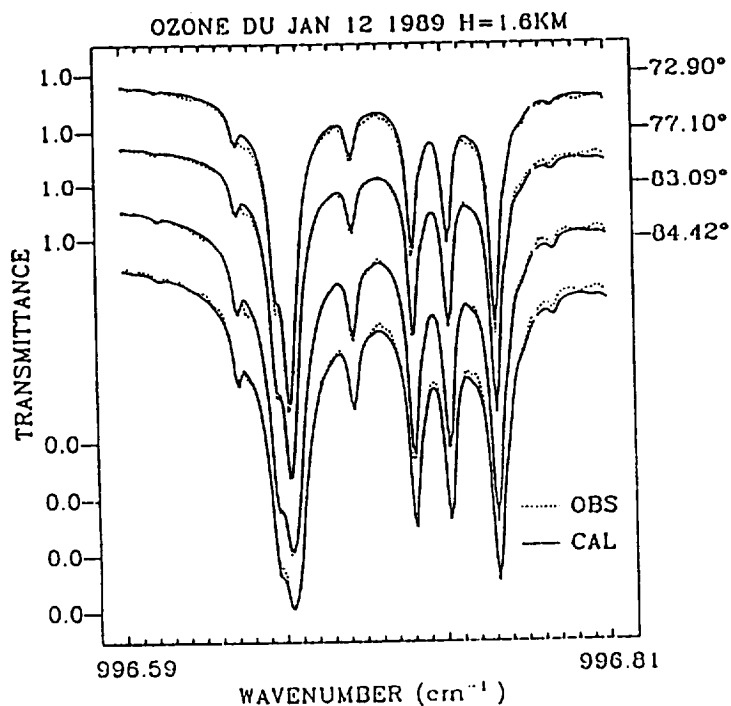


Fig.2. Nonlinear least-squares multi-scan fit of  $\text{O}_3$  with improved line parameters in the  $996 \text{ cm}^{-1}$  region, to solar spectra obtained from Denver, Colorado, during sunset on January 12, 1989, with a modified BOMEM model DA3.002 interferometer used for DU balloon flights. The total column of the fitted profile is  $7.46 \times 10^{18} \text{ molec/cm}^2$ .

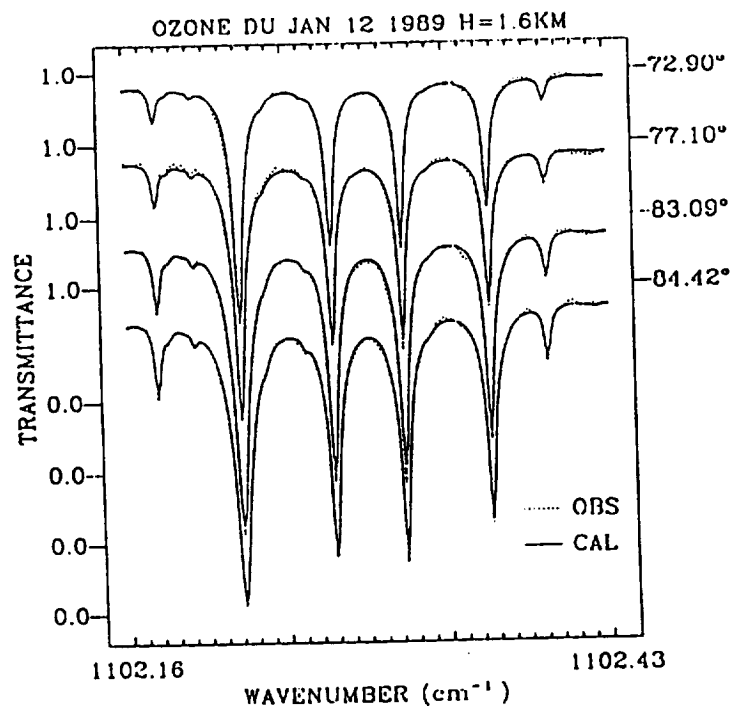


Fig.3. Nonlinear least-squares multi-scan fit of  $O_3$  with improved line parameters in the  $1102\text{ cm}^{-1}$  region, to solar spectra obtained from Denver, Colorado, during sunset on January 12, 1989, with a modified BOMEM model DA3.002 interferometer used for DU balloon flights. The total column of the fitted profile is  $7.33 \times 10^{18}$  molec/cm<sup>2</sup>.

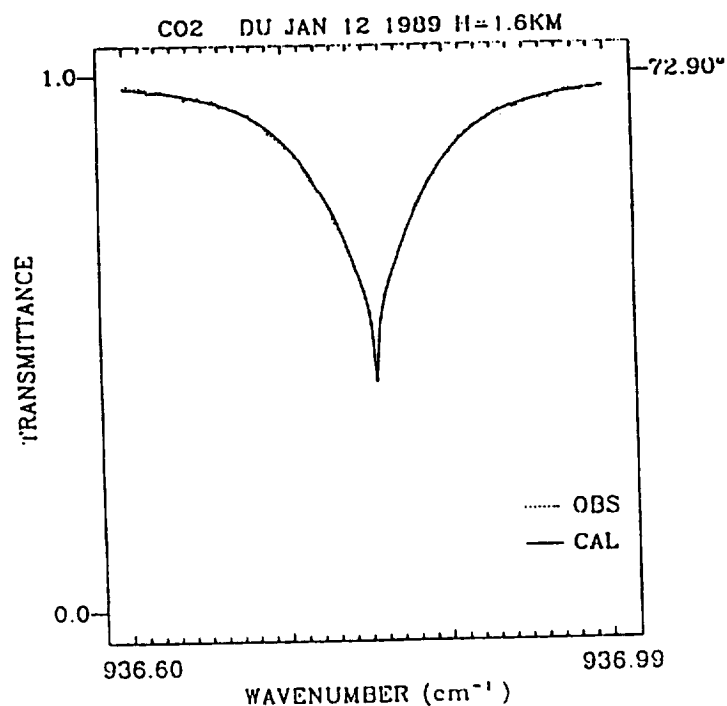


Fig.4. Nonlinear least-squares single scan fit of  $CO_2$  in the  $936\text{ cm}^{-1}$  region from solar spectra obtained from Denver, Colorado during sunset on January 12, 1989, with a modified BOMEM model DA3.002 interferometer used for DU balloon flights.

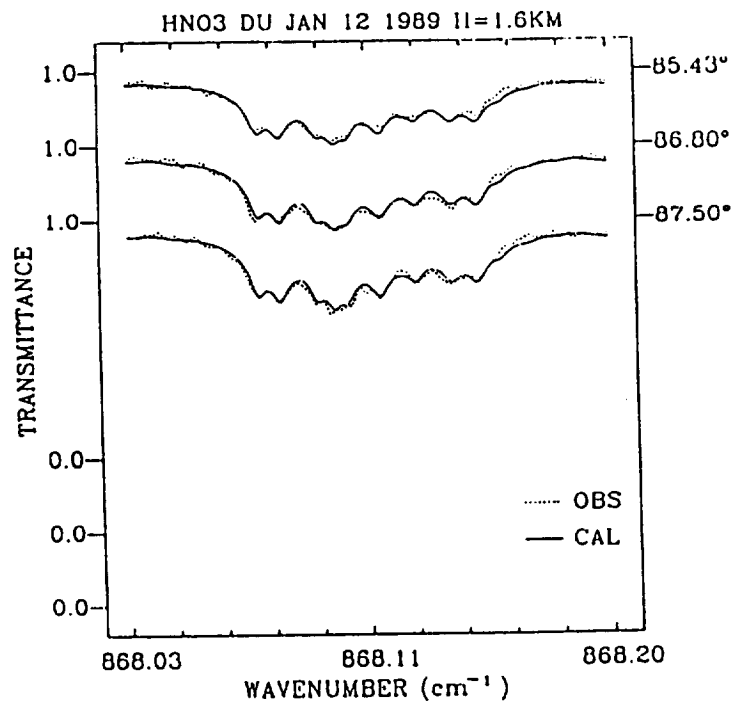


Fig.5. Nonlinear least-squares multi-scan fit of  $\text{HNO}_3$ , with improved line parameters in the  $868 \text{ cm}^{-1}$  region, to solar spectra obtained from Denver, Colorado, during sunset on January 12, 1989, with a modified BOMEM model DA3.002 interferometer used for DU balloon flights. The total column of the fitted profile is  $1.35 \times 10^{16} \text{ molcc/cm}^2$ .

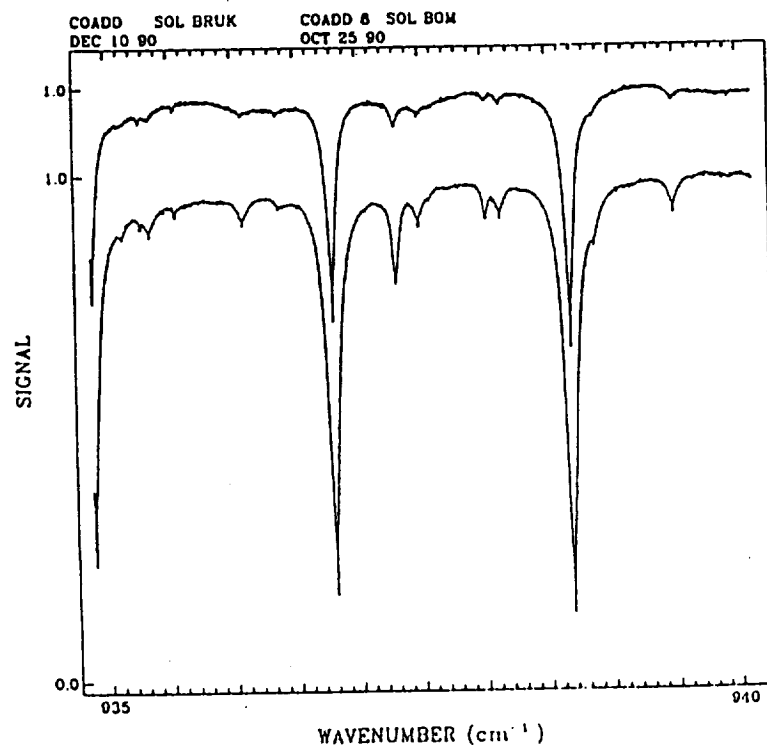


Fig.6. Solar spectra obtained from Denver, Colorado, during preliminary testing of the two interferometer systems BOMEM DA8.002 and BRUKER IFS 120 HR in the  $\text{CO}_2$   $935\text{-}940 \text{ cm}^{-1}$  region.

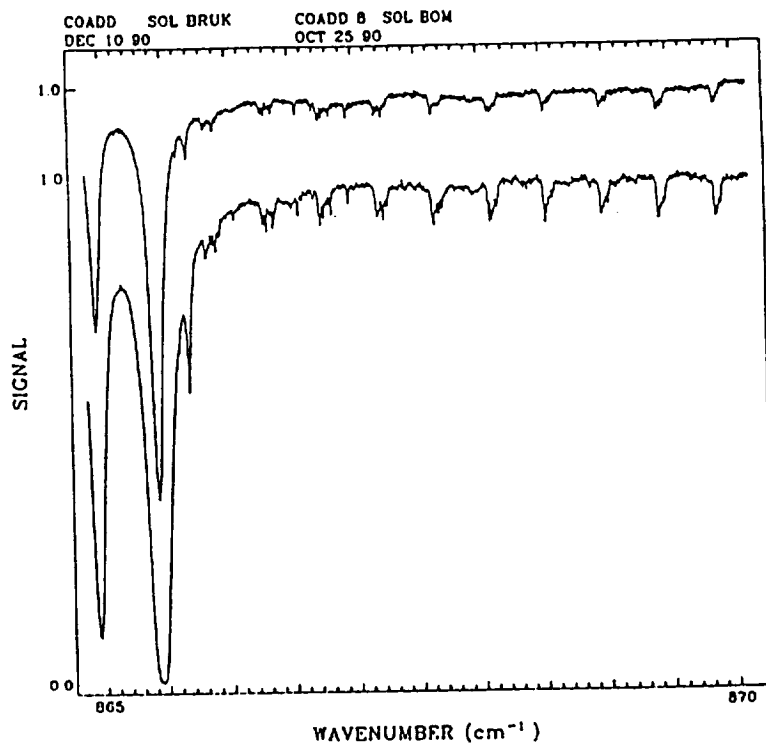


Fig.7.Solar spectra obtained from Denver, Colorado, during preliminary testing of the two interferometer systems BOMEM DA8.002 and BRUKER IFS 120 HR in the  $\text{HNO}_3$ , 865-870  $\text{cm}^{-1}$  region.

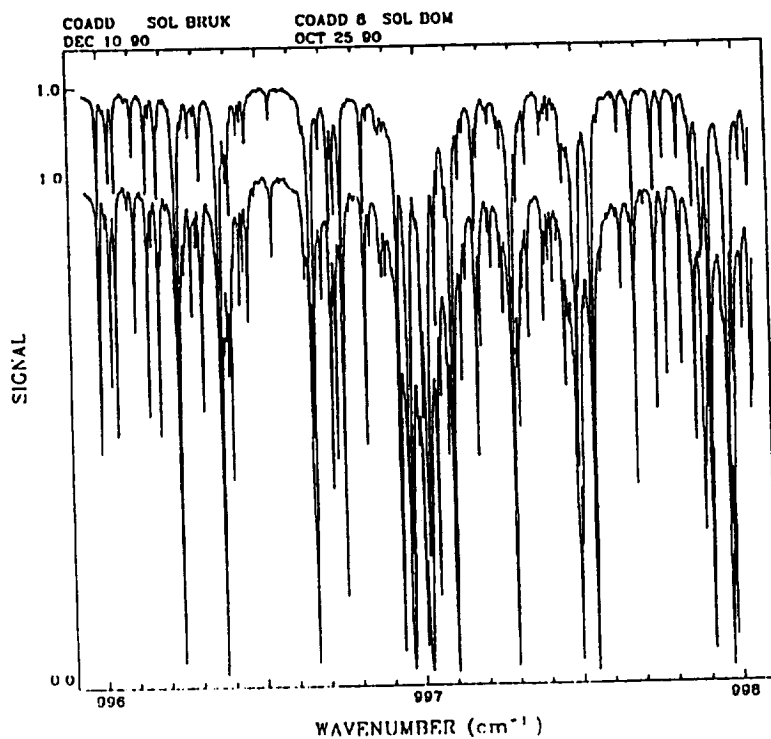


Fig.8.Solar spectra obtained from Denver, Colorado, during preliminary testing of the two interferometer systems BOMEM DA8.002 and BRUKER IFS 120 HR in the  $\text{O}_3$ , 996-998  $\text{cm}^{-1}$  region.

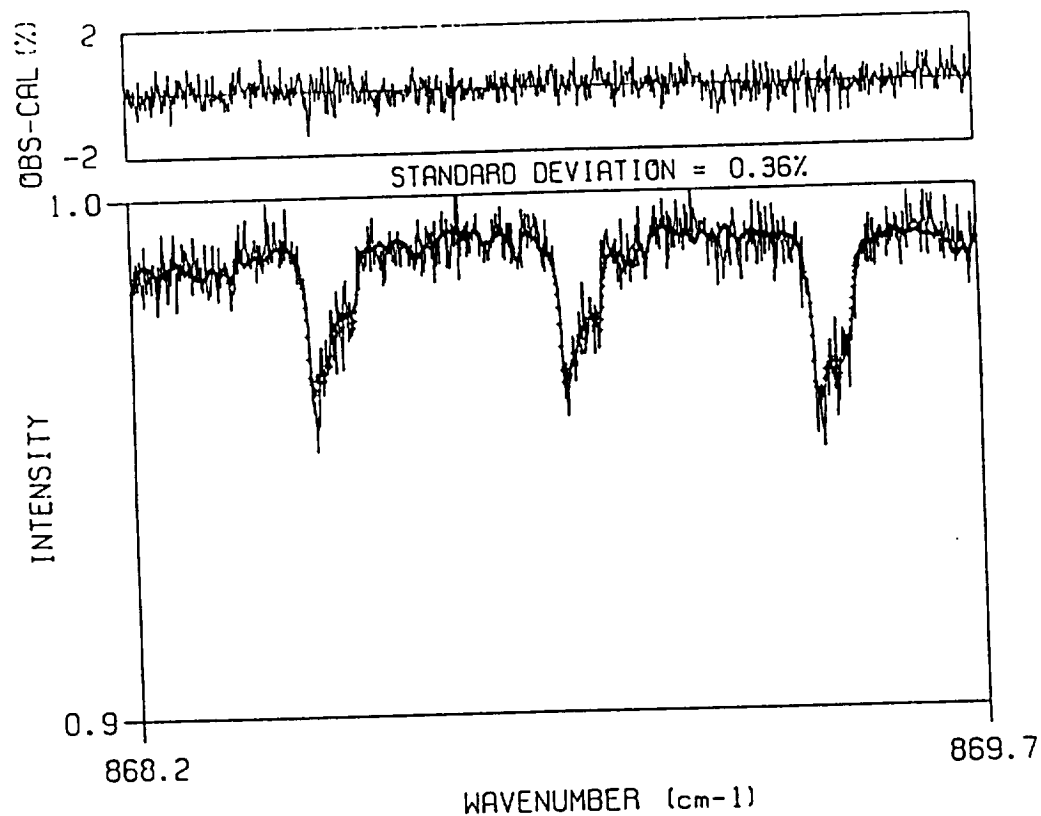


Fig.9. Nonlinear least-squares single scan fit of HNO<sub>3</sub> with improved line parameters in the 868 cm<sup>-1</sup> regions to solar spectra obtained from Denver, Colorado on December 10, 1990, with BRUKER model IFS 120 HR interferometer.

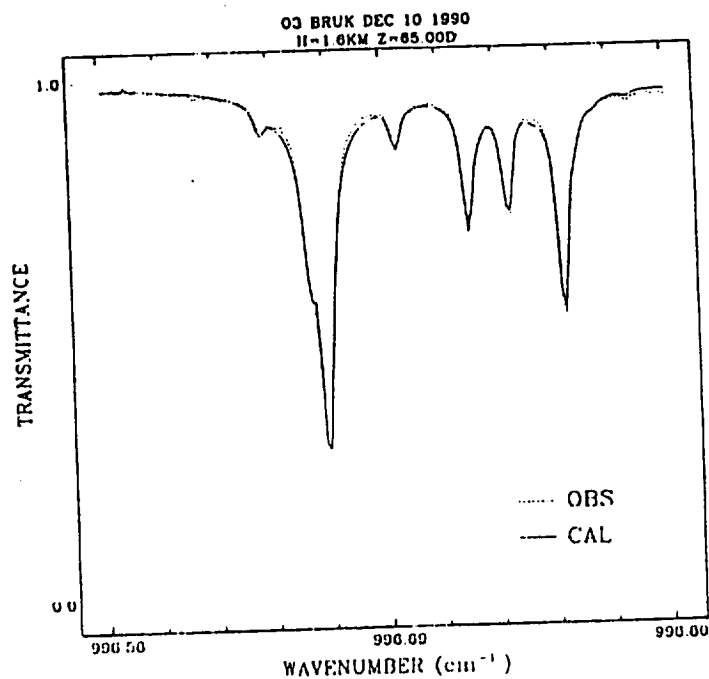


Fig.10. Nonlinear least-squares single scan fit of O<sub>3</sub> with improved line parameters in the 996 cm<sup>-1</sup> regions to solar spectra obtained from Denver, Colorado on December 10, 1990, with BRUKER model IFS 120 HR interferometer.



# Long-Term Trends in the Concentrations of SF<sub>6</sub>, CHClF<sub>2</sub>, and COF<sub>2</sub> in the Lower Stratosphere From Analysis of High-Resolution Infrared Solar Occultation Spectra

C. P. RINSLAND,<sup>1</sup> A. GOLDMAN,<sup>2</sup> F. J. MURCRAY,<sup>2</sup> R. D. BLATHERWICK,<sup>2</sup> J. J. KOSTERS,<sup>2</sup>  
D. G. MURCRAY,<sup>2</sup> N. D. SZE,<sup>3</sup> AND S. T. MASSIE<sup>4</sup>

Long-term trends in the concentrations of SF<sub>6</sub>, CHClF<sub>2</sub> (CFC-22), and COF<sub>2</sub> in the lower stratosphere have been derived from analysis of ca. 1980 and more recent infrared solar occultation spectra recorded near 32°N latitude at ~0.02-cm<sup>-1</sup> resolution. Consistent sets of line parameters and spectral calibration methods have been used in the retrievals to minimize systematic error effects. Quoted error limits are 1 sigma estimated precisions. The SF<sub>6</sub> and CHClF<sub>2</sub> results are based on spectra recorded by balloon-borne interferometers in March 1981 and June 1988 and a comparison of these results with the Atmospheric Trace Molecule Spectroscopy (ATMOS) Experiment/Spacelab 3 measurements obtained in May 1985 near 30°N latitude. In the 13-18 km altitude range the mean measured SF<sub>6</sub> mixing ratio in parts per trillion by volume (pptv) increased from 1.17 ± 0.21 in March 1981 to 2.02 ± 0.20 pptv in June 1988, and the CHClF<sub>2</sub> mixing ratio below 15 km altitude increased from 51 ± 8 pptv in March 1981 to 102 ± 10 pptv in June 1988. The CHClF<sub>2</sub> retrievals used new empirical CHClF<sub>2</sub> line parameters derived from 0.03-cm<sup>-1</sup> resolution laboratory spectra recorded at six temperatures between 203 and 293 K; the derived mixing ratios are ~30% higher than obtained with earlier sets of line parameters, thereby removing a large discrepancy noted previously between IR and in situ measurements of CHClF<sub>2</sub>. Assuming an exponential growth model for fitting the trends, SF<sub>6</sub> and CHClF<sub>2</sub> mean increase rates of 7.4% ± 1.9% and 9.4% ± 1.3% year<sup>-1</sup>, are obtained, respectively, which correspond to cumulative increases by factors of ~1.7 and ~2.0 in the concentrations of these gases over the 7.2-year measurement period. Analysis of spectra recorded in October 1979 and April 1989 yields COF<sub>2</sub> volume mixing ratios that are respectively 0.44 ± 0.17 and 1.21 ± 0.24 times the ATMOS/Spacelab 3 values, from which an average COF<sub>2</sub> increase rate of 10.3 ± 1.8% year<sup>-1</sup> over this time period has been estimated. The present results are compared with previously reported observations and trends and with one-dimensional model calculations. The model calculated trends are in reasonably good agreement with the observations.

## 1. INTRODUCTION

The technique of infrared absorption spectroscopy has been used for many years to measure the concentrations of gases in the Earth's atmosphere. Because of the long time span covered by these observations, there has been considerable recent interest in analyzing the old spectra and comparing the results with newer data to determine the long-term trends of important atmospheric gases. For example, ground-based spectra recorded more than 35 years ago have been studied to estimate the mean trends in the total columns of CH<sub>4</sub> and CO [Rinsland *et al.*, 1985; Rinsland and Levine, 1985; Zander *et al.*, 1989a, b]. IR spectral measurements of the stratosphere do not date back quite as far in time as the ground-based data sets. Moderate resolution (~0.2 cm<sup>-1</sup>) stratospheric observations were first obtained in the late 1960s and early 1970s [e.g., Murcray *et al.*, 1968, 1969, 1975; Goldman *et al.*, 1970], followed by high resolution (~0.02 cm<sup>-1</sup>) data in the late 1970s and early 1980s [e.g., Goldman *et al.*, 1979; Buijs *et al.*, 1980; Murcray, 1984]. We have begun a program of systematic comparison

of the early stratospheric spectra with more recent spectra recorded with the same or similar instrumentation under similar observing conditions (for example, same latitude, all data in the solar occultation mode). An initial analysis of the data revealed clear evidence for rapidly increasing concentrations of three important trace gases that have been the subject of only limited previous stratospheric investigations. In the present paper we report the trends derived for these three gases, SF<sub>6</sub>, CHClF<sub>2</sub>, and COF<sub>2</sub>.

Sulfur hexafluoride (SF<sub>6</sub>) and chlorodifluoromethane (CHClF<sub>2</sub> or CFC-22) are man-made trace atmospheric gases with strong absorption bands in the climatically important 8- to 13-μm window region. SF<sub>6</sub> is widely used as an electrical insulating gas in high-voltage electrical and electronic equipment such as circuit breakers, capacitors, transformers, and microwave components because of its high chemical stability and its ability to impede electric breakdown [e.g., Brown, 1966]. SF<sub>6</sub> has also been used as a meteorological tracer [e.g., Turk *et al.*, 1968; Reiter, 1971; Drivas and Shair, 1974]. CFC-22 is primarily used in refrigeration, but about 35% of the total is used in fluoropolymer production, which results in little release of the gas into the environment [World Meteorological Organization, 1986]. Since both gases are in wide use and their atmospheric lifetimes are believed to be long (perhaps more than 500 years for SF<sub>6</sub> [Ramanathan *et al.*, 1985] and 10-28 years for CFC-22 [World Meteorological Organization, 1982, 1989; Wuebbles, 1983; Hammitt *et al.*, 1987; Golombek and Prinn, 1989; Fisher *et al.*, 1990]), these molecules can be expected to accumulate in our environment. The principal sink for CFC-22 is the reaction with tropospheric OH. Monitoring its trend and ascertaining its

<sup>1</sup>Atmospheric Sciences Division, NASA Langley Research Center, Hampton, Virginia.

<sup>2</sup>Department of Physics, University of Denver, Denver, Colorado.

<sup>3</sup>Atmospheric and Environmental Research Incorporated, Cambridge, Massachusetts.

<sup>4</sup>National Center for Atmospheric Research, Boulder, Colorado.

Copyright 1990 by the American Geophysical Union.

Paper number 90JD01293.  
0148-0227/90/90JD-01293\$05.00

TABLE 1. Parameters for the University of Denver Balloon Flights

Parameter	Value Corresponding to the Flight			
	October 10, 1979	March 23, 1981	June 6, 1988	April 19, 1989
Latitude, °N	32.8	32.8	31.9	34.7
Longitude, °W	106.0	106.0	97.4	103.0
Float altitude, km	33.0 ± 0.5	33.5 ± 0.5	36.5 ± 0.5	36.7 ± 0.5
Scan time, * s	40	40	20/120	20/120
Maximum path difference, † cm	50	50	40/250	40/250
Field of view, arcmin	8	8	10	10
Spectral coverage, cm <sup>-1</sup>	1300–2000	740–1350	720–1300	1400–1960
Tropopause geometric height, km	15.0	10.4	14.4	13.8

\*Time required to record a single spectrum. The two entries for the June 6, 1988 and April 19, 1989 flights are the times required to record the low- and high-resolution interferograms, respectively. Single scans were analyzed from the October 10, 1979 and March 23, 1981 flight observations. In most cases, two scans with the same zero path difference were coadded, and the average spectrum was used in the analysis of the June 6, 1988 and April 19, 1989 flight measurements.

†The entries for the June 6, 1988 and April 19, 1989 flights are the maximum path differences of the low- and high-resolution interferograms, respectively.

emission rates provide a means to derive the atmospheric lifetime of CFC-22 and the global average OH concentration [International Global Atmospheric Chemistry Programme, 1989]. This latter result can provide an independent check on the global average OH concentration deduced recently from the observed methyl chloroform trends [Prinn *et al.*, 1987].

Carbonyl fluoride (COF<sub>2</sub>) is an intermediate product in the decomposition of chlorofluorocarbons in the stratosphere [Rowland and Molina, 1975; Sze, 1978]. The Atmospheric Trace Molecule Spectroscopy (ATMOS) Experiment/Spaceiab 3 (SL3) measurements indicate that COF<sub>2</sub> represents one third of the inorganic fluorine column in the stratosphere, with the remainder contained in HF [Raper *et al.*, 1987]. COF<sub>2</sub> is produced mainly from the decomposition of CCl<sub>2</sub>F<sub>2</sub> [e.g., Rowland and Molina, 1975; Jayanty *et al.*, 1975] and, to a lesser extent, from other chlorofluorocarbons, such as CFC-22 [World Meteorological Organization, 1989]. Carbonyl fluoride is destroyed by photolysis and reaction with O(<sup>1</sup>D) in the stratosphere [Sze, 1978]. Its importance lies in the need to understand the reactions that follow the breakup of the chlorofluorocarbons in the stratosphere. Recently, it has been suggested that COF<sub>2</sub> may react with H<sub>2</sub>O to form HF and CO<sub>2</sub> on the surfaces of polar stratospheric clouds [Wofsy *et al.*, 1990]. Thus observations of COF<sub>2</sub> and HF could help elucidate heterogeneous chemical processes which are important for understanding stratospheric ozone distributions, particularly over polar regions. Carbonyl fluoride is also expected to be an important intermediate in the decomposition of currently proposed alternative fluorocarbons [World Meteorological Organization, 1989].

The measurements and trends reported in this paper are based on the analysis of ~0.02-cm<sup>-1</sup> resolution infrared solar occultation spectra recorded during four stratospheric balloon flights from launch sites near 32°N latitude. The measurements were recorded in October 1979, March 1981, June 1988, and April 1989. All of the balloon flights were conducted by the University of Denver atmospheric spectroscopy group. In addition, we have compared the retrievals with results derived from the infrared solar absorption spectra obtained by the ATMOS experiment during the SL3 shuttle mission in May 1985 (see Farmer, [1987] for an

overview of the ATMOS experiment and the SL3 results). Care has been taken to use consistent sets of line parameters and spectral calibration methods to minimize systematic error effects so as to derive the most reliable long-term trends. All of the measurement data (balloon flight plus the ATMOS results) have been included in deriving the trends. Model calculations are presented to compare with the observed trends. The calculations are based on the Atmospheric and Environmental Research (AER) one-dimensional model [Sze and Ko, 1981] with updated rate data [NASA, 1987]. The model domain is from 0 to 70 km. It includes 150 gas-phase reactions and calculates the concentrations of the oxygen species (O, O(<sup>1</sup>D)), the hydrogen species (H, OH, HO<sub>2</sub>, H<sub>2</sub>O<sub>2</sub>), the nitrogen species (N, NO, NO<sub>2</sub>, HNO<sub>3</sub>, HO<sub>2</sub>NO<sub>2</sub>, N<sub>2</sub>O<sub>5</sub>, NO<sub>3</sub>), the chlorine species (Cl, ClO, OClO, Cl<sub>2</sub>O<sub>2</sub>, HCl, HOCl, ClONO<sub>2</sub>), the bromine species (Br, BrO, BrNO<sub>3</sub>, BrCl, HBr), and the tropospheric source gases (CH<sub>4</sub>, N<sub>2</sub>O, OCS, CS<sub>2</sub>, C<sub>2</sub>H<sub>6</sub>, SF<sub>6</sub>, CH<sub>3</sub>Cl, CCl<sub>4</sub>, CCl<sub>3</sub>F, CCl<sub>2</sub>F<sub>2</sub>, CHClF<sub>2</sub>, CH<sub>3</sub>CCl<sub>3</sub>, CF<sub>3</sub>CCl<sub>3</sub>, and other minor CFC species). The surface fluxes for CCl<sub>3</sub>F and CCl<sub>2</sub>F<sub>2</sub> are based on emission data reported by Gamlen *et al.* [1986]. The emission data for CHClF<sub>2</sub> are uncertain [World Meteorological Organization, 1986]. The atmospheric release rates (10<sup>9</sup> gm yr<sup>-1</sup>) used in the present model calculations are 53, 86, and 95 for the years 1975, 1980, and 1985, respectively.

## 2. BALLOON FLIGHT MEASUREMENTS

Table 1 summarizes important flight and experimental parameters for the four balloon flights. In all four experiments the spectra were recorded at sunset in the solar occultation mode. The two early balloon flights were conducted from Holloman Air Force Base near Alamogordo, New Mexico, on October 10, 1979, and March 23, 1981, using a modified Bomen model DA2.01 interferometer system (optical path difference of 50 cm). High and low sun spectra from these flights (and an earlier one on October 27, 1978) have been reported in an atlas along with a list of the measured positions and corresponding atmospheric and solar line identifications [Goldman *et al.*, 1987]. The launches of the more recent balloon flights occurred from the National



Scientific Balloon Facility (NSBF) near Palestine, Texas, on June 6, 1988, and from Fort Sumner, New Mexico, on April 19, 1989, using a new interferometer, a modified Bomem model DA3.002 system capable of recording spectra with a maximum optical path difference of 250 cm. The new system has been described recently [Murcray *et al.*, 1990], and selected regions of the full resolution spectra from the 1988 flight (and some of the high sun data collected during a balloon flight on November 18, 1987) have been published in an atlas [Goldman *et al.*, 1989a]. A description of the trace gas features observed in the spectra has also been reported [Goldman *et al.*, 1989b]. The full resolution spectra were recorded at tangent heights above 17 km (1988 flight) and above 29 km (1989 flight). Because spectral lines are pressure-broadened at low altitudes, very high resolution observations are less useful in the lower stratosphere and troposphere than at higher altitudes, and for this reason the interferometer was switched to a mode that allowed the rapid recording of spectra with a maximum optical path difference of 40 cm. Only the lower resolution spectra were used for the retrievals reported in this work. When appropriate, the full resolution scans have been analyzed to verify the quality of the line parameters assumed in the analysis.

### 3. DATA ANALYSIS AND RESULTS

As in a number of earlier investigations, the technique of nonlinear least squares spectral fitting has been used to analyze the data. Details and examples of the application of this method to the analysis of solar occultation spectra are presented in papers by Niple [1980], Niple *et al.* [1980], Goldman *et al.* [1980], and Rinsland *et al.* [1982]. Initially, the vertical profiles of SF<sub>6</sub>, CHClF<sub>2</sub>, and COF<sub>2</sub> were retrieved from the balloon flight spectra using the onion-peeling technique [Goldman and Saunders, 1979]. A comparison of the retrieved profiles with the reported ATMOS profiles indicated no differences in the relative vertical distributions of the three gases outside the errors limits of the experiments. Therefore to maximize consistency of the results for the derivation of trends, we assumed the vertical distributions retrieved from the ATMOS observations and derived a single multiplicative scaling factor for each gas relative to the reported ATMOS profile. The scale factors were determined from the individual spectra, and then the average and the standard deviation of these values were computed for each occultation to determine the relative increase (or decrease) in the stratospheric amount relative to the ATMOS observations and a statistical estimate of the

TABLE 2. ATMOS SL3 Profiles Assumed in the Present Analysis

Altitude, km	Volume Mixing Ratio in pptv		
	SF <sub>6</sub> *	CHClF <sub>2</sub> †	COF <sub>2</sub> ‡
14.0	1.42	70.4	5.0‡
16.0	1.42	70.1	10.0‡
18.0	1.42	68.1	20.1
20.0	1.12	64.0	31.2
22.0	0.83	51.7	48.4
24.0	0.83§	44.8	67.4
26.0	0.83§	39.7	82.8
28.0	0.83§	35.3	96.9
30.0	0.83§	33.3§	111
32.0	0.83§	30.1§	118
34.0	0.83§	26.9§	116
36.0	0.83§	21.8§	105
38.0	0.83§	18.6§	89.4
40.0	0.83§	15.4§	73.8§

\*Smoothed values from Rinsland *et al.* [1990].

†Zander *et al.* [1987, Table 4] scaled by 1.28. See text.

‡Retrieved from  $\nu_1$  band manifolds near 1936 cm<sup>-1</sup> [Rinsland *et al.*, 1986, Figure 3, heavy full line].

§Extrapolated value.

scatter in the results. For completeness and because we had to extrapolate the reported volume mixing ratio profiles to higher and lower altitudes, the assumed ATMOS/SL3 vertical distributions of SF<sub>6</sub>, CHClF<sub>2</sub>, and COF<sub>2</sub> are listed in Table 2.

Except as noted below, line parameters were taken from the 1986 Air Force Geophysics Laboratory high-resolution transmission (HITRAN) line list [Rothman *et al.*, 1987]. Correlative pressure-temperature profiles derived from radiosonde and satellite measurements were used in the ray-tracing calculations (M. Gelman and K. W. Johnson, National Meteorological Center (NMC), private communications, 1982, 1989). The NMC analysis also yields an estimate of the tropopause height. The value for each balloon flight is listed in Table 1.

The spectral intervals selected for the analysis are given in Table 3. In addition to retrieving the concentrations of SF<sub>6</sub>, CHClF<sub>2</sub>, and COF<sub>2</sub>, we included intervals to retrieve the concentrations of CH<sub>4</sub>, N<sub>2</sub>O, and CO<sub>2</sub>. These additional gases were included in the analysis because of uncertainties in the instrument pointing angle (about ±0.07° which corresponds to about ±0.5 km in the tangent height, 1 sigma). Following the procedures used to analyze the ATMOS observations (see, for example, Zander *et al.* [1987]), the

TABLE 3. Spectral Regions Analyzed in the Present Study

Spectral Region, cm <sup>-1</sup>	Target Molecules	Primary Interfering Molecules	Data Sets Investigated
828.82–830.00	CH <sup>35</sup> ClF <sub>2</sub>	O <sub>3</sub> , CO <sub>2</sub> , C <sub>2</sub> H <sub>6</sub>	March 1981, June 1988
945.00–949.00	SF <sub>6</sub>	CO <sub>2</sub> , O <sub>3</sub> , H <sub>2</sub> O	March 1981, June 1988
1220.00–1224.50	CH <sub>4</sub> , N <sub>2</sub> O	O <sub>3</sub>	March 1981, June 1988
1231.40–1235.00	CH <sub>4</sub> , N <sub>2</sub> O	COF <sub>2</sub>	March 1981, June 1988
1384.21–1384.70	CO <sub>2</sub>	HDO, O <sub>3</sub> , H <sub>2</sub> O	October 1979, April 1989
1385.00–1385.29	CO <sub>2</sub>	...	October 1979, April 1989
1385.65–1386.10	CO <sub>2</sub>	O <sub>3</sub> , CH <sub>4</sub>	October 1979, April 1989
1936.00–1940.00	COF <sub>2</sub>	CO <sub>2</sub> , H <sub>2</sub> O, O <sub>3</sub> , NO, solar CO	October 1979, April 1989
1952.15–1952.50	CO <sub>2</sub>	solar CO, O <sub>3</sub> , COF <sub>2</sub>	October 1979, April 1989
1955.40–1955.70	CO <sub>2</sub>	...	October 1979, April 1989

tangent altitudes of the individual spectra were adjusted until the retrieved volume mixing ratios (VMRs) of CH<sub>4</sub>, N<sub>2</sub>O, and CO<sub>2</sub> were consistent with measurements in the lower stratosphere.

Ideally, we would have preferred to use lines of N<sub>2</sub> and O<sub>2</sub> to retrieve the tangent heights of the spectra instead of CH<sub>4</sub>, N<sub>2</sub>O, and CO<sub>2</sub> lines because the VMRs of N<sub>2</sub> and O<sub>2</sub> are likely to be constant in the stratosphere to our measurement accuracy, whereas the VMRs of CH<sub>4</sub>, N<sub>2</sub>O, and CO<sub>2</sub> are probably increasing with time. These changes with time complicate the analysis of data sets from different epochs. The S branch lines of the N<sub>2</sub> electric quadrupole (1-0) vibration-rotation band, which are observable in atmospheric spectra near 2400 cm<sup>-1</sup> [e.g., Camy-Peyret et al., 1981; Goldman et al., 1981a], are not included in the spectral regions covered by any of the four balloon flights. Numerous lines of the O<sub>2</sub> electric quadrupole (1-0) vibration-rotation band have been identified in the 1500–1650 cm<sup>-1</sup> region of stratospheric spectra [Goldman et al., 1981a] and are seen in both the 1979 and 1989 balloon flights, but quantitative analysis of these features is hampered at present by the large uncertainty in the absolute values of the electric quadrupole intensities (about ±35%) [Reid et al., 1981; Rothman and Goldman, 1981].

The assumed VMRs for CH<sub>4</sub> and N<sub>2</sub>O were chosen on the basis of accurate measurements from the literature. For CH<sub>4</sub> we selected a reference value at ground level of 1.68 parts per million by volume (ppmv) for 1984.5, which corresponds to the results reported by Steele et al. [1987, Figure 6] for 30°N latitude, and an annual increase of 15.2 pptv obtained by averaging the value of 17.5 pptv reported by Rasmussen and Khalil [1986, Table 1] for 1975 to 1985 and the value of 12.8 pptv reported by Steele et al. [1987] for May 1983 to April 1985. For N<sub>2</sub>O we selected the 1985.0 surface-level reference value of 307.3 parts per billion by volume (ppbv) measured in the Pacific Northwest United States and the mean annual increase of 1.04 ppbv determined from the Pacific Northwest United States measurements and South Pole measurements between 1975 and 1985 [Rasmussen and Khalil, 1986, Table 1]. In the stratosphere we assumed the zonal mean Northern Hemisphere CH<sub>4</sub> and N<sub>2</sub>O profiles (at ~30°N) derived from the ATMOS/SL3 spectra [Gunson et al., 1990, Table 4a]. To account for the expected increases in the stratospheric concentrations of these gases with time, the ATMOS VMRs in each layer were scaled by the ratio of the calculated tropospheric abundance for the time of the balloon flight measurement to the calculated tropospheric abundance for the time of the ATMOS/SL3 flight. Because the stratospheric profiles of CH<sub>4</sub> and N<sub>2</sub>O near 30°N show significant seasonal changes [Jones and Pyle, 1984] and the ATMOS/SL3 profiles show evidence for a "fold" in their vertical distributions between 30 and 40 km which is probably the result of dynamical motions [Gunson et al., 1990], CH<sub>4</sub> and N<sub>2</sub>O features were only used to retrieve the tangent heights of scans within ~5 km of the tropopause, where the lower stratospheric VMRs are very close to those in the troposphere [e.g., Goldan et al., 1980, Figure 17]. The 1986 HITRAN compilation parameters for CH<sub>4</sub> were replaced with improved values determined from recent analysis of high-resolution laboratory spectra [Brown et al., 1989; Champion et al., 1989a, b].

All of the retrieved ATMOS profiles from the SL3 spectra are based on an assumed CO<sub>2</sub> VMR of 330 ppmv below 70

km altitude [Gunson et al., 1990]. For consistency with the ATMOS observations we assumed this profile for the time of the SL3 observations and scaled it in accordance with the mean measured rate of increase of 1.42 ppmv yr<sup>-1</sup> observed at Mauna Loa Observatory between 1974 and 1985 [Thoning et al., 1989]. In addition to the updated CH<sub>4</sub> line parameters [Brown et al., 1989; Champion et al., 1989a, b], the line list used in fitting the CO<sub>2</sub> microwindow regions included O<sub>3</sub> line parameters generated from recent high-resolution laboratory studies [Malathy Devi et al., 1987; Rinsland et al., 1988a; Flaud et al., 1989; Camy-Peyret et al., 1990]. As noted in Table 3, O<sub>3</sub> lines are observable in a number of the microwindow regions. For gases such as O<sub>3</sub> we assumed reference profiles appropriate to mid-latitude Northern Hemisphere conditions [e.g., Smith, 1982].

The precision of the tangent heights, about ±0.2 km (1 sigma), has been estimated from the scatter in the various determinations for each spectrum. There were no obvious differences in the tangent heights estimated from the various gases or different spectral regions. For a well-mixed gas in the lower stratosphere a 0.2 km change in tangent height is equivalent to change of about 3% in the VMR [Gunson et al., 1990]. Systematic errors in the tangent heights are likely to result mostly from uncertainties in the assumed volume mixing ratio profiles of CH<sub>4</sub>, N<sub>2</sub>O, and CO<sub>2</sub>, the assumed spectroscopic line parameters (primarily caused by errors in the line intensities), and the assumed pressure-temperature profiles. Error budget calculations, similar to those performed previously [Rinsland et al., 1983], indicate a total estimated error of ~0.5 km (1 sigma) in the individual tangent heights from the sum of these effects. The tangent heights of the spectra used in the retrievals are as follows: 17.9, 19.1, and 21.7 km, October 10, 1979, flight; 12.4 and 14.3 km, March 23, 1981, flight; 13.8, 14.5, 15.3, and 16.3 km, June 6, 1988, flight; and 19.0, 19.9, 21.1, 22.1, and 22.6 km, April 19, 1989, flight.

### 3.1. SF<sub>6</sub>

Analysis of SF<sub>6</sub> is based on retrievals of the 945.0–949.0 cm<sup>-1</sup> interval which contains the Q branch of the intense  $\nu_3$  band of SF<sub>6</sub> at 947.94 cm<sup>-1</sup>. This feature, which was recently identified in the ATMOS/SL3 spectra [Rinsland et al., 1990], is observable in both the 1981 and 1988 University of Denver balloon flight spectra of the lower stratosphere and upper troposphere.

In this investigation we assumed the same line parameters as adopted in the ATMOS analysis [Rinsland et al., 1990]. The primary modifications to the 1986 HITRAN compilation [Rothman et al., 1987] are the addition of SF<sub>6</sub> line parameters with positions and relative intensities for the  $\nu_3$  band [Bobin et al., 1987], normalized to the band intensity of Schatz and Hornig [1953], and SF<sub>6</sub> air-broadened half widths calculated by Tejwani and Fox [1987]. The ozone lines on the 1986 HITRAN compilation [Rothman et al., 1987] were replaced with a line list derived from analysis of laboratory spectra recorded with the McMath Fourier transform spectrometer on Kitt Peak [Flaud et al., 1990]. Analysis of the ATMOS observations indicated a constant SF<sub>6</sub> VMR of 1.42 ± 0.37 pptv (1 sigma) between 12 and 18 km and a possible decrease in the SF<sub>6</sub> VMR between 18 and 22 km. The evidence for the decline was not conclusive because of the weakness of the SF<sub>6</sub> absorption.

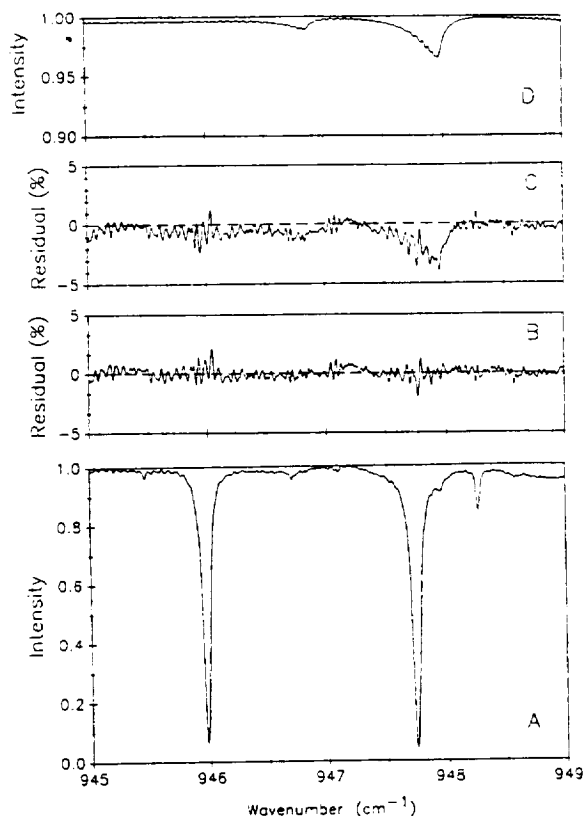


Fig. 1. (a) The SF<sub>6</sub>  $\nu_3$  band Q branch region in a 1981 balloon flight spectrum. (b) spectral fitting residuals obtained by fitting the data for SF<sub>6</sub>, CO<sub>2</sub>, and H<sub>2</sub>O; (c) spectral fitting residuals obtained by fitting the data for CO<sub>2</sub> and H<sub>2</sub>O (no SF<sub>6</sub> lines in the analysis); and (d) a simulation of the absorption by SF<sub>6</sub> only computed for the same atmospheric path and the retrieved SF<sub>6</sub> atmospheric amount. The residuals in Figures 1b and 1c (measured minus calculated values) and the calculated SF<sub>6</sub> absorption spectrum (Figure 1d) are plotted on the same vertical scale, which has been expanded relative to the vertical scale of Figure 1a for clarity. The absorption peaks of the SF<sub>6</sub>  $\nu_3$  and  $\nu_3 + \nu_6 - \nu_6$  Q branches are located near 947.94 and 946.83 cm<sup>-1</sup>, respectively. The spectral data were recorded at sunset from a float altitude of 33.5 km and at an astronomical zenith of 94.92°. The corresponding refracted tangent height is 12.4 km.

As illustrated in Figure 1, SF<sub>6</sub> absorption is weak in the 1981 spectra owing to its extremely low atmospheric abundance, but the Q branch feature is detectable above the noise level of the data. From bottom to top the panels show (Figure 1a) an observed spectrum in the SF<sub>6</sub> Q branch region at a tangent height of 12.4 km; (Figure 1b) the residuals (observed minus calculated intensities) obtained by fitting the data for SF<sub>6</sub>, CO<sub>2</sub>, and H<sub>2</sub>O; (Figure 1c) the residuals obtained by fitting the spectrum for CO<sub>2</sub> and H<sub>2</sub>O without SF<sub>6</sub> lines in the analysis; and (Figure 1d) the calculated absorption by SF<sub>6</sub> alone based on the SF<sub>6</sub> column amount retrieved from the spectrum. The standard deviation of the residuals with SF<sub>6</sub> lines in the analysis is about one-half that achieved without SF<sub>6</sub> lines. The maximum SF<sub>6</sub> absorption in this example (~3%) is less than derived at the same tangent height from both the 1985 ATMOS observations (see Figure 4b of Rinsland et al., [1990] for a sample fit) and the 1988 balloon flight spectra (not shown), indicating a significant increase in the VMR of this gas in the lower stratosphere.

Relative to the ATMOS results, the analysis indicates SF<sub>6</sub> multiplicative scale factors of  $0.82 \pm 0.15$  for the March 1981

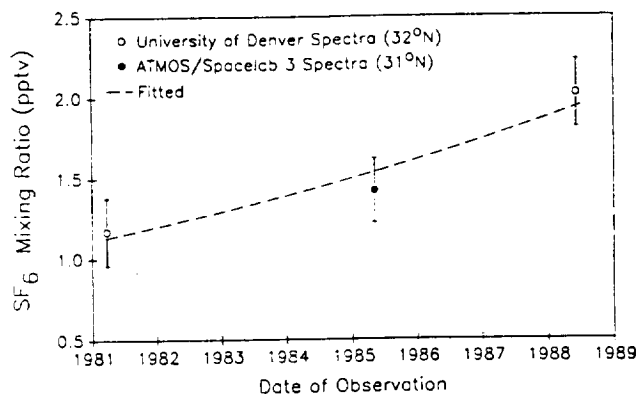


Fig. 2. Mean SF<sub>6</sub> volume mixing ratio below 18 km altitude retrieved from the March 1981 and June 1988 University of Denver balloon flight spectra and the corresponding value retrieved from the ATMOS/SL3 spectra [Rinsland et al., 1990] plotted versus observation date. The error bars are estimated 1-sigma precisions. The dashed line shows a fit to the measurements calculated assuming that the SF<sub>6</sub> volume mixing ratio is increasing at an exponential rate. The derived trend ( $7.4 \pm 1.9\%$  year<sup>-1</sup>, 1 sigma) corresponds to a factor of 1.71 increase in the SF<sub>6</sub> volume mixing ratio between March 1981 and June 1988.

balloon flight and  $1.42 \pm 0.14$  for the June 1988 balloon flight. The error limits indicate the estimated precisions (1 sigma) which were calculated by taking the standard deviation of the SF<sub>6</sub> scale factors retrieved from the individual spectra. The scale factors correspond to SF<sub>6</sub> VMRs in the 12–18 km altitude region of  $1.17 \pm 0.21$  and  $2.02 \pm 0.20$  pptv, respectively. The absolute uncertainties are, of course, larger. Considering the various sources of random error (for example, finite signal-to-noise ratio) and systematic error (for example, the uncertainty in the SF<sub>6</sub> line intensities and air-broadened half widths, uncertainty in the calculation of the interfering absorption lines near the SF<sub>6</sub> Q branch, uncertainty in the derivation of the tangent heights due to CH<sub>4</sub> and N<sub>2</sub>O line parameter errors, retrieval algorithm uncertainties, errors in the assumed pressure-temperature profiles, and instrument distortions such as zero level shift and phase errors), the estimated absolute 1-sigma error limits are about  $\pm 45\%$  and  $\pm 25\%$  for the 1981 and 1988 flight data, respectively. The important sources of systematic error (such as the errors in the assumed line intensities) bias all the retrievals by the same relative amount so that the derived long-term trend is unchanged. The same is also true for the CHClF<sub>2</sub> and COF<sub>2</sub> analyses.

The mean SF<sub>6</sub> volume mixing ratios below 18 km derived from the balloon-borne spectra and the ATMOS spectra [Rinsland et al., 1990] are plotted versus observation date in Figure 2. The dashed line shows the trend computed from a least squares fit to the three observations assuming that the SF<sub>6</sub> VMR is increasing at an exponential rate with time, that is,  $C = C_0 \exp[\beta(t - t_0)]$ , where  $C_0$  is the concentration at time  $t_0$ ,  $C$  is the concentration at time  $t$ , and  $\beta$  is the rate of increase. Assuming this equation, a fit to the results indicates an average SF<sub>6</sub> increase rate between March 1981 and June 1988 of  $7.4 \pm 1.9\%$  year<sup>-1</sup> (1 sigma) which corresponds to a factor of 1.71 increase in the SF<sub>6</sub> VMR. If a linear increase in the SF<sub>6</sub> volume-mixing ratio with time is assumed, a slightly poorer fit to the measurements is obtained, but the difference is not significant given the estimated precision of the data. The measured mean  $7.4 \pm 1.9\%$  year<sup>-1</sup>

(1 sigma) increase rate is less than the AER one-dimensional model calculated rate of 10.3% year<sup>-1</sup> over the 1981 to 1988 period on the basis of known emission data. Work is in progress on estimating the magnitudes of other sources and the sinks of atmospheric SF<sub>6</sub> (M. K. W. Ko et al., manuscript in preparation, 1990).

The present results can be compared with SF<sub>6</sub> trends measured at the surface [Rasmussen and Khalil, 1983] and in the stratosphere [Leifer et al., 1982; Leifer and Juzdan, 1985] and the atmospheric trend inferred from the depth profile of dissolved SF<sub>6</sub> in the northeast Atlantic ocean [Watson and Liddicoat, 1985]. Rasmussen and Khalil [1983] analyzed surface level electron-capture gas chromatography measurements of SF<sub>6</sub> obtained between 1979 and 1983 and derived annual exponential increase rates of  $12.9 \pm 2.6\%$  at the south pole and  $8.6 \pm 2.3\%$  in the pacific northwest and a global average annual rate of  $10.5 \pm 2.4\%$  ( $\pm$  values are the quoted 90% confidence limits). The trend derived from the IR data is slightly less than these results, but the IR and pacific northwest trends overlap within the error limits. The IR results agree very well with the trend and mixing ratios reported by Watson and Liddicoat [1985]. Their best fit to their data was obtained with a linear increase with time,  $C = 0.34 + 0.084(Yr - 1970)$ , where  $Yr$  is the calendar year and  $C$  is the inferred SF<sub>6</sub> atmospheric mixing ratio in pptv. Values computed with this formula and the corresponding measured IR mixing ratios are 1.28 and 1.17 pptv for the 1981 balloon flight, 1.63 and 1.42 pptv for the ATMOS/SL3 mission, and 1.89 and 2.02 pptv for the 1988 balloon flight, respectively. On the basis of electron capture gas chromatographic analysis of air samples, Leifer et al. [1982] estimated that the mean northern hemisphere stratospheric concentration of SF<sub>6</sub> increased by  $61 \pm 20\%$  between 1974 and 1979. Analysis of additional SF<sub>6</sub> measurements from the same program yielded an estimated linear increase rate of 21% year<sup>-1</sup> between April 1974 and November 1983, corresponding to an increase from 0.16 to 0.48 pptv [Leifer and Juzdan, 1985]. On a compound basis this increase is equal to 12% year<sup>-1</sup> which agrees very well with a model calculated increase rate of 14% year<sup>-1</sup> over the decade 1973–1983 (M. K. W. Ko et al., manuscript in preparation, 1990). The smaller rate of increase ( $\sim 7.4\%$  year<sup>-1</sup>) between 1981 and 1988 derived from the infrared data suggests a decline in the percent rate of SF<sub>6</sub> atmospheric accumulation. As noted previously [Watson and Liddicoat, 1985; Rinsland et al., 1990], there appears to be a problem with the calibration of at least some of the reported SF<sub>6</sub> measurements. Our VMRs and those of Watson and Liddicoat [1985] are significantly higher than corresponding values reported by Rasmussen et al. [1981], Rasmussen and Khalil [1983], Leifer et al. [1981, 1982], Leifer and Juzdan [1985], Singh et al. [1977, 1979, 1983], and Krey et al. [1977].

### 3.2. CHClF<sub>2</sub> (CFC-22)

Retrievals of CHClF<sub>2</sub> are based on the narrow, intense absorption feature at 829.05 cm<sup>-1</sup>, which was used for the first spectroscopic detection of CHClF<sub>2</sub> in the lower stratosphere [Goldman et al., 1981b]. On the basis of an extensive analysis of the infrared bands of gas phase CHClF<sub>2</sub>, this feature has been assigned to the  $Q$  branch of  $2\nu_6$  band of CH<sup>35</sup>ClF<sub>2</sub> [Brown et al., 1988]. According to this work, the enhanced intensity of the 829.05-cm<sup>-1</sup>  $Q$  branch results from

the Fermi resonance with the nearby strong  $\nu_4$  fundamental. The rotational structure of the  $2\nu_6$  band has not been analyzed. The 829.05-cm<sup>-1</sup>  $Q$  branch feature is anomalously narrow; even at 0.002-cm<sup>-1</sup> resolution, its width has been reported to be essentially instrument limited [Magill et al., 1986]. Unpublished low-pressure laboratory spectra recorded at the University of Denver show the  $Q$  branch feature narrower at 0.002-cm<sup>-1</sup> resolution than at 0.02-cm<sup>-1</sup> resolution and without recordable fine structure. However, the measured  $Q$  branch width is 0.013 cm<sup>-1</sup> full width half maximum absorption (FWHM) in a 0.002-cm<sup>-1</sup> resolution University of Denver spectrum recorded with 0.31 torr of CHClF<sub>2</sub> in a 5-cm-long absorption cell, indicating that the feature is significantly broader than the interferometer instrument function. The peak absorption by the CH<sup>35</sup>ClF<sub>2</sub>  $2\nu_6$   $Q$  branch is 30% in this spectrum so that the observed broadening is unlikely to be due to saturation effects.

As in previous studies [Zander et al., 1987; Rinsland et al., 1988b, 1989], empirical CHClF<sub>2</sub> line parameters were used to model the unresolved rotational structure of the CH<sup>35</sup>ClF<sub>2</sub>  $2\nu_6$  band  $Q$  branch. We modified the previous sets of parameters based on new 0.03-cm<sup>-1</sup> resolution laboratory measurements recorded at six temperatures between 203 and 293 K. Details of the laboratory investigation and a description of the spectra have been reported by McDaniel et al. [1990]. The measured cross sections are believed to be accurate to 10% or better. A recently reported room temperature measurement of the integrated intensity of the 12- $\mu$ m CHClF<sub>2</sub> bands [Varanasi and Chudamani, 1988] is within 5% of the corresponding value derived from the McDaniel et al. [1990] spectra, in agreement with this error estimate. Because the CH<sup>35</sup>ClF<sub>2</sub>  $Q$  branch feature is unresolved in the McDaniel et al. [1990] laboratory spectra and their cross-section measurements do not properly take into the account the effects of pressure broadening, the selection of the CH<sup>35</sup>ClF<sub>2</sub>  $Q$  branch parameters was also guided by fittings to higher-resolution measurements, the 0.003- and  $\sim 0.02$ -cm<sup>-1</sup> resolution University of Denver stratospheric solar spectra and  $\sim 0.005$ -cm<sup>-1</sup> resolution ground-based solar spectra recorded from Kitt Peak over a range of zenith angles [Rinsland et al., 1989]. The shape of the modeled  $Q$  branch is essentially the same as adopted previously, but the integrated  $Q$  branch intensity at room temperature obtained from the new laboratory measurements is lower by  $\sim 20\%$ . Also, the peak CHClF<sub>2</sub> cross section in the new laboratory measurements increases only by a factor of 1.13 as the temperature is lowered from 293 to 203 K, a significantly smaller increase than is predicted with the earlier data. The combination of these effects produces line intensities at lower stratospheric temperatures that are  $\sim 30\%$  lower than assumed in the past [Zander et al., 1987; Rinsland et al., 1988b, 1989], and therefore the retrieved CHClF<sub>2</sub> VMRs are higher by the same amount. In both the laboratory and atmospheric analyses the vibrational partition function of CHClF<sub>2</sub> was calculated as a function of temperature assuming the harmonic oscillator approximation and the revised assignments and fundamental frequencies reported by Brown et al. [1988]. The assignments and fundamental frequencies of Plyler and Benedict [1951] were assumed in the previous studies [Zander et al., 1987; Rinsland et al., 1988b, 1989]. Over the range of atmospheric temperature ( $\sim 200$ –300 K), this change introduces a difference in the calculated temperature correction to the CHClF<sub>2</sub> line inten-

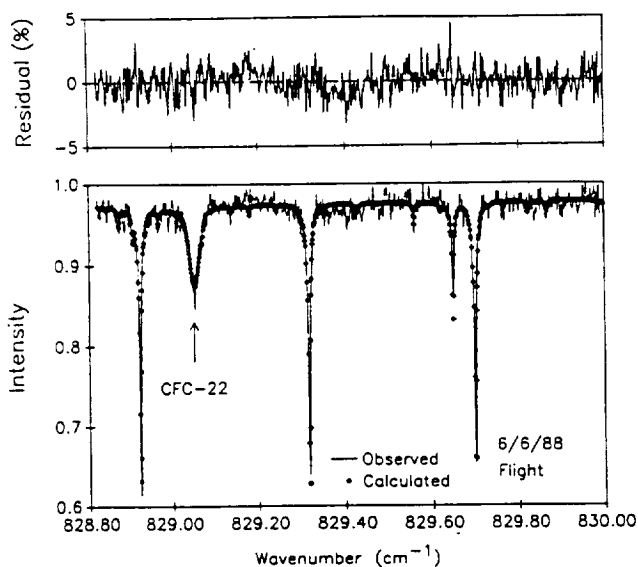


Fig. 3. Example of a least squares fit to a  $0.003\text{-cm}^{-1}$  resolution stratospheric solar occultation spectrum (June 6, 1988, balloon flight) in the region of the unresolved Q branch of  $2\nu_6$  band of  $\text{CH}^{35}\text{ClF}_2$  at  $829.051\text{ cm}^{-1}$ . The spectral data were recorded at sunset from a float altitude of 36.5 km and at an astronomical zenith of  $94.60^\circ$  during the June 6, 1988, balloon flight. The corresponding refracted tangent height is 17.1 km. The residuals (measured minus calculated values) are shown in the upper panel on an expanded vertical scale.

sities of  $<0.4\%$ . The 1986 HITRAN ozone line parameters in this region were replaced with improved values determined in a recent analysis [Pickett *et al.*, 1988].

The stratospheric spectra were analyzed over the  $828.82\text{--}830.00\text{ cm}^{-1}$  interval with the VMRs of both  $\text{CHClF}_2$  and  $\text{O}_3$  included as free parameters in the retrievals. First, the  $0.003\text{-cm}^{-1}$  resolution spectra recorded during the June 1988 balloon flight were fitted over this interval to verify the quality of the line parameters at the highest recorded resolution. Figure 3 illustrates the results obtained from analysis of a spectrum recorded at a tangent height of 17.1 km. As can be seen, the residuals are close to the noise level of the data (the location of the  $\text{CH}^{35}\text{ClF}_2$  Q branch is marked). The lower altitude  $0.025\text{-cm}^{-1}$  resolution scans from the 1988 flight and the  $0.02\text{-cm}^{-1}$  resolution scans from the 1981 flight were then fitted. The ATMOS/SL3 zonal average spectra at  $31^\circ\text{N}$  latitude were also reanalyzed for  $\text{CHClF}_2$  and compared with the retrievals reported previously [Zander *et al.*, 1987]; the agreement between the observed and best fit spectra and the retrieved vertical profile shape are very similar to the earlier results, but the absolute  $\text{CHClF}_2$  VMRs are  $\sim 30\%$  higher than obtained with the previous set of line parameters (for example, the retrieved mean  $\text{CHClF}_2$  VMR below 15 km increased from 55 to 70 pptv). In the final analysis, all of the results have been expressed relative to the reported ATMOS vertical VMR distribution [Zander *et al.*, 1987] scaled by 1.28 to account for the effect of the changes in the  $\text{CHClF}_2$  line parameters.

Figure 4 shows the measured and AER one-dimensional model calculated  $\text{CHClF}_2$  VMRs plotted versus time. In the figure the profile scaling factors of  $0.74 \pm 0.11$  for the March 1981 flight data and  $1.46 \pm 0.15$  for the June 1988 flight data relative to the ATMOS/SL3 observations (error limits are estimated 1-sigma precisions) have been multiplied by 70

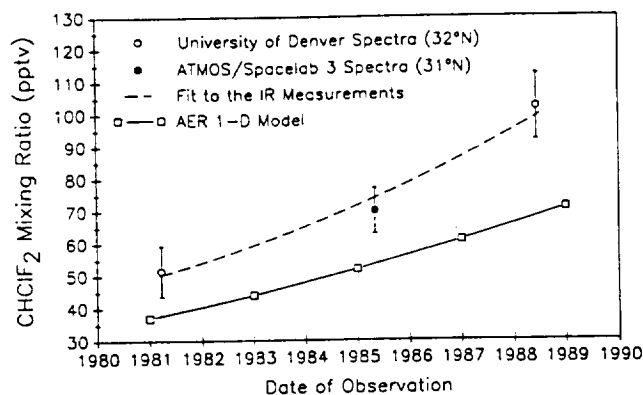


Fig. 4.  $\text{CHClF}_2$  volume mixing ratio below 15 km altitude retrieved from IR solar occultation spectra and corresponding predictions of the AER one-dimensional model plotted versus time. All of the IR results were obtained with the revised  $\text{CHClF}_2$  empirical line parameters described in the text. The error bars are estimated 1-sigma precisions. The dashed line shows a fit to be measurements obtained assuming the  $\text{CHClF}_2$  volume mixing ratio is increasing with time at an exponential rate. The derived trend ( $9.4 \pm 1.3\% \text{ year}^{-1}$ , 1 sigma) corresponds to a factor of 1.97 increase in the  $\text{CHClF}_2$  volume mixing ratio between March 1981 and June 1988.

pptv to convert to VMRs below an altitude of 15 km, where the  $\text{CHClF}_2$  VMR has been assumed to be constant. The dashed line is a fit to the measurements assuming an exponential rate of increase in the VMR during this time period. This curve corresponds to an average  $\text{CHClF}_2$  exponential increase rate of  $9.4 \pm 1.3\% \text{ year}^{-1}$  (1 sigma) which equals a  $\text{CHClF}_2$  VMR increase of a factor of 1.97 between March 1981 and June 1988. As for  $\text{SF}_6$ , a model that assumes a linear increase in the volume mixing ratio with time yields a slightly poorer fit than the exponential increase model, but the results from both are within the estimated precisions of the measurements. The AER one-dimensional model VMRs, which are on average 0.72 times the measurements, correspond to a calculated  $\text{CHClF}_2$  increase rate of  $8.2\% \text{ year}^{-1}$ , slightly lower than the measured IR trend. The calculated global increase rate of  $10.8\% \text{ year}^{-1}$  on October 1, 1984, reported by Golombek and Prinn [1989, Table 2] based on calculations with a global three-dimensional atmospheric circulation and chemistry model, is slightly higher than our measured IR trend. The secular increase in  $\text{CHClF}_2$  is illustrated in Figure 5 where the absorption by  $\text{CHClF}_2$  is compared in nearly equal air mass spectra from the 1981 and 1988 balloon flights.

Measured  $\text{CHClF}_2$  trends have been reported previously by a number of investigators [Fabian, 1986; Fabian *et al.*, 1989; Khalil and Rasmussen, 1981, 1987; Rasmussen and Khalil, 1982, 1983; Watson *et al.*, 1988, Table C-8.1; Rinsland *et al.*, 1989]. As summarized by Rinsland *et al.* [1989], the reported ground-based studies indicate  $\text{CHClF}_2$  increase rates of  $10\text{--}13\% \text{ year}^{-1}$  before 1983, followed by a recent slowdown in the percent rate of  $\text{CHClF}_2$  increase (for example,  $7.1\% \text{ year}^{-1}$  at Cape Grim, Tasmania,  $41^\circ\text{S}$  latitude, for 1986 [Watson *et al.*, 1988]). The only previously reported trend based on stratospheric observations [Fabian *et al.*, 1989] yields a slightly higher rate of increase,  $\sim 10\% \text{ year}^{-1}$  for the 1982–1987 period. The rate of increase derived in the present study is somewhat less than the stratospheric rate of Fabian *et al.* [1989] but more than determi-

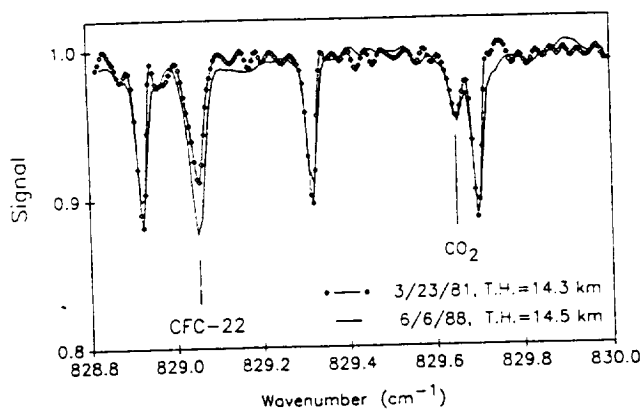


Fig. 5. Comparison of the absorption by CHClF<sub>2</sub> in nearly equal air mass spectra from the 1981 and 1988 balloon flights. The location of the unresolved CHClF<sub>2</sub>  $2\nu_6$  Q branch and a CO<sub>2</sub> line are marked. The other strong features are O<sub>3</sub> lines. The tangent height (T.H.) of each spectrum is given in the lower right corner of the figure. Note that the resolution of the 1981 flight spectrum is about 20% higher than that of the 1988 flight spectrum. Therefore for a given amount of total absorption a measured feature appears slightly narrower and deeper in the 1981 flight spectrum than in the 1988 flight spectrum. The secular increase in CHClF<sub>2</sub> can be noted by comparing the total areas of the CHClF<sub>2</sub> Q branch in the two spectra.

nations of the recent trend infrared from surface-level sampling [Khalil and Rasmussen, 1987; Watson et al., 1988, Table C-8.1]. The trend determined here from the stratospheric infrared observations is also slightly higher than the trend of  $7.8 \pm 1.0\%$  year<sup>-1</sup> (2 sigma) inferred from total column measurements derived from ground-based infrared spectra recorded between December 1980 and May 1988 from Kitt Peak (31.9°N latitude) [Rinsland et al., 1989].

A discrepancy between the infrared and air-sampling VMR measurements of CHClF<sub>2</sub> was noted recently [Rinsland et al., 1988b, 1989]. The magnitude of the difference was estimated as ~30–40% with the infrared results systematically lower than the in situ data. Analysis with the new CHClF<sub>2</sub> absorption cross-section measurements [McDaniel et al., 1990] increases the retrieved infrared CHClF<sub>2</sub> VMRs by ~30%, so that the results of both techniques are now in much better agreement. Predicted atmospheric burdens derived from estimated industrial emissions appear to be lower than in situ measurements [Rasmussen et al., 1980; Khalil and Rasmussen, 1981; Wuebbles, 1983; Fabian, 1986; Fabian et al., 1989] except for the recent model calculations by Golombek and Prinn [1989] who used the production data published by the World Meteorological Organization [1986]. Obviously, reliable estimates of industrial emissions are needed to ascertain whether there is a discrepancy between models and observations. The correction to the IR measurements of CHClF<sub>2</sub> is also important because the absolute calibrations of CHClF<sub>2</sub> and methychloroform (CH<sub>3</sub>CCl<sub>3</sub>) have been identified as important for the determination of average tropospheric hydroxyl radical (OH) concentrations [International Global Atmospheric Chemistry Programme, 1989].

### 3.3. COF<sub>2</sub>

Three bands of COF<sub>2</sub>, the  $\nu_6$  at 774 cm<sup>-1</sup>, the  $\nu_4$  at 1243 cm<sup>-1</sup>, and the  $\nu_1$  at 1944 cm<sup>-1</sup>, have been identified in

high-resolution infrared stratospheric solar occultation spectra [Rinsland et al., 1986; Goldman et al., 1989b]. In the  $\nu_6$  region, only the unresolved Q branch feature has been detected since the manifolds in the P and R branches are rather weak (see Murcray and Goldman [1981] for an example of a COF<sub>2</sub> laboratory spectrum covering this band). Features of the  $\nu_4$  band have been identified throughout the 1220–1260 cm<sup>-1</sup> region of the 1988 balloon flight spectra [Goldman et al., 1989b]. Manifolds of the  $\nu_1$  band are visible in the 1989 balloon flight spectra from about 1930 to 1955 cm<sup>-1</sup>.

The absolute accuracies of COF<sub>2</sub> retrievals are significantly limited by the uncertainties in the COF<sub>2</sub> line parameters. At the time of the first detection of COF<sub>2</sub>, no line-by-line parameters were available for any of the three observable bands. Preliminary profiles derived from measurements of the equivalent width of the  $\nu_6$  band Q branch and spectral fits to several manifolds of the  $\nu_1$  band near 1938 cm<sup>-1</sup> using empirical COF<sub>2</sub> parameters were shown to differ by as much as a factor of 1.5 [Rinsland et al., 1986]. Since then, the  $\nu_6$  band has been analyzed [Thakur et al., 1987; Goldman et al., 1990] and preliminary line-by-line parameters have been generated for both the  $\nu_4$  and  $\nu_1$  regions (see Goldman et al. [1989b] and Brown and Cohen [1989] for descriptions of the parameters for the  $\nu_4$  and  $\nu_1$  regions, respectively), but difficulties remain because of the effects of unmodeled perturbations in the  $\nu_4$  and  $\nu_1$  bands and inconsistencies in the calibrations of the absolute intensities in all three COF<sub>2</sub> bands. As discussed by Goldman et al. [1990], several chemical reactions are known to cause the decomposition of COF<sub>2</sub> in laboratory samples, and impurities have often been reported. To minimize these error effects, the COF<sub>2</sub> trend reported in this paper has been derived from analysis of the  $\nu_1$  band manifolds only.

In the analysis of the  $\nu_1$  region we used the preliminary COF<sub>2</sub> line parameters calculated for the Fermi resonant  $\nu_1$  and  $2\nu_2$  bands by Brown and Cohen [1989], provided to us as a private communication (1989). A mean COF<sub>2</sub> air-broadened half width of 0.0896 cm<sup>-1</sup> atm<sup>-1</sup> at 296 K was calculated by averaging the six microwave N<sub>2</sub>-broadening measurements of Srivastava and Kumar [1976, Table 2]. This value was assumed for all COF<sub>2</sub> lines along with an arbitrary T<sup>-0.75</sup> half width temperature dependence. The vibration partition function for COF<sub>2</sub> was computed with the fundamental frequencies reported by Mallinson et al. [1975] and the standard harmonic oscillator approximation. For O<sub>3</sub> we used the calculated line positions and intensities reported in a number of recent investigations [Malathy Devi et al., 1987; Rinsland et al., 1988a; Camy-Peyret et al., 1990] with O<sub>3</sub> air-broadened half widths computed using the empirical polynomial expression reported by Flaud et al. [1990]. Solar CO lines were simulated as described by Rinsland et al. [1982] using the Minnaert formula.

Simulations with the new O<sub>3</sub> line parameters indicate that O<sub>3</sub> is an important interferent gas in the COF<sub>2</sub>  $\nu_1$  band region. Ozone features with central depths of up to 3% are predicted between 1930 and 1955 cm<sup>-1</sup>. A number of these features have been identified in the balloonborne solar spectra. The strongest O<sub>3</sub> lines in this region are from the  $3\nu_3 - \nu_1$  hot band, which has a band center at 1942.9509 cm<sup>-1</sup> [Camy-Peyret et al., 1990]. Several of the COF<sub>2</sub> manifolds are contaminated by the O<sub>3</sub> absorption, for example, the 1937.522-cm<sup>-1</sup> feature. Ozone laboratory spectra

TABLE 4. Evaluation of Spectral Interference Effects Near Selected Manifolds of the COF<sub>2</sub>  $\nu_1$  Band in the 1936.0–1940.0 cm<sup>-1</sup> Spectral Region

COF <sub>2</sub> Manifold Position, cm <sup>-1</sup> *	Atmospheric and Solar Line Interferences
1936.2587	Slight overlap with two O <sub>3</sub> lines
1936.6820	Slight blending with a solar CO line
1937.1037	Slight blending with a weak CO <sub>2</sub> line
1937.5218	Blended with an O <sub>3</sub> line
1938.3567	Unblended
1938.7736	Blended with a weak solar CO line
1939.1872	Unblended

\*Derived from laboratory spectra [Rinsland *et al.*, 1986, Table 1]. Two COF<sub>2</sub> manifolds with severe blends are not included in the table.

recorded at 0.005-cm<sup>-1</sup> resolution with the McMath Fourier transform spectrometer on Kitt Peak clearly show this overlapping O<sub>3</sub> line. The ATMOS compilation [Brown *et al.*, 1987], which was used in the previous analysis of COF<sub>2</sub>, did not contain any O<sub>3</sub> lines between 1926.89 and 1945.42 cm<sup>-1</sup>, so that the O<sub>3</sub> interference effects were not noticed in the earlier study of COF<sub>2</sub> in the  $\nu_1$  band region [Rinsland *et al.*, 1986].

The 1936.0–1940-cm<sup>-1</sup> region is the most favorable interval for quantitative analysis of the  $\nu_1$  band manifolds of COF<sub>2</sub>. The COF<sub>2</sub> manifolds in this region are near the intensity maximum in the *P* branch of the  $\nu_1$  band. The strongest *R* branch manifolds, which occur near 1950 cm<sup>-1</sup>, are more severely contaminated by O<sub>3</sub> lines. Table 4 presents an evaluation of the interference effects for each of the COF<sub>2</sub> manifolds in the 1936–1940 cm<sup>-1</sup> interval. Although simulations indicate that none of these COF<sub>2</sub> features are isolated from atmospheric and solar interferences at the resolution of the present measurements, the manifolds at 1936.259, 1936.682, 1937.104, 1938.357, and 1939.187 cm<sup>-1</sup> are only slightly contaminated and are believed to be the most favorable COF<sub>2</sub> features for quantitative analysis from our data sets.

Derivation of the COF<sub>2</sub> long-term trend from the balloon-borne spectra is complicated by four factors: (1) the interference problem already mentioned, (2) the weakness of the COF<sub>2</sub> features (at most 3% absorption), (3) the occurrence of complex, relatively strong (~5% of peak intensity) channel spectra in the 1979 flight data (and to a lesser extent in the 1989 flight spectra), and (4) the limited signal-to-rms noise of the 1979 flight spectra (~100) as compared to the 1989 flight spectra (~200). These effects can be seen in Figures 6 and 7 which illustrate the flight data and the results of the least squares spectral fitting analysis.

In the upper panel of Figure 6, 1979 and 1989 flight spectra recorded at tangent heights near 19.0 km are compared with a simulation generated without COF<sub>2</sub> lines. Tick marks at top and beneath each spectrum indicate the locations of the five nearly unblended COF<sub>2</sub> spectral features. All five are easily seen in the 1989 flight spectrum (bottom scan). The features at 1936.259, 1936.682, and 1937.104 cm<sup>-1</sup> appear to be present in the 1979 flight spectrum (middle scan), but the ones at 1938.357 and 1939.187 cm<sup>-1</sup> are not obvious. Two heavy arrows have been drawn beneath the 1979 flight spectrum in regions of minimal absorption near 1936.8 and 1938.3 cm<sup>-1</sup>. The effect of channeling on the shape of the

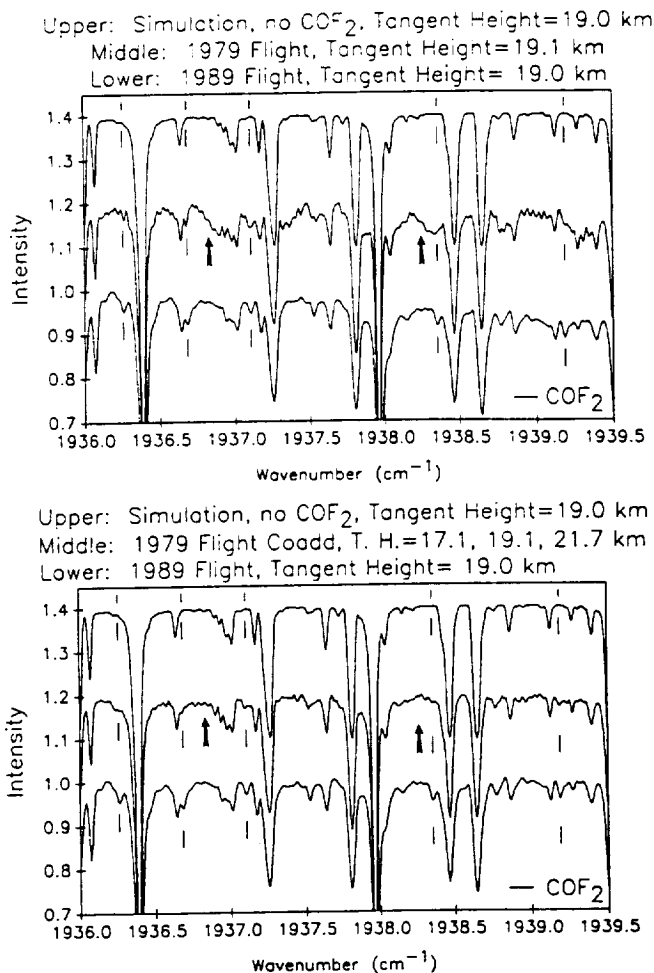


Fig. 6. Comparison of 1979 and 1989 balloon flight spectra in the region of the strongest *P* branch manifolds of the COF<sub>2</sub>  $\nu_1$  band. The data are shown on an expanded vertical scale and are offset vertically for clarity. Only the upper part of each spectrum is shown. Tick marks at top and beneath each spectrum indicate the locations of five COF<sub>2</sub> manifolds with minimal blending. In Figure 5a are plotted a simulation generated without COF<sub>2</sub> lines for a tangent of 19.0 km (top scan), a 1979 flight spectrum recorded at a tangent height of 19.1 km (middle scan), and a 1989 flight spectrum recorded at a tangent height of 19.0 km (bottom scan). Two arrows mark regions containing only weak lines; the effects of channeling and finite signal-to-noise (especially in the 1979 flight data) can be noticed by comparing the measured spectra and the simulation in these regions. In the lower panel the simulation without COF<sub>2</sub> from the upper panel is repeated at top, the middle spectrum is a coadd of 1979 flight spectra recorded at tangent heights of 17.1, 19.1, and 21.7 km, and the lower spectrum is the 1989 flight spectrum recorded at a tangent height of 19.0 km. The measured spectral intensities in the middle and bottom plots have been divided at each wave number by the calculated 100% transmittance level derived from a spectral least squares retrieval analysis of the data; this procedure has been done to remove the effects of channeling from the spectra. Two arrows in each panel mark regions with only relatively weak solar and atmospheric line absorption. The background in these intervals can be used to judge the spectral signal-to-noise and the distortion effects due to channeling.

background and the limited signal-to-noise ratio of the 1979 flight data can be noted by comparing the three spectra in this region.

Some improvement in the visibility of the COF<sub>2</sub> features can be achieved by correcting the background envelope for channeling effects and coadding 1979 flight scans with similar



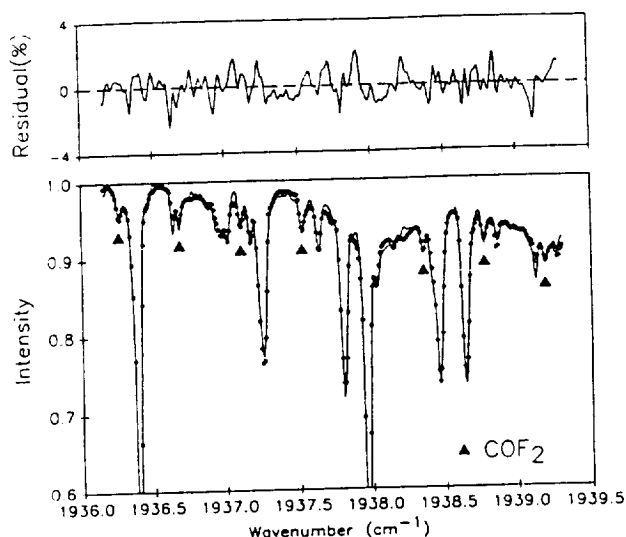


Fig. 7. Example of a least squares fit in the region of the COF<sub>2</sub>  $\nu_1$  band. The lower panel shows the measured spectrum (solid line) and the least squares best fit calculated spectrum (open diamonds). The measured spectrum has been normalized to the highest measured intensity in the interval; only the upper 40% of the spectra are plotted. Solid triangles beneath the spectrum mark the location of the five nearly unblended COF<sub>2</sub> manifolds. The upper panel shows the residuals (observed minus calculated) on an expanded vertical scale. The measured spectrum was recorded during the 1989 balloon flight from a float altitude of  $32.8 \pm 0.5$  km. The astronomical zenith angle and the refracted tangent height of the spectrum are  $94.08^\circ$  and 21.1 km, respectively. The standard deviation of the fit is 0.74%, close to the noise level in the spectrum.

zenith angles to improve the signal-to-noise. In the lower panel of Figure 6, reprocessed spectra from the 1979 and 1989 flights are compared with the same spectral simulation as shown in the upper panel. Each measured spectrum has been divided by the calculated 100% transmission curve determined from the spectral least squares retrieval analysis of the data. Note that the background in the two regions indicated by heavy arrows is now nearly flat, as in the simulation. The channeling correction has preserved the fine spectral structure, as can be seen for example by comparing the weak lines near  $1936.9 \text{ cm}^{-1}$  in the 1979 flight spectrum with the features in the simulation. The 1979 flight spectrum was produced by coadding spectra recorded at tangent heights of 17.1, 19.1, and 21.7 km. The signal-to-noise of the coadded spectrum is improved, although it is still less than the signal-to-noise of the 1989 flight spectrum at bottom. Except for the COF<sub>2</sub> feature at  $1938.357 \text{ cm}^{-1}$ , the marked COF<sub>2</sub> manifolds appear to be present in the coadded 1979 flight spectrum, but their absorption depths are consistently less than measured in the 1989 flight data. Furthermore, recall that the resolution of the 1979 flight spectra is a factor of  $\sim 1.25$  higher than the low-resolution spectra from the 1989 flight, so that features of a given absorption strength should appear narrower and deeper in the 1979 data than in the 1989 data. On the basis of these considerations, the balloon flight measurements indicate a substantial increase in the amount of COF<sub>2</sub> in the lower stratosphere between 1979 and 1989.

As for SF<sub>6</sub> and CHClF<sub>2</sub>, the COF<sub>2</sub> retrievals were referenced to an appropriate ATMOS/SL3 profile. First, the ATMOS analysis was checked by retrieving a COF<sub>2</sub> profile from the ATMOS zonal average sunset spectra ( $30^\circ\text{N}$  lati-

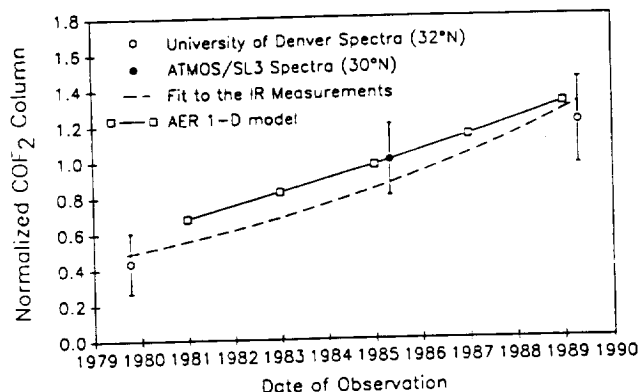


Fig. 8. Comparison between measured and AER one-dimensional calculated trends in lower stratospheric COF<sub>2</sub>. Total columns derived from the October 1979 and April 1989 University of Denver balloon flight spectra have been normalized to the total column calculated for the same ray path assuming a profile retrieved from the ATMOS/SL3 zonal average filter 2 spectra ( $30^\circ\text{N}$  latitude, May 1985) [Rinsland et al., 1986]. The error bars are estimated 1-sigma precisions. The dashed line shows a fit to the measurements obtained with a model that assumes the COF<sub>2</sub> volume mixing ratio is increasing with time at an exponential rate. The derived trend ( $10.3 \pm 1.8\% \text{ year}^{-1}$ , 1 sigma) corresponds to a factor of 2.67 increase in the COF<sub>2</sub> volume mixing ratio between October 1979 and April 1989. The AER one-dimensional model columns have been normalized to a value calculated for the date of the SL3 mission.

tude) using the new set of line parameters and comparing the retrieved profile with the published profile derived from the same spectral region [Rinsland et al., 1986, Figure 3, heavy full line]. The two profiles agree within 5% below an altitude of 38 km. Then, assuming the published ATMOS vertical VMR distribution (Table 2), each balloon flight spectrum was analyzed to retrieve a single multiplicative COF<sub>2</sub> profile scaling factor. The gas amounts of CO<sub>2</sub> and NO were also fitted along with parameters to model the solar CO absorption lines, the background, channel spectra, and the effective instrument line shape. The COF<sub>2</sub> scale factors from the three analyzed spectra from the 1979 flight (tangent heights of 17.1, 19.1, and 21.7 km) were averaged and the standard deviation was computed to derive a scale factor of  $0.44 \pm 0.17$  (1 sigma). The same procedure was used to analyze the 1989 flight spectra. A COF<sub>2</sub> scale factor of  $1.21 \pm 0.24$  (1 sigma) was derived from fitting five spectra with tangent heights between 19.0 and 22.6 km. Figure 7 presents an example of the least-squares fitting results obtained from the 1989 flight spectra.

Figure 8 shows the measured and AER one-dimensional model calculated COF<sub>2</sub> plotted versus time. The dashed line is a fit to the measurements assuming that the concentrations of COF<sub>2</sub> are increasing at an exponential rate. The fitted curve corresponds to an average COF<sub>2</sub> increase rate of  $10.3 \pm 1.8\% \text{ year}^{-1}$  (1 sigma) which is equal to a factor of 2.67 increase over the 9.5-year period (October 1979 to April 1989). Referenced to a base altitude of 18.0 km, the fitted curve corresponds to an increase in the COF<sub>2</sub> total vertical column from  $0.43 \times 10^{14}$  to  $1.20 \times 10^{14}$  molecules  $\text{cm}^{-2}$  over the observation period. The measured increase rate  $10.3 \pm 1.8\% \text{ year}^{-1}$  (1 sigma) is slightly higher than the AER one-dimensional model calculated rate of  $8.3\% \text{ year}^{-1}$  for the same time interval. No other measured or model calculated COF<sub>2</sub> trends have been reported.



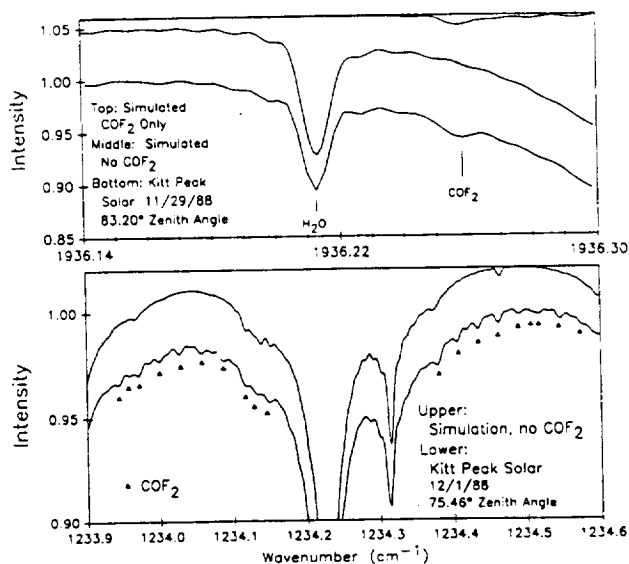


Fig. 9. Spectral features of the CO<sub>2</sub>  $\nu_1$  and  $\nu_4$  bands in 0.0053-cm<sup>-1</sup> resolution solar spectra recorded with the McMath Fourier transform spectrometer and main solar telescope operated by the National Solar Observatory on Kitt Peak near Tucson, Arizona. The upper panel shows the  $\nu_1$  band manifold at 1936.259 cm<sup>-1</sup> in a spectrum recorded at a mean solar astronomical zenith angle of 83.20° on the afternoon of November 29, 1988 (bottom curve), and simulations generated for the same spectral resolution and atmospheric ray path (upper two curves). The simulation are calculations of CO<sub>2</sub> absorption only (top spectrum) and the absorption by all gases except CO<sub>2</sub> (middle spectrum). The tick mark beneath the measured spectrum marks the location of the CO<sub>2</sub> absorption peak as determined from the spectrum at top. The three spectra are offset vertically for clarity. The lower panel presents a simulation of the absorption by all gases except CO<sub>2</sub> (upper curve) and a Kitt Peak solar spectrum recorded at a mean solar astronomical zenith angle of 75.46° on the morning of December 1, 1988 (lower curve). The two spectra are offset vertically for clarity. Solid triangles beneath the measured spectrum indicate the positions of strong CO<sub>2</sub> absorption features determined from line center measurements on a 0.003-cm<sup>-1</sup> resolution laboratory spectrum of CO<sub>2</sub>. The strong features at 1234.226 and 1234.315 cm<sup>-1</sup> are <sup>13</sup>CH<sub>4</sub> and <sup>16</sup>O<sup>12</sup>C<sup>18</sup>O lines, respectively. Weak lines of O<sub>3</sub> and N<sub>2</sub>O have also been identified in this spectral region.

In the future it should be possible to derive the trend in the CO<sub>2</sub> total column from analysis of high-resolution ground-based solar spectra. As illustrated in Figure 9, the strong CO<sub>2</sub>  $\nu_1$  and  $\nu_4$  band features can be seen from Kitt Peak, but they appear as very weak absorptions. High air mass, high signal-to-noise measurements at resolutions greater than 0.01 cm<sup>-1</sup> are required. Care must also be taken to avoid interferences, especially O<sub>3</sub> lines, which are visible in both spectral regions as narrow features, very similar in appearance to the CO<sub>2</sub> absorptions. Because atmospheric transmission in the CO<sub>2</sub>  $\nu_1$  band region is strongly attenuated by tropospheric water vapor absorption, any long-term, ground-based CO<sub>2</sub> measurement program based on measurements of the  $\nu_1$  band manifolds will require observations from dry, high-altitude sites. Observations such as the one illustrated in the upper panel of Figure 9 are seldom possible from Kitt Peak at an altitude of 2.1 km. At present, too few high-quality atmospheric observations of the CO<sub>2</sub>  $\nu_1$  band manifolds have been recorded from Kitt Peak to measure a reliable long-term CO<sub>2</sub> trend. Observations in the  $\nu_4$  band region are potentially more useful since regions less affected

by H<sub>2</sub>O can be selected, but accurate CO<sub>2</sub> total column measurements are not currently possible because of the absence of CO<sub>2</sub> line parameters in the 1230–1235 cm<sup>-1</sup> region which is the best for ground-based remote sensing. The CO<sub>2</sub>  $\nu_1$  and  $\nu_4$  band features have also been identified in high-resolution solar spectra recorded from the Jungfraujoch station at an altitude of 3.58 km (R. Zander, private communication, 1990).

#### 4. SUMMARY AND CONCLUSIONS

Long-term trends in the lower stratospheric concentrations of three trace constituents have been derived from analysis of high resolution infrared solar occultation spectra recorded between 1979 and 1989. The derived average rates of increase are large, 7.4% ± 1.9% year<sup>-1</sup> for SF<sub>6</sub>, 9.4% ± 1.3% year<sup>-1</sup> for CHClF<sub>2</sub>, and 10.3 ± 1.8% year<sup>-1</sup> for CO<sub>2</sub> (1 sigma), and in reasonable agreement with model results. The observed increases illustrate the rapid changes that are taking place in the composition of our upper atmosphere. The derived trends of SF<sub>6</sub> and CHClF<sub>2</sub> are in generally good agreement with the limited number of previously reported stratospheric trend measurements. The CO<sub>2</sub> trend measurements and model calculations are the first such results reported for this molecule. Both SF<sub>6</sub> and CHClF<sub>2</sub> are expected to be well mixed in the upper troposphere and lower stratosphere and thus will exhibit little seasonal or spatial variation. There are, however, significant variations in our calculated model distributions of CO<sub>2</sub>. Hence more frequent measurements are needed to further quantify its temporal trend.

Over the decade of these observations, the IR absorptions of SF<sub>6</sub> and CO<sub>2</sub> increased from only slightly above the limit of detection to features that are readily observable (for example, Figures 5 and 6). For this reason, these gases were only recently identified. On the basis of these studies it was then possible to identify and quantitatively analyze these features in the earlier data sets. In the future, as other gases increase in abundance as the result of anthropogenic emissions, similar cases will occur so that these early IR data sets are likely to provide valuable information on the trends of molecules not yet readily observable. Comparisons of time series of spectra in the 8–13  $\mu$ m atmospheric window may also be useful in accessing of changes in the opacity of this climatically important spectral region.

As demonstrated by this investigation, the systematic analysis of a time series of infrared solar occultation spectra can yield significant new information about the trends of stratospheric gases. The data are precise since no absolute radiance calibration is required, and temperature uncertainties and the attenuation by broad features (for example, aerosols and continua) are unimportant if appropriate features are selected for analysis. However, it is important to use consistent retrieval methods and consistent spectroscopic line lists to minimize systematic error effects. Because of the sensitivity and broad spectral coverage capabilities of high-resolution solar occultation measurements, many species encompassing a wide range in concentration are recorded simultaneously so that a comprehensive analysis of chemical families in such data sets can provide a unique opportunity to study the time history of the chemistry related to the catalytic destruction of stratospheric ozone.

**Acknowledgments.** Research at the University of Denver was supported by NASA and NSF. Acknowledgment is made to the National Center for Atmospheric Research, which is supported by NSF, for computer time used in this research. Research at NCAR was supported by the NASA UARS program under contract S-10782-C. We are grateful to Linda R. Brown of the Jet Propulsion Laboratory for sending us the CH<sub>4</sub> and COF<sub>2</sub> line parameters used in the analysis. The authors also thank B. Bobin of the Laboratoire de Spectrométrie Moléculaire et Instrumentation Laser, Dijon, France, for sending the calculated line parameters for the SF<sub>6</sub>  $\nu_3$  band, and Carolyn Sutton of the STX Corporation for assistance in processing the spectral data at NASA Langley.

## REFERENCES

- Bobin, B., C. J. Bordé, J. Bordé, and C. Bréant, Vibration-rotation molecular constants for the ground and ( $\nu_3 = 1$ ) states of <sup>32</sup>SF<sub>6</sub> from saturated absorption spectroscopy, *J. Mol. Spectrosc.*, **121**, 91-127, 1987.
- Brown, J. A., Sulfur hexafluoride, in *Kirk-Othmer Encyclopedia of Chemical Technology*, 2nd ed., pp. 664-671, J. Wiley, New York, 1966.
- Brown, J. A., D. C. McKean, and J. L. Duncan, Vibrational anharmonicity and Fermi resonances in CHF<sub>2</sub>Cl, *Spectrochim. Acta, Part A*, **44**, 553-565, 1988.
- Brown, L. R., and E. A. Cohen, Assignment of the  $\nu_1$  and  $2\nu_2$  bands of COF<sub>2</sub> at 5.2  $\mu$ m, paper RE7 presented at 44th Symposium on Molecular Spectroscopy, Ohio State Univ., Columbus, June 12-16, 1989.
- Brown, L. R., C. B. Farmer, C. P. Rinsland, and R. A. Toth, Molecular line parameters for the atmospheric trace molecule spectroscopy experiment, *Appl. Opt.*, **26**, 5154-5182, 1987.
- Brown, L. R., M. Loete, and J. C. Hilico, Linestrengths of the  $\nu_2$  and  $\nu_4$  bands of <sup>12</sup>CH<sub>4</sub> and <sup>13</sup>CH<sub>4</sub>, *J. Mol. Spectrosc.*, **133**, 273-311, 1989.
- Buijs, H. L., G. L. Vail, G. Tremblay, and D. J. W. Kendall, Simultaneous measurement of the volume mixing ratios of HCl and HF in the stratosphere, *Geophys. Res. Lett.*, **7**, 205-208, 1980.
- Camy-Peyret, C., J.-M. Flaud, L. Delbouille, G. Roland, J. W. Brault, and L. Testerman, Quadrupole transitions of the  $1 \leftarrow 0$  band of N<sub>2</sub> observed in a high resolution atmospheric spectrum, *J. Phys.*, **42**, L279-L283, 1981.
- Camy-Peyret, C., J.-M. Flaud, C. P. Rinsland, V. Malathy Devi, M. A. H. Smith, and A. Goldman, Line parameters for ozone hot bands in the 4.8- $\mu$ m spectral region, *J. Mol. Spectrosc.*, **139**, 353-360, 1990.
- Champion, J. P., J. C. Hilico, and L. R. Brown, The vibrational ground state of <sup>12</sup>CH<sub>4</sub> and <sup>13</sup>CH<sub>4</sub>, *J. Mol. Spectrosc.*, **133**, 244-255, 1989a.
- Champion, J. P., J. C. Hilico, C. Wenger, and L. R. Brown, Analysis of the  $\nu_2/\nu_4$  dyad of <sup>12</sup>CH<sub>4</sub> and <sup>13</sup>CH<sub>4</sub>, *J. Mol. Spectrosc.*, **133**, 256-272, 1989b.
- Drivas, P. J., and F. H. Shair, A tracer study of pollutant transport and dispersion in the Los Angeles area, *Atmos. Environ.*, **8**, 1155-1163, 1974.
- Fabian, P., Halogenated hydrocarbons in the atmosphere, in *Handbook of Environmental Chemistry*, vol. 4, part A, edited by O. Hutzinger, pp. 24-51, Springer-Verlag, New York, 1986.
- Fabian, P., R. Borchers, H. Dusch, B. C. Krüger, S. Lal, and B. H. Subbaraya, CHClF<sub>2</sub> (CFC-22): Distribution, budget and environmental impact, in *Ozone in the Atmosphere*, edited by R. D. Bojkov and P. Fabian, pp. 294-297, A. Deepak, Hampton, Va., 1989.
- Farmer, C. B., High resolution infrared spectroscopy of the sun and the Earth's atmosphere from space, *Mikrochim. Acta [Wien]*, **3**, 189-214, 1987.
- Fisher, D. A., C. H. Hales, W.-C. Wang, M. K. W. Ko, and N. D. Sze, Model calculations of the relative effects of CFCs and their replacements on global warming, *Nature*, **344**, 513-516, 1990.
- Flaud, J.-M., C. Camy-Peyret, C. P. Rinsland, M. A. H. Smith, and V. Malathy Devi, Line parameters for <sup>16</sup>O<sub>3</sub> bands in the 7- $\mu$ m region, *J. Mol. Spectrosc.*, **134**, 106-112, 1989.
- Flaud, J.-M., C. Camy-Peyret, C. P. Rinsland, V. Malathy Devi, M. A. H. Smith, and A. Goldman, Improved line parameters for ozone bands in the 10- $\mu$ m spectral region, *Appl. Opt.*, in press, 1990.
- Gamlen, P. H., B. C. Lane, P. M. Midgley, and J. M. Steed, The production and release to the atmosphere of CCl<sub>3</sub>F and CCl<sub>2</sub>F<sub>2</sub> (chlorofluorocarbons CFC 11 and CFC 12), *Atmos. Environ.*, **20**, 1077-1085, 1986.
- Goldan, P. D., W. C. Kuster, D. L. Albritten, and A. L. Schmeltkeopf, Stratospheric CFCl<sub>3</sub>, CF<sub>2</sub>Cl<sub>2</sub>, and N<sub>2</sub>O height profile measurements at several latitudes, *J. Geophys. Res.*, **85**, 413-423, 1980.
- Goldman, A., and R. S. Saunders, Analysis of atmospheric infrared spectra for altitude distribution of atmospheric trace constituents-I. Method of analysis, *J. Quant. Spectrosc. Radiat. Transfer*, **21**, 155-161, 1979.
- Goldman, A., T. G. Kyle, D. G. Murcray, F. H. Murcray, and W. J. Williams, Long path atmospheric ozone absorption in the 9-10- $\mu$  region observed from a balloon-borne spectrometer, *Appl. Opt.*, **9**, 565-580, 1970.
- Goldman, A., D. G. Murcray, F. J. Murcray, G. R. Cook, J. W. Van Allen, F. S. Bonomo, and R. D. Blatherwick, Identification of the  $\nu_3$  vibration-rotation band of CF<sub>4</sub> in balloon-borne infrared solar spectra, *Geophys. Res. Lett.*, **6**, 609-612, 1979.
- Goldman, A., D. G. Murcray, F. J. Murcray, and E. Niple, High resolution IR balloon-borne solar spectra and laboratory spectra in the HNO<sub>3</sub> 1720-cm<sup>-1</sup> region: An analysis, *Appl. Opt.*, **19**, 3721-3724, 1980.
- Goldman, A., J. Reid, and L. S. Rothman, Identification of electric quadrupole O<sub>2</sub> and N<sub>2</sub> lines in the infrared atmospheric absorption spectrum due to the vibration-rotation fundamentals, *Geophys. Res. Lett.*, **8**, 77-78, 1981a.
- Goldman, A., F. J. Murcray, R. D. Blatherwick, F. S. Bonomo, F. H. Murcray, and D. G. Murcray, Spectroscopic identification of CHClF<sub>2</sub> (F-22) in the lower stratosphere, *Geophys. Res. Lett.*, **8**, 1012-1014, 1981b.
- Goldman, A., R. D. Blatherwick, F. J. Murcray, J. W. VanAllen, F. H. Murcray, and D. G. Murcray, *New Atlas of Stratospheric IR Absorption Spectra*, vol. 1, *Line Positions and Identifications*, Department of Physics, University of Denver, Denver, Colo., 1987.
- Goldman, A., R. D. Blatherwick, J. J. Kusters, F. J. Murcray, J. W. VanAllen, F. H. Murcray, and D. G. Murcray, *Atlas of Very High Resolution Stratospheric IR Absorption Spectra*, preliminary edition, Department of Physics, University of Denver, Denver, Colo., 1989a.
- Goldman, A., F. J. Murcray, R. D. Blatherwick, J. J. Kusters, F. H. Murcray, D. G. Murcray, and C. P. Rinsland, New spectral features of stratospheric trace gases identified from high resolution infrared balloon-borne and laboratory spectra, *J. Geophys. Res.*, **94**, 14,945-14,955, 1989b.
- Goldman, A., C. P. Rinsland, R. D. Blatherwick, and F. S. Bonomo, Spectroscopic line parameters for the  $\nu_6$  band of carbonyl fluoride (COF<sub>2</sub>), *Appl. Opt.*, **29**, 1860-1863, 1990.
- Golombek, A., and R. G. Prinn, Global three-dimensional model calculations of the budgets and present-day atmosphere lifetimes of CF<sub>2</sub>ClCFCl<sub>2</sub> (CFC-113) and CHClF<sub>2</sub> (CFC-22), *Geophys. Res. Lett.*, **16**, 1153-1156, 1989.
- Gunson, M. R., C. B. Farmer, R. H. Norton, R. Zander, C. P. Rinsland, J. Shaw, and B.-C. Gao, Measurements of CH<sub>4</sub>, N<sub>2</sub>O, CO, H<sub>2</sub>O and O<sub>3</sub> in the middle atmosphere by the ATMOS experiment on Spacelab 3, *J. Geophys. Res.*, in press, 1990.
- Hammit, J. K., F. Camm, P. S. Connell, W. E. Mooz, K. A. Wolf, D. J. Wuebbles, and A. Bamezai, Future emission scenarios for chemicals that may deplete stratospheric ozone, *Nature*, **330**, 711-716, 1987.
- International Global Atmospheric Chemistry Programme, A Core Project of the International Geosphere-Biosphere Programme, edited by I. E. Galbally, p. 38, IAMAP Commission on Atmospheric Chemistry and Global Pollution, Renwick Pride Pty, Albany, New Zealand, 1989.
- Jayanty, R. K. M., R. Simonaitis, and J. Heicklen, The photolysis of chlorofluoromethanes in the presence of O<sub>2</sub> or O<sub>3</sub> at 213.9 nm and their reactions with O(<sup>1</sup>D), *J. Photochem.*, **4**, 381-398, 1975.
- Jones, R. L., and J. A. Pyle, Observations of CH<sub>4</sub> and N<sub>2</sub>O by the NIMBUS 7 SAMS: A comparison with in situ data and two-dimensional numerical model calculations, *J. Geophys. Res.*, **89**, 5263-5279, 1984.
- Khalil, M. A. K., and R. A. Rasmussen, Increase of CHClF<sub>2</sub> in the Earth's atmosphere, *Nature*, **292**, 823-824, 1981.

- Khalil, M. A. K., and R. A. Rasmussen, Chlorocarbons in the southern hemisphere: Concentrations and temporal trends, in *Baseline Atmospheric Program (Australia) 1985*, edited by B. W. Forgan and P. J. Fraser, pp. 26–29, Department of Science/Bureau of Meteorology, Australia, 1987.
- Krey, P. W., R. J. Lagomarsino, and L. E. Toonkel, Gaseous halogens in the atmosphere in 1975, *J. Geophys. Res.*, **82**, 1753–1766, 1977.
- Leifer, R., and R. Juzdan, Measurements of CCl<sub>3</sub>F, CCl<sub>2</sub>F<sub>2</sub>, CCl<sub>4</sub>, N<sub>2</sub>O and SF<sub>6</sub> in the northern hemisphere stratosphere, in *International Council of Scientific Unions Handbook for MAP*, vol. 18, *Extended Abstracts*, edited by S. Kato, pp. 355–358, Special Committee for Solar-Terrestrial Physics Secretariat at University of Illinois, Urbana, Ill., 1985. (Available as N86-27795 from the Natl. Tech. Inf. Serv., Springfield, Va.)
- Leifer, R., K. Sommers, and S. F. Guggenheim, Atmospheric trace gas measurements with a new clean air sampling system, *Geophys. Res. Lett.*, **8**, 1079–1081, 1981.
- Leifer, R., R. Larsen, and L. Toonkel, Trends in stratospheric concentrations of trace gases in the northern hemisphere during the years 1974–1979, *Geophys. Res. Lett.*, **9**, 755–758, 1982.
- Magill, J. V., K. M. Gough, and W. F. Murphy, The vibrational spectrum and normal coordinate analysis of chlorodifluoromethane, CHClF<sub>2</sub>, *Spectrochim. Acta, Part A*, **42a**, 705–715, 1986.
- Malathy Devi, V., J.-M. Flaud, C. Camy-Peyret, C. P. Rinsland, and M. A. H. Smith, Line positions and intensities for the  $\nu_1 + \nu_2$  and  $\nu_2 + \nu_3$  bands of <sup>16</sup>O<sub>3</sub>, *J. Mol. Spectrosc.*, **125**, 174–183, 1987.
- Mallinson, P. D., D. C. McKean, J. H. Holloway, and I. A. Oxtun, Infrared spectra of carbonyl fluorides and general harmonic force field, *Spectrochim. Acta, Part A*, **31a**, 143–159, 1975.
- McDaniel, A. H., C. A. Cantrell, J. A. Davidson, R. E. Shetter, and J. G. Calvert, The temperature dependent, infrared absorption cross sections for the chlorofluorocarbons: CFC-11, CFC-12, CFC-13, CFC-14, CFC-22, CFC-113, CFC-114, and CFC-115, *Atmos. Chem.*, in press, 1990.
- Murcray, D. G., Atmospheric transmission in the 750–2000 cm<sup>-1</sup> region, *J. Quant. Spectrosc. Radiat. Transfer*, **32**, 381–396, 1984.
- Murcray, D. G., and A. Goldman, *CRC Handbook of High Resolution Infrared Laboratory Spectra of Atmospheric Interest*, CRC Press, Boca Raton, Fla., 1981.
- Murcray, D. G., T. G. Kyle, F. H. Murcray, and W. J. Williams, Nitric acid and nitric oxide in the lower stratosphere, *Nature*, **218**, 78–79, 1968.
- Murcray, D. G., F. H. Murcray, W. J. Williams, T. G. Kyle, and A. Goldman, Variation of the infrared solar spectrum between 700 and 2240 cm<sup>-1</sup> with altitude, *Appl. Opt.*, **8**, 2519–2536, 1969.
- Murcray, D. G., F. S. Bonomo, J. N. Brooks, A. Goldman, F. H. Murcray, and W. J. Williams, Detection of fluorocarbons in the stratosphere, *Geophys. Res. Lett.*, **2**, 109–112, 1975.
- Murcray, F. J., J. J. Kusters, R. D. Blatherwick, J. Olson, and D. G. Murcray, High resolution solar spectrometer system for measuring atmospheric constituents, *Appl. Opt.*, **29**, 1520–1525, 1990.
- NASA, Chemical kinetics and photochemical data for use in stratospheric modeling, Evaluation No. 8, *JPL Publ.*, **87-41**, 196 pp., 1987.
- Niple, E., Nonlinear least squares analysis of atmospheric absorption spectra, *Appl. Opt.*, **19**, 3481–3490, 1980.
- Niple, E., W. G. Mankin, A. Goldman, D. G. Murcray, and F. J. Murcray, Stratospheric NO<sub>2</sub> and H<sub>2</sub>O mixing ratio profiles from high resolution infrared solar spectra using nonlinear least squares, *Geophys. Res. Lett.*, **7**, 489–492, 1980.
- Pickett, H. M., et al., The vibrational and rotational spectra of ozone for the (0, 1, 0) and (0, 2, 0) states, *J. Mol. Spectrosc.*, **128**, 151–171, 1988.
- Plyler, E. K., and W. S. Benedict, Infrared spectra of eighteen halogen-substituted methanes, *J. Res. Natl. Bur. Stand.*, **47**, 202–220, 1951.
- Prinn, R., D. Cunnold, R. Rasmussen, P. Simmonds, F. Alyea, A. Crawford, P. Fraser, and R. Rosen, Atmospheric trends in methylchloroform and the global average for the hydroxyl radical, *Science*, **238**, 945–950, 1987.
- Ramanathan, V., R. J. Cicerone, H. B. Singh, and J. T. Kiehl, Trace gas trends and their potential role in climate change, *J. Geophys. Res.*, **90**, 5547–5566, 1985.
- Raper, O. F., C. B. Farmer, R. Zander, and J. H. Park, Infrared spectroscopic measurements of halogenated sink and reservoir gases in the stratosphere with the ATMOS instrument, *J. Geophys. Res.*, **92**, 9851–9858, 1987.
- Rasmussen, R. A., and M. A. K. Khalil, Atmospheric fluorocarbons and methyl chloroform at the South Pole, *Antar. J. U.S.*, **17**, 203–205, 1982.
- Rasmussen, R. A., and M. A. K. Khalil, Rare trace gases at the South Pole, *Antar. J. U.S.*, **18**, 250–252, 1983.
- Rasmussen, R. A., and M. A. K. Khalil, Atmospheric trace gases: Trends and distributions over the last decade, *Science*, **232**, 1623–1624, 1986.
- Rasmussen, R. A., M. A. K. Khalil, S. A. Penkett, and N. J. D. Prosser, CHClF<sub>2</sub> (F-22) in the Earth's atmosphere, *Geophys. Res. Lett.*, **7**, 809–812, 1980.
- Rasmussen, R. A., M. A. K. Khalil, and R. W. Dalluge, Atmospheric trace gases in Antarctica, *Science*, **211**, 285–287, 1981.
- Reid, J., R. L. Sinclair, A. M. Robinson, and A. R. W. McKellar, Observation of electric quadrupole transitions in the fundamental band of O<sub>2</sub> in the 1600-cm<sup>-1</sup> region, *Phys. Rev. A*, **24**, 1944–1949, 1981.
- Reiter, E. R., *Atmospheric Transport Processes*, part 2, *Chemical Tracers*, U.S. Atomic Energy Commission, Washington, D. C., 1971.
- Rinsland, C. P., and J. S. Levine, Free tropospheric carbon monoxide concentrations in 1950 and 1951 deduced from infrared total column amount measurements, *Nature*, **318**, 250–254, 1985.
- Rinsland, C. P., A. Goldman, F. J. Murcray, D. G. Murcray, M. A. H. Smith, R. K. Seals, Jr., J. C. Larsen, and P. L. Rinsland, Stratospheric N<sub>2</sub>O mixing ratio profile from high-resolution balloon-borne solar absorption spectra and laboratory spectra near 1880 cm<sup>-1</sup>, *Appl. Opt.*, **21**, 4351–4355, 1982.
- Rinsland, C. P., A. Goldman, F. J. Murcray, D. G. Murcray, M. A. H. Smith, R. K. Seals, Jr., J. C. Larsen, and P. L. Rinsland, Stratospheric temperature profile from balloon-borne measurements of the 10.4-μm band of CO<sub>2</sub>, *J. Quant. Spectrosc. Radiat. Transfer*, **30**, 327–334, 1983.
- Rinsland, C. P., J. S. Levine, and T. Miles, Concentration of methane in the troposphere deduced from 1951 infrared solar spectra, *Nature*, **318**, 245–249, 1985.
- Rinsland, C. P., R. Zander, L. R. Brown, C. B. Farmer, J. H. Park, R. H. Norton, J. M. Russell III, and O. F. Raper, Detection of carbonyl fluoride in the stratosphere, *Geophys. Res. Lett.*, **13**, 769–772, 1986.
- Rinsland, C. P., M. A. H. Smith, J.-M. Flaud, C. Camy-Peyret, and V. Malathy Devi, Line positions and intensities of the  $2\nu_3$ ,  $\nu_1 + \nu_3$ , and  $2\nu_1$  bands of <sup>16</sup>O<sub>3</sub>, *J. Mol. Spectrosc.*, **130**, 204–212, 1988a.
- Rinsland, C. P., A. Goldman, F. J. Murcray, F. H. Murcray, R. D. Blatherwick, and D. G. Murcray, Infrared measurements of atmospheric gases above Mauna Loa, Hawaii, in February 1987, *J. Geophys. Res.*, **93**, 12,607–12,626, 1988b.
- Rinsland, C. P., D. W. Johnson, A. Goldman, and J. S. Levine, Evidence for a decline in the atmospheric accumulation rate of CHClF<sub>2</sub> (CFC-22), *Nature*, **337**, 535–537, 1989.
- Rinsland, C. P., L. R. Brown, and C. B. Farmer, Infrared spectroscopic detection of sulfur hexafluoride (SF<sub>6</sub>) in the lower stratosphere and upper troposphere, *J. Geophys. Res.*, **95**, 5577–5585, 1990.
- Rothman, L. S., and A. Goldman, Infrared electric quadrupole transitions of atmospheric oxygen, *Appl. Opt.*, **20**, 2182–2184, 1981.
- Rothman, L. S., et al., The HITRAN database: 1986 edition, *Appl. Opt.*, **26**, 4058–4097, 1987.
- Rowland, F. S., and M. J. Molina, Chlorofluoromethanes in the environment, *Rev. Geophys. Space. Phys.*, **13**, 1–35, 1975.
- Schatz, P. N., and D. F. Hornig, Bond moments and derivatives in CF<sub>4</sub>, SiF<sub>4</sub>, and SF<sub>6</sub> from infrared intensities, *J. Chem. Phys.*, **21**, 1516–1530, 1953.
- Singh, H. B., L. J. Salas, and L. A. Cavanaugh, Distribution, sources and sinks of atmospheric halogenated compounds, *J. Air Pollut. Control Assoc.*, **27**, 332–336, 1977.
- Singh, H. B., L. J. Salas, H. Shigeishi, and E. Scribner, Atmospheric halocarbons, hydrocarbons, and sulfur hexafluoride: Global distributions, sources, and sinks, *Science*, **203**, 899–903, 1979.
- Singh, H. B., L. J. Salas, and R. E. Stiles, Selected man-made

- halogenated chemicals in the air and oceanic environment, *J. Geophys. Res.*, **88**, 3675–3683, 1983.
- Smith, M. A. H., Compilation of atmospheric gas concentration profiles from 0 to 50 km, *NASA Tech. Memo.* 83289, 1982. (Available as NTIS 82N22822 from the Natl. Tech. Inf. Serv., Springfield, Va.)
- Srivastava, G. P., and D. Kumar, Microwave pressure broadening studies of carbonyl fluoride, *J. Phys. B.*, **9**, 651–659, 1976.
- Steele, L. P., P. J. Fraser, R. A. Rasmussen, M. A. K. Khalil, T. J. Conway, A. J. Crawford, R. H. Gammon, K. A. Masarie, and K. W. Thoning, The global distribution of methane in the troposphere, *J. Atmos. Chem.*, **5**, 125–171, 1987.
- Sze, N. D., Stratospheric fluorine: A comparison between theory and measurements, *Geophys. Res. Lett.*, **5**, 781–783, 1978.
- Sze, N. D., and M. K. W. Ko, The effects of the rate for OH + HNO<sub>3</sub> and HO<sub>2</sub>NO<sub>2</sub> photolysis on stratospheric chemistry, *Atmos. Environ.*, **15**, 1301–1307, 1981.
- Tejwani, G. D. T., and K. Fox, Calculated self- and foreign-gas-broadened linewidths for SF<sub>6</sub>, *J. Quant. Spectrosc. Radiat. Transfer*, **37**, 541–546, 1987.
- Thakur, K. B., K. Narahari Rao, R. R. Friedl, C. P. Rinsland, and V. Malathy Devi, Analysis of the  $\nu_6$  band of carbonyl fluoride, *J. Mol. Spectrosc.*, **123**, 255–266, 1987.
- Thoning, K. W., P. P. Tans, and W. D. Komhyr, Atmospheric carbon dioxide at Mauna Loa observatory, 2, Analysis of the NOAA GMCC data, 1974–1985, *J. Geophys. Res.*, **94**, 8549–8565, 1989.
- Turk, A., S. M. Edmonds, H. L. Mark, and G. F. Collins, Sulfur hexafluoride as a gas-air tracer, *Environ. Sci. Technol.*, **2**, 44–48, 1968.
- Varanasi, P., and S. Chudamani, Infrared intensities of some chlorofluorocarbons capable of perturbing the global climate, *J. Geophys. Res.*, **93**, 1666–1668, 1988.
- Watson, A. J., and M. I. Liddicoat, Recent history of atmospheric trace gas concentrations deduced from measurements in the deep sea: Application to sulphur hexafluoride and carbon tetrachloride, *Atmos. Environ.*, **19**, 1477–1484, 1985.
- Watson, R. T. and Ozone Trends Panel, M. J. Prather and ad hoc theory panel, and M. J. Kurylo and NASA Panel for Data Evaluation, Present state of knowledge of the upper atmosphere 1988: An assessment report, *NASA Ref. Publ.* 1208, 200 pp., 1988.
- Wofsy, S. C., J. H. Yatteau, R. J. Salawitch, M. B. McElroy, G. C. Toon, W. G. Mankin, and M. T. Coffey, Heterogeneous conversion of COF<sub>2</sub> to HF in polar stratospheric clouds, *Geophys. Res. Lett.*, **17**, 461–464, 1990.
- World Meteorological Organization, The stratosphere 1981 theory and measurements, *Rep. 11*, Geneva, 1982.
- World Meteorological Organization, Atmospheric ozone 1985: Assessment of our understanding of the processes controlling its present distribution and change, *Rep. 16*, Geneva, 1986.
- World Meteorological Organization, Scientific assessment of stratospheric ozone: 1989, Vol. 2, Appendix: AFEAS Report, *Rep. 20*, Geneva, 1989.
- Wuebbles, D. J., Chlorocarbon emission scenarios: Potential impact on stratospheric ozone, *J. Geophys. Res.*, **88**, 1433–1443, 1983.
- Zander, R., C. P. Rinsland, C. B. Farmer, and R. H. Norton, Infrared spectroscopic measurements of halogenated source gases in the stratosphere with the ATMOS instrument, *J. Geophys. Res.*, **92**, 9836–9850, 1987.
- Zander, R., Ph. Demoulin, D. H. Ehhalt, and U. Schmidt, Secular increase of the vertical column abundance of methane derived from IR solar spectra recorded at the Jungfraujoch station, *J. Geophys. Res.*, **94**, 11,029–11,039, 1989a.
- Zander, R., Ph. Demoulin, D. H. Ehhalt, U. Schmidt, and C. P. Rinsland, Secular increase of the total vertical column abundance of carbon monoxide above central Europe since 1950, *J. Geophys. Res.*, **94**, 11,021–11,028, 1989b.
- R. D. Blatherwick, A. Goldman, J. J. Kusters, D. G. Murcray, and F. J. Murcray, Department of Physics, University of Denver, 2112 E. Wesley, Denver, CO 80308.
- S. T. Massie, National Center for Atmospheric Research, Atmospheric Chemistry Division, P.O. Box 3000, Boulder, CO 80307.
- C. P. Rinsland, Atmospheric Sciences Division, NASA Langley Research Center, Mail Code 401A, Hampton, VA 23665.
- N. D. Sze, AER Incorporated, 840 Memorial Drive, Cambridge, MA 02139.

(Received March 16, 1990;  
revised June 14, 1990;  
accepted June 11, 1990.)



# BALLOON-BORNE MEASUREMENTS OF TOTAL REACTIVE NITROGEN, NITRIC ACID, AND AEROSOL IN THE COLD ARCTIC STRATOSPHERE

Y. Kondo<sup>1</sup>, P. Amedieu<sup>2</sup>, W. A. Matthews<sup>3</sup>, D. W. Fahey<sup>4</sup>, D. G. Murcray<sup>5</sup>, D. J. Hofmann<sup>6</sup>,  
P. V. Johnston<sup>3</sup>, Y. Iwasaka<sup>1</sup>, A. Iwata<sup>1</sup>, and W. R. Sheldon<sup>7</sup>

**Abstract.** Total reactive nitrogen ( $\text{NO}_y$ ) between 15 and 29 km was measured for the first time on board a balloon within the Arctic cold vortex. Observations of  $\text{HNO}_3$ , aerosol, and ozone were made by instruments on the same balloon gondola which was launched from Esrange, Sweden ( $68^\circ\text{N}$ ,  $20^\circ\text{E}$ ) on January 23, 1989. The  $\text{NO}_y$  mixing ratio was observed to increase very rapidly from 6 ppbv at 18 km altitude to a maximum of 21 ppbv at 21 km, forming a sharp layer with a thickness of about 2 km. A minimum in the  $\text{NO}_y$  mixing ratio of 5 ppbv was found at 27 km. The measured  $\text{HNO}_3$  profile shows broad similarities to that of  $\text{NO}_y$ . This observation, together with the observed very low column amount of  $\text{NO}_2$ , shows that  $\text{NO}_x$  had been almost totally converted to  $\text{HNO}_3$ , and that  $\text{NO}_y$  was composed mainly of  $\text{HNO}_3$ . The enhanced aerosol concentration between 19 and 22 km suggests that the maximum abundance of  $\text{HNO}_3$  trapped in the form of nitric acid trihydrate (NAT) was about 6 ppbv at 21 km. The sampled air parcels were highly supersaturated with respect to NAT. Although extensive denitrification throughout the stratosphere did not prevail, an indication of denitrification was found at altitudes of 27 and 22 km, and between 18 and 15 km.

## Introduction

Total reactive odd nitrogen defined as  $\text{NO}_y = \text{NO} + \text{NO}_2 + \text{NO}_3 + \text{HNO}_3 + 2(\text{N}_2\text{O}_5) + \text{HO}_2\text{NO}_2 + \text{ClONO}_2$  + aerosol nitrate, plays an important role in the chemistry of the winter polar stratosphere.  $\text{HNO}_3$ , in combination with  $\text{H}_2\text{O}$ , forms aerosols composed of nitric acid trihydrate (NAT) at temperatures higher than that required for water ice particle formation. These aerosols can provide sites for heterogeneous reactions, one of which converts  $\text{HCl}$  and chlorine nitrate ( $\text{ClONO}_2$ , a temporary reservoir of  $\text{ClO}$ ) into reactive chlorine molecules and  $\text{HNO}_3$  [e.g. Solomon *et al.*, 1986; McElroy *et al.*, 1986]. In

bulk these  $\text{H}_2\text{O}$  and NAT aerosols are referred to as polar stratospheric clouds (PSCs). If aerosols grow to a sufficiently large size, gravitational settling can occur, leading to denitrification in the stratosphere. These processes are considered to be essential for the large ozone depletion in the Antarctic stratosphere in spring.

Significant reduction of  $\text{NO}_y$  within the polar vortex has been observed at an altitude of about 20 km in the Antarctic stratosphere during early spring [Fahey *et al.*, 1989a]. In addition, significant amounts of aerosols containing  $\text{HNO}_3$  have been sampled at temperatures above the  $\text{H}_2\text{O}$  frost point [Fahey *et al.*, 1989b]. By contrast, much less is understood about heterogeneous processes occurring in the winter Arctic stratosphere. To investigate heterogeneous processes in that region, instrumented balloons were flown from the Arctic in late January, 1989 as a part of the TECHNOPS campaign organized by the Centre National d'Etude Spatiale (CNES). Parameters which were measured for this purpose included reactive odd nitrogen,  $\text{NO}_y$  between 15 and 29 km, nitric acid, and aerosols.

## Instrumentation

The balloon-borne  $\text{NO}_y$  instrument is based on the principle of the conversion of  $\text{NO}_y$  species into  $\text{NO}$  on a heated gold surface and the subsequent measurement of  $\text{NO}$  by a chemiluminescence detector. A detailed description of the instrument is given in Kondo *et al.* [1989]. For the present experiment, a converter with a diameter larger than that described in Kondo *et al.* [1989] was used to increase the sensitivity. The converter consisted of 19 gold tubes each of which was 30 cm long, with an inner diameter of 5.7 mm and a 0.15 mm wall thickness. They were assembled as a single unit and mounted in a stainless steel tube 50 cm long, with an inner diameter of 30.5 mm. The temperature of the gold converter was controlled to be  $300 \pm 1^\circ\text{C}$ . Laboratory experiments have shown an  $\text{NO}_2$  conversion efficiency as high as  $0.98 \pm 0.02$ , even at 5 mb. Nitric acid in aerosols evaporates in the converter and is therefore measured as  $\text{NO}_y$  [Fahey *et al.*, 1985, 1989a]. As both the velocity of the sampled air through the converter and the ascent velocity of the balloon are a few m/s, no significant enhancement in the sensitivity of particulate  $\text{NO}_y$  should occur. The accuracy of the  $\text{NO}_y$  measurements is estimated to be about 15%.

Other instruments which were mounted on the same gondola were an infrared radiometer from the University of Denver [Murcray *et al.*, 1969], an aerosol counter and an ECC ozonesonde from the University of Wyoming [Hofmann *et al.*, 1989], and a chemiluminescent ozone instrument from the Service d'Aéronomie [Amedieu *et al.* 1987]. The radiometer was designed for measurement of

<sup>1</sup> Research Institute of Atmospherics, Nagoya University, Japan

<sup>2</sup> Service d'Aéronomie, CNRS, France

<sup>3</sup> Physics and Engineering Laboratory, DSIR, New Zealand

<sup>4</sup> Aeronomy Laboratory, NOAA, Colorado

<sup>5</sup> Department of Physics, University of Denver.

<sup>6</sup> Department of Physics and Astronomy, University of Wyoming.

<sup>7</sup> Department of Physics, University of Houston

gas phase  $\text{HNO}_3$ . This was accomplished by measuring at two wavelengths, one at the peak of the gas phase emission and the other outside of the region of gas phase emission but in the region of broad band emission of ice phase  $\text{HNO}_3$  or other emitting aerosols. The  $\text{HNO}_3$  profile was determined by noting the change in the gas phase emission with altitude. The accuracy of the  $\text{HNO}_3$  measurement is about 15%. The aerosol detector was a high-flow ( $200 \text{ cm}^3 \text{ s}^{-1}$ ) optical counter with a short (5 cm) inlet tube insulated from the rest of the scattering chamber to avoid particle evaporation. The accuracy of aerosol mass measurements for small ( $r \approx 0.2 \mu\text{m}$ ) spherical particles is estimated to be about 15%.

Ground based measurements were also conducted to support the balloon measurements: column  $\text{NO}_2$  and ozone amounts were continuously measured by the PEL DSIR, and Nagoya University groups at the Swedish Institute of Space Physics Observatory in Kiruna, using a zenith viewing visible spectrometer [Johnston and McKenzie, 1989]. These measurements were made over the period from 12 January to 28 February, 1989 and will be reported more fully elsewhere.

### Results and discussion

The gondola was flown suspended under a  $10^5 \text{ m}^3$  balloon which was launched from Esrange near Kiruna, Sweden ( $68^\circ\text{N}$ ,  $20^\circ\text{E}$ ) at 1430 UT on January 23, 1989. The ozone and temperature profiles measured during ascent are shown in Figure 1. The altitude was scaled according to the hydrostatic equation using the observed temperature. The approximate potential temperature is given on the right hand side of the figure. It can be seen that the temperature was less than or equal to  $-85^\circ\text{C}$  between 20 and 25 km. Between 22 and 26 km, a reduction of about 25%, compared to typical values of the ozone profile, can be seen; the possible cause for this variation is discussed in Hofmann *et al.* [1989a].

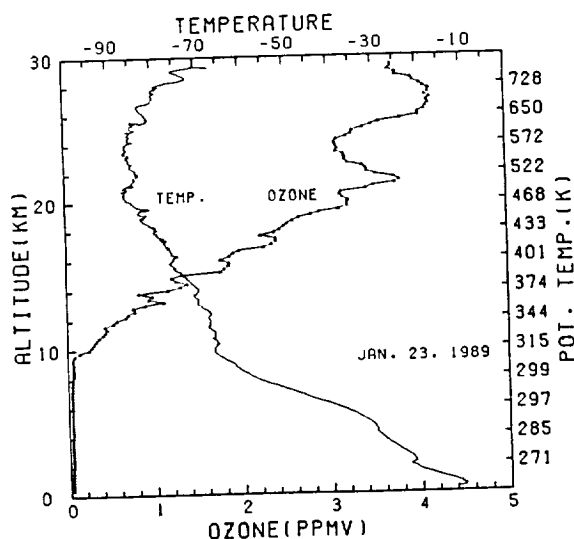


Fig. 1. Temperature (solid line) and ozone profiles (triangles) measured during balloon ascent at Kiruna, Sweden ( $68^\circ\text{N}$ ,  $20^\circ\text{E}$ ) on January 23, 1989.

The  $\text{NO}_y$  and  $\text{HNO}_3$  mixing ratios, also measured during ascent, are shown in Figure 2. It can be seen that the  $\text{NO}_y$  mixing ratio increased very rapidly from 6 ppbv at 18 km altitude to a maximum of 21 ppbv at 21 km, and that the  $\text{NO}_y$  layer centered at 21 km was only 2 km thick. A sharp minimum in the  $\text{NO}_y$  mixing ratio of 5 ppbv at 27 km was also seen. Judging from the potential vorticity maps of January 23 and 24, it is very likely that the present observation was made inside the vortex, but close to the boundary. Aircraft data show that  $2^\circ$  to  $5^\circ$  in latitude poleward of the vortex boundary  $\text{NO}_y$  reached a maximum at potential temperatures between 420 and 470 K [Kawa *et al.*, this issue]. The present  $\text{NO}_y$  profile corresponding to these potential temperatures falls within the range of their  $\text{NO}_y$  values observed a few degrees inside the polar vortex boundary. Our measured column  $\text{NO}_y$  amount integrated from 14.6 to 29.3 km was  $2.0 \times 10^{16} \text{ cm}^{-2}$ .

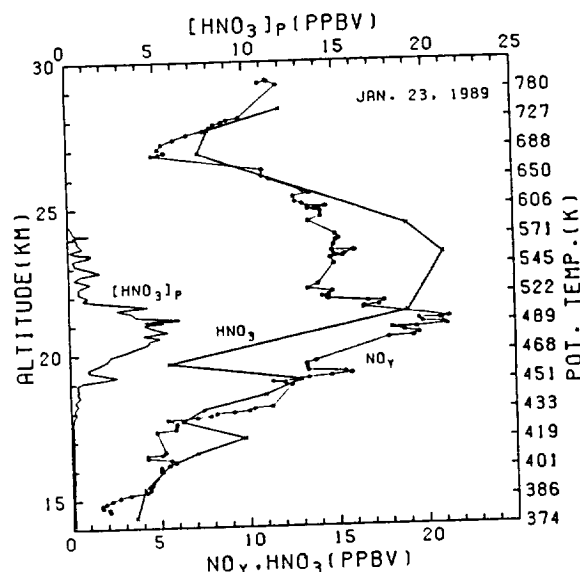


Fig. 2. Profiles of  $\text{NO}_y$  (small open circles),  $\text{HNO}_3$  (crosses), and the calculated  $\text{HNO}_3$  mixing ratio contained in the observed aerosols (thin line) measured at Kiruna on January 23, 1989.

A pronounced layer of aerosol, having a mode radius of about  $0.2 \mu\text{m}$ , was observed between 19 and 22 km, as described in detail in Hofmann *et al.* [1989a]. The  $\text{HNO}_3$  mixing ratio contained in aerosol ( $[\text{HNO}_3]_p$ ) was calculated assuming that all the aerosols were composed of NAT, and is shown as the solid line in Figure 2. In this calculation, the observed concentration of aerosols with radii from 0.2 to  $5 \mu\text{m}$  was used; however aerosol with radii smaller than  $1 \mu\text{m}$  dominated the total volume of  $\text{HNO}_3$ . Below 18 km, aerosols are composed mainly of sulfate and it can be seen that the sulfate particles contributed little to the total volume in the PSC layer between 19 and 23 km, and thus caused little error in the estimate of  $[\text{HNO}_3]_p$ . The peak  $[\text{HNO}_3]_p$  of about 6 ppbv was reached at 21 km. The smoothed profile of  $[\text{HNO}_3]_p$  in Figure 2 is very similar to that of  $[\text{NO}_y]$  when

a constant  $13 \pm 1$  ppbv is subtracted from the  $\text{NO}_y$  profile between 20 and 22 km. It should also be noted that almost all of the small peaks observed in  $[\text{HNO}_3]_p$  exactly match those in  $\text{NO}_y$ .

From Figure 2, the comparison of  $\text{NO}_y$  with  $\text{HNO}_3$  between 15 and 29 km shows good agreement, considering the difference in the methods of the measurements and the likely errors. The derived  $\text{HNO}_3$  mixing ratios were based on the average emission over a range of approximately 60 km detected at an elevation angle of about  $15^\circ$  during the ascent. As is seen from the sharp peak in the  $\text{NO}_y$  and  $[\text{HNO}_3]_p$  profiles between 19 and 21 km, the  $\text{HNO}_3$  mixing ratios are averaged over a larger altitude interval.

The vertical  $\text{NO}_2$  column amount measured by the ground based visible spectrometer on January 23 was about  $0.5 \times 10^{15} \text{ cm}^{-2}$ , a value similar to, or less than that typically observed within the Antarctic vortex in early spring. The uncertainty in the derived vertical column  $\text{NO}_2$  amount is  $\pm 10\%$ . The data sets of  $\text{NO}_y$ ,  $\text{HNO}_3$ , and column  $\text{NO}_2$  indicate that most of the reactive odd nitrogen species were in the form  $\text{HNO}_3$  by the end of January, 1989. By this time nearly all stratospheric  $\text{NO}_x$  in the locale had been converted into  $\text{HNO}_3$ , consistent with the predictions of a simulation model [Douglas and Stolarski, 1989] which includes the effects of heterogeneous processes in PSCs under Arctic winter conditions.

Using the experimental results of Hanson and Mauersberger [1988], the saturation  $\text{HNO}_3$  vapor mixing ratio over NAT for the observed temperature profile has been estimated and is shown in Figure 3 for two assumed  $\text{H}_2\text{O}$  mixing ratios. The  $\text{HNO}_3$  saturation mixing ratio for  $\text{H}_2\text{O} = 4$  ppmv is lower than 3 ppbv between 18 and 24 km. Even for  $\text{H}_2\text{O} = 2$  ppmv, the  $\text{HNO}_3$  saturation mixing ratio is still lower than 3 ppbv between 19 and 21 km. These low  $\text{HNO}_3$  saturation mixing ratios and the observed  $\text{NO}_y$  and  $\text{HNO}_3$  abundances suggest that

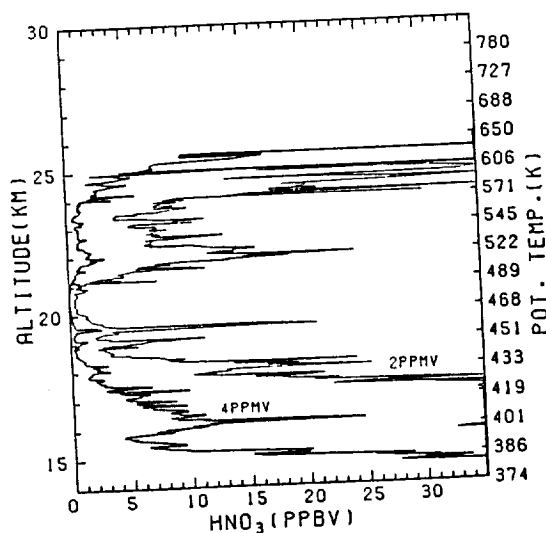


Fig. 3. Calculated equilibrium saturation mixing ratio for  $\text{HNO}_3$  over NAT, using the measured temperature profile on January 23, 1989 and assuming two  $\text{H}_2\text{O}$  vapor mixing ratios, 2 and 4 ppmv.

large enhancements in the aerosol concentration would be present under equilibrium conditions. The absence of an enhanced aerosol concentration therefore indicates a large supersaturation of  $\text{HNO}_3$  with respect to NAT. The aircraft data obtained in the Arctic in January, 1989 [D. W. Fahey, unpublished data, 1989] exhibit similar supersaturation in air parcels below 20 km at the edges of PSC activity. It is possible that the air sampled on board the balloon was in the leading edge of a cloud between 18 and 24 km. The layer in which aerosols were observed showed the greatest supersaturation with respect to NAT.

The  $\text{H}_2\text{O}$  saturation mixing ratio over ice has been calculated using the observed temperature profile; values ranging from 4.6 to 5 ppmv are indicated between 20 and 21 km. The average  $\text{H}_2\text{O}$  mixing ratio observed during the Arctic aircraft campaign was near 5 ppmv inside the polar vortex at altitudes between 18 and 20 km [K. Kelly, unpublished data, 1989].

The  $\text{NO}_y$ /ozone ratio determined using the simultaneously measured ozone profile is shown in Figure 4. Both

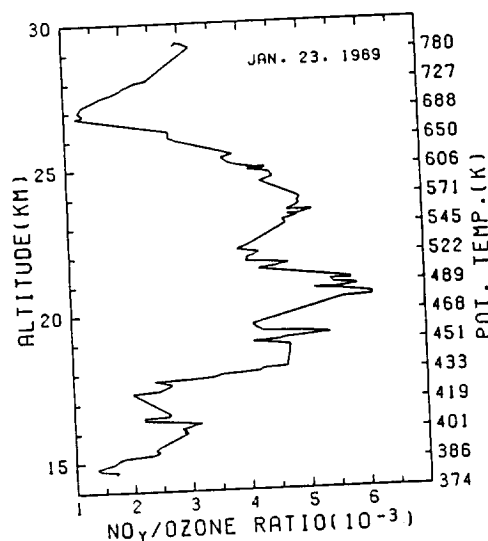


Fig. 4. Ratio of  $\text{NO}_y$  to ozone measured at Kiruna on January 23, 1989.

$\text{NO}_y$  and ozone have relatively long lifetimes for only gas phase chemical processes. This ratio can provide a better indication of possible denitrification than  $\text{NO}_y$  alone since small scale variations will cancel each other [Fahey, unpublished data, 1989]. The aircraft data cited above show a mean value of the  $\text{NO}_y/\text{O}_3$  ratio between 3 and  $5 \times 10^{-3}$  for altitudes between 15 and 20 km for both  $60^\circ$  and  $70^\circ\text{N}$  latitude. Values much less than  $3 \times 10^{-3}$  will indicate the loss in  $\text{NO}_y$ . It should also be noted that ozone profile as shown in Figure 1 does not show signs of enhanced layers that could also result in the decrease in the  $\text{NO}_y/\text{O}_3$  ratio. At around 27 km, a large minimum in the  $\text{NO}_y$ /ozone ratio can be seen. According to the SAM II and lidar measurements in previous years by McCormick *et al.* [1982, 1983], PSCs are sometimes observed up to this altitude. A possible interpretation of the minimum around 27 km is that PSCs had removed  $\text{NO}_y$  from



this region. A dip in the  $\text{NO}_y/\text{ozone}$  ratio around 22 km can also be seen, although it is less pronounced. The measured  $\text{NO}_y/\text{O}_3$  ratio was  $2.5 \pm 1 \times 10^{-3}$  between 15 and 18 km, suggesting again considerable  $\text{NO}_y$  depletion. In the future an important goal should be a background measurement of the winter Arctic stratosphere unperturbed by heterogeneous processes. The degree of denitrification in the data presented here may be better understood when such a background  $\text{NO}_y$  profile is available for comparison.

**Acknowledgments.** We wish to thank CNES for their excellent balloon operations and logistic support at Esrange. The balloon flight was supported by CNES with participation of CNRS. The support of the Ministry of Education, Science and Culture, the Scandinavia-Japan Sasakawa Foundation, the Chemical Manufacturers Association, the NSF Division of Atmospheric Chemistry and Division of Polar Programs, NASA, Esrange, the Swedish Institute of Space Physics, and the Texas Higher Education Coordinating Board are also gratefully acknowledged.

### References

- Aimedieu, P., W. A. Matthews, W. Attmannspacher, R. Hartmannsgruber, J. Cisneros, W. Komhyr, and D. E. Robbins, Comparison of *in situ* stratospheric ozone measurements obtained during the MAP/GLOBUS 1983 campaign, *Planet. Space Sci.*, **35**, 563–585, 1987.
- Douglass, A. R., and R. S. Stolarski, Impact of heterogeneous reactions of stratospheric chemistry of the Arctic, *Geophys. Res. Lett.*, **2**, 131–134, 1989.
- Fahey, D. W., C. S. Eubank, G. Hübner, and F. C. Fehsenfeld, Evaluation of a catalytic reduction technique for the measurement of total reactive odd-nitrogen  $\text{NO}_y$  in the atmosphere, *J. Atmos. Chem.*, **3**, 435–468, 1985.
- Fahey, D. W., D. M. Murphy, C. S. Eubank, K. Kelly, M. H. Proffitt, G. V. Ferry, M. K. W. Ko, M. Loewenstein, and K. R. Chan, Measurements of nitric oxide and total reactive nitrogen in the Antarctic stratosphere: Observations and chemical implications, *J. Geophys. Res.*, in press, 1989a.
- Fahey, D. W., K. K. Kelly, G. V. Ferry, L. R. Poole, J. C. Wilson, D. M. Murphy, M. Loewenstein, and K. R. Chan, *In situ* measurements of total reactive nitrogen, total water, and aerosol in a polar stratospheric cloud in the Antarctic, *J. Geophys. Res.*, **94**, 11299–11315, 1989b.
- Hanson, D., and K. Mauersberger, Laboratory studies of the nitric acid trihydrate: Implications for the south polar stratosphere, *J. Geophys. Res.*, **15**, 855–858, 1988.
- Hofmann, D. J., T. L. Deshler, P. Aimedieu, W. A. Matthews, P. V. Johnston, Y. Kondo, W. R. Sheldon, G. J. Byrne, and J. R. Benbrook, Stratospheric clouds and ozone depletion in the Arctic during January 1989, *Nature*, **340**, 117–121, 1989a.
- Hofmann, D. J., J. M. Rosen, J. W. Harder, and J. V. Hereford, Balloon-borne measurements of aerosol, condensation nuclei, and cloud particles in the stratosphere at McMurdo Station, Antarctica, during the spring of 1987, *J. Geophys. Res.*, **94**, 11253–11269, 1989b.
- Johnston, P. V. and R. C. McKenzie,  $\text{NO}_2$  observation at  $45^\circ$  during the decay phase of solar cycle 21, from 1980 to 1987, *J. Geophys. Res.*, **95**, 3473–3486, 1989.
- Kawa, S. R., D. W. Fahey, L. C. Anderson, M. Loewenstein, and K. R. Chan, Measurements of total reactive nitrogen during the airborne Arctic stratospheric expedition, *Geophys. Res. Lett.*, this issue, 1989.
- Kondo, Y., P. Aimedieu, W. A. Matthews, W. R. Sheldon, and J. R. Benbrook, A mid-latitude balloon-borne observation of total odd nitrogen, in press, *Geophys. Res. Lett.*, 1989.
- McElroy, M. B., R. J. Salawitch, and S. C. Wofsy, Antarctic  $\text{O}_3$ : Chemical mechanisms for the spring decrease, *Geophys. Res. Lett.*, **13**, 1296–1299, 1986.
- McCormick, M. P., H. M. Steele, P. Hamill, W. P. Chu, and T. J. Swisler, Polar stratospheric cloud sightings by SAM II, *J. Atmos. Sci.*, **39**, 1387–1397, 1982.
- McCormick, M. P., C. R. Trepte, and G. S. Kent, Spatial changes in the stratospheric aerosol associated with the north polar vortex, *Geophys. Res. Lett.*, **10**, 941–944, 1983.
- Murcray, D. G., T. G. Kyle, F. H. Murcray, and W. J. Williams, Presence of  $\text{HNO}_3$  in the upper atmosphere, *J. Opt. Soc. Am.*, **59**, 1131–1134, 1969.
- Solomon, S., R. R. Garcia, F. S. Rowland, D. J. Wuebbles, On the depletion of Antarctic ozone, *Nature*, **321**, 755–758, 1986.
- Y. Kondo, Y. Iwasaka, and A. Iwata, Research Institute of Atmospheric Sciences, Nagoya University, Toyokawa, Aichi, Japan.
- P. Aimedieu, Service d'Aéronomie, CNRS, Verrières le Buisson, France.
- W. A. Matthews and P. V. Johnston, Physics and Engineering Laboratory, Lauder, Central Otago, New Zealand.
- D. W. Fahey, Aeronomy Laboratory, NOAA, Boulder, Colorado, USA.
- D. G. Murcray, Department of Physics, University of Denver, Denver, Colorado, USA.
- D. J. Hofmann, Department of Physics and Astronomy, University of Wyoming, Laramie, Wyoming, USA.
- W. R. Sheldon, Department of Physics, University of Houston, Houston, Texas, USA.

(Received October 19, 1989;  
Revised December 6, 1989;  
Accepted December 11, 1989)



# TUNABLE DIODE LASER HETERODYNE SPECTROPHOTOMETRY OF OZONE

P.F. Fogal<sup>1</sup>, C.T. McElroy<sup>2</sup>, A. Goldman<sup>1</sup>, and D.G. Murcray<sup>1</sup>

<sup>1</sup>University of Denver, Denver, CO., USA, 80208-0202

<sup>2</sup>Atmospheric Environment Service, Downsview, Ontario, Canada

## ABSTRACT

Tunable diode laser heterodyne spectrophotometry (TDLHS) has been used to make extremely high resolution ( $< 0.0005 \text{ cm}^{-1}$ ) solar spectra in the 9.6 micron ozone band. Observations have shown that a signal-to-noise ratio of 95:1 (35% of theoretical) for an integration time of 1/8 second can be achieved at a resolution of 0.0005 wavenumbers. The spectral data have been inverted to yield a total column amount of ozone, in good agreement with that measured at the nearby National Oceanographic and Atmospheric Administration (NOAA) ozone monitoring facility in Boulder, Colorado.

## 1. INTRODUCTION

Tunable Diode Laser Heterodyne Spectroscopy (TDLHS) has the ability to produce very high resolution atmospheric spectra. The concept of heterodyning and its applications to instruments for atmospheric measurement have been discussed previously by a number of authors, including Fujii et al. [ 1978 ], Menzies et al. [ 1981 ], Glenar et al. [ 1983 ], and Kostiuik and Mumma [ 1983 ]. In particular, Frerking and Meuhlnner [ 1977 ] have applied TDLHS to the study of atmospheric ozone, with a resolution of  $0.0067 \text{ cm}^{-1}$  and a signal-to-noise ratio of 40. At the University of Denver, the instrument described by Allario et al., [ 1979, 1980 ] has recently produced spectra having a resolution of  $0.0005 \text{ cm}^{-1}$  or better, at wavelengths in the region of the  $9.6 \mu\text{m}$  ozone band. Some of these spectra have been inverted to provide column ozone amounts which were found to be in good agreement with values obtained at the National Oceanographic and Atmospheric Administration (NOAA). A number of the line positions have been compared to the Hitran database [ Rothman et al., 1987 ], with updated ozone lines [ Goldman and Murcray, 1988 ] and in the majority of the cases the frequencies are found to match to better than  $0.001 \text{ cm}^{-1}$ .

## 2. INSTRUMENTATION

The theory behind heterodyne detection is well known, and its application to the TDLHS has been discussed by McElroy et al. [ 1988 ]. The voltage signal-to-noise ratio  $S_V$  [ Blaney, 1975 ],

can be arrived at by considering our photoconductor to be a square-law detector and if we consider the noise bandwidth of the output filter to be on the order of  $1/\tau$ , where  $\tau$  is the post-detection integration time constant of the system. Therefore,

$$S_V = \frac{\eta P_s}{2h\nu B_{IF} (1 + \eta \delta \beta)} \sqrt{2 B_{IF} \tau}$$

where  $\eta$  is the quantum efficiency of the photoconductor,  $\nu$  is the photon frequency,  $B_{IF}$  is the bandwidth of the intermediate frequency,  $\delta = [\exp(h\nu/kT_B) - 1]^{-1}$ , where  $T_B$  is the black-body temperature of the source, and  $\beta = 1$  for a thermal source that completely fills the field-of-view. If values typical to this instrument and atmospheric spectroscopy are used, that is,  $\eta = 0.38$ ,  $T_B = 5500 \text{ K}$ ,  $B_{IF} = 3.1 \text{ MHz}$ ,  $\tau = 0.125 \text{ s}$ ,  $\nu = 3 \cdot 10^{13} \text{ Hz}$ ,  $P_s = 2h\nu\delta\beta B_{IF}$ , and we apply the quantum limit  $h\nu \gg kT_B$ , then  $S_V$  is approximately 1200:1. Other losses such as chopper efficiency (50%) and losses due to the optics (45%) result in a final figure of approximately 260:1.

The University of Denver TDLHS was constructed by the NASA research group in Langley, Virginia. The instrument concept was described by Allario et al. [ 1979, 1980 ]. During the past year of its life at the University of Denver, the instrument has been considerably modified resulting in a reduction in temperature tuning errors and a consequent improvement in wavelength stability. The optical arrangement is more or less unchanged, except for the addition of

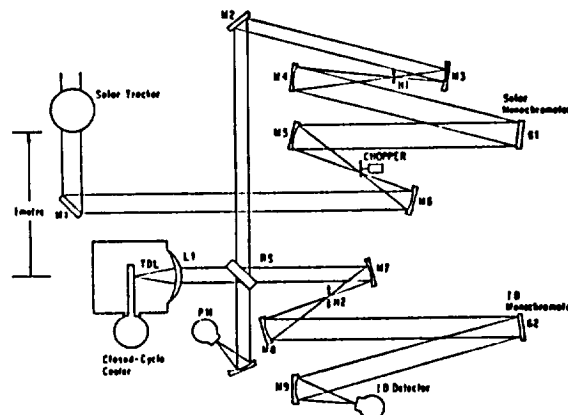


Fig. 1. The optical schematic diagram of the instrument. Mirrors are indicated by the letter M, diffraction gratings by G, the beamsplitter by BS and the lens by L1.

focussing capability at the detector, and is illustrated in Figure 1. Solar radiation is directed into the instrument by means of a clock-driven mirror. The solar tracker directs the light to mirror M1, which reflects it to an off-axis paraboloid M6, which produces an image of the sun at the pin-hole located immediately before the chopper. The light exiting the pinhole is collimated by mirror M5, dispersed by grating G1, and focussed onto the exit pinhole H1 by mirror M4. The light exiting H1 is collimated by mirror M3 and directed towards the beamsplitter BS by mirror M2. Light from the TDL local oscillator is collected by lens L1 and it then falls on the beamsplitter where it combines with the solar beam with phase matching. After the beamsplitter, the composite beam is focussed upon a high-speed mercury-cadmium-tellurium (HgCdTe) photomixer biased as a photoconductor. The heterodyne signal, which contains the spectral information, is then separated from the DC component. The amplified RF signal is then bandpass filtered to set the desired instrumental resolution. Currently, there are 7 different bandpass options available. The highest resolution is derived from a channel having a bandpass that ranges from 1 to 4.1 MHz. After the bandpass filtering, the signal is square-law detected by a broadband RF detector (0.1 to 1 GHz) and subsequently phase-sensitive detected using a dual slope integrator. The integrator is ramped up during the open cycle of the chopper, and then ramped down again during the closed cycle. The phase-sensitive detection process provides a large rejection ratio for sources of noise such as detector thermal noise and other background sources which are unmodulated.

It should be noted, that the signal from the detector RF amplifier is proportional to the square root of the solar intensity, or equivalently, to the solar field strength. After the signal is square-law detected, a signal which is proportional to the solar intensity as well as the local oscillator intensity results. This is the signal which is phase-sensitive detected and then recorded as spectral data.

### 3. SPECTRAL ANALYSIS

The spectra are viewed and manipulated by means of software written for an IBM PC/XT. All of the spectra presented here have had a 3 point (FWHM) triangular filter applied to them. A wavelength calibration is generated through the application of calculated dispersion coefficients. The dispersion coefficients are generally calculated by taking the current scan values for selected lines and then performing a linear or quadratic regression against line positions as determined for the Bomem DA3 interferometer [Murray et al., 1988], which is currently demonstrating an unapodized resolution of  $0.002 \text{ cm}^{-1}$ . For a linear regression, this method generally provides agreement between the wavelength calibration of the spectra of the order of  $10^{-4} \text{ cm}^{-1}$ . In all cases, only fairly narrow, well-defined lines were used in these regressions, one of which is required for each current scan. It is necessary to provide a wavelength scale in this manner, because a sufficiently accurate independent method has not

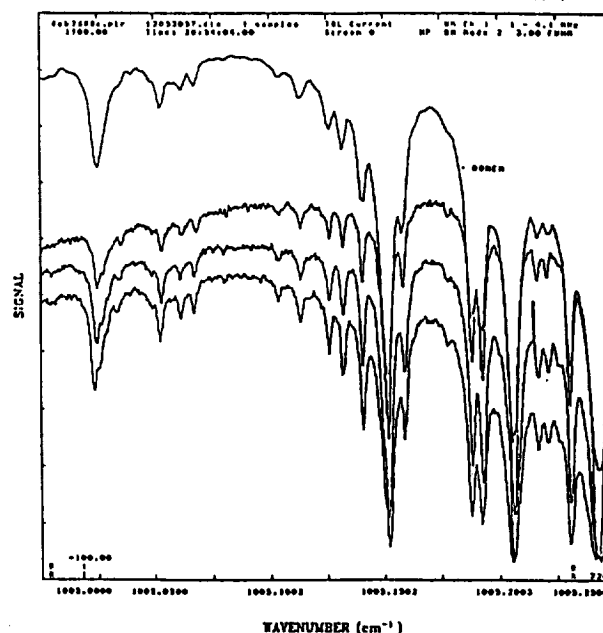


Fig. 2. Comparison of a Bomem solar spectrum to 3 TDLHS solar spectra between  $1005.0$  and  $1005.25 \text{ cm}^{-1}$ . The Bomem spectrum was taken on Oct. 21, 1987 at a zenith angle of  $66.5^\circ$ . The TDLHS spectra were taken on Feb. 26, 1987 at zenith angles of  $54^\circ$ ,  $70^\circ$ , and  $77^\circ$  respectively.

been incorporated into the TDLHS as yet.

The signal-to-noise ratios quoted here were calculated by determining the standard deviation of a number of points in a region where the spectral intensity appeared to be relatively constant. This method could well yield a noise level greater than the actual one, but it is unlikely to yield one that is less. The theoretical signal-to-noise ratio for the  $4.1 \text{ MHz}$  channel is  $260:1$ , while the observed signal-to-noise ratio calculated by this method is  $95:1$ , or  $35\%$  of theoretical.

TDLHS spectra have been compiled in 4 regions. They are as follows:  $996 - 997 \text{ cm}^{-1}$ ,  $1004.9 - 1005.3 \text{ cm}^{-1}$ ,  $1009.6 - 1010.2 \text{ cm}^{-1}$ ,  $1012.0 - 1012.5 \text{ cm}^{-1}$ . The observed TDLHS spectra have been compared to the Hitran database, and to Bomem DA3 spectra taken during October and November of 1987. In each case the higher resolution and signal-to-noise of the TDLHS can be seen. Figure 2 shows three scans taken on February 26, 1988 from  $1005.0$  to  $1005.25 \text{ cm}^{-1}$ . Each scan was calibrated independently as described earlier. The higher resolution can be seen in that the TDLHS can better resolve a number of lines that the Bomem interferometer spectra show as slope changes in the sides of lines. Figure 3 shows a comparison between Bomem and TDLHS spectra in the region  $1009.6 \text{ cm}^{-1}$  to  $1009.8 \text{ cm}^{-1}$ . The TDLHS resolves a line at  $1009.61880 \text{ cm}^{-1}$ , while the Bomem spectrum indicates that there may be a feature at that frequency. A similar phenomenon is seen with the line at  $1009.70334 \text{ cm}^{-1}$ . All the interferometer data were collected by scans of 4 minute duration.

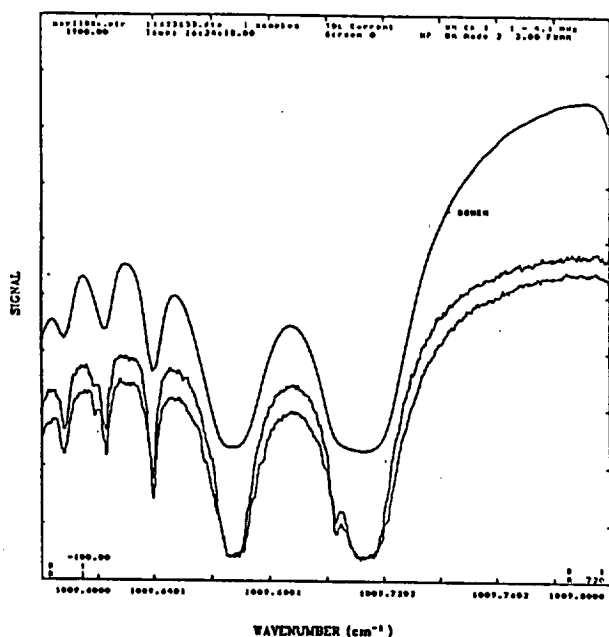


Fig. 3. Comparison of TDLHS solar spectra to a Bomem solar spectrum between 1009.6 and 1009.8  $\text{cm}^{-1}$ . The Bomem is as described in Figure 3, while the TDLHS spectra were taken on May 11, 1988 at zenith angles of 56.5° and 63.5° respectively.

Figure 4 illustrates a spectrum taken January 21, 1987 at the University of Denver (altitude 1.6 km, 39.5°N 105°W). This spectrum was taken while the instrument was in its original configuration, and it has a signal-to-noise ratio of 45:1, or 17% of theoretical. The curves in Figure 5 compare an expanded portion of the observed spectrum taken at 0.0016  $\text{cm}^{-1}$  resolution, to a simulation using line parameters which are the same as those on the Hitran compilation, with the exception of the line positions, which were adjusted to agree with the observed data. The climatological vertical distribution of ozone at mid-latitude was taken as a starting point for a non-linear spectral least squares fitting procedure which scaled the whole profile until the best possible agreement between the two curves was obtained [Goldman et al., 1983]. It can be seen that the three lines shown are not all fit with the same precision. This difference is due to the combined effects of inaccuracies in the compiled line intensities and halfwidths, and the fact that the observed lines result from states of rather different, relatively high, energies and are therefore affected differently by changes in the local temperature.

In order to investigate the possibility that the observed and simulated spectra might be brought into better agreement if the temperature profile of the model atmosphere were changed, the fitting program was run in such a way that the temperature profile could be scaled to achieve the best agreement between the data and the model results. When this was done a slightly different total column amount of ozone was obtained, with no apparent improvement of the fit, with the difference between the two amounts being about

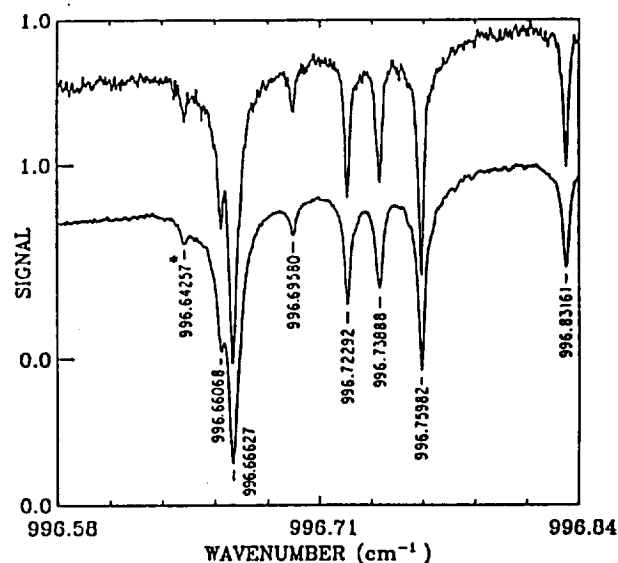


Fig. 4. A solar spectrum taken by the TDLHS on January 21, 1987, at a zenith angle of 60.1°. The upper curve shows data from the 1 to 4.1 MHz channel, while the lower one plots the signal from the 10 to 20 MHz bandpass channel.

8%. The column amounts obtained in these calculations are 344 and 317 m-atm-cm for the fixed and adjusted temperature profiles, respectively. The ozone total column amount determined by the Dobson ozone spectrophotometer at NOAA at Boulder [private communication from W. Komhr and R. Evans, 1987], is 355 m-atm-cm.

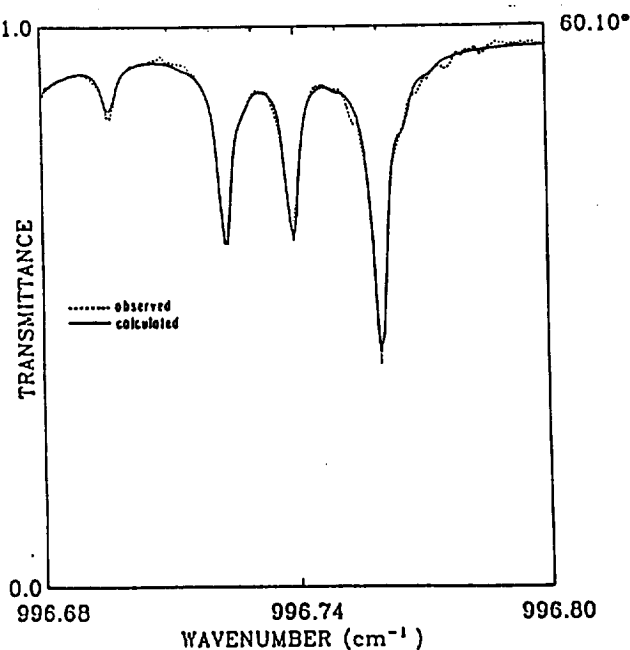


Fig. 5. This figure shows a comparison of the observed data and the results of a spectral simulation over a narrow region containing several ozone lines. The ozone amount was adjusted to give the best fit, and the spectrum shown was calculated with 344 m-atm-cm of ozone in the model atmosphere.

The Dobson total ozone amount was adjusted by 3.9% before being compared to the infrared results, with the reported 369 Dobson unit Boulder measurement corrected to 355 m-atm-cm. This adjustment is needed because the Dobson values are now known to read high compared to ultraviolet and chemical measurements of ozone [ private communication from J.B. Kerr, Atmospheric Environment Service, 1987 ].

#### 4. CONCLUSIONS

The TDLHS is just now beginning to realize its potential. It is hoped that a better selection of TDL's will become available in the not too distant future, thereby increasing the number of spectral regions which can be investigated. The higher resolution of the TDLHS provides the potential to better resolve the spectral lines of absorbers whose lines overlap those of other atmospheric constituents. Higher spectral resolution will provide better resolution of constituent vertical profiles which would benefit line shape inversion studies.

#### ACKNOWLEDGEMENTS

Acknowledgement is made to the National Center for Atmospheric Research, which is sponsored by the National Science Foundation, for computer time used in this research. Funding to support this work was provided by NASA/Langley.

#### REFERENCES

- Allario, F., J. M. Hoell, S. J. Katzberg, J. C. Larsen, 1979: An Experiment Concept to Measure Stratospheric Trace Constituents by Laser Heterodyne Spectroscopy, Proc. NASA Conf. on High Resolution Infrared Spectroscopy Techniques for Atmospheric Measurements, Publ. No. 2134, 57-79.
- Allario, F., J. M. Hoell, and S. J. Katzberg, 1980: An experiment concept to measure stratospheric trace constituents by laser heterodyne spectroscopy, Appl. Phys., **23**, 47-56.
- Blaney, T. G., Signal-to-Noise Ratio and Other Characteristics of Heterodyne Radiation Receivers, 1975: Space Science Reviews, **17**, 691-702.
- Frerking, M. A. and D. J. Muehlner, 1977: Infrared Heterodyne Spectroscopy of Atmospheric Ozone, Appl. Opt., **16**, 526-528.
- Fujii, Y., J. Yamashita, S. Shikata, S. Saito, 1978: Incoherent Optical Heterodyne Detection and its Application to Air Pollution Detection, Appl. Opt., **17**, 3444-3449.
- Glenar, D., T. Kostiuik, D. E. Jennings, D. Buhl, and M. J. Mumma, 1981: Tunable Diode-Laser Heterodyne Spectrometer for Remote Observations near 8  $\mu$ m, Appl. Opt., **21**, 253-259.
- Goldman, A., F. G. Fernald, F. J. Murcray, F. H. Murcray, and D. G. Murcray, 1983: Spectral Least Squares Quantification of Several Atmospheric Gases From High Resolution Infrared Solar Spectra Obtained at the South Pole, J. Quant. Spectrosc. Radiat. Transfer, **29**, 189-204.
- Goldman, A. and D. G. Murcray, 1988: High Resolution Studies of Atmospheric Infrared Emission and Absorption Spectra, Proceedings of the Spie Conference.
- Kostiuk, T., and M. J. Mumma, 1983: Remote Sensing by IR Heterodyne Spectroscopy, Appl. Opt., **22**, 2644-2654.
- McElroy, C. T., A. Goldman, and D. G. Murcray, 1988: Heterodyne Spectrophotometry of Ozone in the 9.6 Micron Band Using a Tunable Diode Laser, submitted to Appl. Opt..
- Menzies, R. T., C. W. Rutledge, R. A. Zanteson, and D. L. Spears, 1981: Balloon-Borne Laser Heterodyne Radiometer for Measurements of Stratospheric Trace Species, Appl. Opt., **20**, 536-544.
- Murcray, F. J., J. J. Kusters, and R. D. Blatherwick, 1988: A Very High Resolution Fourier Transform Spectrometer for Balloon-Borne Applications, Submitted to Appl. Opt..
- Rothman, L. S., R. R. Gamache, A. Goldman, L. R. Brown, R. A. Toth, H. M. Pickett, R. L. Poynter, J. -M. Flaud, C. Camy-Peyret, A. Barbe, N. Husson, C. P. Rinsland, and M. A. H. Smith, 1987: The Hitran Database: 1986 edition, Appl. Opt., **26**, 4058-4097.



# Infrared Measurements of Atmospheric Gases Above Mauna Loa, Hawaii, in February 1987

C. P. RINSLAND

*Atmospheric Sciences Division, NASA Langley Research Center, Hampton, Virginia*

A. GOLDMAN, F. J. MURCRAY, F. H. MURCRAY, R. D. BLATHERWICK, AND D. G. MURCRAY

*Physics Department, University of Denver, Denver, Colorado*

Infrared solar absorption spectra recorded at  $0.02\text{ cm}^{-1}$  resolution from the National Oceanic and Atmospheric Administration (NOAA) Geophysical Monitoring for Climate Change (GMCC) program station at Mauna Loa, Hawaii (latitude  $19.5^\circ\text{N}$ , longitude  $155.6^\circ\text{W}$ , elevation  $3.40\text{ km}$ ), in February 1987 have been analyzed to determine simultaneous total vertical column amounts for 13 atmospheric gases. Average tropospheric concentrations of  $\text{CO}_2$ ,  $\text{N}_2\text{O}$ ,  $\text{CH}_4$ , and  $\text{CHClF}_2$  and the daytime diurnal variations of the total columns of  $\text{NO}$  and  $\text{NO}_2$  have also been inferred. The retrieved total columns (in molecules  $\text{cm}^{-2}$ ) of the nondiurnally varying gases are  $1.6 \pm 0.2 \times 10^{15}$  for  $\text{HCl}$ ,  $5.9 \pm 1.2 \times 10^{15}$  for  $\text{HNO}_3$ ,  $2.0 \pm 0.2 \times 10^{21}$  for  $\text{H}_2^{16}\text{O}$ ,  $4.4 \pm 0.7 \times 10^{18}$  for  $\text{H}_2^{18}\text{O}$ ,  $2.7 \pm 0.1 \times 10^{17}$  for  $\text{HDO}$ ,  $2.3 \pm 0.2 \times 10^{19}$  for  $\text{CH}_4$ ,  $5.0 \pm 0.5 \times 10^{21}$  for  $\text{CO}_2$ ,  $6.7 \pm 0.8 \times 10^{18}$  for  $\text{O}_3$ ,  $4.3 \pm 0.4 \times 10^{18}$  for  $\text{N}_2\text{O}$ ,  $1.0 \pm 0.2 \times 10^{16}$  for  $\text{C}_2\text{H}_6$ , and  $9.7 \pm 2.5 \times 10^{14}$  for  $\text{CHClF}_2$ . We compare the total column measurements of  $\text{HCl}$  and  $\text{HNO}_3$  with previously reported ground-based, aircraft, and satellite measurements. The results for  $\text{HCl}$  are of particular interest because of the expected temporal increase in the concentration of this gas in the stratosphere. However, systematic differences among stratospheric  $\text{HCl}$  total column measurements from 1978 to 1980 and the absence of observations of free tropospheric  $\text{HCl}$  above Mauna Loa make it impossible to obtain a reliable estimate of the trend in the total burden of  $\text{HCl}$ . The measured  $\text{HNO}_3$  total column is consistent with aircraft measurements from  $\sim 12\text{ km}$  altitude. The  $\text{O}_3$  total column deduced from the IR spectra agrees with correlative Mauna Loa Umkehr measurements within the estimated error limits. The column-averaged D/H ratio of water vapor is  $(68 \pm 9) \times 10^{-6}$ , which is  $0.44 \pm 0.06$  times the reference value of  $155.76 \times 10^{-6}$  for standard mean ocean water (SMOW). This large depletion in the D content of water vapor is similar to published measurements of the upper troposphere and lower stratosphere. Average tropospheric concentrations deduced for  $\text{CO}_2$ ,  $\text{N}_2\text{O}$ , and  $\text{CH}_4$  are in good agreement with correlative NOAA GMCC surface data, indicating consistency between the measurement techniques for determining tropospheric volume mixing ratios. Results of the present study indicate that Mauna Loa is a favorable site for infrared monitoring of atmospheric gases. The site is particularly favorable for monitoring the tropospheric volume mixing ratios of long-lived gases, since the high altitude of the tropopause reduces corrections required to account for the decrease in volume mixing ratio in the stratosphere.

## 1. INTRODUCTION

This paper presents the results of a quantitative analysis of absorptions by a number of minor and trace atmospheric gases in  $0.02\text{ cm}^{-1}$  resolution solar absorption spectra recorded at a number of solar zenith angles on 4 days in February 1987 by F. J. Murcray and F. H. Murcray at the National Oceanic and Atmospheric Administration (NOAA) Geophysical Monitoring for Climate Change (GMCC) program station at Mauna Loa, Hawaii (latitude  $19.5^\circ\text{N}$ , longitude  $155.6^\circ\text{W}$ , elevation  $3.40\text{ km}$ ). The spectral data were recorded with a Michelson-type Fourier transform spectrometer, with a maximum path difference of  $50\text{ cm}$  and a scan time of  $62\text{ s}$ . This instrument has been used previously to obtain many balloon-borne, ground-based, and laboratory spectra by the University of Denver spectroscopy group (see Goldman *et al.* [1988] for a description of the instrument and data collection system).

There were a number of reasons for obtaining these observations. First, Mauna Loa is a dry, high-altitude site, where there is a very significant reduction in the spectral interference by the strong  $\text{H}_2\text{O}$  absorptions usually present in IR spectra

recorded from ground-based sites. This reduction allowed us to obtain measurements of several key trace atmospheric gases not usually accessible through ground-based IR observations. For example, we have been able to obtain simultaneous measurements of the daytime diurnal variations of the total columns of  $\text{NO}_2$  and  $\text{NO}$  through observations of  $\text{NO}_2$  lines of the strong  $\nu_3$  band at  $6.2\text{ }\mu\text{m}$  and the weaker  $\nu_1 + \nu_3$  band at  $3.4\text{ }\mu\text{m}$  and of the  $\text{NO}$  lines of the fundamental vibration-rotation band at  $5.3\text{ }\mu\text{m}$ . Second, we were interested in obtaining IR data from a low-latitude station. To our knowledge, no such ground-based IR observations have been obtained previously in the tropics. The spectra compose a permanent record of the state of the atmosphere at the time of the observations and can be compared with spectra from other locations and times to establish latitudinal distributions and temporal trends of minor and trace species. We are in the process of collecting data from a number of sites at different latitudes for this purpose (e.g., South Pole Station, Antarctica, New Zealand, Kitt Peak in Arizona, Mount Evans in Colorado, NASA Langley in Hampton, Virginia). To our knowledge, with the exceptions of ongoing total ozone measurements with a Dobson instrument and visible region measurements of  $\text{NO}_2$  obtained in 1978 [Noxon *et al.*, 1983], the present results provide the only measurements of total col-

Copyright 1988 by the American Geophysical Union.

Paper number 88JD03259.  
0148-0227/88/88JD-03259\$05.00



TABLE 1. Experimental Parameters for the Atmospheric Spectra

Date in 1987	Transition Type	Spectral Region, $\text{cm}^{-1}$	Solar Astronomical Zenith Angle, deg
Feb. 6	sunrise	2450–3300	80.34, 78.24, 77.54
	sunset	2450–3300	78.53, 82.75, 84.86, 86.30
Feb. 8	sunrise	1500–2000	80.60, 69.52, 68.52
	noon	1500–2000	34.48, 48.30
Feb. 9	sunset	1500–2000	63.74, 75.74
Feb. 10	sunrise	750–1300	84.31, 82.87, 81.49, 80.07

umns from Mauna Loa. Our results therefore provide benchmark observations of the total burdens of a number of gases above this site. For gases concentrated primarily in the stratosphere (e.g., HCl and  $\text{HNO}_3$ ), our measured total columns can be compared with values from airborne latitudinal surveys [e.g., Mankin and Coffey, 1983; Girard et al., 1982, 1983]. Our measured ozone total column can be directly compared with correlative Mauna Loa Dobson results. Finally, since Mauna Loa is a NOAA GMCC site, we were interested in using the IR measurements to deduce average tropospheric concentrations of long-lived gases for comparison with the NOAA GMCC site measurements. As will be shown in this paper, our results for  $\text{CO}_2$ ,  $\text{CH}_4$ , and  $\text{N}_2\text{O}$  are in excellent agreement with NOAA GMCC sampling measurements at Mauna Loa. This implies that the Mauna Loa surface sampling measurements of these gases are representative of their average tropospheric concentrations. Because of the high altitude of the tropopause, the stratospheric contribution to the total column is relatively small. Therefore the uncertainty in the assumed mixing ratio distribution in the stratosphere causes only a small uncertainty in the derived mean tropospheric volume mixing ratio. Also, although the height of the tropical tropopause varies on both interannual and annual time scales and with the solar cycle [Gage and Reid, 1981, 1985; Reid and Gage, 1981, 1985], these variations are smaller than at higher latitudes and hence of lesser significance in interpreting time series of IR measurements. For these reasons, we believe that Mauna Loa is more suitable for IR monitoring of the tropospheric concentrations of long-lived gases than higher-latitude sites, where the tropopause is lower and more variable in height.

## 2. DATA AND ANALYSIS METHOD

The spectral data have been analyzed using the technique of nonlinear least squares spectral curve fitting. Details of the application of this method to the analysis of ground-based infrared solar spectra are described in several recent papers [cf. Rinsland et al., 1982a; Goldman et al., 1983, 1987a]. Except as noted in the following discussion, line parameters were taken from the 1986 Air Force Geophysics Laboratory high-resolution transmission (HITRAN) molecular absorption database [Rothman et al., 1987]. Radiosonde soundings from Hilo, Hawaii, on the date of the spectral measurements were used to define the vertical pressure-temperature profile for the analysis. The tropopause was between 17 and 18 km altitude during the observations. The 15°N annual atmosphere from the U.S. Standard Atmosphere (1966) supplements was used to extend the pressure-temperature profile from the upper altitude limit of the soundings (about 30 km) to 100 km. These pressures and temperatures were input to a ray-tracing pro-

gram [Gallery et al., 1983] to calculate the total air mass, mass-weighted pressures, and mass-weighted temperatures for each of 17 layers for the analysis of each spectrum. The total vertical column amount of air above Mauna Loa is calculated to be  $1.44 \times 10^{25}$  molecules  $\text{cm}^{-2}$ .

Table 1 summarizes the spectra included in the present study. The signal-to-rms noise ratio of the spectral data is about 200. It should be recalled that each spectrum provides a simultaneous measurement of a large number of constituents in the same volume of air.

Previous studies [e.g., Goldman et al., 1983, 1987a; Murcray et al., 1987] have shown that the total columns of most gases can be retrieved from the University of Denver ground-based spectra to a precision of several percent and to absolute accuracies of 10–20%. Following the procedures described in these earlier investigations, errors in the total columns have been estimated, based on the sensitivity of the results to changes in the assumed vertical mixing ratio distributions and the assumed pressure-temperature profile and on knowledge of the uncertainties in the spectroscopic line parameters. Examples of sensitivity studies are presented in a previous paper [Goldman et al., 1983].

Narrow lines arising primarily from absorption in the low-pressure stratosphere (e.g., HCl,  $\text{O}_3$ ) show a small asymmetry in the spectral profile indicating residual phase distortion (see, for example, Figures 5 and 9 of this paper), probably caused by incomplete alignment of the instrument during the run. Total columns retrieved, using various assumptions to model the measured line profiles, vary by about 5%. This source of uncertainty has been included in all of the  $1\sigma$  total column error estimates reported later. Phase errors are believed to also distort the shapes of broader lines (e.g.,  $\text{H}_2\text{O}$ ,  $\text{CH}_4$ ,  $\text{N}_2\text{O}$ ), but these effects are difficult to separate from line shape asymmetries caused by pressure-induced line shifts (significant air-broadened line shifts have recently been measured in methane near 7  $\mu\text{m}$  [Rinsland et al., 1988a; Malathy Devi et al., 1988]), errors in the assumed line positions, and line-mixing effects. Note, for example, rather large, second-derivative-type residuals near the  $\text{CH}_4$  and  $\text{CO}_2$  lines in Figure 3, a  $\text{N}_2\text{O}$  line in Figure 6, and the  $\text{CH}_4$  lines in Figure 7.

Ground-based infrared solar spectra also contain information on the vertical distributions of the observable gases. However, the weighting functions in altitude are rather broad. For the present analysis a reference volume mixing ratio profile for each gas [e.g., Smith, 1982] has been scaled by a single multiplicative factor until the best fit to the spectrum is achieved.

## 3. RESULTS

Table 2 lists the spectral regions analyzed in this study. A number of these intervals were used in earlier studies of Uni-

TABLE 2. Spectral Regions Analyzed in the Present Study

Spectral Region, cm <sup>-1</sup>	Target Gases	Other Gases
776.00–776.50	C <sub>2</sub> H <sub>2</sub>	O <sub>3</sub> , CO <sub>2</sub>
828.95–829.20	CHClF <sub>2</sub>	CO <sub>2</sub> , C <sub>2</sub> H <sub>6</sub>
868.00–869.00	HNO <sub>3</sub>	
871.80–873.20	HNO <sub>3</sub>	
1146.40–1146.56	O <sub>3</sub>	
1155.39–1155.56	O <sub>3</sub>	
1163.34–1163.48	O <sub>3</sub>	
1597.97–1598.17	NO <sub>2</sub>	
1599.73–1600.00	NO <sub>2</sub>	
1857.23–1857.35	NO	
1887.48–1887.58	NO	O <sub>3</sub>
1896.95–1897.05	NO	CO <sub>2</sub>
1914.95–1915.05	NO	
2583.10–2583.75	N <sub>2</sub> O	
2621.20–2624.20	HDO, CH <sub>4</sub>	CO <sub>2</sub> , solar OH
2626.35–2626.80	CO <sub>2</sub>	
2632.15–2632.50	CO <sub>2</sub>	HDO
2657.00–2658.00	HDO, CH <sub>4</sub>	
2660.20–2660.80	HDO	
2806.15–2806.55	N <sub>2</sub> O	
2819.20–2819.64	H <sub>2</sub> <sup>16</sup> O, HCl	
2843.55–2843.80	HCl	
2908.70–2911.02	CH <sub>4</sub>	H <sub>2</sub> O
2914.40–2914.70	NO <sub>2</sub>	CH <sub>4</sub>
2925.80–2926.10	HCl	
2976.65–2977.10	C <sub>2</sub> H <sub>6</sub>	O <sub>3</sub>
3155.00–3155.58	H <sub>2</sub> <sup>16</sup> O	CH <sub>4</sub>
3201.30–3201.65	CO <sub>2</sub>	O <sub>3</sub>
3204.50–3204.85	CO <sub>2</sub>	
3205.00–3205.60	H <sub>2</sub> <sup>18</sup> O	

versity of Denver spectra recorded from South Pole Station [Goldman et al., 1987a, 1988; Murcray et al., 1987]. The target molecules are listed along with identifications of additional telluric and solar species occurring in each interval. The regions were selected to provide features that have minimal temperature sensitivity and minimal overlapping interference. The natural isotopic ratios incorporated in the intensities on the 1986 HITRAN compilation [Rothman et al., 1987] have been assumed in the analysis of molecules other than H<sub>2</sub>O; for water vapor the H<sub>2</sub><sup>16</sup>O, H<sub>2</sub><sup>18</sup>O, and HDO isotopes have been analyzed separately.

#### Water Vapor

To analyze for the total column for each isotope, the water vapor line intensities were divided by the isotopic abundance assumed for each on the HITRAN compilation [Rothman et al., 1987, Table IV]. The U.S. Standard Atmosphere (1962) water vapor profile given by McClatchey et al. [1972, Table B1] was scaled by a multiplicative factor in the fittings of all regions. Because of the dryness of the stratosphere and the high altitude of the tropopause in the tropics, the relative contribution of stratospheric H<sub>2</sub>O to the total column is very small. With the assumed vertical H<sub>2</sub>O profile, over 99.9% of the H<sub>2</sub>O molecules in the total vertical column are calculated to be located below the tropopause.

It has proven quite difficult to locate isolated lines with suitable temperature-insensitive intensities for analysis. Figure 1 shows a fit to the primary H<sub>2</sub><sup>16</sup>O line, a 2v<sub>2</sub> band transition at 3155.348 cm<sup>-1</sup> with a lower state energy of 446.511 cm<sup>-1</sup>. Because of overlapping absorption by a methane line on the high wave number wing, the analysis required the simultaneous retrieval of both the H<sub>2</sub><sup>16</sup>O and CH<sub>4</sub> total columns.

The retrieved H<sub>2</sub><sup>16</sup>O total column amount from this interval is  $2.1 \pm 0.4 \times 10^{21}$  molecules cm<sup>-2</sup>. As a check on this result, the 2819.2–2819.64 cm<sup>-1</sup> interval was also analyzed. It contains a more temperature-sensitive 2v<sub>2</sub> band line at 2819.449 cm<sup>-1</sup> (lower state energy of 782.410 cm<sup>-1</sup>) with the P3 (1–0) band H<sup>37</sup>Cl line at 2819.559 cm<sup>-1</sup> overlapping on its high wave number wing. The retrieved H<sub>2</sub><sup>16</sup>O column of  $1.9 \pm 0.2 \times 10^{21}$  molecules cm<sup>-2</sup> is consistent with the result from the 3155.348 cm<sup>-1</sup> line. A weighted average value of  $2.0 \pm 0.2 \times 10^{21}$  molecules cm<sup>-2</sup> has been adopted as the best estimate for the H<sub>2</sub><sup>16</sup>O column. The selected H<sub>2</sub><sup>18</sup>O line at 3205.412 cm<sup>-1</sup>, a 2v<sub>2</sub> band transition with a lower state energy of 172.882 cm<sup>-1</sup>, is isolated and yields a total column of  $4.4 \pm 0.7 \times 10^{18}$  molecules cm<sup>-2</sup>. The fit to this line in the 80.34° solar zenith angle spectrum of February 6, 1987, is shown in Figure 2. There are numerous intervals between 2620 and 2680 cm<sup>-1</sup> that contain isolated HDO lines with temperature-insensitive intensities. The three regions analyzed yield an estimate of  $2.7 \pm 0.1 \times 10^{17}$  molecules cm<sup>-2</sup> for the HDO total column. Figure 3 shows an example of one of the HDO fits.

Standard mean ocean water (SMOW) is the generally accepted standard for reporting isotopic compositions of oxygen and hydrogen in natural samples. According to the IUPAC Commission on Atomic Weights and Isotopic Abundances [1983], recommended values for the D/H and the <sup>18</sup>O/<sup>16</sup>O ratios in SMOW are  $(155.76 \pm 0.05) \times 10^{-6}$  [Hagemann et al., 1970] and  $(2000.20 \pm 0.45) \times 10^{-6}$  [Baertschi, 1976], respectively. Normalized to these reference isotopic concentrations, the measured column amounts correspond to a column-averaged D/H ratio of  $0.44 \pm 0.06$  and a column-averaged <sup>18</sup>O/<sup>16</sup>O ratio of  $1.10 \pm 0.21$ . The deuterium depletion is expected primarily because HDO, the main deuterated constituent, is slightly less volatile, and therefore it preferentially remains in the condensed phase. Large and increasing depletions of D with altitude are predicted [Kaye, 1987]. The same effect should also produce small depletions of <sup>18</sup>O in water vapor; such depletions have been measured [see Kaye, 1987]. At 0°C, Kaye [1987] calculates a depletion that is 9 times larger for D than for <sup>18</sup>O. Assuming the minimum D depletion and the maximum <sup>18</sup>O depletion obtainable from the error limits of our measurements, we calculate a lower limit of ~5 for the ratio of the deuterium to the <sup>18</sup>O depletion in the total column.

The large depletion in D obtained from our total column water vapor measurements is similar to the values determined from other remote sounding measurements, e.g., our study of University of Denver South Pole solar spectra [Goldman et al., 1988], long-path surface measurements with a gas filter correlation spectrometer [Cosden et al., 1977], balloon-borne and aircraft infrared solar spectra of the stratosphere [Rinsland et al., 1984b], and far-infrared thermal emission spectra of the stratosphere [Abbas et al., 1987]. Numerous in situ measurements of D/H in tropospheric water vapor have also been reported, all indicating significant depletions in deuterium relative to SMOW, especially in the middle to upper troposphere (see, for example, Rozanski and Sonntag [1982] and the comprehensive review article on isotopic molecular fractionation in planetary atmospheres by Kaye [1987]). The results show a great deal of variability from measurement to measurement, with a trend of decreasing D depletion with altitude in the troposphere, especially in the lower troposphere. The latter result is supported by analysis of the same

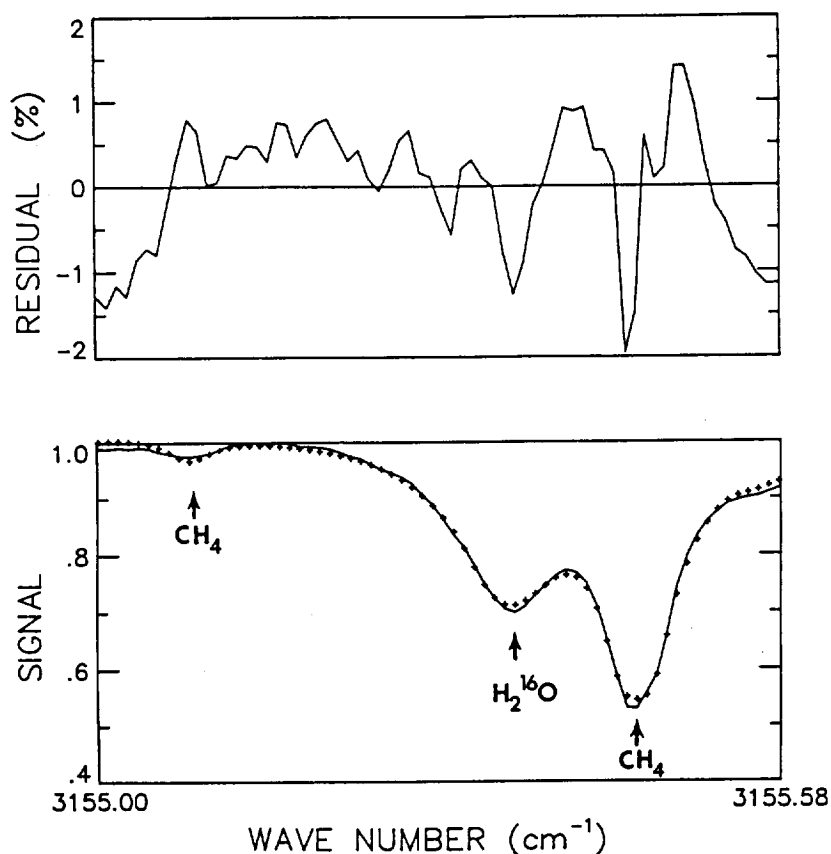


Fig. 1. Comparison between measured (solid curve) and best fit calculated (plus symbols) spectra in the region of  $3155.348\text{ cm}^{-1}$  line of  $\text{H}_2^{16}\text{O}$ . The measured spectrum was recorded at an astronomical zenith angle of  $80.34^\circ$  on February 6, 1987. Residuals (measured minus calculated) are plotted at top on an expanded vertical scale.

$\text{HDO}$  and  $\text{H}_2^{16}\text{O}$  lines in IR solar absorption spectra recorded by G. A. Harvey (NASA Langley Research Center, private communication, 1987) in October 1987 from near sea level at NASA Langley ( $37.1^\circ\text{N}$  latitude,  $76.3^\circ\text{W}$  longitude, elevation 10 m). A column-averaged normalized D/H ratio of 0.75 has been retrieved from these data.

The low abundance of water vapor above Mauna Loa at the time of the observations can be demonstrated by noting that the retrieved  $\text{H}_2\text{O}$  total column is  $\sim 10\%$  lower than a value deduced from similar spectra recorded from South Pole Station on December 3, 1986 [Goldman *et al.*, 1988]. Hence although 0.8 km lower in altitude than nearby Mauna Kea, a well-known site for infrared, submillimeter, and millimeter astronomical observations, Mauna Loa Observatory can also be a very dry observing site. However, wide variations of atmospheric temperature and humidity lead to wide variations in atmospheric  $\text{H}_2\text{O}$  concentrations, so that observations at other times may be more or less favorable in terms of dryness than those reported here.

#### Carbon Dioxide

Four intervals containing temperature-insensitive lines of carbon dioxide have been analyzed. The  $2626$  and  $2632\text{ cm}^{-1}$  intervals each contain a single R branch line of the  $20002\text{--}00001$  band of  $^{16}\text{O}^{12}\text{C}^{18}\text{O}$ . The  $2632\text{ cm}^{-1}$  window was used by Farmer *et al.* [1987] in their analysis of ground-based solar spectra recorded from McMurdo, Antarctica. The  $3201$  and  $3204\text{ cm}^{-1}$  intervals each contain a single line of the  $21103\text{--}$

$00001$  band of  $^{12}\text{C}^{16}\text{O}_2$ . Unpublished  $0.01\text{ cm}^{-1}$  resolution room temperature laboratory spectra of ozone recorded with the McMath Fourier transform spectrometer (M. A. H. Smith, NASA Langley, private communication, 1987) show several lines in the  $3201.30\text{--}3201.65\text{ cm}^{-1}$  analysis interval that are not on the 1986 HITRAN compilation [Rothman *et al.*, 1987]. These  $\text{O}_3$  lines are weak but clearly seen in the Mauna Loa spectra. Their presence has a negligible impact on the  $\text{CO}_2$  retrievals.

The adopted  $\text{CO}_2$  line parameters are reported in Table 3. The positions and intensities for the two  $^{16}\text{O}^{12}\text{C}^{18}\text{O}$  lines are from the study by Malathy Devi *et al.* [1984]; the intensities are  $0.5\text{--}1.0\%$  lower than on the 1986 HITRAN compilation [Rothman *et al.*, 1987]. This small difference results from the effect of a nonzero higher order  $F$ -factor coefficient obtained by Malathy Devi *et al.* [1984] but not included in the HITRAN calculation [Rothman, 1986]. The positions and intensities for the two  $^{12}\text{C}^{16}\text{O}_2$  lines are from the study by Benner *et al.* [1988]. These intensities are about  $5\%$  higher than on the 1986 HITRAN compilation [Rothman *et al.*, 1987]. The air-broadened half widths are from the 1986 HITRAN compilation [Rothman *et al.*, 1987]. A  $T^{-0.75}$  temperature dependence was assumed for the  $\text{CO}_2$  air-broadened half widths. Figure 4 shows an example of a fit to one of the  $^{16}\text{O}^{12}\text{C}^{18}\text{O}$  lines.

An estimate of  $5.0 \pm 0.5 \times 10^{21}$  molecules  $\text{cm}^{-2}$  has been obtained for the total vertical  $\text{CO}_2$  column amount near 1800 UT on February 6, 1987. This corresponds to a column-

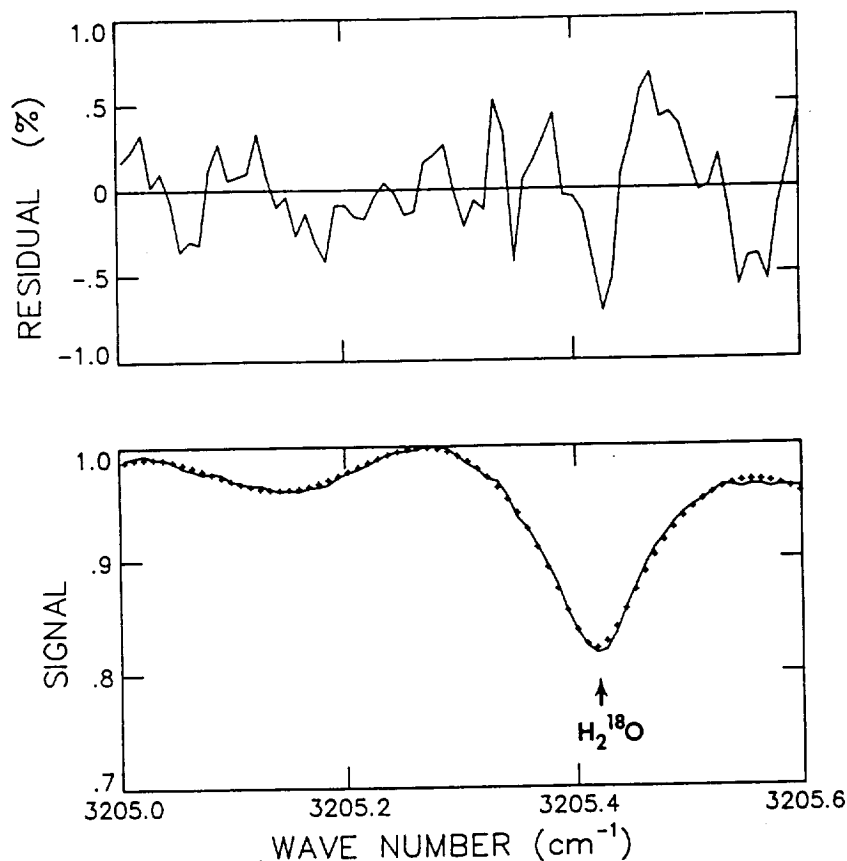


Fig. 2. Comparison between measured (solid curve) and best fit calculated (plus symbols) spectra in the region containing an isolated line of  $\text{H}_2^{18}\text{O}$ . The measured spectrum was recorded at an astronomical zenith angle of  $80.34^\circ$  on February 6, 1987. A channel spectrum with a period of  $0.275\text{ cm}^{-1}$  has been included in modeling the data. Residuals (measured minus calculated) are plotted at top on an expanded vertical scale.

averaged volume mixing ratio (VMR) of  $349 \pm 35$  parts per million by volume (ppmv), in excellent agreement with an unpublished GMCC measurement of 346.7 ppmv at Mauna Loa during the same morning (P. Tans, private communication, 1988). This GMCC value is from a preliminary reduction of the data and is estimated to be accurate to a few tenths of a part per million by volume. The inclusion of a decrease of 7 ppmv from the tropopause to the midstratosphere in the assumed reference  $\text{CO}_2$  vertical distribution, as has been reported by Bischof *et al.* [1985], would raise the retrieved infrared mean tropospheric  $\text{CO}_2$  VMR by only 0.2%.

#### Ozone

Each of the three windows selected for analysis contains an isolated line of the  $\nu_1$  band of  $^{16}\text{O}_3$  with a temperature-insensitive intensity. The adopted line positions and intensities for each are from the study of Flaud *et al.* [1987]. The 1986 HITRAN compilation intensities for these lines are 0.917–0.926 times the Flaud *et al.* [1987] intensities. The air-broadened  $\text{O}_3$  half widths from the 1986 HITRAN compilation [Rothman *et al.*, 1987], which result from the calculations of Gamache and Rothman [1985], have been multiplied by 1.07 to agree with the recent laboratory measurements of Smith *et al.* [1988]. The adopted line parameters are given in Table 4. A  $T^{-0.76}$  temperature dependence has been assumed for the  $\text{O}_3$  air-broadened half widths [Gamache, 1985].

Figure 5 gives an example of one of the ozone fits. As noted in section 1, the line shape is slightly asymmetric. This asym-

metry has been modeled in the calculation of the best fit spectra.

From the fittings, the total vertical column amount of ozone above Mauna Loa on the morning of February 10, 1987, is estimated to be  $6.67 \pm 0.80 \times 10^{18}$  molecules  $\text{cm}^{-2}$  or  $248 \pm 30$  Dobson units (DU). The agreement between the various retrievals is 4%; this value has been adopted as the estimate of the precision. The rather large error estimate is dominated by the estimated 10% uncertainty in the absolute intensity scale for the  $\text{O}_3$  lines [Flaud *et al.*, 1987]. There is an urgent need for laboratory studies to improve the absolute accuracy of infrared ozone line intensities.

Umkehr spectrophotometric measurements of total column ozone were obtained at Mauna Loa on the same morning as our IR spectral measurements. The measured value of 235 DU (R. D. Evans, personal communication, 1988) is slightly lower than our value of  $248 \pm 30$  DU, but in agreement within our measurement uncertainty. If the 1986 HITRAN  $\text{O}_3$  parameters [Rothman *et al.*, 1987] are assumed in our retrievals, a total  $\text{O}_3$  column of 275 DU, 1.18 times the correlative Umkehr measurements, is obtained. This significantly poorer agreement suggests that there is need to update the HITRAN parameters using the results of Flaud *et al.* [1987] and Smith *et al.* [1988].

#### Nitrous Oxide

Two spectral intervals in the 3- to 4- $\mu\text{m}$  region have been analyzed to retrieve the  $\text{N}_2\text{O}$  total column amount. The lower

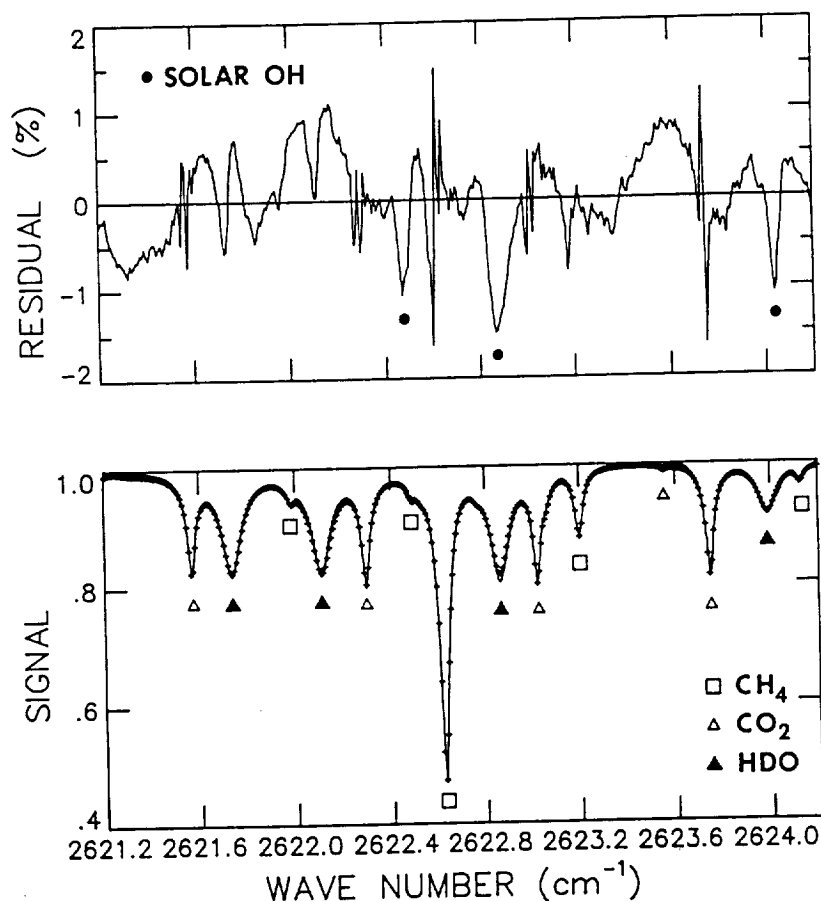


Fig. 3. Comparison between measured (solid curve) and best fit calculated (plus symbols) spectra in a region containing several lines of HDO. The measured spectrum was recorded at an astronomical zenith angle of 80.34° on February 6, 1987. Residuals (measured minus calculated) are plotted at top on an expanded vertical scale.

interval, 2583.10–2583.75  $\text{cm}^{-1}$ , is dominated by the R26 line of the  $^{14}\text{N}_2^{16}\text{O}$  20 $^0$ 0–00 $^0$ 0 band at 2583.385  $\text{cm}^{-1}$ , with a lower state energy of 294.059  $\text{cm}^{-1}$ . For a 2°K error in temperature, the intensity per molecule of this line changes by less than 1% between 200 and 300 K. The 2806.15–2806.65  $\text{cm}^{-1}$  interval contains the R9 line of the  $^{14}\text{N}_2^{16}\text{O}$  01 $^1$ 1–00 $^0$ 0 band. Figure 6 shows an example of the fitting results for this region. A relative profile with a constant  $\text{N}_2\text{O}$  VMR in the troposphere and a decreasing VMR in the stratosphere, based on in situ measurements and satellite measurements of the Nimbus 7 Stratospheric and Mesospheric Sounder (SAMS) instrument has been assumed. The stratospheric values were obtained from the equatorial data presented in Figure 9 of Jones and Pyle [1984]; a smooth curve was drawn through the in situ data from 15 to 35 km and extended to higher altitude with

the SAMS annual mean profile. Approximately 91% of the  $\text{N}_2\text{O}$  total vertical column is located below the tropopause.

The total columns obtained from the fittings agree to better than 5% and yield a total vertical column amount of  $4.3 \pm 0.4 \times 10^{18}$  molecules  $\text{cm}^{-2}$ , which corresponds to a column-averaged VMR of  $299 \pm 25$  parts per billion by volume (ppbv). An estimate of  $308 \pm 30$  ppbv for the mean VMR in the troposphere is obtained from the retrieved total column amount and the assumed vertical distribution, in excellent agreement with a value of  $306.2 \pm 2.0$  ppbv, obtained from a preliminary reduction of the Mauna Loa NOAA GMCC flask sample measurements of January 26, 1987, the date closest to the recording of our infrared spectra (J. W. Elkins, unpublished measurements, 1988).

Recently, Conner *et al.* [1987] have reported three  $\text{N}_2\text{O}$

TABLE 3.  $\text{CO}_2$  Line Parameters Adopted in the Analysis

Position	Intensity	Half Width	Lower State Energy	Transition
2626.62961	$4.319 \times 10^{-25}$	0.0769	100.1374	R16 20002–00001 628
2632.36693	$3.514 \times 10^{-25}$	0.0715	220.8681	R24 20002–00001 628
3201.47684	$4.958 \times 10^{-25}$	0.0715	234.0829	R24 21103–00001 626
3204.76075	$5.114 \times 10^{-25}$	0.0695	316.7693	R28 21103–00001 626

Positions are given in  $\text{cm}^{-1}$ , intensities in  $\text{cm}^{-1}/\text{molecule cm}^{-2}$  at 296 K, half widths in  $\text{cm}^{-1} \text{atm}^{-1}$  at 296 K, and lower state energies in  $\text{cm}^{-1}$ . Transitions are in HITRAN compilation format [Rothman, 1986].

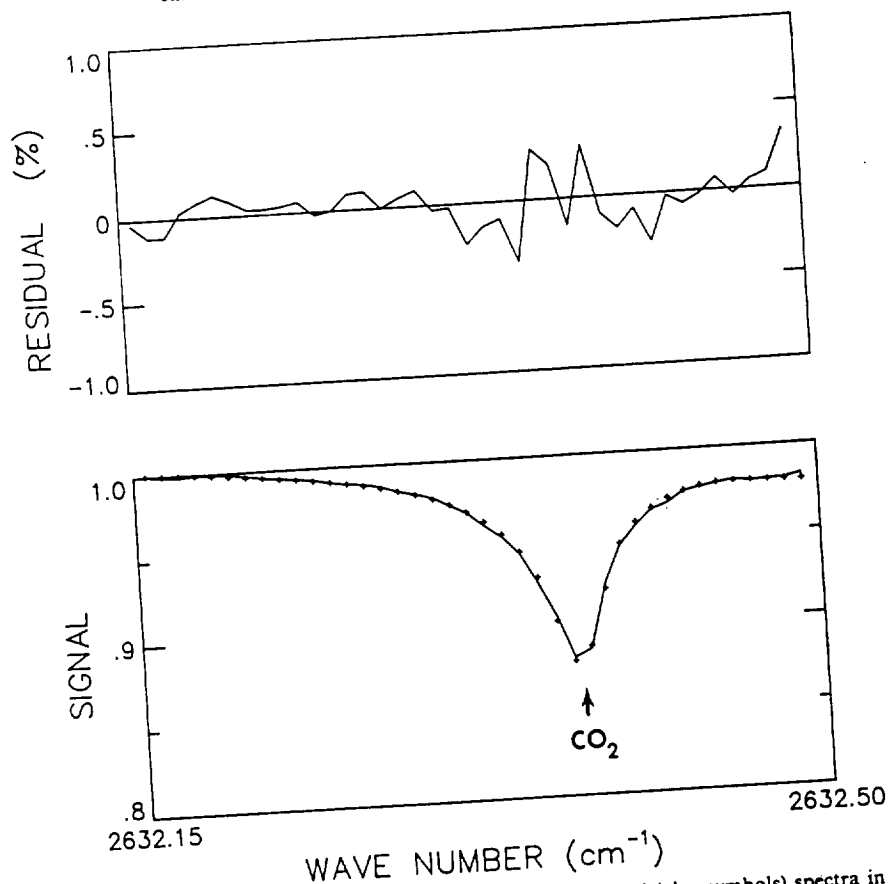


Fig. 4. Comparison between measured (solid curve) and best fit calculated (plus symbols) spectra in the region of an isolated line of carbon dioxide. The measured spectrum was recorded at an astronomical zenith angle of  $77.54^\circ$  on February 6, 1987. Residuals (measured minus calculated) are plotted on an expanded vertical scale at top. The  $\text{CO}_2$  line is the R24 transition of the 20002-00001 band of the  $^{16}\text{O}^{12}\text{C}^{18}\text{O}$  isotopic species.

stratospheric VMR profiles derived from mm-wave spectrometric observations obtained from Mauna Kea in June 1983 and in May and June 1986. The retrieved profiles agree reasonably well with the SAMS satellite profiles, except above 40 km, where the Mauna Kea VMRs are about a factor of 2 higher than the SAMS VMRs. Because the upper stratosphere contributes only a small amount to the  $\text{N}_2\text{O}$  total column, this difference has a negligible effect on our IR retrievals; the inferred mean tropospheric  $\text{N}_2\text{O}$  VMR is decreased 0.3% by assuming the Conner *et al.* [1987] stratospheric distribution instead of the SAMS stratospheric distribution.

#### Methane

Three intervals in the 3- to 4- $\mu\text{m}$  region were selected for retrieval of the  $\text{CH}_4$  total column amount. The primary interval, 2908.70–2911.02  $\text{cm}^{-1}$ , contains three strong lines of the

$\nu_2 + \nu_4$  band of  $^{12}\text{CH}_4$ , with intensities that are nearly independent of temperature (lower state energies of 219.9  $\text{cm}^{-1}$ ). An example of a fit is shown in Figure 7. This interval was utilized in a previous study of University of Denver spectra recorded from South Pole Station [Goldman *et al.*, 1988]. As for  $\text{N}_2\text{O}$ , a vertical profile shape with a constant VMR in the troposphere and a vertical decrease in VMR in the stratosphere based on in situ and SAMS instrument data has been assumed. The stratospheric values were obtained by drawing a smooth curve through the tropical ( $10^\circ\text{S}$  to  $10^\circ\text{N}$  latitude) data presented in Figure 5 of Jones and Pyle [1984]. Approximately 90% of the  $\text{CH}_4$  total vertical column is located below the tropopause.

The retrievals yield an estimate of  $2.3 \pm 0.2 \times 10^{19}$  molecules  $\text{cm}^{-2}$  for the total  $\text{CH}_4$  vertical column. This amount corresponds to a column-averaged mixing ratio of  $1.60 \pm 0.14$

TABLE 4.  $\text{O}_3 \nu_1$  Band Line Parameters Adopted in the Analysis

Position	Intensity	Half Width	Lower State Energy	Rotational Assignment					
				$J'$	$K_a'$	$K_c'$	$J''$	$K_a''$	$K_c''$
1146.4715	$3.95 \times 10^{-22}$	0.0723	372.4103	29	4	26	28	3	25
1155.5132	$2.84 \times 10^{-22}$	0.0699	189.0092	14	7	7	13	6	8
1163.4222	$2.57 \times 10^{-22}$	0.0700	253.8827	16	8	8	15	7	9

Positions are given in  $\text{cm}^{-1}$ , intensities in  $\text{cm}^{-1}/\text{molecule cm}^{-2}$  at 296 K, half widths in  $\text{cm}^{-1} \text{atm}^{-1}$  at 296 K, and lower state energies in  $\text{cm}^{-1}$

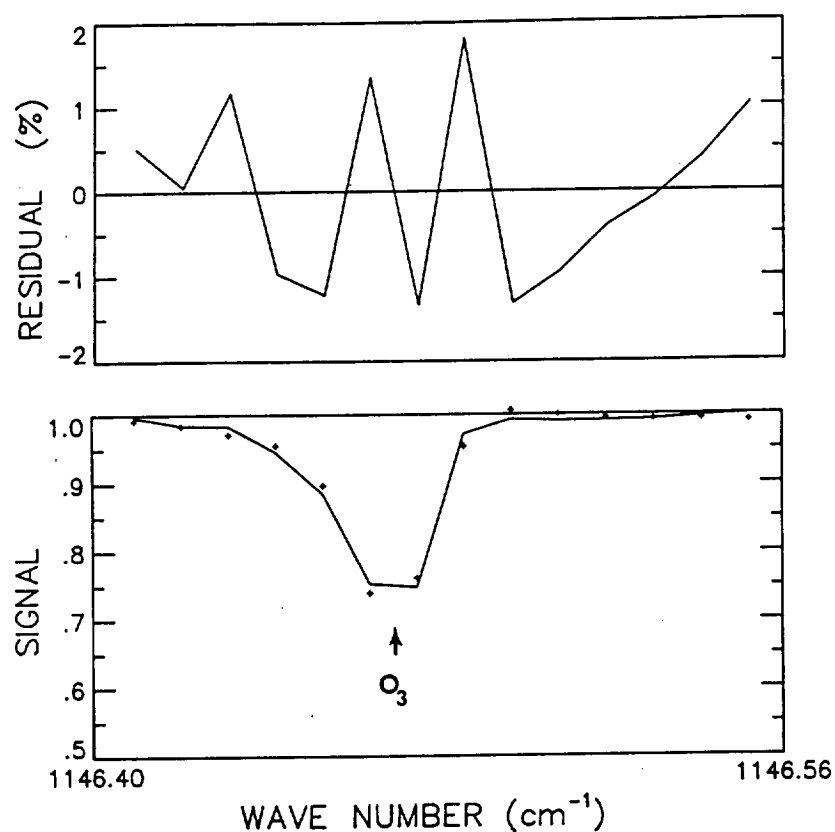


Fig. 5. Comparison between measured (solid curve) and best fit calculated (plus symbols) spectra in the region of an isolated line of ozone. The measured spectrum was recorded at an astronomical zenith angle of 80.07° on February 10, 1987. Residuals (measured minus calculated) are plotted at top on an expanded vertical scale.

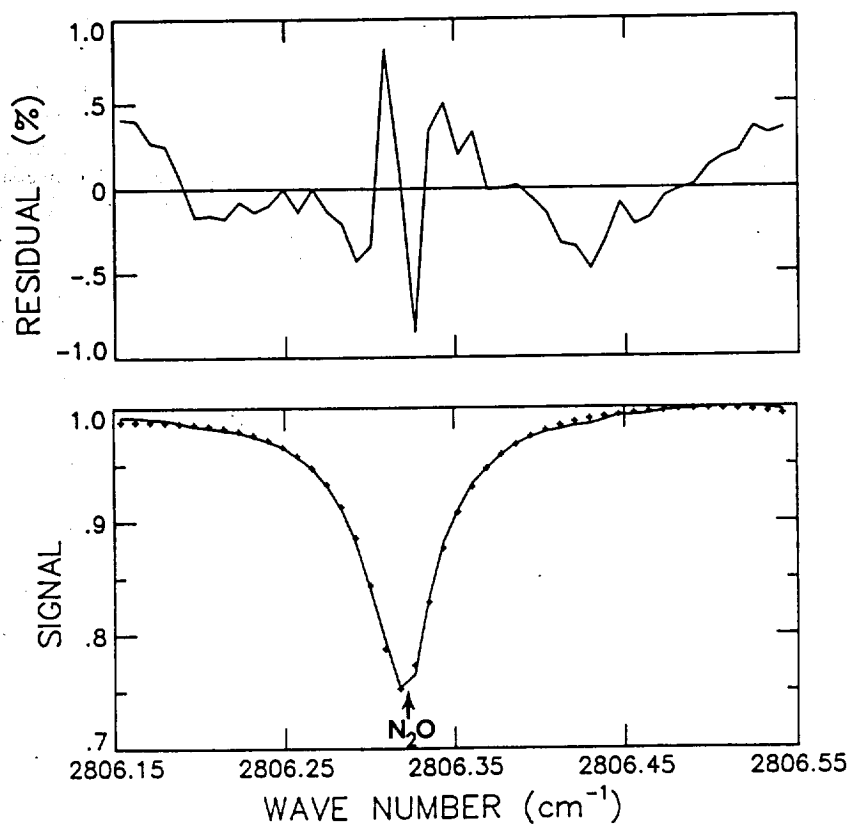


Fig. 6. Comparison between measured (solid curve) and best fit calculated (plus symbols) spectra in the region of the R9 line of the <sup>14</sup>N<sub>2</sub><sup>16</sup>O 01<sup>1</sup>-00<sup>0</sup> band. The measured spectrum was recorded at an astronomical zenith angle of 80.34° on February 6, 1987. Residuals (measured minus calculated) are plotted at top on an expanded vertical scale.

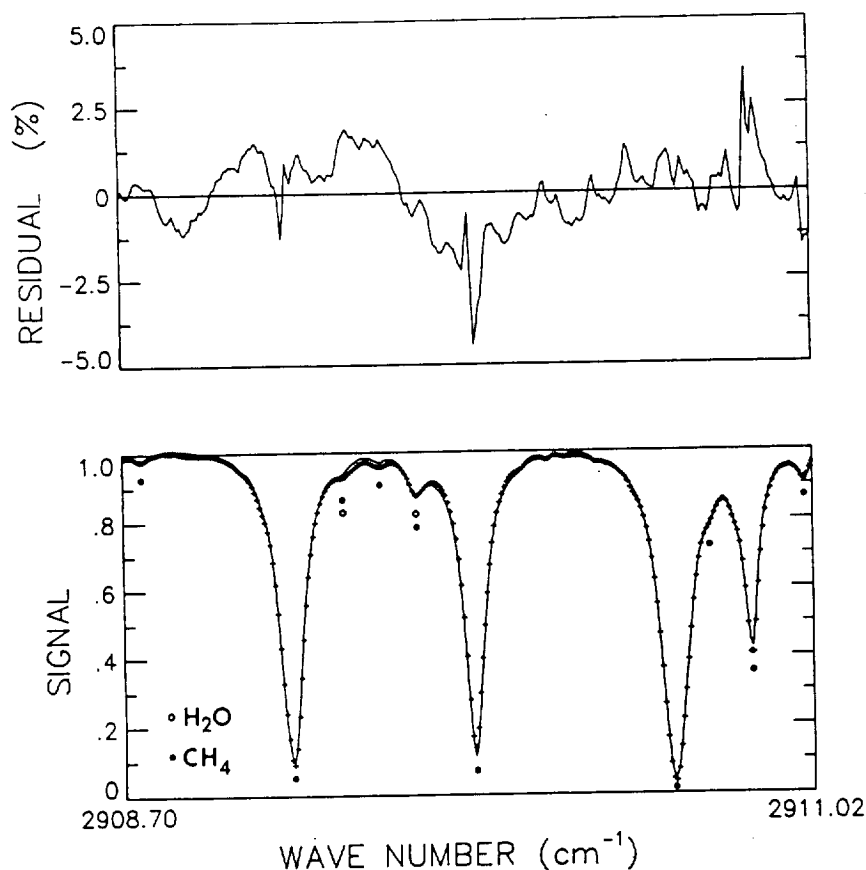


Fig. 7. Comparison between measured (solid curve) and best fit calculated (plus symbols) spectra in a region dominated by methane absorption. The measured spectrum was recorded at an astronomical zenith angle of  $80.34^\circ$  on February 6, 1987. Residuals (measured minus calculated) are plotted in the upper panel on an expanded vertical scale.

ppmv. An estimated mean tropospheric VMR of  $1.64 \pm 0.16$  ppm is obtained from the measured total column and the assumed vertical distribution. This value can be compared with data from flask samples collected at Mauna Loa within minutes of our infrared observations. The measured hourly averaged  $\text{CH}_4$  concentration of 1.665 ppmv between 1700 and 1800 UT on February 6, 1987 (L. P. Steele, unpublished data, 1988) agrees within 2% with our nearly simultaneous infrared data. (See Steele *et al.* [1987] for a discussion of the calibration of the Mauna Loa  $\text{CH}_4$  NOAA GMCC data.)

Comparisons of infrared mean tropospheric VMR and the NOAA GMCC surface measurements are potentially useful for detecting deviations from a uniform  $\text{CH}_4$  volume mixing ratio in the troposphere. A constant VMR profile is indicated by measurements obtained at northern hemisphere mid-latitudes by collection of flask samples from aircraft [Ehhalt and Heidt, 1973; Reichle and Condon, 1979]. Also, the data of Rasmussen and Khalil [1982] show no conclusive evidence for differences in  $\text{CH}_4$  volume mixing ratios measured above and below the tropical boundary layer. However, a comparison by Steele *et al.* [1987] of the very precise NOAA GMCC data sets from Cape Kumukahi and Mauna Loa, Hawaii, which are in close geographic proximity but separated by 3.34 km in altitude, indicates that on average the Mauna Loa  $\text{CH}_4$  concentrations are lower than the Cape Kumukahi values by 22 ppbv ( $\sim 1.5\%$ ). No conclusive evidence for differences in the seasonal cycles at these two sites was found. Vertical profile gradients that vary with season have been measured in the mid-latitudes of the southern hemisphere; these data also

show a significant reduction of the surface level  $\text{CH}_4$  seasonal cycle in the middle troposphere and the absence of a seasonal cycle in the upper troposphere [Fraser *et al.*, 1984, 1986]. Additional infrared spectral measurements from Mauna Loa at various times of the year would allow an opportunity to compare the seasonal variation in these results with those determined from the NOAA GMCC site data.

#### Nitric Acid

The  $\text{HNO}_3$  vertical distribution assumed in the analysis was obtained by combining measurements and model predictions. In the stratosphere we have adopted the  $20^\circ\text{N}$  latitude February 1979 monthly mean volume mixing ratios measured by the Limb Infrared Monitor of the Stratosphere (LIMS) experiment aboard the Nimbus 7 satellite [Gille *et al.*, 1984]. Below 12 km altitude we have adopted the calculated  $\text{HNO}_3$  volume mixing ratios from profile A of Logan *et al.* [1981, Figure 12a], scaled by 0.225 to agree with the average daytime concentration of 18 parts per trillion by volume (pptv) measured at the Mauna Loa NOAA GMCC station by Galasyn *et al.* [1987] during February 1985. Volume mixing ratios between 12 km altitude and the tropopause were obtained by smoothly extending the upper and lower altitude distributions, using the reference  $\text{HNO}_3$  profile of Smith [1982] as a guide. Our reference  $\text{HNO}_3$  distribution corresponds to a total vertical column amount of  $5.9 \times 10^{15}$  molecules  $\text{cm}^{-2}$ . About 86% of the  $\text{HNO}_3$  molecules are located in the stratosphere. About 96% of the  $\text{HNO}_3$  molecules are above 12 km altitude, the



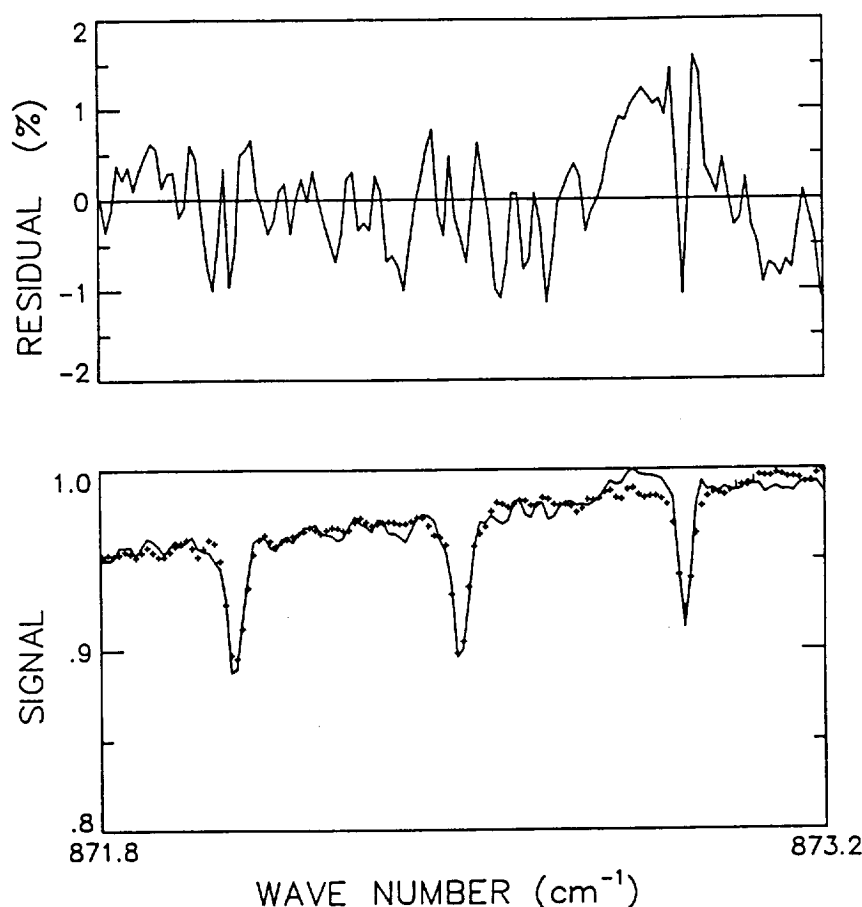


Fig. 8. Comparison between measured (solid curve) and best fit calculated (plus symbols) spectra in a region containing three  $P$ -branch manifolds of the  $\nu_3$  band of nitric acid ( $\text{HNO}_3$ ). The measured spectrum was recorded at an astronomical zenith angle of  $84.31^\circ$  on February 10, 1987. Residuals (measured minus calculated) are plotted at top on an expanded vertical scale.

approximate base altitude of previously reported aircraft total column amount surveys.

Two spectral intervals containing a number of strong  $P$ -branch manifolds of the  $\nu_3$  band of  $\text{HNO}_3$  were analyzed, assuming the 1986 HITRAN compilation line parameters [Rothman *et al.*, 1987]. Total column amounts retrieved from four spectra using these two intervals agree to 5%, a value we have adopted as the estimate of the precision. The average retrieved total column amount of  $5.9 \times 10^{15}$  molecules  $\text{cm}^{-2}$  is estimated to have an absolute accuracy of 20%, based on sensitivity studies similar to those reported by Murcray *et al.* [1987]. Figure 8 shows an example of the fitting results.

Results of a number of surveys of the latitudinal variation of the total vertical column amount of  $\text{HNO}_3$  are collected in Figure 2 of Murcray *et al.* [1987]. At the latitude of Mauna Loa, these values range from about  $4$  to  $6 \times 10^{15}$  molecules  $\text{cm}^{-2}$ . Hence our Mauna Loa result is located in the upper part of the range of these measurements.

As noted above, measurements and model predictions suggest that the troposphere contributes only a relatively small amount to our measured total column. However, our infrared data were recorded in winter, when the  $\text{HNO}_3$  surface concentrations at Mauna Loa are lowest [Galasyn *et al.*, 1987]. Highest concentrations were measured during the late summer. Assuming the average daytime surface concentration of 97 pptv measured in August to scale the same vertical

distribution shape [Logan *et al.*, 1981, Figure 12a, profile A], we calculate a total vertical column of  $\text{HNO}_3$  below 12 km altitude of  $1.4 \times 10^{15}$  molecules  $\text{cm}^{-2}$ , about 24% of our measured total column. Hence seasonal changes in the tropospheric column amount need to be considered in interpreting a time series of  $\text{HNO}_3$  total columns measured from the ground, even from a remote site such as Mauna Loa. Although a diurnal cycle (higher concentrations during the upslope wind hours of 0900–2100 LT) in the ground-level concentrations at Mauna Loa was also observed, Galasyn *et al.* [1987] believe these changes are the result of depletion through dry deposition on the mountain's elevated surface and are unlikely to be reflected in the free troposphere. The daytime measurements of Galasyn *et al.* [1987] are consistent with GAMETAG measurements of free tropospheric  $\text{HNO}_3$  [Huebert and Lazrus, 1980] obtained during the same time of the year (see Galasyn *et al.* [1987] for a discussion).

#### Hydrogen Chloride

As in two recent ground-based studies [Goldman *et al.*, 1987a; Farmer *et al.*, 1987], we adopted the  $P_2$  transition of  $\text{H}^{35}\text{Cl}$  at  $2843.625 \text{ cm}^{-1}$  and the  $R_1$  transition of  $\text{H}^{35}\text{Cl}$  at  $2925.897 \text{ cm}^{-1}$  as the principal lines for the atmospheric quantification of hydrogen chloride. The total columns derived from the fittings of these two lines agree to better than 5%. An example of a fit to the  $R_1$  line is shown in Figure 9.

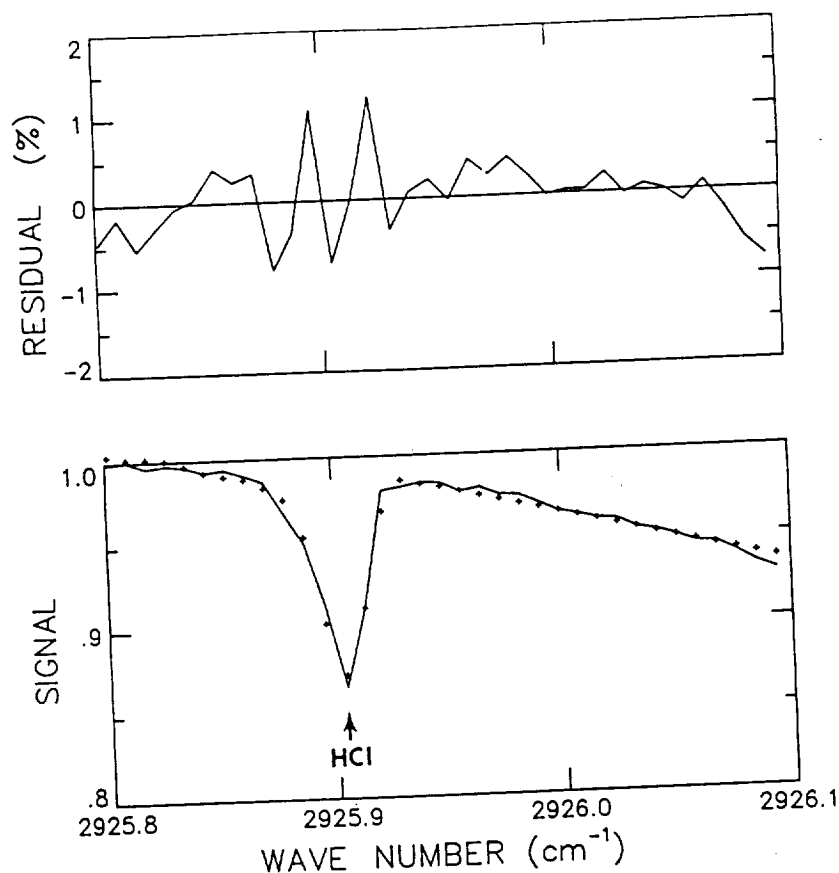


Fig. 9. Comparison between measured (solid curve) and best fit calculated (plus symbols) spectra in the region of the R1 line of the (1-0) band of  $\text{H}^{35}\text{Cl}$ . The measured spectrum was recorded at an astronomical zenith angle of  $77.54^\circ$  on February 6, 1987. Residuals (measured minus calculated) are plotted in the upper panel on an expanded vertical scale.

The HCl lines are narrow, even at the highest zenith angles, indicating that most of the HCl molecules are located in the upper atmosphere. As concluded by Goldman *et al.* [1986], the measurements show little sensitivity to the details of the tropospheric HCl profile; the fitting results and retrieved total column amount change very little for low and medium concentrations of tropospheric HCl in the model.

The retrieved total column amount of  $1.6 \pm 0.2 \times 10^{15}$  molecules  $\text{cm}^{-2}$  is plotted in Figure 10 along with aircraft observations and model predictions of the HCl stratospheric column abundance, as presented in Figures 11-12 of the *World Meteorological Organization (WMO)* [1986] report. Our measured total column is about a factor of 2 higher than three measurements obtained between  $18.3^\circ\text{N}$  and  $24.5^\circ\text{N}$  latitude in 1978 [Mankin and Coffey, 1983]. However, the Mauna Loa column is very close to the measurement of  $1.5 \pm 0.5 \times 10^{15}$  molecules  $\text{cm}^{-2}$  for the total HCl column near  $25^\circ\text{N}$  in 1980 [Girard *et al.*, 1982]. The latter measurement was subsequently revised upward to  $2.0 \pm 0.5 \times 10^{15}$  molecules  $\text{cm}^{-2}$ , because of changes in the assumed spectroscopic parameters [Girard *et al.*, 1983]. The rather large discrepancy between these two sets of aircraft total column amount measurements needs to be resolved before the present data can be used to derive any information about the long-term trend in the HCl total column. Additional measurements are needed to assess the seasonal and short-term variability of the total column and to determine the contribution of tropospheric HCl to the total column.

#### Ethane

As in three recent studies [Rinsland *et al.*, 1987; Dang-Nhu and Goldman, 1987; Goldman *et al.*, 1988], we have utilized the unresolved  $\nu_7$  band  $^P\text{Q}_3$  subbranch at  $2976.8 \text{ cm}^{-1}$  for quantification of atmospheric  $\text{C}_2\text{H}_6$ . Line parameters for  $\text{H}_2\text{O}$  and  $\text{CH}_4$  were adopted from the 1986 HITRAN compilation [Rothman *et al.*, 1987]. Line parameters for  $\text{C}_2\text{H}_6$  and  $\text{O}_3$  were taken from the study by Rinsland *et al.* [1987]. The adopted  $\text{C}_2\text{H}_6$  parameters agree closely with the values derived independently by Dang-Nhu and Goldman [1987]. A total  $\text{C}_2\text{H}_6$  column amount of  $1.0 \pm 0.2 \times 10^{16}$  molecules  $\text{cm}^{-2}$  has been retrieved assuming the one-dimensional model vertical distribution of Ko and Sze [1984], as presented in Figure 11-7 of WMO [1986]. Figure 11 shows an example of the fitting results.

The Mauna Loa total column amount corresponds to a mean  $\text{C}_2\text{H}_6$  volume mixing ratio of 0.70 ppbv. This result is similar to corresponding values obtained from ground-based infrared spectral measurements at northern mid-latitudes [Zander *et al.*, 1982; Coffey *et al.*, 1985; Rinsland and Levine, 1986; Dang-Nhu and Goldman, 1987] and is a factor of  $\sim 3$  higher than similar measurements from South Pole Station [Goldman *et al.*, 1988]. Since latitudinal surveys of  $\text{C}_2\text{H}_6$  concentrations in clean air at remote sites near the surface show maxima at northern mid-latitudes with strong concentration gradients in the northern tropics [Singh *et al.*, 1979; Rudolph and Ehhalt, 1981; Singh and Salas, 1982; Rasmussen and

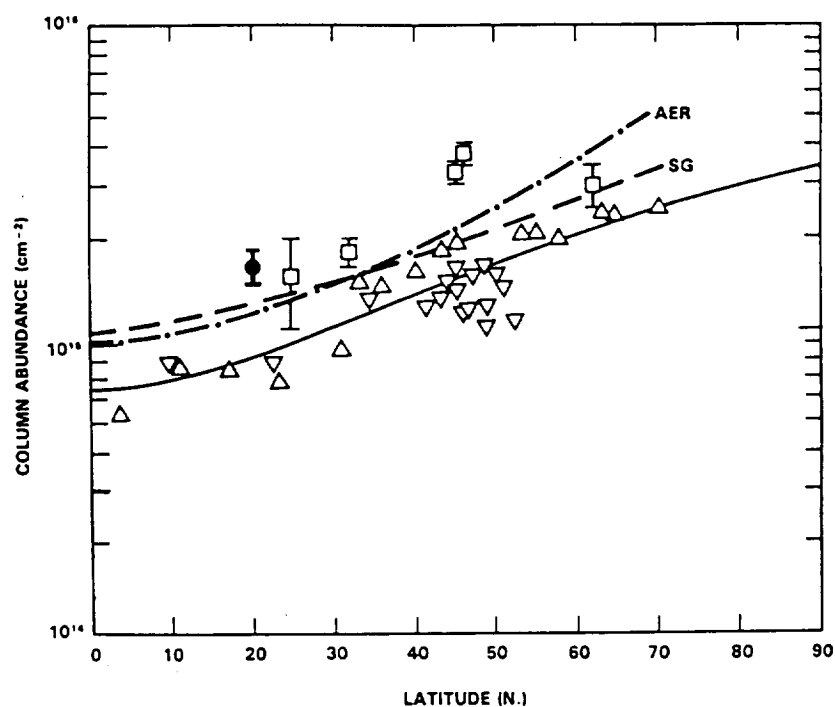


Fig. 10. Variation of the column abundance of HCl with latitude in the northern hemisphere. The solid circle at 19.5°N latitude represents the Mauna Loa measurement from this study. The open triangles are the aircraft measurements of Mankin and Coffey [1983], and the open squares are the aircraft data of Girard *et al.* [1982]. The solid line is the parametric fit derived by Mankin and Coffey [1983] from their data. The dashed lines are model predictions: the line labeled AER from Ko *et al.* [1985] and that labeled SG from Solomon and Garcia [1984].

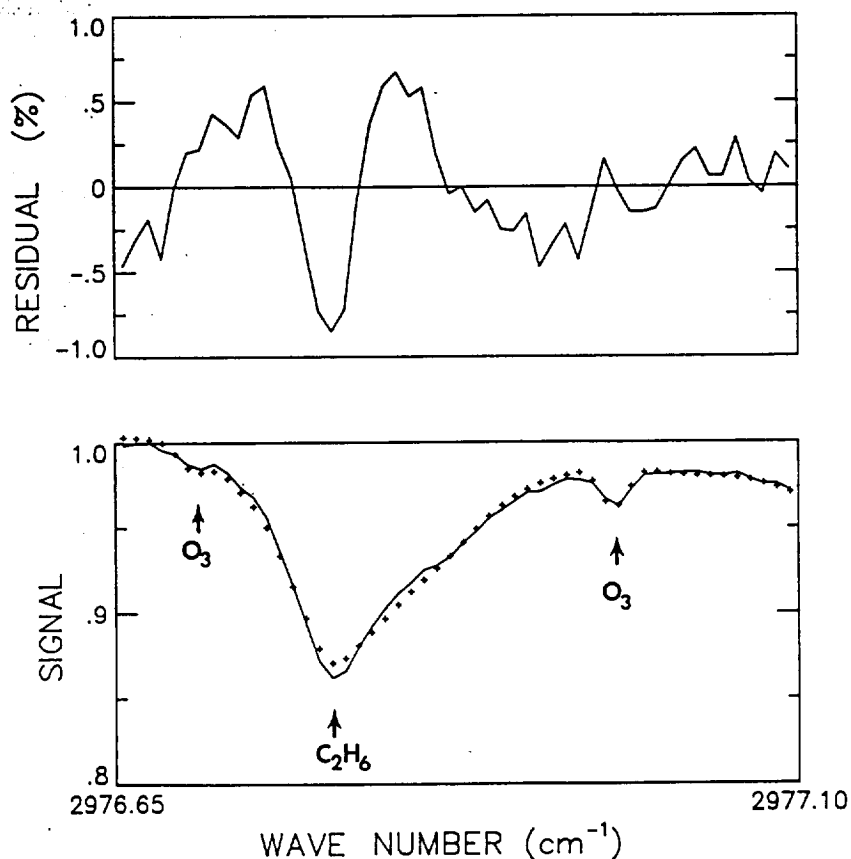


Fig. 11. Comparison between measured (solid curve) and best fit calculated (plus symbols) spectra in the region of the unresolved  $^3Q_3$  subbranch of the  $\nu_1$  band of ethane ( $C_2H_6$ ). The measured spectrum was recorded at an astronomical zenith angle of 80.34° on February 6, 1987. Residuals (measured minus calculated) are plotted at top on an expanded vertical scale.

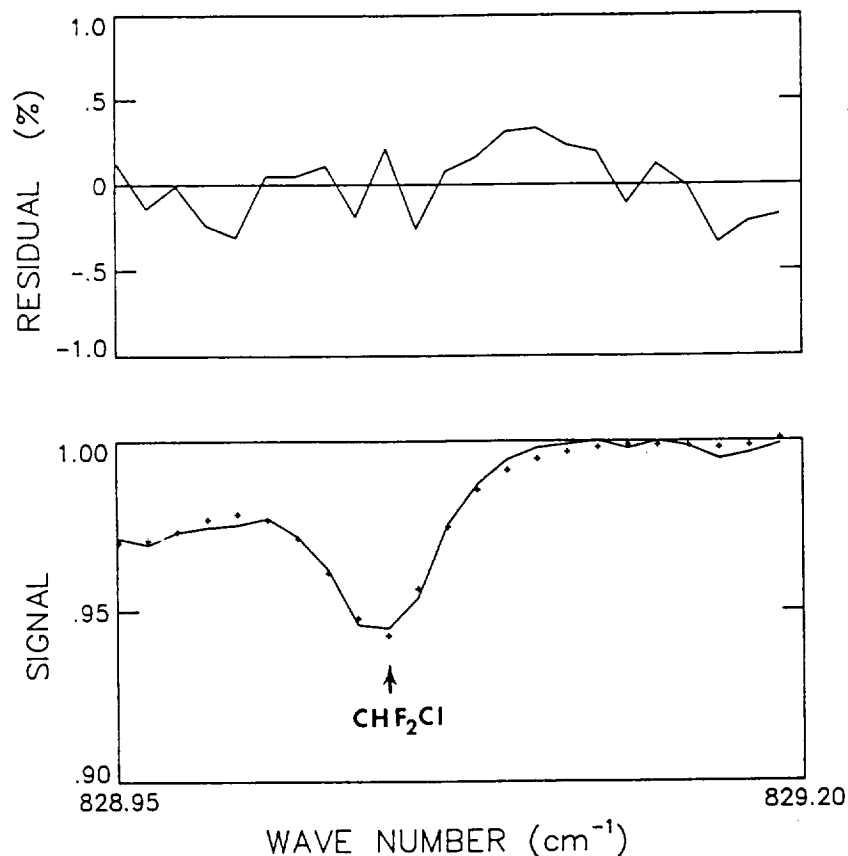


Fig. 12. Comparison between measured (solid curve) and best fit calculated (plus symbols) spectra in the region of the  $2\nu_2$  band Q branch of  $\text{CHClF}_2$ . The measured spectrum was recorded at an astronomical zenith angle of  $84.31^\circ$  on February 10, 1987. Residuals (measured minus calculated) are plotted at top on an expanded vertical scale.

Khalil, 1982; Ehhalt and Rudolph, 1984; Blake and Rowland, 1986], the similarity between the Mauna Loa and the northern mid-latitude mean VMRs is surprising. The rather high Mauna Loa total column may result from the seasonal cycle of  $\text{C}_2\text{H}_6$ ; the present measurements were obtained in winter, when  $\text{C}_2\text{H}_6$  concentrations are reported to be the highest [Tille *et al.*, 1985; Blake and Rowland, 1986]. However, in another study, Singh and Salas [1982] did not find any evidence for a seasonal cycle during 1979–1981 at Point Arena, California ( $39^\circ\text{N}$ ). Additional Mauna Loa spectral measurements during other seasons would be useful to quantify the seasonal cycle of  $\text{C}_2\text{H}_6$ .

#### Difluorochloromethane (CFC-22)

Figure 12 shows an example of a fit to the narrow, intense  $2\nu_2$  Q branch of  $\text{CHClF}_2$  at  $829.05\text{ cm}^{-1}$ . This feature has been used previously for atmospheric quantifications from ground-based [Zander *et al.*, 1983], balloon-borne [Goldman *et al.*, 1981a], and space-shuttle-borne solar spectra [Zander *et al.*, 1987]. The spectroscopic parameters adopted for  $\text{CHClF}_2$  were provided by L. R. Brown (Jet Propulsion Laboratory, private communication, 1987) and are based on fittings to room-temperature and low-temperature laboratory spectra recorded at  $0.005\text{ cm}^{-1}$  resolution with the McMath Fourier transform spectrometer at the National Solar Observatory on Kitt Peak. These parameters are described by Brown *et al.* [1987] and Zander *et al.* [1987]. Parameters for additional gases in the window region (only  $\text{CO}_2$  and  $\text{C}_2\text{H}_6$  are significant contaminants) were taken from the 1986 HITRAN com-

pilation [Rothman *et al.*, 1987]. The  $\text{CHClF}_2$  vertical distribution reported by Zander *et al.* [1987] was assumed in the fittings.

An estimate of  $9.7 \pm 2.5 \times 10^{14}\text{ molecules cm}^{-2}$  has been derived for the total vertical column of  $\text{CHClF}_2$  above Mauna Loa. This corresponds to a column-averaged VMR of  $68 \pm 17$  pptv, close to column-averaged values from Kitt Peak ( $31.9^\circ\text{N}$  latitude) solar spectra of  $67 \pm 16$  pptv on April 26, 1981, and  $90 \pm 18$  pptv on March 6, 1982 [Zander *et al.*, 1983]. Since the  $\text{CHClF}_2$  volume mixing ratio decreases above the tropopause [Fabian *et al.*, 1985; Zander *et al.*, 1987], the tropospheric VMR is slightly higher than the column-averaged VMR; an estimate of  $78 \pm 20$  pptv for the mean tropospheric VMR is obtained from our value and the vertical distribution we have assumed. This result can be compared with previously reported infrared and in situ measurements of the troposphere. A profile covering the 10- to 30-km altitude range at  $30^\circ\text{N}$  was deduced from infrared spectra recorded with the Atmospheric Trace Molecule Spectroscopy (ATMOS) instrument from the space shuttle in May 1985 [Zander *et al.*, 1987]. The Mauna Loa mean tropospheric VMR estimate is slightly higher than the ATMOS value of  $55 \pm 5$  pptv at 10 km. Unfortunately,  $\text{CHClF}_2$  is not currently being measured at Mauna Loa. Published surface sampling measurements indicate that the concentration of  $\text{CHClF}_2$  is increasing by about 12–16% per year [Khalil and Rasmussen, 1981; Fabian *et al.*, 1985; Fabian, 1986]. The inferred Mauna Loa tropospheric VMR is 0.71 times an estimated northern hemisphere surface value of 110 pptv, derived by extending the trend in

TABLE 5. Simultaneous NO and NO<sub>2</sub> Vertical Column Amounts

Astronomical Zenith Angle, deg	Date in 1987	Total Vertical Column Amount, 10 <sup>15</sup> molecules cm <sup>-2</sup>	
		NO	NO <sub>2</sub>
80.60 M	Feb. 8	2.02 (20)	...
80.34 M	Feb. 6	...	1.30 (26)
78.24 M	Feb. 6	...	1.25 (24)
77.54 M	Feb. 6	...	1.40 (28)
69.52 M	Feb. 8	2.29 (23)	1.69 (17)
68.84 M	Feb. 8	2.34 (23)	1.88 (19)
48.30 N	Feb. 8	2.68 (27)	2.10 (21)
34.48 N	Feb. 8	2.80 (28)	2.51 (25)
63.74 A	Feb. 9	3.11 (31)	...
75.74 A	Feb. 9	2.59 (26)	...
78.53 A	Feb. 6	...	2.93 (29)
82.75 A	Feb. 6	...	2.60 (26)
84.86 A	Feb. 6	...	2.59 (26)
86.30 A	Feb. 6	...	2.81 (28)

M, morning scan; N, noon scan; A, afternoon scan. Values in parentheses are the estimated precision of the measurements in units of the last digit.

the 1976–1982 data in Figure 7 of Fabian [1986] to February 1987.

The discrepancy between the IR and the extrapolated surface sampling data may be caused by (1) an error in the calibration of the surface sampling data, (2) a slower increase in the surface level CHClF<sub>2</sub> VMRs from 1982 to 1987 than as-

sumed by us, (3) errors in the CHClF<sub>2</sub> line parameters utilized in the spectroscopic analysis, (4) a decrease in the CHClF<sub>2</sub> VMR with altitude in the troposphere, or (5) a combination of the above-mentioned factors.

#### Nitric Oxide

The daytime diurnal variation of NO has been measured from three spectra recorded during the early morning of February 8, 1987, two spectra recorded near noon on the same day, and two spectra obtained during the late afternoon of February 9, 1987.

As in our recent study of infrared spectra recorded from South Pole Station [Murray *et al.*, 1987], the well-isolated NO lines at 1857.275 cm<sup>-1</sup> (P5.5) and 1914.990 cm<sup>-1</sup> (R11.5) were selected as primary features for the analysis. Spectral fitting retrievals were also run with the less favorable NO lines at 1887.523 cm<sup>-1</sup> (R2.5) and 1896.990 cm<sup>-1</sup> (R5.5). The R2.5 line is overlapped by a weak O<sub>3</sub> line at 1887.580 cm<sup>-1</sup>, and the R5.5 line is overlapped by a weak CO<sub>2</sub> line at 1897.023 cm<sup>-1</sup>. The nitric oxide lines (actually unresolved  $\lambda$  doublets with component separations of 0.011 cm<sup>-1</sup>) are weak features in the Mauna Loa spectra with maximum absorptions of ~5% or less.

Table 5 lists the retrieved NO total vertical column amounts. These values were determined assuming the 1986 HITRAN spectroscopic line parameters [Rothman *et al.*, 1987] and an NO vertical VMR distribution for clean tropospheric conditions [Rinsland *et al.*, 1984a, Table 3]. Figure 13 shows an example of the fitting results. The precision of the NO total

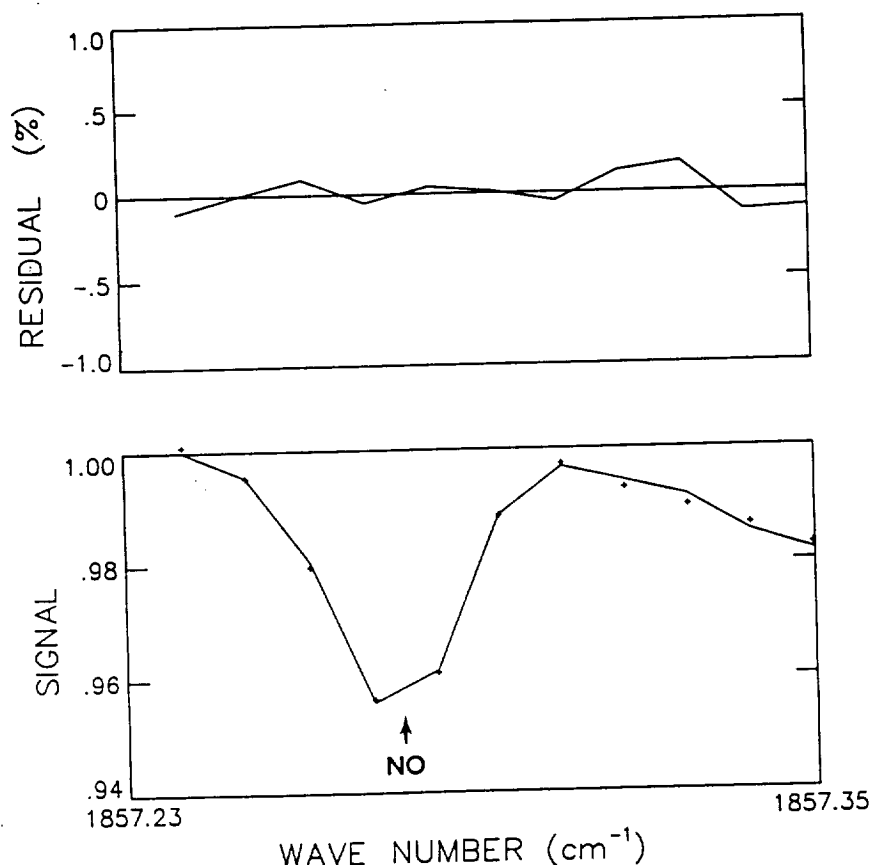


Fig. 13. Comparison between measured (solid curve) and best fit calculated (plus symbols) spectra in the region of the P5.5 line of NO at 1857.275 cm<sup>-1</sup>. The measured spectrum was recorded at an astronomical zenith angle of 80.60° on the morning of February 8, 1987.

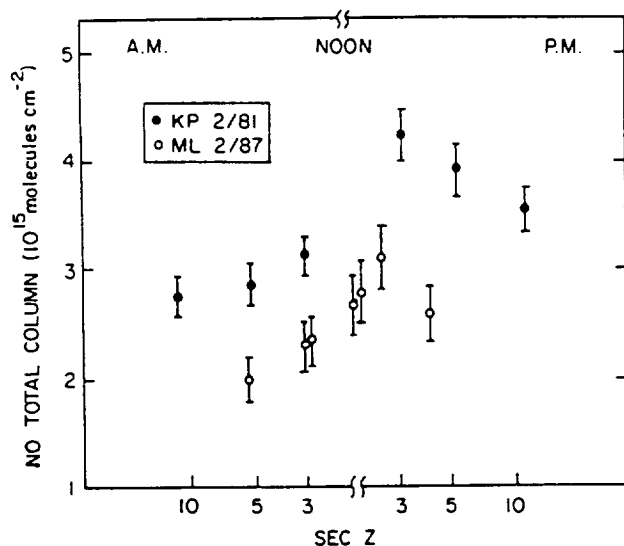


Fig. 14. NO vertical column amounts measured above Kitt Peak (KP) on February 23, 1981, and above Mauna Loa (ML) on February 8-9, 1987, versus sec  $z$ , where  $z$  is the solar astronomical zenith angle. The vertical error bars indicate the estimated precisions. See text for details.

columns in Table 5 is  $\sim 10\%$ , based on the agreement of the individual retrievals from each spectrum and on photochemical model studies of errors resulting from the assumption of an NO vertical profile shape that does not change with time [Rinsland et al., 1984a]. The absolute accuracies of the total columns are lower,  $\sim 20\%$ , since the values also depend on the accuracies of the assumed NO spectral line parameters, the assumed pressure-temperature profile, and the assumed shape of the vertical NO profile distribution; furthermore, as noted previously, they are affected by the inaccuracies in the modeling of the phase distortions in the spectral line profiles.

Uncertainty in the values of the NO line intensities is a major source of potential systematic error. The intensities on the 1986 HITRAN compilation [Rothman et al., 1987] were calculated by Gillis and Goldman [1982] and are normalized to agree with the high-resolution measurements of individual  $P$ - and  $R$ -branch lines by Mandin et al. [1980]. Although this normalization is supported by the integrated absorption measurements of Holland et al. [1983], a number of other studies have obtained intensities that are  $\sim 10$ - $15\%$  lower [see Ballard et al., 1988]. A  $10\%$  uncertainty in the intensities has been assumed in our error budget calculations.

Figure 14 compares the present results with total columns retrieved from a series of  $0.01\text{ cm}^{-1}$  resolution solar absorption spectra recorded from Kitt Peak (latitude  $31.9^\circ\text{N}$ , longitude  $111.6^\circ\text{W}$ ,  $2.095\text{ km}$  altitude) on February 23, 1981. It is reasonable to compare these results, since the two sets of measurements were obtained at nearly the same time of year from sites separated by only  $12.4^\circ$  in latitude and were derived using the same analysis techniques (nonlinear least squares spectral fitting). Also, the NO line parameters assumed for both studies are from the same calculation [Gillis and Goldman, 1982]. The daytime diurnal changes derived from the two sets of measurements are consistent: an increase in the NO total column during the morning, late afternoon values about  $40$ - $50\%$  higher than in the morning, and a decline in the total NO column prior to sunset. The Mauna Loa data include two measurements obtained near noon. These values are  $\sim 12\%$

lower than the afternoon measurement at a zenith angle of  $63.74^\circ$ , suggesting that the peak in the total column occurs sometime in the early afternoon, rather than at noon. However, since this difference is very close to our estimated precision, we believe that additional measurements need to be obtained to confirm this result.

At the same time of day, the Mauna Loa total column is  $\sim 0.7$  times the Kitt Peak total column. This substantial difference conflicts with the aircraft stratospheric total column measurements of Coffey et al. [1981] which, as shown in their Figure 9, indicate no significant latitudinal gradient below  $35^\circ\text{N}$  in winter (however, their higher-latitude data show a clear decrease in the total column above  $40^\circ\text{N}$  in winter). Since the Kitt Peak and Mauna Loa data were obtained on single days in February 1981 and February 1987, it is possible that this discrepancy may be caused by variability and/or long-term trends, rather than a latitudinal gradient in the total column of NO. Additional aircraft and ground-based measurements are needed to resolve this discrepancy. From analysis of aircraft IR measurements obtained in November 1976 near  $20^\circ\text{N}$  latitude, Girard et al. [1979] report a total column of  $5.0 \times 10^{15}\text{ molecules cm}^{-2}$  above  $11\text{ km}$  at sunset, nearly a factor of 2 higher than the total columns measured in the late afternoon from Mauna Loa and the total column of  $3.08 \times 10^{15}\text{ molecules cm}^{-2}$  above  $12\text{ km}$ , measured at sunset on February 12, 1978, near  $22.6^\circ\text{N}$  latitude [Coffey et al., 1981].

#### Nitrogen Dioxide

As noted previously [Murcray et al., 1987], the intense  $\nu_3$  band of  $\text{NO}_2$  near  $6.2\text{ }\mu\text{m}$  is usually unobservable in ground-based solar spectra because of overlapping strong absorption by intense water vapor lines. Under especially dry conditions,  $\text{NO}_2$  absorption features can be detected in several small ( $\sim 2$ - $5\text{ cm}^{-1}$  wide) windows between  $1585$  and  $1610\text{ cm}^{-1}$ . These lines have been observed in solar spectra recorded from South Pole Station [Murcray et al., 1987] and are clearly seen in the low to intermediate air mass Mauna Loa spectra, where signal-to-rms noise ratios of  $200$ - $500$  are achieved in the  $\text{NO}_2$  window regions. Figure 15 shows the best window region in one of the Mauna Loa spectra; identifications of the observable atmospheric and solar features are given. Unfortunately, water vapor absorption is much stronger in the high air mass Mauna Loa spectra and, primarily for this reason, these spectra have too low a signal-to-noise ratio to obtain good quantitative results on  $\text{NO}_2$ .

To study the daytime diurnal variation of the total column of  $\text{NO}_2$ , a total of 11 solar spectra have been utilized. Four of the spectra are the low to moderate air mass spectra showing the  $\text{NO}_2\text{ }\nu_3$  band features; they are the same spectra that were used in the analysis of NO. To obtain  $\text{NO}_2$  total columns near sunrise and sunset, we analyzed three spectra recorded in the early morning and four recorded in the late afternoon of February 6, 1987. They show weak features of the  $\nu_1 + \nu_3$  band of  $\text{NO}_2$  near  $3.4\text{ }\mu\text{m}$ , which is about 20 times weaker than the  $6.2\text{-}\mu\text{m }\nu_3$  band. The  $\nu_1 + \nu_3$  band occurs in a relatively clear transmission region and has been utilized previously for ground-based IR studies of atmospheric  $\text{NO}_2$  [Camy-Peyret et al., 1983; Flaud et al., 1983, 1988; Murcray et al., 1987]. As in these studies, we have derived total columns from the  $\text{NO}_2$  feature at  $2914.65\text{ cm}^{-1}$ , a composite of several closely spaced transitions. This feature is fairly well isolated, but is weak in

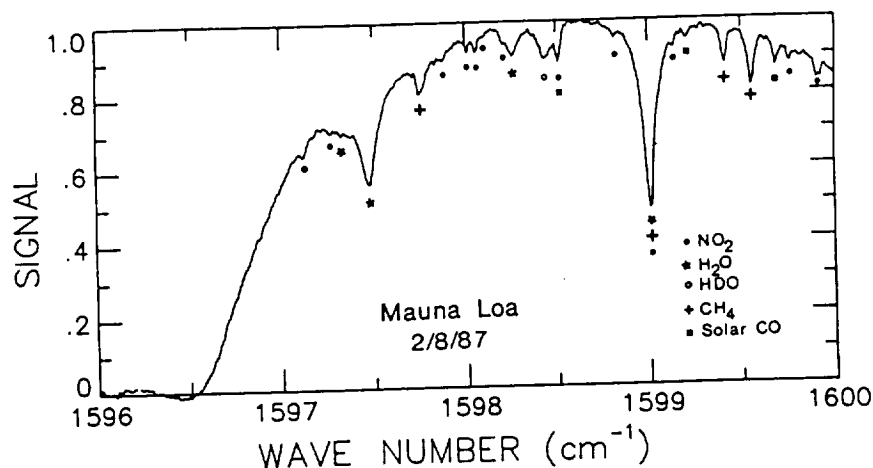


Fig. 15. Portion of a solar spectrum in a region containing absorption features of the  $\nu_3$  band of  $\text{NO}_2$ . The data were recorded on the morning of February 8, 1987, at an astronomical zenith angle of  $69.52^\circ$ . The atmospheric and solar features are identified.

the measured spectra, with maximum absorption depths ranging from 0.5% (early morning spectra) to 1.5% (late afternoon spectra). A fairly wide interval ( $2914.40\text{--}2914.70\text{ cm}^{-1}$ ) was analyzed so as to include the strong  $\text{CH}_4$  line at  $2914.4986\text{ cm}^{-1}$ . The  $\text{CH}_4$  total columns retrieved from this line agree to 5%, thus verifying that the measured  $\text{NO}_2$  diurnal changes are not an artifact of our analysis method.

The  $\text{NO}_2$  vertical mixing ratio distribution adopted in the analysis assumes low volume mixing ratios of  $\text{NO}_2$  in the troposphere, consistent with the narrow line widths of the  $\text{NO}_2$  features in the solar spectra and visible region sunrise and sunset solar absorption measurements from Mauna Loa, which indicate a mean  $\text{NO}_2$  mixing ratio of 30 pptv at  $3.0 \pm 0.5\text{ km}$  altitude [Noxon, 1981]. Our assumed vertical distribution has been obtained by smoothly joining the tropospheric and lower stratospheric mixing ratios from profile "3N" of Noxon [1981, Figure 3] with the stratospheric volume mixing ratios of Camy-Peyret et al. [1983, Table 3] at 21 km altitude. With this distribution, 38% of the total vertical column is located below the tropopause. The mean altitude of  $\text{NO}_2$  molecules in the assumed vertical distribution is 23 km, as compared to a mean altitude of  $\sim 30\text{ km}$  derived from measurements at Mauna Loa in February 1978 [Noxon et al., 1983].

Line positions and intensities for the  $\nu_3$  and the  $\nu_2 + \nu_3 - \nu_2$   $\text{NO}_2$  bands in the  $6.2\text{-}\mu\text{m}$  region, obtained from C. Camy-Peyret and J.-M. Flaud (private communication, 1984), are from the calculation described by Camy-Peyret et al. [1982]. Line positions and intensities for the  $\nu_1 + \nu_3$  and the  $\nu_1 + \nu_2 + \nu_3 - \nu_2$   $\text{NO}_2$  bands in the  $3.4\text{-}\mu\text{m}$  region were taken from the 1986 HITRAN compilation [Rothman et al., 1987]; the calculation of these parameters is described by Perrin et al. [1982]. An air-broadened half width of  $0.063\text{ cm}^{-1}\text{ atm}^{-1}$  at 296 K with a  $T^{-0.968}$  temperature dependence [Malathy Devi et al., 1982a, b] was assumed for all  $\text{NO}_2$  lines. Absorption by other atmospheric gases in the selected regions (see Table 2) was calculated with the parameters from the 1986 HITRAN compilation [Rothman et al., 1987] and the mixing ratios retrieved from the other regions. Solar CO lines of the fundamental vibration-rotation sequence of bands are observable in the  $6\text{-}\mu\text{m}$  Mauna Loa spectra (see Figure 15), but simulations of this absorption generated using the procedure

described by Rinsland et al. [1982b] and studies of high Sun spectra recorded during University of Denver balloon flights [Goldman et al., 1987b, c] indicate negligible interference by solar CO lines in the selected windows.

The retrieved  $\text{NO}_2$  total columns are listed in Table 5. On the basis of considerations similar to those described for the NO analysis, the precisions of the  $\text{NO}_2$  total columns are estimated to be  $\sim 10\%$  for values deduced from the  $6.2\text{-}\mu\text{m}$  features and  $\sim 10\text{--}20\%$  for values deduced from the much weaker  $3.4\text{-}\mu\text{m}$  feature. The line parameters are well determined in both regions, with uncertainties of only  $\sim 5\%$ , so that only a small error is believed to result by combining retrievals from the two spectral regions. A previous study has shown that the  $3.4\text{-}$  and  $6.2\text{-}\mu\text{m}$   $\text{NO}_2$  bands yield consistent quantitative results [Coffey et al., 1986]. The absolute accuracies are only slightly poorer than the estimated precisions:  $\sim 15\%$  for the retrievals from the  $6.2\text{-}\mu\text{m}$  features and  $\sim 15\text{--}25\%$  for the retrievals from the  $3.4\text{-}\mu\text{m}$  feature.

Since previous ground-based studies show no evidence for differences in the  $\text{NO}_2$  diurnal cycle over 3 days of observations [Flaud et al., 1988], all of the Mauna Loa data have been combined to study the  $\text{NO}_2$  diurnal cycle. Figure 16 presents a plot of the Mauna Loa measurements, along with total columns retrieved from  $0.01\text{ cm}^{-1}$  resolution solar absorption spectra recorded from Kitt Peak at nearly the same time of the year, February 23, 1981, [Camy-Peyret et al., 1983] and March 1–2, 1986, [Flaud et al., 1988]. The latter measurements were obtained as part of a study of the diurnal variation of the  $\text{NO}_2$  total column from daytime observations using the Sun as the source and nighttime observations using the Moon as the source. The same set of line parameters have been assumed in the three studies. Within the estimated precisions, all of the measurements overlap. All three data sets are consistent with a continuous increase of the  $\text{NO}_2$  total column with time throughout the day, with a more rapid rise during the morning than in the afternoon. Total columns deduced from solar spectra recorded from Kitt Peak on September 20, 1982, [Flaud et al., 1983] show a diurnal variation similar to the results plotted in Figure 16; however, the absolute amounts in September 1982 were nearly a factor of 2 smaller than on the other dates.

Noxon et al. [1983] obtained an extensive set of daytime

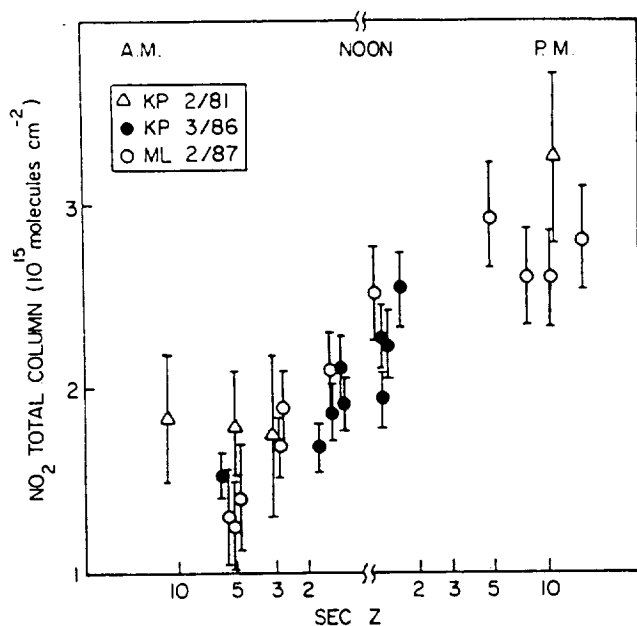


Fig. 16.  $\text{NO}_2$  vertical column amounts measured above Kitt Peak (KP) on February 23, 1981, and March 1–2, 1986, and above Mauna Loa (ML) on February 6, 8–9, 1987, versus sec  $z$ , where  $z$  is the solar astronomical zenith angle. The vertical bars indicate the estimated precisions. See text for details.

$\text{NO}_2$  measurements from the Mauna Loa NOAA GMCC station. The data were acquired during most of 1978 by visible spectral region spectrophotometers, which ran automatically and recorded spectra of the zenith sky for subsequent analysis. In February 1978, evening twilight  $\text{NO}_2$  column abundances averaged  $\sim 3.7 \times 10^{15}$  molecules  $\text{cm}^{-2}$  and morning twilight abundances averaged  $\sim 2.3 \times 10^{15}$  molecules  $\text{cm}^{-2}$ , with short-term fluctuations of  $\sim 0.5 \times 10^{15}$  molecules  $\text{cm}^{-2}$  [Noxon *et al.*, 1983, Figure 1]. It is not possible to make an exact comparison of these results with our measurements, since the data of Noxon *et al.* [1983] refer to times much closer to sunrise and sunset than our data. However, in both the morning and evening, the total columns derived from our highest air mass spectra are significantly lower than the corresponding values of Noxon *et al.* [1983]. Also, our late afternoon total columns are nearly a factor of 2 higher than those near sunrise, whereas the corresponding ratio of the Noxon *et al.* [1983] data is  $\sim 1.6$ . Since both the visible and the infrared methods are frequently used for measuring atmospheric  $\text{NO}_2$ , we believe it would be useful to obtain simultaneous measurements with both techniques in the future to resolve such discrepancies.

#### 4. OTHER GASES

The two most abundant chlorofluorocarbons,  $\text{CF}_2\text{Cl}_2$  and  $\text{CFCI}_3$ , show strong absorption features in the 8- to 12- $\mu\text{m}$  region of the Mauna Loa spectra. However, the lack of accurate spectroscopic parameters precludes quantification of the total columns at this time. Work is in progress on the calculation of parameters for the  $923\text{ cm}^{-1}$   $\text{CF}_2\text{Cl}_2$   $Q$  branches (see Deroche and Goldman [1987] and Rinsland *et al.* [1988b] for discussions).

Very weak absorption is observable at the position of the R19 line of the  $\nu_3$  band of  $\text{C}_2\text{H}_2$  (acetylene) at  $776.0818\text{ cm}^{-1}$ . However, this absorption is too close to the noise level of the

present spectra to obtain a definitive identification of  $\text{C}_2\text{H}_2$ . An upper limit for the total vertical column of  $1.5 \times 10^{15}$  molecules  $\text{cm}^{-2}$  has been estimated by scaling a  $\text{C}_2\text{H}_2$  vertical distribution calculated for medium OH in the troposphere [Goldman *et al.*, 1981b, Figure 2] by a single multiplicative factor, until an absorption feature 3 times the rms noise level is predicted. This upper limit total column is slightly less than total columns of  $2.28 \pm 0.34 \times 10^{15}$  molecules  $\text{cm}^{-2}$  on February 23, 1981, and  $2.00 \pm 0.30 \times 10^{15}$  molecules  $\text{cm}^{-2}$  on October 1, 1982, derived from analysis of Fourier transform infrared (FTIR) spectra recorded at the National Solar Observatory on Kitt Peak [Rinsland *et al.*, 1985]. Observations at higher air masses (the present spectra cover zenith angles of  $84.31^\circ$  or less) should permit the identification and quantitative measurement of  $\text{C}_2\text{H}_2$  from Mauna Loa.

A number of additional atmospheric gases have strong IR absorption bands outside the regions covered by the Mauna Loa observations. Of these, four have been detected using similar IR instrumentation and could be readily monitored from Mauna Loa. These gases and their most favorable IR bands are OCS ( $\nu_3$  band at  $2062\text{ cm}^{-1}$ ), CO (1–0 band at  $2117\text{ cm}^{-1}$ ), HCN ( $\nu_3$  band at  $3311\text{ cm}^{-1}$ ), and HF (1–0 band at  $3961\text{ cm}^{-1}$ ).

#### 5. SUMMARY AND CONCLUSIONS

The measurements and main conclusions of this study may be summarized as follows:

1. A series of high and low air mass infrared solar spectra were collected from Mauna Loa, Hawaii, on 4 days in February 1987. These spectra have been analyzed to deduce total vertical column amounts of 13 atmospheric gases.

2. The mean D/H ratio of the total water vapor column was  $0.44 \pm 0.06$  times the reference value of  $155.76 \times 10^{-6}$  for SMOW, indicating a large depletion in the deuterium content similar to previous measurements of the upper troposphere and lower stratosphere.

3. Within the measurement uncertainties, there is agreement between ozone total columns deduced from the infrared spectra and correlative Umkehr observations.

4. Mean tropospheric volume mixing ratios of  $\text{CO}_2$ ,  $\text{CH}_4$ , and  $\text{N}_2\text{O}$  deduced from our IR observations agree with correlative NOAA GMCC measurements within the measurement uncertainties. This implies that the NOAA GMCC surface volume mixing ratios are good measures of the mean volume mixing ratios of these gases in the troposphere.

5. The measured  $\text{HNO}_3$  total column agrees within the errors with published aircraft and satellite measurements of the total stratospheric column. Published sampling measurements from Mauna Loa show a significant seasonal cycle in the surface level concentrations of  $\text{HNO}_3$ , with minimum values near the time of our IR measurements. On the basis of these data, tropospheric  $\text{HNO}_3$  is estimated to contribute only a small amount to our measured total column. A significant tropospheric contribution is predicted for late summer.

6. Although the measured HCl total column is about a factor of 2 higher than aircraft total column measurements obtained near the same latitude 9 years earlier by Mankin and Coffey [1983], discrepancies between these aircraft values and the higher aircraft values reported by Girard *et al.* [1982, 1983] and the absence of measurements to assess the concentrations of HCl in the troposphere above Mauna Loa



make it impossible at present to derive information about long-term trends in the HCl total column from our data.

7. The mean tropospheric volume mixing ratio of CHClF<sub>2</sub> deduced from the infrared spectra is about 30% lower than a value obtained from an extrapolation of in situ surface data to the date of our infrared observations.

8. Simultaneous measurements of the daytime diurnal variations of the total columns of NO and NO<sub>2</sub> have been obtained. To our knowledge, these are the first such observations that have been reported.

The column amounts reported here were obtained from spectra recorded with a resolution of 0.02 cm<sup>-1</sup>. Absolute accuracies of about 10% have been achieved. The good agreement between the IR and the GMCC data is encouraging. It is important to recall that several of the sources of error are systematic (for example, the uncertainties in the assumed line intensities) and that these effects are eliminated or reduced significantly when results are normalized to study a time series of measurements. Hence additional sets of IR measurements obtained from Mauna Loa and analyzed in the same way should yield precise information on seasonal and long-term trends for a number of important atmospheric species.

Observations with a new interferometer operating at a resolution of 0.002 cm<sup>-1</sup> are planned from Mauna Loa and should yield improved results. The increased resolution should permit details of the altitude distributions to be derived from analysis of the observed pressure-broadening effects as a function of solar zenith angle. Such effects are apparent in HNO<sub>3</sub> features recorded in initial solar observations from the University of Denver. Improved information on the vertical profile is necessary, for example, in interpreting secular trends in HCl, since significant variability of the tropospheric profile may mask increases observed in the stratospheric total column [WMO, 1986].

**Acknowledgments.** Research at the University of Denver was supported by NASA. Acknowledgment is made to the National Center for Atmospheric Research, which is supported by the National Science Foundation, for computer time used in this research. We are grateful to Linda R. Brown of the Jet Propulsion Laboratory for allowing use of the ATMOS parameters for CHClF<sub>2</sub>. We also thank Carolyn Sutton of STX Corporation for processing the data at NASA Langley, Susan Edwards of NASA Langley for assistance in preparing this manuscript, and an anonymous referee for a number of helpful, detailed comments.

#### REFERENCES

- Abbas, M. M., J. Guo, B. Carli, F. Mencaraglia, A. Bonetti, M. Carlotti, and I. G. Nolt, Stratospheric O<sub>3</sub>, H<sub>2</sub>O, and HDO distributions from balloon-based far-infrared observations, *J. Geophys. Res.*, **92**, 8354-8364, 1987.
- Baertschi, P., Absolute <sup>18</sup>O content of standard mean ocean water, *Earth Planet. Sci. Lett.*, **31**, 341-344, 1976.
- Ballard, J., W. B. Johnston, B. J. Kerridge, and J. J. Remedios, Experimental spectral line parameters in the 1-0 band of nitric oxide, *J. Mol. Spectrosc.*, **127**, 70-82, 1988.
- Benner, D. C., V. Malathy Devi, C. P. Rinsland, and P. S. Ferry-Leeper, Absolute intensities of CO<sub>2</sub> lines in the 3140-3410 cm<sup>-1</sup> spectral region, *Appl. Opt.*, **27**, 1588-1597, 1988.
- Bischof, W., R. Borchers, P. Fabian, and B. C. Krüger, Increased concentration and vertical distribution of carbon dioxide in the stratosphere, *Nature*, **316**, 708-710, 1985.
- Blake, D. R., and F. S. Rowland, Global atmospheric concentrations and source strength of ethane, *Nature*, **321**, 231-233, 1986.
- Brown, L. R., C. B. Farmer, C. P. Rinsland, and R. A. Toth, Molecular line parameters for the atmospheric trace molecule spectroscopy experiment, *Appl. Opt.*, **26**, 5154-5182, 1987.
- Camy-Peyret, C., J.-M. Flaud, A. Perrin, and K. Narahari Rao, Improved line parameters for the ν<sub>3</sub> and ν<sub>2</sub> + ν<sub>3</sub> - ν<sub>2</sub> bands of <sup>14</sup>N<sup>16</sup>O<sub>2</sub>, *J. Mol. Spectrosc.*, **95**, 72-79, 1982.
- Camy-Peyret, C., J.-M. Flaud, J. Laurent, and G. M. Stokes, First infrared measurement of atmospheric NO<sub>2</sub> from the ground, *Geophys. Res. Lett.*, **10**, 35-38, 1983.
- Coffey, M. T., W. G. Mankin, and A. Goldman, Simultaneous spectroscopic determination of the latitudinal, seasonal and diurnal variability of stratospheric N<sub>2</sub>O, NO, NO<sub>2</sub>, and HNO<sub>3</sub>, *J. Geophys. Res.*, **86**, 7331-7341, 1981.
- Coffey, M. T., W. G. Mankin, A. Goldman, C. P. Rinsland, G. A. Harvey, V. Malathy Devi, and G. M. Stokes, Infrared measurements of atmospheric ethane (C<sub>2</sub>H<sub>6</sub>) from aircraft and ground-based solar absorption spectra in the 3000 cm<sup>-1</sup> region, *Geophys. Res. Lett.*, **12**, 199-202, 1985.
- Coffey, M. T., W. G. Mankin, and A. Goldman, Stratospheric NO<sub>2</sub> retrieved from solar absorption spectra in the ν<sub>3</sub> and ν<sub>1</sub> + ν<sub>3</sub> infrared bands, *Appl. Opt.*, **25**, 2460-2462, 1986.
- Conner, B. J., R. L. de Zafra, P. M. Solomon, A. Parrish, J. W. Barrett, and M. Jaramillo, Nitrous oxide in the tropical middle atmosphere, observed by ground-based mm-wave spectrometry, *Geophys. Res. Lett.*, **14**, 1254-1257, 1987.
- Cosden, T. H., et al., Data compendium for atmospheric laser propagation studies conducted at Cape Canaveral, Florida, February-May 1977, *NRL Memo. Rep. 3611*, 123 pp., Nav. Res. Lab., Washington, D. C., 1977.
- Dang-Nhu, M., and A. Goldman, Line parameters for C<sub>2</sub>H<sub>6</sub> in the 3000 cm<sup>-1</sup> region, *J. Quant. Spectrosc. Radiat. Transfer*, **38**, 159-161, 1987.
- Deroche, J.-C., and A. Goldman, Line-by-line calculation of CF<sub>2</sub>Cl<sub>2</sub> (F-12) absorption profile in the 923 cm<sup>-1</sup> region, paper presented at 10th Colloquium on High-Resolution Molecular Spectroscopy, Dijon, France, Sept. 14-18, 1987.
- Ehlt, D. H., and L. E. Heidt, Vertical profiles of CH<sub>4</sub> in the troposphere and stratosphere, *J. Geophys. Res.*, **78**, 5265-5271, 1973.
- Ehlt, D. H., and J. Rudolph, On the importance of light hydrocarbons in multiphase atmospheric systems, *Ber. Kernforschungsanlage Jülich, D-5170*, 1-43, 1984.
- Fabian, P., Halogenated hydrocarbons in the atmosphere, in *The Handbook of Environmental Chemistry*, vol. 4, part A, edited by O. Hutzinger, pp. 23-51, Springer-Verlag, New York, 1986.
- Fabian, P., R. Borchers, B. C. Krüger, S. Lal, and S. A. Penkett, The vertical distribution of CHClF<sub>2</sub> (CFC-22) in the stratosphere, *Geophys. Res. Lett.*, **12**, 1-3, 1985.
- Farmer, C. B., G. C. Toon, P. W. Schaper, J.-F. Blavier, and L. L. Lowes, Stratospheric trace gases in the spring 1986 Antarctic atmosphere, *Nature*, **329**, 126-130, 1987.
- Flaud, J.-M., C. Camy-Peyret, D. Cariolle, J. Laurent, and G. M. Stokes, Daytime variation of atmospheric NO<sub>2</sub> from ground-based infrared measurements, *Geophys. Res. Lett.*, **10**, 1104-1107, 1983.
- Flaud, J.-M., C. Camy-Peyret, V. Malathy Devi, C. P. Rinsland, and M. A. H. Smith, The ν<sub>1</sub> and ν<sub>3</sub> bands of <sup>16</sup>O<sub>3</sub>: Line positions and intensities, *J. Mol. Spectrosc.*, **124**, 209-217, 1987.
- Flaud, J.-M., C. Camy-Peyret, J. W. Brault, C. P. Rinsland, and D. Cariolle, Nighttime and daytime variation of atmospheric NO<sub>2</sub> from ground-based infrared measurements, *Geophys. Res. Lett.*, **15**, 261-264, 1988.
- Fraser, P. J., M. A. K. Khalil, R. A. Rasmussen, and L. P. Steele, Tropospheric methane in the mid-latitudes of the southern hemisphere, *J. Atmos. Chem.*, **1**, 125-135, 1984.
- Fraser, P. J., P. Hyson, R. A. Rasmussen, A. J. Crawford, and M. A. K. Khalil, Methane, carbon monoxide, and methylchloroform in the southern hemisphere, *J. Atmos. Chem.*, **4**, 3-42, 1986.
- Gage, K. S., and G. C. Reid, Solar variability and the secular variation in the tropical tropopause, *Geophys. Res. Lett.*, **8**, 187-190, 1981.
- Gage, K. S., and G. C. Reid, Response of the tropical tropopause to El Chichón and the El Niño of 1982-1983, *Geophys. Res. Lett.*, **12**, 195-197, 1985.
- Galasyn, J. F., K. L. Tschudy, and B. J. Huebert, Seasonal and diurnal variability of nitric acid vapor and ionic aerosol species in the remote free troposphere at Mauna Loa, Hawaii, *J. Geophys. Res.*, **92**, 3105-3113, 1987.
- Gallery, W. O., F. X. Kneizys, and S. A. Clough, Air mass computer program for atmospheric transmittance/radiance calculation: FSCATM, *Environ. Res. Pap. 828 (AFGL-TR-83-0065)*, 145 pp., Air Force Geophys. Lab., Bedford, Mass., 1983.

- Gamache, R. R., Temperature dependence of  $N_2$ -broadened half-widths of ozone, *J. Mol. Spectrosc.*, **114**, 31–41, 1985.
- Gamache, R. R., and L. S. Rothman, Theoretical  $N_2$ -broadened half-widths of  $^{16}O_3$ , *Appl. Opt.*, **24**, 1651–1656, 1985.
- Gille, J. C., et al., Accuracy and precision of the nitric acid concentrations determined by the Limb Infrared Monitor of the Stratosphere Experiment on Nimbus 7, *J. Geophys. Res.*, **89**, 5179–5190, 1984.
- Gillis, J. R., and A. Goldman, Nitric oxide IR line parameters for the upper atmosphere, *Appl. Opt.*, **21**, 1161–1163, 1982.
- Girard, A., J. Besson, R. Giraudet, and L. Gramont, Correlated seasonal and climatic variations of trace constituents in the stratosphere, *Pure Appl. Geophys.*, **117**, 381–394, 1979.
- Girard, A., L. Gramont, N. Louisnard, S. Le Boiteux, and G. Fergant, Latitudinal variation of  $HNO_3$ ,  $HCl$ , and  $HF$  vertical column density above 11.5 km, *Geophys. Res. Lett.*, **9**, 135–138, 1982.
- Girard, A., G. Fergant, L. Gramont, O. Lado-Bordowsky, J. Laurent, S. Le Boiteux, M. P. Lemaître, and N. Louisnard, Latitudinal distribution of ten stratospheric species deduced from simultaneous spectroscopic measurements, *J. Geophys. Res.*, **88**, 5377–5392, 1983.
- Goldman, A., F. J. Murcray, R. D. Blatherwick, F. S. Bonomo, F. H. Murcray, and D. G. Murcray, Spectroscopic identification of  $CHClF_2$  (F-22) in the lower stratosphere, *Geophys. Res. Lett.*, **8**, 1012–1014, 1981a.
- Goldman, A., F. J. Murcray, R. D. Blatherwick, J. R. Gillis, F. S. Bonomo, F. H. Murcray, D. G. Murcray, and R. J. Cicerone, Identification of acetylene ( $C_2H_2$ ) in infrared atmospheric absorption spectra, *J. Geophys. Res.*, **86**, 12,413–12,446, 1981b.
- Goldman, A., F. G. Fernald, F. J. Murcray, F. H. Murcray, and D. G. Murcray, Spectral least squares quantification of several atmospheric gases from high-resolution infrared solar spectra obtained at the south pole, *J. Quant. Spectrosc. Radiat. Transfer*, **29**, 189–204, 1983.
- Goldman, A., F. J. Murcray, R. D. Blatherwick, and D. G. Murcray, Quantification of  $HCl$  from high-resolution, ground-based, infrared solar spectra in the  $3000\text{ cm}^{-1}$  region, *J. Quant. Spectrosc. Radiat. Transfer*, **36**, 385–387, 1986.
- Goldman, A., F. J. Murcray, F. H. Murcray, and D. G. Murcray, Quantification of  $HCl$  from high-resolution infrared solar spectra obtained at the south pole in December 1986, *Geophys. Res. Lett.*, **14**, 622–623, 1987a.
- Goldman, A., R. D. Blatherwick, F. J. Murcray, J. W. VanAllen, F. H. Murcray, and D. G. Murcray, New atlas of stratospheric IR absorption spectra, vol. I. Line positions and identifications, Sept. 1987 ed., Dep. of Phys., Univ. of Denver, Denver, Colo., 1987b.
- Goldman, A., R. D. Blatherwick, F. J. Murcray, J. W. VanAllen, F. H. Murcray, and D. G. Murcray, New atlas of stratospheric IR absorption spectra, vol. II. The spectra, Sept. 1987 ed., Dep. of Phys., Univ. of Denver, Denver, Colo., 1987c.
- Goldman, A., F. J. Murcray, F. H. Murcray, D. G. Murcray, and C. P. Rinsland, Measurements of several atmospheric gases above the south pole in December 1986 from high-resolution 3- to 4- $\mu\text{m}$  solar spectra, *J. Geophys. Res.*, **93**, 7069–7074, 1988.
- Hagemann, R., G. Nief, and E. Roth, Absolute isotopic scale for deuterium analysis of natural waters. Absolute D/H ratio of SMOW, *Tellus*, **22**, 712–715, 1970.
- Holland, R. F., M. C. Vasquez, W. H. Beattie, and R. S. McDowell, Absorptivity of nitric oxide in the fundamental vibrational band, *J. Quant. Spectrosc. Radiat. Transfer*, **29**, 435–438, 1983.
- Huebert, B. J., and A. L. Lazrus, Tropospheric gas-phase and particulate nitrate measurements, *J. Geophys. Res.*, **85**, 7322–7328, 1980.
- IUPAC Commission on Atomic Weights and Isotopic Abundances, Isotopic compositions of the elements 1981, *Pure Appl. Chem.*, **55**, 1119–1136, 1983.
- Jones, R. L., and J. A. Pyle, Observations of  $CH_4$  and  $N_2O$  by the Nimbus 7 SAMS: A comparison with in situ data and two-dimensional numerical model calculations, *J. Geophys. Res.*, **89**, 5263–5279, 1984.
- Kaye, J. A., Mechanisms and observations for isotope fractionation of molecular species in planetary atmospheres, *Rev. Geophys.*, **25**, 1609–1658, 1987.
- Khalil, M. A. K., and R. A. Rasmussen, Increase of  $CHClF_2$  in the Earth's atmosphere, *Nature*, **292**, 823–824, 1981.
- Ko, M. K. W., and N. D. Sze, Diurnal variation of  $ClO$ : Implications for the stratospheric chemistries of  $ClONO_2$ ,  $HOCl$ , and  $HCl$ , *J. Geophys. Res.*, **89**, 11,619–11,632, 1984.
- Ko, M. K. W., K. K. Tung, D. K. Weisenstein, and N. D. Sze, A zonal mean model of stratospheric tracer transport in isentropic coordinates: Numerical simulations for nitrous oxide and nitric acid, *J. Geophys. Res.*, **90**, 2313–2329, 1985.
- Logan, J. A., M. J. Prather, S. C. Wofsy, and M. B. McElroy, Tropospheric chemistry: A global perspective, *J. Geophys. Res.*, **86**, 7210–7254, 1981.
- Malathy Devi, V., B. Fridovich, G. D. Jones, D. G. S. Snyder, and A. Neuendorffer, Temperature dependence of the widths of  $N_2$ -broadened lines of the  $\nu_3$  band of  $^{14}N^{16}O_2$ , *Appl. Opt.*, **21**, 1537–1538, 1982a.
- Malathy Devi, V., B. Fridovich, G. D. Jones, D. G. S. Snyder, P. P. Das, J.-M. Flaud, C. Camy-Peyret, and K. Narahari Rao, Tunable diode laser spectroscopy of  $NO_2$  at 6.2  $\mu\text{m}$ , *J. Mol. Spectrosc.*, **93**, 179–195, 1982b.
- Malathy Devi, V., C. P. Rinsland, and D. C. Benner, Absolute intensity measurements of  $CO_2$  bands in the  $2395\text{--}2680\text{ cm}^{-1}$  region, *Appl. Opt.*, **23**, 4067–4075, 1984.
- Malathy Devi, V., C. P. Rinsland, M. A. H. Smith, and D. C. Benner, Air-broadened Lorentz halfwidths and pressure-induced line shifts in the  $\nu_4$  band of  $^{13}CH_4$ , *Appl. Opt.*, **27**, 2296–2308, 1988.
- Mandin, J.-Y., C. Amiot, and G. Guelachvili, Intensity and self-broadening coefficient measurements from Fourier transform spectra: Application to the nitric oxide fundamental band, *Ann. Phys.*, **5**, 91–112, 1980.
- Mankin, W. G., and M. T. Coffey, Latitudinal distributions and temporal changes of stratospheric  $HCl$  and  $HF$ , *J. Geophys. Res.*, **88**, 10,776–10,784, 1983.
- McClatchey, R. A., R. W. Fenn, J. E. A. Selby, F. E. Volz, and J. S. Garing, Optical properties of the atmosphere, 3rd ed., *Rep. AFRL-72-0497, ERP 411*, Air Force Cambridge Res. Lab., Bedford, Mass., 1972.
- Murcray, F. J., F. H. Murcray, A. Goldman, D. G. Murcray, and C. P. Rinsland, Infrared measurements of several nitrogen species above the south pole in December 1980 and November–December 1986, *J. Geophys. Res.*, **92**, 13,373–13,376, 1987.
- Noxon, J. F.,  $NO_2$  in the mid-Pacific troposphere, *Geophys. Res. Lett.*, **8**, 1223–1226, 1981.
- Noxon, J. F., W. R. Henderson, and R. B. Norton, Stratospheric  $NO_2$ , 3, The effects of large-scale horizontal transport, *J. Geophys. Res.*, **88**, 5240–5248, 1983.
- Perrin, A., J.-M. Flaud, and C. Camy-Peyret, Calculated line positions and intensities for the  $\nu_1 + \nu_3$  and  $\nu_1 + \nu_2 + \nu_3 - \nu_2$  bands of  $^{14}N^{16}O_2$ , *Infrared Phys.*, **22**, 343–348, 1982.
- Rasmussen, R. A., and M. A. K. Khalil, Latitudinal distributions of trace gases in and above the boundary layer, *Chemosphere*, **11**, 227–235, 1982.
- Reichle, H. G., Jr., and E. P. Condon, Vertical profiles of  $CO$  and  $CH_4$  in the lower and middle troposphere over the eastern United States January 1978, *Geophys. Res. Lett.*, **6**, 949–951, 1979.
- Reid, G. C., and K. S. Gage, On the annual variation in height of the tropical tropopause, *J. Atmos. Sci.*, **38**, 1928–1938, 1981.
- Reid, G. C., and K. S. Gage, Interannual variations in the height of the tropical tropopause, *J. Geophys. Res.*, **90**, 5629–5635, 1985.
- Rinsland, C. P., and J. S. Levine, Identification and measurement of atmospheric ethane ( $C_2H_6$ ) from a 1951 infrared solar spectrum, *Appl. Opt.*, **25**, 4522–4525, 1986.
- Rinsland, C. P., M. A. H. Smith, P. L. Rinsland, A. Goldman, J. W. Brault, and G. M. Stokes, Ground-based infrared spectroscopic measurements of atmospheric hydrogen cyanide, *J. Geophys. Res.*, **87**, 11,119–11,125, 1982a.
- Rinsland, C. P., A. Goldman, F. J. Murcray, D. G. Murcray, M. A. H. Smith, R. K. Seals, Jr., J. C. Larsen, and P. L. Rinsland, Stratospheric  $N_2O$  mixing ratio profile from high-resolution, balloon-borne solar absorption spectra and laboratory spectra near  $1880\text{ cm}^{-1}$ , *Appl. Opt.*, **21**, 4351–4355, 1982b.
- Rinsland, C. P., R. E. Boughner, J. C. Larsen, G. M. Stokes, and J. W. Brault, Diurnal variations of atmospheric nitric oxide: Ground-based infrared spectroscopic measurements and their interpretation with time-dependent photochemical model calculations, *J. Geophys. Res.*, **89**, 9613–9622, 1984a.
- Rinsland, C. P., et al., Simultaneous stratospheric measurements of  $H_2O$ ,  $HDO$ , and  $CH_4$  from balloon-borne and aircraft infrared solar absorption spectra and tunable diode laser laboratory spectra of  $HDO$ , *J. Geophys. Res.*, **89**, 7259–7266, 1984b.
- Rinsland, C. P., A. Goldman, and G. M. Stokes, Identification of

- atmospheric  $C_2H_2$  lines in the 3230–3340  $cm^{-1}$  region of high-resolution solar absorption spectra recorded at the National Solar Observatory, *Appl. Opt.*, 24, 2044–2046, 1985.
- Rinsland, C. P., R. Zander, C. B. Farmer, R. H. Norton, and J. M. Russell III, Concentrations of ethane ( $C_2H_6$ ) in the lower stratosphere and upper troposphere and acetylene ( $C_2H_2$ ) in the upper troposphere deduced from Atmospheric Trace Molecule Spectroscopy/Spacelab 3 spectra, *J. Geophys. Res.*, 92, 11,951–11,964, 1987.
- Rinsland, C. P., V. Malathy Devi, M. A. H. Smith, and D. C. Benner, Measurements of air-broadened and nitrogen-broadened Lorentz width coefficients and pressure-shift coefficients in the  $\nu_4$  and  $\nu_2$  bands of  $^{12}CH_4$ , *Appl. Opt.*, 27, 631–651, 1988a.
- Rinsland, C. P., A. Goldman, F. J. Murcray, F. H. Murcray, D. G. Murcray, and J. S. Levine, Infrared measurements of increased  $CF_2Cl_2$  (CFC-12) absorption above the south pole, *Appl. Opt.*, 27, 627–630, 1988b.
- Rothman, L. S., Infrared energy levels and intensities of carbon dioxide, 3, *Appl. Opt.*, 25, 1795–1816, 1986.
- Rothman, L. S., et al., The HITRAN database: 1986 edition, *Appl. Opt.*, 26, 4058–4097, 1987.
- Rozanski, K., and C. Sonntag, Vertical distribution of deuterium in atmospheric water vapour, *Tellus*, 34, 135–141, 1982.
- Rudolph, J., and D. H. Ehhalt, Measurements of  $C_2$ – $C_3$  hydrocarbons over the North Atlantic, *J. Geophys. Res.*, 86, 11,959–11,964, 1981.
- Singh, H. B., and L. J. Salas, Measurement of selected light hydrocarbons over the Pacific Ocean: Latitudinal and seasonal variations, *Geophys. Res. Lett.*, 9, 842–845, 1982.
- Singh, H. B., L. J. Salas, H. Shigeishi, and E. Scribner, Atmospheric halocarbons, hydrocarbons, and sulfur hexafluoride: Global distributions, sources, and sinks, *Science*, 203, 899–903, 1979.
- Smith, M. A. H., Compilation of atmospheric gas concentration profiles from 0 to 50 km, *NASA Tech. Memo*, 83289, NASA Langley Res. Cent., Hampton, Va., 1982. (Available as NTIS 82N22822 from the Natl. Tech. Inf. Serv., Springfield, Va.)
- Smith, M. A. H., C. P. Rinsland, V. Malathy Devi, D. C. Benner, and K. B. Thakur, Measurements of air-broadened and nitrogen-broadened half-widths and shifts of ozone lines near 9  $\mu m$ , *J. Opt. Soc. Am. B*, 5, 585–592, 1988.
- Solomon, S., and R. R. Garcia, On the distributions of long-lived tracers and chlorine species in the middle atmosphere, *J. Geophys. Res.*, 89, 11,633–11,644, 1984.
- Steele, L. P., P. J. Fraser, R. A. Rasmussen, M. A. K. Khalil, T. J. Conway, A. J. Crawford, R. H. Gammon, K. A. Masarie, and K. W. Thoning, The global distribution of methane in the troposphere, *J. Atmos. Chem.*, 5, 125–171, 1987.
- Tille, K. J. W., M. Savelsberg, and K. Bächmann, Airborne measurements of nonmethane hydrocarbons over western Europe: Vertical distributions, seasonal cycles of mixing ratios and source strengths, *Atmos. Environ.*, 19, 1751–1760, 1985.
- World Meteorological Organization, Atmospheric ozone 1985: Assessment of our understanding of the processes controlling its present distribution and change, *Rep. 16*, Geneva, Switzerland, 1986.
- Zander, R., G. Stokes, and J. Brault, Detection, par voie spectroscopique, de l'acétylène et de l'éthane dans l'atmosphère terrestre, à partir d'observations solaires infrarouges au sol, *C. R. Seances Acad. Sci., Ser. 2*, 295, 583–586, 1982.
- Zander, R., G. M. Stokes, and J. W. Brault, Simultaneous detection of FC-11, FC-12, and FC-22, through 8 to 13 micrometers IR solar observations from the ground, *Geophys. Res. Lett.*, 10, 521–524, 1983.
- Zander, R., C. P. Rinsland, C. B. Farmer, and R. H. Norton, Infrared spectroscopic measurements of halogenated source gases in the stratosphere with the ATMOS instrument, *J. Geophys. Res.*, 92, 9836–9850, 1987.
- R. D. Blatherwick, A. Goldman, D. G. Murcray, F. H. Murcray, and F. J. Murcray, Physics Department, University of Denver, Denver, CO 80208.
- C. P. Rinsland, Atmospheric Sciences Division, MS 401A, NASA Langley Research Center, Hampton, VA 23665.

(Received May 3, 1988;  
revised July 12, 1988;  
accepted July 12, 1988.)



# Infrared Measurements of Several Nitrogen Species Above the South Pole in December 1980 and November–December 1986

F. J. MURCRAY, F. H. MURCRAY, A. GOLDMAN, AND D. G. MURCRAY

*Physics Department, University of Denver, Denver, Colorado*

C. P. RINSLAND

*Atmospheric Sciences Division, NASA Langley Research Center, Hampton, Virginia*

Ground-based high-resolution infrared solar absorption spectra recorded from the Amundsen-Scott south pole station have been analyzed to determine total vertical column amounts of  $\text{HNO}_3$  in December 1980 and November 1986, and  $\text{NO}$ ,  $\text{NO}_2$ , in November–December 1986.

## INTRODUCTION

In December 1980 and November–December 1986, the University of Denver atmospheric spectroscopy group recorded numerous high-resolution infrared solar absorption spectra from the Amundsen-Scott south pole station. These spectra were obtained by Frank J. Murcay and Frank H. Murcay with a Michelson-type Fourier transform spectrometer and show absorption features of a number of minor and trace atmospheric gases with a minimum of atmospheric water vapor absorption. Quantifications of the total column amounts of  $\text{O}_3$ ,  $\text{CH}_4$ ,  $\text{N}_2\text{O}$ , and  $\text{H}_2\text{O}$  from the 1980 observations [Goldman *et al.*, 1983] and  $\text{HCl}$  from the 1986 observations [Goldman *et al.*, 1987] have been reported along with an atlas of the  $750\text{--}960\text{ cm}^{-1}$  spectral region [Blatherwick *et al.*, 1982]. In the present study, we report measurements of  $\text{HNO}_3$  total column amounts deduced from both data sets and  $\text{NO}$ , and  $\text{NO}_2$  total column amounts from the 1986 data set. Nitric acid may be important in the chemistry which creates the spring Antarctic ozone minimum, since it may condense in the cold winter polar stratosphere and become the dominant component of polar stratospheric clouds [Toon *et al.*, 1986; Crutzen and Arnold, 1986]. The present measurements were obtained shortly after the austral spring ozone minimum and define for the first time the ambient levels of these nitrogen species immediately following the breakup of the polar vortex.

## ANALYSIS OF $\text{HNO}_3$ OBSERVATIONS

Spectral intervals near  $870\text{ cm}^{-1}$  for which the best agreement is obtained between measured and calculated  $\text{HNO}_3$  absorption features have been selected for quantitative analysis from spectra obtained on December 5, 1980, and November 26, 1986. The most prominent absorptions contained in this region are the regularly spaced P-branch manifolds of the  $\text{HNO}_3$   $\nu_5$  band. The nearly constant solar zenith angle of the south pole observations allowed the coadding of several spectral scans on each day, yielding a signal-to-rms-noise of about 300 near  $870\text{ cm}^{-1}$ . The resolution of the 1980 and 1986 spectra are  $0.02$  and  $0.04\text{ cm}^{-1}$ ,

respectively. A multiparameter nonlinear least squares spectral fitting method, the same utilized to quantify gas amounts in previous ground-based spectra analysis studies [Rinsland *et al.*, 1982; Goldman *et al.*, 1983, 1986], has been employed along with the line parameters of the 1986 HITRAN compilation [Rothman *et al.*, 1987]. The  $\text{HNO}_3$  parameters covering the  $870\text{ cm}^{-1}$  region in the HITRAN compilation were generated at the University of Denver [Goldman and Gillis, 1984] and have been applied previously to the analysis of stratospheric solar absorption spectra obtained during a balloon flight [Goldman *et al.*, 1984]. However, a constant air-broadened half-width of  $0.13\text{ cm}^{-1}\text{ atm}^{-1}$  at  $296\text{ K}$  is assumed on the 1986 HITRAN compilation [Rothman *et al.*, 1987], whereas a constant air-broadened halfwidth of  $0.10\text{ cm}^{-1}\text{ atm}^{-1}$  at  $296\text{ K}$  was assumed in two previous atmospheric studies of  $\text{HNO}_3$  [Goldman *et al.*, 1980, 1984]. This difference changes the retrieved  $\text{HNO}_3$  total column amounts by less than 5%. The major interference near the spectral region used is due to water vapor. Under the conditions that exist at the south pole, this interference is minimal.

Figure 1 illustrates the agreement between measured and best fit calculated spectra. All of the observed features in the fitted region are attributable to  $\text{HNO}_3$  [Blatherwick *et al.*, 1982]. A total of six parameters have been adjusted simultaneously in this fitting, five of which are instrumental parameters to model the level and slope of the 100% transmission curve, the shift in frequency ( $\text{cm}^{-1}$ ) between the measured and computed spectrum, and the amplitude and phase of a weak channel spectrum (period  $\approx 1.0\text{ cm}^{-1}$ ) observed in the data. The remaining parameter is a multiplicative scaling factor that converts an assumed relative mixing ratio in each layer to an absolute value. Notice that the calculated 100% transmittance level (dashed curve in Figure 1) is several percent above the measured spectrum. This difference results from the many overlapping weak fundamental and hot band lines of  $\text{HNO}_3$  in this region. The presence of an unresolved  $\text{HNO}_3$  "continuum" in this region has also been noted in laboratory studies [Brockman *et al.*, 1978]. The  $\text{HNO}_3$  reference mixing ratio profile of Smith [1982] has been assumed in the analysis. The effective instrument line shape function has been determined from fittings of  $\text{O}_3$  lines near  $780\text{ cm}^{-1}$ . These lines show an asymmetric shape in the data

Copyright 1987 by the American Geophysical Union.

Paper number 7D0666.

0148-0227/87/007D-0666\$02.00

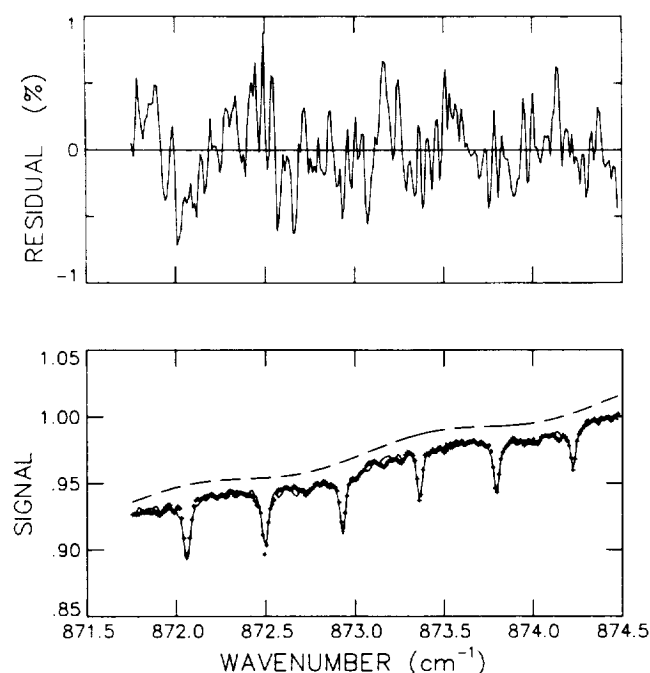


Fig. 1. (bottom) Comparison between a ground-based solar absorption spectrum (solid line) recorded at the south pole on December 5, 1980, at an astronomical zenith angle of  $67.7^\circ$  and a least squares best fit to the data (crosses). The intensities of the measured spectrum have been normalized to the highest intensity in the fitted region. The dashed curve indicates the modeled 100% transmittance level. (top) Residuals are measured minus calculated values.

indicating residual instrumental distortions. Radiosonde soundings from the south pole on the date of the measurements have been used to define the atmospheric pressure-temperature profiles.

Fittings to the  $867.0$  to  $870.0\text{ cm}^{-1}$  and  $871.75$  to  $874.50\text{ cm}^{-1}$  regions were run and found to yield total column amounts consistent to 10%. The average results and their estimated total absolute uncertainties (1 sigma) are  $1.6 (0.3) \times 10^{16}$  molecules  $\text{cm}^{-2}$  for the December 1980 spectra and  $1.4 (0.4) \times 10^{16}$  molecules  $\text{cm}^{-2}$  for the November 1986 data. The two measurements agree within the combined total uncertainties. The sources of error and the estimated uncertainty in the  $\text{HNO}_3$  total vertical column amount resulting from each are (1) uncertainty due to instrument effects (noise, channel spectra, line shape distortions, and zero level shifts) ( $\pm 10\%$  in the 1980 data and  $\pm 20\%$  in the 1986 data), (2) uncertainty in the assumed  $\text{HNO}_3$  relative mixing ratio distribution ( $\pm 5\%$ ), (3) uncertainty in the assumed  $\text{HNO}_3$  line intensities ( $\pm 15\%$ ), (4) uncertainty in the assumed  $\text{HNO}_3$  air-broadened half-widths and their temperature dependences ( $\pm 5\%$ ), and (5) uncertainty in the assumed pressure-temperature profile ( $\pm 5\%$ ).

As a check on the analysis method used in this study, a solar spectrum recorded on July 10, 1976, at  $0.06\text{ cm}^{-1}$  resolution from Mt. Evans near Denver, Colorado (elevation  $4.3\text{ km}$ ) by the University of Denver atmospheric sciences group and a solar spectrum (G. M. Stokes, Battelle Observatory, private communication, 1984) recorded on October 6, 1982, at  $0.005\text{ cm}^{-1}$  resolution with the McMath Fourier transform spectrometer on Kitt Peak ( $31.9^\circ\text{N}$  latitude,  $111.6^\circ\text{W}$  longitude, elevation  $2095\text{ m}$ ) were fitted in the  $870$

$\text{cm}^{-1}$  region to retrieve the  $\text{HNO}_3$  total vertical column amounts. The derived values,  $0.98 (0.20) \times 10^{16}$  molecules  $\text{cm}^{-2}$  from the Mt. Evans spectrum and  $1.0 (0.2) \times 10^{16}$  molecules  $\text{cm}^{-2}$  from the Kitt Peak spectrum, are within the range of previous measurements obtained near the same latitudes (see below).

A number of surveys have measured the latitudinal variation of the total vertical column amount of  $\text{HNO}_3$ , although only a few of these studies include measurements in the southern hemisphere. Figure 2 shows the northern and southern hemisphere survey results included in a recent assessment document [WMO, 1986] along with the present measurements at  $90^\circ\text{S}$ . Also included are total column amounts [Gille *et al.*, 1984] inferred from profiles obtained by the limb infrared monitor of the stratosphere (LIMS) experiment aboard the Nimbus 7 satellite and the measurements of Williams *et al.* [1982], the only total column amounts obtained south of  $64^\circ\text{S}$  latitude. The latter results, which agree very well with the LIMS total columns in the range of overlapping measurements ( $48^\circ\text{S}$  to  $64^\circ$ ), were derived from analysis of aircraft emission spectra with a band model and indicate a rapid latitudinal increase from  $1.2 (0.2) \times 10^{16}$  molecules  $\text{cm}^{-2}$  at  $53^\circ\text{S}$  to  $3.4 (0.7) \times 10^{16}$  molecules  $\text{cm}^{-2}$  at  $89^\circ\text{S}$  during the second half of November in 1978. The south pole spectra were recorded at nearly the same time of year in 1980 and 1986 but yield total vertical column amounts nearly a factor of 2 lower than the corresponding value from the Williams *et al.* [1982] study. Because of the difference in the measurement techniques (emission versus absorption), methods of analysis (band model versus line-by-line and spectral least squares), it is likely that systematic sources of error may contribute to this difference.

#### ANALYSIS OF NO OBSERVATIONS

The well-isolated nitric oxide lines at  $1857.275\text{ cm}^{-1}$  and  $1914.990\text{ cm}^{-1}$  were utilized in fittings of a spectrum recorded on November 28, 1986. These lines, which have been used in previous studies of spectra recorded with balloon-borne and aircraft-borne interferometers [Murray *et al.*, 1980; Blatherwick *et al.*, 1980; Coffey *et al.*, 1981], are relatively weak in the present data set with maximum absorptions of less than 10%.

Assuming the line parameters of the 1986 HITRAN compilation [Rothman *et al.*, 1987] and the reference vertical distribution of Smith [1982], total vertical column amounts of  $5.42 \times 10^{15}$  and  $5.27 \times 10^{15}$  molecules  $\text{cm}^{-2}$  are derived from the  $1857.275$  and  $1914.990\text{ cm}^{-1}$  lines, respectively. The mean value,  $5.34 \times 10^{15}$  molecules  $\text{cm}^{-2}$ , is estimated to be accurate to about 12%. The NO line widths are narrower than those of nearby  $\text{CO}_2$  and  $\text{H}_2\text{O}$  lines; tests assuming different NO vertical distributions indicate that most of the NO column resides about the tropopause.

Latitude surveys of NO total column amounts are summarized in Figure 10–21 of WMO Report 16 [WMO, 1986]. These show a small amount of data in the southern hemisphere and none at high southern latitudes. The northern hemisphere data shows no indication of a latitudinal gradient, however the small number of observations coupled with the scatter in the values make it difficult to draw any definite conclusions. The values reported by Girard *et al.* [1979] of  $6 \times 10^{15}$  molecules  $\text{cm}^{-2}$  at the equator and  $4 \times 10^{15}$  molecules  $\text{cm}^{-2}$  at  $50^\circ\text{S}$  were derived for the total column above  $11\text{ km}$

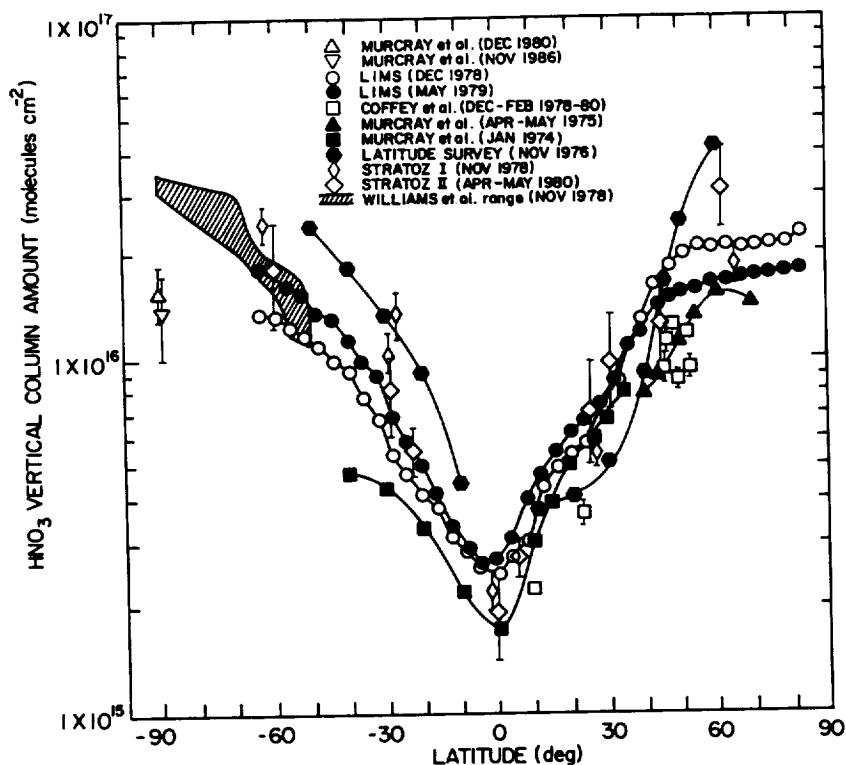


Fig. 2. Latitudinal variation of the total vertical column amount of  $\text{HNO}_3$ . The LIMS measurements are from Figure 13 of Gille *et al.* [1984]. The November 1976 latitude survey mission results were reported by Girard [1979]. STRATOZ I and STRATOZ II results were reported by Girard *et al.* [1980] and Girard *et al.* [1983], respectively.

with no measurable difference at sunrise and sunset. Our south pole column is slightly higher than the  $60^\circ\text{S}$  value of Girard *et al.* [1983], but additional measurements are needed before a reliable latitude trend can be established for NO in the southern hemisphere.

#### ANALYSIS OF $\text{NO}_2$ OBSERVATIONS

The  $\text{NO}_2$  feature at  $2914.65\text{ cm}^{-1}$ , a composite of several closely spaced transitions of the  $\nu_1 + \nu_3$  band, was selected for the quantitative analysis assuming the 1986 HITRAN line parameters [Rothman *et al.*, 1987]. This feature is weak (less than 5% absorption) but well isolated in the present spectra. It has been used in previous ground-based studies of atmospheric  $\text{NO}_2$  [Camy-Peyret *et al.*, 1983; Flaud *et al.*, 1983]. Assuming the reference vertical distribution of Smith [1982], a value of  $8.03 (0.96) \times 10^{15}$  molecules  $\text{cm}^{-2}$  is estimated for the total vertical column amount on December 3, 1986.

In all previous ground-based spectra, the intense  $\nu_3$  band of  $\text{NO}_2$  near  $6\text{ }\mu\text{m}$  is unobservable because of overlapping strong absorption by  $\text{H}_2\text{O}$ . In the south pole data the reduced  $\text{H}_2\text{O}$  amounts allow the identification of several isolated  $\nu_3$  band  $\text{NO}_2$  features. However, because these lines occur in the wings of strong  $\text{H}_2\text{O}$  lines, they are less favorable for quantitative analysis than the  $3\text{ }\mu\text{m}$  features. Recently, it has been shown that both the  $3\text{ }\mu\text{m}$  and  $6\text{ }\mu\text{m}$   $\text{NO}_2$  bands yield consistent quantitative results [Coffey *et al.*, 1986].

Measurements of the vertical column of daytime  $\text{NO}_2$  versus latitude are summarized in Figures 10–22 of WMO Report 16 [WMO, 1986]. This assessment includes three sets of southern hemisphere spring measurements, but all were obtained north of  $50^\circ\text{S}$ . A more valid comparison is possible with the visible absorption total columns measured at Syowa Station ( $69.0^\circ\text{S}$ ,  $39.6^\circ\text{E}$ ) in Antarctica [Shibasaki *et al.*,

1986]. The results of Shibasaki *et al.* show seasonal variation with a winter minimum of  $1 \times 10^{15}$  molecules  $\text{cm}^{-2}$ , and a summer maximum of  $7 \times 10^{15}$  molecules  $\text{cm}^{-2}$ . Keys and Johnston [1986] find a similar seasonal variation of total column  $\text{NO}_2$  at Arrival Heights, Antarctica. Measurements in early December 1984 [Shibasaki *et al.*, 1986] indicate a total column of about  $6.8 \times 10^{15}$  molecules  $\text{cm}^{-2}$ , slightly lower than our south pole results.

#### DISCUSSION

The column amounts reported here were obtained after the ozone "hole" had disappeared over the south pole. Low readings of the total ozone were observed with the south pole Dobson instrument until November 15, 1986. While the data were obtained after the hole disappeared they are close enough in time that some residual effects may be present in the data. The data when compared with other data sets obtained earlier at the south pole or at other sites at lower latitudes show a number of interesting features. The first is the change in  $\text{HNO}_3$  column amount between 1978 and 1980. As noted in the discussion, the measurements were made using different techniques which may result in some systematic errors; however, other tests indicate that these, if present, are small.

The column amounts for both NO and  $\text{NO}_2$  are higher than observed at low latitudes. This is not unexpected, since, as was emphasized by Farman *et al.* [1985] during the Antarctic summer (particularly the south pole), there is no diurnal change and compounds such as  $\text{N}_2\text{O}_5$  which are formed at night will not be present at concentrations present at lower latitudes. Thus the NO and  $\text{NO}_2$  will be present at higher levels. The  $\text{NO}_2$  observations at other Antarctic sites [Keys and Johnston, 1986; Shibasaki *et al.*, 1986] show the buildup

in NO<sub>2</sub> column as the hours of daylight increases. As noted in the discussion, the NO<sub>2</sub> results agree with other observations; however, the NO results do not agree with the conclusion reached by WMO [1986] that the NO column is constant with latitude at a value near  $3 \times 10^{15}$  molecules cm<sup>-2</sup>.

**Acknowledgments.** The authors thank C. R. Trepte of ST Systems Corp. (STX) for his help in obtaining the correlative pressure-temperature profiles. Research at the University of Denver was supported by NSF under grant DPP-8118005 and by NASA. Acknowledgment is made to the National Center for Atmospheric Research, which is supported by NSF, for computer time used in this research.

#### REFERENCES

- Blatherwick, R. D., A. Goldman, D. G. Murcray, G. R. Cook, and J. W. Van Allen, Simultaneous mixing ratio profiles of stratospheric NO and NO<sub>2</sub> as described from balloon-borne infrared solar spectra, *Geophys. Res. Lett.*, **7**, 471–473, 1980.
- Blatherwick, R. D., F. J. Murcray, F. H. Murcray, A. Goldman, and D. G. Murcray, Atlas of South Pole IR solar spectra, *Appl. Opt.*, **21**, 2658–2659, 1982.
- Brockman, P., C. H. Bair, and F. Allario, High resolution spectral measurements of the HNO<sub>3</sub> 11.3 μm band using tunable diode lasers, *Appl. Opt.*, **17**, 91–100, 1978.
- Camy-Peyret, C., J. M. Flaud, J. Laurent, and G. M. Stokes, First infrared measurement of atmospheric NO<sub>2</sub> from the ground, *Geophys. Res. Lett.*, **10**, 35–38, 1983.
- Coffey, M. T., W. G. Mankin, and A. Goldman, Simultaneous spectroscopic determination of the latitudinal, seasonal, and diurnal variability of stratospheric N<sub>2</sub>O, NO, NO<sub>2</sub>, and HNO<sub>3</sub>, *J. Geophys. Res.*, **86**, 7331–7341, 1981.
- Coffey, M. T., W. G. Mankin, and A. Goldman, Stratospheric NO<sub>2</sub> retrieval from solar absorption spectra in the  $\nu_3$  and  $\nu_1 + \nu_3$  bands, *Appl. Opt.*, **25**, 2460–2462, 1986.
- Crutzen, P. J., and F. Arnold, Nitric acid cloud formation in the cold Antarctic stratosphere: A major cause for the springtime 'ozone hole,' *Nature*, **324**, 651–655, 1986.
- Farman, J. C., R. J. Murgatroyd, A. M. Silnickas, and B. A. Thrush, Ozone photochemistry in the Antarctic stratosphere in summer, *Q. J. R. Meteorol. Soc.*, **111**, 1013, 1985.
- Flaud, J. M., C. Camy-Peyret, D. Cariolle, J. Laurent, and G. M. Stokes, Daytime variation of atmospheric NO<sub>2</sub> from ground-based infrared measurements, *Geophys. Res. Lett.*, **10**, 1104–1107, 1983.
- Gille, J. C., J. M. Russell, III, P. L. Bailey, E. E. Remsberg, L. L. Gordley, W. F. Evans, H. Fischer, B. W. Bandrud, A. Girard, J. E. Harries, and S. A. Beck, Accuracy and precision of the nitric acid concentrations determined by the limb infrared monitor of the stratosphere experiment on NIMBUS 7, *J. Geophys. Res.*, **89**, 5179–5190, 1984.
- Girard, A., J. Besson, R. Giraudet, and L. Gramont, Correlated seasonal and climatic variations of trace constituents in the stratosphere, *Pure Appl. Geophys.*, **117**, 381–394, 1979.
- Girard, A., L. Gramont, D. Imbault, J. Laurent, M. P. Lemaître, S. Boiteus, and N. Louisnard, Contribution à l'étude des variations dans la composition de la stratosphère en fonction de la latitude: Résultats de la mission STRATOZ, *Proc. Quadrenn. Int. Ozone Symp.*, 704–711, 1980.
- Girard, A., G. Fergant, L. Gramont, O. Lado-Bordowsky, J. Laurent, S. Le Boiteux, M. P. Lemaître, and N. Louisnard, Latitudinal distribution of ten stratospheric species deduced from simultaneous spectroscopic measurements, *J. Geophys. Res.*, **88**, 5377–5392, 1983.
- Goldman, A., and J. R. Gillis, Line parameters and line-by-line calculations for molecules of stratospheric interest, progress report, Physics Department, Univ. of Denver, Denver, Colo., 1984.
- Goldman, A., D. G. Murcray, and E. Niple, High resolution IR balloon-borne solar spectra and laboratory spectra in the HNO<sub>3</sub> 1720-cm<sup>-1</sup> region: An analysis, *Appl. Opt.*, **19**, 3721–3724, 1980.
- Goldman, A., F. G. Fernald, F. J. Murcray, F. H. Murcray, and D. G. Murcray, Spectral least squares quantification of several atmospheric gases from high resolution infrared solar spectra obtained at the South Pole, *J. Quant. Spectrosc. Radiat. Transfer*, **29**, 189–204, 1983.
- Goldman, A., J. R. Gillis, C. P. Rinsland, F. J. Murcray, and D. G. Murcray, Stratospheric HNO<sub>3</sub> quantification from line-by-line nonlinear least-squares analysis of high-resolution balloon-borne solar absorption spectra in the 870-cm<sup>-1</sup> region, *Appl. Opt.*, **23**, 3252–3255, 1984.
- Goldman, A., F. J. Murcray, R. D. Blatherwick, and D. G. Murcray, Quantification of HCl from high resolution, ground-based, infrared solar spectra in the 3000 cm<sup>-1</sup> region, *J. Quant. Spectrosc. Radiat. Transfer*, **36**, 385–387, 1986.
- Goldman, A., F. J. Murcray, F. H. Murcray, and D. G. Murcray, Quantification of HCl from high resolution infrared solar spectra obtained at the South Pole in December 1986, *Geophys. Res. Lett.*, in press, 1987.
- Keys, J. G., and P. V. Johnston, Stratospheric NO<sub>2</sub> and O<sub>3</sub> in Antarctica: Dynamic and chemically controlled variations, *Geophys. Res. Lett.*, **13**, 1260–1263, 1986.
- Murcray, D. G., D. B. Barker, J. N. Brooks, A. Goldman, J. J. Kusters, F. H. Murcray, and W. J. Williams, Variation of HNO<sub>3</sub> total column density with latitude and season and a measurement of stratospheric CF<sub>2</sub>Cl<sub>2</sub>, *Proc. Conf. Clim. Impact Assess. Program*, **4**, 432, 1975a.
- Murcray, D. G., D. B. Barker, J. N. Brooks, A. Goldman, and W. J. Williams, Seasonal and latitudinal variation of the stratospheric concentration of HNO<sub>3</sub>, *Geophys. Res. Lett.*, **2**, 223–225, 1975b.
- Murcray, F. J., A. Goldman, D. G. Murcray, G. R. Cook, J. W. Van Allen, and R. D. Blatherwick, Identification of isolated NO lines in balloon-borne infrared solar spectra, *Geophys. Res. Lett.*, **7**, 673–676, 1980.
- Rinsland, C. P., M. A. H. Smith, P. L. Rinsland, A. Goldman, J. W. Brault, and G. M. Stokes, Ground-based infrared spectroscopic measurements of atmospheric hydrogen cyanide, *J. Geophys. Res.*, **87**, 11,119–11,125, 1982.
- Rothman, L. S., R. P. Gamache, A. Goldman, L. R. Brown, R. A. Toth, H. Pickett, R. P. Poynter, J. M. Flaud, C. Camy-Peyret, A. Barbe, N. Husson, C. P. Rinsland, and M. A. H. Smith, The HITRAN database: 1986 edition, *Appl. Opt.*, in press, 1987.
- Shibasaki, K., N. Iwagami, and T. Ogawa, Stratospheric nitrogen dioxide observed by ground-based and balloon-borne techniques at Syowa Station (69.0°S, 39.6°E), *Geophys. Res. Lett.*, **13**, 1268–1271, 1986.
- Smith, M. A. H., Compilation of atmospheric gas concentration profiles from 0 to 50 km, *NASA Tech. Memo.*, TM-83289, 1982.
- Toon, O. B., P. Hamill, R. P. Turco, and J. Pinto, Condensation of HNO<sub>3</sub> and HCl in the winter polar stratosphere, *Geophys. Res. Lett.*, **13**, 1284–1287, 1986.
- Williams, W. J., J. J. Kusters, and D. G. Murcray, Nitric acid column densities over Antarctica, *J. Geophys. Res.*, **87**, 8976–8980, 1982.
- WMO, Atmospheric ozone 1985: Assessment of our understanding of the process controlling its present distribution and change, *Rep. 16*, World Meteorol. Organ, Geneva, Switzerland, 1986.

A. Goldman, D. G. Murcray, F. J. Murcray, and F. H. Murcray, Physics Department, University of Denver, Denver, CO 80208.  
C. P. Rinsland, Atmospheric Sciences Division, NASA Langley Research Center, Hampton, VA 23665.

(Received May 5, 1987;  
revised August 11, 1987;  
accepted August 12, 1987.)



## QUANTIFICATION OF HCl FROM HIGH RESOLUTION INFRARED SOLAR SPECTRA OBTAINED

AT THE SOUTH POLE IN DECEMBER 1986

A. Goldman, F.J. Murcray, F.H. Murcray, and D.G. Murcray

Department of Physics, University of Denver

**Abstract** - Ground-based infrared solar spectra at  $0.02\text{ cm}^{-1}$  resolution obtained at the Amundsen-Scott South Pole station in December 1986 have been analysed for the atmospheric content of HCl. Nonlinear least-squares spectral fitting applied to the spectra yields a total HCl column amount of  $(6.4 \pm 0.8) \times 10^{15}\text{ molec/cm}^2$ , most being stratospheric. This amount is larger than that extrapolated from earlier results on the latitudinal distribution of atmospheric HCl.

This Letter reports the determination of HCl total column amount above the South Pole, from ground based solar spectra observations made at the Amundsen-Scott station (altitude 2.85km) in December 1986, by F.J.M. and F.H.M. The spectra were recorded with a  $0.02\text{ cm}^{-1}$  resolution Michelson type interferometer, the same system used to record many balloon-borne, ground based and laboratory spectra by the University of Denver atmospheric spectroscopy group. The South Pole solar spectra were obtained during November 26 - December 3, 1986 and covered large portions of the  $3\text{--}15\text{ }\mu\text{m}$  region. The nearly constant solar zenith angle allowed the co-adding of several spectral scans from a single day for improved signal to noise ratio. The data analysis methods and spectroscopic data base used are similar to those used previously [Goldman et al., 1983, Goldman et al., 1986], applying nonlinear least-squares spectral fitting for the quantification of HCl. Radiosonde ascents from the South Pole (kindly provided by NOAA, Boulder, Colorado) were used to establish the atmospheric temperature-pressure profiles.

Figure 1 shows a typical analysis of the  $2923\text{--}2929\text{ cm}^{-1}$  region, which is dominated by strong  $\text{CH}_4$  lines with some weak  $\text{H}_2\text{O}$  lines, surrounding the quite isolated  $\text{H}^{35}\text{Cl R1}$  line at  $2925.9\text{ cm}^{-1}$ . For the present analysis, the  $\text{CH}_4$  line parameters were updated [Rothman et al., 1987], but for consistency of comparisons with other recent studies, the previous HCl line parameters were retained (however, the updated HCl parameters lead to only 1% decrease in the column amount). The residual phase distortions, not fully accounted for by the fitted synthetic spectrum, required a more specific fitting for the  $\text{H}^{35}\text{Cl R1}$  line over a narrower interval. This is presented in Figure 2, which also shows a small asymmetry in the spectral profile (probably due to incomplete adjustment of the instrument). The narrow interval analysis (with larger weight assigned to the high wavenumber half of the line)

yields a total HCl column amount of  $(6.4 \pm 0.8) \times 10^{15}\text{ molec/cm}^2$ , most of which is stratospheric, as concluded from spectral fittings with various HCl and temperature-pressure profiles [Goldman et al., 1986]. The HCl in these spectra being mostly stratospheric could have been expected for a high observation point in a low tropopause region such as the south pole. However, the sensitivity of the current spectra (at  $0.02\text{ cm}^{-1}$  resolution and a single solar zenith angle) to the altitude distribution of HCl is limited [Goldman et al., 1983]. Several other HCl lines are quite isolated on the South Pole spectra, such as the R1 and P2  $\text{H}^{35}\text{Cl}$  lines, and these lead to practically the same HCl column amounts. The complete set of the South Pole solar spectra in the  $3\text{ }\mu\text{m}$  region, collected during the week of the measurements, shows no significant change in the HCl amounts.

This is the first HCl measurement reported from the South Pole and is of particular interest to current studies of the chemistry and dynamics of the Antarctic atmosphere. Previous measure-

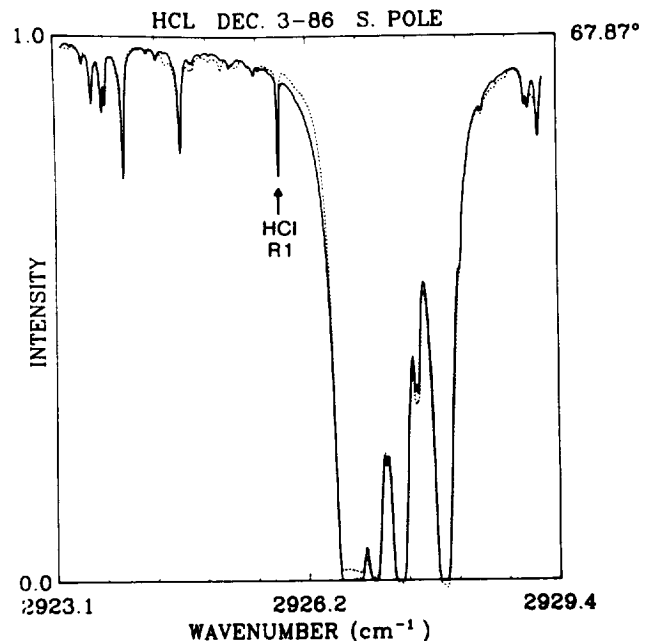


Fig. 1. Solar spectrum (dotted line) obtained from the South Pole on December 3, 1986 and nonlinear least-squares fit (solid line) in the  $2923\text{--}2929\text{ cm}^{-1}$  region. The amplitude is the measured signal, normalized to the maximum envelope value over the interval. The marked feature at  $2925.9\text{ cm}^{-1}$  is the  $(0\text{--}1)\text{ H}^{35}\text{Cl R1}$  line. The solar zenith angle was fixed at  $67.87^\circ$ .

Copyright 1987 by the American Geophysical Union.

Paper Number 7L6546.

0094-8276/87/007L-6546\$03.00

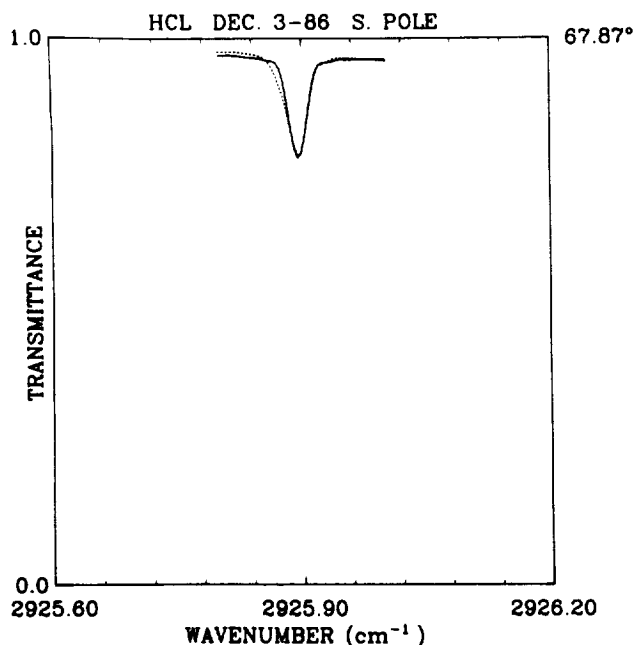


Fig. 2. Nonlinear least-squares fit of the  $\text{H}^{35}\text{Cl}$  R1 absorption line at  $2925.9\text{cm}^{-1}$  in the solar spectrum of Fig. 1. The amplitude is plotted on a transmittance scale. The total HCl column amount of the fitted profile is  $(6.4 \pm 0.8) \times 10^{15}$  molec/cm<sup>2</sup>.

ments and assessments [Mankin et. al., 1983, Molina et. al., 1985] of the latitudinal dependence of stratospheric HCl show total column values above 12km increasing from  $0.7 \times 10^{15}$  molec/cm<sup>2</sup> near the equator, to  $2.7 \times 10^{15}$  molec/cm<sup>2</sup> at 70°N, with an extrapolated value of  $3.4 \times 10^{15}$  molec/cm<sup>2</sup> at 90°N. South latitude measurements [Girard et. al., 1983] of HCl column above 11.5km show values increasing from  $0.8 \times 10^{15}$  molec/cm<sup>2</sup> at 1°S to  $2.7 \times 10^{15}$  molec/cm<sup>2</sup> at 60°S, implying a symmetrical North-South distribution for these latitudes. While there are unresolved difficulties in assessing the tropospheric HCl content and variability, it has been established that most of the HCl total column is stratospheric, and that it has been increasing with time, at an annual rate of 5% per year.

The present result for the column amount of HCl above the South Pole is larger than the extrapolated values from the northern or southern latitude's results, even if we assume a temporal increase of 5% per year as has been reported by Mankin et al [1983]. It is probably characteristic of the Antarctic atmosphere at the end of the period of the spring ozone depletion.

Work is in progress on the quantification of several other atmospheric trace constituents observable in the 1986 South Pole Solar spectra

reported here. Further measurements need to be made for monitoring HCl and other species during the ozone depletion periods.

**Acknowledgments.** This research was supported in part by the National Science Foundation Division of Polar Programs, and in part by the Fluorocarbon Program Panel of the Chemical Manufacturers Association. Acknowledgment is made to the National Center for Atmospheric Research, which is supported by NSF, for computer time used in this research. Discussions with W.G. Mankin on the trends of stratospheric HCl are acknowledged.

## References

- Girard, A., G. Fergant, L. Gramont, O. Lado-Borodowsky, J. Laurent, S. Le Boiteux, M.P. Lemaître and N. Louisnard, Latitudinal Distribution of Ten Stratospheric Species Deduced from Simultaneous Spectroscopic Measurements, *J. Geophys. Res.*, **88**, 5377-5392, 1983.
- Goldman, A., F.G. Fernald, F.J. Murcray, F.H. Murcray, and D.G. Murcray, Spectral Least Squares Quantification of Several Atmospheric Gases from High Resolution Infrared Solar Spectra Obtained at the South Pole, *J. Quant. Spectrosc. Radiat. Transfer*, **29**, 189-204, 1983.
- Goldman, A., F.J. Murcray, R.D. Blatherwick, and D.G. Murcray, Quantification of HCl from High Resolution Ground-Based Infrared Solar Spectra in the  $3000\text{cm}^{-1}$  Region, *J. Quant. Spectrosc. Radiat. Transfer*, **36**, 385-387, 1986.
- Mankin, W.G., and M.T. Coffey, Latitudinal Distributions and Temporal Changes of Stratospheric HCl and HF, *J. Geophys. Res.*, **88**, 10,776-10,784, 1983.
- Molina, M.J., R. deZafra, P. Fabian, C.B. Farmer, W.G. Mankin, N.D. Sze, J. Waters and R.J. Zander, Halogenated Species, Chap. 11 in *Atmospheric Ozone, 1985: Assessment of our Understanding of the Processes Controlling its Present Distribution and Change*, WMO Report No. 16; WMO, B.P. 5, Geneva, Switzerland, 1986.
- Rothman, L.S., R.R. Gamache, A. Goldman, L.R. Brown, R.A. Toth, H. Pickett, R.P. Poynter, J.- M. Flaud, C. Camy-Peyret, A. Barbe, N. Husson, M.A.H. Smith and C.P. Rinsland, *The HITRAN Database: 1986 Edition*, in press, *Appl. Opt.*, 1987.
- A. Goldman, F.J. Murcray, F.H. Murcray, and D.G. Murcray, Department of Physics, University of Denver, Denver, CO 80208

(Received March 20, 1987;  
accepted April 20, 1987.)



UPPER LIMITS FOR STRATOSPHERIC  $\text{H}_2\text{O}_2$  and  $\text{HOCl}$  FROM HIGH  
RESOLUTION BALLOON-BORNE INFRARED SOLAR ABSORPTION SPECTRAJ. C. Larsen<sup>1</sup>, C. P. Rinsland<sup>2</sup>,  
A. Goldman<sup>3</sup>, D. G. Murcray<sup>3</sup>, and F. J. Murcray<sup>3</sup><sup>1</sup>SASC Technologies, Inc., Hampton, VA<sup>2</sup>Atmospheric Sciences Division, NASA Langley Research Center, Hampton, VA<sup>3</sup>University of Denver, Denver, CO

**Abstract.** Solar absorption spectra from two stratospheric balloon flights have been analyzed for the presence of  $\text{H}_2\text{O}_2$  and  $\text{HOCl}$  absorption in the 1230.0 to 1255.0  $\text{cm}^{-1}$  region. The data were recorded at 0.02  $\text{cm}^{-1}$  resolution during sunset with the University of Denver interferometer system on October 27, 1978 and March 23, 1981. Selected spectral regions were analyzed with the technique of nonlinear least squares spectral curve fitting. Upper limits of 0.33 ppbv for  $\text{H}_2\text{O}_2$  and 0.36 ppbv for  $\text{HOCl}$  near 28 km are derived from the 1978 flight data while upper limits of 0.44 ppbv for  $\text{H}_2\text{O}_2$  and 0.43 ppbv for  $\text{HOCl}$  at 29.5 km are obtained from the 1981 flight data.

## Introduction

Hydrogen peroxide ( $\text{H}_2\text{O}_2$ ) is thought to play a significant role in the  $\text{HO}_x$  chemical family where it acts as a reservoir and sink gas. The importance of  $\text{HOCl}$  with respect to the diurnal variation of  $\text{ClO}$  in the upper stratosphere has recently been discussed by Ko and Sze [1984]. Several attempts have been made to detect  $\text{H}_2\text{O}_2$ . The most recent is an upper limit of 0.05 ppbv at 26.5 km from spectra obtained with a Fourier transform spectrometer operating in the far-infrared [Chance and Traub, 1984]. A tentative measurement of 1.1 ppbv from 27 to 35 km has been reported by Waters et al. [1981] from the emission of  $\text{H}_2\text{O}_2$  at 204.574 GHz. Analysis of infrared solar absorption spectra obtained with a grating spectrometer yielded an upper limit of 1.0 ppbv at 20 km for  $\text{H}_2\text{O}_2$  [Murcray et al., 1978]. No measurements or attempted measurements of  $\text{HOCl}$  have been reported to our knowledge. Clearly, additional observations are needed to expand the measurement data sets of these two species. This paper describes the analysis carried out to derive upper limit profiles for  $\text{H}_2\text{O}_2$  and  $\text{HOCl}$  from infrared solar spectra obtained during two stratospheric balloon flights.

## Observations and Spectral Analysis

Spectra were recorded at 0.02  $\text{cm}^{-1}$  resolution with a Michelson interferometer during two balloon flights from Alamogordo, NM (32.8°N, 106.0°W) on October 27, 1978 and March 23, 1981 from float altitudes of 39.1 km and 33.5 km, respectively. Selected flight spectra have been published in an atlas along with the positions and identifications of the atmospheric and solar features [Goldman et

al., 1985]. For each flight, a sequence of scans obtained during sunset was selected for analysis to provide altitude coverage from the balloon float altitude down to approximately 23 km.

The spectral data were analyzed with the technique of nonlinear least squares curve fitting [cf., Goldman et al., 1980]. There are several advantages in using this technique in an upper limit study. Since the profiles of the major absorbers can be obtained from the fitting process, the contribution of the weak interfering lines of these gases can be properly included in the analysis. The analysis also defines the background level, the noise level of the spectrum, and the effective instrument line shape.

National Meteorological Center pressure-temperature profiles were assumed in the ray-tracing calculations. Mixing ratios of  $\text{CH}_4$ ,  $\text{N}_2\text{O}$  and  $\text{CO}_2$  were included as unknowns in the fitting procedure. To simulate the absorption of  $\text{H}_2\text{O}_2$  the 30°S profile for April (equivalent to September, 30°N) from Miller et al. [1981] was multiplied by a factor of 3.1 to yield a peak mixing ratio of 0.64 ppbv near 33 km.

Except as noted below, the line parameters were taken from the 1982 AFGL compilations [Rothman et al., 1983a, b]. Recent laboratory measurements of air-broadened  $\text{CH}_4$  half-widths [C. Rinsland, unpublished data, 1984] and the positions and intensities of weak hot band and  $^{13}\text{CH}_3\text{D}$  lines [L. Brown, private communication, 1984] have been added to the set of line parameters. The  $\text{H}_2\text{O}_2$  line intensities in the AFGL compilation were multiplied by 0.78 to account for hot bands which were present in the room temperature integrated intensity measurements of Valero et al. [1981] but not included in the normalization of the relative intensities [J. Hillman, private communication, 1985]. Estimates of the line parameter uncertainties are developed in a following section.

The selection of the 1230.0 to 1255.0  $\text{cm}^{-1}$  region for analysis was based on a tradeoff between maximizing the expected absorption of  $\text{H}_2\text{O}_2$  and  $\text{HOCl}$  and minimizing the interference from  $\text{CH}_4$ ,  $\text{N}_2\text{O}$  and  $\text{CO}_2$ . Narrow window regions covering the stronger features of both gases were identified and are listed in Table 1. These regions were first surveyed for the presence of  $\text{H}_2\text{O}_2$  or  $\text{HOCl}$  by comparing the fits obtained with and without simulated absorption of these gases. From these results, a single region for each gas was selected for detailed study from which the altitude dependent upper limit was derived. The line parameters for the spectral features used in each region are listed in Table 2.

Figure 1 shows the fitting results for the 93.6° scan (1978 flight) with the mixing ratio of  $\text{H}_2\text{O}_2$  set to zero in all layers. The observed spectrum has been normalized to the highest

Copyright 1985 by the American Geophysical Union.

Paper number 5L6634

0094-8276/85/005L-6634\$03.00

TABLE 1. Spectral Regions (cm<sup>-1</sup>) Considered in this Study

H <sub>2</sub> O <sub>2</sub>	HOCl
1241.2-1242.5	1231.0-1232.0
1242.9-1244.0	1233.0-1234.9*
1246.6-1247.4*	1250.0-1251.0
1248.2-1249.4	1254.0-1254.8
1250.0-1255.0	

\*Selected for Detailed Study

intensity in the region. The line identifications [Goldman et al., 1985] are indicated. The two weak features indicated with question marks persist over several scans and are also present in the 1981 flight spectra. They appear to be real and not noise but identification of these features has not yet been possible. The standard deviation of the fit is 0.44%. The larger amplitude residuals are due to minor inadequacies in the modeling of the instrument line shape and the complex channel spectra present in the data. Figure 2 shows a fit in the same region except that H<sub>2</sub>O<sub>2</sub> absorption has been simulated using the scaled H<sub>2</sub>O<sub>2</sub> mixing ratio profile. The background level and slope and the amplitude, period and phase of the channel spectra were constrained to the values obtained from the fit without H<sub>2</sub>O<sub>2</sub> absorption. The simulated H<sub>2</sub>O<sub>2</sub> absorption features (arrows) are clearly above the noise level. Analysis of the other window regions for the 1978 flight yielded similar results. Coincidences between very weak spectral features and the simulated H<sub>2</sub>O<sub>2</sub> absorption occurred occasionally in both data sets but identification of a consistent series of H<sub>2</sub>O<sub>2</sub> lines was not possible.

The altitude dependent mixing ratio upper limit is derived as follows. For each scan a known column amount of H<sub>2</sub>O<sub>2</sub> is placed in the tangent layer and the fit repeated. The H<sub>2</sub>O<sub>2</sub> column amount is then adjusted to reduce the depth of the simulated H<sub>2</sub>O<sub>2</sub> absorption to the local peak-to-peak noise level. To illustrate this procedure horizontal dashed lines are drawn on the residual plot of Figure 1 near the strongest H<sub>2</sub>O<sub>2</sub> feature to define the peak-to-peak noise level (~0.8%). The H<sub>2</sub>O<sub>2</sub> residual in Figure 2 is almost 2.0% so the H<sub>2</sub>O<sub>2</sub> column amount would have to be decreased by a factor of 2.5 in this example to reduce the depth of the H<sub>2</sub>O<sub>2</sub> absorption to the peak-to-peak noise level. Note that this procedure is equivalent to requiring the H<sub>2</sub>O<sub>2</sub> feature to have a depth of 4 times the standard deviation ( $\sigma$ ) of the local noise. We feel that this procedure produces a

conservative upper limit since an absorption feature greater than 4 $\sigma$  could be positively detected in most cases. An upper limit average mixing ratio for each scan is calculated by assuming the entire H<sub>2</sub>O<sub>2</sub> absorber amount is contained in a 5-km thick tangent layer. To account for experimental uncertainties, the estimated error shown in Table 3 has been added to the average mixing ratio value to obtain the final upper limit estimate. The resulting upper limit profile for the 1978 flight is plotted in Figure 3 at the air-mass-weighted effective altitudes for the 5-km thick layers. Figure 3 also contains the upper limit profile derived from the 1981 flight data. Although the noise level in these spectra is slightly lower than that in the 1978 flight data, this improvement is offset by a slightly degraded instrument resolution.

The same analysis procedure was carried out for HOCl using the spectral regions listed in Table 1. As with H<sub>2</sub>O<sub>2</sub>, the simulated HOCl absorption lines occasionally coincided with weak spectral features, but we were unable to positively detect HOCl. The inferred upper limit profiles are shown in Figure 4. The noise levels in all scans but one are similar to those found in the noisiest scan in the H<sub>2</sub>O<sub>2</sub> region. This decreased sensitivity tends to cancel the improvement expected from the greater HOCl intensities. The overall effect results in HOCl upper limit profiles similar to those for H<sub>2</sub>O<sub>2</sub>.

#### Error Analysis

The primary sources of error are the viewing geometry and the spectral line parameters used in

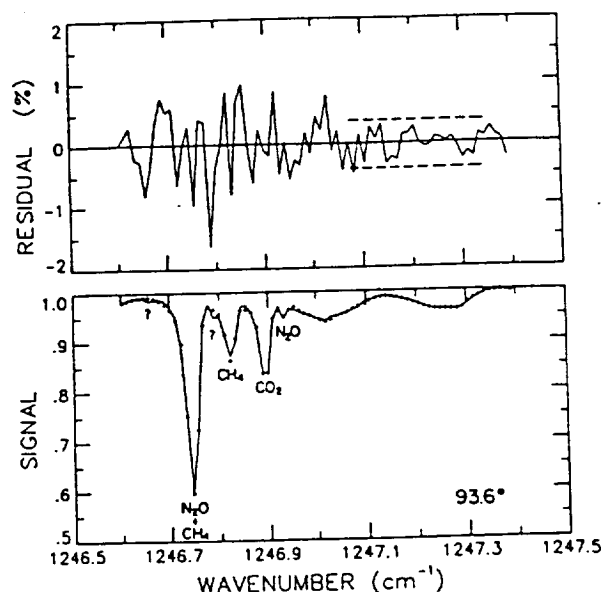


Fig. 1. Comparison between a solar absorption spectrum (solid line) obtained at an astronomical zenith angle of 93.6° (27.1 km tangent altitude, 1978 flight) and a least-squares best fit to the data (crosses). Residuals are shown in the upper portion of the figure (observed-calculated). Horizontal dashed lines indicate the peak-to-peak noise level near the strongest H<sub>2</sub>O<sub>2</sub> feature. Spectral identifications are given below the corresponding features.

TABLE 2. Spectral Line Parameters Adopted in This Study

	Wavenumber cm <sup>-1</sup>	Intensity(296°) cm/molec	J'K'K" A C	J''K''K''' A C
H <sub>2</sub> O <sub>2</sub>	1247.1660	0.788E-20	9 1 9	10 1 10
	1247.1810	0.235E-19	9 1 8	10 1 9
HOCl	1234.6251	0.146E-19	3 0 3	4 0 4
	1234.6313	0.146E-19	6 2 4	7 2 5
	1234.6316	0.146E-19	6 2 5	7 2 6

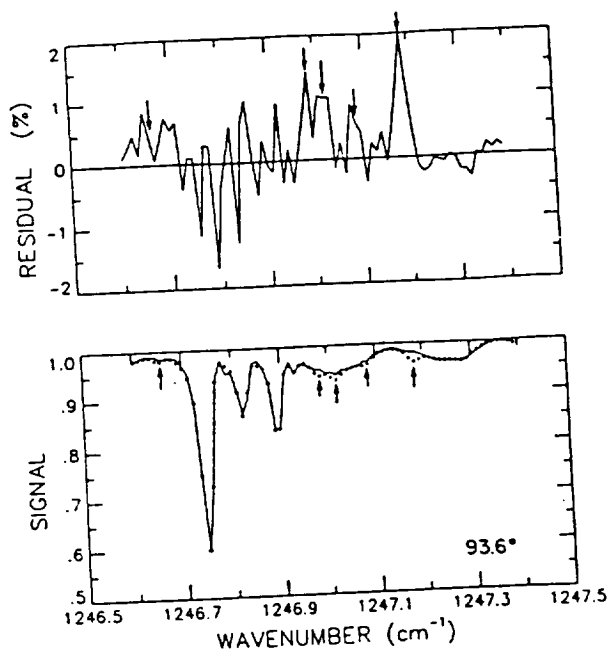


Fig. 2. Similar to Figure 1 except that simulated H<sub>2</sub>O<sub>2</sub> absorption using a scaled photochemical model profile (see text) is included in the calculations. Arrows indicate simulated H<sub>2</sub>O<sub>2</sub> absorption features.

the simulations. We will assume that the errors are independent of one another with normal distributions so that the total error due to a combination of errors may be obtained from the square root of the sum of the squares (RSS) of the individual values. Estimates of the measurement uncertainties due to the viewing geometry are shown in Table 3. Line intensities for both species on the 1982 AFGL compilation were calculated by normalizing theoretically calculated relative intensities with laboratory measurements of the total band intensity. The total band intensity of H<sub>2</sub>O<sub>2</sub> [Valero et al., 1981] was measured with an accuracy of 5%. We will assume an additional uncertainty of 5% in the total band intensity due to the hot band correction and another 15% uncertainty in the theoretically calculated relative line intensities. For HOCl the total band intensity uncertainty is estimated to be approximately 25% [Su et. al, 1979] and a

TABLE 3. Error Estimates

Geometry Uncertainties		Resulting Error in Mixing Ratio
Balloon Float Altitude <sup>1</sup>	± 0.5km	10.0%
Solar Zenith Angle <sup>1</sup>	± 0.05°	10.0%
RSS Error		14.1%
Line Intensity Uncertainties		RSS Total Error
H <sub>2</sub> O <sub>2</sub>	16.6%	21.8%
HOCl	29.2%	32.4%

<sup>1</sup>Maximum Error in Tangent Layer Air Mass for all Scans in Both Flights

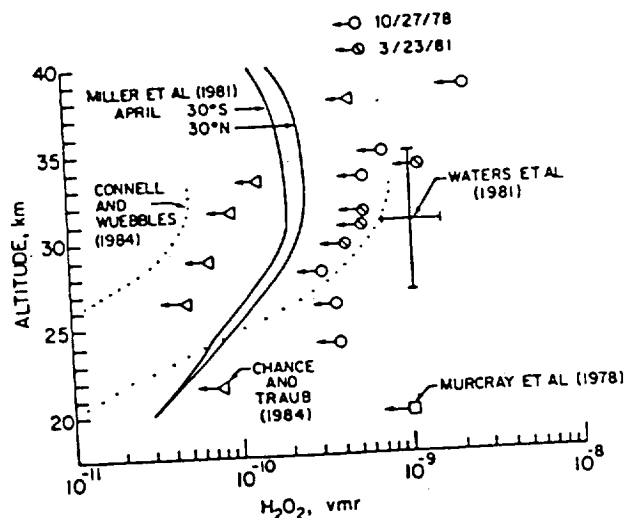


Fig. 3. Mixing ratio profiles from photochemical model calculations and measurements. The circles (1978 flight) and the circles with bars (1981 flight) indicate the H<sub>2</sub>O<sub>2</sub> upper limit profiles obtained in this work.

relative line intensity uncertainty of 15% is assumed. Estimates of the total experimental error are then calculated by combining the line intensity uncertainties and geometry errors as shown in Table 3.

#### Discussion and Conclusions

The H<sub>2</sub>O<sub>2</sub> and HOCl upper limit profiles derived from the two balloon flights are compared to other available measurements and photochemical calculations in Figures 3 and 4. The H<sub>2</sub>O<sub>2</sub> upper limits obtained in this work are consistent with those obtained by Chance and Traub [1984] from their January 1983 far-infrared balloon flight measurements at 32°N. The considerably lower far-infrared upper limit can be attributed to two

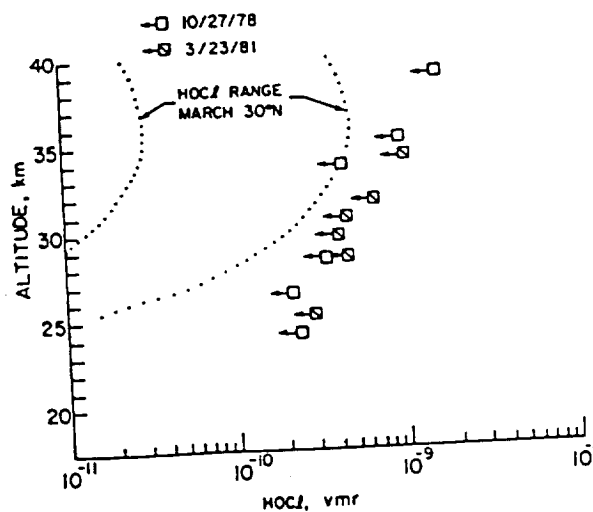


Fig. 4. Mixing ratio profiles from photochemical model calculations and measurements. The squares (1978 flight) and the squares with bars (1981 flight) indicate the HOCl upper limit profiles obtained in this work.

factors: larger line intensities in the far-infrared and the definition of the detection limits. We have used a more conservative 4 $\sigma$  detection limit while Traub and Chance used a 2 $\sigma$  limit. Both the near-infrared and far-infrared upper limits are below the mean mixing ratio obtained by Waters et al. [1981] for February 1981 at 32°N and, hence, it seems unlikely this tentative identification is correct. The dotted profiles in Figure 3 from Connell and Wuebbles [1984] indicate the possible range in calculated  $\text{H}_2\text{O}_2$  profiles taking into consideration uncertainties in the reaction rates controlling  $\text{H}_2\text{O}_2$  and the variability of other species involved in the chemical scheme. The upper limits derived from both flights are consistent with this range from 28 to 35 km.

The upper limits are dependent on the assumptions adopted for the vertical mixing ratio distribution in the upper limit calculation. For example, if we assume the vertical variation of the 30°S Miller et al. mixing ratio profile for  $\text{H}_2\text{O}_2$  and analyze scan 4 of the 1978 flight (tangent altitude = 27.1 km) with the 4 $\sigma$  detection criterion, the resulting upper limit profile has a peak mixing ratio of 0.31 ppbv at 33 km (including total estimated errors).

For  $\text{HOCl}$  only model calculations are available for comparison. Sunset concentrations corresponding to March 30°N conditions [M. Natarajan, private communication, 1985] obtained from diurnal photochemical model calculations using the recommended reaction rates in JPL Publication 83-62 were scaled by a model uncertainty factor of 4 at all altitudes [Callis, private communication, 1985] to produce a minimum and maximum range of calculated  $\text{HOCl}$  mixing ratios (dotted profiles in Figure 4). The model uncertainty factor of 4 results from uncertainties in reaction rates, photolysis cross sections and measurement uncertainties of other species needed to infer  $\text{HOCl}$ . This range would be shifted to slightly lower mixing ratios for October conditions. The measured upper limits from both flights are considerably larger than the maximum expected range except for the October 1978 flight upper limit at 33.6 km which approaches the maximum predicted mixing ratio.

The first balloon flight with the new University of Denver 0.004  $\text{cm}^{-1}$  resolution interferometer is planned for the near future. Spectra obtained with this instrument should improve the detection sensitivity by a factor of 2 to 2.5 for both  $\text{H}_2\text{O}_2$  and  $\text{HOCl}$ . At this level, infrared measurements should provide better constraints on photochemical model predictions of both stratospheric mixing ratio profiles, particularly  $\text{H}_2\text{O}_2$ . Our error analysis indicates that additional measurements of the infrared intensities of both species will be needed for accurate quantitative analysis of these spectra. Values for the  $\text{H}_2\text{O}_2$  and  $\text{HOCl}$  lines in the window regions listed in Table 1 would be most helpful.

**Acknowledgements.** We thank L. Brown of JPL for sending us her unpublished  $\text{CH}_4$  line parameters.

#### References

Chance, K. V. and W. A. Traub, An Upper Limit for

- Stratospheric Hydrogen Peroxide, *J. Geophys. Res.*, **89**, 11655-11660, 1984.
- Connell, P. S. and D. J. Wuebbles, Aspects of the Comparison of Stratospheric Trace Species Measurements with Photochemical Models, *Proceedings of the Quadrennial Ozone Symposium*, edited by C. S. Zerefos and A. Ghazi, 61-65, D. Reidel, Hingham, Mass., 1984.
- Goldman, A., R. D. Blatherwick, F. J. Murcray, J. W. VanAllen, F. H. Murcray, and D. G. Murcray, "New Atlas of Stratospheric IR Absorption Spectra," University of Denver, 1985.
- Goldman, A., D. G. Murcray, F. J. Murcray, and E. Niple, High Resolution IR Balloon-Borne Solar Spectra and Laboratory Spectra in the  $\text{HNO}_3$  1720- $\text{cm}^{-1}$  Region: An Analysis, *Appl. Opt.*, **19**, 3721-3724, 1980.
- Ko, M. K. W. and N. D. Sze, Diurnal Variation of  $\text{ClO}$ : Implications for the Stratospheric Chemistries of  $\text{ClONO}_2$ ,  $\text{HOCl}$  and  $\text{HCl}$ , *J. Geophys. Res.*, **89**, 11619-11632, 1984.
- Miller, C., D. L. Filkin, A. J. Owens, J. M. Steed, and J. P. Jesson, A Two-Dimensional Model of Stratospheric Chemistry and Transport, *J. Geophys. Res.*, **86**, 12039-12065, 1981.
- Murcray, D. G., W. J. Williams, D. B. Barker, A. Goldman, C. Bradford and G. Cook, Measurements of Constituents of Interest in the Chemistry of the Ozone Layer Using IR Techniques, *Proceedings of the WMO Symposium on the Geophysical Aspects and Consequences of Change in the Composition of the Stratosphere*, WMO No. 511, 61-68, Toronto, June, 1978.
- Rothman, L. S., R. R. Gamache, A. Barbe, A. Goldman, J. R. Gillis, L. R. Brown, R. A. Toth, J.-M. Flaud, and C. Camy-Peyret, AFGL Atmospheric Absorption Line Parameters Compilation: 1982 Edition, *Appl. Opt.*, **22**, 2247-2256, 1983a.
- Rothman, L. S., A. Goldman, J. R. Gillis, R. R. Gamache, H. M. Pickett, R. L. Poynter, N. Husson, and A. Chedin, AFGL Trace Gas Compilation: 1982 Version, *Appl. Opt.*, **22**, 1616-1627, 1983b.
- Su, F., J. G. Calvert, C. R. Lindley, W. M. Uselman and J. H. Shaw, A Fourier Transform Infrared Kinetic Study of  $\text{HOCl}$  and its Absolute Integrated Infrared Band Intensities, *J. Phys. Chem.*, **83**, 912-920, 1979.
- Valero, F. P., D. Goorvitch, F. S. Bonomo, and R. W. Boese, Intensity of the Hydrogen Peroxide  $\nu_6(b)$  Band Around 1266  $\text{cm}^{-1}$ , *Appl. Opt.*, **20**, 4097-4101, 1981.
- Waters, J. W., J. C. Hardy, R. F. Jarnot, and H. M. Pickett, Chlorine Monoxide Radical, Ozone and Hydrogen Peroxide: Stratospheric Measurements by Microwave Limb Sounding, *Science*, **214**, 61-64, 1981.

J. C. Larsen, SASC Technologies, Inc.,  
17 Research Drive, Hampton, VA, 23666  
A. Goldman, D. G. Murcray, F. J. Murcray,  
Dept. of Physics, Univ. of Denver, Denver, CO,  
80208  
C. P. Rinsland, Mail Stop 401A,  
NASA Langley Research Center, Hampton, VA, 23665

(Received July 9, 1985;  
accepted August 1, 1985.)





# Tentative Identification of the $780\text{-cm}^{-1}$ $\nu_4$ Band $Q$ Branch of Chlorine Nitrate in High-Resolution Solar Absorption Spectra of the Stratosphere

C. P. RINSLAND,<sup>1</sup> A. GOLDMAN,<sup>2</sup> D. G. MURCRAY,<sup>2</sup> F. J. MURCRAY,<sup>2</sup> F. S. BONOMO,<sup>2</sup> R. D. BLATHERWICK,<sup>2</sup> V. MALATHY DEVI,<sup>3</sup> M. A. H. SMITH,<sup>1</sup> and P. L. RINSLAND<sup>4</sup>

Absorption by the  $Q$  branch of the  $\nu_4$  band of  $\text{ClONO}_2$  at  $780.2\text{ cm}^{-1}$  has been tentatively identified in a series of  $0.02\text{-cm}^{-1}$ -resolution balloon-borne solar absorption spectra of the stratosphere. The spectral data were recorded at sunset from a float altitude of  $33.5\text{ km}$  during a balloon flight from Holloman Air Force Base ( $32.8^\circ\text{N}$ ,  $106.0^\circ\text{W}$ ) near Alamogordo, New Mexico, on March 23, 1981. A preliminary  $\text{ClONO}_2$  vertical profile has been determined from the stratospheric spectra by using the technique of nonlinear least squares spectral curve fitting and new spectroscopic parameters deduced from high-resolution laboratory spectra of  $\text{ClONO}_2$  and  $\text{O}_3$ .

## INTRODUCTION

Models of the photochemistry of the stratosphere predict that chlorine nitrate ( $\text{ClONO}_2$ ) is an important temporary reservoir of stratospheric chlorine. At night,  $\text{ClO}$  is believed to combine in a three-body reaction with  $\text{NO}_2$  to form chlorine nitrate. During daylight, chlorine nitrate is destroyed by photolysis to form free chlorine and  $\text{NO}_3$ .

As a technique, infrared spectroscopy has the potential to provide important quantitative measurements of stratospheric chlorine nitrate. Laboratory measurements have shown that relatively strong  $Q$  branches of  $\text{ClONO}_2$  occur at  $780$ ,  $809$ ,  $1292$ , and  $1738\text{ cm}^{-1}$  [Miller *et al.*, 1967; Graham *et al.*, 1977; Murcray and Goldman, 1981; Murcray *et al.*, 1984]. Evidence for absorption by the  $1292\text{-cm}^{-1}$   $Q$  branch has been reported on the basis of analysis of a series of  $0.02\text{-cm}^{-1}$ -resolution balloon-borne stratospheric solar absorption spectra recorded during sunset from a float altitude of  $39.1\text{ km}$  [Murcray *et al.*, 1979]. The  $780\text{-cm}^{-1}$  spectral region was covered at a resolution of  $0.2\text{ cm}^{-1}$  during an earlier balloon flight [Williams *et al.*, 1976]. Ozone and carbon dioxide have many absorption lines in this spectral region, and under the spectral resolution achieved on that flight, it was not possible to separate absorption that might be due to  $\text{ClONO}_2$  from absorption by interfering lines [Murcray *et al.*, 1977]. Since that time, additional laboratory spectra of  $\text{ClONO}_2$  and  $\text{O}_3$  and new stratospheric solar absorption spectra have been recorded that cover the  $780\text{-cm}^{-1}$  region at higher resolution. In the present paper we report a detailed study of these spectra that has led to the tentative identification of the  $\nu_4$  band  $Q$  branch of  $\text{ClONO}_2$  as a significant contributor to the observed stratospheric absorption near  $780.21\text{ cm}^{-1}$ .

## LABORATORY SPECTRA

Several samples of chlorine nitrate were given to the University of Denver in 1976 by L. C. Glasgow of E. I. DuPont de Nemours and Co. These samples were prepared by reaction of  $\text{Cl}_2\text{O}$  with  $\text{N}_2\text{O}_5$  at low temperature (typically starting at  $-78^\circ\text{C}$  and slowly heating to  $0^\circ\text{C}$  in 15 hours) [Schmeisser, 1967] and were purified by trap-to-trap distillations. A cold trap at  $-78^\circ\text{C}$  eliminated  $\text{HNO}_3$ ,  $\text{NO}_2$ , and  $\text{N}_2\text{O}_5$ , and a cold trap at  $-118^\circ\text{C}$  eliminated  $\text{Cl}_2$  (L. C. Glasgow, private communication, 1976) [Zahniser *et al.*, 1977; Kurylo, 1977]. Analysis of the samples by IR, UV, and mass spectroscopy showed the purity to be greater than 99%, with the principal contaminant being  $\text{NO}_2$  [Birks *et al.*, 1977].

Upon receipt of the  $\text{ClONO}_2$  (in a stainless steel cylinder), it was kept at  $-196^\circ\text{C}$  with liquid nitrogen until ready for use. The entire sample was transferred by warming the cylinder to  $-84^\circ\text{C}$  (ethyl acetate slush bath), passing the  $\text{ClONO}_2$  vapor through a  $-118^\circ\text{C}$  trap (ethyl bromide slush), and freezing in a glass trap at  $-196^\circ\text{C}$  under high vacuum. All of the glass was flamed out whenever  $\text{ClONO}_2$  was to be handled in the vacuum system. Cells and the glass vacuum system were conditioned with  $\text{ClONO}_2$  at several torrs pressure for 10–15 min, followed by pumping to high vacuum, and repeating this procedure if it was felt to be necessary.

If the sample was stored for prolonged periods (1 year or more) or had been thawed and refrozen many times, it was checked by distilling at  $-84^\circ\text{C}$ , discarding the first and last cuts, and keeping about 90% of the sample as a heart cut. This cut was evaluated by making an infrared spectrum to observe impurity bands and by measuring the vapor pressure at one or more temperatures. The vapor pressure was measured either with a slush of cyclopentanone at  $-51.3^\circ\text{C}$ , where  $\text{ClONO}_2$  has a vapor pressure of 13 torr, or with ethyl acetate at  $-84^\circ\text{C}$ , where  $\text{ClONO}_2$  has a vapor pressure of 1.5 torr. The chlorine nitrate was so stable in storage and handling that this occasional distillation was adequate to keep the sample pure.

Infrared cell windows for  $\text{ClONO}_2$  were  $\text{AgCl}$ ,  $\text{NaCl}$ , or  $\text{CaF}_2$ , of which the latter two were least affected by the sample. So long as the cell and vacuum system were kept absolutely dry by pumping and flame desiccation,  $\text{ClONO}_2$  could be kept in the cell for many hours with little deterioration. This stability of anhydrous  $\text{ClONO}_2$  has been noted by

<sup>1</sup> Atmospheric Sciences Division, NASA Langley Research Center, Hampton, Virginia.

<sup>2</sup> Department of Physics, University of Denver, Denver, Colorado.

<sup>3</sup> Department of Physics, College of William and Mary, Williamsburg, Virginia.

<sup>4</sup> Flight Electronics Division, NASA Langley Research Center, Hampton, Virginia.

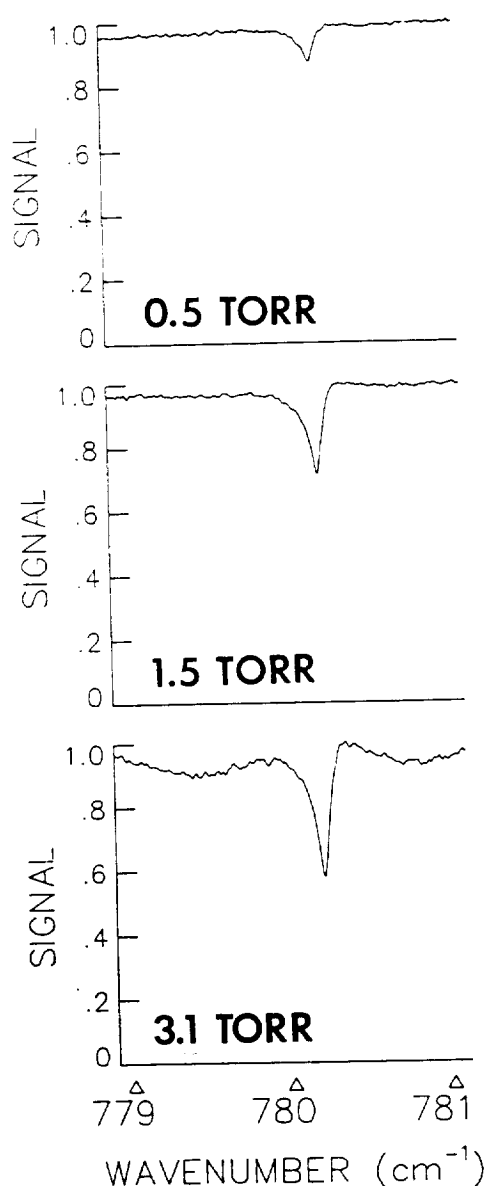


Fig. 1. Room-temperature laboratory spectra of  $\text{ClONO}_2$  in the region of the  $\nu_4$  band  $Q$  branch. All three scans were obtained at  $\approx 0.02\text{-cm}^{-1}$  resolution and with a 5-cm absorption path.

others [Kurylo, 1977; Molina *et al.*, 1977; Kurylo and Manning, 1977].

Figure 1 shows the  $779.0\text{--}781.0\text{ cm}^{-1}$  region of laboratory spectra obtained with  $\text{ClONO}_2$  pressures of 0.5, 1.5, and 3.1 torr in a 5-cm cell. The spectral data were recorded at room temperature and at  $0.02\text{-cm}^{-1}$  resolution with the same Fourier transform interferometer used to obtain the stratospheric spectra. Even at the high resolution and low pressures of these measurements, the  $Q$  branch is unresolved but considerably broader than the width of the instrumental line shape function. The  $Q$  branch feature is clearly asymmetric: the absorption decreases more rapidly on the high wave number side of the peak than on the low wave number side. Additional spectra obtained with a new interferometer at  $0.004\text{-cm}^{-1}$  resolution also do not show any fine structure within the  $Q$  branch. The background in the 1.5-torr and 3.1-torr scans show a sinusoidal modulation in this interval with a period of  $\approx 1.3\text{ cm}^{-1}$ . In the analysis this modulation has

been modeled as a channel spectrum with the expressions derived by Niple *et al.* [1980]. However, since the amplitude of the modulation increases with  $\text{ClONO}_2$  pressure, it may be due at least in part to unresolved weaker  $\text{ClONO}_2$  absorption. No modulation was detected in the background of the 0.5-torr scan. Plots of the  $750\text{--}840\text{ cm}^{-1}$  and  $1250\text{--}1330\text{ cm}^{-1}$  intervals of the 1.5-torr and 3.1-torr scans are contained in a compilation of high-resolution infrared spectra of atmospheric interest [Murray *et al.*, 1984].

Unfortunately, line positions and assignments have not been reported for the  $\nu_4$  band of  $\text{ClONO}_2$ . For this reason we were forced to adopt an empirical model to analyze the laboratory measurements. The unresolved shape in the  $Q$  branch region is simple, and after trying a number of empirical forms, a good fit to the data was obtained by using a model with only four adjustable parameters. The values of these parameters have been determined from the analysis of the data with the technique of nonlinear least squares spectral curve fitting. From these results a listing of parameters for "artificial"  $\text{ClONO}_2$  lines has been generated for use in the analysis of the stratospheric spectra.

We have assumed that the absorption by the  $\nu_4$  band  $Q$  branch can be represented by a series of evenly spaced Voigt lines with an exponential distribution of intensities. The position  $\nu$  ( $\text{cm}^{-1}$ ) of line  $n$  has been calculated from

$$\nu = \nu_0 + \delta n \quad (1)$$

where

$$n = 0, \pm 1, \pm 2, \pm 3, \pm 4, \dots \quad (2)$$

A value of  $0.002\text{ cm}^{-1}$  has been assumed for the line spacing

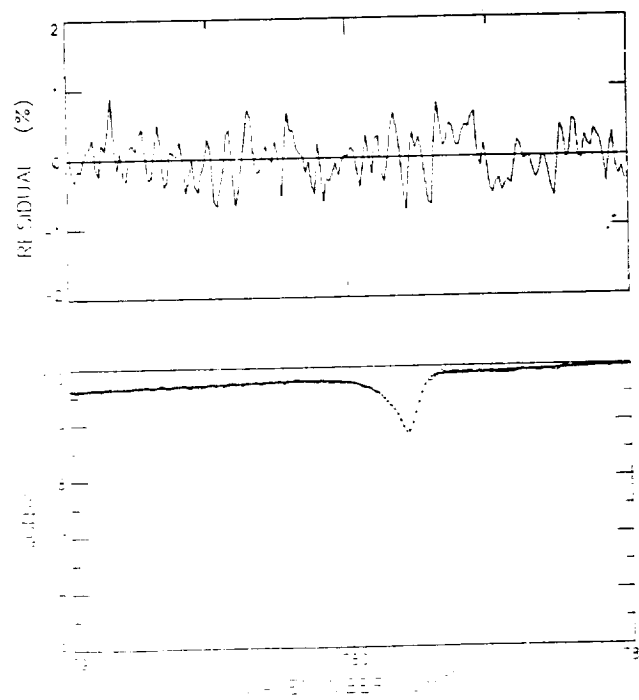


Fig. 2. Comparison in the region of the  $\nu_4$  band  $Q$  branch of  $\text{ClONO}_2$  between a laboratory spectrum recorded at room temperature with about 0.5 torr of  $\text{ClONO}_2$  in a 5-cm absorption path (solid line) and a least squares best fit to the data (crosses). The measured spectrum has been normalized to the peak intensity in the interval: the upper half of the spectrum is plotted. Residuals (observed-calculated) are plotted at top.

8. The intensity  $S$  (in  $\text{cm}^{-1}/\text{molecule cm}^{-2}$  at 296 K) has been calculated from

$$\begin{aligned} S &= S_v \exp [A(\nu - \nu_0)] & \nu < \nu_0 \\ S &= S_v & \nu = \nu_0 \\ S &= S_v \exp [-B(\nu - \nu_0)^2] & \nu > \nu_0 \end{aligned} \quad (3)$$

In (3),  $\nu_0$  corresponds to the position of the absorption peak of the  $\text{ClONO}_2$   $Q$  branch. The values of  $\nu_0$ ,  $S_v$ ,  $A$ , and  $B$  have been derived from the least squares fits. Since neither quantum assignments nor measurements of the temperature dependence of the absorption are available, an arbitrary value of  $300 \text{ cm}^{-1}$  has been adopted for the lower state energy of all lines. Runs were made with Lorentz half-widths  $\gamma_0$  of 0.1 and  $0.2 \text{ cm}^{-1} \text{ atm}^{-1}$  at 296 K to study the sensitivity of the results to the assumed half-width.

The analysis of the laboratory spectra with the technique of nonlinear least squares spectral curve fitting followed the procedures described in previous papers [Goldman et al., 1980; Rinsland et al., 1983a]. In the present work a subroutine was added to the analysis program to generate a line list from values for  $\nu_0$ ,  $S_v$ ,  $A$ , and  $B$ . These four parameters and two parameters for the background level and slope were adjusted simultaneously in fitting the 182 measured intensities between 779.0 and  $781.0 \text{ cm}^{-1}$ . For the 1.5 and 3.1 torr scans, parameters for the amplitude and phase of the channel spectrum were added; the period was held fixed at  $1.3 \text{ cm}^{-1}$  in the analysis. The Fourier transform technique [cf. Niple et al., 1980] has been used to convolve the infinite resolution transmittances with the instrument line shape function.

Figure 2 shows the agreement between the 0.5-torr laboratory spectrum and the least squares best fit to the data. The differences in the upper panel are observed minus calculated intensities expressed as a fraction of the maximum measured

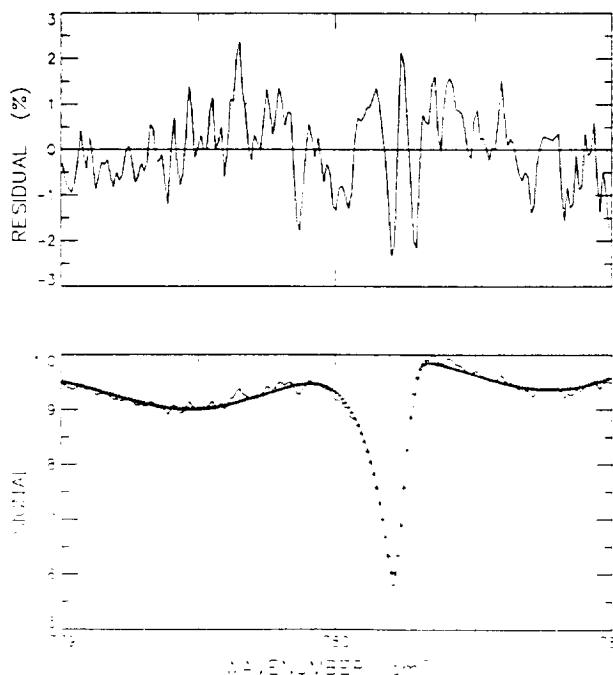


Fig. 3. Comparison in the region of the  $\nu_4$  band  $Q$  branch of  $\text{ClONO}_2$  between a laboratory spectrum recorded at room temperature with about 3.1 torr of  $\text{ClONO}_2$  in a 5-cm absorption path (solid line) and a least squares best fit to the data (crosses). The format is the same as in Figure 2.

intensity in the fitted region. The rms residual is 0.3% for this scan. The fits are slightly poorer for the 1.5-torr and 3.1-torr scans. The rms residuals for these spectra are 0.5% and 0.9%, respectively. The fit to the 3.1-torr scan is shown in Figure 3. As can be seen from this plot, the calculated spectrum slightly underestimates the absorption in the strongest part of the  $Q$  branch. For all three scans the rms residual of the fit was the same for assumed Lorentz half-widths of 0.1 and  $0.2 \text{ cm}^{-1} \text{ atm}^{-1}$  at 296 K.

Table 1 presents the parameters derived from the fits to the three laboratory scans, assuming half-widths  $\gamma_0$  of 0.1 and  $0.2 \text{ cm}^{-1} \text{ atm}^{-1}$  at 296 K for all lines and that the measured pressure is due entirely to  $\text{ClONO}_2$ . Also listed is the sum of individual line intensities  $S_{\text{tot}}$ . For the three scans the parameter values derived from the fits are nearly independent of the assumed half-width. The agreement between the values determined from the 0.5-torr and 1.5-torr scans is quite good, but slightly lower values for  $S_v$  and  $S_{\text{tot}}$  were obtained from the analysis of the 3.1-torr scan. This difference is believed to result from the inadequacies in the simple model used to analyze the laboratory spectra and possibly from the decay of  $\text{ClONO}_2$  in the sample. Nitric acid was observed as a decomposition product in the 3.1-torr scan. The positions of  $\text{HNO}_3$  features in the  $865\text{--}875 \text{ cm}^{-1}$  region were measured from this scan and compared to calibrated positions from the University of Denver Atlas of Stratospheric Absorption Spectra [Goldman et al., 1983a]. The average of the differences between the observed and reference positions was used as a calibration factor for the determination of  $\nu_0$  for this scan. Absorption by  $\text{HNO}_3$  was not detected in the 0.5-torr scan and is very weak in the 1.5-torr scan. The values of  $\nu_0$  listed for these two scans are uncalibrated.

Because of sample impurities, the values of  $S_v$  and  $S_{\text{tot}}$  in Table 1 are lower limits. To obtain an estimate of the partial pressure of  $\text{HNO}_3$ , the  $\text{HNO}_3$  features identified in the 3.1-torr spectrum were analyzed with the technique of nonlinear least squares spectral curve fitting. A  $\text{HNO}_3$  volume mixing ratio of  $0.04 \pm 0.01$  was derived from a fit to the  $867.0\text{--}870.0 \text{ cm}^{-1}$  region with the line parameters generated by Goldman et al. [1984]. Absorption by  $\text{HNO}_3$  is much weaker in the 1.5-torr scan. A volume mixing ratio of  $0.03 \pm 0.015$  was estimated for this spectrum from the absorption depth of the  $\nu_3$  band  $Q$  branch at  $879 \text{ cm}^{-1}$ . An upper limit of 0.10 for the  $\text{HNO}_3$  volume mixing ratio in the 0.5-torr spectrum was estimated from the same spectral region. No other contaminants have been identified in the  $750\text{--}1300 \text{ cm}^{-1}$  region covered by these spectra. However, similar laboratory spectra of  $\text{ClONO}_2$  covering the  $1200\text{--}2000 \text{ cm}^{-1}$  region show absorption by the  $\nu_3$  band of  $\text{NO}_2$  near  $1600 \text{ cm}^{-1}$ . Also, it is important to note that contaminants with only weak or diffuse bands in the intervals covered in the laboratory spectra would not be identified.

We compared the peak absorptivity ( $a = \ln(I_0/I)/pl$ ) derived from our laboratory spectra (assuming pure  $\text{ClONO}_2$  samples) with the values measured by Graham et al. [1977] after they corrected for the decay of  $\text{ClONO}_2$ . The values measured from our 0.5-torr, 1.5-torr, and 3.1-torr scans are 38, 35, and  $28 \text{ cm}^{-1} \text{ atm}^{-1}$  at STP, respectively. The lower value for the 3.1-torr scan probably results from the difficulty in determining the background (100% transmittance) level caused by the stronger absorption of  $\text{ClONO}_2$  in that spectrum. The absorptivities derived by Graham et al. are a

TABLE 1. Parameters Obtained From the Analysis of the ClONO<sub>2</sub> Laboratory Spectra

Parameter	0.5-torr ClONO <sub>2</sub>		1.5-torr ClONO <sub>2</sub>		3.1-torr ClONO <sub>2</sub>	
	$\gamma_0 = 0.1$	$\gamma_0 = 0.2$	$\gamma_0 = 0.1$	$\gamma_0 = 0.2$	$\gamma_0 = 0.1$	$\gamma_0 = 0.2$
$\nu_0$	780.1999*	780.2013*	780.2058*	780.2035*	780.2138†	780.2114†
<i>A</i>	13.5056	13.3694	11.1699	11.3714	11.6282	11.8626
<i>B</i>	0.8503	0.9296	0.9063	0.8348	0.7993	0.7232
<i>S<sub>v</sub></i>	$2.798 \times 10^{-21}$	$2.813 \times 10^{-21}$	$2.604 \times 10^{-21}$	$2.576 \times 10^{-21}$	$2.117 \times 10^{-21}$	$2.106 \times 10^{-21}$
<i>S<sub>tot</sub></i>	$1.636 \times 10^{-19}$	$1.629 \times 10^{-19}$	$1.703 \times 10^{-19}$	$1.688 \times 10^{-19}$	$1.377 \times 10^{-19}$	$1.376 \times 10^{-19}$

For all three spectra, absorption path is 5 cm,  $T = 22^\circ\text{C}$ . Units are  $\text{cm}^{-1} \text{atm}^{-1}$  at 296 K for the half-width  $\gamma_0$ ,  $\text{cm}^{-1}$  for  $\nu_0$ , cm for *A* and *B*, and  $\text{cm}^{-1}/\text{molecule cm}^{-2}$  at 296 K for *S<sub>v</sub>* and *S<sub>tot</sub>*.

\* Uncalibrated position.

† Calibrated position, see text.

strong function of the resolution of the measurements. At the highest resolution ( $0.0625 \text{ cm}^{-1}$ ) a value of  $49 \text{ cm}^{-1} \text{atm}^{-1}$  at STP was determined for pure ClONO<sub>2</sub>. This result is about 25% higher than our values. In assessing this difference it should be noted that Graham et al. assign an uncertainty of 25% to their results and that our measurements were obtained at a resolution of  $0.02 \text{ cm}^{-1}$ . The integrated intensity obtained in the present study is considerably larger than that derived from earlier spectra obtained at the University of

Denver [Murcray et al., 1977]. This difference is believed to result from an unrecognized contaminant in the samples used in the previous analysis.

#### OZONE LABORATORY SPECTRA

Laboratory spectra of nearly pure ozone were recorded at room temperature and  $0.005 \text{ cm}^{-1}$  resolution with the Fourier transform spectrometer in the McMath solar telescope complex at the National Solar Observatory. Ozone for the

TABLE 2. Line Positions (in  $\text{cm}^{-1}$ ) and Relative Intensities (in  $10^{-23} \text{ cm}^{-1}/\text{molecule cm}^{-2}$  at 296 K) of <sup>16</sup>O<sub>3</sub> Lines Derived From the Laboratory Spectra

Line Position	Identification							Line Intensity	
	Band	<i>J'</i>	<i>K<sub>a</sub>'</i>	<i>K<sub>c</sub>'</i>	<i>J''</i>	<i>K<sub>a</sub>''</i>	<i>K<sub>c</sub>''</i>	This Study	AFGL 82†
779.02223	1	12	12	0	12	11	1	1.581	2.39
779.06323	1	44	3	41	43	2	42	0.697	0.447
779.10190	2	29	9	21	28	8	20	1.261	1.19
779.27584	1	56	6	50	55	5	51	0.505	0.288
779.33482	1	27	9	19	26	8	18	22.37	21.7
779.42190	1	37	8	30	36	7	29	9.897	8.27
779.42983	1	48	7	41	47	6	42	2.78†	1.60
779.59247	1	18	10	8	17	9	9	30.50	34.5
779.60550	2	20	10	10	19	9	11	2.382†	2.01
779.66458	1	23	15	9	24	14	10	0.245	0.307
779.78004	1	49	7	43	48	6	42	1.813	1.33
779.81850	2	11	11	1	10	10	0	2.342†	2.55
780.06893	1	28	9	19	27	8	20	21.03	19.8
780.10383	1	38	8	30	37	7	31	8.742	7.22
780.21479	2	41	8	34	40	7	33	0.469	0.312
780.36367	1	19	10	10	18	9	9	29.48†	32.6
780.53592	2	31	9	23	30	8	22	1.187	0.966
780.61120	2	12	11	1	11	10	2	2.062	2.45
780.64074	1	50	7	43	49	6	44	1.717	1.10
780.65060	1	14	14	0	15	13	3	0.664	0.03
780.77906	1	39	8	32	38	7	31	7.680	6.27
780.79861	1	29	9	21	28	8	20	19.75	17.9
780.83348	1	51	7	45	50	6	44	1.541	0.901
781.11794	2	22	10	12	21	9	13	1.752	1.77
781.13098	1	20	10	10	19	9	11	27.90	30.7
781.18143	1	11	11	1	10	10	0	29.56	39.1
781.24633	2	32	9	23	31	8	24	0.728	0.865
781.39999	2	13	11	3	12	10	2	1.555	2.35
781.45019	1	40	8	32	39	7	33	7.067	5.42
781.50707	2	43	8	36	42	7	35	0.269†	0.253
781.52387	1	30	9	21	29	8	22	17.92	16.2
781.77864	1	50	13	37	50	12	38	0.316	0.329
781.80619	1	53	7	47	52	6	46	1.139	0.599
781.83912	1	52	7	45	51	6	46	1.210	0.736
781.86810	2	23	10	14	22	9	13	1.850	1.64
781.89446	1	21	10	12	20	9	11	26.77	28.8
781.95190	2	33	9	25	32	8	24	0.992	0.773
781.97890	1	12	11	1	11	10	2	29.62	37.6

\* Band 1,  $\nu_2$ ; band 2,  $2\nu_2 - \nu_2$ .

† Absolute intensity values from the 1982 compilation [Rothman et al., 1983].

‡ Relative intensity value is less accurate because of overlapping absorption.

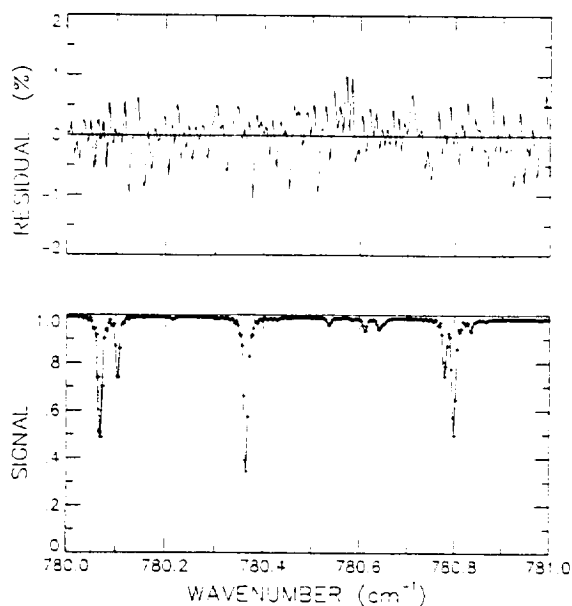


Fig. 4. Comparison in the 780.0–781.0-cm<sup>-1</sup> region between a laboratory spectrum recorded at room temperature with about 23.2 torr of ozone in a 50-cm cell (solid line) and a least squares best fit to the data (crosses). The format is the same as in Figure 2.

measurements was generated from natural oxygen by using the silent electric discharge technique [cf. *Meunier et al.*, 1982]. In the present analysis, spectra obtained with total pressures of 8.1 torr and 23.2 torr in a 50-cm absorption path have been analyzed. Because of the problem of ozone decomposition, only relative intensities and line positions have been derived from the data. For both scans a signal-to-rms noise ratio in the 780-cm<sup>-1</sup> region of  $\approx 500$  was achieved with an integration time of 1 hour.

The 779.0–782.0 cm<sup>-1</sup> region was covered by analyzing consecutive segments 1 cm<sup>-1</sup> wide with the technique of nonlinear least squares spectral curve fitting. Starting values for the ozone positions and intensities were obtained from the 1982 Air Force Geophysics Laboratory (AFGL) line parameters compilation [*Rothman et al.*, 1983a]. These parameters were calculated as described by *Goldman et al.* [1982]. Lines with absorption depths at line center of less than  $\approx 1\%$  of the background intensity were included in the calculations but with position and intensity values fixed to those listed in the 1982 AFGL compilation. For the 23.2-torr scan this criterion corresponds to an intensity value of about  $2.0 \times 10^{-24}$  cm<sup>-1</sup>/molecule cm<sup>-2</sup> at 296 K. A self-broadened half-width of 0.115 cm<sup>-1</sup> atm<sup>-1</sup> at 296 K was assumed for the weaker O<sub>3</sub> lines. This value is the average of 22 measurements obtained in the 3- and 5- $\mu$ m regions by *Meunier et al.* [1982]. The half-widths of the stronger lines were included as free parameters in the analysis.

Table 2 presents the line positions and relative intensities derived from the analysis of the 23.2-torr scan. The identifications are based on the comparisons of the measured positions and intensities with values in the 1982 AFGL compilation [*Rothman et al.*, 1983a]. The line positions have been calibrated with respect to accurate N<sub>2</sub>O line positions in the 1255–1282 cm<sup>-1</sup> region from the tables of *Olson et al.* [1981]. For the stronger unblended lines the positions determined from the 8.1-torr and 23.2-torr spectra agree to  $\approx 0.00015$  cm<sup>-1</sup>. The accuracy of the positions decreases with line intensity and is estimated to be  $\approx 0.003$  cm<sup>-1</sup> for the

weaker and blended lines. Based also on the comparison of the results obtained from the 8.1-torr and 23.2-torr spectra, the relative intensities are estimated to be accurate to 10% for strong, unblended lines and to about 50% for the weakest lines. Although only relative line intensities have been determined from the lab spectra, 26 of the 38 measured values are within 30% of absolute intensities in the 1982 AFGL compilation (also listed in Table 2). However, some significant discrepancies can be noted; in particular the line

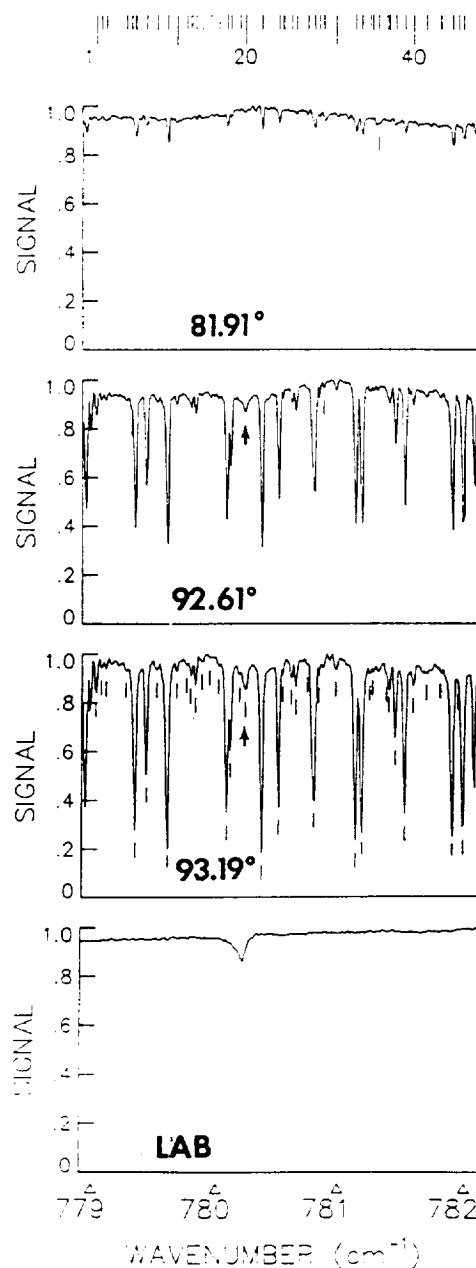


Fig. 5. Stratospheric and laboratory spectra (0.02-cm<sup>-1</sup> resolution) in the region of the  $\nu_2$  band Q branch of ClONO<sub>2</sub>. The upper three spectra were recorded at the float altitude of 33.5 km during a balloon flight on March 23, 1981, from Holloman Air Force Base, New Mexico, with the University of Denver interferometer system. The astronomical zenith angles are indicated for each scan. The tangent heights are 27.0 km and 23.8 km for the 92.61° and 93.19° scans, respectively. The bottom scan was obtained in the laboratory at room temperature with about 0.5 torr of ClONO<sub>2</sub> in a 5-cm absorption path. Arrows in two of the stratospheric scans indicate an absorption feature tentatively identified as a blend of CO<sub>2</sub>, ClONO<sub>2</sub>, and O<sub>3</sub>.

TABLE 3. Parameters for the March 23, 1981, University of Denver Balloon Flight

Parameter	Value
Latitude	32.8°N
Longitude	106.0°W
Float altitude	33.5 ± 0.5 km
Scan time	40 s
Maximum path difference	50 cm
Field of view	8 arcmin
Pointing accuracy	~0.05°
Spectral coverage	740 – 1350 cm <sup>-1</sup>
Continuum signal to rms noise at 780 cm <sup>-1</sup>	150
Tropopause height	10.4 km

at 780.6505 cm<sup>-1</sup> is observed to be much stronger than indicated by the 1982 AFGL compilation. Perhaps, this difference is due to an overlapping line from an unassigned hot band. The line widths measured from the 23.2-torr scan are only slightly larger than the width of the instrument line shape function; for this reason the self-broadened widths derived from this spectrum are believed to be not very accurate and are not reported.

The weak O<sub>3</sub> line at 780.2148 cm<sup>-1</sup> occurs close to the position of the strongest absorption by ClONO<sub>2</sub>. When the 23.2-torr laboratory spectrum is plotted on an expanded vertical scale, there is an indication that this line is blended with about a factor of 2 weaker, unassigned O<sub>3</sub> line centered near 780.206 cm<sup>-1</sup>. This weaker feature is near the noise level of the present data; higher signal to noise and increased resolution are needed to determine if this weaker O<sub>3</sub> line is real.

Figure 4 shows the agreement obtained in the 780.0–781.0 cm<sup>-1</sup> region between the 23.2-torr laboratory and best-fit calculated spectra. As in Figure 3 the residuals (observed-calculated) in the upper panel are expressed as a percentage of the maximum intensity measured in the region. The rms residual is 0.35%, very close to the noise level of the data. Similar results were obtained from the fits to the 779.0–780.0 cm<sup>-1</sup> and 781.0–782.0 cm<sup>-1</sup> regions.

#### STRATOSPHERIC SPECTRA AND ANALYSIS

The stratospheric solar absorption spectra analyzed in this work were recorded during sunset with a Michelson-type Fourier transform interferometer with an apodized FWHM (full width at half maximum) resolution of 0.02 cm<sup>-1</sup>. The balloon flight was performed from Holloman Air Force Base near Alamogordo, New Mexico, on March 23, 1981. Table 3 summarizes important flight and experimental parameters and their estimated uncertainties.

Figure 5 shows the 779.0–782.0 cm<sup>-1</sup> interval in balloon flight spectra recorded under high sun and low sun conditions and in the 0.5-torr laboratory spectrum of ClONO<sub>2</sub>. The solar and atmospheric features identified in the stratospheric spectra are marked beneath one of the scans and are repeated and numbered at top. Table 4 lists the corresponding line positions and identifications. These identifications are based on comparisons between the observed spectra and simulated spectra generated with the line parameters and vertical profiles discussed below and on the agreement between the measured and reference line positions. An arrow beneath the low sun stratospheric scans indicates the feature corresponding in position to the strongest absorption by the  $\nu_4$  band Q branch of ClONO<sub>2</sub>. Based on the consider-

ations discussed in this section, we tentatively identify this feature as a blend of ClONO<sub>2</sub>, CO<sub>2</sub>, and O<sub>3</sub>. The other identifications, except for a few minor changes, which result from comparisons of the balloon spectra with the new O<sub>3</sub> laboratory spectra, are from the University of Denver Atlas of Stratospheric Solar Absorption Spectra [Goldman *et al.*, 1983a].

Line positions and intensities for O<sub>3</sub> were taken from the analysis of the Kitt Peak laboratory spectra. The transition-dependent air-broadened half-widths calculated recently for 296 K by Gamache *et al.* [1984] were assumed in the analysis (R. R. Gamache, private communication, 1984). For ClONO<sub>2</sub> the line list was calculated with our simple empirical model assuming the values of *A* and *B* derived from fitting the 0.5-torr lab scan with  $\gamma_0 = 0.1$  cm<sup>-1</sup> atm<sup>-1</sup> at 296 K, 1.25 times the value of *S<sub>v</sub>* derived from the same analysis (scaled to agree with the measurements of Graham *et al.* [1977]) and the average of the two calibrated values of  $\nu_0$  determined from the fit to the 3.1-torr lab scan. Line parameters for CO<sub>2</sub>, NO<sub>2</sub>, and HCN were taken from the 1982 Air Force Geo-

TABLE 4. Identification of Atmospheric and Solar Features in the 779.0–781.0 cm<sup>-1</sup> Region

Sequence Number	Position, cm <sup>-1</sup>	Molecular Identification
1	779.021	O <sub>3</sub>
2	779.064	O <sub>3</sub>
3	779.105	O <sub>3</sub>
4	779.263	O <sub>3</sub>
5	779.305	H <sub>2</sub> O
6	779.335	O <sub>3</sub>
7	779.424	O <sub>3</sub>
8	779.508	CO <sub>2</sub> , O <sub>3</sub> ?
9	779.592	O <sub>3</sub>
10	779.667	CO <sub>2</sub> , O <sub>3</sub>
11	779.746	CO <sub>2</sub> , O <sub>3</sub>
12	779.780	O <sub>3</sub>
13	779.818	O <sub>3</sub>
14	779.870	O <sub>3</sub>
15	779.933	O <sub>3</sub>
16	780.004	O <sub>3</sub>
17	780.070	O <sub>3</sub> , CO <sub>2</sub>
18	780.103	O <sub>3</sub>
19	780.180	?
20	780.227	ClONO <sub>2</sub> ?, CO <sub>2</sub> , O <sub>3</sub>
21	780.363	O <sub>3</sub>
22	780.504	CO <sub>2</sub> , O <sub>3</sub>
23	780.540	O <sub>3</sub>
24	780.609	O <sub>3</sub>
25	780.648	O <sub>3</sub>
26	780.741	O <sub>3</sub>
27	780.794	O <sub>3</sub>
28	780.834	O <sub>3</sub>
29	780.871	O <sub>3</sub> , solar OH
30	780.971	CO <sub>2</sub>
31	781.130	O <sub>3</sub>
32	781.180	O <sub>3</sub>
33	781.245	O <sub>3</sub>
34	781.267	CO <sub>2</sub>
35	781.311	O <sub>3</sub> , solar OH
36	781.381	O <sub>3</sub>
37	781.399	O <sub>3</sub>
38	781.450	O <sub>3</sub>
39	781.523	O <sub>3</sub>
40	781.591	O <sub>3</sub> , CO <sub>2</sub>
41	781.692	CO <sub>2</sub> , O <sub>3</sub>
42	781.800	O <sub>3</sub>
43	781.893	O <sub>3</sub> , solar OH
44	781.938	O <sub>3</sub>
45	781.978	O <sub>3</sub>

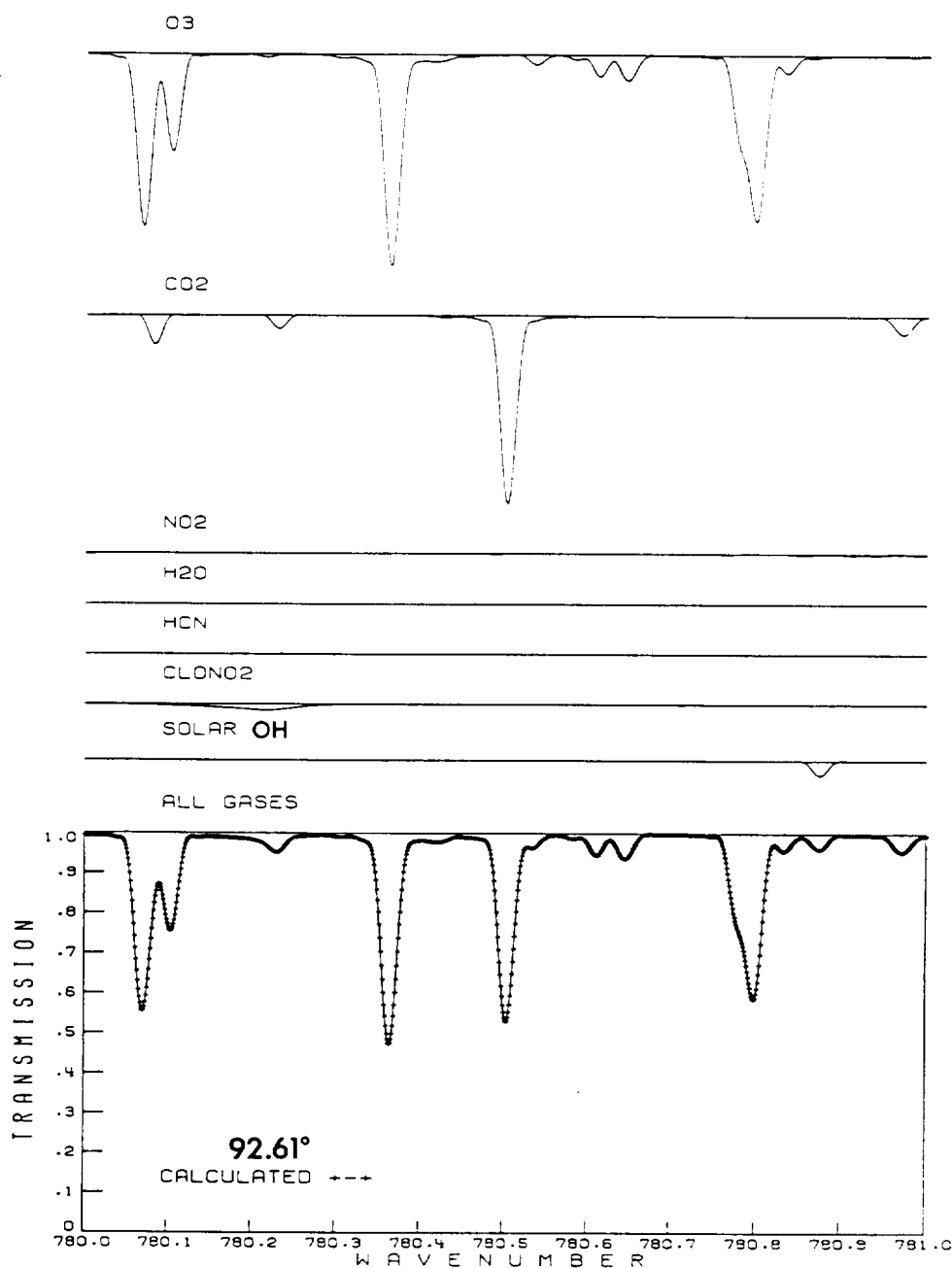


Fig. 6. Simulation of the spectral region containing the  $\text{ClONO}_2$   $\nu_4$  band  $Q$  branch. The upper portion of the plot shows the transmittance spectrum calculated for each gas; the transmittance spectrum for the sum of the gases is plotted at bottom. The vertical scaling for each gas is the same, but the calculated spectra have been offset vertically for clarity. In all cases the infinite resolution spectrum has been convolved with the instrument profile function corresponding to the University of Denver instrument.

physics Laboratory (AFGL) major and trace gas compilations [Rothman *et al.*, 1983a, b]. Several lines of solar OH have been identified in this spectral region [Goldman *et al.*, 1983a]; their absorption has been simulated by assuming a Doppler line shape and the positions and intensities at 6000 K calculated by Goldman *et al.* [1983b]. The temperature dependence of the air-broadened half-width has been assumed to be  $T^{-0.65}$  for  $\text{O}_3$  [Colmont and Monnanteuil, 1984],  $T^{-0.75}$  for  $\text{CO}_2$ , and  $T^{-0.5}$  for the other gases.

A 12-layer model was adopted for the analysis of one high-sun ( $81.91^\circ$ ) and six low-sun spectra. Isothermal layer boundaries were defined by the tangent altitudes of the

refracted rays of the low sun scans (23.8, 27.0, 28.4, 29.6, 30.6, and 33.2 km), the balloon float altitude (33.5 km), and selected points above the balloon (35, 40, 45, 50, 70, and 100 km). The ray-tracing calculations were made with the FSCATM program from FASCOD1B [Gallery *et al.*, 1983], assuming a correlative pressure-temperature profile derived from global satellite and radiosonde measurements (M. Gelman, private communication, 1982).

A simulation of the region containing the  $\text{ClONO}_2$   $\nu_4$  band  $Q$  branch is shown in Figure 6 for conditions corresponding to the  $92.61^\circ$  scan (tangent height, 27.0 km). The absorption by each of the gases is shown in the upper part of the figure.

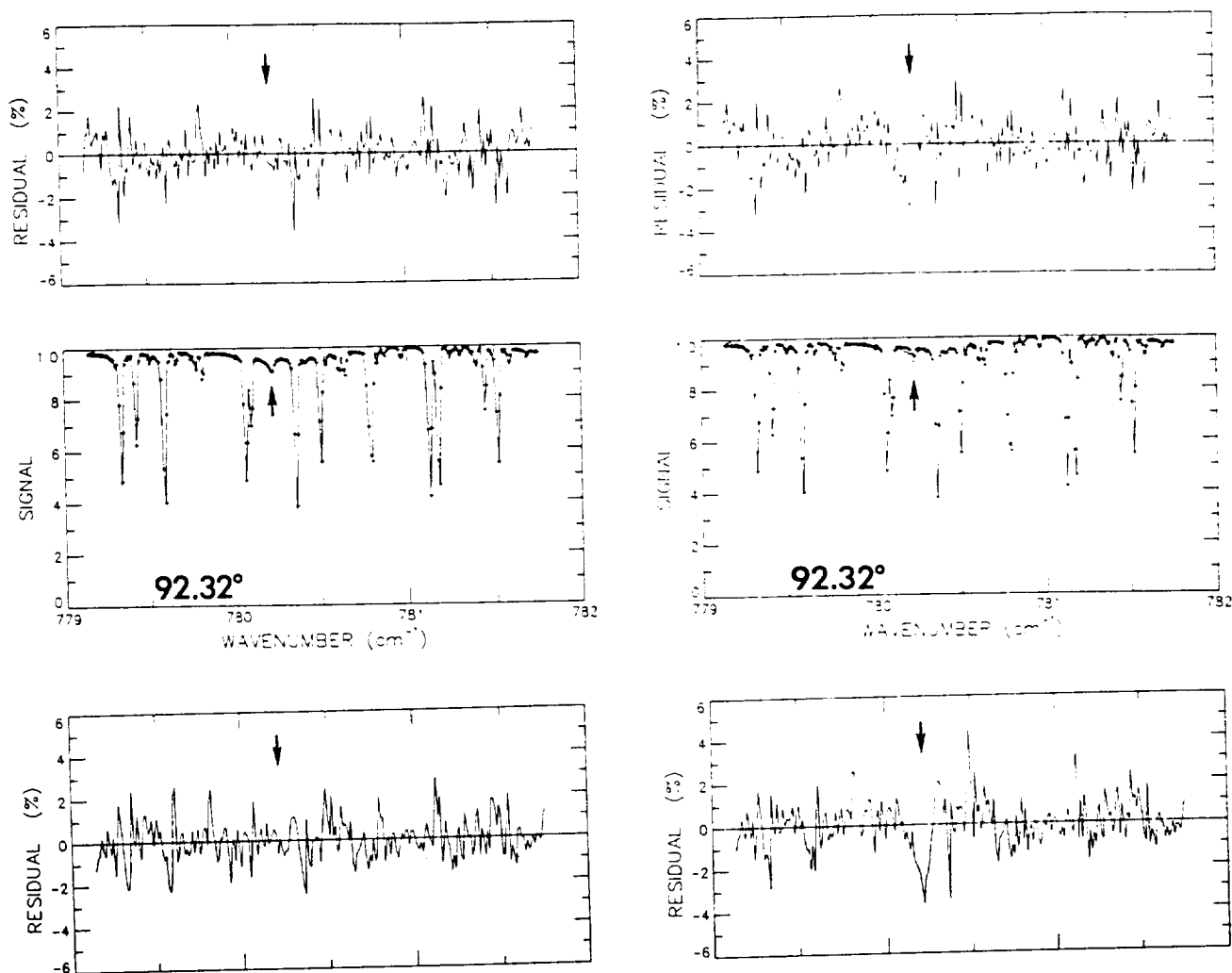


Fig. 7. Fitting results for the 92.32°, 92.61°, and 93.19° stratospheric spectra with  $\text{ClONO}_2$  lines (left) and without  $\text{ClONO}_2$  lines (right) included in the analysis. The measured spectra have been normalized to the peak intensity in the interval; residuals (observed-calculated) are plotted above each scan. Arrows mark the location of the strongest absorption by the  $\text{ClONO}_2$   $\nu_4$   $Q$  branch. The tangent altitudes of the scans (top to bottom) are 28.4, 27.0, and 23.8 km.

The vertical scaling for each gas is the same, but the calculated spectra have been displaced vertically for clarity. At bottom the calculated spectrum obtained with all gases is plotted at the same vertical scale. The average daytime  $\text{ClONO}_2$  profile from the model calculations of Miller *et al.* [1981] and a constant  $\text{CO}_2$  mixing ratio of 325 ppmv have been assumed. The profiles for other gases are from Smith [1982]. The absorption by  $\text{ClONO}_2$  is calculated to be considerably broader than the width of single lines. The  $\text{ClONO}_2$  absorption depth is computed to be 1.5% at the strongest part of the  $Q$  branch. In this region the  $\text{ClONO}_2$  absorption is overlapped by lines of  $\text{CO}_2$  and  $\text{O}_3$ . The  $\text{CO}_2$  line is the stronger of the two, and its position is  $0.018 \text{ cm}^{-1}$  higher than the  $\text{ClONO}_2$  peak at  $780.213 \text{ cm}^{-1}$ . Absorption by  $\text{NO}_2$ ,  $\text{H}_2\text{O}$ , and  $\text{HCN}$  is calculated to be negligible in this interval.

Because of the overlapping absorption by  $\text{CO}_2$  and  $\text{O}_3$ , the region near the  $\text{ClONO}_2$   $\nu_4$  band  $Q$  branch was analyzed with the technique of nonlinear least squares, spectral curve fitting. Details of the application of this procedure to the analysis of University of Denver stratospheric spectra have been described in several previous publications [Niple *et al.*, 1980; Goldman *et al.*, 1980; Rinsland *et al.*, 1982, 1983b]. In

the present work a relatively wide interval ( $779.14\text{--}781.75 \text{ cm}^{-1}$ ) has been included in the fit to improve the accuracy in establishing the background and to permit the comparison of the quality of the fit within and away from the  $\text{ClONO}_2$   $Q$  branch region. In addition to the  $\text{ClONO}_2$  profile, the  $\text{O}_3$  profile was derived from the analysis. However, only the  $\text{O}_3$  profile shape is well determined, since the assumed  $\text{O}_3$  line intensities are relative rather than absolute values. The profiles of  $\text{CO}_2$ ,  $\text{HCN}$ ,  $\text{H}_2\text{O}$ , and  $\text{NO}_2$  were constrained to initial values. Additional parameters were included to model the background level and slope, weak channel spectra (with periods between  $1.1$  and  $2.5 \text{ cm}^{-1}$ ), and minor residual phase distortions in the instrument line shape.

Figure 7 presents the fitting results obtained for the three lowest sun scans with (left panels) and without (right panels)  $\text{ClONO}_2$  lines included in the analysis. The measured intensities have been normalized to the peak intensity in the fitted region. Arrows beneath the spectra and in the residual plots mark the position of the strongest absorption by  $\text{ClONO}_2$ , as determined from the laboratory spectra. Without  $\text{ClONO}_2$  lines the absorption in the  $Q$  branch region is underestimated in the calculated spectra, and a weak broad feature results in all three residual plots. The rms residuals without  $\text{ClONO}_2$



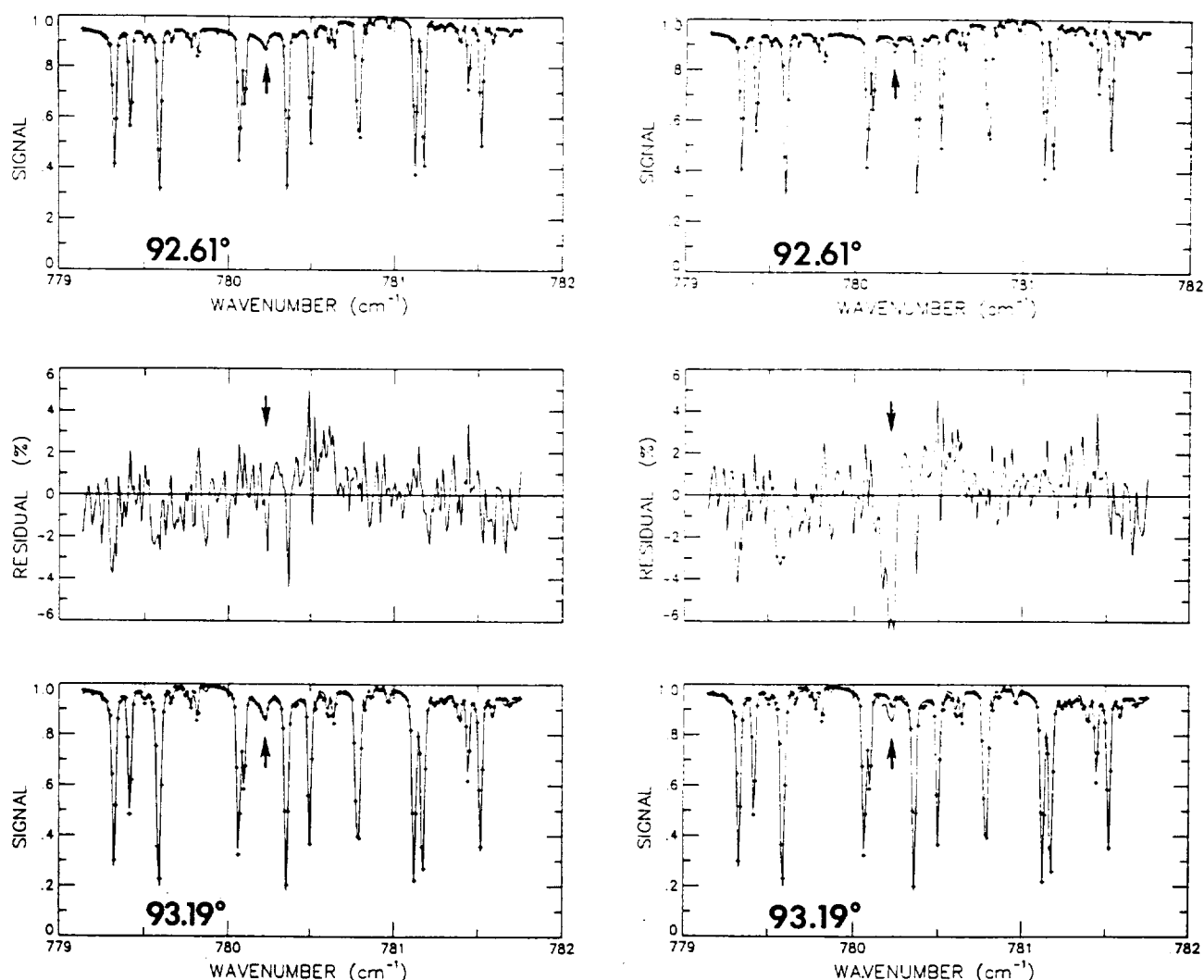


Fig. 7. (continued)

lines in the fit (top to bottom) are 1.0%, 1.1%, and 1.7%. The fits with  $\text{ClONO}_2$  lines included in the analysis are considerably better in the  $\text{ClONO}_2$   $Q$  branch region. The rms residuals with  $\text{ClONO}_2$  lines in the fit (top to bottom) are 0.9%, 1.0%, and 1.4%.

Figure 8 compares the 0.5-torr laboratory spectrum of  $\text{ClONO}_2$  and the residuals obtained for the 92.61° and 93.19° scans without  $\text{ClONO}_2$  lines in the analysis. Despite the difference in the temperature of the laboratory run ( $\approx 22^\circ\text{C}$ ) and that of the stratosphere and the problem of the contribution from the overlapping lines of  $\text{CO}_2$  and  $\text{O}_3$ , there is fairly good agreement in both the position and shape of the broad feature in the residuals and the  $\text{ClONO}_2$  absorption in the laboratory spectrum. The large residuals near  $780.36\text{ cm}^{-1}$  result from errors in fitting a strong  $\text{O}_3$  line; note that these residuals have a sharper appearance than those of the broad feature.

Since  $\text{CO}_2$  and  $\text{O}_3$  lines are calculated to produce discernible absorption near the  $\text{ClONO}_2$   $Q$  branch position, it is important to try to determine if errors in the parameters assumed for these lines could cause the large residuals noted in the fits. The overlapping carbon dioxide line is R29 from the temperature-sensitive 12201-03301 band of  $^{12}\text{C}^{16}\text{O}_2$ . To our knowledge there have not been any recent measure-

ments reported for this band. However, the position for this line in the 1982 AFGL compilation should be accurate to  $0.001\text{ cm}^{-1}$  or better, since the molecular constants for both the upper and lower levels have been derived from numerous experimental measurements [see Rothman et al., 1983a, Table II]. The 1982 AFGL compilation lists three additional lines of this band in the fitted region: R28 at  $779.508\text{ cm}^{-1}$ , R30 at  $780.976\text{ cm}^{-1}$ , and R31 at  $781.692\text{ cm}^{-1}$ . The line positions measured from the stratospheric spectra agree with these values to  $0.001\text{ cm}^{-1}$  for R28 and R31 and to  $0.005\text{ cm}^{-1}$  for R30, which is blended with another  $\text{CO}_2$  line of about the same intensity. Only weak  $\text{O}_3$  lines are listed near these line positions in the 1982 AFGL compilation [Rothman et al., 1983a]. The new  $\text{O}_3$  lab spectra also do not show measurable  $\text{O}_3$  absorption in the vicinity of these  $\text{CO}_2$  lines. Minor contamination of the R28 and R31 lines by  $\text{O}_3$  is likely, however, since an atlas of  $0.04\text{-cm}^{-1}$  resolution laboratory spectra [Damon et al., 1981] obtained with 40 times more  $\text{O}_3$  in the path than used in the Kitt Peak experiment show absorption near the positions of both lines. Despite these limitations, the quality of the fits to all three of these  $\text{CO}_2$  features in the stratospheric spectra suggests that this  $\text{CO}_2$  band has been simulated fairly well in our analysis. Figure 9 shows an example of a fit near the R31 line on an expanded

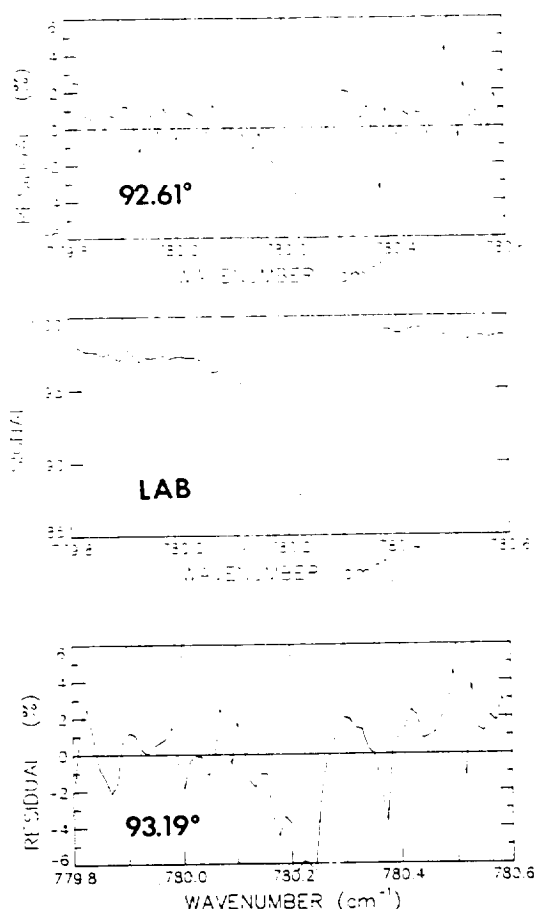


Fig. 8. Comparison in the region of the  $\text{ClONO}_2$   $\nu_4$  band Q branch between the residuals (observed-calculated) obtained without  $\text{ClONO}_2$  lines in the analysis and a room-temperature laboratory spectrum of  $\text{ClONO}_2$  recorded with about 0.5 torr of  $\text{ClONO}_2$  in a 5-cm path. The astronomical zenith angles of the corresponding stratospheric scans are indicated for the residual plots. A calibration factor has been added to the wave numbers to convert from a relative to an absolute scale.

scale. An analysis of the  $\text{CO}_2$  bands in this region is planned (L. R. Brown, private communication, 1984).

The overlapping  $\text{O}_3$  line at  $780.215 \text{ cm}^{-1}$  is very weak in our 23.2-torr laboratory spectrum. To obtain an upper limit for its possible contribution to the absorption, the retrievals were repeated with the intensity of this line increased by a factor of 2. Figure 10 compares the residuals in the  $\text{ClONO}_2$  region with and without the doubling of the  $\text{O}_3$  line intensity. No  $\text{ClONO}_2$  lines were included in the analysis. The changes in the residuals are very small, and thus we conclude that most of the absorption near  $780.2 \text{ cm}^{-1}$  cannot be explained by  $\text{O}_3$ .

The stratospheric spectra were also analyzed assuming the  $\text{O}_3$  line parameters on the 1982 AFGL compilation [Rothman *et al.*, 1983a]. These parameters produce considerably poorer fits to the stratospheric spectra than those obtained with the values listed in Table 2. An extensive analysis of the new  $\text{O}_3$  lab data is in progress.

Of the seven scans analyzed, only the four with the largest zenith angles ( $92.03^\circ$ ,  $92.32^\circ$ ,  $92.61^\circ$ , and  $93.19^\circ$ ) show sufficient absorption to derive quantitative values for  $\text{ClONO}_2$ . The  $92.03^\circ$  scan has been used to determine an average mixing ratio of 0.5 ppbv above the tangent altitude of 29.6 km. The absorption is very weak, and the uncertainty of this

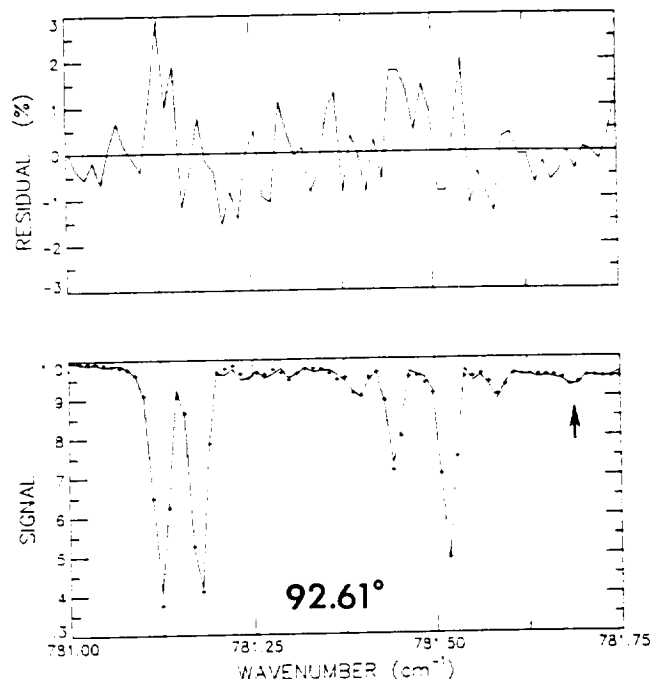


Fig. 9. The R31 line of the 12201-03301 band of  $^{12}\text{C}^{16}\text{O}_2$  (arrow) in measured and least squares, best fit stratospheric spectra. The results displayed were obtained as part of the fit to the  $92.61^\circ$  scan with  $\text{ClONO}_2$  lines included in the analysis.

value is estimated to be  $\pm 80\%$ . Values of 1.1, 1.0, and 0.9 ppbv were retrieved from the  $92.32^\circ$ ,  $92.61^\circ$ , and  $93.19^\circ$  scans, respectively. The uncertainties in these mixing ratios are estimated to be  $\pm 60\%$ . The uncertainties for all four measured values are total uncertainties, which include the effects of the dominant sources of error: (1) influence of instrument noise, (2) the uncertainty in the simulation of the overlapping  $\text{CO}_2$  and  $\text{O}_3$  absorption, (3) the uncertainty in the fit to the background level in the  $\text{ClONO}_2$  region, and (4) the uncertainty in the intensity and shape of the  $\text{ClONO}_2$   $\nu_4$  band Q branch at stratospheric temperatures.

As a check of the results, retrievals were also made using equivalent width measurements. Within the uncertainties the mixing ratios inferred with this procedure were found to be consistent with the values determined from the least squares fits. For example an equivalent width of  $0.00450 \text{ cm}^{-1}$  was measured for the  $780.16\text{--}780.28 \text{ cm}^{-1}$  interval of the  $92.61^\circ$

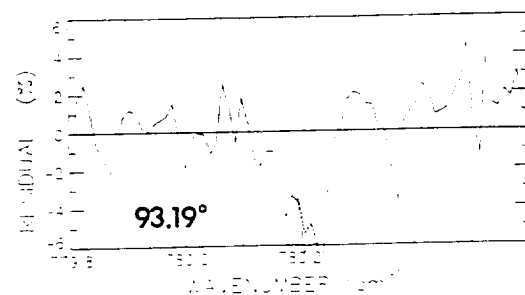


Fig. 10. The effect on the residuals (observed-calculated) of doubling the assumed intensity of the  $780.215\text{-cm}^{-1}$  line of  $\text{O}_3$ . The results are shown for the  $93.19^\circ$  scan (tangent height, 23.8 km). The solid line shows the residuals obtained with the intensity value listed in Table 2. The dashed line indicates the residuals obtained with the  $\text{O}_3$  intensity doubled. For both fits, no  $\text{ClONO}_2$  lines were included in the analysis.

scan (tangent height of 27.0 km). The equivalent widths of the overlapping CO<sub>2</sub> and O<sub>3</sub> lines are calculated to be 0.00066 cm<sup>-1</sup> and 0.00016 cm<sup>-1</sup>, respectively. The difference between the measured equivalent width and the sum of the calculated CO<sub>2</sub> and O<sub>3</sub> equivalent widths is 0.00371 cm<sup>-1</sup>. Using this difference together with an integrated intensity of  $1.38 \times 10^{-19}$  cm<sup>-1</sup>/molecule cm<sup>-2</sup> for ClONO<sub>2</sub> in this region and a total air mass of  $2.83 \times 10^{25}$  molecules cm<sup>-2</sup>, an average mixing ratio of 0.95 ppbv is obtained (assuming the absorption is on the linear part of the curve of growth).

### DISCUSSION

Our analysis has shown that an absorption feature observed near 780.227 cm<sup>-1</sup> in a sequence of stratospheric spectra is too strong and too broad to be attributed solely to known lines of CO<sub>2</sub> and O<sub>3</sub>. Although the additional absorption coincides closely with the ClONO<sub>2</sub>  $\nu_4$  band *Q* branch in position and shape, the identification must be regarded as tentative because of the following considerations:

1. It was not possible to identify the 809-cm<sup>-1</sup> and 1292-cm<sup>-1</sup> bands of ClONO<sub>2</sub> in the same set of spectra. The relatively weak  $\nu_3$  fundamental at 809 cm<sup>-1</sup> falls in a short gap in the flight data caused by the real-time filter used with the University of Denver instrument. High-resolution laboratory spectra [Murcray and Goldman, 1981; Murcray et al., 1984] indicate the  $\nu_2$  fundamental *Q* branch is considerably broader than the *Q* branches of the  $\nu_3$  and  $\nu_4$  bands. The  $\nu_2$  strongest absorption extends over the 1291–1293 cm<sup>-1</sup> region. This region was covered during a balloon flight made on October 27, 1978. A ClONO<sub>2</sub> profile was determined from those data based on the assumption that a broadband absorption occurring in this region was due to ClONO<sub>2</sub> [Murcray et al., 1979]. It should be emphasized that the 1292-cm<sup>-1</sup> band results were based on simple equivalent width estimates and the assumption that all the broadband absorption is due to ClONO<sub>2</sub>. Thus the ClONO<sub>2</sub> profile from this earlier flight is not on as firm a spectroscopic basis as the current analysis. A complete analysis of the 1292-cm<sup>-1</sup> region has not been performed because of the lack of suitable spectroscopic parameters for HNO<sub>3</sub> and ClONO<sub>2</sub> in this region. Current plans call for nonlinear least squares analysis of this region with empirical line parameters for ClONO<sub>2</sub> (similar to those used here for the 780-cm<sup>-1</sup> *Q* branch) and HNO<sub>3</sub> spectroscopic line parameters for which work is in progress (A. Maki, private communication, 1984).

2. The line parameters derived from the new laboratory data for O<sub>3</sub> and ClONO<sub>2</sub> produce considerable improvements in the least squares fits to the stratospheric spectra, but the residual plots indicate that problems remain in modeling the experimental data. The poorest fit is obtained for the 93.19° scan, and for this spectrum the rms residual is about twice the rms-noise of the data. These systematic problems are believed to be due mostly to minor inaccuracies in the assumed line parameters (particularly the positions and intensities of the weaker O<sub>3</sub> lines), and their presence makes it difficult to analyze a feature as weak as the ClONO<sub>2</sub> *Q* branch.

3. A weak line appears at 780.180 cm<sup>-1</sup> in the 93.19° scan and is also observed in the four lower sun scans obtained during this flight (zenith angles of 94.64° to 95.15°, corresponding to tangent altitudes of 14.2 km to 8.1 km). A line from the 2 $\nu_2$ - $\nu_2$  band of O<sub>3</sub> is listed at 780.177 cm<sup>-1</sup> in the 1982 AFGL compilation [Rothman et al., 1983a], but its

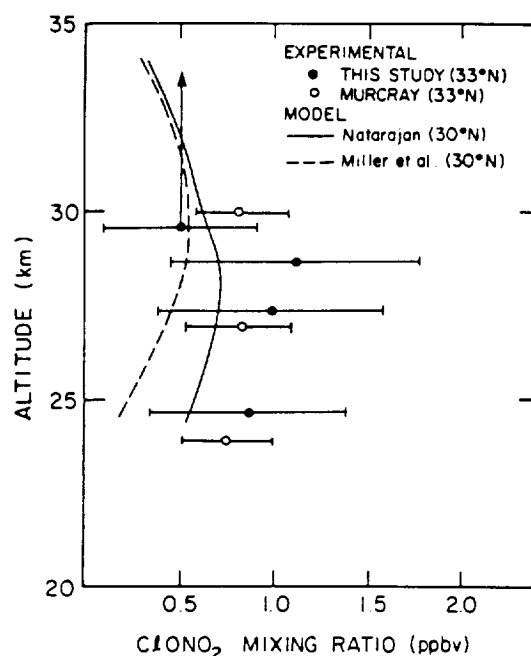


Fig. 11. Comparison of measured profiles (from this study and from the study of Murcray et al. [1979]) and model profiles (M. Natarajan, private communication, 1984, and from the study of Miller et al. [1981]) of ClONO<sub>2</sub>.

intensity is calculated to be too weak to account for the observed line. Both the new O<sub>3</sub> laboratory spectra and the atlas of Damon et al. [1981] show no obvious absorption at this frequency. The presence of this unassigned line has only a minor influence on the fit to the 93.19° scan, but its occurrence points out the potential pitfalls of relying on a single, weak feature for a spectroscopic identification.

In Figure 11 the two experimental ClONO<sub>2</sub> mixing ratio profiles determined from University of Denver stratospheric spectra are plotted along with a daytime-averaged ClONO<sub>2</sub> profile for 30°N (dashed line) calculated by Miller et al. [1981] and a sunset ClONO<sub>2</sub> profile (M. Natarajan, private communication, 1984) calculated for March at 30°N (solid line) with the model of Callis et al. [1983] and recent reaction rates [NASA Panel for Data Evaluation, 1983]. The experimental mixing ratios are higher on average than the calculated values, but the experimental error bars are large. The two experimental profiles agree at all altitudes within the uncertainties. There is better agreement between the experimental and the model profile shapes, but it is difficult to draw firm conclusions because of the large uncertainties in the experimental values.

### SUMMARY AND CONCLUSIONS

We have reported a tentative identification of the 780-cm<sup>-1</sup>  $\nu_4$  band *Q* branch of ClONO<sub>2</sub> on the basis of an analysis of 0.02-cm<sup>-1</sup> resolution balloon-borne stratospheric solar absorption spectra and new high-resolution laboratory spectra of ClONO<sub>2</sub> and O<sub>3</sub>. The preliminary altitude profile deduced from the data is similar to photochemical model predictions and to the results obtained previously from the 1292-cm<sup>-1</sup> band [Murcray et al., 1979], but the experimental values have large uncertainties owing to the difficulties of the measurements. We caution that only limited significance should be attached to the differences between the measured

and model profiles in view of the large experimental uncertainties and the tentative nature of our results.

Improved stratospheric and laboratory spectra will be necessary to obtain a firm identification of  $\text{ClONO}_2$  (which should be based on more than one feature in the same set of spectra) and to accurately quantify its vertical profile. In the near future we hope to use a narrow-band filter to record high-resolution stratospheric solar absorption spectra covering the  $780\text{-cm}^{-1}$  and  $809\text{-cm}^{-1}$   $Q$  branches of  $\text{ClONO}_2$ . These measurements should have the higher signal-to-noise ratio needed to better study the weak, broad absorption feature detected at the position of the  $780\text{-cm}^{-1}$   $Q$  branch. In the laboratory, additional spectra of  $\text{ClONO}_2$  and  $\text{O}_3$  are needed. A key issue for  $\text{ClONO}_2$  remains the possibility that the integrated intensities have been underestimated because of unrecognized contaminants in the sample. Both the absolute intensities and shapes of the  $\text{ClONO}_2$   $Q$  branches need to be measured at stratospheric temperatures. Improved line parameters for the weak  $\text{O}_3$  lines in the  $780\text{-cm}^{-1}$  and  $809\text{-cm}^{-1}$  regions would improve least squares fits to stratospheric spectra.

**Acknowledgments.** Research at the University of Denver was supported by NASA, the Chemical Manufacturers Association, and the National Science Foundation. Research at the College of William and Mary was supported by NASA. The authors thank R. R. Gamache of the University of Lowell Center for Atmospheric Research for communicating his calculated  $\text{O}_3$  air-broadened half-widths to us prior to publication and Burnie S. Williams of NASA Langley, Rob Hubbard, Mike Brown, James W. Brault, and Greg Ladd of the National Solar Observatory for their assistance in obtaining the  $\text{O}_3$  laboratory spectra. We also thank Robert K. Seals, Jr., of NASA Langley and Carolyn H. Sutton of Systems and Applied Sciences Corporation for helpful comments and Susan Edwards of NASA Langley for typing the manuscript. The National Solar Observatory is operated by the Association of Universities for Research in Astronomy under contract with the National Science Foundation.

## REFERENCES

- Birks, J. W., B. Shoemaker, T. J. Leck, R. A. Borders, and L. J. Hart, Studies of reactions of importance in the stratosphere, 2. Reactions involving chlorine nitrate and chlorine dioxide, *J. Chem. Phys.*, **66**, 4591-4598, 1977.
- Callis, L. B., M. Natarajan, and R. E. Boughner, On the relationship between the greenhouse effect, atmospheric photochemistry, and species distribution, *J. Geophys. Res.*, **88**, 1401-1426, 1983.
- Colmont, J. M., and N. Monnanteuil, Measurements of  $\text{N}_2$ ,  $\text{O}_2$ , and air-broadened linewidths of ozone in the millimeter region: Temperature dependence of the linewidths, *J. Mol. Spectrosc.*, **104**, 122-128, 1984.
- Damon, E., R. L. Hawkins, and J. H. Shaw, A spectrum of ozone from  $760$  to  $5800\text{-cm}^{-1}$ , interim technical report, *Res. Found. Proj.* 761420/711626, Ohio State Univ., Columbus, 1981.
- Gallery, W. O., F. X. Kneizys, and S. A. Clough, Air mass computer program for atmospheric transmittance/radiance calculation: FSCATM, *Environ. Res. Pap.* 828 (AFGL-TR-83-0065), 145 pp., Air Force Geophys. Lab., Bedford, Mass., 1983.
- Gamache, R. R., R. W. Davies, and L. S. Rothman, Theoretical  $\text{N}_2$ ,  $\text{O}_2$ , and air-broadened halfwidths of  $^{16}\text{O}_3$  calculated by quantum Fourier transform theory with realistic collision dynamics, paper presented at 39th Symposium on Molecular Spectroscopy, Ohio State Univ., Columbus, 1984.
- Goldman, A., D. G. Murcray, F. J. Murcray, and E. Niple, High resolution IR balloon-borne solar spectra and laboratory spectra in the  $\text{HNO}_3$   $1720\text{-cm}^{-1}$  region: An analysis, *Appl. Opt.*, **19**, 3721-3724, 1980.
- Goldman, A., J. R. Gillis, D. G. Murcray, A. Barbe, and C. Secroun, Analysis of the  $\nu_2$  and  $2\nu_2-\nu_2$  ozone bands from high-resolution infrared atmospheric spectra, *J. Mol. Spectrosc.*, **96**, 279-287, 1982.
- Goldman, A., R. D. Blatherwick, F. J. Murcray, J. W. Van Allen, F. H. Murcray, and D. G. Murcray, New Atlas of Stratospheric IR Absorption Spectra, vol. 1, Line Positions and Identifications; vol. 2, The Spectra, report, Dep. Phys., Univ. Denver, Denver, Colo., 1983a.
- Goldman, A., J. R. Gillis, and J. A. Coxon, Spectral line parameters for the pure rotation bands of solar OH, *J. Quant. Spectrosc. Radiat. Transfer*, **29**, 469-470, 1983b.
- Goldman, A., J. R. Gillis, C. P. Rinsland, F. J. Murcray, and D. G. Murcray, Stratospheric  $\text{HNO}_3$  quantification from line-by-line, nonlinear least-squares analysis of high-resolution balloon-borne solar absorption spectra in the  $870\text{-cm}^{-1}$  region, *Appl. Opt.*, **23**, 3252-3255, 1984.
- Graham, R. A., E. C. Tuazon, A. M. Winer, J. N. Pitts, Jr., L. T. Molina, L. Beaman, and M. J. Molina, High resolution infrared absorptivities for gaseous chlorine nitrate, *Geophys. Res. Lett.*, **4**, 3-5, 1977.
- Kurylo, M. J., Flash photolysis resonance fluorescence investigation of the reaction of  $\text{O}(^3\text{P})$  atoms with  $\text{ClONO}_2$ , *Chem. Phys. Lett.*, **49**, 467-470, 1977.
- Kurylo, M. J., and R. G. Manning, Flash photolysis resonance fluorescence investigation of the reaction of  $\text{Cl}(^2\text{P})$  atoms with  $\text{ClONO}_2$ , *Chem. Phys. Lett.*, **48**, 279-283, 1977.
- Meunier, C., P. Marche, and A. Barbe, Intensities and air broadening coefficients of  $\text{O}_3$  in the 5- and 3- $\mu\text{m}$  regions, *J. Mol. Spectrosc.*, **95**, 271-275, 1982.
- Miller, R. H., D. L. Bernitt, and I. C. Hisatsune, Infrared spectra of isotopic halogen nitrates, *Spectrochim. Acta*, **23A**, 223-236, 1967.
- Miller, C., D. L. Filkin, A. J. Owens, J. M. Steed, and J. P. Jesson, A two-dimensional model of stratospheric chemistry and transport, *J. Geophys. Res.*, **86**, 12,039-12,065, 1981.
- Molina, L. T., J. E. Spencer, and M. J. Molina, The rate constant for the reaction of  $\text{O}(^3\text{P})$  atoms with  $\text{ClONO}_2$ , *Chem. Phys. Lett.*, **45**, 158-162, 1977.
- Murcray, D. G., and A. Goldman, *CRC Handbook of High Resolution Infrared Laboratory Spectra of Atmospheric Interest*, CRC Press, Boca Raton, Fla., 1981.
- Murcray, D. G., A. Goldman, W. J. Williams, F. H. Murcray, F. S. Bonomo, C. M. Bradford, G. R. Cook, P. L. Hanst, and M. J. Molina, Upper limit for stratospheric  $\text{ClONO}_2$  from balloon-borne infrared measurements, *Geophys. Res. Lett.*, **4**, 227-230, 1977.
- Murcray, D. G., A. Goldman, F. H. Murcray, F. J. Murcray, and W. J. Williams, Stratospheric distribution of  $\text{ClONO}_2$ , *Geophys. Res. Lett.*, **6**, 857-859, 1979.
- Murcray, D. G., F. J. Murcray, F. S. Bonomo, A. Goldman, and R. D. Blatherwick, High resolution IR Laboratory Spectra, *Appl. Opt.*, **23**, 3502, 1984.
- NASA Panel for Data Evaluation, Chemical kinetics and photochemical data for use in stratospheric modelling, Evaluation 6, *Publ.* 83-62, Jet Propul. Lab., Pasadena, Calif., 1983.
- Niple, E., W. G. Mankin, A. Goldman, D. G. Murcray, and F. J. Murcray, Stratospheric  $\text{NO}_2$  and  $\text{H}_2\text{O}$  mixing ratio profiles from high resolution infrared solar spectra using nonlinear least squares, *Geophys. Res. Lett.*, **7**, 489-492, 1980.
- Olson, W. B., A. G. Maki, and W. J. Lafferty, Tables of  $\text{N}_2\text{O}$  absorption lines for the calibration of tunable infrared lasers from  $522\text{-cm}^{-1}$  to  $657\text{-cm}^{-1}$  and from  $1115\text{-cm}^{-1}$  to  $1340\text{-cm}^{-1}$ , *J. Phys. Chem. Ref. Data*, **10**, 1065-1084, 1981.
- Rinsland, C. P., A. Goldman, F. J. Murcray, D. G. Murcray, M. A. H. Smith, R. K. Seals, Jr., J. C. Larsen, and P. L. Rinsland, Stratospheric  $\text{N}_2\text{O}$  mixing ratio profile from high-resolution balloon-borne solar absorption spectra and laboratory spectra near  $1880\text{-cm}^{-1}$ , *Appl. Opt.*, **21**, 4351-4355, 1982.
- Rinsland, C. P., D. C. Benner, D. J. Richardson, and R. A. Toth, Absolute intensity measurements of the  $(11^0_0)_1 \leftarrow 00^0_0$  band of  $\text{CO}_2$  at  $5.2\text{-}\mu\text{m}$ , *Appl. Opt.*, **22**, 3805-3809, 1983a.
- Rinsland, C. P., A. Goldman, F. J. Murcray, D. G. Murcray, M. A. H. Smith, R. K. Seals, Jr., J. C. Larsen, and P. L. Rinsland, Stratospheric temperature profile from balloon-borne measurements of the  $10.4\text{-}\mu\text{m}$  band of  $\text{CO}_2$ , *J. Quant. Spectrosc. Radiat. Transfer*, **30**, 327-334, 1983b.
- Rothman, L. S., R. R. Gamache, A. Barbe, A. Goldman, J. R. Gillis, L. R. Brown, R. A. Toth, J.-M. Flaud, and C. Camy-Peyret, AFGL atmospheric absorption line parameters compilation: 1982 edition, *Appl. Opt.*, **22**, 2247-2256, 1983a.

- Rothman, L. S., A. Goldman, J. R. Gillis, R. R. Gamache, H. M. Pickett, R. L. Poynter, N. Husson, and A. Chedin, AFGL trace gas compilation: 1982 version, *Appl. Opt.*, **22**, 1616-1627, 1983b.
- Schmeisser, M., Chlorine (I) nitrate, *Inorg. Syn.*, **9**, 127-130, 1967.
- Smith, M. A. H., Compilation of atmospheric gas concentration profiles from 0 to 50 km, *Techn. Memor.* 83289, NASA Langley Res. Center, Hampton, Va., 1982.
- Williams, W. J., J. J. Kusters, A. Goldman, and D. G. Murcay, Measurements of stratospheric halocarbon distributions using infrared techniques, *Geophys. Res. Lett.*, **3**, 379-382, 1976.
- Zahniser, M. S., J. S. Chang, and F. Kaufman, Chlorine nitrate: Kinetics of formation by  $\text{ClO} + \text{NO}_2 + \text{M}$  and of reaction with OH, *J. Chem. Phys.*, **67**, 997-1003, 1977.
- R. D. Blatherwick, F. S. Bonomo, A. Goldman, D. G. Murcay, and F. J. Murcay, Department of Physics, University of Denver, Denver, CO 80208.
- V. Malathy Devi, Department of Physics, College of William and Mary, Williamsburg, VA 23185.
- C. P. Rinsland and M. A. H. Smith, Atmospheric Sciences Division, NASA Langley Research Center, Hampton, VA 23665.
- P. L. Rinsland, Flight Electronics Division, NASA Langley Research Center, Hampton, VA 23665.

(Received January 3, 1985;  
revised March 22, 1985;  
accepted March 26, 1985.)



a concentrated load applied at the center. The ground state was recorded with all the apertures open. The subsequent exposures were taken by opening in turn only two apertures, one each on the two segments, and sequentially loading the object.

The exposure times were all equal, and care was taken to ensure linearity of the recording. After processing, the specklegram was placed in the Fourier filtering setup, and various fringe patterns were photographed by filtering at the respective halos. Figure 2 shows the photographs for a  $x$  shear of 2 mm and central deflections of 5, 10, 15, and 20  $\mu\text{m}$ , respectively.

This method includes the earlier methods described in Refs. 1 and 2 as special cases. It provides a more convenient method to multiplex any amount of information on the same plate. The split-lens arrangement provides a flexibility to apply shears of desired magnitude and direction. If flexibility is not a primary requirement, a normal camera lens with an appropriate aperture mask and a custom-made wedge plate covering half of the lens can be used.

## References

1. C. Joenathan, R. K. Mohanty, and R. S. Sirohi, "Multiplexing in Speckle Shear Interferometry," *Opt. Acta* **31**, 681 (1984).
2. C. Joenathan, R. K. Mohanty, and R. S. Sirohi, "On Methods of Multiplexing in Speckle Shear Interferometry," *Optik* **69**, 8 (1984).
3. R. Krishna Murthy, R. S. Sirohi, and M. P. Kothiyal, "Speckle Shearing Interferometry: A New Method," *Appl. Opt.* **21**, 2865 (1982).

## Identification of atmospheric $\text{C}_2\text{H}_2$ lines in the 3230–3340- $\text{cm}^{-1}$ region of high resolution solar absorption spectra recorded at the National Solar Observatory

Curtis P. Rinsland, Aaron Goldman, and Gerald M. Stokes

Curtis Rinsland is with NASA Langley Research Center, Atmospheric Sciences Division, Hampton, Virginia 23665; Aaron Goldman is with University of Denver, Physics Department, Denver, Colorado 80208; and Gerald Stokes is with Battelle Observatory, Battelle Pacific Northwest Laboratories, P.O. Box 999, Richland, Washington 99352.

Received 18 March 1985.

The 3230–3340- $\text{cm}^{-1}$  interval of 0.01- $\text{cm}^{-1}$  resolution solar absorption spectra recorded with the McMath interferometer of the National Solar Observatory on Kitt Peak (31.9°N, 111.6°W, altitude 2095 m) has been searched for the presence of absorption lines of atmospheric acetylene ( $\text{C}_2\text{H}_2$ ). A total of 12 lines belonging to the strong  $\nu_3$  and  $\nu_2 + \nu_4 + \nu_5$  bands has been identified in this interval. Several of these lines are well isolated in the solar spectra and are suitable for ground-based monitoring of seasonal and long term trends in the column amounts of atmospheric  $\text{C}_2\text{H}_2$ . In this Letter, we report the identification and analysis of selected atmospheric  $\text{C}_2\text{H}_2$  lines in a representative set of Kitt Peak solar spectra.

Figure 1 is a plot of small spectral intervals containing the two atmospheric  $\text{C}_2\text{H}_2$  lines selected as most favorable for quantitative analysis. The sequence of scans shown covers the 1850–5500- $\text{cm}^{-1}$  region and was obtained on the morning of 23 Feb. 1981. The signal-to-rms noise ratio of the spectra

is  $\approx 1000$  in the  $\text{C}_2\text{H}_2$  region. The  $\text{C}_2\text{H}_2$  lines are marked. Based on the positions and assignments reported in a recent laboratory study,<sup>1</sup> the line at 3250.6633  $\text{cm}^{-1}$  is identified as P13 of the  $\nu_2 + \nu_4 + \nu_5$  band, and the line at 3304.9686  $\text{cm}^{-1}$  is identified as R9 of the same band. The measured positions in the solar spectra agree with the laboratory values to 0.002  $\text{cm}^{-1}$ . Lines of  $\text{H}_2\text{O}$  at 3250.938 and 3305.172  $\text{cm}^{-1}$  are also indicated in the figure.

The P2 line of the  $\nu_3$  band of HCN is observed at 3305.544  $\text{cm}^{-1}$ , just outside the interval shown in the figure. The  $\text{C}_2\text{H}_2$  and  $\text{H}_2\text{O}$  lines are broad in the solar spectra, indicating they result from gases concentrated predominately in the troposphere where pressure broadening is important. Simulations with the line parameters discussed below and the atmospheric trace gas concentration profiles of Smith<sup>2</sup> indicate both  $\text{C}_2\text{H}_2$  lines are located in the far wings of broad strong lines but that no interfering absorption occurs near the  $\text{C}_2\text{H}_2$  line centers.

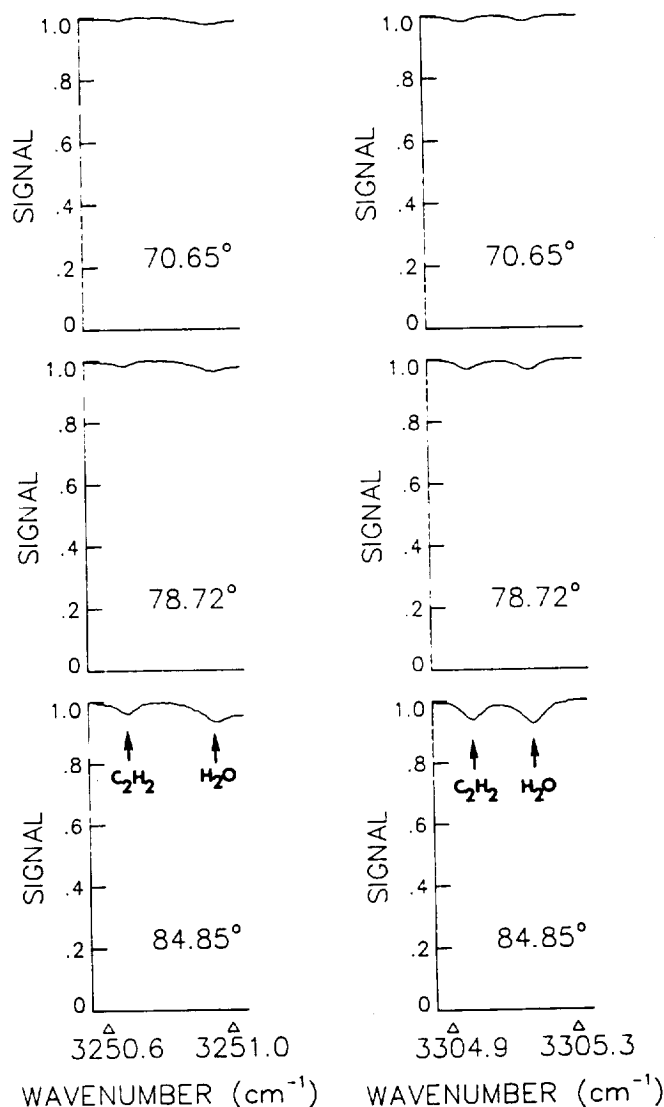


Fig. 1. Sequence of solar absorption spectra in the regions of the P13 and R9 lines of the  $\nu_2 + \nu_4 + \nu_5$  band of  $\text{C}_2\text{H}_2$ . The average solar zenith angles are indicated. Lines of  $\text{C}_2\text{H}_2$  and  $\text{H}_2\text{O}$  are marked. The data were recorded during the morning of 23 Feb. 1981. Additional details concerning these spectra are given by Rinsland *et al.*<sup>14</sup>

Table I. Total Vertical Column Amounts  $u_{C_2H_2}$  (in  $10^{18}$  molecules  $cm^{-2}$ ) and Corresponding Average Tropospheric Volume Mixing Ratios  $\beta$  (in ppbv) of  $C_2H_2$  above Kitt Peak

Line <sup>a</sup>	Position (cm <sup>-1</sup> )	23 Feb. 1981 <sup>b</sup>		1 Oct. 1982 <sup>c</sup>	
		$u_{C_2H_2}$	$\beta$	$u_{C_2H_2}$	$\beta$
P13	3250.6633	2.23	0.20	2.14	0.15
R9	3304.9686	2.34	0.21	1.86	0.13
Average		2.28 <sup>d</sup>	0.20	2.00 <sup>d</sup>	0.14

<sup>a</sup> In the  $\nu_2 + \nu_4 + \nu_5$  band of  $^{12}C_2H_2$ .

<sup>b</sup> Tropopause geopotential altitude = 10.4 km.

<sup>c</sup> Tropopause geopotential altitude = 15.6 km.

<sup>d</sup> Estimated uncertainty  $\pm 15\%$ , estimated precision  $\pm 10\%$ .

However, long path laboratory spectra of  $CO_2$  obtained with the McMath interferometer show that there is minor contamination of the 3304.9686- $cm^{-1}$  line by the P46 line of the 22202-01101 band of  $^{12}C^{16}O_2$ .<sup>3</sup> This interfering  $CO_2$  line also appears in the  $CO_2$  atlas of Smith *et al.*<sup>4</sup> Long path length laboratory spectra of  $N_2O$ ,<sup>5</sup>  $CH_4$ ,<sup>6</sup> and  $O_3$  (Ref. 7) indicate that both  $C_2H_2$  lines are free of overlap by weak lines of these molecules.

The  $C_2H_2$  line positions, intensities, and lower state energies for the analysis were taken from the 1982 AFGL trace gas compilation.<sup>8</sup> Since, to our knowledge, no measurements of air-broadened halfwidths of  $C_2H_2$  have been reported, we assumed the same dependence with  $|m|$  ( $m = J'' + 1$  for R-branch lines and  $m = -J''$  for the P-branch lines, where  $J''$  is the lower state rotational quantum number), as measured for  $N_2$  broadening in the  $(\nu_4 + \nu_5)$  band of  $^{12}C_2H_2$ .<sup>9</sup> These values are 0.0842  $cm^{-1} atm^{-1}$  at 296 K for R9 and, by linear interpolation, 0.0803  $cm^{-1} atm^{-1}$  at 296 K for P13. Since the background level of the P13 line is affected by strong nearby lines of  $H_2O$  and the background level of the R9 lines is affected by strong nearby lines of  $H_2O$  and  $CO_2$ , these lines were included in the calculations assuming the parameters listed in the 1982 AFGL major gas compilation.<sup>10</sup> The position of the interfering P46 line of the 22202-01101 band of  $^{12}C^{16}O_2$  was changed from the 1982 AFGL value<sup>10</sup> of 3305.0394  $cm^{-1}$  to the laboratory value<sup>3</sup> of 3304.9482  $cm^{-1}$ . The 1982 AFGL intensity for this  $CO_2$  line<sup>10</sup> is in good agreement with a preliminary intensity value determined from laboratory spectra.<sup>3</sup>

*In situ* measurements indicate very low stratospheric concentrations of  $C_2H_2$  at 32°N latitude.<sup>11</sup> Therefore, as a preliminary estimate, we have assumed that the  $C_2H_2$  mixing ratio by volume is constant within the troposphere and that there are no  $C_2H_2$  molecules above the altitude of the tropopause. Spectral data obtained in Feb. 1981 and Oct. 1982 were analyzed with the technique of nonlinear least-squares curve fitting. Examples of the application of this procedure to retrieve information about the abundance and vertical distribution of atmospheric gases from ground-based solar absorption spectra are given in several recent papers.<sup>12-14</sup> Table I presents the total vertical column amounts and corresponding mean tropospheric mixing ratios deduced from analysis of the solar spectra. The retrieved average tropospheric mixing ratio values of 0.14 and 0.20 ppbv are slightly lower than ground level mixing ratios of 0.3 ppbv determined over the Atlantic at 30°N latitude<sup>15</sup> and 0.4 ppbv determined over the eastern Pacific at the same latitude.<sup>16</sup> Since measurements<sup>11</sup> and calculations<sup>11,17</sup> indicate that the  $C_2H_2$  mixing ratio decreases with altitude in the troposphere, the differences between the reported ground level measurements and our results for the average troposphere above 2.1 km are reasonable. Results of the fits to the solar absorption spectra are illustrated in Fig. 2.

R-branch lines near 770  $cm^{-1}$  of the  $\nu_5$  band have been used previously for spectroscopic measurements of atmospheric  $C_2H_2$ . Goldman *et al.*<sup>17</sup> determined a preliminary upper tropospheric mixing ratio of 25 pptv near 9 km from solar absorption spectra obtained during a balloon flight from Holloman Air Force Base near Alamogordo, N.M. (32°N, 106°W). Zander *et al.*<sup>18</sup> analyzed a different set of Kitt Peak solar spectra than used in the present analysis and determined a mean  $C_2H_2$  mixing ratio of  $27 \pm 6$  pptv. It is interesting to note that this latter value is almost an order of magnitude lower than derived in the present study. Although some of this difference is probably due to differences in the methods of analysis (the equivalent width method was used by Zander *et al.*<sup>18</sup>) and uncertainties in the assumed values for the spectroscopic line parameters, the pressure-temperature profile, and the shape of the gas concentration profile with altitude, its magnitude seems too large to result entirely from these factors. On the other hand, our vertical column amounts for Feb. 1981 and Oct. 1982 differ by only 14% so that large variability in the total abundance of atmospheric  $C_2H_2$  above Kitt Peak is unlikely. We plan to analyze additional Kitt Peak solar spectra to determine the range of seasonal variations in the  $C_2H_2$  vertical column amount.

The  $C_2H_2$  lines reported here were also confirmed by Coffey and Mankin<sup>19</sup> from analysis of their stratospheric solar absorption spectra obtained at 0.06- $cm^{-1}$  resolution from an aircraft at 12-km altitude. While most of the  $C_2H_2$  lines in the 3200-3400- $cm^{-1}$  region are partially or totally overlapped by other atmospheric lines, the 3250.66- and 3304.97- $cm^{-1}$  lines are quite isolated and show 3-5% absorption in spectra obtained with zenith angles of 91-93°. The nearby P2 HCN line at 3305.544  $cm^{-1}$  absorbs ~5% in these spectra. Unfortunately, the available aircraft spectra do not allow an accu-

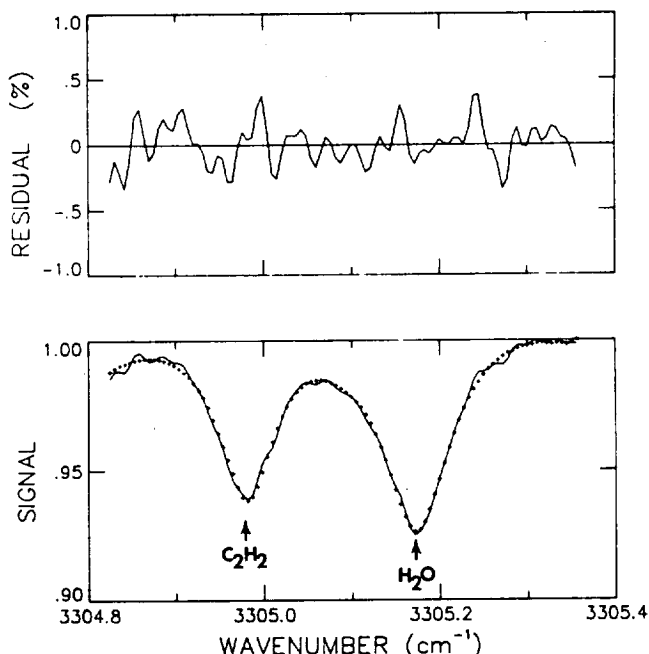


Fig. 2. Comparison between the solar absorption spectrum recorded at an average astronomical zenith angle of 84.85° (solid line) and least-squares best fit to the data (crosses) in the region of the R9 line of the  $\nu_2 + \nu_4 + \nu_5$  band of  $C_2H_2$ . The measured spectrum has been normalized to the highest intensity value in the fitted interval. Lines  $C_2H_2$  and  $H_2O$  are identified.



rate quantitative determination of the  $C_2H_2$  column amount or mixing ratio.

The opportunity to compare the current work with the NCAR aircraft spectra is greatly appreciated. Research at the University of Denver was supported in part by NASA and in part by the National Science Foundation. Research at Battelle Observatory was supported by the Carbon Dioxide Research Division of the Department of Energy under contract DE-AC06-76RL01830. The National Solar Observatory is operated by the Association of Universities for Research in Astronomy, Inc., under contract with NSF.

## References

1. C. P. Rinsland, A. Baldacci, and K. Narahari Rao, "Acetylene Bands Observed in Carbon Stars: A Laboratory Study and an Illustrative Example of its Application to IRC + 10216," *Astrophys. J. Suppl.* **49**, 487 (1982).
2. M. A. H. Smith, "Compilation of Atmospheric Gas Concentration Profiles from 0 to 50 km," NASA Tech. Memor. 83289 (1982).
3. D. C. Benner and V. Malathy Devi, College of William and Mary; private communication (1985).
4. D. H. Smith, M. L. Hoke, R. A. Hawkins, and J. H. Shaw, "A Spectrum of Carbon Dioxide from 800 to 5500  $cm^{-1}$ ," Interim. Tech. Rep., RF Project 761420/711626, Ohio State U., Columbus (1981).
5. R. L. Hawkins, R. J. Nordstrom, and J. H. Shaw, "The Spectrum of  $N_2O$  between 800 and 5200  $cm^{-1}$ ," Interim. Tech. Rep., RF Project 761420/711626, Ohio State U., Columbus (1980).
6. H. Baddar, M. L. Hoke, R. L. Hawkins, and J. H. Shaw, "A Spectrum of Methane from 700 to 5500  $cm^{-1}$ ," Interim. Tech. Rep., RF Project 761420/711626, Ohio State U., Columbus (1984).
7. E. Damon, R. L. Hawkins, and J. H. Shaw, "A Spectrum of Ozone from 760 to 5800  $cm^{-1}$ ," Interim. Tech. Rep., RF Project 761420/711626, Ohio State U., Columbus (1981).
8. L. S. Rothman *et al.*, "AFGL Trace Gas Compilation: 1982 Version," *Appl. Opt.* **22**, 1616 (1983).
9. J. R. Podolske, M. Loewenstein, and P. Varanasi, "Diode Laser Line Strength Measurements of the  $(\nu_4 + \nu_5)^0$  Band of  $^{12}C_2H_2$ ," *J. Mol. Spectrosc.* **107**, 241 (1984).
10. L. S. Rothman *et al.*, "AFGL Atmospheric Absorption Line Parameters Compilation: 1982 Edition," *Appl. Opt.* **22**, 2247 (1983).
11. J. Rudolph, D. H. Ehhalt, and A. Khedim, "Vertical Profiles of Acetylene in the Troposphere and Stratosphere," *J. Atmos. Chem.* **2**, 117 (1984).
12. C. P. Rinsland, M. A. H. Smith, P. L. Rinsland, A. Goldman, J. W. Brault, and G. M. Stokes, "Ground-based Infrared Spectroscopic Measurements of Atmospheric Hydrogen Cyanide," *J. Geophys. Res.* **87**, 11119 (1982).
13. A. Goldman, F. G. Fernald, F. J. Murcray, F. H. Murcray, and D. J. Murcray, "Spectral Least Squares Quantification of Several Atmospheric Gases from High Resolution Infrared Solar Spectra Obtained at the South Pole," *J. Quant. Spectrosc. Radiat. Transfer* **29**, 189 (1983).
14. C. P. Rinsland, R. E. Boughner, J. C. Larsen, G. M. Stokes, and J. W. Brault, "Diurnal Variations of Atmospheric Nitric Oxide: Ground-Based Infrared Spectroscopic Measurements and their Interpretation with Time-Dependent Photochemical Model Calculations," *J. Geophys. Res.* **89**, 9613 (1984).
15. J. Rudolph, D. H. Ehhalt, A. Khedim, and C. Jebsen, "Latitudinal Profiles of Some  $C_2-C_6$  Hydrocarbons in the Clean Troposphere over the Atlantic," Preprint Volume: *Second Symposium on the Composition of the Nonurban Troposphere*, 25-28 May 1982, Williamsburg, Va. (American Meteorological Society, Boston, 1982), pp. 284-286.
16. H. B. Singh and J. L. Salas, "Measurement of Selected Light Hydrocarbons over the Pacific Ocean: Latitudinal and Seasonal Variations," *Geophys. Res. Lett.* **9**, 842 (1982).
17. A. Goldman *et al.*, "Identification of Acetylene ( $C_2H_2$ ) in Infrared Atmospheric Absorption Spectra," *J. Geophys. Res.* **86**, 12143 (1981).
18. R. Zander, G. Stokes, and J. Brault, "Détection, par voie spectroscopique, de l'acétylène et de l'éthane dans l'atmosphère terrestre, à partir d'observations solaires infrarouges au sol," *C. R. Acad. Sci. Paris* **295**, 583 (1982).
19. M. T. Coffey and W. G. Mankin, National Center for Atmospheric Research; private communication (1985).

## Model studies of retrospective dispersive correlation spectroscopy

Ralph W. Nicholls

York University, Centre for Research in Experimental Space Science, 4700, Keele Street, Downsview, Ontario M3J 1P3.

Received 4 March 1985.

0003-6935/85/142046-03\$02.00/0.

© 1985 Optical Society of America.

The principle of analog dispersive correlation spectroscopy was first proposed in 1964.<sup>1-4</sup> It uses a field spectrum (e.g., the absorption of skylight by a contaminant plume) dispersed along a focal surface at which an analog mask of alternate transparent and opaque slits, characteristic of the absorption spectral features of the contaminant species, is located. The mask is oscillated mechanically in the dispersion direction, and the total signal passing through it is focused on a photoelectric detector. The correlation between the field spectrum and the mask function is inferred by phase sensitive signal detection (with respect to the mask oscillation frequency). After suitable calibration this signal can be interpreted diagnostically as a quantitative measure of the concentration (or column density) of the contaminant in the optical path. This principle is the basis of commercial correlation spectrometers used to monitor plumes of contaminants such as  $SO_2$  in the atmosphere.

The purpose of this Letter is to examine using a simple analytical model the extension of the analog method to retrospective correlative interrogation of a digital field spectrum with a numerical mask function which can also be specified in digital terms. Digital recording of atmospheric spectra is now common.<sup>5</sup> It is far easier to adapt numerically specified mask functions to the characteristic spectral fingerprints of contaminant molecular species than mechanically to fabricate and install suitable analog masks, one for each spectrum of interest.

If  $\lambda$  is the wavelength,  $I(\lambda)$  is the field spectrum intensity distribution, and  $M(\lambda)$  is the mask function, the correlogram between  $I$  and  $M$  when they differ in register in the dispersion direction by  $z$  is

$$C(z) = \int I(\lambda)M(\lambda - z)d\lambda. \quad (1)$$

Furthermore, if  $I(\lambda)$  is the result of optically thin extinction of a sky spectrum  $I_0(\lambda)$  by a contaminant slab of path length  $X$  and number density  $N$ , then

$$I(\lambda) = I_0(\lambda) \exp[-NX\sigma(\lambda)] = I_0(\lambda)[1 - NX\sigma(\lambda)]. \quad (2)$$

$NX$  is called the column density of absorbers in the slab, and  $\sigma(\lambda)$  is the absorption cross section per molecule.

Equation (1) can be rewritten as



A SEARCH FOR FORMIC ACID IN THE UPPER TROPOSPHERE: A TENTATIVE IDENTIFICATION OF THE 1105- $\text{cm}^{-1}$   $\nu_6$  BAND Q BRANCH IN HIGH-RESOLUTION BALLOON-BORNE SOLAR ABSORPTION SPECTRAA. Goldman<sup>1</sup>, F. H. Murcray<sup>1</sup>, D. G. Murcray<sup>1</sup>, and C. P. Rinsland<sup>2</sup><sup>1</sup>Department of Physics, University of Denver, Denver, Colorado 80208<sup>2</sup>Atmospheric Sciences Division, NASA Langley Research Center, Hampton, Virginia 23665

**Abstract.** Infrared solar absorption spectra recorded at 0.02- $\text{cm}^{-1}$  resolution during a balloon flight from Alamogordo, N.M. (33°N), on March 23, 1981, have been analyzed for the possible presence of absorption by formic acid (HCOOH). An absorption feature at 1105  $\text{cm}^{-1}$  has been tentatively identified in upper tropospheric spectra as due to the  $\nu_6$  band Q branch. A preliminary analysis indicates a concentration of  $\sim 0.6$  ppbv and  $\sim 0.4$  ppbv near 8 and 10 km, respectively.

Two recent studies have reported ground-level measurements of vapor phase formic acid (HCOOH) in both urban and nonurban environments [Dawson et al., 1980; Hanst et al., 1982]. Formic acid has also been identified as a major acidic component of rain in remote regions [Galloway et al., 1982]. Because these measurements suggest that HCOOH may be widely distributed in the environment, we have examined 0.02- $\text{cm}^{-1}$  resolution solar absorption spectra recorded with a balloon-borne interferometer for the possible presence of HCOOH absorption. An absorption feature has been found in upper tropospheric scans which agrees well with the position and shape of the  $\nu_6$  band Q branch at 1104.86  $\text{cm}^{-1}$ . We report here our analysis which suggests the possible occurrence of a significant amount of HCOOH in the upper troposphere.

Figures 1a and 1b show the 1100-1108  $\text{cm}^{-1}$  spectral region in two scans recorded with the University of Denver interferometer system. The spectral data were obtained during a balloon flight from Alamogordo, N.M. (33°N) on March 23, 1981. Each scan was acquired in 40 seconds during sunset from a float altitude of  $33.5 \pm 0.5$  km. The observed features are identified in the University of Denver stratospheric atlas [Goldman et al., 1983]. The dominant absorber in this interval is atmospheric  $\text{O}_3$ . The  $\text{O}_3$  lines show maximum absorption in the 93.21° scan, in accordance with the well-known mid-stratospheric peak in the vertical  $\text{O}_3$  distribution. The  $\text{H}_2\text{O}$  lines increase in strength over the full range of observed solar zenith angles, as is also expected from knowledge of the  $\text{H}_2\text{O}$  profile.

In the lowest scan, which was recorded at an astronomical zenith angle of 95.58° (tangent altitude = 7.7 km), a broad absorption feature is superimposed on the lines near 1105  $\text{cm}^{-1}$ . The pattern of this broad absorption is difficult to recognize in Figure 1b because of numerous overlapping strong lines (of  $\text{O}_3$ ). It has been found that this broad absorption can be studied better

by ratioing the 95.58° spectrum to a higher sun spectrum with a nearly equal amount of  $\text{O}_3$  absorption. In the ratio spectrum, the  $\text{O}_3$  lines are then largely cancelled. The 94.71° scan (tangent altitude = 14.7 km) has been found well suited for this purpose.

Figure 2 compares a laboratory spectrum of HCOOH (upper plot) and the atmospheric 95.58°/94.71° ratio spectrum (lower plot). Comparison with Figures 1a and 1b shows the  $\text{O}_3$  lines are almost completely removed in the atmospheric ratio spectrum; the broad feature near 1105  $\text{cm}^{-1}$  remains in addition to the lines of  $\text{H}_2\text{O}$ . The modulation of the background results from a complex residual channel spectrum which is not cancelled completely in the ratioing procedure. The laboratory spectrum in Figure 2 was recorded at 0.06- $\text{cm}^{-1}$  resolution and 22°C [Murcray and Goldman, 1981]. Comparison between the stratospheric ratio scan and the laboratory scan indicates good agreement in the position and the shape of the 1105- $\text{cm}^{-1}$  feature. Figure 3 presents versions of the same spectra convolved with a triangular response function with a full width at half maximum of 1.0  $\text{cm}^{-1}$ . These spectra show clearer agreement in the stratospheric and laboratory band shape of the 1105- $\text{cm}^{-1}$  feature. The strong residual  $\text{H}_2\text{O}$  lines are marked with asterisks in the atmospheric spectrum.

The integrated absorption of the broad 1105- $\text{cm}^{-1}$  feature in the 95.58°/94.71° atmospheric spectrum is  $\sim 0.21 \text{ cm}^{-1}$ . A weak feature also appears with the same position and shape in the 95.29° scan (tangent height = 9.8 km); an equivalent width of  $\sim 0.06 \text{ cm}^{-1}$  has been measured from the 95.29°/94.71° ratio spectrum. A preliminary estimate for the HCOOH profile has been derived from these equivalent widths and an integrated Q branch intensity of  $\sim 28 \text{ cm}^{-2} \text{ atm}^{-1}$ , averaged from  $\sim 20 \text{ cm}^{-2} \text{ atm}^{-1}$  estimated from the University of Denver laboratory data and  $\sim 36 \text{ cm}^{-2} \text{ atm}^{-1}$  estimated from other laboratory data [Maker and Niki, 1983]. Assuming that no HCOOH molecules occur above the tropopause height of 10.4 km and that the measured absorption is on the linear part of the curve of growth, an onion-peeling inversion yields mixing ratios of  $\sim 0.6$  ppbv between 7.7 and 9.8 km and  $\sim 0.4$  ppbv between 9.8 and 10.4 km (estimated accurate to within a factor of two). These concentrations are close to the ground level values measured in the southwest U.S.A. during clean conditions [Dawson et al., 1980] but are an order of magnitude larger than predicted for the vapor phase in a recent study of aqueous-phase cloud chemistry [Chameides and Davis, 1983].

Although the observed shape and close frequency coincidence support the conclusion that the observed atmospheric feature is due to HCOOH,

Copyright 1984 by the American Geophysical Union.

Paper number 4L6024.

0094-8276/84/004L-0024\$03.00

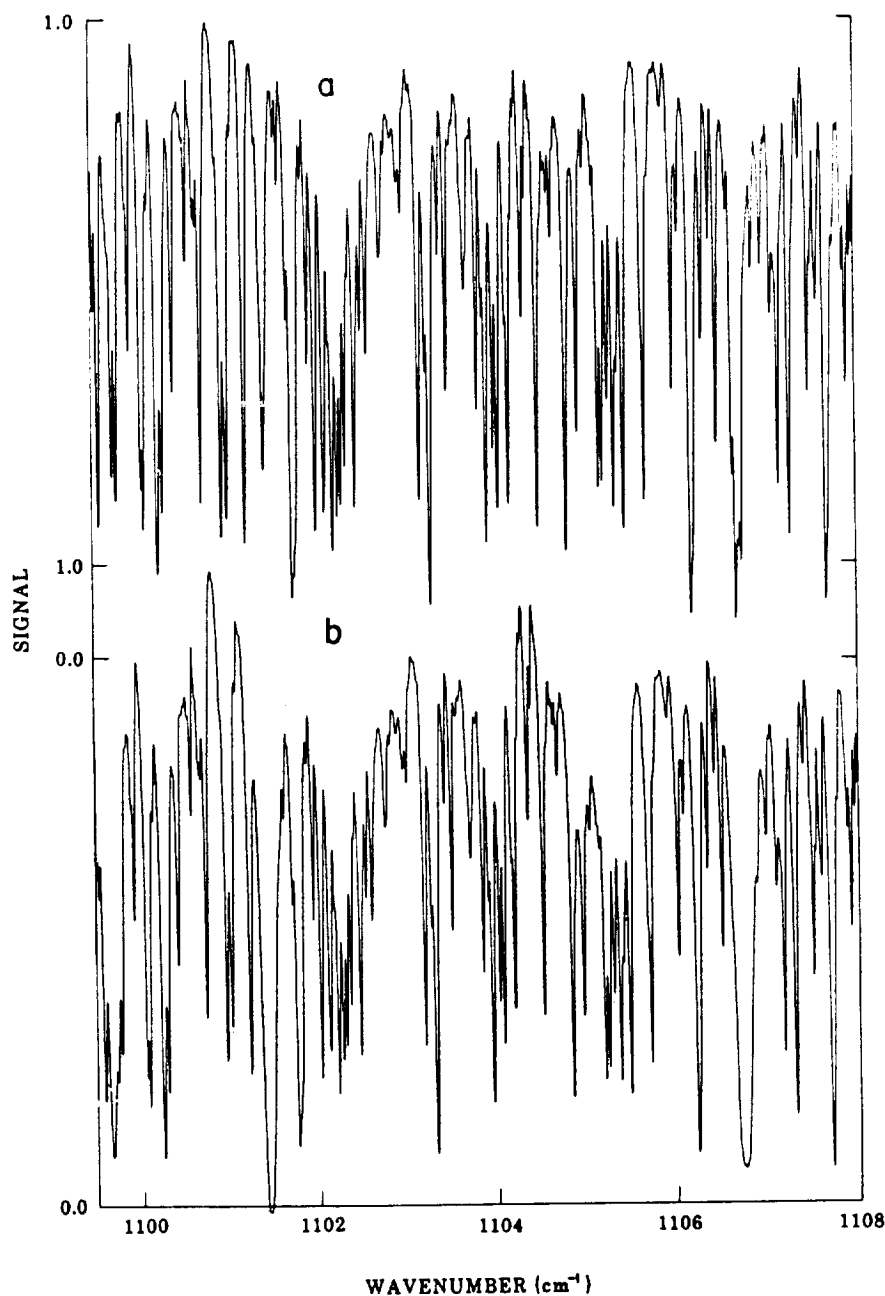


Fig. 1. Solar absorption spectra obtained from a float altitude of 33.5 km during a balloon flight from Alamogordo, N.M. (33°N) on March 23, 1981. The scaling for both scans is the same, but they have been displaced vertically for clarity. The zero levels are indicated at left. The astronomical zenith angles and tangent heights are 94.71° and 14.7 km for a, 95.58° and 7.7 km for b, respectively.

this identification must be regarded as tentative because it results from a single, broad feature. Also, the occurrence of a complex residual channel spectrum in the data makes it difficult to be certain that the observed feature is real. Unfortunately, it has not been possible to identify the 1105-cm<sup>-1</sup> feature in ground-based solar absorption spectra because of interference by a weak, broad water vapor line near the location of the strongest HCOOH absorption. The  $\nu_3$  band, centered near 1776.5 cm<sup>-1</sup>, also has a prominent Q branch and is about an order of magnitude stronger than the 1105-cm<sup>-1</sup> band.

Unfortunately, in low sun scans this region is strongly absorbed by H<sub>2</sub>O lines, as seen on the currently available balloon-borne scans at the University of Denver from the 10/10/79 flight. It is hoped that spectra recorded during a future balloon flight in that region with higher resolution and higher signal-to-noise will provide an opportunity to look for absorption by HCOOH. The 1220-cm<sup>-1</sup> HCOOH band, which appears stronger than the 1105-cm<sup>-1</sup> band in standard chemical infrared catalogs, has been found to be due to the formic acid dimer [Maker and Niki, 1983] and therefore should not be absorbing in the atmosphere.

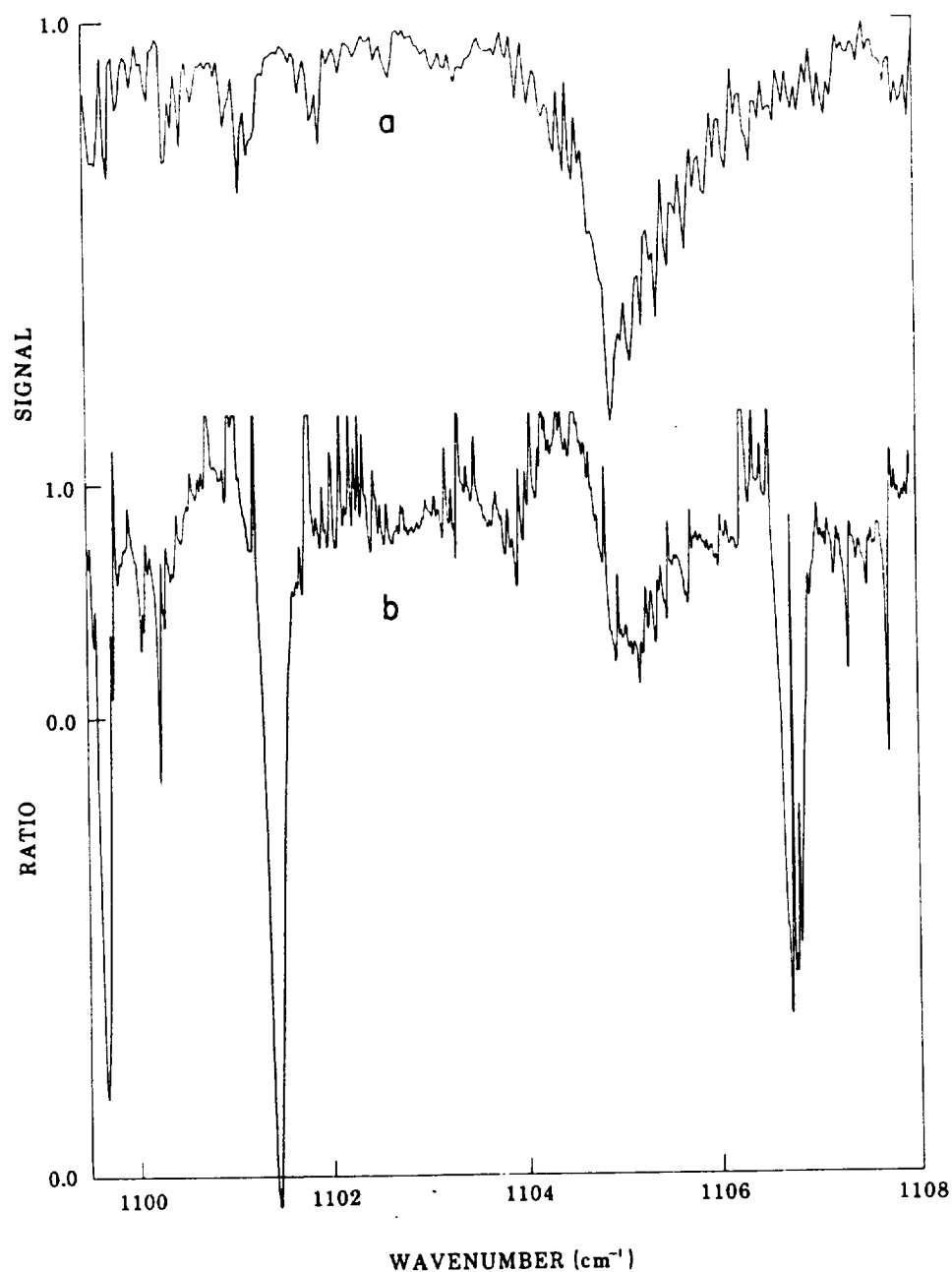


Fig. 2. Laboratory and atmospheric spectra in the region of the  $\text{HCOOH } 1105\text{-cm}^{-1}$  Q branch. Spectrum a is a laboratory scan recorded at  $0.06\text{-cm}^{-1}$  resolution with 1.6 Torr of  $\text{HCOOH}$  in a 10 cm path cell at  $22^\circ\text{C}$ . Spectrum b was determined from the point-by-point ratio of the  $95.58^\circ$  and  $94.71^\circ$  atmospheric scans.

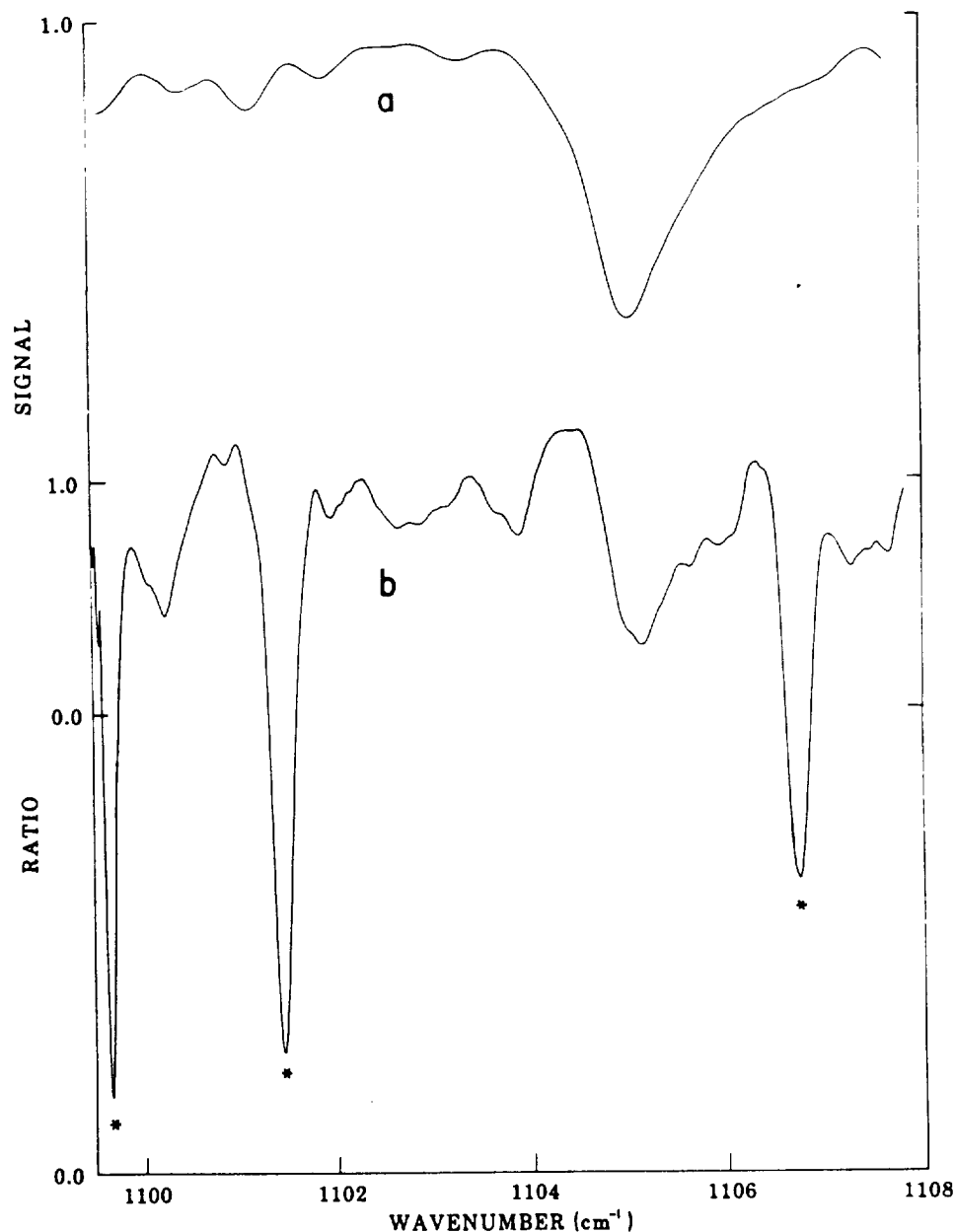


Fig. 3. Filtered versions of the same laboratory spectrum (a) and atmospheric ratio spectrum (b) as shown in Figure 2. Water vapor lines are marked with asterisks in spectrum b.

**Acknowledgments.** Research at the University of Denver is supported by NASA and NSF. We thank Ervin Weinberger of ASW Controls and Instruments of Downsview, Ontario, Canada, and Paul Maker and Hiromi Niki of Ford Motor Company, Dearborn, Michigan, for useful discussions concerning the infrared spectrum of formic acid.

#### References

- Chameides, W. L., and D. D. Davis, Aqueous-phase source of formic acid in clouds, *Nature*, **304**, 427-429, 1983.
- Dawson, G. A., J. C. Farmer, and J. L. Moyers, Formic and acetic acids in the atmosphere of the southwest U.S.A., *Geophys. Res. Lett.*, **7**, 725-728, 1980.
- Galloway, J. N., G. E. Likens, W. C. Keene, and J. M. Miller, The composition of precipitation in remote areas of the world, *J. Geophys. Res.*, **87**, 8771-8786, 1982.
- Goldman, A., R. D. Blatherwick, F. J. Murcray, J. W. Van Allen, F. H. Murcray, and D. G. Murcray, New atlas of stratospheric IR absorption spectra, Vol. I, Line positions and identifications, Vol. II, The spectra, Department of Physics, University of Denver, 1983.
- Hanst, P. L., N. W. Wong, and J. Bragin, A long-path infra-red study of Los Angeles smog, *Atmos. Environ.*, **16**, 969-981, 1982.
- Maker, P. D. and H. Niki, private communication, 1983.
- Murcray, D. G., and A. Goldman, *Handbook of High Resolution Infrared Laboratory Spectra of Atmospheric Interest*, CRC Press, 1981.

(Received January 13, 1984;  
accepted February 2, 1984.)



## QUANTIFICATION OF HCl FROM HIGH RESOLUTION INFRARED SOLAR SPECTRA OBTAINED

AT THE SOUTH POLE IN DECEMBER 1986

A. Goldman, F.J. Murcray, F.H. Murcray, and D.G. Murcray

Department of Physics, University of Denver

**Abstract** - Ground-based infrared solar spectra at  $0.02\text{ cm}^{-1}$  resolution obtained at the Amundsen-Scott South Pole station in December 1986 have been analysed for the atmospheric content of HCl. Nonlinear least-squares spectral fitting applied to the spectra yields a total HCl column amount of  $(6.4 \pm 0.8) \times 10^{15}$  molec/cm<sup>2</sup>, most being stratospheric. This amount is larger than that extrapolated from earlier results on the latitudinal distribution of atmospheric HCl.

This Letter reports the determination of HCl total column amount above the South Pole, from ground based solar spectra observations made at the Amundsen-Scott station (altitude 2.85km) in December 1986, by F.J.M. and F.H.M. The spectra were recorded with a  $0.02\text{ cm}^{-1}$  resolution Michelson type interferometer, the same system used to record many balloon-borne, ground based and laboratory spectra by the University of Denver atmospheric spectroscopy group. The South Pole solar spectra were obtained during November 26 - December 3, 1986 and covered large portions of the  $3\text{--}15\text{ }\mu\text{m}$  region. The nearly constant solar zenith angle allowed the co-adding of several spectral scans from a single day for improved signal to noise ratio. The data analysis methods and spectroscopic data base used are similar to those used previously [Goldman et al., 1983, Goldman et al., 1986], applying nonlinear least-squares spectral fitting for the quantification of HCl. Radiosonde ascents from the South Pole (kindly provided by NOAA, Boulder, Colorado) were used to establish the atmospheric temperature-pressure profiles.

Figure 1 shows a typical analysis of the  $2923\text{--}2929\text{ cm}^{-1}$  region, which is dominated by strong  $\text{CH}_4$  lines with some weak  $\text{H}_2\text{O}$  lines, surrounding the quite isolated  $\text{H}^{35}\text{Cl}$  R1 line at  $2925.9\text{ cm}^{-1}$ . For the present analysis, the  $\text{CH}_4$  line parameters were updated [Rothman et al., 1987], but for consistency of comparisons with other recent studies, the previous HCl line parameters were retained (however, the updated HCl parameters lead to only 1% decrease in the column amount). The residual phase distortions, not fully accounted for by the fitted synthetic spectrum, required a more specific fitting for the  $\text{H}^{35}\text{Cl}$  R1 line over a narrower interval. This is presented in Figure 2, which also shows a small asymmetry in the spectral profile (probably due to incomplete adjustment of the instrument). The narrow interval analysis (with larger weight assigned to the high wavenumber half of the line)

yields a total HCl column amount of  $(6.4 \pm 0.8) \times 10^{15}$  molec/cm<sup>2</sup>, most of which is stratospheric, as concluded from spectral fittings with various HCl and temperature-pressure profiles [Goldman et al., 1986]. The HCl in these spectra being mostly stratospheric could have been expected for a high observation point in a low tropopause region such as the south pole. However, the sensitivity of the current spectra (at  $0.02\text{ cm}^{-1}$  resolution and a single solar zenith angle) to the altitude distribution of HCl is limited [Goldman et al., 1983]. Several other HCl lines are quite isolated on the South Pole spectra, such as the R1 and P2  $\text{H}^{35}\text{Cl}$  lines, and these lead to practically the same HCl column amounts. The complete set of the South Pole solar spectra in the  $3\text{ }\mu\text{m}$  region, collected during the week of the measurements, shows no significant change in the HCl amounts.

This is the first HCl measurement reported from the South Pole and is of particular interest to current studies of the chemistry and dynamics of the Antarctic atmosphere. Previous measure-

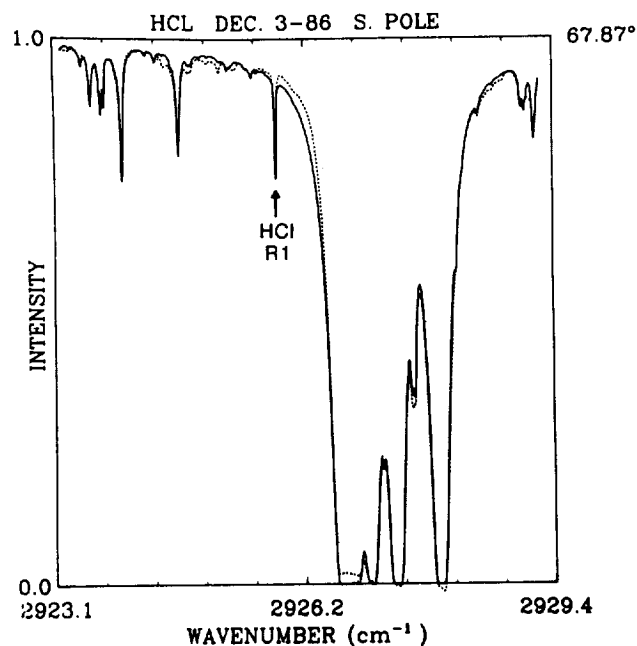


Fig. 1. Solar spectrum (dotted line) obtained from the South Pole on December 3, 1986 and nonlinear least-squares fit (solid line) in the  $2923\text{--}2929\text{ cm}^{-1}$  region. The amplitude is the measured signal, normalized to the maximum envelope value over the interval. The marked feature at  $2925.9\text{ cm}^{-1}$  is the (0-1)  $\text{H}^{35}\text{Cl}$  R1 line. The solar zenith angle was fixed at  $67.87^\circ$ .

Copyright 1987 by the American Geophysical Union.

Paper Number 7L6546.

0094-8276/87/007L-6546\$03.00



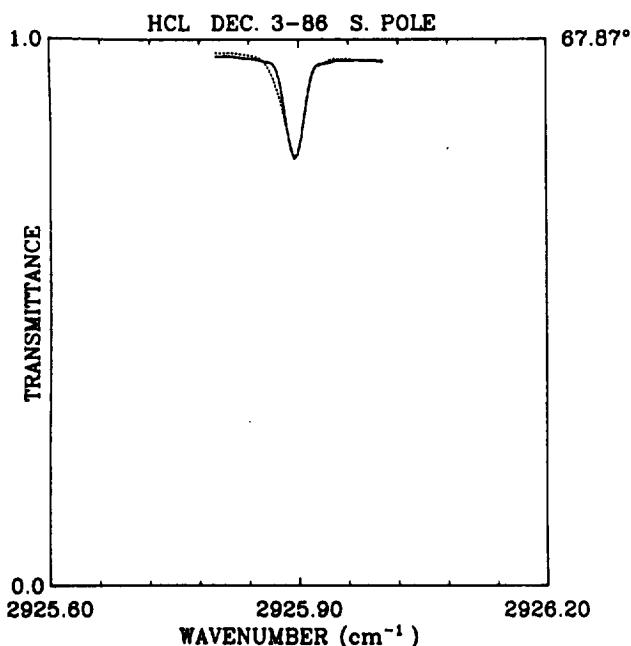


Fig. 2. Nonlinear least-squares fit of the  $\text{H}^{35}\text{Cl}$  R1 absorption line at  $2925.9\text{cm}^{-1}$  in the solar spectrum of Fig. 1. The amplitude is plotted on a transmittance scale. The total HCl column amount of the fitted profile is  $(6.4 \pm 0.8) \times 10^{15}$  molec/cm<sup>2</sup>.

ments and assessments [Mankin et. al., 1983, Molina et. al., 1985] of the latitudinal dependence of stratospheric HCl show total column values above 12km increasing from  $0.7 \times 10^{15}$  molec/cm<sup>2</sup> near the equator, to  $2.7 \times 10^{15}$  molec/cm<sup>2</sup> at 70°N, with an extrapolated value of  $3.4 \times 10^{15}$  molec/cm<sup>2</sup> at 90°N. South latitude measurements [Girard et. al., 1983] of HCl column above 11.5km show values increasing from  $0.8 \times 10^{15}$  molec/cm<sup>2</sup> at 1°S to  $2.7 \times 10^{15}$  molec/cm<sup>2</sup> at 60°S, implying a symmetrical North-South distribution for these latitudes. While there are unresolved difficulties in assessing the tropospheric HCl content and variability, it has been established that most of the HCl total column is stratospheric, and that it has been increasing with time, at an annual rate of 5% per year.

The present result for the column amount of HCl above the South Pole is larger than the extrapolated values from the northern or southern latitude's results, even if we assume a temporal increase of 5% per year as has been reported by Mankin et al [1983]. It is probably characteristic of the Antarctic atmosphere at the end of the period of the spring ozone depletion.

Work is in progress on the quantification of several other atmospheric trace constituents observable in the 1986 South Pole Solar spectra

reported here. Further measurements need to be made for monitoring HCl and other species during the ozone depletion periods.

**Acknowledgments.** This research was supported in part by the National Science Foundation Division of Polar Programs, and in part by the Fluorocarbon Program Panel of the Chemical Manufacturers Association. Acknowledgment is made to the National Center for Atmospheric Research, which is supported by NSF, for computer time used in this research. Discussions with W.G. Mankin on the trends of stratospheric HCl are acknowledged.

#### References

- Girard, A., G. Fergant, L. Gramont, O. Lado-Borodowsky, J. Laurent, S. Le Boiteux, M.P. Lemaitre and N. Louisnard, Latitudinal Distribution of Ten Stratospheric Species Deduced from Simultaneous Spectroscopic Measurements, *J. Geophys. Res.*, **88**, 5377-5392, 1983.
- Goldman, A., F.G. Fernald, F.J. Murcray, F.H. Murcray, and D.G. Murcray, Spectral Least Squares Quantification of Several Atmospheric Gases from High Resolution Infrared Solar Spectra Obtained at the South Pole, *J. Quant. Spectrosc. Radiat. Transfer*, **29**, 189-204, 1983.
- Goldman, A., F.J. Murcray, R.D. Blatherwick, and D.G. Murcray, Quantification of HCl from High Resolution Ground-Based Infrared Solar Spectra in the  $3000\text{cm}^{-1}$  Region, *J. Quant. Spectrosc. Radiat. Transfer*, **36**, 385-387, 1986.
- Mankin, W.G., and M.T. Coffey, Latitudinal Distributions and Temporal Changes of Stratospheric HCl and HF, *J. Geophys. Res.*, **88**, 10,776-10,784, 1983.
- Molina, M.J., R. deZafra, P. Fabian, C.B. Farmer, W.G. Mankin, N.D. Sze, J. Waters and R.J. Zander, Halogenated Species, Chap. 11 in *Atmospheric Ozone, 1985: Assessment of our Understanding of the Processes Controlling its Present Distribution and Change*, WMO Report No. 16; WMO, B.P. 5, Geneva, Switzerland, 1986.
- Rothman, L.S., R.R. Gamache, A. Goldman, L.R. Brown, R.A. Toth, H. Pickett, R.P. Poynter, J.-M. Flaud, C. Camy-Peyret, A. Barbe, N. Husson, M.A.H. Smith and C.P. Rinsland, The HITRAN Database: 1986 Edition, in press, *Appl. Opt.*, 1987.
- A. Goldman, F.J. Murcray, F.H. Murcray, and D.G. Murcray, Department of Physics, University of Denver, Denver, CO 80208

(Received March 20, 1987;  
accepted April 20, 1987.)

